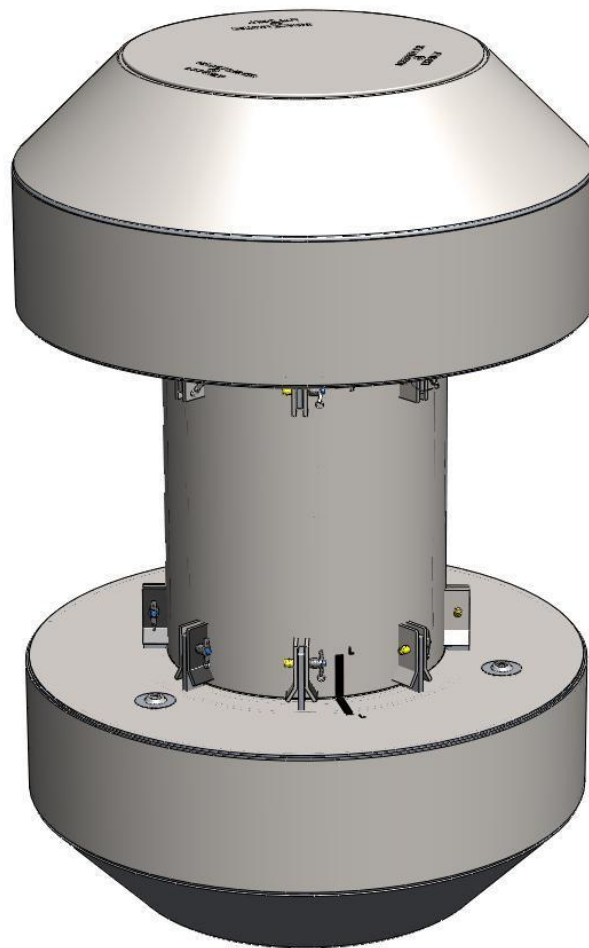




DOCKET 71-9341

BEA Research Reactor Package



Safety Analysis Report

AREVA Federal Services LLC

Revision 2
November 2009

TABLE OF CONTENTS

1.0 GENERAL INFORMATION 1.1-1

1.1 Introduction..... 1.1-1

1.2 Package Description..... 1.2-1

1.2.1 Packaging..... 1.2-1

1.2.2 Contents 1.2-5

1.2.3 Special Requirements for Plutonium 1.2-7

1.2.4 Operational Features 1.2-7

1.3 Appendices..... 1.3-1

1.3.1 References..... 1.3-1

1.3.2 Glossary of Terms and Acronyms 1.3-2

1.3.3 Packaging General Arrangement Drawings..... 1.3-4

2.0 STRUCTURAL EVALUATION 2.1-1

2.1 Structural Design 2.1-1

2.1.1 Discussion 2.1-1

2.1.2 Design Criteria 2.1-2

2.1.3 Weights and Centers of Gravity..... 2.1-6

2.1.4 Identification of Codes and Standards for Package Design..... 2.1-6

2.2 Materials 2.2-1

2.2.1 Material Properties and Specifications 2.2-1

2.2.2 Chemical, Galvanic, or Other Reactions 2.2-1

2.2.3 Effects of Radiation on Materials 2.2-2

2.3 Fabrication and Examination 2.3-1

2.3.1 Fabrication 2.3-1

2.3.2 Examination 2.3-1

2.4 General Standards for All Packages 2.4-1

2.4.1 Minimum Package Size 2.4-1

2.4.2 Tamper-Indicating Feature 2.4-1

2.4.3 Positive Closure 2.4-1

2.4.4 Valves 2.4-1

2.4.5 Package Design..... 2.4-1

2.4.6 External Temperatures 2.4-1

2.4.7 Venting..... 2.4-2

2.5 Lifting and Tie-down Standards for All Packages 2.5-1

2.5.1 Lifting Devices..... 2.5-1

2.5.2 Tie-down Devices 2.5-1

2.6 Normal Conditions of Transport..... 2.6-1

2.6.1 Heat 2.6-1

2.6.2 Cold..... 2.6-7

2.6.3 Reduced External Pressure 2.6-9

2.6.4 Increased External Pressure 2.6-9

2.6.5 Vibration 2.6-10

2.6.6 Water Spray 2.6-11

2.6.7 Free Drop 2.6-11

2.6.8	Corner Drop	2.6-15
2.6.9	Compression	2.6-15
2.6.10	Penetration	2.6-15
2.7	Hypothetical Accident Conditions	2.7-1
2.7.1	Free Drop	2.7-1
2.7.2	Crush	2.7-18
2.7.3	Puncture	2.7-18
2.7.4	Thermal	2.7-20
2.7.5	Immersion – Fissile	2.7-22
2.7.6	Immersion – All Packages	2.7-22
2.7.7	Deep Water Immersion Test	2.7-22
2.7.8	Summary of Damage	2.7-23
2.8	Accident Conditions for Air Transport of Plutonium	2.8-1
2.9	Accident Conditions for Fissile Material Packages for Air Transport	2.9-1
2.10	Special Form	2.10-1
2.11	Fuel Rods	2.11-1
2.12	Appendices	2.12-1
2.12.1	References	2.12.1-1
2.12.2	Certification Test Plan	2.12.2-1
2.12.3	Certification Test Results	2.12.3-1
2.12.4	Stress Analysis Finite Element Models	2.12.4-1
2.12.5	Impact Limiter Performance Evaluation	2.12.5-1
2.12.6	Analysis Software Descriptions	2.12.6-1
2.12.7	Seal Performance Tests	2.12.7-1
2.12.8	Fuel Basket Stress Analysis	2.12.8-1
3.0	THERMAL EVALUATION	3.1-1
3.1	Description of Thermal Design	3.1-1
3.1.1	Design Features	3.1-1
3.1.2	Content's Decay Heat	3.1-3
3.1.3	Summary Tables of Temperatures	3.1-4
3.1.4	Summary Tables of Maximum Pressures	3.1-4
3.2	Material Properties and Component Specifications	3.2-1
3.2.1	Material Properties	3.2-1
3.2.2	Technical Specifications of Components	3.2-3
3.3	Thermal Evaluation for Normal Conditions of Transport	3.3-1
3.3.1	Heat and Cold	3.3-1
3.3.2	Maximum Normal Operating Pressure	3.3-3
3.3.3	Vacuum Drying Operations	3.3-4
3.4	Thermal Evaluation for Hypothetical Accident Conditions	3.4-1
3.4.1	Initial Conditions	3.4-1
3.4.2	Fire Test Conditions	3.4-2
3.4.3	Maximum Temperatures and Pressure	3.4-2
3.4.4	Maximum Thermal Stresses	3.4-3
3.5	Appendices	3.5-1
3.5.1	References	3.5-2
3.5.2	Computer Analysis Results	3.5-4

3.5.3	Analytical Thermal Model.....	3.5-4
3.5.4	'Last-A-Foam' Response under HAC Conditions.....	3.5-35
4.0	CONTAINMENT	4.1-1
4.1	Description of the Containment System	4.1-1
4.1.1	Containment Boundary	4.1-1
4.1.2	Containment Penetrations	4.1-1
4.1.3	Seals	4.1-1
4.1.4	Welds	4.1-2
4.1.5	Closure	4.1-2
4.2	Containment Under Normal Conditions of Transport	4.2-1
4.3	Containment Under Hypothetical Accident Conditions	4.3-1
4.4	Leakage Rate Tests for Type B Packages.....	4.4-1
4.4.1	Fabrication Leakage Rate Tests	4.4-1
4.4.2	Maintenance/Periodic Leakage Rate Tests	4.4-1
4.4.3	Preshipment Leakage Rate Tests	4.4-1
4.5	Appendix.....	4.5-1
4.5.1	References.....	4.5-1
5.0	SHIELDING EVALUATION	5.1-1
5.1	Description of Shielding Design.....	5.1-1
5.1.1	Design Features.....	5.1-1
5.1.2	Summary Table of Maximum Radiation Levels.....	5.1-1
5.2	Source Specification	5.2-1
5.2.1	Gamma Source.....	5.2-1
5.2.2	Neutron Source	5.2-6
5.3	Shielding Model.....	5.3-1
5.3.1	Configuration of Source and Shielding	5.3-1
5.3.2	Material Properties.....	5.3-2
5.4	Shielding Evaluation.....	5.4-1
5.4.1	Methods.....	5.4-1
5.4.2	Input and Output Data.....	5.4-1
5.4.3	Flux-to-Dose Rate Conversion	5.4-2
5.4.4	External Radiation Levels.....	5.4-2
5.5	Appendices.....	5.5-1
5.5.1	References.....	5.5-1
5.5.2	Detailed MITR-II Results	5.5-1
5.5.3	Sample Input Files	5.5-7
6.0	CRITICALITY EVALUATION.....	6.1-1
6.1	Description of Criticality Design.....	6.1-1
6.1.1	Design Features.....	6.1-1
6.1.2	Summary Table of Criticality Evaluation.....	6.1-1
6.1.3	Criticality Safety Index	6.1-2
6.2	Fissile Material Contents	6.2-1
6.2.1	MURR Fuel Element	6.2-1
6.2.2	MITR-II Fuel Element	6.2-2
6.2.3	ATR Fuel Element	6.2-3
6.2.4	TRIGA Fuel Element.....	6.2-4

6.3	General Considerations	6.3-1
6.3.1	Model Configuration.....	6.3-1
6.3.2	Material Properties.....	6.3-2
6.3.3	Computer Codes and Cross-Section Libraries.....	6.3-2
6.3.4	Demonstration of Maximum Reactivity	6.3-3
6.4	Single Package Evaluation.....	6.4-1
6.4.1	Configuration	6.4-1
6.4.2	Results.....	6.4-3
6.5	Evaluation of Package Arrays under Normal Conditions of Transport.....	6.5-1
6.5.1	Configuration	6.5-1
6.5.2	Results.....	6.5-1
6.6	Package Arrays under Hypothetical Accident Conditions	6.6-1
6.6.1	Configuration	6.6-1
6.6.2	Results.....	6.6-2
6.7	Fissile Material Packages for Air Transport.....	6.7-1
6.8	Benchmark Evaluations	6.8-1
6.8.1	Applicability of Benchmark Experiments	6.8-1
6.8.2	Bias Determination	6.8-2
6.9	Appendices.....	6.9-1
6.9.1	References.....	6.9-1
6.9.2	Parametric Evaluations to Determine the Most Reactive Fuel Geometries	6.9-1
6.9.3	Sample Input Files	6.9-14
7.0	PACKAGE OPERATIONS.....	7.1-1
7.1	Procedures for Loading the Package.....	7.1-1
7.1.1	Preparation for Loading	7.1-1
7.1.2	Loading of Contents.....	7.1-1
7.1.3	Preparation for Transport.....	7.1-4
7.2	Procedures for Unloading the Package.....	7.2-1
7.2.1	Receipt of Package from Carrier.....	7.2-1
7.2.2	Removal of Contents.....	7.2-1
7.3	Preparation of an Empty Package for Transport.....	7.3-1
7.4	Preshipment Leakage Rate Test.....	7.4-1
7.4.1	Gas Pressure Rise Leakage Rate Test Acceptance Criteria.....	7.4-1
7.4.2	Determining the Test Volume and Test Time.....	7.4-1
7.4.3	Performing the Gas Pressure Rise Leakage Rate Test.....	7.4-2
7.4.4	Optional Preshipment Leakage Rate Test.....	7.4-2
7.5	Appendix.....	7.5-1
7.5.1	References.....	7.5-1
8.0	ACCEPTANCE TESTS AND MAINTENANCE PROGRAM.....	8.1-1
8.1	Acceptance Tests	8.1-1
8.1.1	Visual Inspection and Measurements	8.1-1
8.1.2	Weld Examinations.....	8.1-1
8.1.3	Structural and Pressure Tests.....	8.1-1
8.1.4	Fabrication Leakage Rate Tests.....	8.1-2
8.1.5	Component and Material Tests	8.1-6

BRR Package Safety Analysis Report

8.1.6	Shielding Integrity Tests	8.1-13
8.1.7	Thermal Tests.....	8.1-14
8.2	Maintenance Program	8.2-1
8.2.1	Structural and Pressure Tests	8.2-1
8.2.2	Maintenance/Periodic Leakage Rate Tests	8.2-1
8.2.3	Component and Material Tests	8.2-3
8.2.4	Thermal Tests.....	8.2-4
8.3	Appendix.....	8.3-1
8.3.1	References.....	8.3-1

1.0 GENERAL INFORMATION

This section presents a general introduction and description of the BEA Research Reactor (BRR) package. The BRR package is used to transport fuel elements that have been irradiated in various test and research reactors, including the University of Missouri Research Reactor (MURR), the Massachusetts Institute of Technology Nuclear Research Reactor (MITR-II), Advanced Test Reactor (ATR), and Training, Research, Isotopes, General Atomics (TRIGA) reactors. This application seeks authorization of the BRR package as a Type B(U)F-96 shipping container in accordance with the provisions of Title 10, Part 71 of the Code of Federal Regulations [1].

The major components comprising the package are discussed in Section 1.2.1, *Packaging*, and illustrated in Figure 1.2-1 through Figure 1.2-7. A glossary of terms is presented in Appendix 1.3.2, *Glossary of Terms and Acronyms*. Detailed drawings of the package design are presented in Appendix 1.3.3, *Packaging General Arrangement Drawings*.

1.1 Introduction

The BRR package has been developed to transport irradiated research reactor fuel. The fuel is primarily of two basic types: highly enriched aluminum-uranium plate fuel, and TRIGA fuel of varying enrichments. Within the package, the fuel is contained in basket structures specifically designed for each fuel type, and that provide for optimum heat rejection and criticality control.

The packaging consists of a payload basket, a lead-shielded cask body, an upper shield plug, a closure lid, and upper and lower impact limiters. The package is of conventional design and utilizes ASTM Type 304 stainless steel as its primary structural material. The package is designed to provide leaktight containment of the radioactive contents under all NCT and HAC.¹

The BRR package may be used in a pool or hot cell environment. The cask body is provided with a drain port, and is intended for use with a drying system to ensure that water is not present during transport. The package is designed to be transported singly, with its longitudinal axis vertical, by highway truck or by rail in exclusive use. When loaded and prepared for transport, the BRR package is 119.5 inches long, 78 inches in diameter (over the impact limiters), and weighs 32,000 lb.

Based on the criticality assessment provided in Chapter 6, *Criticality Evaluation*, the criticality safety index for the BRR package is zero.

¹ Leaktight is defined as a maximum of 1×10^{-7} reference-cm³/sec, air leakage per ANSI N14.5-1997 [2].

1.2 Package Description

This section presents a basic description of the BRR package components and construction. General arrangement drawings are provided in Appendix 1.3.3, *Packaging General Arrangement Drawings*.

1.2.1 Packaging

The BRR package consists of a payload basket (of a design that is specific for the fuel being transported), a lead–shielded cask body, a separate, removable upper shield plug, a closure lid, twelve closure bolts, and upper and lower impact limiters containing polyurethane foam. Except for the closure bolts and impact limiter attachments, the package is of primarily welded construction, using Type 304 austenitic stainless steel. These components will now be discussed in detail.

1.2.1.1 Cask Body

The BRR cask body is a right circular cylinder 77.1 inches long and 38 inches in diameter (not including the impact limiter attachments and the thermal shield). It is composed of upper and lower massive end structures connected by inner and outer shells. Thick lead shielding is located between the two circular shells, in the lower end structure, and in the shield plug. The payload cavity has a diameter of 16 inches and a length of 54 inches.

The massive end structures may be cast from ASTM A351, Grade CF8A, or forged from ASTM A182, Type F304. The lower end structure contains a drain to allow removal of water from the payload cavity. The inner shell may be cast from ASTM A451, Grade CPF8A, or forged from ASTM A182, Type F304. The outer shell may be made from ASTM A240, Type 304 plate, or optionally cast from ASTM A451, Grade CPF8A or forged from ASTM A182, Type F304. The outer shell may have up to two, full penetration longitudinal seam welds. The inner shell is one inch thick, and is welded to each end structure using a full penetration weld. The outer shell is two inches thick, and is connected to each end structure using a full penetration weld. The weld of the outer shell to the upper end structure is made after lead pour.

The cask is lifted using four, 1–8 UNC threaded holes in the upper end structure, that may be optionally fitted with heavy duty thread inserts. See Zone D2 of sheet 3 of drawing 1910–01–01–SAR.

On the outside of the outer shell, in the region not covered by the impact limiters, is a thermal shield composed of an outer sheet of 12 gauge (0.105–inch thick) Type 304 stainless steel, separated from the outer shell by small strips of the same 12 gauge material.

A set of eight receptacles are attached to the outer shell at each end of the exposed region of the cask (total of 16 receptacles), that serve as impact limiter attachments (see Zone A4 of sheet 2 of drawing 1910–01–01–SAR). The receptacles consist of two closely spaced plates, 1/2–inches thick, that pass through the thermal shield and attach directly to the outer shell using a full penetration groove weld with a 1/2–inch fillet reinforcement on one side. Each impact limiter features eight, 3/4–inch thick blades that pass between the receptacle plates on the cask body. The attachment is completed by passing a one inch diameter, stainless steel ball lock pin through the three plates. The ball lock pins therefore act in double shear. Each impact limiter is retained by eight such attachments.

All lead shielding is made from ASTM B29, chemical lead, or optionally, from lead per Federal Specification QQ–L–171E, Grade A or C. The lead shield on the side of the cask body is cast–

BRR Package Safety Analysis Report

in-place through the upper end structure, and is nominally 8 inches thick. The shield at the bottom is made from lead sheet material that is packed firmly into place, and is 7.7 inches thick. The bottom lead cavity is closed using a one inch thick plate secured with a full penetration groove weld, see Zone A6/7 of sheet 3 of drawing 1910-01-01-SAR.

The removable shield plug is located at the top of the payload cavity. The outer shell is made from Type 304 plate material of 1/2-inch, 3/8-inch, 1-inch, and 1/2-inch thickness. See Zone D2 of sheet 4 of drawing 1910-01-01-SAR. The cavity is filled with lead sheet material that is packed firmly into place. The total thickness of the plug is 11.2 inches, and the lead thickness is 9.7 inches. The plug rests on a shoulder located approximately half way along the length of the plug. A corresponding shoulder is located in the upper end structure of the cask body to support the shield plug. A 3/4-inch diameter pipe passes through the plug to ensure proper draining and drying of the cask. The pipe is oriented approximately diagonally to prevent a deleterious shine path. The shield plug is lifted using a central, 1/2-13 UNC threaded hole.

The closure lid is made from 2-inch thick, ASTM A240, Type 304 stainless steel plate. It is attached to the cask using 12, 1-8 UNC bolts made of ASTM A320, Grade L43 material, with hardened steel washers. The bolts are plated with electroless nickel per MIL-DTL-26074 Rev. F Class 1 Grade B, and tightened to a torque of 220 ± 20 ft-lb. The mating holes in the cask body may be optionally fitted with heavy duty thread inserts. The mating surface of the lid features a step relief located at the bolt circle. This relief prevents any contact from occurring between the lid and the body outside of the bolt circle, thus preventing prying loads from being applied to the closure bolts. The closure lid includes two O-ring seals made from butyl rubber of 3/8-inch cross sectional diameter. The inner O-ring is the containment seal, and the outer is the test seal. The seals are retained in dovetail grooves in the lid. The O-ring material (including the sealing washers, see below) is made from Rainier Rubber R-0405-70, and subject to the tests given in Section 8.1.5.2.

The BRR package provides a single level of leaktight containment. The containment boundary of the BRR package consists of the following elements. Unless noted, all elements are made of ASTM Type 304 stainless steel in various product forms.

- The lower massive end structure (including the passage to the drain port)
- The inner cylindrical shell
- The upper massive end structure
- The containment O-ring seal (the inner seal in the closure lid)
- The closure lid
- The vent port in the closure lid
- The drain port in the lower end structure

The containment boundary is shown in Figure 1.2-12.

As noted above, the BRR package features two ports that are part of the containment boundary: a vent port in the closure lid, and a drain port in the lower end structure. Both ports are closed with threaded plugs made of ASTM B16 brass and sealed with butyl rubber sealing washers. A

threaded brass cover is used to protect the port plugs. A seal test port is located between the containment O-ring seal and test O-ring seals, and is not part of containment.

1.2.1.2 Impact Limiters

Impact limiters are attached to each end of the BRR package, having essentially identical design, and are shown in drawing 1910-01-02-SAR. Each limiter is 78 inches in diameter and 34.6 inches long overall, with a conical section 15 inches long towards the outer end. The impact limiter design consists of Type 304 stainless steel shells and approximately 9 lb/ft³ polyurethane foam. The external shells (except for the end plate) are 1/4 inches thick, and the internal shells (that interface with the cask body) are 1/2 inches thick. The outer end plate is 1/2 inches thick. The closure end impact limiter features three reinforced, 1/2-13UNC holes for lifting of the impact limiter only. The polyurethane foam is rigid, closed-cell, and is poured in place. On the side that mates with the cask, the annular sheet features three plastic melt-out plugs designed to relieve pressure in the HAC fire event. The attachment of the impact limiters to the cask body is described in Section 1.2.1.1, *Cask Body*.

1.2.1.3 Baskets

There are four baskets used with the BRR package, one for each type of fuel transported, and are shown in drawing 1910-01-03-SAR. The baskets are made from welded construction using Type 304 stainless steel in plate, bar, pipe, and tubular forms. Each basket has a diameter of 15.63 inches and a length of 53.45 inches, and features a number of cavities that fit the size and shape of the fuel. The cavities are sized to minimize free play between the fuel and the basket, while ensuring free insertion and removal of the elements. The baskets are open on the top, and the fuel is located at the top end, nearest the shield plug. The baskets are designed to freely drain water when the cask is lifted out of the spent fuel pool.

1.2.1.3.1 MURR

The MURR basket consists of an outer rolled shell, an inner pipe, and thick radial plates that form eight pie-shaped cavities for the fuel in a circular array. The bottom of the fuel cavities is formed by a 3/8-inch thick plate that is welded to the inside of the shell. The lifting bar divides the interior of the inner tube in half and prevents loading any fuel within the inner tube. The MURR basket is shown in Figure 1.2-4.

1.2.1.3.2 MITR-II

The MITR-II basket consists of eleven diamond-shaped tubes that match the shape and size of the fuel. Three tubes are arranged side-by-side in the center, and eight tubes are arrayed around the outside. Tubes are held in place by a top plate, a bottom support plate, and a central support plate. The bottom support plate is 1/2-inches thick. A 14-inch diameter, 1/4-inch thick circular shell forms the lower portion of the basket. The MITR-II basket is shown in Figure 1.2-5.

1.2.1.3.3 ATR

The ATR basket consists of a rolled outer shell, an inner pipe, and radial plates that form eight pie-shaped cavities for the fuel in a circular array. Since the outer shell is somewhat smaller than the cask cavity, the ATR basket features four circular ribs having an outer diameter of 15.63 inches. The bottom support plate is 1/2-inch thick. The lifting bar divides the interior of the inner tube in half and prevents loading any fuel within the inner tube. The ATR basket is shown in Figure 1.2-6.

1.2.1.3.4 TRIGA

The TRIGA basket consists of an array of 19 tubes having a 2-inch outer diameter and an 11-gauge wall thickness. The tubes are held in place by a top plate, a bottom support plate, and a central support plate. A 13-inch diameter, 1/4-inch thick circular shell forms the lower portion of the basket. The short spacer pedestal and the adjustable spacer pedestal are used to customize the fuel cavity for various TRIGA fuel lengths. The TRIGA basket is shown in Figure 1.2-7.

1.2.1.4 Gross Weight

The gross weight of the BRR package, including the cask, impact limiters, and maximum payload, is 32,000 lb. A summary of overall component weights is shown in Table 2.1-2 and discussed in Section 2.1.3, *Weights and Centers of Gravity*.

1.2.1.5 Neutron Moderation and Absorption

The BRR package maintains criticality control by means of limitation of the quantity of fissile material present and by maintaining a safe configuration of the material under all NCT and HAC. The design of the BRR package does not include any components whose principal purpose is the absorption of neutrons. A more detailed description of the package criticality control functions is given in Chapter 6, *Criticality Evaluation*.

1.2.1.6 Receptacles, Valves, Testing and Sampling Ports

The BRR package closure lid contains a vent port and a containment seal test port. A body drain port is located on the side of the lower end of the cask. There are no valves or receptacles used in the BRR package.

1.2.1.7 Heat Dissipation

The dissipation of heat from the BRR package is entirely passive. The impact limiters are painted white to reduce the absorption of solar heat. A thermal shield is used on the cask body to limit the temperature of the lead gamma shield in the HAC fire event. A more detailed description of the package thermal design is given in Chapter 3, *Thermal Evaluation*.

1.2.1.8 Lifting and Tie-down Devices

Other than the threaded holes in the top of the cask body, there are no lifting or tie-down devices that are a structural part of the BRR package. The package is secured to the transport vehicle

using structures that interface with the surfaces of the upper and lower impact limiters. The package rests on a lower frame that is attached to the vehicle. An upper frame contacts the upper impact limiter and is attached to the vehicle using cables or the equivalent. There are no provisions to lift the package with the impact limiters installed.

1.2.1.9 Pressure Relief System

There is no pressure relief system in the BRR package.

1.2.1.10 Shielding

Biological shielding of gamma radiation is provided by a combination of lead and the thick steel shells of the BRR package. Hydrogenous neutron shielding is not necessary and none is included in the package design. Details of the gamma shielding are provided in Section 1.2.1.1, *Cask Body*. A full assessment of the shielding design is provided in Chapter 5, *Shielding Evaluation*.

1.2.2 Contents

The BRR package may contain up to 8 irradiated MURR fuel elements, up to 11 irradiated MITR-II fuel elements, up to 8 irradiated ATR fuel elements, and up to 19 irradiated TRIGA fuel elements. Only one fuel element is allowed per basket location. Details for each fuel type are provided in the following paragraphs.

1.2.2.1 MURR

The MURR fuel element may be irradiated to a maximum burnup of 180 MWD (218,196 MWD/MTU, or a U-235 depletion of 30.9%). The minimum cooling time is 180 days after reactor shutdown.

Each fresh MURR element contains 775.0 ± 7.8 g U-235, enriched up to 93 wt.%. The weight percents of the remaining uranium isotopes are 1.2 wt.% U-234, 0.7 wt.% U-236, and 5.0 – 7.0 wt.% U-238. The MURR fuel element fissile material is uranium aluminide (UAl_x).

Each MURR fuel element contains 24 curved fuel plates. Fuel plate 1 has the smallest radius, while fuel plate 24 has the largest radius, as shown in Figure 1.2-8. The fuel “meat” is a mixture of uranium metal and aluminum, while the cladding and structural materials are an aluminum alloy. The fuel plates are rolled to shape and swaged into the two fuel element side plates. The fissile material (uranium aluminide) is nominally 0.02-in thick for all 24 plates. Fuel element side plates are fabricated of ASTM B 209, aluminum alloy 6061-T6 or 6061-T651 and are approximately 0.15-in thick. The fuel plates are typically spaced with a 0.08-in gap between plates.

The MURR element overall length, including irradiation growth, is 32.75 inches. The bounding weight of one assembly is 15 lb. The maximum decay heat per fuel element is 158 W.

1.2.2.2 MITR-II

The MITR-II fuel element may be irradiated to a maximum burnup of 225 MWD (418,500 MWD/MTU, or a U-235 depletion of 59.3%). The minimum cooling time is 930 days after reactor shutdown.

Each fresh MITR-II element contains 510.0 +3.0/-10.0 g U-235, enriched up to 93 wt.%. The weight percents of the remaining uranium isotopes are 1.2 wt.% U-234, 0.7 wt.% U-236, and 5.0 – 7.0 wt.% U-238. Like the MURR fuel element, the MITR-II fuel element fissile material is uranium aluminide (UAl_x).

Each MITR-II fuel element contains 15 flat fuel plates, as shown in Figure 1.2-9. The fuel plates are fabricated and swaged into the two fuel element side plates. The fuel “meat” is a mixture of uranium metal and aluminum, while the cladding and structural materials are an aluminum alloy. The fissile material (uranium aluminide) is nominally 0.03-in thick and the cladding is nominally 0.025-in thick. Fuel element side plates are fabricated of ASTM B 209, aluminum alloy 6061-T6 and are approximately 0.19-in thick. The fuel plates are nominally 0.08 inches apart.

The MITR-II element overall length, including irradiation growth, is 26.52 inches. The bounding weight of one assembly is 10 lb. The maximum decay heat per assembly is 30 W.

1.2.2.3 ATR

The ATR fuel element may be irradiated to a maximum burnup of 480 MWD¹ (491,155 MWD/MTU, or a U-235 depletion of 58.6%). The minimum cooling time is 1,670 days (4.6 years) after reactor shutdown.

There are two general classes of ATR fuel element, XA and YA. The XA fuel element has a fresh fuel loading of 1,075 ± 10 g U-235. The weight percents of the remaining uranium isotopes are 1.2 wt.% U-234 (max), 0.7 wt.% U-236 (max), and 5.0 – 7.0 wt.% U-238. Like the MURR and MITR-II fuel elements, the fuel element fissile material is uranium aluminide (UAl_x).

The XA fuel element is further subdivided into fuel element types 7F, 7NB, 7NBH. In the 7F fuel element, all 19 fuel plates are loaded with enriched uranium in an aluminum matrix with the eight outer plates (1 through 4 and 16 through 19) containing boron as a burnable poison. The fuel element with the greatest reactivity is the 7NB that contains no burnable poison. The 7NBH fuel element is similar to the 7NB fuel element except that it contains one or two borated plates. The YA fuel element is identical to the 7F fuel element except that plate 19 of the YA fuel element is an aluminum alloy plate containing neither uranium fuel nor boron burnable poison. The YA fuel element has a fresh fuel loading of 1,022.4 ± 10 g U-235. A second YA fuel element design (YA-M) has the side plate width reduced by 15 mils.

The ATR fuel elements contain 19 curved fuel plates. A section view of an ATR fuel element is given in Figure 1.2-10. Note that an intact ATR fuel element has end boxes (as shown on Figure 1.2-10), although these end boxes are removed prior to insertion in the BRR package. The fuel

¹ The element burnup of 480 MWD should not be a limit for licensing purposes because the element burnup is typically not known in units of MWD. The final U-235 mass within an element is computed and recorded by ATR staff.

plates are rolled to shape and swaged into the two fuel element side plates. Fuel plate 1 has the smallest radius, while fuel plate 19 has the largest radius. The fissile material (uranium aluminide) is nominally 0.02-in thick for all 19 plates. Fuel element side plates are fabricated of ASTM B 209, aluminum alloy 6061-T6 or 6061-T651 and are approximately 0.19-in thick. The fuel plates are typically spaced with a 0.08-in gap between plates.

The ATR element overall length, after removal of the end box structures, 51.0 inches max. The bounding weight of one assembly is 25 lb. The maximum decay heat per assembly is 30 W.

1.2.2.4 TRIGA

Many different types of TRIGA fuel elements have been fabricated over the past several decades. TRIGA fuel elements utilize a zirconium hydride fuel matrix. The BRR package is limited to five specific TRIGA fuel types:

1. 8 wt.% uranium aluminum clad element (General Atomics catalog number 101)
2. 8.5 wt.% uranium stainless steel clad element (General Atomics catalog number 103)
3. 8.5 wt.% uranium stainless steel clad element, high enriched uranium (General Atomics catalog number 109). This fuel element is sometimes referred to in the literature as a Fuel Life Improvement Program (FLIP) element.
4. 20 wt.% uranium stainless steel clad element (General Atomics catalog number 117). This fuel element is sometimes referred to in the literature as a FLIP-LEU-I element.
5. 8.5 wt.% uranium stainless steel clad element, instrumented (General Atomics catalog number 203).

Basic fresh fuel data used to describe the various TRIGA fuel elements are summarized in Table 1.2-1. The maximum length of an element, including irradiation growth, is 45.50 inches. Non-instrumented fuel elements are somewhat shorter. For all fuel elements, spacers are utilized within the TRIGA baskets.

The maximum burnup and minimum cooling time varies for the five fuel element types and is summarized in Table 1.2-2. The two FLIP elements have significantly higher U-235 loadings and hence much larger burnups and longer cooling times. The bounding weight of any TRIGA fuel element is 10 lb. The maximum decay heat per element is 20 W.

1.2.3 Special Requirements for Plutonium

The BRR package may contain plutonium in excess of 20 Ci as a consequence of irradiation of the reactor fuel. As such, the plutonium is in solid form within the fuel matrix. Table 1.2-3 summarizes the plutonium activity for each of the four fuel types, both on a per-element and per-package basis. The maximum quantity of plutonium for the BRR package is 873 Ci.

1.2.4 Operational Features

The BRR package is of conventional design and is not complex to operate. Operational features are depicted on the drawings provided in Appendix 1.3.3, *Packaging General Arrangement*

BRR Package Safety Analysis Report

Drawings. Operating procedures and instructions for loading, unloading, and preparing an empty package for transport are provided in Chapter 7, *Package Operations*.

Table 1.2-1 – TRIGA Fresh Fuel Characteristics

Parameter	GA Cat. # 101	GA Cat. # 103	GA Cat. # 109	GA Cat. # 117	GA Cat. # 203
General Description	8 wt.% aluminum clad	8.5 wt.% stainless steel clad	8.5 wt.% stainless steel clad, HEU	20 wt.% stainless steel clad	8.5 wt.% instrumented stainless steel clad
Active Fuel Length (in)	14	15	15	15	15
Fuel Pellet OD (in)	1.41	1.44	1.44	1.44	1.44
U (wt.% in fuel)	8.0	8.5	8.5	20	8.5
U (g)	180	195	196	504	195
U-235 (wt.% in U)	20	20	70	20	20
U-235 (g)	36	39	137	101	39
H/Zr	1.0	1.7	1.6	1.6	1.7
Erbium (wt.%)	0	0	1.3	0.5	0
Zirconium Center Rod Length (in)	n/a	15.0	15.0	15.0	15.0
Overall Element Length (in)**	28.37	28.90	28.90	29.68	45.25
Cladding OD (in)	1.48	1.48	1.48	1.48	1.48
Cladding Thickness (in)	0.03	0.02	0.02	0.02	0.02
Graphite Reflector Length Top/Bottom (in)	4.0 / 4.0 *	2.6 / 3.7	2.6 / 3.7	2.6 / 3.7	3.1 / 3.4
Graphite Reflector OD (in)	1.4	1.4	1.4	1.4	1.4
Molybdenum Disc (Y/N)	No	Yes	Yes	Yes	Yes
Samarium Trioxide Disc (Y/N)	Yes (prior to 1964)	Yes (prior to 1964)	No	No	No
Zr Fuel Matrix Mass (g)	2,070	2,088	2,060	2,060	2,088

* Graphite reflector dimensions provided for an active fuel length of 14-in. If the active fuel length is reduced, the top and bottom reflectors increase equally in length, and the overall column stackup of fuel and reflector remains fixed at 22-in.

** Length does not include irradiation growth.

Table 1.2-2 – TRIGA Fuel Parameters

Fuel Type	Maximum U-235 depletion (%)	Maximum Burnup (MWD/MTU)	Minimum Decay Time
GA Cat. # 101 (Aluminum-clad standard)	22.42	36,953	28 days
GA Cat. # 103/203 (Stainless steel-clad standard)	20.72	34,111	28 days
GA Cat. # 109 (FLIP)	59.74	339,368	1 year
GA Cat. # 117 (FLIP-LEU-I)	43.81	75,415	1 year

Table 1.2-3 – Plutonium Activity

Plutonium Activity per Fuel Element (Ci)				
Isotope	MURR	MITR-II	ATR	TRIGA
Pu-238	1.63E+00	1.21E+01	8.38E+00	7.19E-01
Pu-239	1.03E-01	1.01E-01	1.90E-01	2.33E-01
Pu-240	4.91E-02	7.39E-02	1.38E-01	1.70E-01
Pu-241	1.19E+01	3.70E+01	4.60E+01	4.48E+01
Pu-242	3.66E-05	3.69E-04	4.93E-04	2.44E-04
Total	1.37E+01	4.93E+01	5.48E+01	4.59E+01
Plutonium Activity per BRR Package (Ci)				
Isotope	MURR	MITR-II	ATR	TRIGA
Pu-238	1.30E+01	1.33E+02	6.70E+01	1.37E+01
Pu-239	8.26E-01	1.11E+00	1.52E+00	4.42E+00
Pu-240	3.93E-01	8.12E-01	1.10E+00	3.23E+00
Pu-241	9.56E+01	4.07E+02	3.68E+02	8.51E+02
Pu-242	2.93E-04	4.06E-03	3.95E-03	4.64E-03
Total	1.10E+02	5.42E+02	4.38E+02	8.73E+02

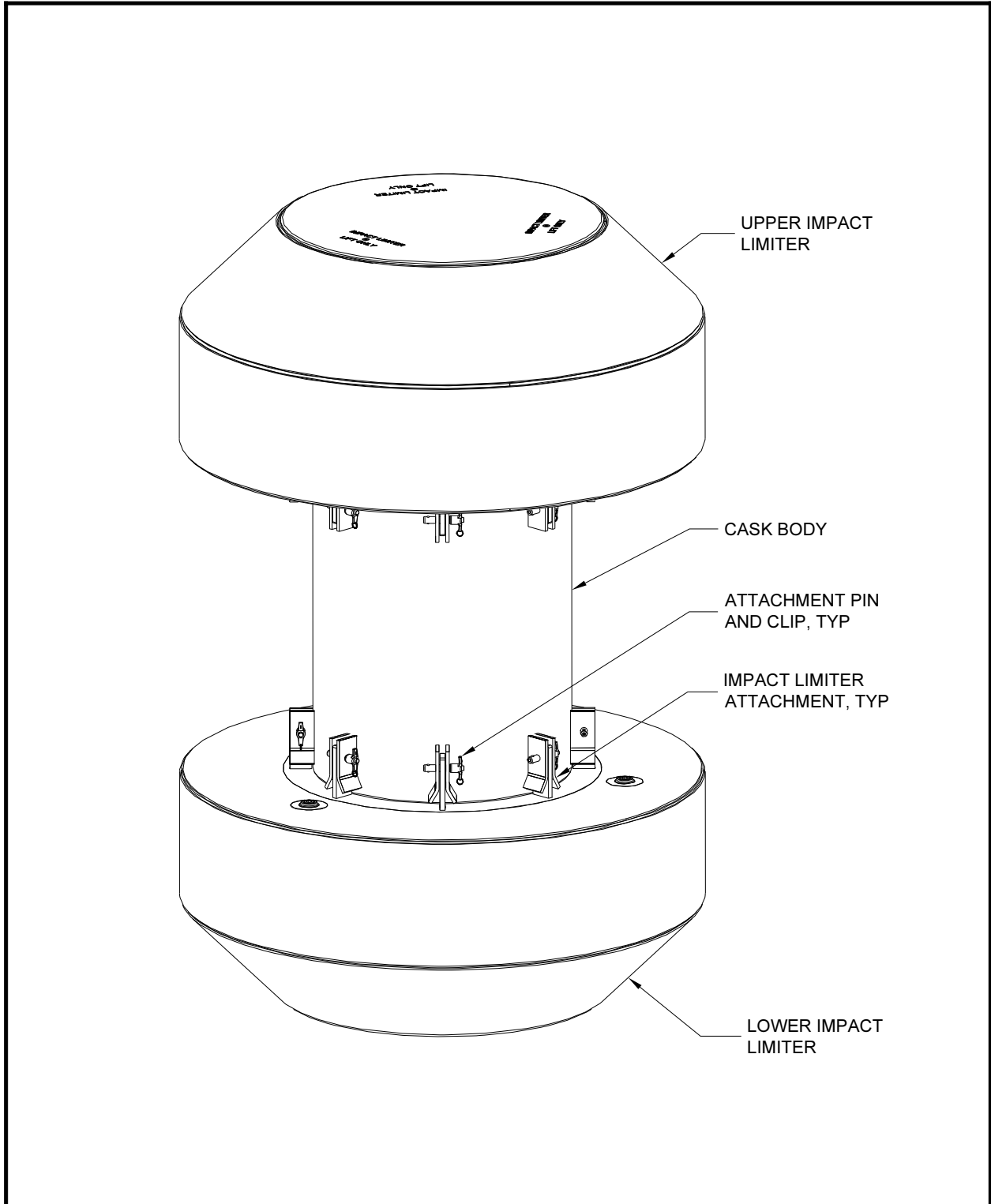


Figure 1.2-1 – BRR Packaging Components

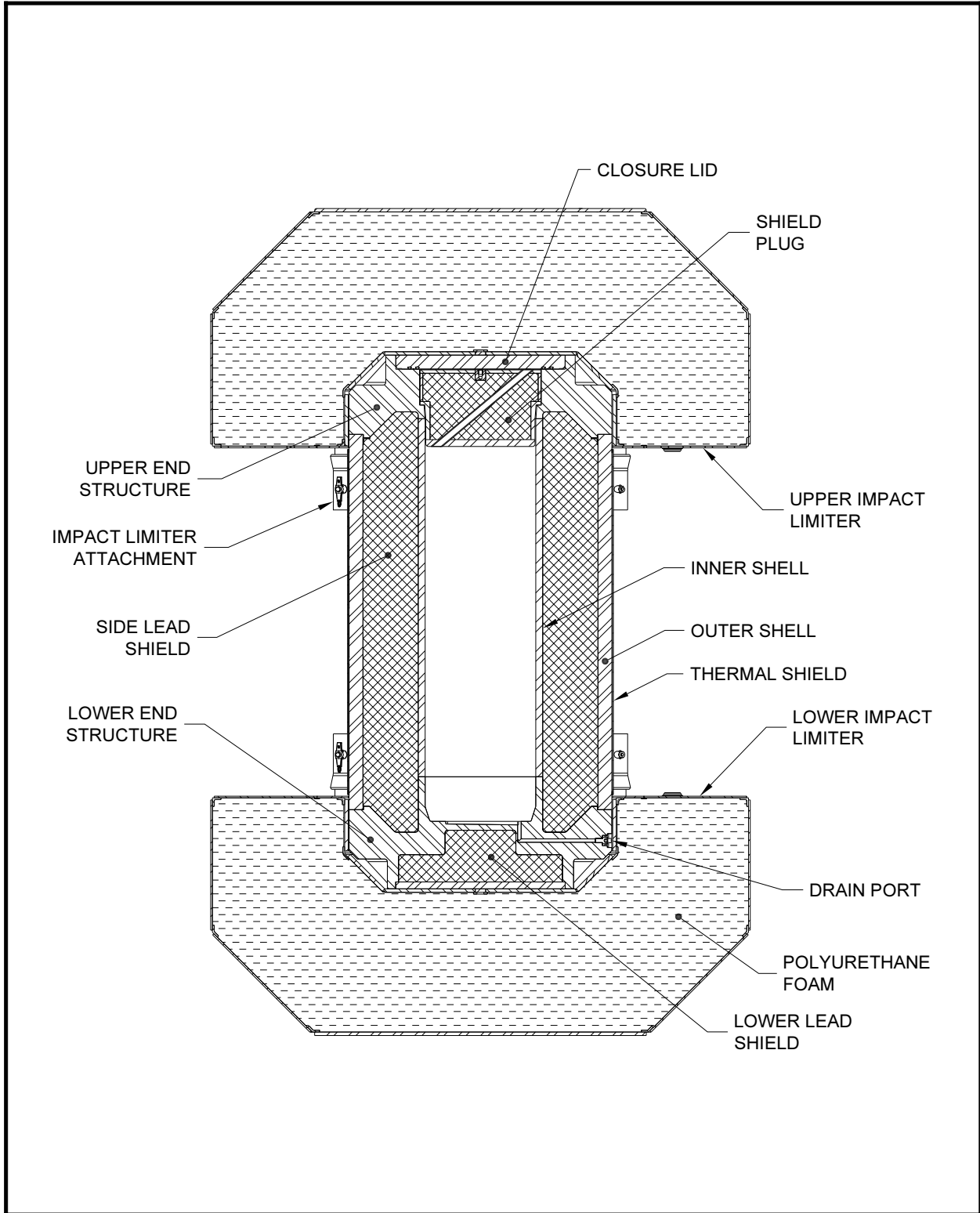


Figure 1.2-2 – BRR Package Cross Section

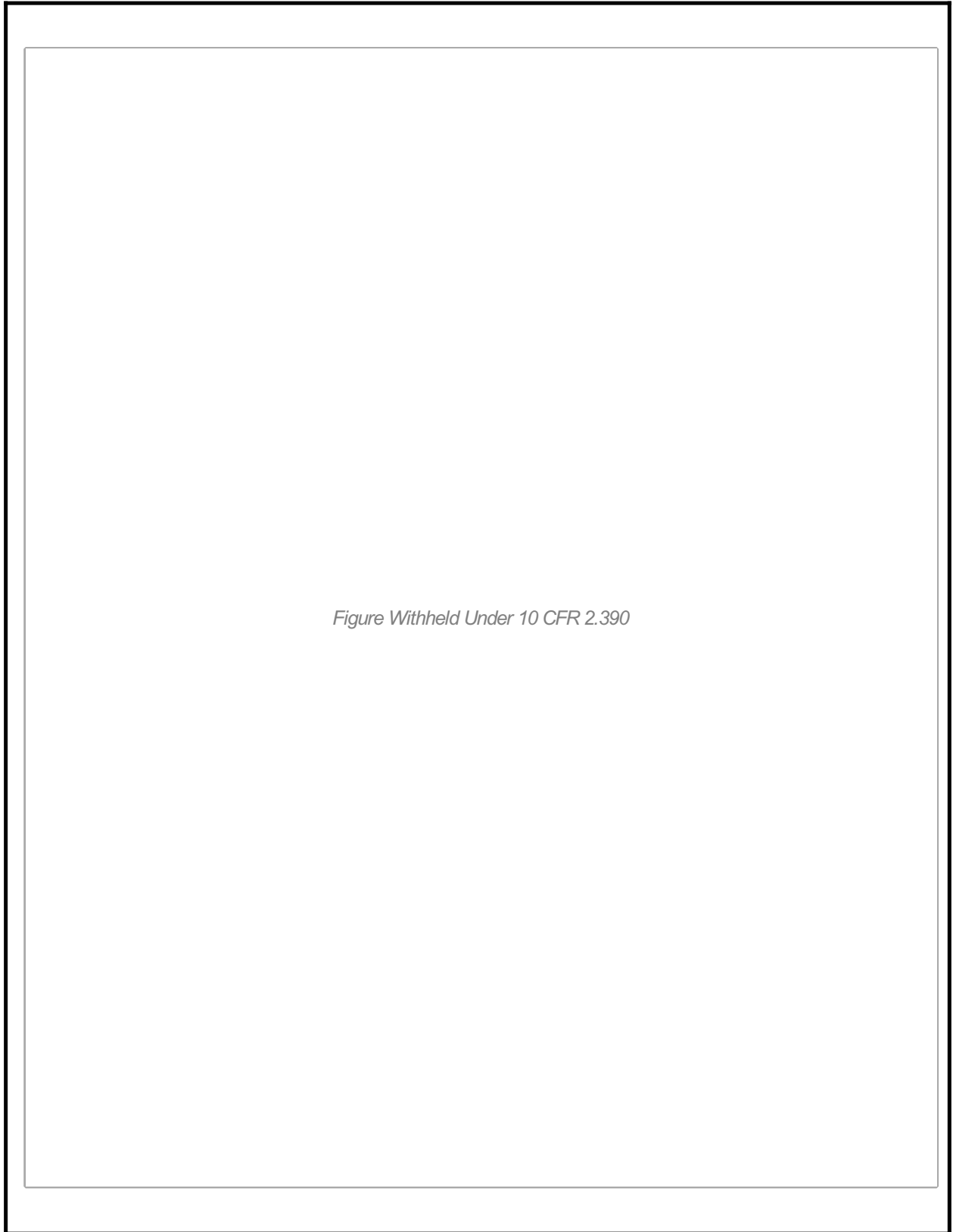


Figure 1.2-3 – BRR Package Dimensions

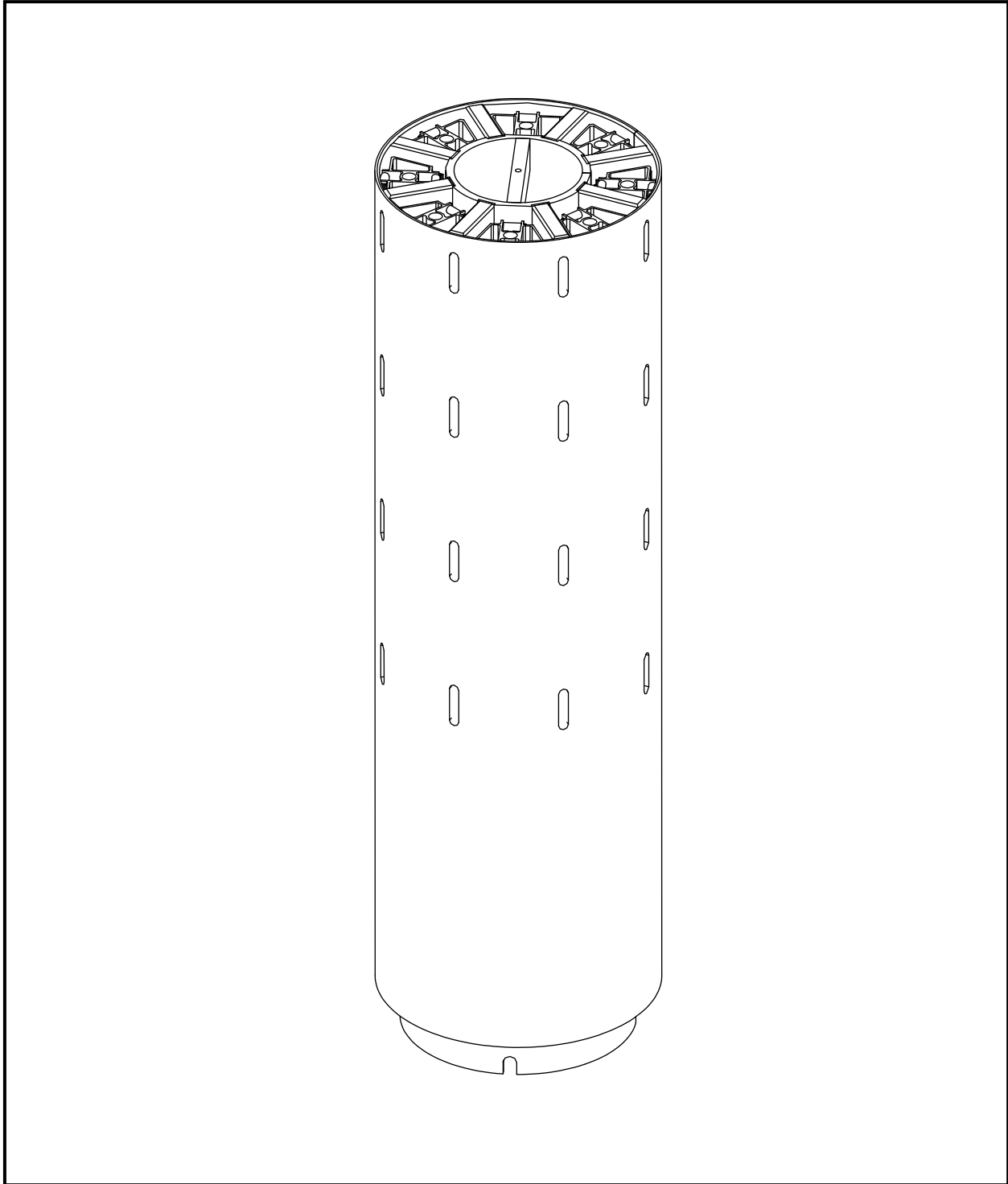


Figure 1.2-4 – MURR Fuel Basket

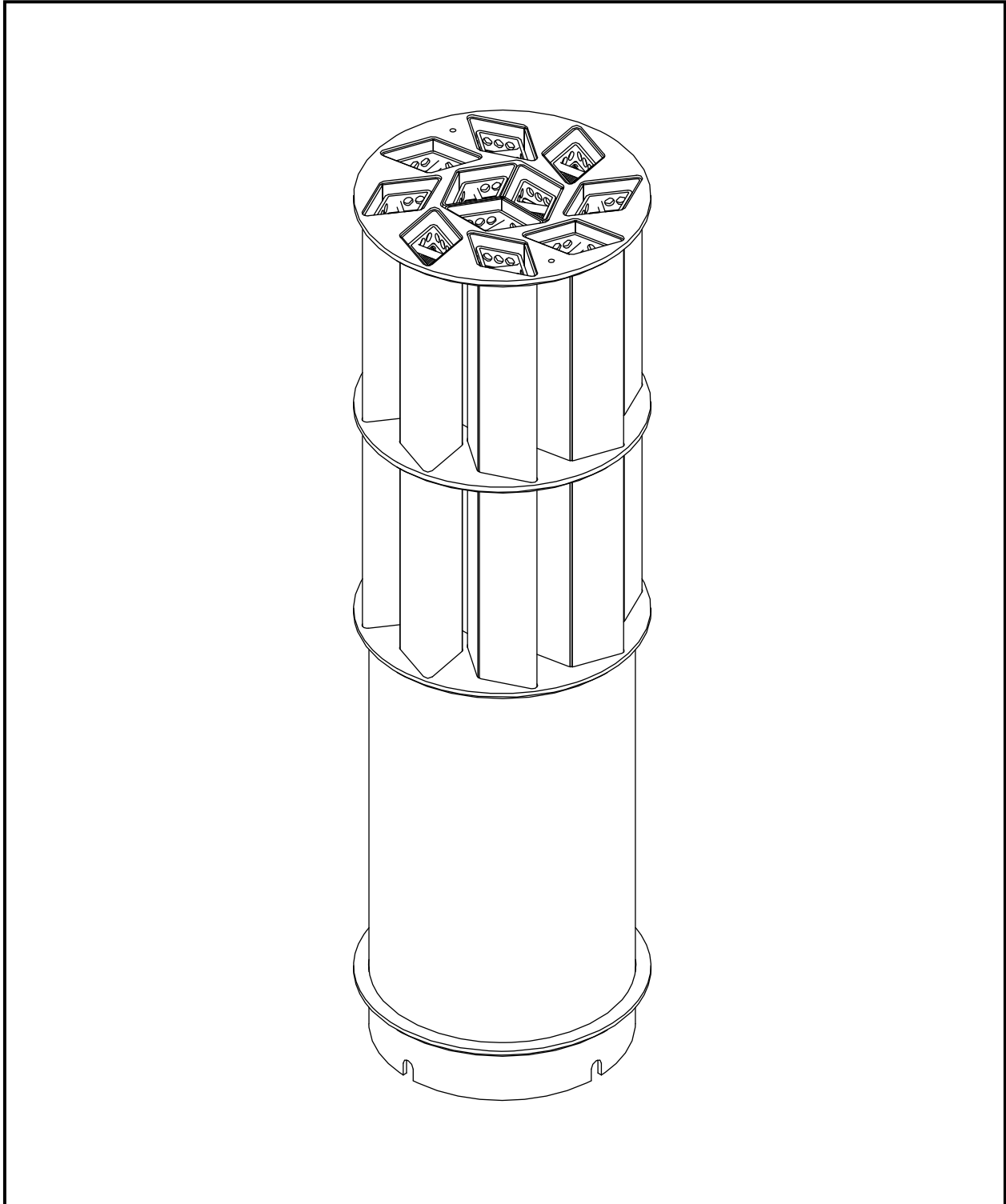


Figure 1.2-5 – MITR-II Fuel Basket

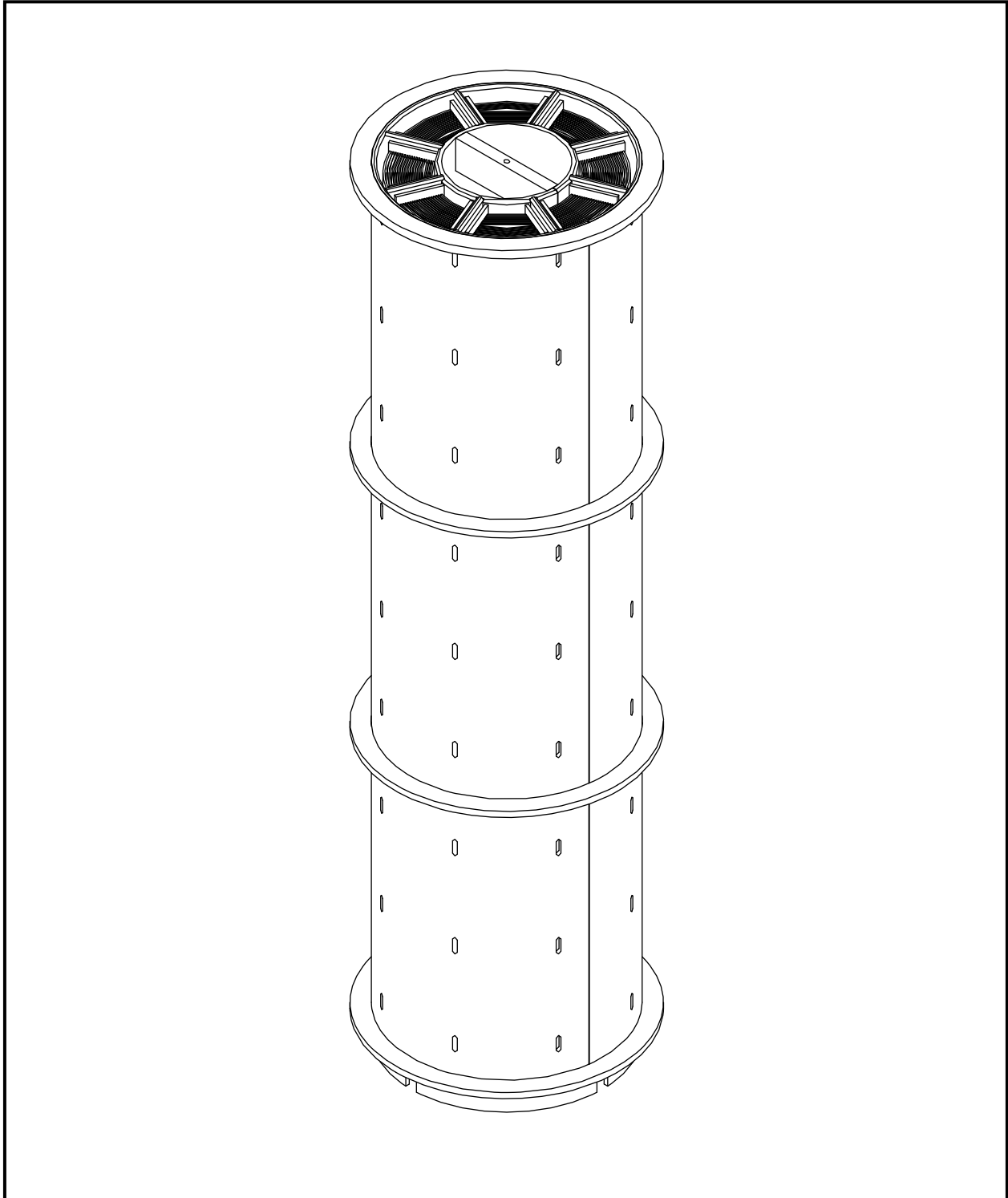


Figure 1.2-6 –ATR Fuel Basket

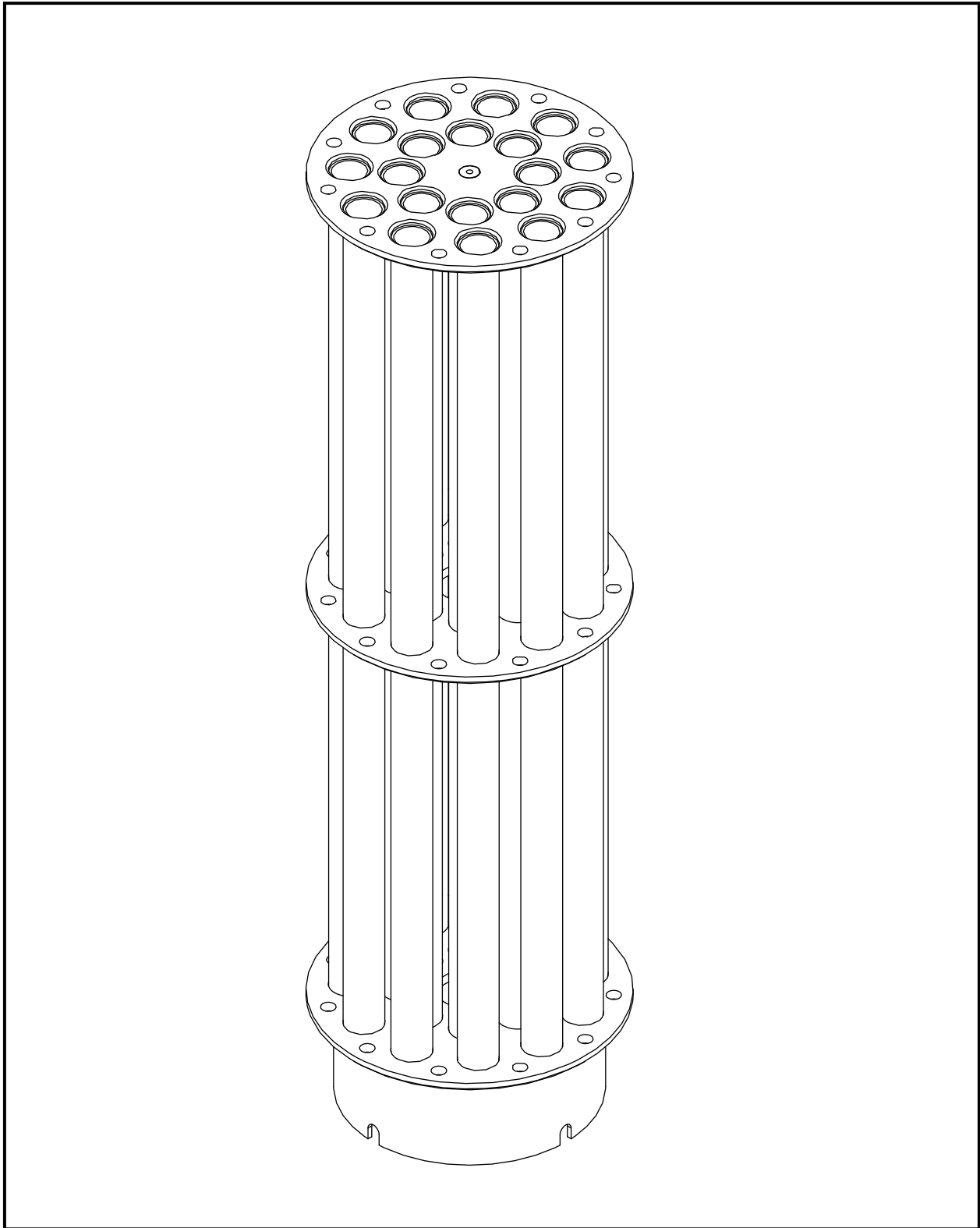


Figure 1.2-7 – TRIGA Fuel Basket

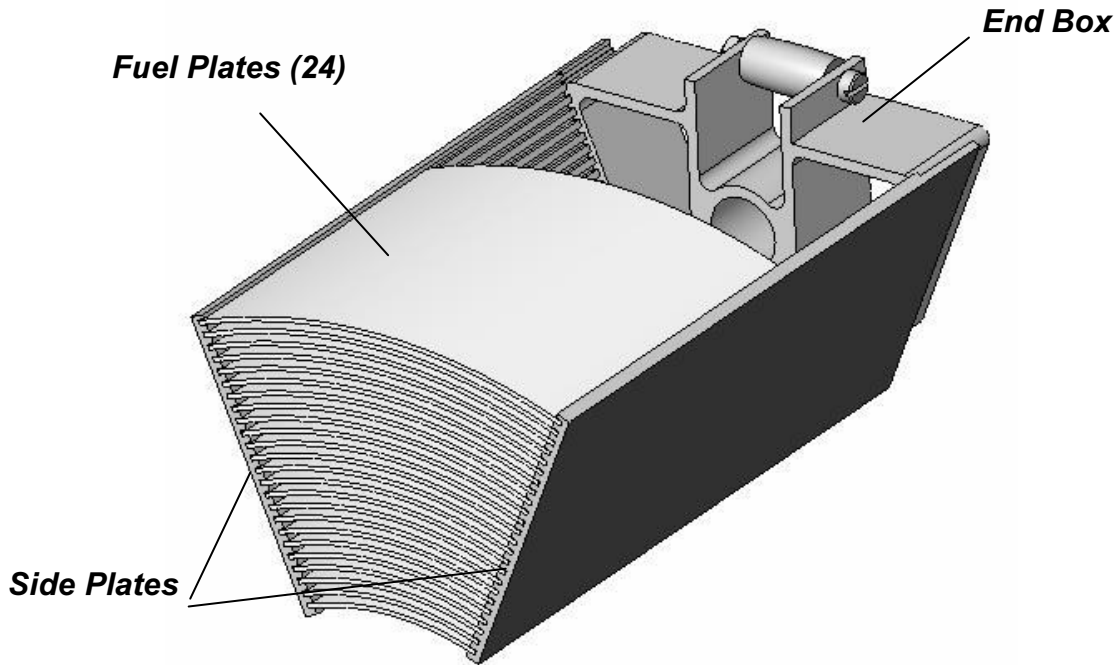


Figure 1.2-8 – MURR Fuel Element – Section View

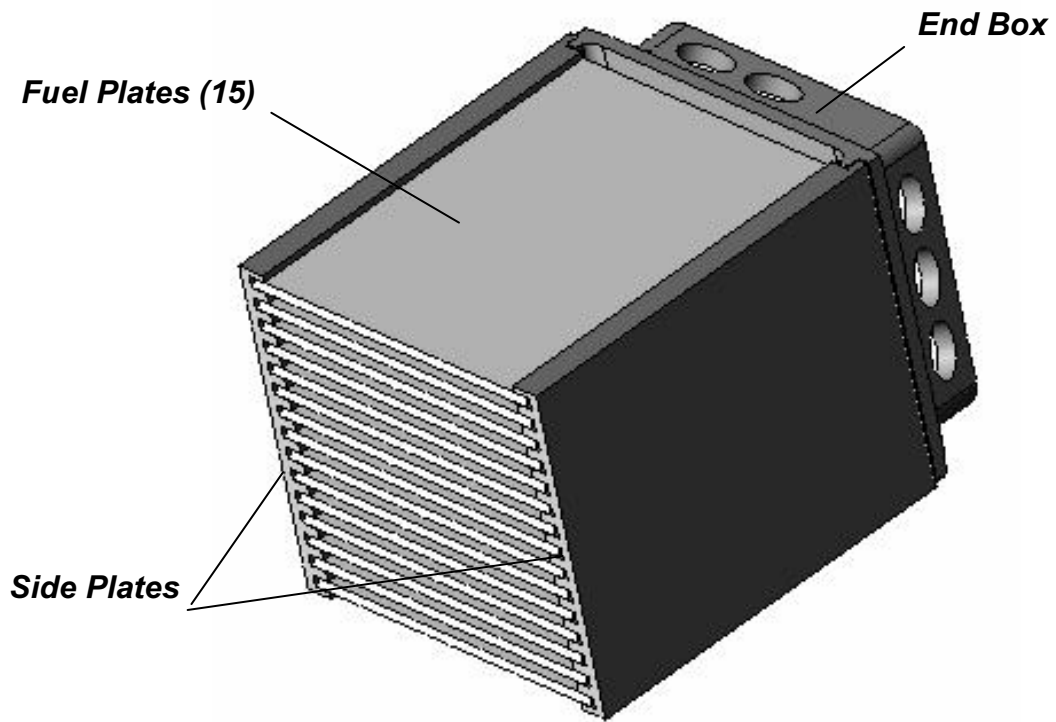
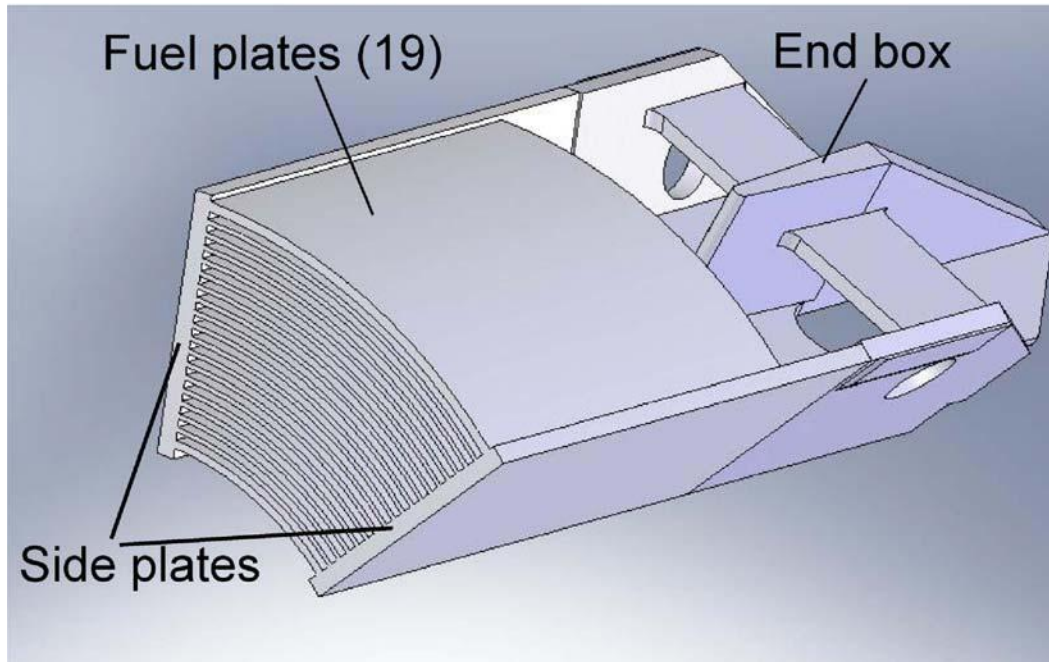


Figure 1.2-9 – MITR-II Fuel Element – Section View



Note: The end box shown in this figure will be removed prior to insertion in the BRR package.

Figure 1.2-10 – ATR Fuel Element – Section View

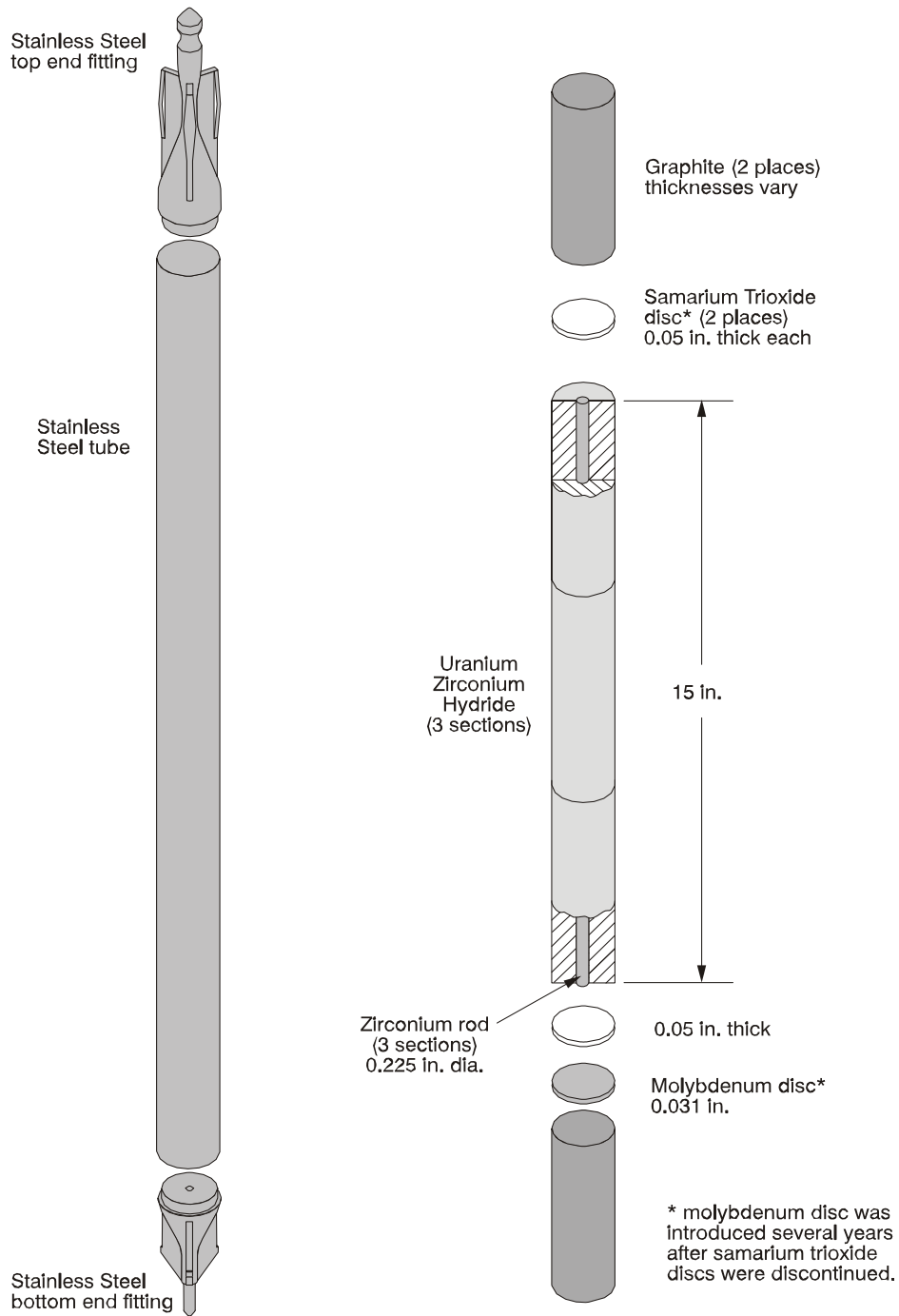


Figure 1.2-11 – TRIGA Fuel Element (Stainless Steel Clad)

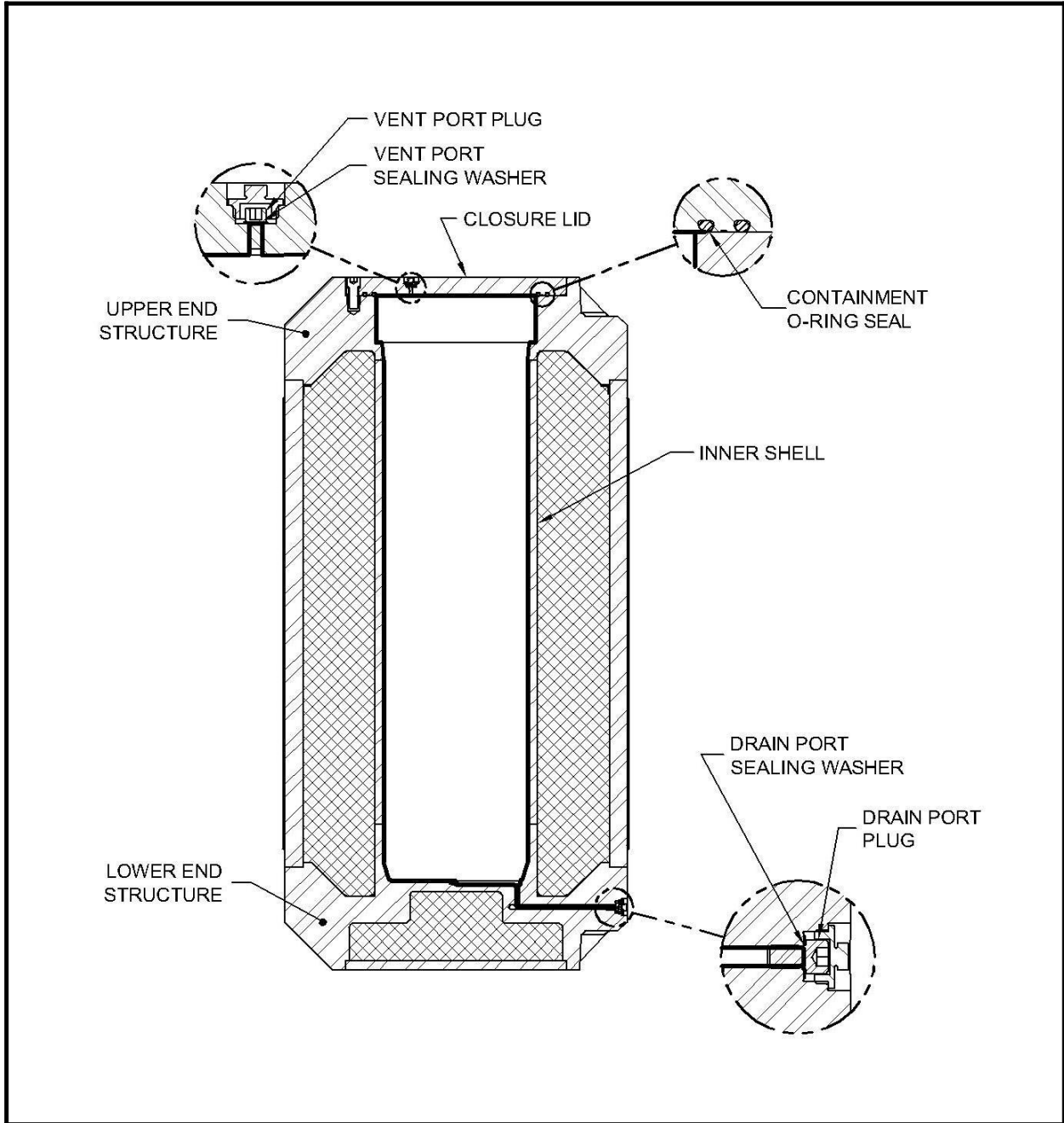


Figure 1.2-12 – BRR Package Containment Boundary

1.3 Appendices

1.3.1 References

1. Title 10, Code of Federal Regulations, Part 71 (10 CFR 71), Packaging and Transportation of Radioactive Material, 1-1-08 Edition.
2. ANSI N14.5-1997, *American National Standard for Radioactive Materials – Leakage Tests on Packages for Shipment*, American National Standards Institute (ANSI), Inc.

1.3.2 Glossary of Terms and Acronyms

ANSI –	American National Standards Institute.
ASME B&PV Code –	American Society of Mechanical Engineers Boiler and Pressure Vessel Code.
ASTM –	American Society for Testing and Materials.
ATR –	Advanced Test Reactor.
AWS –	American Welding Society.
Basket –	Structure that supports the fuel within the payload cavity.
Blade –	Part of impact limiter attachment, integral with the impact limiter. See <i>Receptacle</i> , below.
Cask Body –	BRR package component consisting of the inner shell, outer shell, upper and lower end structures, side and lower lead shielding.
Closure Lid –	Plate that completes the containment boundary. It contains the vent port, the test port, the containment O-ring seal, and the test O-ring seal.
Closure Bolts –	Fasteners that secure the closure lid to the body.
Containment O-ring Seal –	Inner elastomeric seal, retained in the closure lid, that forms part of the containment boundary.
Drain port –	Containment penetration at the lower end of the cask body through which water is drained from the cask during operations. Closed with the drain port plug, that is protected by a dust cover.
FLIP –	Fuel Life Improvement Program
GA –	General Atomics.
HAC –	Hypothetical Accident Conditions.
HEU –	High Enriched Uranium.
LEU –	Low Enriched Uranium.
Lower End Structure –	Part of the cask body. Massive structural element made of casting or forging that connects to both inner and outer cask body shells, and that contains the lower lead shielding and drain port. Interfaces with the lower impact limiter.
MITR-II –	Massachusetts Institute of Technology Nuclear Research Reactor.
MNOP –	Maximum Normal Operating Pressure.
MURR –	University of Missouri Research Reactor.

BRR Package Safety Analysis Report

NCT –	Normal Conditions of Transport.
OD –	Outer Diameter.
Sealing Washers –	Integrated metal and elastomer seals that are used with the vent, test, and drain ports.
Shield Plug –	A removable plug that serves as the upper shielding.
Receptacle –	The pair of plates, attached to the cask, that accepts the impact limiter blade and create the impact limiter attachment.
Test O-ring Seal –	Outer elastomeric seal, retained in the closure lid, used to allow leakage rate testing of the containment seal.
Test port –	Opening located between the containment O-ring seal and the test O-ring seal in the closure lid, used to test the leakage rate of the containment O-ring seal. Closed with the test port plug, which is protected by a dust cover.
Thermal Shield –	Thin sheet attached to the outside of the outer shell, forming a thin air gap that inhibits heat transfer into the package during the HAC fire event.
TRIGA –	Training, Research, Isotopes, General Atomic.
Upper End Structure –	Part of the cask body. Massive structural element made of casting or forging that connects to both inner and outer cask body shells, and interfaces with the closure lid, shield plug, and upper impact limiter.
Vent port –	Containment penetration located in the closure lid which is used to vent the cavity and to introduce helium for leakage rate testing during operations. Closed with the vent port plug, that is protected by a dust cover.

1.3.3 Packaging General Arrangement Drawings

The packaging general arrangement drawings consist of:

- 1910-01-01-SAR, BRR Package Assembly SAR Drawing, 4 sheets
- 1910-01-02-SAR, BRR Package Impact Limiter SAR Drawing, 2 sheets
- 1910-01-03-SAR, BRR Package Fuel Baskets SAR Drawing, 3 sheets

8

7

6

5

4

3

2

DWG NO 1910-01-01-SAR REV 2 SH 1

1

D

D

C

C

B

B

A

A

Figure Withheld Under 10 CFR 2.390

		AREVA Federal Services LLC Packaging Projects Tacoma, WA 98402	
DWG TITLE			
BRR PACKAGE ASSEMBLY SAR DRAWING			
SCALE: SHOWN		WT. ~ LBS	
REV: 2		SHEET 1 OF 4	
DWG NO.		1910-01-01-SAR	
DWG SIZE		D	
CADFILE: 19100101SAR2.SLDDRW			

8

7

6

5

4

3

2

1

1

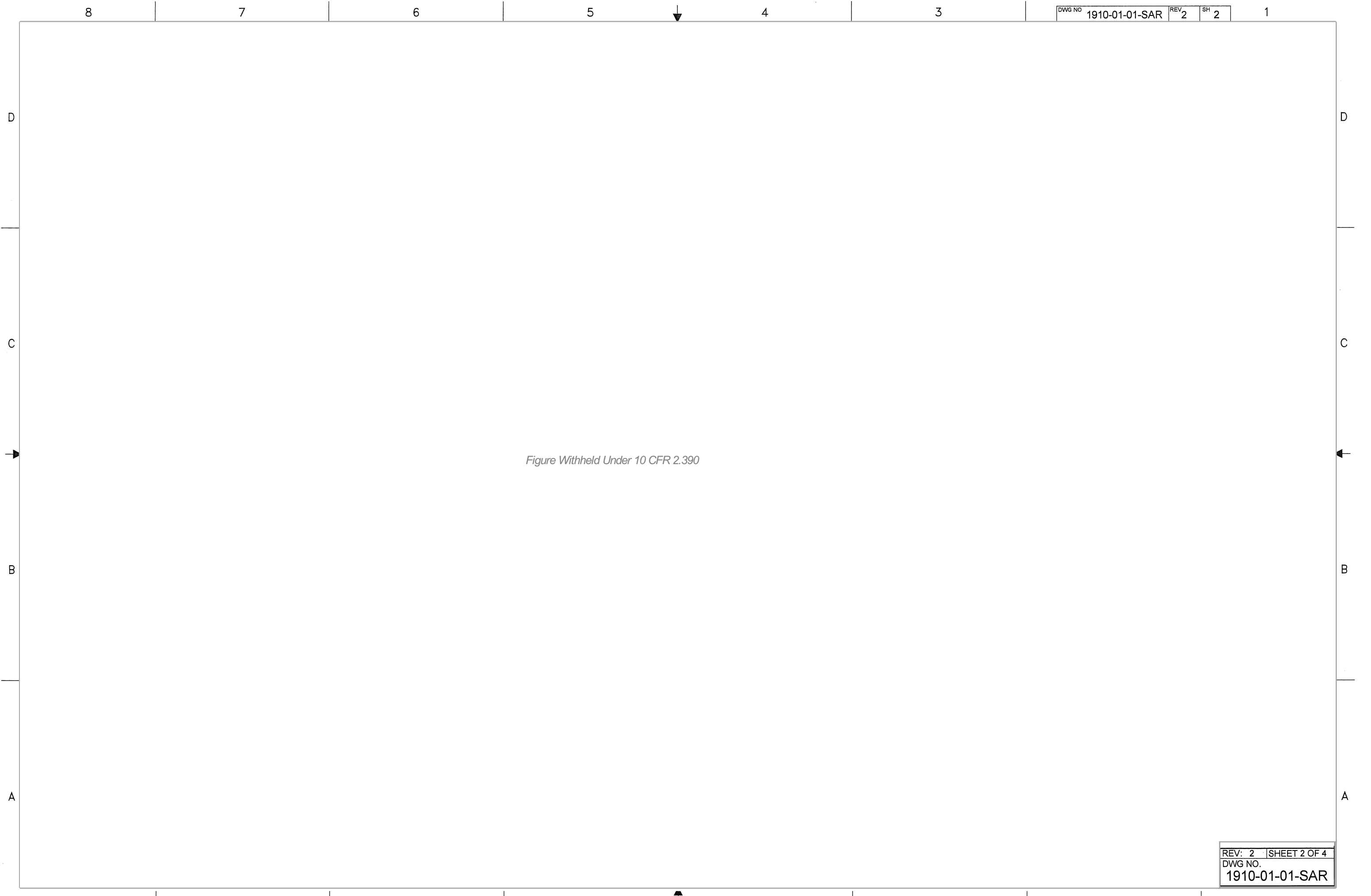


Figure Withheld Under 10 CFR 2.390

8

7

6

5

4

3

DWG NO 1910-01-01-SAR

REV 2

SH 3

1

D

D

C

C

B

B

A

A

Figure Withheld Under 10 CFR 2.390

REV: 2 SHEET 3 OF 4
DWG NO.
1910-01-01-SAR

8

7

6

5

4

3

2

1

Figure Withheld Under 10 CFR 2.390

Figure Withheld Under 10 CFR 2.390

		AREVA Federal Services LLC Packaging Projects Tacoma, WA 98402	
DWG TITLE			
BRR PACKAGE IMPACT LIMITER SAR DRAWING			
SCALE: NOTED		WT. ~ 2252 LBS	
REV: 0		SHEET 1 OF 2	
DWG SIZE	DWG NO.	1910-01-02-SAR	
D	CADFILE: 19100102SAR0.SLDDRW		
DWG - 3001276-000			

8

7

6

5

4

3

DWG NO 1910-01-02-SAR

REV 0

SH 2

1

D

D

C

C

B

B

A

A

Figure Withheld Under 10 CFR 2.390

8

7

6

5

4

3

2

1

REV: 0 SHEET 2 OF 2
DWG NO.
1910-01-02-SAR

8

7

6

5

4

3

D

D

C

C

B

B

A

A

Figure Withheld Under 10 CFR 2.390

		AREVA Federal Services LLC Packaging Projects Tacoma, WA 98402	
DWG TITLE		BRR PACKAGE FUEL BASKETS SAR DRAWING	
SCALE: SHOWN		WT. ~ LBS	
REV: 2		SHEET 1 OF 3	
DWG NO.		1910-01-03-SAR	
DWG SIZE		D	
CADFILE: 19100103SAR2.SLDDRW		DWG - 3001277-002	

8

7

6

5

4

3

2

1



Figure Withheld Under 10 CFR 2.390



Figure Withheld Under 10 CFR 2.390

2.0 STRUCTURAL EVALUATION

This section presents evaluations demonstrating that the BRR package meets all applicable structural criteria. The BRR package, consisting of a fuel basket, cask assembly, and impact limiters, is evaluated and shown to provide adequate protection for the payload. Normal conditions of transport (NCT) and hypothetical accident condition (HAC) evaluations are performed to address 10 CFR 71 [1] performance requirements. The primary method of performance demonstration is by analysis. Analytic demonstration techniques comply with the methodology presented in NRC Regulatory Guides 7.6 [2] and 7.8 [3]. Impact limiter performance in the free drop and puncture drop events is demonstrated by certification testing utilizing a half-scale certification test unit (CTU). A discussion of the tests performed is given in Appendix 2.12.2, *Certification Test Plan*, and results of the certification tests are provided in Appendix 2.12.3, *Certification Test Results*.

2.1 Structural Design

2.1.1 Discussion

The BRR package is designed to transport irradiated research reactor fuel. An isometric view of the cask is shown in Figure 1.2-1, a cross section view is shown Figure 1.2-2, and basic dimensions in Figure 1.2-3. The four types of fuel basket are shown in Figure 1.2-4 through Figure 1.2-7. The BRR package consists of a fuel basket, a cask body (which includes the gamma shielding), a shield plug, a closure lid, and two impact limiters. The payload cavity is 16 inches in diameter and 54 inches long. A lead shield plug of 11.2 inches in thickness is located at the top of the cavity. The inner (containment) shell is 1 inch thick, and the outer structural shell is 2 inches thick. The shells are welded to massive cast or forged end structures. The radial lead thickness is 8 inches, and the bottom lead thickness is 7.7 inches. A 12-gauge thermal shield is attached to the outside of the structural shell.

The closure lid is 2 inches thick and is attached with 12, 1-8 UNC socket head cap screws. Containment is afforded by a 3/8-inch cross-sectional diameter butyl O-ring seal. A test O-ring seal is used to provide a cavity for helium leak testing of the containment seal. The closure lid features vent and test ports and the bottom of the cask features a drain port. Impact limiters are located at each end of the cask to mitigate free drop and puncture drop impact. Each impact limiter has a 1/4-inch thick outer stainless steel shell which envelops a nominally 9 lb/ft³ polyurethane foam impact absorbing material. Each impact limiter is attached using eight, 1-inch diameter ball-lock pins.

There are four different kinds of payload basket, one each for MURR, MITR-II, ATR, and TRIGA fuel elements. Each fuel element cavity conforms to the overall geometric shape of the fuel, to ensure a nominally uniform support for the fuel elements under impact conditions.

All important structures are made from ASTM Type 304 stainless steel. The closure bolts are made from ASTM A320, Grade L43 alloy steel. Gamma shielding is made from ASTM B29, Chemical Lead, or equivalent lead. A comprehensive discussion of the BRR package design and configuration is provided in Section 1.2, *Package Description*.

2.1.2 Design Criteria

Proof of performance for the BRR package is achieved primarily by analysis. Impact limiter performance is demonstrated by half-scale certification testing. The acceptance criteria for analytic assessments are in accordance with Regulatory Guide 7.6. These design criteria meet the following safety requirements of 10 CFR §71.51:

1. For normal conditions of transport, there shall be no loss or dispersal of radioactive contents, as demonstrated to a sensitivity of 10^{-6} A₂ per hour, no significant increase in external radiation levels, and no substantial reduction in the effectiveness of the packaging.
2. For hypothetical accident conditions, there shall be no escape of radioactive material exceeding a total amount A₂ in one week, and no external radiation dose rate exceeding one rem per hour at one meter from the external surface of the package.

The BRR package is conservatively designated a Category I container, which is the highest and most stringent category [4]. Per NUREG/CR-3019 [5] and NUREG/CR-3854 [6], the cask components are classified as follows:

- Containment components are classified as ASME Code, Section III, Subsection NB [7].
- Fuel basket components are classified as ASME Code, Section III, Subsection NG [8].
- The outer shell, thermal shield, and impact limiter attachments are classified as ASME Code, Section III, Subsection NF [9]. However, the outer shell is conservatively analyzed to the requirements of Subsection NB.

The remainder of this section presents the detailed acceptance criteria used for analytic structural assessments of the BRR package.

2.1.2.1 Containment and Criticality Control Structures

A summary of allowable stresses used for containment and criticality control structures is presented in Table 2.1-1. Containment structures include the inner shell, massive end structures, and the closure lid. Criticality control structures include the fuel baskets. The allowable stresses shown in Table 2.1-1 are consistent with Regulatory Guide 7.6, and the ASME Code, Section III, Subsections NB and NG, and Appendix F. Peak stresses are further discussed in Section 2.1.2.3.2, *Fatigue Assessment*, and buckling in Section 2.1.2.3.3, *Buckling Assessment*. Closure bolts are evaluated utilizing NUREG/CR-6007 [10]. Furthermore, stress intensity in the cask closure region which could affect compression of the containment O-ring seal is limited to the lesser of the value shown in Table 2.1-1, or the yield strength.

2.1.2.2 Other Structures

Impact limiter structures, including the steel shells, energy-absorbing foam, and attachment structures, are expected to permanently deform under NCT and HAC. The impact limiter performance criteria are:

- Limit impact magnitude such that cask component stress and deflection criteria are met.
- Prevent "hard" contact of a rigid part of the cask with the ground due to excessive deformation of the foam.

BRR Package Safety Analysis Report

- Maintain attachment to the cask and sufficient structural integrity subsequent to the HAC free drop and puncture drop events that the containment O-ring seal is protected from excessive temperature in the subsequent HAC fire event.

The performance of the impact limiters is discussed in Sections 2.7.1, *Free Drop*, and 2.7.3, *Puncture*. The thermal performance of the undamaged and damaged limiters is evaluated in Chapter 3, *Thermal Evaluation*.

The allowable stress for lifting components of the BRR package is limited to a maximum of one-third of the minimum yield strength of the material in the lifting load path, per the requirements of 10 CFR §71.45(a).

Since the BRR package is not attached to the conveyance using any structural part of the package, tiedown structural criteria are not required.

2.1.2.3 Miscellaneous Structural Failure Modes

2.1.2.3.1 Brittle Fracture

With the exception of the closure lid bolts, all structural components of the BRR package are fabricated of austenitic stainless steel. Austenitic stainless steels do not undergo a ductile-to-brittle transition in the temperature range of interest (i.e., down to -40 °F), and thus do not need to be evaluated for brittle fracture. The closure lid bolts are fabricated from ASTM A320, Grade L43 alloy steel bolting material. This material is specifically intended for low temperature service. In addition, per Section 5 of NUREG/CR-1815 [11], bolts are not considered as fracture-critical components because multiple load paths exist and bolting systems are generally redundant, as is the case with the BRR package. Therefore, brittle fracture is not a failure mode of concern.

2.1.2.3.2 Fatigue Assessment

2.1.2.3.2.1 Normal Operating Cycles

Normal operating cycles do not present a fatigue concern for the BRR package components over its service life. The basis for this conclusion is reached using the six criteria of Article NB-3222.4(d) of the ASME Boiler and Pressure Vessel Code. A summary of the six criteria and their application are discussed below. The service life of the package is 25 years with up to 20 shipments per year for a maximum of 500 shipments in the service life.

(1) Atmospheric to Service Pressure Cycle: The total number of atmospheric-to-operating pressure cycles during normal operations does not exceed the number of cycles on the fatigue curve corresponding to a value of $S_a = 3S_m$ for Type 304 stainless steel. From Section 2.2.1, *Material Properties and Specifications* at a bounding temperature of 250 °F per Section 2.6.1.1, *Summary of Pressures and Temperatures*, the S_m value for Type 304 stainless steel is 20 ksi, which corresponds to an alternating stress value of $S_a = 3S_m = 60$ ksi. The corresponding number of cycles for a value of $S_a = 60$ ksi is greater than 10,000 from Figure I-9.2.1 and Table I-9.1 of the ASME Code [12]. The package undergoes one atmospheric-to-operating pressure cycle per shipment, therefore the package will experience 500 atmospheric-to-operating pressure cycles in its life. Since the

BRR Package Safety Analysis Report

allowable number of cycles is greater than the maximum expected number of cycles, the first criterion is satisfied.

(2) Normal Service Pressure Fluctuation: The specified full range of pressure fluctuations during normal service does not exceed the quantity $1/3 \times \text{Design Pressure} \times (S_a/S_m)$, where the Design Pressure is 25 psi, S_a is the value obtained from the Type 304 stainless steel design fatigue curve for the total specified number of significant pressure fluctuations (SPF), and S_m is the allowable stress intensity for the material at the service temperature. The total number of service cycles is based on the fill gas extreme temperature range as stated below. Conservatively, two complete temperature cycles are assumed to occur for each of the 500 lifetime shipments for a total quantity of 1,000 pressure fluctuation cycles. From Table I-9.1, $S_a = 119,000$ psi for 1,000 cycles. The value of S_m was defined above as 20 ksi at service temperature. The limiting full range of pressure fluctuations (FRF) becomes:

$$\text{FRF}_{\text{LIMIT}} = 1/3 \times \text{Design Pressure} \times (S_a/S_m) = 49.6 \text{ psi}$$

Next, the maximum pressure fluctuations in the package will be determined. Of note, the maximum pressure fluctuations will be conservatively assumed to be above the significance level, and therefore the value SPF does not need to be computed. The bulk average fill gas temperature varies between the extremes of $T_1 = -40$ °F and a conservative bounding temperature of $T_2 = 400$ °F. The maximum pressure (conservatively assuming that atmospheric pressure corresponds to -40 °F) is:

$$\frac{P_2}{P_1} = \frac{T_2}{T_1} \Rightarrow P_2 = P_1 \left(\frac{T_2}{T_1} \right) = 14.7 \left(\frac{400 + 460}{-40 + 460} \right) = 30.1 \text{ psia}$$

The resulting pressure fluctuation is $\text{FRF} = 30.1 - 14.7 = 15.4$ psi, which is less than $\text{FRF}_{\text{LIMIT}} = 49.6$ psi presented above and therefore, the second criterion is satisfied.

(3) Temperature Difference — Startup and Shutdown: The temperature between adjacent points of a package component during normal service does not exceed $1/2(S_a/E\alpha)$, where S_a is the design fatigue curve value taken from Table I-9.1 for Figure I-9.2.1 of the ASME Code for Type 304 stainless steel for the total specified number of temperature difference fluctuations, E is the modulus of elasticity, and α is the mean coefficient of thermal expansion, all evaluated at temperature. The total number of temperature fluctuations will not exceed the number of uses of the package, which is 500 as calculated above. It will be conservative to use the value of S_a from Table I-9.1 of the ASME Code for 1,000 cycles, which is 119,000 psi. From Section 2.2.1, *Material Properties and Specifications* at a bounding temperature of 250 °F, the value of the mean thermal expansion coefficient is $\alpha = 9.1(10^{-6})/\text{°F}$ and the modulus of elasticity, $E = 27.3(10^6)$ psi. Therefore, the value of $1/2(S_a/E\alpha) = 1/2(119,000/[27.3(10^6)9.1(10^{-6})]) = 240$ °F. Since the package design temperature is 250 °F under ambient conditions of 100 °F, the temperature difference between any two adjacent points cannot approach the 240 °F value. Thus, the third criterion is satisfied.

(4) Temperature Difference — Normal Service: The temperature difference between any two adjacent points does not change during normal service by more than the quantity $1/2(S_a/E\alpha)$, where S_a , E , and α are as defined above. However, normal operating temperatures of the containment boundary are largely determined by the steady heat load, and any changes in

BRR Package Safety Analysis Report

temperature due to changes in ambient conditions, warm-up, or cool-down will be relatively slow and even due to the large thermal mass of the package. Therefore, the fourth criterion is satisfied.

(5) Temperature Difference — Dissimilar Materials: The fifth criterion is concerned with dissimilar materials. Since the containment boundary is constructed entirely of Type 304 stainless steel, dissimilar materials are not of concern. Therefore the fifth criterion is satisfied.

(6) Mechanical Loads: The specified full range of mechanical loads does not result in load stresses whose range exceeds the S_a design fatigue curve for the total specified number of load fluctuations. The only repeating mechanical loads will be those associated with lifting the package and tightening of the closure bolts.

Lifting. As the containment boundary is handled twice for each transport cycle (load and unload), the maximum number of cycles is $2 \times 500 = 1,000$. From Table I-9.1, $S_a = 119,000$ psi for 1,000 cycles. Of note, each load stress excursion will be conservatively assumed to be above the significance level, and therefore the actual significance level does not need to be computed. Lifting stress is limited by 10 CFR §71.45(a) to a value of one-third of the material's minimum yield strength. For a design temperature of 250 °F, the minimum yield strength of Type 304 stainless steel is 23,700 psi. Thus, one-third of the minimum yield strength is $23,700/3 = 7,900$ psi. As $119,000$ psi $\gg 7,900$ psi, the sixth criterion is satisfied for lifting.

Closure bolts. The maximum stress intensity developed in the closure bolts during normal operations, given in Section 2.6.1.5, *Closure Bolts*, is bounded by a value of $S_{max} = 55,000$ psi. This stress includes preload stress, thermal stress, and a conservative inclusion of 50% of the applied preload torque as a residual torsion stress. From Table 2.2-3, the ASME allowable stress for the bolting material, S_m , at 250 °F is 32,450 psi. As defined by Table I-9.1 of the ASME B&PV Code, the Maximum Nominal Stress (MNS) of 55,000 psi is less than $2.7S_m$ (i.e., $2.7(32,450) = 87,615$ psi). Per NB-3232.3(c), a stress concentration factor of four shall be applied to one-half the value of S_{max} , i.e., $4(0.5S_{max}) = 4 \times 0.5 \times 55,000 = 110,000$ psi. Per NB-3232.3(d), the alternating stress must be adjusted for the elastic modulus used in the fatigue curves. The modulus at a temperature of 250 °F is $26.9(10^6)$ psi and the modulus used for the fatigue curve, per Table I-9.1 is $30(10^6)$ psi. The adjusted alternating stress is:

$$S_{ALT} = \frac{30}{26.9} 110 = 123 \text{ ksi}$$

From Table I-9.1 for figure I-9.4, the service cycles allowed for a stress of 123 ksi is 670. Since closure bolts are tightened twice per package service cycle, the allowable number of package service cycles is half of this value. Therefore the closure bolts should be replaced every $670/2 = 335$ service cycles for the package, and the sixth criterion is satisfied for closure bolts.

Summary: The previous discussion verifies that fatigue failure of the packaging containment boundary due to normal operating cycles is not a concern, per Section III, Subsection NB, Article NB-3222.4(d) of the ASME Code. Therefore the resistance of the BRR package to fatigue is adequate to ensure a minimum 25 year service life of up to 20 shipments per year.

2.1.2.3.2.2 Normal Vibration Over the Road

Fatigue associated with normal vibration over the road is addressed in Section 2.6.5, *Vibration*.

2.1.2.3.3 Buckling Assessment

Buckling, per Regulatory Guide 7.6, is an unacceptable failure mode for the containment vessel. The intent of this provision is to preclude large deformations that would compromise the validity of linear analysis assumptions and quasi-linear stress allowable limits, as given in Paragraph C.6 of Regulatory Guide 7.6.

Buckling investigations contained herein consider the outer shell of the BRR package. The outer and inner shells of the cask are closely connected through the massive end structures, thus, the two shells act to strengthen each other. One shell cannot buckle independently of the other. However, the strength of the inner shell for buckling considerations is conservatively ignored.

The shell buckling analysis is performed using the methodology of ASME B&PV Code Case N-284-2 [13]. Consistent with Regulatory Guide 7.6 philosophy, factors of safety corresponding to ASME Boiler and Pressure Vessel Code, Level A and Level D service conditions are employed. For NCT (Service Level A), the factor of safety is 2.0, and for HAC (Service Level D), the factor of safety is 1.34. Buckling analysis details are provided in Section 2.6.4, *Increased External Pressure*, Section 2.7.1, *Free Drop*, and Section 2.7.6, *Immersion – All Packages*.

2.1.3 Weights and Centers of Gravity

The maximum gross weight of the BRR package is 32,000 lb. The packaging component weights are summarized in Table 2.1-2, and the fuel basket and fuel weights in Table 2.1-3. The center of gravity (CG) of the package is located 38.7 inches from the bottom outside surface of the cask body. Note that this is directly on the geometric center of the package. The mass moment of inertia of the cask about a transverse axis through the center of gravity (including impact limiters, as prepared for transport) is 63,246 in-lb-s².

2.1.4 Identification of Codes and Standards for Package Design

The BRR package, without regard to content, is conservatively designated a Category I package. Per the guidance of NUREG/CR-3854, the appropriate design criteria for the containment is Section III, Subsection NB of the ASME B&PV Code. Consequently, the design of the containment boundary is based on the methodology of Regulatory Guide 7.6, and load cases are applied and combined according to Regulatory Guide 7.8. The outer shell is conservatively included under the NB criteria. The closure bolts are designed using the guidance of NUREG/CR-6007.

For the design of the baskets as criticality control components, the criteria is taken from Section III, Subsection NG of the ASME B&PV Code. For other structures such as the thermal shield, impact limiter shells, and impact limiter attachments, the criteria is taken from Section III, Subsection NF of the ASME B&PV Code.

Table 2.1-1 – Containment and Criticality Control Structure Allowable Stress Limits

Stress Category	NCT	HAC
General Primary Membrane Stress Intensity	S_m	Lesser of: $2.4S_m$ $0.7S_u$
Local Primary Membrane Stress Intensity ^①	$1.5S_m$	Lesser of: $3.6S_m$ S_u
Primary Membrane + Bending Stress Intensity	$1.5S_m$	Lesser of: $3.6S_m$ S_u
Range of Primary + Secondary Stress Intensity	$3.0S_m$	Not Applicable
Pure Shear Stress	$0.6S_m$	$0.42S_u$ ^②
Peak	Per Section 2.1.2.2.2, <i>Fatigue Assessment</i>	
Buckling	Per Section 2.1.2.2.3, <i>Buckling Assessment</i>	
<i>Containment Fasteners:</i> ^③		
Average Tensile Stress Intensity	S_m ^④	Lesser of: S_y $0.7S_u$
Average Tensile + Average Shear + Bending + Residual Torsion Stress Intensity	$1.35S_m$ for $S_u > 100$ ksi	Not Applicable

Notes:

1. This stress category does not apply to criticality control structures (Subsection NG).
2. For criticality control structures, the limit is the lesser of twice the NCT limit ($2 \times 0.6S_m = 1.2S_m$) or $0.42S_u$, per NG-3225.
3. Containment fastener stress limits are in accordance with NUREG/CR-6007.
4. S_m is defined as $(2/3)S_y$ as recommended by NUREG/CR-6007.

Table 2.1-2 – BRR Package Component Weights

Item	Weight, lb	CG, inches
Cask body ^①	25,400	---
Removable shield plug	950	---
Closure lid	280	---
Upper impact limiter	2,300	---
Lower impact limiter	2,300	---
Total empty package	31,230	38.6 ^④
MURR Fuel basket ^② (loaded)	770	32.7 ^③
MITR-II Fuel basket ^② (loaded)	400	32.7 ^③
ATR Fuel basket ^② (loaded)	650	27.1 ^③
TRIGA Fuel basket ^② (loaded)	480	28.1 ^③
Total package, including MURR fuel (maximum)	32,000	38.7^④
Total package, including MITR-II fuel	31,630	38.6 ^④
Total package, including ATR fuel	31,880	38.6 ^④
Total package, including TRIGA fuel	31,710	38.6 ^④

Notes:

1. Includes all shells, end structures, and lead.
2. Individual basket and fuel weights are given in Table 2.1-3. Although ATR fuel is the heaviest at 200 lb, the MURR basket plus fuel weight is greatest overall.
3. Measured from the bottom surface of the basket.
4. Measured from the bottom outside surface of the cask body.

Table 2.1-3 – BRR Package Basket and Fuel Weights

Design	Weight (lb)			
	Empty Basket	Fuel Element × Quan.	Combined Fuel	Total
MURR	650	15 × 8	120	770
MITR-II	290	10 × 11	110	400
ATR	450	25 × 8	200	650
TRIGA	290	10 × 19	190	480

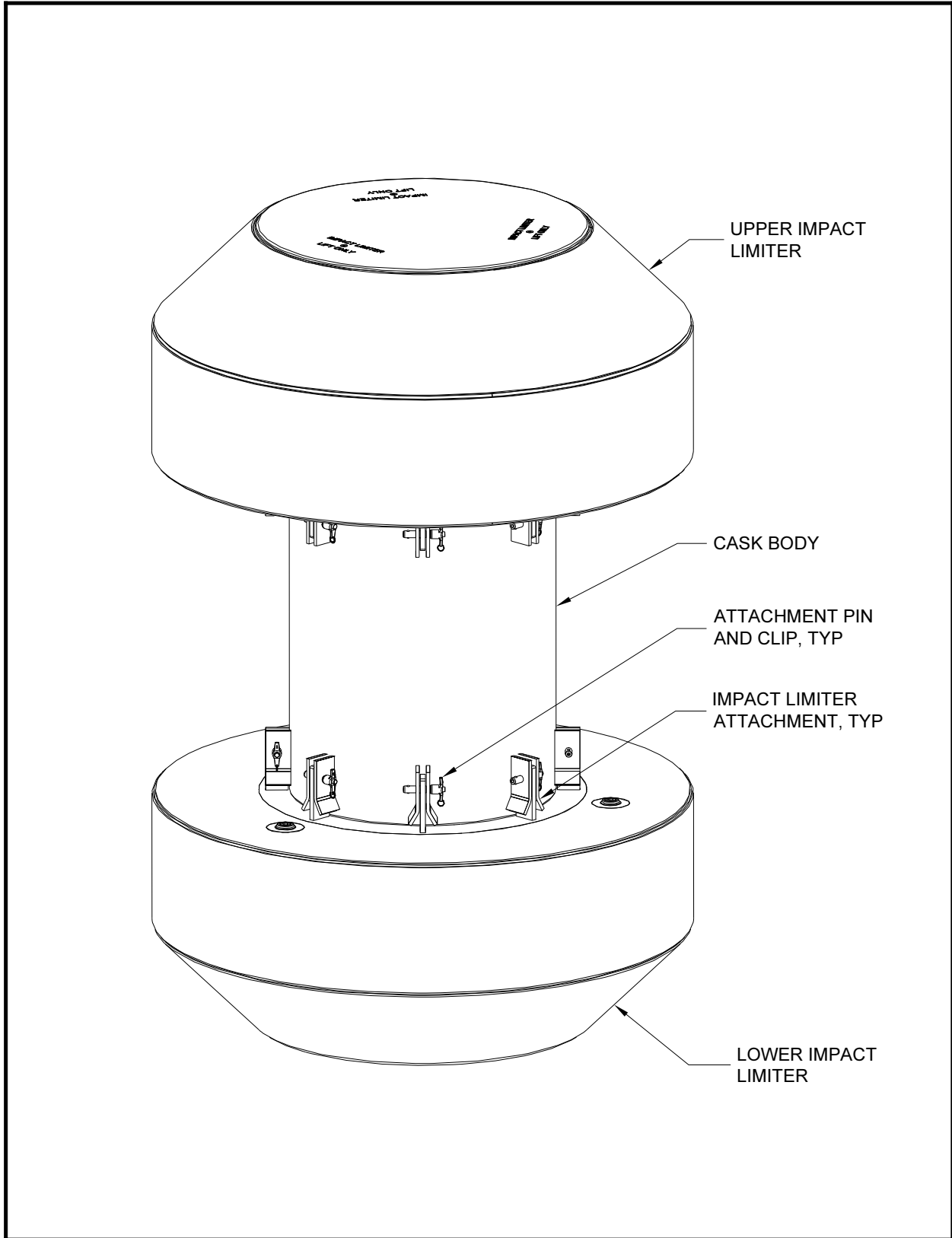


Figure 2.1-1 – BRR Packaging Components

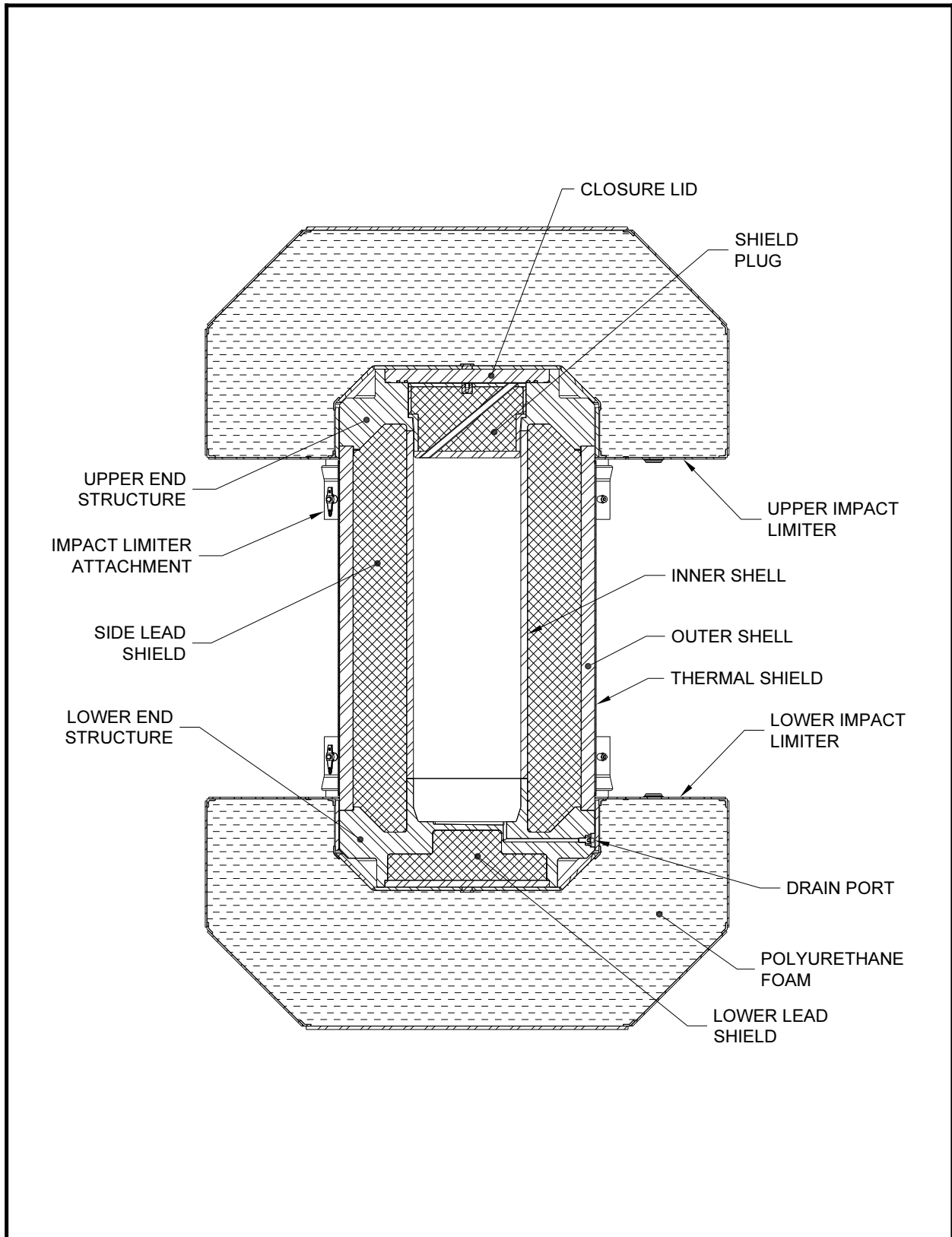


Figure 2.1-2 – BRR Package Cross Section

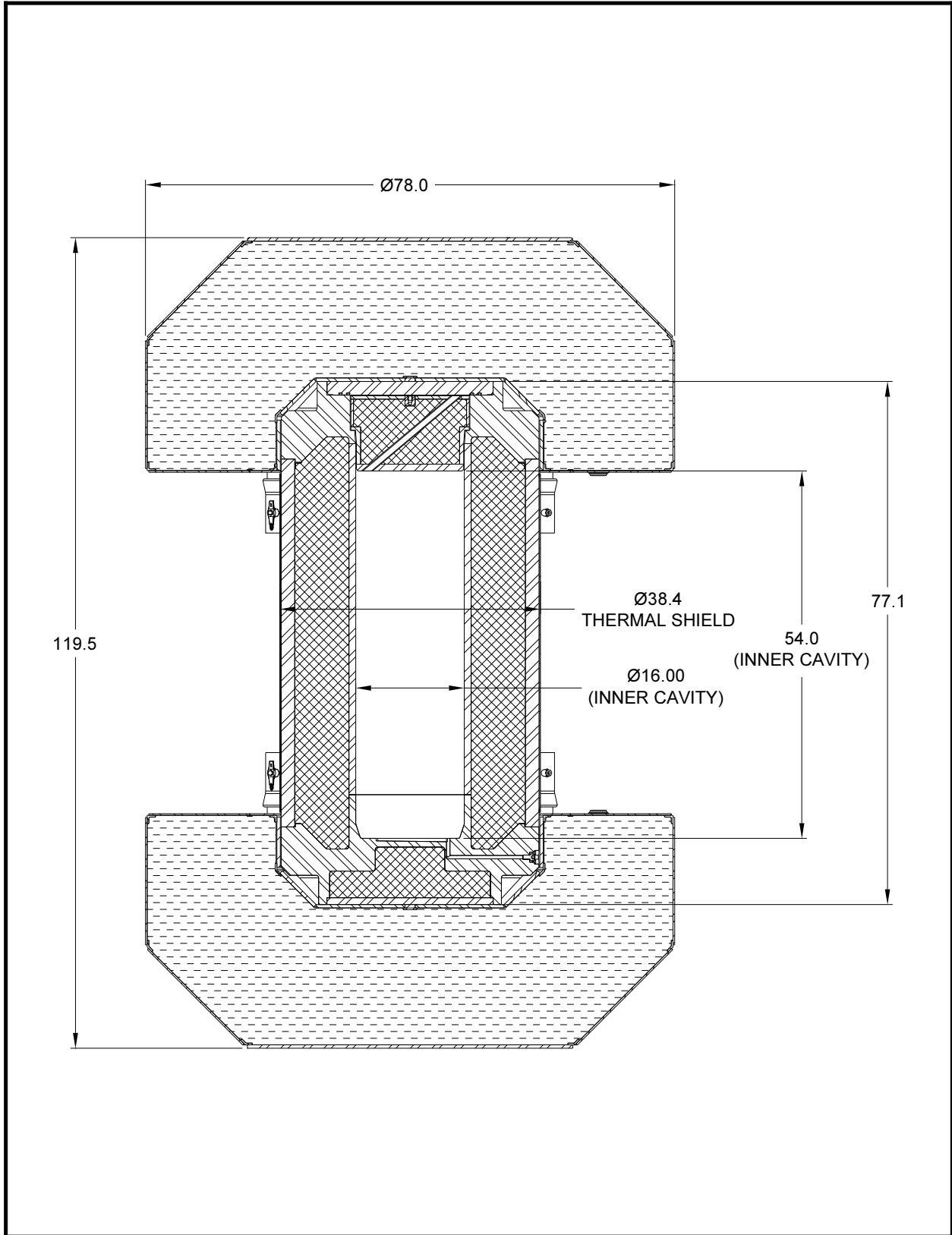


Figure 2.1-3 – BRR Package Dimensions

2.2 Materials

The BRR package structural components, including the impact limiter shells, are fabricated primarily from Type 304 stainless steel in various product forms. The gamma shielding is made from ASTM B29, Chemical Lead, or equivalent lead. Polyurethane foam is used for impact energy absorption. Other materials performing a structural function are ASTM B16 UNS C36000 brass alloy (for the test, vent, and drain port plugs), and ASTM A320, L43, alloy steel for the closure lid bolts. Austenitic stainless steel is used for the heavy duty thread inserts used for the closure bolt holes and lifting holes in the upper end structure. The ball lock pins that attach the impact limiters to the cask are made from 17-4PH stainless steel. The containment O-ring seal is made from butyl rubber. Plastic is used for the fire-consumable vent plugs in the foam cavities. The drawings presented in Appendix 1.3.3, *Packaging General Arrangement Drawings*, delineate the specific materials used for each BRR package component.

2.2.1 Material Properties and Specifications

Table 2.2-1 through Table 2.2-6 present the mechanical properties for the structural materials used in the BRR package. The density of stainless steel is 0.29 lb/in³, and Poisson's ratio is 0.3. The density of lead is 0.41 lb/in³ and Poisson's ratio is 0.45. Data is interpolated or extrapolated from the available data, as necessary, as noted in the tables.

The performance of the BRR package in free drop and puncture events is partially dependent on the energy-absorbing performance of polyurethane foam. The foam is poured in place within the impact limiter steel shells. Nominally 9 lb/ft³ polyurethane foam is used. Section 8.1.5.1, *Polyurethane Foam* presents the details of acceptance tests for this material. The nominal, room-temperature crush properties of the polyurethane foam component are given in Table 2.2-6. Properties for both "parallel to rise" and "perpendicular to rise" are given. The "rise" direction is parallel to the force of gravity during solidification, and is oriented to be parallel to the cylindrical axis of the impact limiters.

2.2.2 Chemical, Galvanic, or Other Reactions

The materials of construction of the BRR package will not have significant chemical, galvanic or other reactions in air or water environments. These materials have been previously used, without incident, in radioactive material packages for transport of similar payload materials such as the RH-TRU 72-B (NRC Docket 9212) and the NAC LWT (NRC Docket 9225). The polyurethane foam is fully enveloped by sheets of stainless steel and welded closed. The foam is a rigid, closed-cell (non-water absorbent) material that is free of halogens and chlorides, as discussed in Section 8.1.5.1, *Polyurethane Foam*. The lead gamma shielding is fully encased in a stainless steel weldment and cannot be affected by water or atmospheric moisture.

The brass alloy vent port plug used in the closure lid is very corrosion resistant. Any damage that could occur to the material is easily detectable since the fitting is handled each time the BRR package is loaded and unloaded. Similarly, the alloy steel closure bolts, which are plated with corrosion-resistant nickel plating, can be readily inspected at each use for the presence of corrosion.

BRR Package Safety Analysis Report

The butyl elastomer that is used for the containment O-ring seals contains no corrosives that would react with or adversely affect the BRR package. This material is organic in nature and noncorrosive to the stainless steel containment boundary of the BRR package.

A successful RAM packaging history combined with successful use of these fabrication materials in similar industrial environments ensures that the integrity of the BRR package will not be compromised by any chemical, galvanic or other reactions.

2.2.3 Effects of Radiation on Materials

The radiation associated with the decay of spent fuel will have no effect on the austenitic stainless steel comprising the structural components of the BRR package. Since the payload of the BRR package is heavily shielded, the radiation exposure of the overpack materials (including the polyurethane foam) is negligible. The butyl rubber containment seal, which is also located outside of the gamma shielding, likewise receives a negligible exposure. For these reasons, there will be no deleterious radiation effects on the packaging, and the requirements of 10 CFR §71.43(d) are met.

Table 2.2-1 – Mechanical Properties of Wrought Type 304 Stainless Steel

Material Specification	Temperature (°F)	①	②	③	④	⑤
		Yield Strength, S _y (psi)	Ultimate Strength, S _u (psi)	Allowable Strength, S _m (psi)	Elastic Modulus, E (×10 ⁶ psi)	Thermal Expansion Coefficient, α (×10 ⁻⁶ /°F)
ASTM A240 ASTM A249 ASTM A276 ASTM A479 Type 304	-40	30,000	75,000	20,000	28.9	8.2
	-20	30,000	75,000	20,000	28.8	8.2
	70	30,000	75,000	20,000	28.3	8.5
	100	30,000	75,000	20,000	28.1	8.6
	200	25,000	71,000	20,000	27.5	8.9
	300	22,400	66,200	20,000	27.0	9.2
	400	20,700	64,000	18,600	26.4	9.5
	500	19,400	63,400	17,500	25.9	9.7
	600	18,400	63,400	16,600	25.3	9.8
700	17,600	63,400	15,800	24.8	10.0	
800	16,900	62,800	15,200	24.1	10.1	

- Notes:
- ① ASME Code, Section II, Part D, Table Y-1.
 - ② ASME Code, Section II, Part D, Table U.
 - ③ ASME Code, Section II, Part D, Table 2A.
 - ④ ASME Code, Section II, Part D, Table TM-1, Material Group G. Values for -40 °F and -20 °F interpolated from 70 °F and -100 °F.
 - ⑤ ASME Code, Section II, Part D, Table TE-1, Material Group 3, Mean Coefficient. Values for -40 °F and -20 °F extrapolated from 70 °F and 100 °F.

Table 2.2-2 – Mechanical Properties of Forged and Cast Type 304 Stainless Steel

Material Specification	Temperature (°F)	①	②	③	④	⑤
		Yield Strength, S_y (psi)	Ultimate Strength, S_u (psi)	Allowable Strength, S_m (psi)	Elastic Modulus, E ($\times 10^6$ psi)	Thermal Expansion Coefficient, α ($\times 10^{-6}$ /°F)
ASTM A182 Type F304, ASTM A351 Type CF8, and ASTM A451, Type CPF8 ⑥	-40	30,000	70,000	20,000	28.9	8.2
	-20	30,000	70,000	20,000	28.8	8.2
	70	30,000	70,000	20,000	28.3	8.5
	100	30,000	70,000	20,000	28.1	8.6
	200	25,000	66,300	20,000	27.5	8.9
	300	22,400	61,800	20,000	27.0	9.2
	400	20,700	59,700	18,600	26.4	9.5
	500	19,400	59,200	17,500	25.9	9.7
	600	18,400	59,200	16,600	25.3	9.8
	700	17,600	59,200	15,800	24.8	10.0
800	16,900	58,600	15,200	24.1	10.1	

- Notes:
- ① ASME Code, Section II, Part D, Table Y-1.
 - ② ASME Code, Section II, Part D, Table U.
 - ③ ASME Code, Section II, Part D, Table 2A.
 - ④ ASME Code, Section II, Part D, Table TM-1, Material Group G. Values for -40 °F and -20 °F interpolated from 70 °F and -100 °F.
 - ⑤ ASME Code, Section II, Part D, Table TE-1, Material Group 3, Mean Coefficient. Values for -40 °F and -20 °F extrapolated from 70 °F and 100 °F.
 - ⑥ Optional cast materials are ASTM A351 Type CF8A and ASTM A451 Type CPF8A. The yield, ultimate, and allowable strengths of these materials are higher than the values in this table at all temperatures with one exception: the allowable strength, S_m , is not given for a temperature of 800 °F. However, since the BRR package temperatures never exceed 700 °F, this limitation does not apply.

Table 2.2-3 – Mechanical Properties of ASTM A320, Grade L43 Alloy Bolting Material

Material Specification	Temperature (°F)	① Yield Strength, S_y (psi)	② Ultimate Strength, S_u (psi)	③ Allowable Strength, S_m (psi)	④ Elastic Modulus, E (×10⁶ psi)	⑤ Thermal Expansion Coefficient, α (×10⁻⁶ /°F)
ASTM A320 Grade L43	-40	105,000	125,000	35,000	28.3	6.2
	-20	105,000	125,000	35,000	28.2	6.3
	70	105,000	125,000	35,000	27.8	6.4
	100	105,000	125,000	35,000	27.6	6.5
	200	99,000	125,000	33,000	27.1	6.7
	300	95,700	125,000	31,900	26.7	6.9
	400	91,800	125,000	30,600	26.2	7.1
	500	88,500	125,000	29,500	25.7	7.3
	600	84,300	125,000	28,100	25.1	7.4
	700	79,200	125,000	26,400	24.6	7.6

- Notes:
- ① ASME Code, Section II, Part D, Table Y-1.
 - ② ASME Code, Section II, Part D, Table Y-1.
 - ③ ASME Code, Section II, Part D, Table 4.
 - ④ ASME Code, Section II, Part D, Table TM-1, Material Group B. Values for -40 °F and -20 °F interpolated from 70 °F and -100 °F.
 - ⑤ ASME Code, Section II, Part D, Table TE-1, Material Group 1, Mean Coefficient. Values for -40 °F and -20 °F extrapolated from 70 °F and 100 °F.

Table 2.2-4 – Mechanical Properties of Lead Shielding

Material Specification	Temperature (°F)	① Tensile Yield Strength, S_y (psi)	① Tensile Ultimate Strength, S_u (psi)	① Tensile Proportional Limit (psi)	② Elastic Modulus, E (×10⁶ psi)	② Thermal Expansion Coefficient, α (×10⁻⁶ /°F)
ASTM B29 Chemical Lead or Fed Spec QQ-L-121E, Gr. A or C	-99	---	---	---	2.50	15.3
	70	---	---	---	2.34	16.1
	100	584	1,585	276	2.30	16.2
	175	509	1,158	293	2.20	16.6
	250	498	839	277	2.09	17.0
	325	311	639	189	1.96	17.5
	440	---	---	---	1.74	18.5
620	---	---	---	1.36	20.4	

Notes: ① WADC Technical Report 57-695, ASTIA Document No. 151165, “Determination of the Mechanical Properties of a High Purity Lead and a 0.05% Copper-Lead Alloy,” April 1958, by Thomas Tietz, Stanford Research Center, pp. 14, 21, for copperized lead.
 ② NUREG/CR-0481, SAND77-1872, “An Assessment of Stress-Strain Data Suitable for Finite Element Elastic-Plastic Analysis of Shipping Containers,” H. J. Rack and G. A. Knorovsky, Sept. 1978, p. 66.

Table 2.2-5 – Mechanical Properties of Brass Material

Material	Minimum Mechanical Properties
ASTM B16, UNS C36000, Temper H02	Yield Strength, $\sigma_y = 25,000$ psi Ultimate Strength, $\sigma_u = 55,000$ psi

Table 2.2-6 – Nominal Material Properties of 9 lb/ft³ Polyurethane Foam

Property	Direction	Room Temperature Value
Compressive Strength, S	Axial (Parallel-to-Rise)	280 psi @ 10% Strain 306 psi @ 40% Strain 758 psi @ 70% Strain
	Radial (Perpendicular-to-Rise)	278 psi @ 10% Strain 303 psi @ 40% Strain 767 psi @ 70% Strain

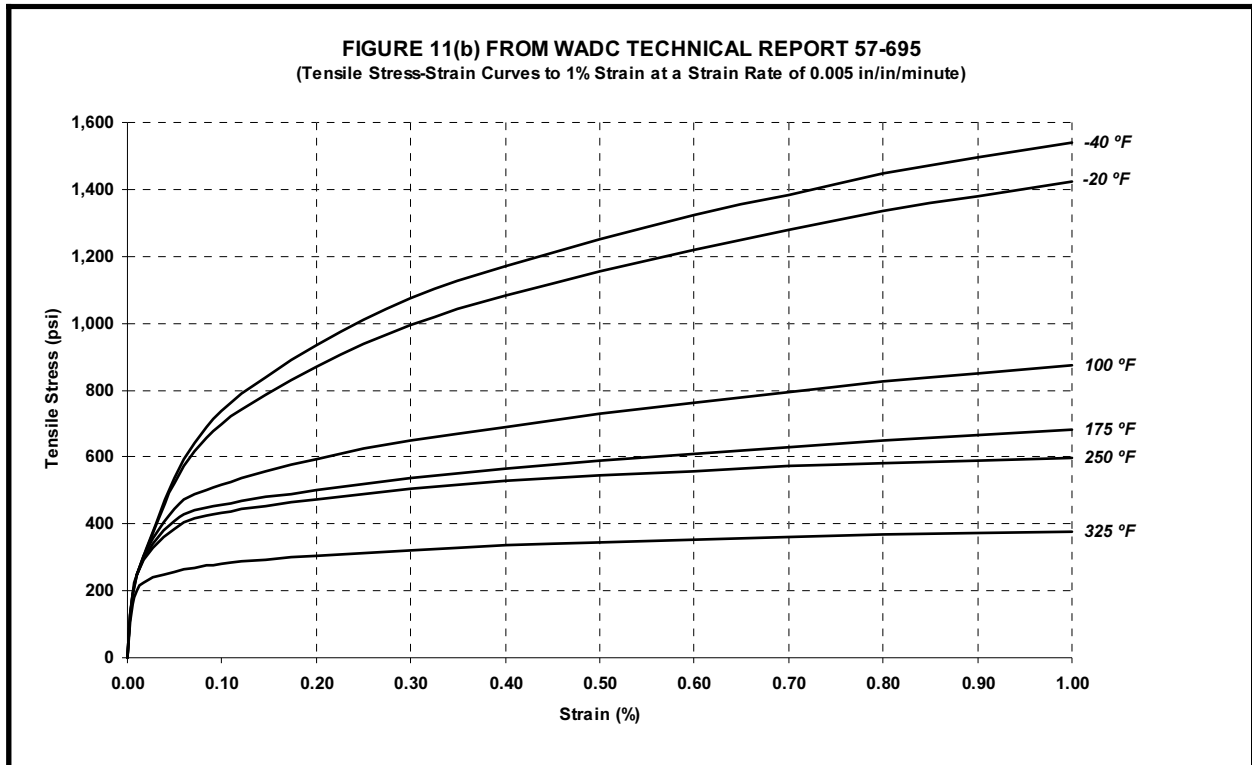


Figure 2.2-1 – Tensile Stress-Strain Curves for Lead Shielding (Source: see note 1 of Table 2.2-4)

2.3 Fabrication and Examination

2.3.1 Fabrication

The BRR package is fabricated using conventional metal forming and joining techniques. All welding procedures and welding personnel must be qualified in accordance with Section IX of the ASME Boiler and Pressure Vessel Code [14]. Containment boundary welds, as well as the welds at each end of the outer shell, are full penetration joints. All non-containment joints are fabricated in accordance with the requirements delineated on the drawings in Appendix 1.3.3, *Packaging General Arrangement Drawings*. The containment shell and outer shell fabrications shall comply with the tolerance requirements of the ASME Code, Subsection NE, Article NE-4220 [15]. Article NE-4220 is selected because the package cylindrical shells are verified for buckling performance using the ASME Code Case N-284-2. This Code Case is for Section III, Division 1, Class MC construction, and is based on the fabrication requirements of NE-4222, as stated in Section 1120 of the Code Case. Therefore, it is appropriate to fabricate the BRR package using shell tolerances from NE-4220, rather than NB-4220.

The polyurethane foam and butyl rubber O-rings are procured using written procedures. See Section 8.1.5, *Component Tests*, for details of the fabrication and performance requirements of these components.

2.3.2 Examination

Each of the materials performing a significant safety function must meet the ASTM specifications delineated on the drawings in Appendix 1.3.3, *Packaging General Arrangement Drawings*. Safety-significant materials not having an ASTM designation are controlled by means of written procedures whose requirements are summarized in Section 8.1.5, *Component Tests*.

Forgings are subject to ultrasonic and liquid penetrant inspection per the ASME Code, Subsection NB, Article NB-2540 [16]. Castings are subject to radiographic and liquid penetrant inspection per the ASME Code, Subsection NB, Article NB-2570 [17].

All welds are subject to visual examination per AWS D1.6 [18]. The welds between the inner containment shell and either end structure, the welds between the outer shell and either end structure, and the longitudinal weld(s) in the outer shell, if any, are examined by ultrasonic inspection in accordance with the ASME Code, Subsection NB, Article NB-5000, and Section V, Article 4 [20]. Optionally, the weld between the inner containment shell and the lower end structure may be examined by radiographic inspection in accordance with the ASME Code, Subsection NB, Article NB-5000, and Section V, Article 2 [19]. All welds on the BRR package, except seal welds, are liquid penetrant inspected on the final pass in accordance with the ASME Code, Subsection Nx, Article Nx-5000, and Section V, Article 6 [21]. The appropriate Subsection for the containment welds and outer shell welds is NB; for other cask body welds and the impact limiter shells, NF; and for the fuel baskets, NG.

Each BRR package will also be subjected to the following tests:

- An internal pressure test, in which the containment boundary is pressurized to 125% of the design pressure per the ASME Code [22], or 150% of the MNOP, per 10 CFR §71.85(b),

whichever is greater. The pressure test requirements are described in Section 8.1.3.2, *Containment Boundary Pressure Testing*.

- Containment boundary leakage rate test, which includes helium leakage rate tests of the containment boundary, the closure lid containment O-ring seal, the vent port containment O-ring seal, and the drain port containment O-ring seal. The leakage rate test requirements are described in Section 8.1.4, *Fabrication Leakage Rate Tests*.
- A test to ensure the integrity of the lead gamma shielding. The gamma test requirements are described in Section 8.1.6, *Shielding Integrity Test*.

2.4 General Standards for All Packages

This section defines the general standards for all packages. The BRR package meets all requirements delineated for this section.

2.4.1 Minimum Package Size

The minimum dimension of the BRR package is approximately 38.5 inches (the package diameter). Thus, the 4-in. minimum requirement of 10 CFR §71.43(a) is satisfied.

2.4.2 Tamper-Indicating Feature

A tamper-indicating seal is made by passing a lock wire through a hole in one of the upper impact limiter attachments. The wire passes through both the blade (impact limiter) and receptacle (cask body) components comprising the attachment. The upper impact limiter covers the closure lid and vent port. The wire must be destroyed in order to remove the impact limiter, thus providing evidence of possible tampering. Thus, the requirement of 10 CFR §71.43(b) is satisfied.

2.4.3 Positive Closure

The BRR package cannot be opened unintentionally. The impact limiters, which are each secured with eight, 1-inch diameter ball lock pins, fully conceal all cask openings. Thus, the requirements of 10 CFR §71.43(c) are satisfied.

2.4.4 Valves

The containment boundary of the BRR package does not contain any valves. The closure lid contains one vent port, and the lower end structure contains one drain port, which penetrate the containment boundary and which are closed with brass port plugs. Both ports are closed and tested during pre-shipment leak testing of the BRR package. The ports are protected from inadvertent use or from tampering by the impact limiters as described above. Thus, the requirements of 10 CFR §71.43(e) are satisfied.

2.4.5 Package Design

As shown in Chapter 2.0, *Structural Evaluation*, Chapter 3.0, *Thermal Evaluation*, and Chapter 5.0, *Shielding Evaluation*, the structural, thermal, and shielding requirements, respectively, of 10 CFR §71.43(f) are satisfied for the BRR package.

2.4.6 External Temperatures

As shown in Table 3.3-1 from Section 3.3, *Thermal Evaluation for Normal Conditions of Transport*, the maximum accessible surface temperature with maximum internal decay heat load and no insolation is bounded by 185 °F. This satisfies the limit of 10 CFR §71.43(g) for exclusive use shipments.

2.4.7 Venting

The BRR package does not include any features intended to allow continuous venting of the containment boundary during transport. Thus, the requirements of 10 CFR §71.43(h) are satisfied.

2.5 Lifting and Tie-down Standards for All Packages

2.5.1 Lifting Devices

The BRR package is lifted from four lift points located in the upper massive end structure. Lifting devices are installed in threaded holes containing optional alloy steel inserts. The failure mode of the lifting device is via shear tearout of the threads. Since the parent material is Type 304 stainless steel, it is conservative to consider the case in which the alloy steel inserts are not used.

The cask will be lifted using two cables, each attached to two lifting devices on the same side of the cask to preclude any crossing of the cables. In this way, both cables will have the same seating in the crane hook, and carry the same load. Consequently, all four lift points will experience the same lifting load. Although normal operating procedures call for the cask to be lifted without the lower impact limiter, it is conservatively assumed for the purpose of this analysis that it is in place during lifting. Since the upper impact limiter must be removed prior to installation of the lifting devices, lifting the cask with the upper limiter in place is impossible. The weight of the loaded cask with bottom impact limiter is:

$$W = 32,000 - 2,300 = 29,700 \text{ lb}$$

where the maximum package weight is 32,000 lb, and the upper impact limiter weight is 2,300 lb, from Table 2.1-2. For this calculation, a bounding weight of 30,000 lb is used. Since the weight will be evenly distributed among the four lifting devices, the load on each cask lift point is $F = 30,000/4 = 7,500$ lb.

The governing shear area is based on the hole thread specification, which is 1-8 UNC-2B. From [23], $A_i = 2.3256 \text{ in}^2/\text{in}$. The shear stress in the inner threads is

$$\tau_i = \frac{F}{A_i L} = 2,150 \text{ psi}$$

where the minimum thread length, $L = 1.5$ inches. At the NCT hot bounding temperature of 250 °F, the yield strength of the Type 304 parent material from Table 2.6-1 is 23,700 psi. The margin of safety is

$$MS = \frac{23,700(0.6)}{2,150(3)} - 1 = +1.20$$

where the factor of 0.6 in the numerator accounts for the shear failure mode and the factor of 3 in the denominator ensures that a minimum factor of safety of 3 is present. In the case of lifting overload, the device will strip out of the parent material without damage to the cask. Therefore, the requirements of 10 CFR §71.45(a) are met.

2.5.2 Tie-down Devices

During transport, the BRR package rests on a steel pallet, and is held down to the pallet by means of a steel frame which rests on top of the upper impact limiter. The upper impact limiter covers the lifting holes described in the section just above, and the steel tiedown frame covers

BRR Package Safety Analysis Report

the threaded holes in the upper impact limiter, thus these holes could not be erroneously used for tiedown. The steel tiedown frame is attached by wire ropes or equivalent to the conveyance, so that a nominal downward load is applied to keep the BRR package in place. In this configuration, the package contacts only the pallet on the bottom and the steel frame on the top, and therefore has no integral tie-down devices which are a structural part of the package. Therefore, per 10 CFR §71.45(b)(1), no evaluation of tie-down devices is required.

2.6 Normal Conditions of Transport

When subjected to normal conditions of transport (NCT) as specified in 10 CFR §71.71, the BRR package meets the performance requirements specified in Subpart E of 10 CFR 71. This is demonstrated in the following subsections where each NCT condition is addressed and shown to meet the applicable design criteria. Load combinations used in this section are consistent with Regulatory Guide 7.8.

2.6.1 Heat

The normal heat condition, as defined in 10 CFR §71.71(c)(1), is evaluated in Section 3.0, *Thermal Evaluation*. The bounding temperatures and pressures for use in structural analyses are summarized in the following section. Material properties and stress limits, consistent with the design criteria shown in Table 2.1-1, are summarized for the relevant bounding temperatures in Table 2.6-1.

2.6.1.1 Summary of Pressures and Temperatures

The bounding maximum temperatures for the 100 °F ambient NCT condition of the BRR package are presented in Table 3.1-1 of Chapter 3, *Thermal Evaluation*. For purposes of structural evaluation, the bounding fuel basket temperature is 400 °F. All components of the cask body, including the end structures, shells, shield plug, lead, closure lid and bolts, and elastomer seals, are bounded by a temperature of 250 °F. The bulk average polyurethane foam in both limiters is bounded by a temperature of 150 °F.

The initial pressure in the package at assembly is ambient, i.e., 14.7 psia. As determined in Section 3.3.2, *Maximum Normal Operating Pressure*, the maximum normal operating pressure (MNOP) can be conservatively defined to be 10 psig. The design pressure of the BRR package is 25 psig, which is significantly higher than the MNOP.

2.6.1.2 Differential Thermal Expansion

Acceptable minimum clearances are maintained, including consideration of worst-case tolerances, between the cask, the fuel baskets, and the fuel.

2.6.1.2.1 Baskets

The baskets for each fuel type have a nominal length of 53.45 inches with a tolerance of ± 0.12 inches, giving a maximum length of 53.57 inches. The cask cavity, with the shield plug installed, has a nominal length of 54.0 inches, with a tolerance of ± 0.1 inches, for a minimum length of $L_{\text{Cask-min}} = 53.9$ inches. The length of the basket at a bounding temperature of 400 °F is:

$$L_{\text{Bsk}} = 53.57[1 + \alpha(400 - 70)] = 53.74 \text{ inches}$$

where the coefficient of thermal expansion, α , is taken from Table 2.6-1 for Type 304 stainless steel at 400 °F as $9.5(10^{-6})$ in/in/°F, and the reference temperature is 70 °F. The cask cavity thermal expansion is conservatively ignored. The minimum axial clearance at the NCT hot temperature is:

$$CLR_{\text{Bsk-Axi}} = L_{\text{Cask-min}} - L_{\text{Bsk}} = 0.16 \text{ inches}$$

All baskets have a nominal outer diameter of 15.63 inches with a tolerance of ± 0.12 inches, giving a maximum diameter of 15.75 inches. The cask cavity has a diameter of 16.0 inches, with a tolerance of ± 0.1 inches, for a minimum diameter of $D_{\text{Cask-min}} = 15.9$ inches. The diameter of the basket at a bounding temperature of 400 °F is:

$$D_{\text{Bsk}} = 15.75[1 + \alpha(400 - 70)] = 15.80 \text{ inches}$$

where the coefficient of thermal expansion is the same as above. Again, the cask cavity thermal expansion is ignored. The minimum diametral clearance at the NCT hot temperature is:

$$CLR_{\text{Bsk-Dia}} = D_{\text{Cask-min}} - D_{\text{Bsk}} = 0.10 \text{ inches}$$

Therefore, the thermal expansion of the baskets is not of concern.

2.6.1.2.2 Fuel

The fuel types transported in the BRR Package are made primarily of aluminum. The TRIGA type also includes a stainless steel clad version, but its thermal expansion behavior will be governed by the aluminum clad configuration. At the bounding fuel temperature of 400 °F, the thermal expansion coefficient of 6061 aluminum alloy, $\alpha_{\text{Al-400}} = 13.6(10^{-6})$ in/in/°F, per Table TE-3 of the ASME Code, Section II, Part D. As an example of the minimum clearance calculation, the MITR-II fuel type case is shown in detail.

From Section 1.2.2.2, *MITR-II*, the maximum length of the MITR-II fuel element (including variation, irradiation growth, and margin) is 26.52 inches. At 400 °F, the fuel length is:

$$L_{\text{MIT-Fuel}} = 26.52[1 + \alpha_{\text{Al-400}}(400 - 70)] = 26.64 \text{ inches}$$

The basket fuel cavity length is 26.88 inches, with a tolerance of ± 0.12 , giving a minimum length of 26.76 inches at 70 °F. At a bounding temperature of 400 °F, the cavity length is:

$$L_{\text{MIT-Cav}} = 26.76[1 + \alpha(400 - 70)] = 26.84 \text{ inches}$$

where the thermal expansion coefficient for Type 304 stainless steel is the same as used above. The minimum axial clearance between the MITR-II fuel assembly and the basket cavity at the NCT hot temperature is:

$$CLR_{\text{Fuel-Axi}} = L_{\text{MIT-Cav}} - L_{\text{MIT-Fuel}} = 0.20 \text{ inches}$$

The minimum axial clearances of each fuel type are shown in Table 2.6-2.

2.6.1.2.3 Lead

Due to different thermal expansion coefficients, the lead gamma shielding creates a stress in the inner shell under NCT hot conditions. An upper bound interface pressure between the lead and the inner shell is now determined, and applied as a pressure load to the finite element model and to the buckling analysis. First, note that the lead and the cask inner and outer shells are all in contact, and are stress-free, at the point of solidification of the lead at 620 °F. As the cask and lead cool, the lead contracts more than the stainless steel, and an interface pressure develops between the lead and the inner shell. This interface pressure is a function of the amount of

interference between the lead and inner shell, and of the yield point of the lead at the NCT temperature. Due to the effects of material creep, the interface pressure will diminish over a relatively short period of time, thus reducing the resulting inner shell stresses. However, the effects of lead creep are conservatively neglected. The amount of interference between the lead and the inner shell depends upon the free state radii of these components, both at their respective NCT temperatures. The free state outer radius of the inner shell at the NCT hot temperature is

$$r_{ioh} = r_{io} [1 + \alpha_{s200}(T_{sh} - 70)] = 9.010 \text{ inches}$$

where the outer free state radius of the inner shell at room temperature, $r_{io} = 9$ inches, the lower bound NCT hot case temperature of the shell, $T_{sh} = 200$ °F, and the coefficient of thermal expansion of the inner shell material at 200 °F is $\alpha_{s200} = 8.9(10^{-6})$ /°F from Table 2.2-1. Note that the interface pressure calculation is conservative for lower bound temperatures, since the lead will contract more and apply a larger pressure.

To determine the free state radii of the lead under NCT temperatures, it is necessary to start with the radii of the steel shells at the lead solidification point at 620 °F, at which point all of the components are in stress free contact. The radii of the lead/steel interfaces at 620 °F are

$$r_{Li620} = r_{io620} = r_{io} [1 + \alpha_{s620}(620 - 70)] = 9.049 \text{ inches}$$

$$r_{Lo620} = r_{oi620} = r_{oi} [1 + \alpha_{s620}(620 - 70)] = 17.092 \text{ inches}$$

where r_{Li620}/r_{io620} represent the inner lead/steel interface radius, and r_{Lo620}/r_{oi620} represents the outer lead/steel interface radius at 620 °F. In these equations, the room temperature outer radius of the inner shell, $r_{io} = 9$ inches, the inner radius of the outer shell, $r_{oi} = 17$ inches, and the thermal expansion coefficient of the shells at 620 °F, $\alpha_{s620} = 9.84(10^{-6})$ /°F. These values are then used to find the free state lead dimensions at the NCT temperature of lead as follows. Note that two thermal expansion terms are used (first contracting the lead from 620 °F to 70 °F, then expanding it from 70 °F to the hot lead temperature), since the thermal expansion coefficients given in Table 2.2-4 are based on 70 °F. The NCT hot case temperature of the lead is given a conservative lower bound of $T_{Lh} = 200$ °F as discussed above.

$$r_{Lih} = r_{Li620} [1 - \alpha_{L620}(620 - 70) + \alpha_{L200}(T_{Lh} - 70)] = 8.967 \text{ inches}$$

$$r_{Loh} = r_{Lo620} [1 - \alpha_{L620}(620 - 70) + \alpha_{L200}(T_{Lh} - 70)] = 16.937 \text{ inches}$$

where r_{Lih} is the free state inner radius of the lead, and r_{Loh} is the outer radius, at NCT. From Table 2.2-4, the thermal expansion coefficient of the lead from 620 °F to 70 °F, $\alpha_{L620} = 20.4(10^{-6})$ /°F, and from 70 °F to T_{Lh} , the corresponding coefficient is $\alpha_{L200} = 16.7(10^{-6})$ /°F. Next, the interference between the inner shell and the lead will be found. Since the lead has a relatively low yield stress, the interface pressure between the inner shell and the lead will be governed by the lead yield stress, which in turn depends on the location of the lead stress state on the lead stress-strain curve. The hoop strain in the lead is equal to u/r , where u represents the radial displacement of the inner surface, and r is the inner radius, of the lead. The interface pressure can be conservatively maximized by assuming that the cask inner shell is rigid, and that therefore all of the radial interference is taken by the lead. The radial interference is

$$u = r_{ioh} - r_{Lih} = 0.043 \text{ inches}$$

The maximum lead strain is then

$$\varepsilon_{Lh} = \frac{u}{r_{Lih}} (100) = 0.480 \%$$

Stress-strain curves for lead at various temperatures are reproduced in Figure 2.2-1. The hoop stress at a temperature of 200 °F, corresponding to a maximum strain of 0.480% may be conservatively bounded by a value of $\sigma_{Lh} = 600$ psi. It may be observed from the figure that the actual stress would be somewhat lower. The maximum sustainable interface pressure can be backed out of the equation for hoop stress in a thick walled cylinder, Table 32, Case 1a [25], as

$$p_h = \frac{\sigma_{Lh}}{\frac{r_{Loh}^2 + r_{Lih}^2}{r_{Loh}^2 - r_{Lih}^2}} = 337 \text{ psi}$$

In the finite element thermal stress analysis discussed in Section 2.6.1.3.2, a conservative upper bound external pressure of 350 psi is applied to the inner shell to represent the worst case lead contraction loading.

2.6.1.3 Stress Calculations

2.6.1.3.1 Stresses Due to Pressure Loading

The finite element model described in Appendix 2.12.4, *Stress Analysis Finite Element Models*, is loaded with the internal maximum design pressure of 25 psi, without thermal loading, and gives the result discussed in Section 2.12.4.4.1, *Case No. 1, Design Pressure Only*, and shown in Figure 2.12.4-5. The maximum overall stress intensity which results from the model, which bounds both the primary membrane and membrane plus bending stress, is 281 psi, located at the midpoint of the cavity bottom. Since this value is less than the lowest (primary membrane) stress allowable, as shown in Section 2.6.1.4, *Comparison with Allowable Stresses*, it is not necessary to identify the individual stress components.

Since the FEA model does not include the closure lid, the stress due to pressure on the lid is computed manually. From [25], Table 24, Case 10a for a simply supported, uniformly loaded plate, the bending moment is:

$$M = \frac{qa^2(3+\nu)}{16} = 668 \text{ in-lb/in}$$

where the radius, $a = 22.75/2 = 11.38$ inches, the design pressure, $q = 25$ psig, conservatively applied over the entire area within the bolt circle, and $\nu = 0.3$. The stress in the closure lid is:

$$\sigma = \frac{6M}{t^2} = 1,002 \text{ psi}$$

where the lid thickness, $t = 2.0$ inches. As shown, the stress in the closure lid is bounding over the stress in the cavity bottom.

2.6.1.3.2 Stresses Due to Thermal Loading

The same finite element model is loaded with 25 psi internal pressure, as well as with the structural temperatures shown in Figure 2.12.4-3 and the lead contraction pressure determined in Section 2.6.1.2.3, *Lead*, and gives the result discussed in Section 2.12.4.4.2, *Case No. 2, Lead Shrinkage Pressure With Thermal*, and shown in Figure 2.12.4-6. The structural temperatures are originally obtained from the SINDA® thermal model described in Chapter 3, *Thermal Evaluation*, and are imported into the stress analysis as described in Appendix 2.12.4.2.1, *Thermal Loads*. The maximum overall stress intensity due to pressure and thermal gradient loading is 6,933 psi and occurs at the top of the inner shell cross section. Since this value is less than the lowest (primary membrane) stress allowable, as shown in Section 2.6.1.4, *Comparison with Allowable Stresses*, it is not necessary to identify the individual stress components.

2.6.1.4 Comparison with Allowable Stresses

From Table 2.1-1, the limit on primary membrane plus bending stress is $1.5S_m$. At the bounding temperature of 250 °F given in Section 2.6.1.1, *Summary of Pressures and Temperatures*, the value of $1.5S_m$ for Type 304 is 30,000 psi from Table 2.6-1. Applying this limit to the bounding stress intensity of 1,002 psi given in Section 2.6.1.3.1, *Stresses Due to Pressure Loading*, the margin of safety is:

$$MS = \frac{30,000}{1,002} - 1 = +28.9$$

From Table 2.1-1, the limit on the range of primary plus secondary stress intensity is $3S_m$. For the range of stress intensity of 6,933 psi given in Section 2.6.1.3.2, *Stresses Due to Thermal Loading*, the margin of safety is:

$$MS = \frac{(3.0)20,000}{6,933} - 1 = +7.65$$

As shown, all margins of safety for the NCT warm condition are positive.

2.6.1.5 Closure Bolts

Twelve closure bolts attach the closure lid to the cask opening. The closure lid is sized such that support against lateral loads (in the plane of the lid) is obtained from the fit between the lid and the cask opening, thus preventing any shear loading of the closure bolts. In addition, the lid is prepared with a 1/16-inch deep step located on the bolt circle which extends to the outer edge of the lid. The step prevents any bolt prying or significant bolt bending from occurring as a result of lid deformation.

The closure bolts are tightened to 220 ± 20 ft-lb of torque, or a maximum of 240 ft-lb. From Section 4.2 of [10], the maximum non-prying tensile force per bolt due to the preload, F_{a_max} , is found from:

$$F_{a_max} = \frac{Q_{max}}{(K)(Db)} = 19,200 \text{ lb}$$

where $Q_{max} = 240 \times 12 = 2,880$ in-lb is the maximum bolt torque, $K = 0.15$ is the nut factor for a lubricated bolt (approximately equal to the average of the values for lubricated surfaces in

BRR Package Safety Analysis Report

Table 4.1 of [10]), and $D_b = 1.0$ inches is the nominal diameter of the closure bolt. The maximum residual torsion is 50% of the applied torsion, or:

$$M_{tr} = 0.5(Q_{max}) = 1,440 \text{ in} - \text{lb}$$

From Section 4.4 of [10], the maximum non-prying tensile force per bolt, F_{a_max} , due to pressure loads are:

$$F_{a_max} = \frac{\pi D_l g^2 (P_{li} - P_{lo})}{4 N_b} = 789 \text{ lb}$$

where $D_l g = 18.25$ inches is the diameter of the pressure boundary, i.e., the inner (containment) O-ring seal, $P_{li} = 25 \text{ psig} + 14.7 \text{ psia} = 39.7 \text{ psia}$ is the internal pressure, $P_{lo} = 3.5 \text{ psia}$ is the NCT cold external reduced pressure from Section 2.6.3, *Reduced External Pressure*, and $N_b = 12$ is the quantity of closure bolts. From this it is clear that the preload force is governing over the pressure force.

Even though the temperatures of the closure lid and bolts are the same, a thermally induced loading is applied to the closure bolts due to the difference in thermal expansion coefficient between the ASTM A320 L43 alloy steel closure bolts and the Type 304 stainless steel closure lid. From Section 4.5 of [10], the maximum non-prying tensile force due to thermal expansion effects is:

$$F_a = \frac{\pi}{4} D_b^2 (E_b) [a_l(T_l) - a_b(T_b)] = 8,747 \text{ lb}$$

where the modulus of elasticity of the bolt, $E_b = 26.9(10^6)$ psi, the thermal expansion coefficient of the closure lid, $a_l = 9.1(10^{-6})$ in/in/°F, and the thermal expansion coefficient of the bolt, $a_b = 6.8(10^{-6})$ in/in/°F, all from Table 2.6-1. The change in temperature of both components, $T_l = T_b = (250 - 70) = 180$ °F, where the bounding temperature of the components is 250 °F, and the ambient temperature is 70 °F.

The average axial bolt stress corresponding to these loadings is:

$$S_{ba} = 1.2732 \frac{(19,200 + 8,747)}{D_{ba}^2} = 46,158 \text{ psi}$$

where the load term in the numerator is the sum of the preload and thermal loads, and the stress diameter, $D_{ba} = D_b - 0.9743(p) = 0.878$ inches, where D_b is 1.0 inches and the pitch, p , is 0.125 for the 1-8 UNC bolt. The residual torsional stress is:

$$S_{bt} = \frac{5.093(M_{tr})}{D_{ba}^2} = 9,514 \text{ psi}$$

From Table 2.1-1, for NCT the allowable average tensile stress is $S_m = (2/3)S_y$, which from Table 2.6-1 is equal to 64,900 psi at the NCT hot temperature of 250 °F. The margin of safety is:

$$MS_{S_{ba}} = \frac{64,900}{S_{ba}} - 1 = +0.41$$

Combining the axial and residual torsional shear stresses, the maximum closure bolt stress intensity is:

$$S_{bi} = \sqrt{S_{ba}^2 + 4S_{bt}^2} = 49,926 \text{ psi}$$

As noted at the beginning of this section, bolt shear or prying loads are precluded by the design of the closure lid. From Table 2.1-1, the allowable stress intensity is $1.35S_m$ for cases where S_y is greater than 100 ksi. The margin of safety is:

$$MS_{S_{bi}} = \frac{1.35(64,900)}{49,926} - 1 = +0.75$$

Thus the closure bolts are not of concern for the NCT hot condition, including the reduced external pressure load case.

2.6.2 Cold

For the cold condition, a -40 °F steady state ambient temperature is utilized per Regulatory Guide 7.8 [3], with zero insolation and zero decay heat. This results in a uniform temperature of -40 °F throughout the cask. The materials of construction for the SEC transportation cask are not adversely affected by the -40 °F condition, including brittle fracture, which is evaluated in Section 2.1.2.3.1, *Brittle Fracture*.

In Section 2.6.1.2, *Differential Thermal Expansion*, the interface pressure between the cask inner shell and the lead gamma shielding was evaluated at the NCT maximum temperature. Since the lead will contract further at lower temperatures, that analysis is now repeated for the NCT cold condition. As discussed in Section 2.6.1.2, the lead and the cask inner and outer shells are all in contact, and stress free, at the point of solidification of the lead at 620 °F. As the cask and lead cool, the lead contracts more than the stainless steel, and an interface pressure develops between the lead and the inner shell. This interface pressure is a function of the amount of interference between the lead and inner shell, and of the yield point of the lead at the cold temperature. As stated in Section 2.6.1.2, material creep in the lead will reduce the interface pressure over time, but the effect is conservatively neglected. In addition, the entire strain history of the lead is assumed to occur at a temperature of -40 °F, which further maximizes the lead interface pressure. The amount of interference between the lead and the inner shell depends upon the free state radii of these components, both at -40 °F. The free state outer radius of the inner shell at -40 °F is:

$$r_{ioc} = r_{io} [1 + \alpha_{s-40} (-40 - 70)] = 8.992 \text{ inches}$$

where the outer free state radius of the inner shell at room temperature, $r_{io} = 9$ inches, and the coefficient of thermal expansion of the shell at -40 °F, $\alpha_{s-40} = 8.2(10^{-6})/^{\circ}\text{F}$ from Table 2.6-1.

To determine the free state radii of the lead at -40 °F, it is necessary to start with the radii of the steel shells at the lead solidification point at 620 °F, at which point all of the components are in stress free contact. The radii of the lead/steel interfaces at 620 °F were found in Section 2.6.1.2. The value $r_{Li620} = 9.049$ inches represents the inner radius of the lead and $r_{Lo620} = 17.092$ inches represents the outer lead radius. These values are then used to find the free state lead dimensions at the cold temperature of -40 °F as follows. Note that two thermal expansion terms are used (first contracting the lead from 620 °F to 70 °F, then contracting it further from 70 °F to -40 °F), since the thermal expansion coefficients given in Table 2.2-4 are based on 70 °F.

$$r_{Lic} = r_{Li620} [1 - \alpha_{L620} (620 - 70) + \alpha_{L-40} (-40 - 70)] = 8.932 \text{ inches}$$

$$r_{Loc} = r_{Lo620} [1 - \alpha_{L620} (620 - 70) + \alpha_{L-40} (-40 - 70)] = 16.871 \text{ inches}$$

BRR Package Safety Analysis Report

where r_{Lic} is the free state inner radius of the lead, and r_{Loc} is the outer radius, at -40 °F. From Table 2.2-4, the thermal expansion coefficient of the lead from 620 °F to 70 °F, $\alpha_{L620} = 20.4(10^{-6})/^{\circ}\text{F}$, and from 70 °F to -40 °F, $\alpha_{L-40} = 15.6(10^{-6})/^{\circ}\text{F}$. Since the lead has a relatively low yield stress, the interface pressure between the inner shell and the lead will be governed by the lead yield stress, which in turn depends on the location of the lead stress state on the lead stress-strain curve. The hoop strain in the lead is equal to u/r , where u represents the radial displacement of the inner surface, and r is the inner radius of the lead. The interface pressure can be conservatively maximized by assuming that the inner shell is rigid, and therefore all of the radial interference is taken by the lead. The radial interference is

$$u = r_{ioc} - r_{Lic} = 0.060 \text{ inches}$$

The maximum lead strain is then

$$\epsilon_{Lh} = \frac{u}{r_{Lic}} (100) = 0.671 \%$$

Stress-strain curves for lead at various temperatures are reproduced in Figure 2.2-1. From the curve representing a lead temperature of -40 °F, the maximum lead stress corresponding to a strain of 0.671% is bounded by $\sigma_{Lc} = 1,400$ psi. The maximum sustainable interface pressure can be backed out of the equation for hoop stress in a thick walled cylinder, Table 32, Case 1a [25], as

$$p_c = \frac{\sigma_{Lc}}{\frac{r_{Loc}^2 + r_{Lic}^2}{r_{Loc}^2 - r_{Lic}^2}} = 787 \text{ psi}$$

Using this external pressure, the inner shell membrane stress is

$$\sigma_i = \frac{p_c r_{avg}}{t} = 6,690 \text{ psi}$$

where r_{avg} is the minimum average inner shell radius, 8.5 inches, and t is the wall thickness of 1 inch. From Table 2.6-1, the allowable primary membrane stress intensity (S_m) is $20,000$ psi. The margin of safety is

$$MS = \frac{20,000}{6,690} - 1 = +1.99$$

Therefore, the NCT cold condition is not of concern.

Since the coefficient of thermal expansion of the closure lid material is slightly larger than that of the bolting material, a reduction in closure bolt preload will occur at the NCT cold condition. Using the terminology of [10], the reduction in preload is:

$$F_a = \frac{\pi}{4} D_b^2 (E_b) [a_l(T_l) - a_b(T_b)] = -4,890 \text{ lb}$$

where the bolt nominal diameter, $D_b = 1.0$ inches, the bolt modulus of elasticity, $E_b = 28.3(10^6)$ psi, the coefficient of thermal expansion of the lid material, $a_l = 8.2(10^{-6})$ in/in/°F for Type 304 stainless steel, the coefficient of thermal expansion of the bolt material, $a_b = 6.2(10^{-6})$ in/in/°F for A320 L43 alloy steel, and $T_l = T_b = -40 - 70 = -110$ °F. The material properties are taken from

Table 2.6-1. The minimum bolt preload torque is 220 ft-lb minus 20 ft-lb, or $Q_{min} = 2,400$ in-lb. The minimum bolt preload force is:

$$F_{a_min} = \frac{Q_{min}}{K(Db)} = 16,000 \text{ lb}$$

where Db is defined above and $K = 0.15$, consistent with the definition in Section 2.6.1.5, *Closure Bolts*. Thus, the reduction in preload due to differential thermal expansion is only $4,890/16,000 \times 100 = 31\%$, and a large positive preload force remains at the NCT minimum temperature of -40 °F.

2.6.3 Reduced External Pressure

The effect of reduced external pressure of 3.5 psia, per 10 CFR §71.71(c)(3), is considered negligible for the BRR package compared to other design loadings. This conclusion is based on the NCT structural analyses presented in Section 2.6.1, *Heat*, demonstrating the structural integrity for a 25 psig internal design pressure. Based on the Maximum Normal Operating Pressure (MNOP) of 10 psig, the reduced external pressure conditions would cause a pressure of 21.2 psig. Therefore, the 25 psig internal design pressure analysis is conservatively bounding for the reduced external pressure case.

2.6.4 Increased External Pressure

The effect of an increased external pressure of 20 psia, per 10 CFR §71.71(c)(4), is acceptable for the BRR package. Consistent with Regulatory Guide 7.8, this loading corresponds to an ambient temperature of -20 °F, no insolation, no decay heat, and minimum internal pressure. Additionally, the fabrication stress resulting from the shrinking of the radial lead shield of $p_c = 787$ psi (see Section 2.6. 2, *Cold*) is included as a radial pressure on the outside of the inner shell. Note that the lead shrinkage stress corresponds to a temperature of -40 °F, which results in a conservatively higher shrinkage stress than would occur at the required ambient temperature of -20 °F. Conservatively, the inner shell is evaluated neglecting the outer shell, even though the external pressure would be applied to the much stronger outer shell rather than the inner shell.

Since the cask is closed under ambient conditions, the internal pressure in the cask at a temperature of -20 °F is

$$p_i = p_{amb} \frac{(-20 + 460)}{(70 + 460)} = 12.2 \text{ psia}$$

where p_{amb} is 14.7 psia. Therefore the net external differential gas pressure $p_o = 20 - 12.2 = 7.8$ psi. The combined external pressure on the inner shell is $p_{ext} = p_c + p_o = 794.8$ psi. An upper bound value of $p_{ext} = 800$ psi is used. The compressive hoop stress is:

$$\sigma_\theta = p_{ext} \frac{r_{avg}}{t} = 6,800 \text{ psi}$$

where the mean inner shell radius, $r_{avg} = 8.5$ inches, and the thickness, $t =$ one inch. The compressive axial stress, obtained by supporting the pressure load from the entire cask cross section over the inner shell cross section, is:

BRR Package Safety Analysis Report

$$\sigma_{\phi} = \frac{P_o \pi r_{\text{cask}}^2}{2 \pi r_{\text{avg}} t} = 169 \text{ psi}$$

where $r_{\text{cask}} = 38.4/2 = 19.2$ inches. Using Mohr's circle, the maximum shear stress is:

$$\sigma_{\phi\theta} = \frac{1}{2}(\sigma_{\theta} - \sigma_{\phi}) = 3,316 \text{ psi}$$

The maximum stress intensity is twice this value, or $SI = 6,632$ psi. From Table 2.6-1, the allowable membrane stress intensity for the inner shell is 20,000 psi. The margin of safety is:

$$MS = \frac{20,000}{6,632} - 1 = +2.02$$

The possibility of buckling of the inner shell is evaluated using [13]. Consistent with Regulatory Guide 7.6, a factor of safety corresponding to ASME Code, Service Level A is employed. In this case, the applicable factor of safety is 2.00 for normal conditions, as specified in [13]. The analysis used a modulus of elasticity of $28.8(10^6)$ psi, corresponding to -20 °F. Buckling analysis geometry and loading parameters are listed in Table 2.6-3 and results of the analysis in Table 2.6-4. As shown, all interaction check values, including the maximum value of 0.5974, are less than unity, as required. Thus, the increased external pressure load case is not of concern for the BRR package.

2.6.5 Vibration

The effects of vibration normally incident to transport are shown to be insignificant. Draft ANSI Standard N14.23 [24] identifies peak truck trailer vibration inputs. Table 2 of [24] shows peak vibration accelerations of a trailer bed as a function of package and tiedown system natural frequency. For the frequency range 0 to 5 Hz, and conservatively assuming a light package, Table 2 gives peak accelerations (99% level) of 2g in the vertical direction, and 0.1g in both the lateral and longitudinal directions. All other frequency ranges give significantly lower acceleration levels. Due to cask symmetry, the vertical load of $\pm 2g$ governs the $\pm 0.1g$ in the lateral and longitudinal directions.

Design fatigue curves are taken from Figure I-9.2.1 and Table I-9.2.2 of [12] for the Type 304 stainless steel cask material, from which the allowable amplitude, S_a , of the alternating stress component (1/2 of the alternating stress range) as a function of number of loading cycles may be obtained. Table I-9.2.2 extends the fatigue allowable data to the endurance limit, which is used in the fatigue assessment of transportation vibration. The allowable amplitude, S_a , from Table I-9.2.2 for Type 304 stainless steel cask material at 10^{11} cycles is 13,600 psi. This value is adjusted based on the ratio of room temperature elastic modulus of $28.3(10^6)$ psi, which is the basis for Table I-9.2.2, and the elastic modulus at NCT maximum temperature, as follows:

$$S_a = 13,600 \left[\frac{27.3(10^6)}{28.3(10^6)} \right] = 13,119 \text{ psi}$$

where $27.3(10^6)$ psi is the elastic modulus at the bounding temperature of all cask components of 250 °F from Table 2.2-1.

The BRR package is transported vertically. In this orientation, the closure lid experiences the $\pm 2g$ loading transverse to the plane of the lid. The weight of the shield plug is conservatively assumed to act with the weight of the lid in responding to the vibratory input. From Table 2.1-2, the weight of the shield plug is 950 lb, and the weight of the lid is 280 lb, for a total of $W = 1,230$ lb. The lid is modeled as a simply supported plate with an effective outer radius equal to the bolt circle of 22.75 inches. Under a load of $2g$, the maximum bending moment in the plate (at the center) is found from Table 24, Case 10a of [25], and is:

$$M = 2K_M qa^2 = 161.7 \text{ in} - \text{lb/in}$$

where the factor 2 is the vibrational load, $K_M = 0.20625$ for $r_o = 0$ from [25], the bolt circle radius, $a = 22.75/2 = 11.375$ inches, and q is the 1-g plate loading, equivalent to a pressure, found from:

$$q = \frac{W}{A} = 3.03 \text{ psi}$$

where W is defined above and A is the area defined by the bolt circle, equal to 406.5 in^2 . The stress in the closure lid is:

$$\sigma = \frac{6M}{t^2} = 242.6 \text{ psi}$$

where the thickness of the closure lid, $t = 2$ inches. For the allowable amplitude, S_a , found above, equal to 13,119 psi, the margin of safety against fatigue of the closure lid due to vibration is:

$$MS = \frac{13,119}{242.6} - 1 = +53.1$$

Therefore, fatigue of the BRR package due to transportation vibration is not of concern.

2.6.6 Water Spray

The materials of construction used in the BRR package are not affected by the water spray test identified in 10 CFR §71.71(c)(6).

2.6.7 Free Drop

Section 10 CFR §71.71(c)(7) specifies a free drop from a height of 2 ft for a package weight between 22,000 and 33,100 lb. The governing orientations of end and side are evaluated for the NCT free drop event. The choice of governing orientations is discussed in further detail in Appendix 2.12.2, *Certification Test Plan*. NCT free drop impacts are developed in Appendix 2.12.5, *Impact Limiter Performance Evaluation*. A value of 40g is chosen to bound the calculated impact magnitude for all NCT drop orientations.

Cask body stresses are analyzed for the NCT free drop using the same finite element model identified in Section 2.6.1.3, *Stress Calculations*, and which is also used for evaluation of the HAC free drop event. The model is loaded by a global, quasi-static acceleration field consistent with an impact of 40g. The cask stress analysis for NCT is identical with the analysis for HAC, with the following exceptions:

BRR Package Safety Analysis Report

- Thermal stresses are included in the NCT stress analyses
- The applied quasi-static acceleration field corresponds to the NCT free drop impact of 40g
- Allowable stresses are lower, in accordance with Regulatory Guide 7.6 recommendations.

As discussed in Section 2.7.1.4, *Oblique Drop*, cask stresses are governed by those resulting from the end and side drop orientations. The stress analyses for NCT free drop are given in Sections 2.6.7.1, *NCT End Free Drop*, and 2.6.7.2, *NCT Side Free Drop*.

2.6.7.1 NCT End Free Drop

The construction of the finite element model is discussed in Appendix 2.12.4, *Stress Analysis Finite Element Models*. Temperature loading is applied as discussed in that appendix. The end drop case is evaluated for both top down and bottom down orientations by applying a quasi-static acceleration of 40g. Five analyses are performed:

- Cask body stress
- Closure bolt stress
- Closure lid stress
- Lower closure plate weld stress
- End drop buckling evaluation

Cask Body Stress. From Section 2.12.4.4.3, *Case No. 3, NCT Bottom-down End Drop*, the maximum stress intensity resulting from the bottom-down impact of 40g is 15,202 psi, located at the outside surface of the bottom end structure, as shown in Figure 2.12.4-8. From Table 2.1-1, the limit on primary membrane stress is S_m . At the bounding temperature of 250 °F, the value of S_m for Type 304 is 20,000 psi from Table 2.6-1. Conservatively applying the membrane stress limit to the maximum stress intensity of 15,202 psi, the margin of safety is:

$$MS = \frac{20,000}{15,202} - 1 = +0.32$$

From Section 2.12.4.4.4, *Case No. 4, NCT Bottom-down End Drop With Thermal*, the maximum stress intensity resulting from the bottom-down impact of 40g with thermal loads included is 14,586 psi, located at the top of the inner shell cross section, as shown in Figure 2.12.4-9. From Table 2.1-1, the limit on the range of primary plus secondary stress intensity is $3S_m$. The margin of safety is:

$$MS = \frac{(3.0)20,000}{14,586} - 1 = +3.11$$

From Section 2.12.4.4.6, *Case No. 6, NCT Top-down End Drop*, the maximum stress intensity resulting from the top-down impact of 40g is 13,248 psi, located at the top of the inner shell, as shown in Figure 2.12.4-13. From Table 2.1-1, the limit on primary membrane stress is S_m . Conservatively applying the membrane stress limit to the maximum stress intensity of 13,248 psi, the margin of safety is:

$$MS = \frac{20,000}{13,248} - 1 = +0.51$$

From Section 2.12.4.4.7, *Case No. 7, NCT Top-down End Drop With Thermal*, the maximum stress intensity resulting from the top-down impact of 40g with thermal loads included is 13,258 psi, located at the top of the inner shell, as shown in Figure 2.12.4-14. From Table 2.1-1, the limit on the range of primary plus secondary stress intensity is $3S_m$. The margin of safety is:

$$MS = \frac{(3.0)20,000}{13,258} - 1 = +3.53$$

As shown, all cask body margins of safety for the NCT end free drop condition are positive.

Closure bolt stress. In the top-down orientation, the non-prying closure bolt load is calculated according to Section 4.6 of [10] using:

$$F_a = \frac{1.34 \sin(\xi_i)(DLF)(a_i)(W_l + W_c)}{N_b} = 9,380 \text{ lb}$$

where the impact angle, $\xi_i = 90^\circ$ for the end drop impact, the dynamic load factor, $DLF = 1.05$ as discussed in Section 2.7.1.2, *End Drop*, the impact magnitude, $a_i = 40g$ as discussed above, the weight of the lid, $W_l = 280 \text{ lb}$, and the weight of the contents, $W_c = 1,720 \text{ lb}^1$ from Table 2.1-2, and the quantity of bolts, $N_b = 12$. Note that no support for the lid is assumed from the inner surface of the impact limiter.

The sum of all applied loads (the NCT free drop load plus the load due to the design pressure, equal to 789 lb as determined in Section 2.6.1.5, *Closure Bolts*) is equal to $9,380 + 789 = 10,169 \text{ lb}$. This value is however much less than the sum of preload (19,200 lb) and thermal expansion load (8,747 lb). Therefore, the bolt load in the NCT free drop event is governed by the preload plus thermal load, and the margins of safety calculated in Section 2.6.1.5, *Closure Bolts*, are not affected by the free drop event.

Closure lid stress. In Section 2.7.1.2, *Free Drop*, the bending stress in the closure lid is calculated for the top-down HAC free drop under an impact load of 120g. The only difference in the case of the NCT free drop is that the impact is one-third as large, i.e., 40g. The following calculations rely on data given in Section 2.7.1.2. Since the total weight in the end drop is 2,000 lb, the applied load is $2,000 \times 40 = 80,000 \text{ lb}$. Since the area of the lid is $A_{\text{lid}} = 406.9 \text{ in}^2$, the uniform load on the lid is:

$$q = \frac{80,000}{A_{\text{lid}}} + 25 = 221.6 \text{ psi}$$

where the second term accounts for the design pressure of 25 psig. The uniform load in the HAC case is 614.8 psi, and the resulting stress is 25,865 psi. Using a ratio, the stress under the NCT free end drop is

$$\sigma_{\text{NCT}} = \frac{221.6}{614.8} 25,865 = 9,323 \text{ psi}$$

¹ This weight consists of the shield plug plus the heaviest basket/fuel combination.

From Table 2.1-1, the allowable membrane plus bending stress is equal to $1.5S_m$. From Table 2.6-1, $1.5S_m$ is equal to 30,000 psi at the NCT hot temperature of 250 °F. The margin of safety on the closure lid is:

$$MS = \frac{30,000}{9,323} - 1 = +2.22$$

Thus, the allowable stress is satisfied for the closure lid in the NCT end drop.

Lower closure plate weld stress. In Section 2.7.1.2, *Free Drop*, the combined stress in the lower closure plate weld is calculated for the top-down HAC free drop under an impact load of 120g. The resulting stress is 49,165 psi. This stress includes both fixed-edge bending effects as well as shear loading. Since the NCT impact is 40g and the HAC impact is 120g, the stress corresponding to the NCT free drop is:

$$\sigma_{\text{NCT}} = \sigma_{\text{HAC}} \frac{40}{120} = 16,388 \text{ psi}$$

From Table 2.1-1, the membrane plus bending stress allowable is $1.5S_m$, which from Table 2.6-1 is equal to 30,000 psi for Type 304 at 250 °F. The margin of safety is:

$$MS = \frac{30,000}{16,388} - 1 = +0.83$$

Thus, the allowable stress is satisfied for the lower closure plate weld stress in the NCT end drop.

End drop buckling evaluation. The cask shells are subject to buckling loads in the end drop orientation. Due to its much greater stiffness compared to the inner shell, the cask outer shell will carry most of the axial loading. The NCT case is essentially the same as the HAC case evaluated in Section 2.7.1.2, *End Drop*, except for the different impact load and factor of safety required by Code Case N-284-2 [13]. Since the HAC end drop is evaluated for an impact of 120g and the NCT for 40g, the axial stress in the NCT buckling evaluation is:

$$\sigma_{\phi\text{-NCT}} = \sigma_{\phi\text{-HAC}} \times \frac{40}{120} = 2,372 \text{ psi}$$

where $\sigma_{\phi\text{-HAC}} = 7,117$ psi from Section 2.7.1.2, *End Drop*. No other stresses are applied for the end drop buckling evaluation. The outer shell is conservatively assumed to carry the entire axial load without assistance from the inner shell. Thermal stress, which is tensile in the outer shell, is conservatively ignored. Shell dimensions are taken from Table 2.6-5. The factor of safety is equal to 2.00, consistent with Code Case N-284-2 for NCT. The results are shown in Table 2.6-6. As shown, all interaction parameters are less than unity, as required. Therefore, buckling of the cask shells in the NCT free drop will not occur.

2.6.7.2 NCT Side Free Drop

The NCT side free drop is evaluated using the same finite element model which was used for the end drop case. The quasi-static acceleration of 40g also applies to the side drop, since it bounds the calculated side drop impact as discussed in Appendix 2.12.5, *Impact Limiter Performance*

BRR Package Safety Analysis Report

Evaluation. The side drop orientation is governing over the slapdown orientation as discussed in Section 2.7.1.4, *Oblique Drop*.

From Section 2.12.4.4.9, *Case No. 9, NCT Side Drop*, the maximum stress intensity resulting from the side drop impact of 40g is 18,935 psi, located at the bottom outside edge of the lower lead cavity, as shown in Figure 2.12.4-19. From Table 2.1-1, the limit on primary membrane stress is S_m . At the bounding temperature of 250 °F, the value of S_m for Type 304 is 20,000 psi from Table 2.6-1. Conservatively applying the membrane stress limit to the maximum stress intensity of 18,935 psi, the margin of safety is:

$$MS = \frac{20,000}{18,935} - 1 = +0.06$$

From Section 2.12.4.4.10, *Case No. 10, NCT Side Drop With Thermal*, the maximum stress intensity resulting from the side drop impact of 40g with thermal loads included is 22,704 psi, located at the shield plug shelf, as shown in Figure 2.12.4-20. From Table 2.1-1, the limit on the range of primary plus secondary stress intensity is $3S_m$. Conservatively applying the membrane stress limit to the maximum stress intensity of 22,704 psi, the margin of safety is:

$$MS = \frac{(3.0)20,000}{22,704} - 1 = +1.64$$

As shown, all cask body margins of safety for the NCT side free drop condition are positive.

2.6.8 Corner Drop

The BRR package is not required to be evaluated for the corner drop condition, since 10 CFR §71.71(c)(8) applies only to rectangular fiberboard or wood packages weighing less than 110 lb or to cylindrical fiberboard or wood packages weighing less than 220 lb. The weight of the BRR package exceeds these limits and therefore does not need to be evaluated for the NCT corner drop.

2.6.9 Compression

The BRR package is not required to be evaluated for the compression condition, since 10 CFR §71.71(c)(9) applies only to packages weighing less than 11,000 lb. The weight of the BRR package exceeds this limit, and therefore does not need to be evaluated for compression.

2.6.10 Penetration

The impact of a 1.25-inch diameter, hemispherically ended, 13-lb steel bar, per 10 CFR §71.71(c)(10), dropped vertically from a height of 40 inches, has no significant effect on the BRR package. Slight denting of the thermal shield on the outside of the cask can occur, but the bar cannot penetrate or rip into the shield, and cannot harm the impact limiters or impact limiter attachments. Therefore, this test has no significant effect on the package.

Table 2.6-1 – Summary of NCT Design Parameters

Parameter	Body, Closure Lid (Type 304)	Closure Bolts (A320, Grade L43)	Baskets (all Type 304)
NCT Hot Bounding Temperature, °F	250	250	400
Coefficient of Thermal Expansion, α , (in/in/°F)	9.1×10^{-6}	6.8×10^{-6}	9.5×10^{-6}
Elastic Modulus, psi	27.3×10^6	26.9×10^6	26.4×10^6
Design Stress, S_m , psi	20,000	64,900	18,600
Yield Stress, S_y , psi	23,700	97,350	20,700
Primary Membrane Stress Intensity (P_m), psi	$S_m = 20,000$	n/a*	$S_m = 18,600$
Primary Membrane + Bending Stress Intensity ($P_m + P_b$), psi	$1.5S_m = 30,000$	n/a*	$1.5S_m = 27,900$
Primary Membrane + Bending + Secondary Stress Intensity ($P_m + P_b + Q$), psi	$3.0S_m = 60,000$	n/a*	$3.0S_m = 55,800$
NCT Cold Bounding Temperature, °F	-40	-40	-40
Coefficient of Thermal Expansion, α , (in/in/°F)	8.2×10^{-6}	6.2×10^{-6}	8.2×10^{-6}
Elastic Modulus, psi	28.9×10^6	28.3×10^6	28.9×10^6

* Bolting allowable stresses are discussed in the sections where they are used.

Table 2.6-2 – Axial Clearance of Fuel

Type	Max. fuel len., 70°F, in.	Max. fuel len., 400 °F, in.	Basket cavity len., 70 °F, in.	Basket cavity, less 0.12 in. tol.	Min basket cavity len., 400 °F, in.	Axial clearance, min, in.*
MURR	32.75	32.90	33.13	33.01	33.13	0.21
MITR-II	26.52	26.64	26.88	26.76	26.86	0.20
ATR	51.00	51.23	51.38	51.26	51.44	0.19
TRIGA	45.50	45.70	45.88**	45.76	45.90	0.20

* Axial clearance is equal to column 6 (min basket cavity length at 400 °F) minus column 3 (max fuel length at 400 °F).

**Total cavity length of 48.00 inches, minus a 2.12-inch long, short spacer.

Table 2.6-3 – Increased External Pressure Buckling Evaluation: Geometry and Loads

	Inner shell dimensions, inches	Applied stress, psi	
Inner Dia.	16.0	σ_{ϕ}	169
Outer Dia.	18.0	σ_{θ}	6,800
Length*	62.0	$\sigma_{\phi\theta}$	3,316

* Bounding length used.

Table 2.6-4 – Increased External Pressure: N-284-2 Results

Parameter	Value	Remarks
Capacity Reduction Factors (-1511)		
$\alpha_{\phi L} =$	0.2795	
$\alpha_{\theta L} =$	0.8000	
$\alpha_{\phi\theta L} =$	0.8000	
Plasticity Reduction Factors (-1610)		
$\eta_{\phi} =$	0.0524	
$\eta_{\theta} =$	0.2811	
$\eta_{\phi\theta} =$	0.0410	
Theoretical Buckling Values (-1712.1.1)		
$C_{\phi} =$	0.6050	
$\sigma_{\phi eL} =$	2,049,882 psi	
$C_{\theta r} =$	0.0387	
$\sigma_{\theta eL} = \sigma_{reL} =$	133,985 psi	
$C_{\theta h} =$	0.0387	
$\sigma_{\theta eL} = \sigma_{heL} =$	133,985 psi	
$C_{\phi\theta} =$	0.1619	
$\sigma_{\phi\theta eL} =$	548,683 psi	
Elastic Interaction Equations (-1713.1.1)		
$\sigma_{xa} =$	286,471 psi	
$\sigma_{ha} =$	52,394 psi	
$\sigma_{ra} =$	52,394 psi	
$\sigma_{\tau a} =$	219,473 psi	
Axial + Shear \Rightarrow Check (c):	0.0008	<1 \therefore OK (see note*)
Hoop + Shear \Rightarrow Check (d):	0.1300	<1 \therefore OK
Inelastic Interaction Equations (-1714.2.1)		
$\sigma_{xc} =$	15,000 psi	
$\sigma_{rc} =$	14,730 psi	
$\sigma_{\tau c} =$	9,000 psi	
Max(Axial,Hoop) \Rightarrow Check (a):	0.4616	<1 \therefore OK
Axial + Shear \Rightarrow Check (b):	0.1470	<1 \therefore OK
Hoop + Shear \Rightarrow Check (c):	0.5974	<1 \therefore OK

*Note: Elastic interaction checks (a), (b), (e), and (f) are not applicable.

Table 2.6-5 – NCT Free Drop Buckling Evaluation: Geometry and Loads

	Outer shell dimensions, inches	Applied stress, psi	
Inner Dia.	34.0	σ_{ϕ}	2,372
Outer Dia.	38.0	σ_{θ}	0
Length*	55.0	$\sigma_{\phi\theta}$	0

* Bounding length used.

Table 2.6-6 – NCT Free Drop: N-284-2 Results

Parameter	Value	Remarks
Capacity Reduction Factors (-1511)		
$\alpha_{\phi L} =$	0.2279	
$\alpha_{\theta L} =$	0.8000	
$\alpha_{\phi\theta L} =$	0.8000	
Plasticity Reduction Factors (-1610)		
$\eta_{\phi} =$	0.0568	
$\eta_{\theta} =$	0.0850	
$\eta_{\phi\theta} =$	0.0232	
Theoretical Buckling Values (-1712.1.1)		
$C_{\phi} =$	0.6050	
$\sigma_{\phi eL} =$	1,831,806 psi	
$C_{\theta r} =$	0.1150	
$\sigma_{\theta eL} = \sigma_{reL} =$	348,340 psi	
$C_{\theta h} =$	0.1078	
$\sigma_{\theta eL} = \sigma_{heL} =$	326,534 psi	
$C_{\phi\theta} =$	0.2527	
$\sigma_{\phi\theta eL} =$	765,157 psi	
Elastic Interaction Equations (-1713.1.1)		
$\sigma_{xa} =$	208,750 psi	
$\sigma_{ha} =$	130,614 psi	
$\sigma_{ra} =$	139,336 psi	
$\sigma_{\tau a} =$	306,063 psi	
Axial + Shear \Rightarrow Check (c):	0.0114	<1 \therefore OK (see note*)
Hoop + Shear \Rightarrow Check (d):	0.0000	<1 \therefore OK
Inelastic Interaction Equations (-1714.2.1)		
$\sigma_{xc} =$	11,850 psi	
$\sigma_{rc} =$	11,850 psi	
$\sigma_{\tau c} =$	7,110 psi	
Max(Axial,Hoop) \Rightarrow Check (a):	0.2002	<1 \therefore OK
Axial + Shear \Rightarrow Check (b):	0.2002	<1 \therefore OK
Hoop + Shear \Rightarrow Check (c):	0.0000	<1 \therefore OK

*Note: Elastic interaction checks (a), (b), (e), and (f) are not applicable.

2.7 Hypothetical Accident Conditions

When subjected to the hypothetical accident conditions (HAC) as specified in 10 CFR §71.73 [1], the BRR package meets the performance requirements specified in Subpart E of 10 CFR 71. This is demonstrated in the following subsections, where each accident condition is addressed and the cask shown to meet the applicable design criteria. The method of demonstration is primarily by analysis. The loads specified in 10 CFR §71.73 are applied sequentially, per Regulatory Guide 7.8 [3]. Resulting stresses are maintained below the limits established by Regulatory Guide 7.6 [2]. Dynamic testing of impact limiter performance is discussed in Section 2.12.3, *Certification Test Results*. A summary of cumulative damage is provided in Section 2.7.8, *Summary of Damage*.

2.7.1 Free Drop

Subpart F of 10 CFR 71 requires that a 30 ft free drop be considered. The free drop is to occur onto a flat, essentially unyielding, horizontal surface, and the cask is to strike the surface in an orientation for which maximum damage is expected. Several impact orientations and bounding ambient environments are considered. In order to minimize the number of specific analyses that must be performed, the worst case maximum cold drop impact loads are conservatively applied to the cask using material properties and allowables corresponding to maximum (warm) Normal Conditions of Transport (NCT) temperatures.

2.7.1.1 Impact Forces and Deformations

In Section 2.1.2.2, *Other Structures*, the design criteria of the impact limiters of the BRR Package includes the requirement to limit the free drop impact such that cask component stress and deflection criteria are met. The impact and deformation response of the impact limiters is evaluated and discussed in Appendix 2.12.5, *Impact Limiter Performance Evaluation*. This appendix also includes a comparison of the analysis results to the results obtained from the half-scale certification testing of the impact limiters. The tests are described in Appendix 2.12.2, *Certification Test Plan*, and in Appendix 2.12.3, *Certification Test Results*. The analysis results contributed to informing the choice of physical test orientations. The half-scale test impacts (tests D1, D2R, and D3) were all lower than predicted. The maximum predicted impact in full-scale is 86.8g for the secondary impact in the 15° oblique slapdown orientation. All of the calculations in this section utilize a bounding HAC impact of 120g, which is nearly 40% higher than the maximum result obtained from either test or analysis. Although no NCT tests were performed, the same conservative prediction techniques were used to set the bounding NCT impact at 40g, as described in Appendix 2.12.5, *Impact Limiter Performance Evaluation*.

The second design criterion of the impact limiters is to prevent "hard" contact of a rigid part of the cask with the ground due to excessive deformation of the foam. Since all of the certification testing was performed at the cold condition in order to obtain the maximum impact, the maximum crush deformation, which occurs at the maximum NCT hot temperature, could not be obtained directly from the testing. However, as the crush distances obtained from the half-scale test were found to be below the predicted cold case values, it is conservative not to adjust the predicted hot case crush distances downward. The maximum predicted hot case crush distance

occurs in the 15° oblique secondary impact event, and amounts to 15.9 inches, or 83.2% of the available crush distance. Not only is the majority of the foam in the limiter at a lower value of strain than this maximum value, the value is well within the range in which strain energy absorption is effective. The bounding bulk average foam temperature used for the analysis of 150 °F conservatively bounds the temperature predicted in the thermal analysis.

The final requirement is that the impact limiter structures and attachments to the cask maintain sufficient integrity subsequent to the HAC free drop and puncture drop events so that the containment O-ring seal is protected from excessive temperature in the subsequent HAC fire event. As documented in Appendix 2.12.3, *Certification Test Results*, while the original design did not meet this requirement, the final design of the attachment structures did meet it, as demonstrated by half-scale test. Section 2.7.1.7, *Impact Limiter Attachments*, shows that the final design is stronger than the successfully tested design. In addition, the worst-case damage to the impact limiter shells as a result of the puncture tests is fully accounted for in the thermal model, as discussed in Chapter 3, *Thermal Evaluation*.

For these reasons, the performance of the impact limiters is considered acceptable.

2.7.1.2 End Drop

The HAC end orientation free drop is evaluated using a combination of computer and manual calculations using an acceleration of 120g as discussed in Section 2.7.1.1, *Impact Forces and Deformations*. Stresses in the cask body are evaluated using the finite element model described in Appendix 2.12.4, *Stress Analysis Finite Element Models*. Both bottom down and top down impact orientations are considered. Including manual calculations, eight analyses of the HAC end drop are performed:

- Cask body stress
- Closure bolt stress
- Closure lid stress
- Lower closure plate weld stress
- Shield plug shell stress
- Buckling evaluation
- Lead slump evaluation
- Fuel basket stress is discussed in Section 2.7.1.5, *Basket Stress Analysis*.

Cask body stress. From Section 2.12.4.4.5, *Case No. 5, HAC Bottom-down End Drop*, the maximum stress intensity resulting from the bottom-down impact of 120g is 45,681 psi, located at the outside surface of the bottom end structure, as shown in Figure 2.12.4-10. The stress is linearized through the lower massive end structure cross section, Figure 2.12.4-11, and the maximum primary membrane stress is 22,680 psi. From Table 2.1-1, the limit on primary membrane stress is the lesser of $2.4S_m$ and $0.7S_u$, which for Type 304 cast or forged material (see Table 2.2-2) is $0.7S_u = 44,835$ psi at 250 °F. The margin of safety is:

BRR Package Safety Analysis Report

$$MS = \frac{44,835}{22,680} - 1 = +0.98$$

The maximum membrane plus bending stress through the lower massive end structure cross section is 43,080 psi. The allowable membrane plus bending stress, from Table 2.1-1, is the lesser of $3.6S_m$ or S_u , which for Type 304 cast or forged material is $S_u = 64,050$ psi at 250 °F. The margin of safety is:

$$MS = \frac{64,050}{43,080} - 1 = +0.49$$

From Section 2.12.4.4.8, *Case No. 8, HAC Top-down End Drop*, the maximum stress intensity resulting from the bottom-down impact of 120g is 40,140 psi, located at the top of the inner shell, as shown in Figure 2.12.4-15. The stress is linearized through the inner shell cross section, Figure 2.12.4-16, and the maximum primary membrane stress is 22,720 psi. From Table 2.1-1, the limit on primary membrane stress is the lesser of $2.4S_m$ and $0.7S_u$, which for Type 304 cast or forged material (see Table 2.2-2) is $0.7S_u = 44,835$ psi at 250 °F. The margin of safety is:

$$MS = \frac{44,835}{22,720} - 1 = +0.97$$

The maximum membrane plus bending stress through the inner shell cross section is 33,400 psi. The allowable membrane plus bending stress, from Table 2.1-1, is the lesser of $3.6S_m$ or S_u , which for Type 304 cast or forged material is $S_u = 64,050$ psi at 250 °F. The margin of safety is:

$$MS = \frac{64,050}{33,400} - 1 = +0.92$$

As shown, all cask body margins of safety for the HAC end free drop condition are positive.

Closure bolt stress. In the top-down orientation, the non-prying closure bolt load is calculated according to Section 4.6 of [10] using:

$$F_a = \frac{1.34 \sin(\xi)(DLF)(a_i)(W_l + W_c)}{N_b} = 28,140 \text{ lb}$$

where the impact angle, $\xi = 90^\circ$ for the end drop impact, the dynamic load factor, $DLF = 1.05$ as discussed below, the impact magnitude, $a_i = 120g$ for the HAC impact, the weight of the lid, $W_l = 280$ lb, and the weight of the contents, $W_c = 1,720$ lb¹ from Table 2.1-2, and the quantity of bolts, $N_b = 12$. Note that no support for the lid is assumed from the inner surface of the impact limiter.

The sum of all applied loads (the HAC free drop load of 28,140 lb plus the load due to the design pressure, equal to 789 lb as determined in Section 2.6.1.5, *Closure Bolts*) is equal to $28,140 + 789 = 28,929$ lb. This value exceeds the preload of 19,200 lb. The average tensile stress is:

$$S_{ba} = 1.2732 \frac{F_a}{D_{ba}^2} = 47,779 \text{ psi}$$

¹ This weight consists of the shield plug plus the heaviest basket/fuel combination.

BRR Package Safety Analysis Report

where the value of D_{ba} was computed as 0.878 inches in Section 2.6.1.5, *Closure Bolts*. From Table 2.1-1, the allowable average tensile stress intensity for HAC is the lesser of $0.7S_u$ or S_y , which for the ASTM A320 L43 bolting material is $0.7S_u = 87,500$ psi at 250 °F. The margin of safety is:

$$MS = \frac{87,500}{47,779} - 1 = +0.83$$

The dynamic load factor (DLF) used in this section and in Section 2.6.7.1, *NCT End Free Drop*, is calculated using NUREG/CR-3966 [26] (this quantity is called the DAF in that document). In Section 2.2.3 of [26], an estimated impact pulse duration is developed assuming a constant impact acceleration:

$$t_1 = \frac{Mv_o}{F_{\max}}$$

This equation, however, underestimates the duration of a varying pulse such as a sinusoidal pulse, which is the closest shape to an actual, measured pulse. For a sinusoidal pulse, from Newton's Second Law:

$$F = Ma = MA \sin \omega t$$

The area under the pulse is the total change in velocity. Since the impact velocity is v_o , and the package comes to a complete stop during impact, the change in velocity is simply v_o . This can be written:

$$v_o = A \int_0^{\pi} \sin \omega t dt = -\frac{A}{\omega} \cos \omega t \Big|_0^{\pi} = \frac{2A}{\omega}$$

From this,

$$\omega = \frac{2A}{v_o}$$

Since the pseudo-frequency of the pulse is a full sine wave (two pulse lengths), the pulse length is equal to:

$$t_1 = \frac{T_1}{2} = \frac{1/f}{2} = \frac{2\pi/\omega}{2} = \frac{\pi}{\omega}$$

Substituting from above,

$$t_{1-HAC} = \frac{\pi v_o}{2A} = \frac{828.6}{A}$$

where v_o is the impact speed for a 30-foot free drop of 527.5 in/s. Parameter A is the acceleration, in/s². For the bounding impact acceleration of 120g, equivalent to $A = 46,368$ in/s², the pulse length of the sinusoidal impact time history is $t_{1-HAC} = 0.018$ s, which compares well with the duration of the end drop impact pulse accelerometer traces shown in Section 2.12.3.7, *Accelerometer Plots*.

For the NCT impact, the impact velocity for the two foot free drop is 136.2 in/s, and the bounding impact is 40g. The corresponding impact pulse length is:

$$t_{1-NCT} = \frac{\pi v_o}{2A} = 0.014 \text{ s}$$

BRR Package Safety Analysis Report

The frequency of the closure lid is found using [25], Table 36, Case 11a. The lowest mode frequency for a flat circular plate, assuming a simply supported edge, is found from:

$$f = \frac{K_n}{2\pi} \sqrt{\frac{Dg}{wr^4}} = 650 \text{ Hz}$$

where $K_1 = 4.99$, $g = 386.4 \text{ in/s}^2$, and the lid bolt radius, $r = 11.38$ inches. Since from Table 2.1-2, the weight of the lid, $W = 280 \text{ lb}$ and the area, $A_{\text{lid}} = \pi r^2 = 406.9 \text{ in}^2$, the weight per unit area, $w = W/A_{\text{lid}} = 0.688 \text{ psi}$. Parameter D is found from:

$$D = \frac{Et^3}{12(1-\nu^2)} = 20.0(10^6) \text{ in-lb}$$

where $E = 27.3(10^6) \text{ psi}$ for Type 304 steel at 250 °F, $\nu = 0.3$, and the thickness, $t = 2.0$ inches. The period of the lid is equal to $1/f$, or $T = 1/650 = 0.00154 \text{ s}$. The amplification factor for a half sine wave is given in Figure 2-15 of [26]. The abscissa of the figure is the ratio t_1/T . The smallest value of the ratio occurs in the NCT impact, where $t_{1\text{-NCT}} = 0.014 \text{ s}$:

$$\frac{t_{1\text{-NCT}}}{T} = 9.09$$

This value exceeds the range shown in the figure. The corresponding ratio for HAC, where t_1 equals 0.018 s, is even larger. As the curve is clearly tending toward unity, it is concluded that the DLF may be conservatively bounded by a value of 1.05 for both NCT and HAC.

Closure lid stress. In the top-down drop orientation, the closure lid supports both the contents weight and its self-weight against the impact load of 120g. The lid is a solid, 2-inch thick plate made of Type 304 stainless steel. The outer diameter of the lid will be taken as the bolt circle, since that is the location of the step (see Section 2.6.1.5, *Closure Bolts*, for a discussion of the lid step). The bolt circle diameter is 22.75 inches. The self-weight of the lid is 280 lb, and the maximum contents weight is 1,720 lb (including the shield plug and the maximum basket/fuel weight), from Table 2.1-2. The total weight is $1,720 + 280 = 2,000 \text{ lb}$. For an impact of 120g, the total force applied to the lid is $2,000 \times 120 = 240,000 \text{ lb}$. From above, the area of the lid, $A_{\text{lid}} = 406.9 \text{ in}^2$.

The lid will be considered as uniformly loaded. This is somewhat conservative, since the shield plug is very stiff, and will consequently shift some of the load toward the edges of the lid, lessening the bending stress. In addition, the internal design pressure is 25 psig. The uniform load is:

$$q = \frac{240,000}{A_{\text{lid}}} + 25 = 614.8 \text{ psi}$$

From [25], Table 24, Case 10a for a simply supported, uniformly loaded plate, the bending moment is:

$$M = \frac{qa^2(3+\nu)}{16} \text{DLF} = 17,243 \text{ in-lb/in}$$

where the radius, $a = 22.75/2 = 11.38$ inches, $\nu = 0.3$, and the dynamic load factor, $\text{DLF} = 1.05$ as discussed above. The stress is:

BRR Package Safety Analysis Report

$$\sigma = \frac{6M}{t^2} = 25,865 \text{ psi}$$

where the plate thickness, $t = 2.0$ inches. The allowable membrane plus bending stress, from Table 2.1-1, is the lesser of $3.6S_m$ or S_u , which, from Table 2.2-1, is equal to 68,600 psi for ASTM A240, Type 304 at 250 °F. The margin of safety is:

$$MS = \frac{68,600}{25,865} - 1 = +1.65$$

Thus, the allowable stress is satisfied for the closure lid in the HAC end drop.

As noted in Section 2.1.2.1, *Containment and Criticality Control Structures*, a stress intensity in the cask closure region (such as the closure lid) which could affect compression of the containment O-ring seal is limited to the lesser of the Table 2.1-1 allowable, or the yield strength. For ASTM A240, Type 304 at 250 °F, the yield strength from Table 2.6-1 is 23,700 psi. The calculated value of stress exceeds the yield stress by approximately 5%. However, as noted above, the calculation is conservative, and the impact magnitude of 120g is very conservative. As found in Table 2.12.5-11, the actual calculated end drop impact is 74.4g, which bounds an even lower actual impact recorded in the certification testing. Therefore it is evident that the actual stress in the closure lid is well below the yield stress of the lid material.

Lower closure plate weld stress. In the bottom-down drop orientation, the lower closure plate supports both the lower lead shield hydrostatic pressure and its self-weight against the impact load of 120g. The closure plate is a solid, 1-inch thick plate made of Type 304 stainless steel. The outer diameter of the plate is $d = 24.5$ inches and connected by a full penetration weld to the adjacent massive end structure. The area of the closure plate is:

$$A_{cp} = \frac{\pi}{4} d^2 = 471.4 \text{ in}^2$$

The self-weight of the closure plate is:

$$W_{cp} = A_{cp} \rho_{ss} = 136.7 \text{ lb}$$

where the density of steel is $\rho_{ss} = 0.29 \text{ lb/in}^3$. The weight of the lower lead is modeled as two separate hydrostatic loads based the inner and outer lead depths above the upper surface of the closure plate (see Section 2.12.4.2.2, *Free Drop Impact Loads*). The maximum hydrostatic pressure will be conservatively applied to the entire plate. The hydrostatic force is:

$$F = \rho \cdot h \cdot A_{cp} = 1,488.2 \text{ lb}$$

where the maximum depth of the lead column, $h = 7.7$ inches and the density of lead is 0.41. The total weight is $1,488.2 \text{ lb} + 136.7 \text{ lb} = 1,624.9 \text{ lb}$. For an impact of 120g, the total force applied to the closure plate is $1,624.9 \times 120 = 194,988 \text{ lb}$.

Conservatively the closure plate will be considered as uniformly loaded. The uniform load is:

$$q = \frac{194,988}{A_{cp}} = 413.6 \text{ psi}$$

From [25], Table 24, Case 10b for a fixed edge, uniformly loaded plate, the maximum bending moment at the edge of the plate is:

BRR Package Safety Analysis Report

$$M = \frac{qa^2}{8} DLF = 8,146 \text{ in-lb/in}$$

where the radius, $a = 24.5/2 = 12.25$ inches and the dynamic load factor, $DLF = 1.05$ as discussed above. The stress is:

$$\sigma = \frac{6M}{t^2} = 48,876 \text{ psi}$$

where the plate thickness, $t = 1.0$ inches. The shear stress at the fixed end of the closure plate is:

$$\tau = \frac{194,988}{24.5\pi t} DLF = 2,660 \text{ psi}$$

The maximum stress intensity is determined by combining the component stresses using Mohr's circle as follows:

$$SI = \sqrt{\sigma^2 + 4\tau^2} = 49,165 \text{ psi}$$

The allowable membrane plus bending stress found above is equal to 68,600 psi for ASTM A240, Type 304 at 250 °F. The margin of safety is:

$$MS = \frac{68,600}{49,165} - 1 = +0.40$$

Thus, the allowable stress is satisfied for the closure plate in the HAC end drop.

Shield plug shell stress. In a bottom-down end drop, the shield plug lead will be supported by the lower plate of the shield plug shell. The one-inch thick plate is 15.8 inches in diameter and connected by a complete joint penetration weld to the adjacent cylindrical shell. The weight of the lead in the shield plug, plus the self-weight of the lower steel plate, will be conservatively bounded by utilizing the weight of the full shield plug, from Table 2.1-2, of 950 lb. To simplify the calculation, the lead will be treated very conservatively as a liquid. The entire weight of 950 lb will therefore be applied as a pressure to the plate inner surface.

The area of the plate is:

$$A_p = \frac{\pi}{4} 15.8^2 = 196.1 \text{ in}^2$$

For the end drop impact of 120g, the total loading per unit area of the plate is:

$$q = \frac{950 \times 120}{A_p} = 581.3 \text{ psi}$$

It will be further conservatively assumed that the plate has a simply supported edge. From [25], Table 24, Case 10a, the maximum moment at the center of the plate is:

$$M_c = \frac{qa^2(3+\nu)}{16} DLF = 7,856.7 \text{ in-lb/in}$$

where the plate radius, $a = 15.8/2 = 7.9$ inches and the DLF is defined as equal to 1.05 above. The maximum stress is:

BRR Package Safety Analysis Report

$$\sigma_c = \frac{6M_c}{t^2} = 47,140 \text{ psi}$$

where the thickness, $t = 1$ inch. The allowable membrane plus bending stress found above is equal to 68,600 psi for ASTM A240, Type 304 at 250 °F. The margin of safety is:

$$MS = \frac{68,600}{47,140} - 1 = +0.46$$

The side wall and weld are checked by establishing moment equilibrium between the bottom plate and cylindrical shell, solving for the common moment, and calculating the stress. The direct tension stress is also added.

The slope at the outer edge of the bottom plate is the sum of the slope of a simply supported plate with a pressure load q , and the slope from a restoring moment, M_o , applied in the opposite direction by the cylindrical shell. The pressure load causes the plate to deflect downward, and the moment causes it to deflect upward. The slope due to the pressure load, θ_d (see [25], Table 24, Case 10a) is:

$$\theta_d = \frac{qa^3}{8D_p(1+\nu)}$$

The slope due to the moment load (see [25], Table 24, Case 13a, for $r_o = a$) is:

$$\theta_m = K_\theta \frac{M_o a}{D_p}$$

The parameter D_p is:

$$D_p = \frac{Et_p^3}{12(1-\nu^2)} = 2.5(10^6) \text{ in-lb}$$

where $E = 27.3(10^6)$ psi, $\nu = 0.3$, and the plate thickness, $t_p = 1.0$ inches. The sum of these two slopes is:

$$\theta_d + \theta_m = 0.0098 - 2.338(10^{-6})M_o$$

where the lead hydrostatic pressure, $q = 581.3$ psi, the radius to the meridian of the cylindrical shell, $a = 7.6$ inches, and $K_\theta = -0.76923$.

The corresponding slope of a cylindrical shell under the action of an end moment is found from [25], Table 29, Case 3, as:

$$\theta_w = \frac{M_o}{D_w \lambda} \frac{C_{12}}{C_{11}}$$

Note that the notation for the slope has substituted θ for ψ for consistency. In addition, the sign value of the slope has been redefined to be opposite to that given in the introduction to Table 29 [25], thus, the negative sign has been omitted from the equation. The parameter λ is:

$$\lambda = \left[\frac{3(1-\nu^2)}{R^2 t_w^2} \right]^{1/4} = 0.602$$

BRR Package Safety Analysis Report

where $R = a = 7.6$ inches, and the thickness of the cylindrical wall, $t_w = 0.6$ inches. The parameter D_w is:

$$D_w = \frac{Et_w^3}{12(1-\nu^2)} = 5.4(10^5) \text{ in-lb}$$

Since the length of the lower cylindrical shell is $L = 5$ inches, the parameter λL is 3.01 inches. Parameters C_{12} and C_{11} are essentially identical, so their ratio is unity. The slope of the shell can now be evaluated as:

$$\theta_w = \frac{M_o}{D_w \lambda} \frac{C_{12}}{C_{11}} = 3.076(10^{-6}) M_o$$

Setting $\theta_w = \theta_d + \theta_m$,

$$3.076(10^{-6}) M_o = 0.0098 - 2.338(10^{-6}) M_o$$

Solving, $M_o = 1,810.1$ in-lb/in. The stress in the cylindrical shell is:

$$\sigma_m = \frac{6M_o}{t_w^2} \text{ DLF} = 31,677 \text{ psi}$$

To this stress, the direct tension stress is added. The area of the weld to the cylindrical shell is:

$$A_s = \frac{\pi}{4} (OD^2 - ID^2) = 28.65 \text{ in}^2$$

where the shell outer diameter, $OD = 15.8$ inches and the inner diameter, $ID = 14.6$ inches. The direct stress is therefore:

$$\sigma_D = \frac{950 \times 120}{A_s} \text{ DLF} = 4,178 \text{ psi}$$

The stress sum in the weld is:

$$\sigma_{\text{Sum}} = \sigma_m + \sigma_D = 35,855 \text{ psi}$$

For a full penetration weld, the allowable stress is the same as determined above. The margin of safety is:

$$MS = \frac{68,600}{35,855} - 1 = +0.91$$

Thus, the allowable stress is satisfied for the shield plug lower plate stress and lower plate weld stress in the HAC end drop.

Buckling evaluation. In the end drop orientation, the outer shell will carry most of the axial loads due to its much greater stiffness compared to the inner shell. Therefore, end drop buckling analysis may be conservatively performed by considering only the outer shell. The outer shell, which is cooler than the inner shell, is subject to tensile thermal stress, but for the buckling evaluation, the thermal stress on the outer shell is conservatively neglected. Since the inner shell is neglected, lead shrinkage pressure, which only affects the inner shell, is not considered. The maximum cold HAC impact of 120g is conservatively applied along with the bounding hot temperature case of 250 °F.

The only applied stress is axial, and assumes a bottom-down end drop configuration, for which the weight supported by the outer shell is larger than for the top-down case. The total weight

BRR Package Safety Analysis Report

supported by the outer shell is the sum of the total cask body (25,400 lb), less the side lead and bottom lead (see below), the closure lid (280 lb), the shield plug (950 lb), and the upper impact limiter (2,300 lb). Weight values are taken from Table 2.1-2.

The weights for the side and bottom lead are calculated using a lead density of 0.41 lb/in³. The side lead has an outer diameter of 34.0 inches (outer shell ID), an inner diameter of 18.0 inches (inner shell OD), and a lower-bound length (cylindrical length only) of 55.0 inches. The conservatively underestimated weight of the side lead is:

$$W_{\text{pbs}} = \frac{\pi}{4} (34.0^2 - 18.0^2) (55.0) (0.41) = 14,735 \text{ lb}$$

The bottom lead has a large diameter of 23.7 inches and a length of 4.2 inches, and a small diameter of 10.3 inches and a length of 3.5 inches. The weight of the bottom lead is:

$$W_{\text{pbb}} = \frac{\pi}{4} [(23.7^2) (4.2) + (10.3^2) (3.5)] (0.41) = 879 \text{ lb}$$

Conservatively, the bottom lead weight will be underestimated by 100 lb, so that $W_{\text{pbb}} = 779 \text{ lb}$. The total weight supported by the outer shell is therefore:

$$W_{\text{tot}} = 25,400 - 14,735 - 779 + 280 + 950 + 2,300 = 13,416 \text{ lb}$$

The weight used is conservative, since it underestimates the removed weight of the side lead and bottom lead, and includes the lower end structure as part of the cask body weight, even though it is not supported by the outer shell. The cross sectional area of the outer shell is:

$$A_{\text{OS}} = \frac{\pi}{4} (38.0^2 - 34.0^2) = 226.2 \text{ in}^2$$

The axial stress is:

$$\sigma_{\phi} = \frac{W_{\text{tot}}}{A_{\text{OS}}} (120) = 7,117 \text{ psi}$$

No other stresses are applied in the end drop. Shell dimensions are taken from Table 2.7-1. The factor of safety is equal to 1.34, consistent with Code Case N-284-2 for HAC. The results are shown in Table 2.7-2. As shown, all interaction parameters, including the maximum value of 0.4024 are less than unity, as required. Therefore, buckling of the cask shells in the HAC free drop will not occur.

Lead Slump. In the end drop, impact forces act on the lead gamma shield which could cause a reconfiguration of the lead in the direction of impact. As shown in the evaluation of the cask body stress above, the steel shells which enclose the lead will not significantly deform, but the lead could experience flow strains causing a gap to appear at the upper surface of the lead. In the following analysis, the lead is conservatively treated as a fluid, having no resistance to flow from impact forces. The lead will therefore occupy the lower portion of the volume available within the lead cavity. The difference between the cavity volume and the lead volume defines the maximum possible gap at the top of the lead. Of note, since the shield plug and bottom lead shield are installed manually, using small scraps and lead wool hammered into place to fill all cavities, lead slump cannot occur. The following analysis applies only to the side cavity in which lead is poured in the molten state.

BRR Package Safety Analysis Report

The amount of lead installed in the side cavity of the BRR cask body is assumed to correspond to the volume of the cavity at the point of solidification of the lead of 620 °F. At this point, there is no difference between the volume of the cavity and the volume of the lead. As the cask cools to the minimum HAC temperature of -20 °F, the lead will shrink more than the cavity due to the greater thermal expansion coefficient of lead than steel, generating a volume difference. Assuming the lead behaves as a fluid in the end drop concentrates this volume difference at one end or the other of the cask cavity, which constitutes the lead slump gap. This gap is further evaluated in Chapter 5, *Shielding Evaluation*.

To simplify calculations, the side lead shield is assumed to have a fully rectangular cross section, i.e., the lead cavity is assumed to have square corners at the full length. This simplification does not have a significant affect on the calculation. The lead cavity at the assumed fabrication temperature of 70 °F has an inner diameter of 18 inches (the inner shell OD), an outer diameter of 34 inches (the outer shell ID), and a length of 60.9 inches. The volume therefore is:

$$V_{\text{CAV-RT}} = \frac{\pi}{4}(34^2 - 18^2)60.9 = 39,795 \text{ in}^3$$

It will be convenient to define a volumetric expansion relation. Note that, for a general case:

$$V_C = L_C^3$$

$$L_H = L_C(1 + \alpha\Delta T)$$

where V_C and L_C are the original (cold state) volume and length, respectively, L_H is the expanded (hot) length, and α and ΔT are the thermal expansion coefficient and the change in temperature, respectively. Since the expanded (hot) volume is:

$$V_H = L_H^3 = L_C^3(1 + \alpha\Delta T)^3,$$

Then:

$$V_H = V_C(1 + \alpha\Delta T)^3$$

From Table 2.2-4, the thermal expansion coefficient of steel between 70 °F and 620 °F is $\alpha_{s620} = 9.84(10^{-6})\text{in/in/}^\circ\text{F}$. The lead cavity and lead volumes at the lead solidification temperature are then:

$$V_{\text{CAV620}} = V_{\text{L620}} = V_{\text{CAV-RT}}(1 + \alpha_{s620}\Delta T_{70-620})^3 = 40,445 \text{ in}^3$$

Next, calculate the volume of the lead at 70 °F and at -20 °F. This must be done in two steps because the thermal expansion coefficients are referenced to 70 °F. The thermal expansion of lead between 620 °F and 70 °F is $\alpha_{L620} = 20.4(10^{-6})\text{in/in/}^\circ\text{F}$, and between 70 °F and -20 °F is $\alpha_{L-20} = 15.7(10^{-6})\text{in/in/}^\circ\text{F}$, as shown in Table 2.2-4.

$$V_{\text{L-RT}} = V_{\text{L620}}(1 - \alpha_{L620}\Delta T_{620-70})^3 = 39,099 \text{ in}^3$$

$$V_{\text{L-20}} = V_{\text{L-RT}}(1 - \alpha_{L-20}\Delta T_{70--20})^3 = 38,933 \text{ in}^3$$

The volume of the cavity at -20 °F, utilizing the thermal expansion coefficient between 70 °F and -20 °F of $\alpha_{s-20} = 8.2(10^{-6})\text{in/in/}^\circ\text{F}$, is:

$$V_{\text{CAV-20}} = V_{\text{CAV-RT}} (1 - \alpha_{s-20} \Delta T_{70--20})^3 = 39,707 \text{ in}^3$$

The difference in volume between the cavity and the lead at the HAC free drop temperature of -20 °F is:

$$\Delta V_{-20} = V_{\text{CAV-20}} - V_{\text{L-20}} = 774 \text{ in}^3$$

The volume of the cavity per inch of length is:

$$\Delta V_{/\text{in}} = \frac{\pi}{4} (34^2 - 18^2) = 653 \text{ in}^3 / \text{in}$$

The lead slump dimension (the gap between the top of the lead cavity and the top of the lead) therefore has a bounding value of:

$$x_{\text{slump}} = \frac{\Delta V_{-20}}{\Delta V_{/\text{in}}} = 1.185 \text{ in}$$

This value is conservative since it takes no credit for any resistance to flow of the lead material. The effect of this gap is evaluated in Chapter 5, *Shielding Evaluation*.

2.7.1.3 Side Drop

The HAC side orientation free drop is evaluated using the finite element model described in Appendix 2.12.4, *Stress Analysis Finite Element Models*, and an acceleration of 120g as discussed in Section 2.7.1.1, *Impact Forces and Deformations*.

From Section 2.12.4.4.11, *Case No. 11, HAC Side Drop*, the maximum stress intensity resulting from the side drop impact of 120g is located at the bottom outside edge of the lower lead cavity as shown in Figure 2.12.4-21. The stress is linearized through the lower closure plate cross section, Figure 2.12.4-22, and the maximum primary membrane stress is 16,330 psi. From Table 2.1-1, the limit on primary membrane stress is the lesser of $2.4S_m$ and $0.7S_u$, which for Type 304 cast or forged material is $0.7S_u = 44,835$ psi at 250 °F. The margin of safety is:

$$MS = \frac{44,835}{16,330} - 1 = +1.75$$

The maximum membrane plus bending stress resulting through the lower closure plate cross section is 51,990 psi. The allowable membrane plus bending stress, from Table 2.1-1, is the lesser of $3.6S_m$ or S_u , which for Type 304 cast or forged material is $S_u = 64,050$ psi at 250 °F. The margin of safety is:

$$MS = \frac{64,050}{51,990} - 1 = +0.23$$

As shown, all cask body margins of safety for the HAC side drop condition are positive.

2.7.1.4 Oblique Drop

For the HAC free drop, the BRR package can strike the ground in any primary orientation. As shown in the following discussion, the cask stresses for all oblique drop orientations are conservatively bounded by the side drop (horizontal) orientation when performed using an impact of 120g. This evaluation is based on the axial, shear, and moment forces in the cask

BRR Package Safety Analysis Report

shells as derived in NUREG/CR-3966 [26]. It is shown that, for the specific impact forces developed in the HAC oblique free drops, the cask shell stress intensity is governed by the side drop case.

In Section 2.2 of [26], the maximum axial force, R, shear force, V, and bending moment, M, in the cask shells are given for the primary oblique impact as:

$$\begin{aligned} R_p &= F_p \sin(\theta) \\ V_p &= F_p \cos(\theta) \\ M_p &= (4/27) F_p L \cos(\theta) \end{aligned}$$

where the subscript p indicates the primary impact event, L is the overall length of the cask, θ is the primary impact angle with respect to the horizontal, and F_p is the maximum primary impact limiter force. For the subsequent secondary (slapdown) impact, the maximum values of the above parameters are:

$$\begin{aligned} R_s &= 0 \\ V_s &= F_s \\ M_s &= (4/27) F_s L \end{aligned}$$

where the subscript s indicates the secondary impact event, and F_s is the maximum secondary impact limiter force. In the horizontal side drop impact, the maximum values of the above parameters are:

$$\begin{aligned} R_h &= 0 \\ V_h &= F_h \\ M_h &= (1/4) F_h L \end{aligned}$$

where the subscript h indicates the horizontal case, and F_h is the maximum impact limiter force in the side drop. The cask shell stresses resulting from these applied forces and moments can be calculated as follows:

$$\begin{aligned} \sigma_a &= \frac{R_i}{A} \\ \tau &= \frac{V_i}{A} \\ \sigma_b &= \frac{M_i c}{I} \end{aligned}$$

where σ_a is the axial stress, τ the shear stress, and σ_b the bending stress in the cask shells, and where A is the cross sectional area of the cask shells, and I is the moment of inertia. The maximum stress intensity in the cask shells is determined by combining the component stresses using Mohr's circle as follows:

$$SI = \frac{\sigma_a + \sigma_b}{2} \pm \sqrt{\left(\frac{\sigma_a + \sigma_b}{2}\right)^2 + \tau^2}$$

For purposes of comparison, it is only necessary to consider one shell, for example, the inner shell. The cross sectional area of the inner shell is

$$A = (\pi/4)(d_o^2 - d_i^2) = 53.4 \text{ in}^2$$

and the moment of inertia is

$$I = (\pi/64)(d_o^4 - d_i^4) = 1,936 \text{ in}^4$$

where $d_o = 18.0$ inches and $d_i = 16.0$ inches. The parameter $c = 18.0/2 = 9.0$ inches, and the length between the center of the cylindrical portion of each impact limiter is $L = 70$ inches.

The maximum force on each impact limiter in the HAC 30 ft, horizontal side drop for the bounding impact value of $g_h = 120g$ and an overall cask weight of $W = 32,000$ lb is:

$$F_h = \frac{Wg_h}{2} = 1.920(10^6) \text{ lb}$$

The worst case oblique free drop is the shallow-angle side slapdown orientation at a primary impact angle of 15° , as discussed in Appendix 2.12.5, *Impact Limiter Performance Evaluation*. The primary and secondary impact limiter forces are found using the calculated maximum deformation at cold conditions and the force-deflection curves corresponding to the impact orientation. From Table 2.12.5-11, the maximum primary deformation for the 15° impact case is 10.7 inches, and from Table 2.12.5-12, the maximum secondary deformation is 12.1 inches. From Figure 2.12.5-4 (primary impact at 15°), the maximum crush force at the primary deformation of 10.7 inches is bounded by a value of 1,049,000 lb, and from Figure 2.12.5-3 (secondary impact, taken at 0°), the maximum crush force at the secondary deformation of 12.1 inches is bounded by a value of 1,220,000 lb.

The resulting cask shell forces and maximum combined stress intensities are shown in Table 2.7-3. Since only the inner shell properties are used, the stress intensity is relative, and is used for comparison between the different cases only. The stress values in the table therefore do not represent actual inner shell stress intensity. As shown, the stress intensity is greatest in the horizontal side drop case at the bounding value of $120g$. Since, according to Section 2.7.1.1, *Impact Forces and Deformations*, the actual impacts are lower than the calculated values, the difference between the actual loading in the oblique impacts and the bounding side drop is even greater. Therefore, the side drop stress analyses, detailed in Section 2.7.1.3, *Side Drop*, are enveloping for all oblique drop orientations.

2.7.1.5 Fuel Basket Stress Analysis

Each of the four fuel baskets is evaluated for structural integrity in the governing free drop orientations of end and side. The maximum cold impact acceleration of $120g$ is used, but conservatively the material allowable stresses are evaluated at the maximum NCT temperature of 400°F . Allowable stresses are taken from Table 2.1-1. Each basket is analyzed for several modes of failure which are applicable to its design, including bending, weld shear, and buckling. Bounding weights for the baskets and fuel are given in Table 2.1-3.

The smallest margin of safety of any of these evaluations is $+0.12$, for the shear load on the TRIGA basket spacer pedestal screw. All of the evaluations and corresponding margins of safety are summarized in Table 2.7-4. The analysis details are provided in Appendix 2.12.8, *Fuel Basket Stress Analysis*. Therefore, the BRR package fuel baskets are adequate to support the fuel in all HAC free drops.

In the HAC side drop impact orientation, the fuel baskets apply a load to the inside of the inner shell. The heaviest basket is for MURR fuel, but this basket has no ribs and the load is well distributed. The next-heaviest basket, for ATR fuel (650 lb), has four ribs. The top rib is a 0.5-inch thick plate with a 0.19-inch chamfer, for a land width of 0.31 inches. The middle two ribs are made from 0.38-inch thick plate with 0.19-inch chamfers, for a land width of 0.19 inches each. The lowest rib is made from 0.50-inch thick plate with a 0.13-inch step and a 0.19-inch chamfer, for a land width of 0.18 inches. The diameter of each rib is 15.63 inches. The projected bearing area of the ribs against the inner shell is:

$$A = 15.63(0.31 + 0.19 + 0.19 + 0.18) = 13.60 \text{ in}^2$$

The side load, using the bounding side drop impact of 120g, is:

$$P = 650(120) = 78,000 \text{ lb}$$

The bearing stress is:

$$\sigma = \frac{P}{A} = 5,735 \text{ psi}$$

The other two baskets, the MITR-II and the TRIGA, are considerably lighter and not bounding. At the bounding fuel basket temperature of 400 °F, the minimum yield strength of the inner shell material, from Table 2.2-2, is 20,700 psi. Since this stress is over three times larger than the bearing stress, bearing yield of the basket ribs or of the inner shell will not occur.

2.7.1.6 Fuel Impact Deformation

During the end drop, the fuel elements may experience a separate, internal impact with the cask or basket structures. This impact could occur if, during the period of package free fall, the fuel was in contact with the upper end of its cavity, which would be possible due to the zero-g environment of free fall. When the package strikes the ground, the velocity of the cask would begin to decrease, but the fuel would continue to fall freely until impact with the lower end occurred. When the gap between the fuel and the cask was traversed, the fuel would hit the cavity end. The fuel would have the full free drop velocity, v_o , but the cask cavity would be traveling in the same direction with a lower velocity. See Figure 2.7-1.

To simplify calculations, it will be conservatively assumed that, at the moment of impact with the fuel, the cask inner contact surface is motionless and unyielding. Further, it will be assumed that the deceleration of the package during the period of fuel traversing the gap is constant and equal to the maximum bounding deceleration of 120g. The fuel will therefore experience an equivalent free drop. This analysis will determine the magnitude of the free drop impact and determine the effect on the fuel elements.

At the moment of impact with the ground, both the cask and fuel have a velocity of v_o . The cask immediately begins to decelerate according to:

$$v(t) = at + v_o$$

The distance the cask travels until the moment of impact with the fuel is:

$$x_c = a \int_0^T t dt = \frac{1}{2} at^2 + v_0 t \Big|_0^T = \frac{1}{2} aT^2 + v_0 T$$

where T is the time of fuel impact, and $x_c = 0$ at $t = 0$ (the time of package impact). Note that during time T, the fuel has traveled the distance the cask has traveled, plus the initial gap between the fuel and cask. Alternately, it can be stated that the fuel has traveled $v_0 T$, since its velocity is unchanged during this interval. Therefore:

$$x_c + \text{GAP} = v_0 T, \quad \text{or}$$

$$x_c = v_0 T - \text{GAP}$$

Substituting this into the formula for x_c above,

$$x_c = \frac{1}{2} aT^2 + v_0 T = v_0 T - \text{GAP}$$

Simplifying,

$$T = \left(\frac{-2\text{GAP}}{a} \right)^{1/2}$$

Since the difference in velocity between the fuel and the cask at time T is equal to the decay in velocity over the interval, equal to (aT) , the difference can be written as:

$$\Delta v = aT = a \left(\frac{-2\text{GAP}}{a} \right)^{1/2} = (-2a\text{GAP})^{1/2}$$

(Note that since the acceleration is negative (deceleration), the quantity under the square root will be positive.) The energy associated with a change in velocity, Δv , is equivalent to the energy of a free drop height, h. Since:

$$h = \frac{\Delta v^2}{2g_g}$$

then the equivalent free drop height of the fuel element in the BRR package impact is:

$$h = \bar{g}\text{GAP}$$

where g_g is the acceleration due to gravity, and the deceleration in g-units, $\bar{g} = a/g_g = 120g$. The energy to be dissipated during the impact of the fuel is equal to Wh, or:

$$E = W\bar{g}\text{GAP}$$

where W is the weight of a fuel element. If this energy is absorbed in the fuel structure by volumetric plastic flow, the energy absorbed is related to the volume of flow according to:

$$E = V\sigma_f$$

where σ_f is the flow stress of the material, equal to the average of the yield and ultimate tensile strengths. Solving this for the volume,

$$V = \frac{W\bar{g}\text{GAP}}{\sigma_f}$$

Since the material flow is assumed to occur on the fuel cross section, the deformation length is equal to the volume divided by the cross-sectional area of the fuel element, $L = V/A_{xc}$, or:

$$L = \frac{W\bar{g}GAP}{\sigma_f A_{xc}}$$

This formula will be evaluated for the bounding fuel case. The fuel is made from 6061-T6 aluminum material. From the ASME B&PV Code, Section II, Part D, Table Y-1, the yield strength at a temperature of 400 °F is equal to 13.3 ksi. Since this material does not appear in Table U, an ultimate tensile strength at temperature is not readily available. Conservatively, the yield strength will be used for the flow strength as defined above. Therefore, $\sigma_f = 13,300$ psi.

The total gap value, GAP, consists of a) the free space between the fuel element and the basket cavity length, plus b) the difference between the cask cavity and the basket length. Parameter a), denoted as L_{FB} , is calculated by subtracting the fuel length from the basket cavity length, and is listed in Table 2.7-5. Parameter b) is found by subtracting the basket length (equal to 53.45 inches in all cases) from the cask cavity length of 54.0 inches, and is equal to 0.55 inches. The total fuel gap is therefore:

$$GAP = L_{FB} + 0.55$$

Due primarily to its larger gap and weight, the ATR fuel is the governing case. The maximum deformation length of any fuel element is therefore:

$$L = \left(\frac{W}{A_{xc}} \right) \frac{\bar{g}GAP}{\sigma_f} = 0.096 \text{ inches}$$

The fuel bounding weights, cross-sectional areas, and W/A_{xc} ratios are presented in Table 2.7-5. The bounding fuel weights are taken from Table 2.1-3. The areas are calculated from CAD drawings of the fuel active region cross section, and do not consider the end structures. The end structures are considered sacrificial since a) they do not contain any fissile material and b) the criticality analysis discussed in Section 6.3.1 does not model the end structures, and determines the most reactive axial position of the active length of the fuel as if the end structures were absent. Since the fuel end structures do not serve a safety function, they are ignored in the axial deformation analysis.

This maximum deformation length, which is just below $1/10^{\text{th}}$ of an inch, is negligible from a structural, shielding, or criticality perspective. Therefore fuel behavior in the HAC end drop is acceptable.

2.7.1.7 Impact Limiter Attachments

As reported in Appendix 2.12.3, *Certification Test Results*, the initial design of the impact limiter attachments was not adequate, since they did not securely retain the primary impact limiter in the 15° oblique slapdown free drop impact. The redesigned attachments are shown in the drawings in Appendix 1.3.3, *Packaging General Arrangement Drawings*. One half-scale certification test limiter was refurbished, as far as possible, to incorporate the revised design and retested to confirm its adequacy. The attachment load path of the refurbished test article, when converted to full-scale, was conservatively less strong than the revised design, as shown by the comparison

shown in Table 2.7-6. Note: in the table, the blade is the attachment component integral to the impact limiter, and the receptacle is the pair of plates, attached to the cask, that accept the blade.

As detailed in Section 2.12.3.6, *Confirmatory Test of Attachments*, the 15° oblique slapdown free drop was repeated, followed by a puncture test. The attachments that experienced the greatest loads from the puncture test were the same ones that experienced the greatest loads in the free drop test. The result was that the impact limiter was securely retained on the test cask. The only measurable change to the refurbished attachment hardware was a negligible elongation of one of the blade holes by 0.07 inches (full-scale). Other than that slight deformation, there were no signs of distress or impending failure in any other feature located in the attachment load path. Of note, no other free drop or puncture drop test orientation caused any significant damage to the original, smaller design of the attachments. Therefore the impact limiter attachments are adequate to securely retain the impact limiter in the worst-case series of free drop and puncture events.

2.7.2 Crush

Since the weight of the BRR package exceeds 1,100 lb, the crush test specified in 10 CFR §71.73(c)(2) does not apply.

2.7.3 Puncture

The BRR package is evaluated for puncture resistance under HAC as defined in 10 CFR §71.73(c)(3). The puncture event is defined as a free drop from a height of 40 inches onto a vertical, cylindrical mild steel bar, 6 inches in diameter, in an orientation and in a location for which maximum damage is expected. Puncture performance of the BRR package is divided into two categories: puncture on the impact limiters, which was evaluated by half-scale certification test, and puncture of the package body, which is evaluated by analysis.

2.7.3.1 Puncture on the Impact Limiters

Appendix 2.12.2, *Certification Test Plan*, discusses the strategy used to evaluate the puncture performance of the impact limiters under the worst-case conditions, including the test objectives and success criteria. Section 2.12.2.4.1, *Test Sequence and Damage Accumulation*, identifies the five puncture tests that were performed on the half-scale certification test unit. The results of these tests is summarized below. Details are to be found in Appendix 2.12.3, *Certification Test Results*. The configuration of each test is shown schematically in Figure 2.12.3-2.

Test P1. This test was designed to show that the puncture bar would not penetrate beyond the impact limiter shell located on the flat bottom. This protects the closure lid from direct puncture bar loading, and prevents possible excessive loss of foam for protection in the HAC fire event. This test was performed subsequent to the end free drop test. The bar impacted the shell at an oblique angle through the cask c.g., which would enhance its ability to perforate the plate. The result shown in Figure 2.12.3-12 demonstrates that the impact limiter shell prevents perforation by the bar.

Test P2. This test was designed to show that the puncture bar would not create a significant exposure of foam adjacent to the cask (and containment seal) or dislodge the impact limiter from

the end of the cask. Although Figure 2.12.3-2 shows the impact occurring on the same side as the slapdown free drop primary damage, it was found that it would be much more challenging to impact the side opposite to this damage, since that is the azimuth location where the attachments experienced the greatest loading in the free drop. This test was successfully repeated (test P2C) after the redesign of the impact limiter attachments, and subsequent to the repeated 15° oblique slapdown free drop (test D2C). As shown in Figure 2.12.3-40, the impact with the bar did not perforate the shell or expose any foam, and the discussion in Section 2.12.3.6.4, *Examination of Attachments*, documents that the impact limiter was not dislodged by the impact.

Test P3. This test was designed to show that the puncture bar would not enter the impact limiter through a side impact on the limiter shell (in this case, the secondary slapdown damage area caused by the 15° oblique slapdown free drop) and rip open a large area that could compromise the performance in the subsequent HAC fire event. As shown in Figure 2.12.3-34, no perforation of the shell occurred.

Test P4. This test was designed to show that the puncture bar damage from impact on the c.g.-over-corner free drop damage would be acceptable. The bar impacted the thinner shell material (formerly the conical portion of the limiter shell, before the free drop deformation occurred), adjacent to the thicker bottom plate material. As shown in Figure 2.12.3-29, the exposure of foam from this test was modest, and is bounded by a large margin by the exposure of foam from test P5.

Test P5. This test was originally designed to apply an oblique impact on a damaged portion of the shell to determine that the exposure of foam would be acceptable. When it was determined that the limiter shell corner joint between the top flat annular portion and the cylindrical side had developed a crack in the secondary 15° oblique slapdown free drop, this test was used to accumulate the maximum amount of damage in that area. The orientation of the test is shown in Figure 2.12.3-30. The impact with the bar opened up the cracked region and peeled back part of the annular plate, exposing the underlying foam. The final configuration is shown in Figure 2.12.3-31 and Figure 2.12.3-32. Since this test is clearly governing above the other puncture tests regarding the HAC fire event, it is used in modeling the fire event as discussed in Section 3.4, *Thermal Evaluation for Hypothetical Accident Conditions*. It is worth noting that a design change was made subsequent to this test, aimed at preventing this breach of the joint from recurring. The design shown in Appendix 1.3.3, *Packaging General Arrangement Drawings*, includes the stronger joint. The details of the change are discussed in Section 2.12.3.3, *Test Unit Configuration*. However, as just noted, in spite of the design change, the result from the half-scale puncture test P5 was conservatively used for the HAC fire event analysis.

2.7.3.2 Puncture on the Cask Body

The puncture resistance of the outer surface of the cask body is evaluated using Nelms' Equation [27], which is used to determine the resistance to puncture of lead-backed stainless steel shells. For the NCT hot case temperature of 250 °F, the ultimate strength of the Type 304 outer shell (assuming the lower strength cast or forged option) is $S_u = 64,050$ psi from Table 2.2-2. The bounding weight of the BRR package, including impact limiters, is $W = 32,000$ lb. The required thickness of the outer shell to resist puncture is:

$$t = \left(\frac{W}{S_u} \right)^{0.71} = 0.61 \text{ inches}$$

The thickness of the outer shell is 2 inches. The margin of safety on the cask outer shell thickness is:

$$MS = \frac{2.0}{0.61} - 1 = +2.28$$

Therefore, puncture of the BRR package is not of concern.

2.7.4 Thermal

The BRR package is designed to withstand the HAC 30 minute fire specified in 10 CFR §71.73(c)(4). The thermal evaluation is presented in Section 3.4, *Thermal Evaluation under Hypothetical Accident Conditions*.

2.7.4.1 Summary of Pressures and Temperatures

As shown in Table 3.1-2, the maximum internal cask pressure as a result of the HAC fire event is 8.8 psig. This is lower than the bounding value of MNOP of 10 psig, and significantly lower than the design pressure of 25 psig stated in Section 2.6.1.1, *Summary of Temperatures and Pressures*. Package component stresses were calculated for an internal pressure of 25 psig in Section 2.6.1.3, *Stress Calculations*, and are compared to allowable stress at the higher HAC temperature in Section 2.7.4.3, *Stress Calculations*.

From Table 3.1-1, as a result of the HAC fire event, the maximum temperature of any part of the cask (except closure bolts) may be bounded by a temperature of 710 °F. The maximum temperature of the closure bolts is considered to be the same as that of the closure lid, bounded by a temperature of 350 °F. Conservatively, all stainless steel components will be assumed to be made from cast or forged Type 304 material, which has a lower ultimate strength than plate material. From Table 2.2-2, $S_u = 59,140$ psi at 710 °F. The value of S_u for the closure bolts at 350 °F is equal to 125,000 psi, from Table 2.2-3.

2.7.4.2 Differential Thermal Expansion

Differential expansion under NCT is evaluated in Section 2.6.1.2.1, *Baskets*. In that case, the basket was given a uniform bounding temperature of 400 °F, and the thermal expansion of the cask was conservatively neglected. The resulting minimum axial clearance is shown as 0.16 inches, and the minimum diametral clearance is 0.10 inches. In the HAC fire event, from Table 3.1-1, the peak basket temperature is given as 437 °F. Since the basket temperature is locally only 37 °F hotter than the uniform NCT assumption, and in consideration of the significant thermal expansion of the cask cavity dimensions (for example, the inner shell peak temperature is 393 °F), the clearance between the basket and the cask will not be significantly affected by the cask temperatures resulting from the fire event.

Similarly, the fuel axial clearance was evaluated using a uniform bounding temperature of 400 °F in Section 2.6.1.2.2, *Fuel*, and found to have a minimum value of 0.19 inches. Given that the local peak fuel temperature, from Table 3.1-1 is only 451 °F, and that the NCT evaluation again

neglected the thermal expansion of the cask components, the clearance between the fuel and the basket will not be significantly affected by the cask temperatures resulting from the fire event.

2.7.4.3 Stress Calculations

Cask stress due to the internal design pressure of 25 psig is presented in Section 2.6.1.3.1, *Stresses Due to Pressure Loading*, as equal to 1,002 psi. This corresponds to the stress in the outer fiber of the closure lid, and is classified as a membrane plus bending stress. This stress clearly bounds the stress generated under an internal pressure in the HAC fire event of 8.8 psig, and the margin of safety may be conservatively calculated using this stress along with the lower fire case allowable stress determined in Section 2.7.4.1, *Summary of Temperatures and Pressures*. The margin of safety is:

$$MS = \frac{59,140}{1,002} - 1 = +58.0$$

The primary load on the closure bolts is governed by the preload force, calculated in Section 2.6.1.5, *Closure Bolts*, as equal to 19,200 lb. The stress is:

$$S_{bs} = 1.2732 \frac{19,200}{D_{ba}^2} = 31,711 \text{ psi}$$

where the stress diameter, $D_{ba} = 0.878$ inches from Section 2.6.1.5. From Table 2.1-1, the allowable average tensile stress intensity for HAC is the lesser of $0.7S_u$ or S_y , which for the ASTM A320 L43 bolting material is $0.7S_u = 87,500$ psi at 350 °F. The margin of safety is:

$$MS = \frac{87,500}{31,711} - 1 = +1.76$$

Per Regulatory Guide 7.6, paragraph C.7, the extreme range of stress must be considered. Of all the various allowable stresses corresponding to the different conditions evaluated (including fabrication stresses and normal conditions of transport), the largest allowable stress is equal to the material ultimate strength, S_u . It is therefore conservative to assume that S_u bounds all stresses actually developed in the structure. For Type 304 stainless steel, $S_u = 75,000$ psi at 70 °F. The maximum possible stress intensity range is twice this value, or 150,000 psi. Applying a factor of four to account for possible stress concentrations at structural discontinuities gives a total elastic stress range of 600,000 psi. The alternating component is one-half of this value, or 300,000 psi. To account for temperature effects, this value of alternating stress is factored by the ratio of modulus of elasticity. This ratio is formed between the modulus of elasticity at room temperature (at which the test data applies directly) and the modulus of elasticity at the maximum temperature, conservatively bounded by a temperature of 710 °F for any structural part of the package. The adjusted stress is

$$S_{alt} = 300,000 \frac{E_{70^\circ\text{F}}}{E_{710^\circ\text{F}}} = 343,725 \text{ psi}$$

where $E_{70^\circ\text{F}} = 28.3(10^6)$ psi and $E_{710^\circ\text{F}} = 24.7(10^6)$ psi. Per Figure I-9.2.1 and Table I-9.1 of the ASME Code [9], the allowable value for S_{alt} at 10 cycles is 708,000 psi. The margin of safety is

$$MS = \frac{708,000}{343,725} - 1 = +1.06$$

Considering the significant conservatism used in the underlying assumptions (e.g., use of allowable stress rather than smaller actual stresses, assuming worst case stresses are fully reversing, use of the maximum factor of stress concentration), it is apparent that the actual margin of safety is larger than 1.06. Thus, the requirement of paragraph C.7 of Regulatory Guide 7.6 is met.

2.7.5 Immersion – Fissile

An immersion test for fissile material packages is required by 10 CFR §71.73(c)(5). The criticality evaluation presented in Chapter 6, *Criticality Evaluation*, assumes optimum hydrogenous moderation of the contents, thereby conservatively addressing the effects and consequences of water in-leakage.

2.7.6 Immersion – All Packages

An immersion test for all packages is required by 10 CFR §71.73(c)(6), in which a separate, undamaged specimen must be subjected an equivalent pressure of 21.7 psig. Since the BRR package is evaluated to the much greater hydrostatic pressure of the deep immersion test (see the next section), this test does not need to be evaluated.

2.7.7 Deep Water Immersion Test (for Type B Packages Containing More than $10^5 A_2$)

For Type B packages containing an activity of more than $10^5 A_2$, 10 CFR §71.61 requires that an undamaged containment system withstand an external pressure of $p_o = 290$ psig for a period of not less than one hour without collapse, buckling, or inleakage of water. This test will not have a significant effect on the BRR package. Although a temperature is not specified for this test, a lead shrinkage (fabrication) stress corresponding to a temperature of -40 °F, taken from Section 2.6.2, *Cold*, will be conservatively applied in addition to the specified hydrostatic pressure. The lead shrinkage pressure is $p_c = 787$ psi. Conservatively, the inner shell is evaluated neglecting the outer shell, even though the external pressure would be applied to the much stronger outer shell.

The internal pressure in the cask is assumed to be ambient, thus the net external pressure across the inner shell on its outer cylindrical surface is equal to a sum of the applied hydrostatic pressure of 290 psig and the lead shrinkage pressure of 787 psi, or a total of:

$$p_{cyl} = 290 + 787 = 1,077 \text{ psi}$$

The compressive hoop stress is:

$$\sigma_{\theta} = p_{cyl} \frac{r_{avg}}{t} = 9,155 \text{ psi}$$

where the mean inner shell radius, $r_{avg} = 8.5$ inches, and the thickness, $t =$ one inch. The compressive axial stress, obtained by supporting the hydrostatic pressure load, p_o , from the entire cask end cross section over the inner shell cross section, is:

$$\sigma_{\phi} = \frac{P_o \pi r_{\text{cask}}^2}{2 \pi r_{\text{avg}} t} = 6,289 \text{ psi}$$

where $r_{\text{cask}} = 38.4/2 = 19.2$ inches. Using Mohr's circle, the maximum shear stress is:

$$\sigma_{\theta\theta} = \frac{1}{2}(\sigma_{\theta} - \sigma_{\phi}) = 1,433 \text{ psi}$$

The possibility of buckling of the inner shell is evaluated using [13]. Consistent with Regulatory Guide 7.6, a factor of safety corresponding to ASME Code, Service Level D is employed. In this case, the applicable factor of safety is 1.34 for hypothetical accident conditions, as specified in [13]. The analysis used a modulus of elasticity of $28.3(10^6)$ psi, corresponding to 70 °F. Buckling analysis geometry and loading parameters are listed in Table 2.7-7 and results of the analysis in Table 2.7-8. As shown, all interaction parameters, including the maximum value of 0.4286, are less than unity, as required. Thus, the deep water immersion test is not of concern for the BRR package.

2.7.8 Summary of Damage

From the analyses presented, it is shown that the HAC sequence does not result in significant damage to the BRR package, and that all stress criteria established for HAC in Section 2.1.2, *Design Criteria*, are satisfied. The margins of safety resulting from the analyses performed in this section are shown in Table 2.7-9.

The BRR cask body and internal components were evaluated primarily by analysis, and the impact limiters and attachments were evaluated by test. The test results confirmed that the impact acceleration of 120g used in the analyses was bounding for all free drop orientations. The tests are summarized below.

The analysis of the cask body and internal components under free drop impact included the cask body structure, the closure lid, the closure bolts, and the shield plug shell. Bounding orientations of end and side drop were evaluated. A demonstration that the side drop governs over the worst-case slapdown is provided in Section 2.7.1.4, *Oblique Drop*. The cask body was analyzed using finite element analysis, in which the cask was loaded by self-weight and contents weight, and supported by the impact limiters. Conservatively, the lead shielding was considered to act as a fluid, having no structural strength. The minimum margin of safety from the finite element analysis, which corresponded to the side drop impact case, was +0.23. All of the manual evaluations resulted in larger margins of safety, as shown in Table 2.7-9. The end drop buckling analysis of the package shells, performed using ASME Code Case N-284-2, resulted in a maximum check value of 0.4024, which is well below the limit of unity, as required by the Code Case. An evaluation of lead slump in the end drop orientation was performed, and resulted in a bounding value of 1.185 inches. This value was used in the shielding evaluation documented in Chapter 5.0, *Shielding Evaluation*. An analysis of the fuel baskets was performed as documented in Appendix 2.12.8, *Fuel Basket Stress Analysis*. Each basket was evaluated for governing modes of failure, with a minimum margin of safety of +0.12. A summary of the margins of safety for the fuel baskets is provided in Table 2.7-4. An analysis of the puncture test on the cask body was performed using Nelms' equation, and resulted in a margin of safety of +2.28. Therefore, since all margins of safety are positive, the criteria of Section 2.1.2, *Design Criteria*, are satisfied for the BRR package.

The impact limiter design was tested using half-scale, prototypic certification test units and a dummy cask body. The impact limiters successfully performed their role in limiting the impact acceleration to a value considerably lower than the value of 120g used for stress analysis. In addition, the test showed that the calculated maximum strain in the energy-absorbing polyurethane foam of 83.2% was conservative. Some exposure of the foam was produced by the worst-case sequence of free drop and puncture tests. The final configuration of the impact limiter shell and of the exposed foam was included in the HAC fire event thermal model as described in Section 3.5.3.7, *Description of Thermal Model for HAC Conditions*. The impact limiter attachments, subsequent to a redesign and retest under the worst-case free drop and puncture conditions, successfully retained the impact limiters on the cask. Therefore the impact limiters satisfy their design criteria established in Section 2.1.2.2, *Other Structures*.

Table 2.7-1 – HAC Free Drop Buckling Evaluation: Geometry and Loads

	Outer shell dimensions, inches	Applied stress, psi	
Inner Dia.	34.0	σ_{ϕ}	7,117
Outer Dia.	38.0	σ_{θ}	0
Length (bounding)	55.0	$\sigma_{\phi\theta}$	0

Table 2.7-2 – HAC Free Drop: N-284-2 Results

Parameter	Value	Remarks
Capacity Reduction Factors (-1511)		
$\alpha_{\phi L} =$	0.2279	
$\alpha_{\theta L} =$	0.8000	
$\alpha_{\phi\theta L} =$	0.8000	
Plasticity Reduction Factors (-1610)		
$\eta_{\phi} =$	0.0568	
$\eta_{\theta} =$	0.0850	
$\eta_{\phi\theta} =$	0.0232	
Theoretical Buckling Values (-1712.1.1)		
$C_{\phi} =$	0.6050	
$\sigma_{\phi eL} =$	1,831,806 psi	
$C_{\theta r} =$	0.1150	
$\sigma_{\theta eL} = \sigma_{reL} =$	348,340 psi	
$C_{\theta h} =$	0.1078	
$\sigma_{\theta eL} = \sigma_{heL} =$	326,534 psi	
$C_{\phi\theta} =$	0.2527	
$\sigma_{\phi\theta eL} =$	765,157 psi	
Elastic Interaction Equations (-1713.1.1)		
$\sigma_{xa} =$	311,567 psi	
$\sigma_{ha} =$	194,946 psi	
$\sigma_{ra} =$	207,964 psi	
$\sigma_{\tau a} =$	456,810 psi	
Axial + Shear \Rightarrow Check (c):	0.0228	<1 \therefore OK (see note*)
Hoop + Shear \Rightarrow Check (d):	0.0000	<1 \therefore OK
Inelastic Interaction Equations (-1714.2.1)		
$\sigma_{xc} =$	17,687 psi	
$\sigma_{rc} =$	17,687 psi	
$\sigma_{\tau c} =$	10,612 psi	
Max(Axial,Hoop) \Rightarrow Check (a):	0.4024	<1 \therefore OK
Axial + Shear \Rightarrow Check (b):	0.4024	<1 \therefore OK
Hoop + Shear \Rightarrow Check (c):	0.0000	<1 \therefore OK

*Note: Elastic interaction checks (a), (b), (e), and (f) are not applicable.

Table 2.7-3 – Cask Shell Force and Stress Comparison

Case	Impact Limiter Force, lb	Axial Force, R, lb	Shear Force, V, lb	Bending Moment, M, in-lb	Relative Stress Intensity, psi
Side Drop	1.920(10 ⁶)	0	1.920(10 ⁶)	33.600(10 ⁶)	164,077*
15°, Primary	1.049(10 ⁶)	271,501	1.013(10 ⁶)	10.508(10 ⁶)	59,940*
15°, Secondary	1.220(10 ⁶)	0	1.220(10 ⁶)	12.652(10 ⁶)	66,647*

*Stress for comparison purposes only; not actual inner shell stress.

Table 2.7-4 – Fuel Basket Stress Analysis Results

Analysis Description	Reference Section ^①	Margin of Safety
MURR Basket		
Fuel Support Plate Bending		+8.32
Outer Shell Slot Welds		+3.00
Buckling of Lower Shell		Pass ^②
MITR-II Basket		
Buckling of Lower Shell		Pass ^②
Buckling of Fuel Tubes		+5.71
Side Drop Bending		+4.90
ATR Basket		
Fuel Support Plate Bending		+10.2
Outer Shell Slot Welds		+1.02
Side Drop Bending		+4.16
TRIGA Basket		
Fuel Support Plate Bending		+0.65
Shear Load on Spacer Screw		+0.12
Buckling of Fuel Tubes		Pass ^②
Side Drop Bending		+1.81

Notes:

1. Calculational details are presented in Appendix 2.12.8, *Fuel Basket Stress Analysis*.
2. Interaction equation checks are less than unity, as required by [13].

Table 2.7-5 – Fuel Impact Deformation Results

Fuel Type	W, lb	L _{FB}	A _{xc} , in ²	W/A _{xc} , lb/in ²	GAP	L, in
MURR	15	0.38	4.584	3.27	1.18	0.035
MITR-II	10	0.36	3.814	2.62	1.17	0.028
ATR	25	0.38	3.961	6.31	1.68	0.096
TRIGA	10	0.37	1.72*	5.81	1.18	0.062

*TRIGA fuel has 0.03-inch thick cladding for aluminum clad and 0.02-inch thick cladding for stainless steel clad fuel. Since the entire fuel cross-section is made of a strong material (fuel pellet of UZrH), the area used is that of the entire pellet cross-section of 1.48 inches.

Table 2.7-6 – Impact Limiter Attachment Comparisons

Feature Description	Refurbished Test article (Full-scale Equiv.)	Final Production Design (per Appendix 1.3.3)	Remarks
Blade and receptacle material	ASTM Type 304	ASTM Type 304	Same
Blade thickness, in.	3/4	3/4	Same
Blade width, in.	3.0	3.3	Improved
Hole diameter in blade, in.	1.13	1.13	Same
Hole-to-blade edge, in.	0.94	1.06	Improved
Blade weld to limiter inner shell structure	3/8-in. fillet on both sides	3/8-in. fillet on both sides	Same
Receptacle plate thickness, in.	3/8	1/2	Improved
Ball lock pin diameter, in.	1.0	1.0	Same
Pin material	Carbon steel	Stainless steel	Improved
Pin rated double shear strength, lb	65,600	73,500	Improved
Attachment quantity per limiter	6	8	Improved

Table 2.7-7 – Deep Immersion Test: Geometry and Loads

	Inner shell dimensions, inches	Applied stress, psi	
Inner Dia.	16.0	σ_{ϕ}	6,289
Outer Dia.	18.0	σ_{θ}	9,155
Length (bounding)	62.0	$\sigma_{\phi\theta}$	1,433

Table 2.7-8 – Deep Immersion Test: N-284-2 Results

Parameter	Value	Remarks
Capacity Reduction Factors (-1511)		
$\alpha_{\phi L} =$	0.2850	
$\alpha_{\theta L} =$	0.8000	
$\alpha_{\phi\theta L} =$	0.8000	
Plasticity Reduction Factors (-1610)		
$\eta_{\phi} =$	0.0523	
$\eta_{\theta} =$	0.2856	
$\eta_{\phi\theta} =$	0.0417	
Theoretical Buckling Values (-1712.1.1)		
$C_{\phi} =$	0.6050	
$\sigma_{\phi eL} =$	2,014,294 psi	
$C_{\theta r} =$	0.0387	
$\sigma_{\theta eL} = \sigma_{reL} =$	128,711 psi	
$C_{\theta h} =$	0.0387	
$\sigma_{\theta eL} = \sigma_{heL} =$	128,711 psi	
$C_{\phi\theta} =$	0.1619	
$\sigma_{\phi\theta eL} =$	539,157 psi	
Elastic Interaction Equations (-1713.1.1)		
$\sigma_{xa} =$	428,445 psi	
$\sigma_{ha} =$	76,843 psi	
$\sigma_{ra} =$	76,843 psi	
$\sigma_{\tau a} =$	321,885 psi	
Axial + Shear \Rightarrow Check (c):	0.0147	<1 \therefore OK (see note*)
Hoop + Shear \Rightarrow Check (d):	0.1192	<1 \therefore OK
Inelastic Interaction Equations (-1714.2.1)		
$\sigma_{xc} =$	22,388 psi	
$\sigma_{rc} =$	21,943 psi	
$\sigma_{\tau c} =$	13,433 psi	
Max(Axial,Hoop) \Rightarrow Check (a):	0.4172	<1 \therefore OK
Axial + Shear \Rightarrow Check (b):	0.2923	<1 \therefore OK
Hoop + Shear \Rightarrow Check (c):	0.4286	<1 \therefore OK

*Note: Elastic interaction checks (a), (b), (e), and (f) are not applicable.

Table 2.7-9 – Minimum Margins of Safety from HAC Evaluations

Component	Loading Condition	Minimum Margin of Safety
<i>Free Drop</i>		
Cask body (FEA)	End drop, bottom down, membrane stress	+0.98
	End drop, bottom down, membrane + bending	+0.49
	End drop, top down, membrane stress	+0.97
	End drop, top down, membrane + bending stress	+0.92
	Side drop, membrane stress	+1.75
	Side drop, membrane + bending stress	+0.23
Lower closure plate	End drop, bottom down, membrane + bending	+0.40
Closure bolts	End drop, top down	+0.83
Closure lid	End drop, top down	+1.65
Shield plug shell lower plate	End drop, bottom down, assuming simple support, stress at center	+0.46
	End drop, bottom down, assuming fixed edge support, stress at edge (weld)	+0.91
Cask outer shell	End drop, buckling (Code Case N-284-2)	0.4024*
<i>Puncture</i>		
Cask outer shell	Nelms' Equation	+2.28
<i>Thermal</i>		
Containment boundary	Internal pressure, fire conditions	+58.0
Closure bolts	Internal pressure, fire conditions	+1.76
Cask	Range of stress	+1.06

*Maximum check value must be less than unity.

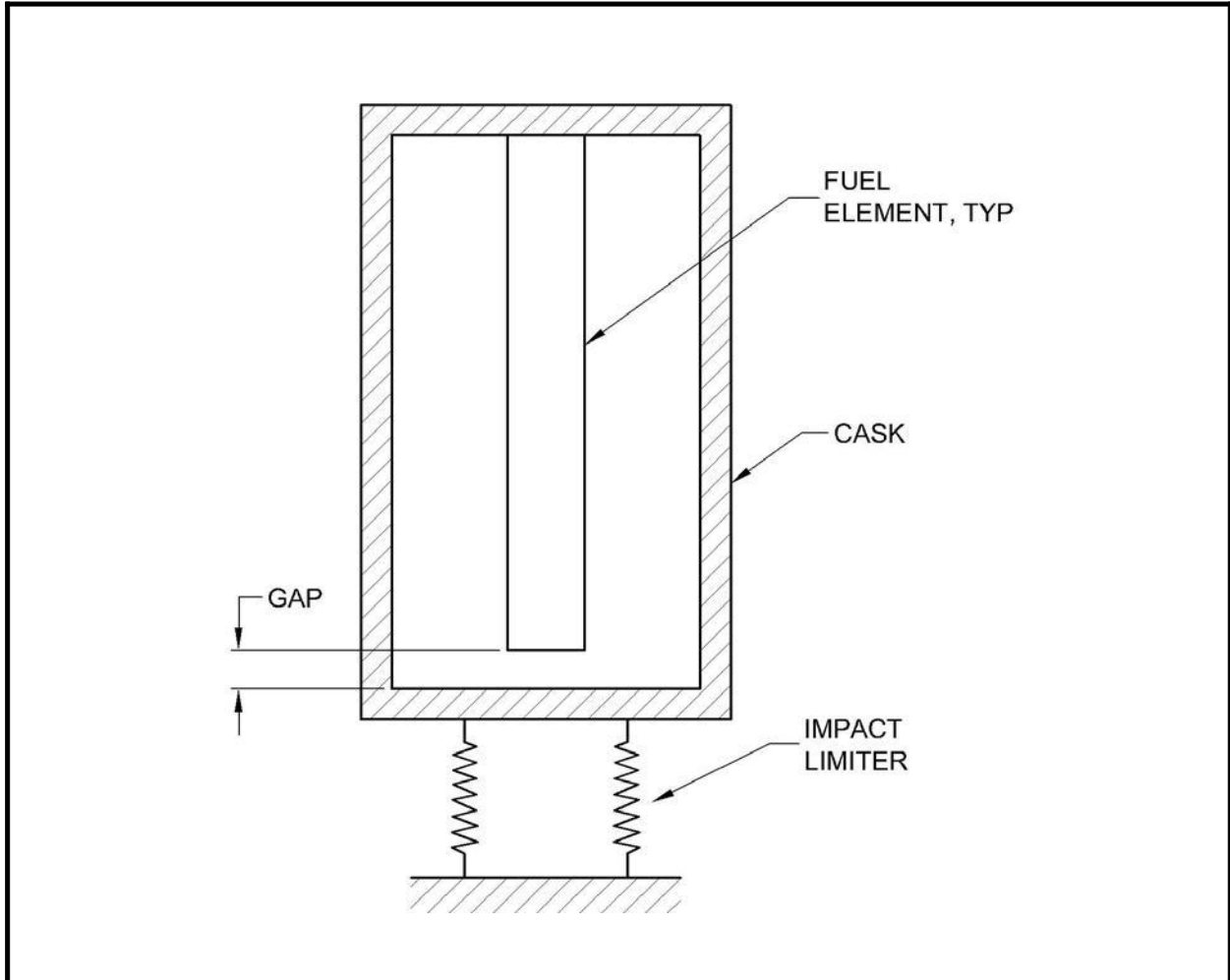


Figure 2.7-1 – Cask Cavity and Fuel During Free End Drop

2.8 Accident Conditions for Air Transport of Plutonium

This section does not apply, since air transport is not used for the BRR package.

2.9 Accident Conditions for Fissile Material Packages for Air Transport

This section does not apply, since air transport is not used for the BRR package.

2.10 Special Form

This section does not apply, since special form is not claimed for the BRR package.

2.11 Fuel Rods

This section does not apply, since fuel rod cladding is not credited with containment in the BRR package.

2.12 Appendices

- 2.12.1 References
- 2.12.2 Certification Test Plan
- 2.12.3 Certification Test Results
- 2.12.4 Stress Analysis Finite Element Models
- 2.12.5 Impact Limiter Performance Evaluation
- 2.12.6 Impact Analysis Software Descriptions
- 2.12.7 Seal Performance Tests
- 2.12.8 Fuel Basket Stress Analysis

2.12.1 References

1. Title 10, Code of Federal Regulations, Part 71 (10 CFR 71), *Packaging and Transportation of Radioactive Material*, 01-01-08 Edition.
2. U. S. Nuclear Regulatory Commission, Regulatory Guide 7.6, *Design Criteria for the Structural Analysis of Shipping Cask Containment Vessels*, Revision 1, March 1978.
3. U. S. Nuclear Regulatory Commission, Regulatory Guide 7.8, *Load Combinations for the Structural Analysis of Shipping Casks for Radioactive Material*, Revision 1, March 1989.
4. U. S. Nuclear Regulatory Commission, Regulatory Guide 7.11, *Fracture Toughness Criteria of Base Material for Ferritic Steel Shipping Cask Containment Vessels with a Maximum Wall Thickness of 4 Inches (0.1 m)*, June 1991.
5. R. E. Monroe, H. H. Woo, and R. G. Sears, *Recommended Welding Criteria for Use in the Fabrication of Shipping Containers for Radioactive Materials*, NUREG/CR-3019, UCRL-53044, March 1985.
6. L. E. Fischer, W. Lai, *Fabrication Criteria for Shipping Containers*, NUREG/CR-3854, UCRL-53544, U.S. Nuclear Regulatory Commission, March 1985.
7. American Society of Mechanical Engineers (ASME) Boiler and Pressure Vessel Code, Section III, *Rules for Construction of Nuclear Facility Components*, Division 1 – Subsection NB, *Class 1 Components*, 2007 Edition.
8. American Society of Mechanical Engineers (ASME) Boiler and Pressure Vessel Code, Section III, *Rules for Construction of Nuclear Facility Components*, Division 1 – Subsection NG, *Core Support Structures*, 2007 Edition.
9. American Society of Mechanical Engineers (ASME) Boiler and Pressure Vessel Code, Section III, *Rules for Construction of Nuclear Facility Components*, Division 1 – Subsection NF, *Supports*, 2007 Edition.
10. G.C. Mok, L.E. Fischer, S.T. Hsu, *Stress Analysis of Closure Bolts for Shipping Casks*, NUREG/CR-6007, UCRL-ID-110637, U.S. Nuclear Regulatory Commission, April 1992.
11. W.R. Holman, R. T. Langland, *Recommendations for Protecting Against Failure by Brittle Fracture in Ferritic Steel Shipping Containers Up to Four Inch Thick*, NUREG/CR-1815, UCRL-53013, August 1981.
12. American Society of Mechanical Engineers (ASME) Boiler and Pressure Vessel Code, Section III, *Rules for Construction of Nuclear Facility Components*, Appendix I, *Design Stress Intensity Values, Allowable Stresses, Material Properties, and Design Fatigue Curves*, 2007 Edition.
13. American Society of Mechanical Engineers (ASME) Boiler and Pressure Vessel Code, Section III, *Rules for Construction of Nuclear Power Plant Components*, Division 1, Class MC, Code Case N-284-2, *Metal Containment Shell Buckling Design Methods*, 2007 Edition.
14. American Society of Mechanical Engineers (ASME) Boiler and Pressure Vessel Code, Section IX, *Qualification Standard for Welding and Brazing Procedures, Welders, Brazers, and Welding and Brazing Operators*, 2007 Edition.

BRR Package Safety Analysis Report

15. American Society of Mechanical Engineers (ASME) Boiler and Pressure Vessel Code, Section III, *Rules for Construction of Nuclear Facility Components*, Division 1 – Subsection NE, *Class MC Components*, Article NE-4220, 2007 Edition.
16. American Society of Mechanical Engineers (ASME) Boiler and Pressure Vessel Code, Section III, *Rules for Construction of Nuclear Facility Components*, Division 1 – Subsection NB, *Class 1 Components*, Article NB-2540, 2007 Edition.
17. American Society of Mechanical Engineers (ASME) Boiler and Pressure Vessel Code, Section III, *Rules for Construction of Nuclear Facility Components*, Division 1 – Subsection NB, *Class 1 Components*, Article NB-2570, 2007 Edition.
18. ANSI/AWS D1.6:2007, *Structural Welding Code–Stainless Steel*, American Welding Society (AWS).
19. American Society of Mechanical Engineers (ASME) Boiler and Pressure Vessel Code, Section III, *Rules for Construction of Nuclear Facility Components*, Division 1 – Subsection NB, *Class 1 Components*, and Section V, *Nondestructive Examination*, Article 2, *Radiographic Examination*, 2007 Edition.
20. American Society of Mechanical Engineers (ASME) Boiler and Pressure Vessel Code, Section III, *Rules for Construction of Nuclear Facility Components*, Division 1 – Subsection NB, *Class 1 Components*, and Section V, *Nondestructive Examination*, Article 4, *Ultrasonic Examination Methods for Welds*, 2007 Edition.
21. American Society of Mechanical Engineers (ASME) Boiler and Pressure Vessel Code, Section III, *Rules for Construction of Nuclear Facility Components*, Division 1 – Subsection NB, *Class 1 Components*, and Section V, *Nondestructive Examination*, Article 6, *Liquid Penetrant Examination*, 2007 Edition.
22. American Society of Mechanical Engineers (ASME) Boiler and Pressure Vessel Code, Section III, *Rules for Construction of Nuclear Facility Components*, Division 1 – Subsection NB, *Class 1 Components*, Article NB-6220, 2007 Edition.
23. Boucher, R. C., *Strength of Threads*, Product Engineering, November 27, 1961.
24. ANSI N14.23, *Design Basis for Resistance to Shock and Vibration of Radioactive Material Packages Greater Than One Ton in Truck Transport (DRAFT)*, 1980, American National Standards Institute, Inc, New York.
25. Roark's Formulas for Stress and Strain, Sixth Edition, McGraw-Hill, New York, 1989.
26. T.A. Nelson and R. C. Chun, *Methods for Impact Analysis of Shipping Casks*, NUREG/CR-3966, UCID-20639, U.S. Nuclear Regulatory Commission, November 1987.
27. A. Nelms, *Structural Analysis of Shipping Casks, Effect of Jacket Physical Properties and Curvature on Puncture Resistance*, ORNL-TM-1312, Vol. 3, Oak Ridge National Laboratory, 1968.
28. General Plastics Manufacturing Company, *Design Guide for Use of Last-A-Foam® FR-3700 For Crash & Fire Protection of Radioactive Material Shipping Containers*, Issue 004.
29. NRC Docket No. 71-9295, *Mixed Oxide Fresh fuel Package Safety Analysis Report*, Revision 7, July 2008.

30. G. D. Sjaardema and G. W. Wellman, *Numerical and Analytical Methods for Approximating the Eccentric Impact Response (Slapdown) of Deformable Bodies*, SAND88-0616 (UC-71), Sandia National Laboratories.
31. **SCANS** (*Shipping Cask ANalysis System*), *A Microcomputer Based Analysis System for Shipping Cask Design Review*, NUREG/CR-4554 (UCID-20674), Lawrence Livermore National Laboratory.
32. American Society of Mechanical Engineers (ASME) Boiler and Pressure Vessel Code, Section III, *Rules for Construction of Nuclear Facility Components*, Division 1 – Subsection NG, *Core Support Structures*, Article NG-3350, 2007 Edition.
33. American Society of Mechanical Engineers (ASME) Boiler and Pressure Vessel Code, Section III, *Rules for Construction of Nuclear Facility Components*, Appendix F, *Rules for Evaluation of Service Loadings with Level D Service Limits*, 2007 Edition.
34. General Plastics Manufacturing Company, *General Plastics Last-A-Foam® FR-3700 For Crash & Fire Protection of Radioactive Material Shipping Containers*, June 1997.

2.12.2 Certification Test Plan

This appendix describes the certification tests that were performed on the BEA Research Reactor package impact limiters. The justification for choosing the specific tests is presented and discussed. Since this material served for test planning purposes, the future tense is used. The results of the tests is provided in Appendix 2.12.3, *Certification Test Results*.

Because the BRR package includes a conventional, austenitic stainless steel cask shielded by lead and closed by a bolted lid, testing of the cask body is not necessary. The licensing basis for the cask body is by analysis. Physical testing will focus only on the impact limiters and attachments. The licensing basis for the impact limiters will be a combination of half-scale physical test and analysis. Free drop and puncture drop damage of steel-shell, polyurethane foam-filled impact limiters can be adequately modeled using scaled test specimens with appropriate scaling factors.

The test unit configuration will therefore consist of a half-scale dummy cask and half-scale prototypic impact limiters and attachments. Testing will consist of free drops and puncture drops. Test data will consist of measured accelerations and measurements of the damaged configuration.

2.12.2.1 Certification Objective

The objective of the certification test program is to demonstrate the adequacy of the BRR package impact limiter design. The impact limiters were designed using computer software to predict the impact (maximum at cold temperature) and the crush deformation (maximum at hot temperature). Refer to Appendix 2.12.5, *Impact Limiter Performance Evaluation*. The certification tests will demonstrate the performance of the limiters in both the hypothetical accident condition (HAC) free drop and puncture drop events. Free drop impact and crush deformation results will be used to benchmark the computer program for use in non-tested orientations or conditions. Puncture drop deformation results will be used to demonstrate impact limiter structural integrity and in the HAC thermal analysis as discussed below.

Several orientations will be tested to ensure that the worst-case series of free and puncture drop events has been considered. The maximum combination of free and puncture drop deformation will be used in the thermal analysis to show that under these worst-case conditions, the elastomer containment O-ring seal temperatures do not exceed safe limits during the HAC fire event.

Since a half-scale test unit will be used, a scaling of the various test parameters is necessary. All of the dimensions of the test unit will be one half of the full-scale design. Dimensional results from the half-scale model (e.g., crush distance) must be multiplied by a factor of two to obtain the full-scale equivalent result. Similarly, the measured accelerations must be divided by two to convert to full-scale. The test unit weight will be 1/8 the weight of the full-scale design, and the rotational moment of inertia will be 1/32 of the full-scale package.

2.12.2.2 Initial Test Conditions

2.12.2.2.1 Temperature

To confirm the maximum free drop impact accelerations that have been obtained from computer analysis, the free drops must occur at or near the minimum temperature of -20 °F, due to the increase in crush strength of the energy absorbing materials (polyurethane foam) with decreasing

BRR Package Safety Analysis Report

temperature. The maximum crush, which occurs at the maximum NCT temperature, will be obtained by first benchmarking the computer code using the cold case impacts and deformations, and then performing runs with material properties at maximum temperature. Consequently, free drop impacts will occur with the foam material at a bulk average temperature at or near -20 °F. A temperature somewhat below -20 °F is desirable. However, to facilitate testing, a small deviation of as much as 10 °F (to -10 °F) is permissible, since the difference can be accounted for analytically.

Puncture damage depends on the perforation resistance of the shell and the compressive/shearing behavior of the foam subsequent to perforation. Perforation resistance is least at cold temperature, since the underlying foam is stronger and supports a greater shearing action of the edge of the puncture bar. Subsequent to perforation, if that occurs, the 9 lb/ft³ (pcf) foam used for the BRR package impact limiters will not present a significant resistance to the puncture bar, regardless of strength. Therefore, the cold condition is worst-case when perforation resistance is of primary interest. However, since most puncture drop tests are expected to perforate the thinner shells regardless of temperature, only the puncture drop tests on the thicker shell (the flat, circular shell located at the end of the impact limiter, which is expected to resist perforation) needs to be performed at the cold, -20 °F temperature. As for the free drop, a small deviation up to a bulk foam temperature of -10 °F is acceptable.

2.12.2.2 Test Facilities and Instrumentation

The certification drop and puncture testing will be conducted using a drop pad having a mass of at least 10 times the weight of the certification test unit (CTU), or at least 40,000 lb. The top of the pad will be covered by an embedded steel plate of adequate thickness such that the drop pad will represent an essentially unyielding surface. The half-scale puncture bar will be a 3-in diameter bar of mild steel, mounted perpendicular to the drop pad, and having an edge radius not exceeding 1/8-inch. The bar will be reinforced by gussets at its base and fastened securely to the pad. The length of the bar will permit the bar to do maximum damage before the package becomes supported by the drop pad, and it will be at least 8 inches long. More than one length of bar may be used. Puncture bars will not be reinforced beyond what is necessary to provide rigidity at the baseplate joint.

CTU temperature will be measured by means of thermocouples embedded in the foam. As a minimum, the region of foam expected to undergo crush deformation will be monitored.

The primary means of recording the results of the certification testing will be physical measurements and observations of the CTU before and after testing. In addition, each free drop impact will be recorded using active accelerometers.

2.12.2.3 Certification Test Unit Configuration

The certification tests will be performed using a test unit consisting of a dummy cask assembled with prototypic, half-scale impact limiters. The impact limiter attachments, including the welds of the mating attachments to the dummy cask, will be prototypic. The dummy cask will be made of steel and lead, and possess a weight of 1/8 of the weight of the full-scale cask (consistent with half-scale). The dummy cask's impact limiter interface dimensions and features, and its overall length, will be in prototypic half-scale.

The impact limiters will be constructed using the same materials and details as the full-scale limiters, using half-scale dimensions. The polyurethane foam will use the same procurement specification,

including crush properties, as the full-scale components. Lifting features will be omitted from the half-scale components. Prior to testing, the impact limiters will receive a certificate of compliance with all fabrication drawing and specification requirements.

2.12.2.3 Identification of Worst-Case Test Orientations

The objectives of the certification test program are:

1. To confirm maximum free drop impact accelerations obtained from computer calculations.
2. To calibrate or benchmark the computer program, in order to validate calculations for orientations not tested.
3. To demonstrate the general structural integrity of the impact limiter during impact.
4. To demonstrate the effectiveness of the impact limiter attachments in both free drop and puncture drop events.
5. To demonstrate that the puncture bar will not penetrate the circular end plate of the upper impact limiter shell.
6. To quantify the worst-case puncture damage for the HAC fire event thermal analysis.

These objectives will now be discussed under the headings of free drop impact and puncture damage.

2.12.2.3.1 Free Drop Impact Objectives

The computer analysis documented in Appendix 2.12.5, *Impact Limiter Performance Evaluation*, shows that the governing free drop orientation for impact is the 15° slapdown secondary impact in the cold case, at 87g (full scale). Similarly, the governing crush damage occurs for the primary impact in the 15° slapdown orientation in the hot case, at a strain of 81%. The c.g.-over-corner impact is next closest in damage severity, having a maximum strain of 76% in the hot case. Therefore, the 15° slapdown and c.g.-over-corner orientations should be considered for the certification test. In addition, since the end drop orientation is of critical importance to the analysis of the cask body shells, the closure lid bolts, and lead slump, the end drop orientation should also be considered.

The 15° slapdown test in the cold condition will directly result in the worst-case impact occurring in the 30-foot free drop. The primary impact crush deformation will not be the worst-case, since the worst-case occurs at maximum temperature. However, the impact analysis will be benchmarked for the cold case, and by subsequently adjusting the foam and steel properties for hot temperatures, the maximum crush can be demonstrated using a computer calculation.

The end drop test will directly result in the maximum impact occurring in the 30-foot end drop. This data can be used to ensure that the impact used in the quasi-static finite element analysis for the end drop is adequately bounding.

The c.g.-over-corner free drop will not result in the worst-case deformation that could occur in that orientation, which occurs at hot temperature. However, using the same benchmarking technique as for the slapdown test, the maximum crush deformation for this orientation can be readily calculated. Of note, this test could be performed using hot temperature, but it is more convenient

BRR Package Safety Analysis Report

to use the naturally occurring temperature, so long as it is adequately characterized to support the benchmarking procedure.

The finite element analysis which is documented in Chapter 2.0, *Structural Evaluation*, will include both the end drop orientation and the side drop orientation. From the data collected in other drop tests, the impact analysis software can adequately predict a bounding impact acceleration for the side drop. Therefore, a side drop orientation does not need to be performed.

The licensing strategy for demonstrating the adequacy of the impact limiter attachments depends upon test. The multiplicity of the free drops considered above (along with puncture drops, see below) ensures that this can be done solely by means of the test results. Furthermore, the general integrity of the impact limiter shells and joints, and the energy absorbing efficiency of the foam at cold temperatures, can also be clearly demonstrated with the proposed tests.

2.12.2.3.2 Puncture Drop Objectives

The circular plate on the end of the upper impact limiter is designed to prevent perforation by the puncture bar. This prevents concentrated puncture loads from occurring directly on the closure lid. Perforation of the conical or side cylindrical impact limiter shells is expected, however the possible orientation of the bar with respect to the closure lid would either be too oblique to be damaging to the lid, or would impact the relatively strong end structure. To demonstrate the puncture resistance of the plate, an end puncture should be considered. The angle should be somewhat oblique to enhance perforation. Per Section 10 CFR §71.73(a), the puncture should follow the free drops, and should occur on the surface impacted in the end drop, if determined to be the worst orientation.

As a part of achieving the worst-case damage to bound the fire event thermal analysis, a puncture on the c.g.-over-corner free drop damage should be considered. The bar should be oriented so that the potential penetration depth is not hindered by the resistance of the cask end structure. This would also examine the possibility that significant damage could occur from the cask rolling off of the bar, if the impact limiter becomes impaled on it. The resulting puncture damage measurements can be added to the hot case bounding free drop damage calculation to obtain the worst-case from this sequence of events.

Another possibility is that the puncture bar could penetrate the conical region from a side, or near-side orientation, and rip deeply into the limiter in a direction more or less parallel to the cask end surface, and either cause a chimney to occur, or rip out a large section of the limiter as the cask is rolling off of the bar, if the impact limiter becomes impaled on it. This action might be somewhat limited by the fact that the bar orientation would not be toward the c.g., allowing the package to rotate away from the damage site. This test could be located on the slapdown primary or secondary free drop damage.

The cask drain port, located in the cask lower end structure, is closed using an elastomer O-ring seal that may be damaged in the HAC fire event. Therefore, exposure of the end structure side could allow excessive temperatures in the drain port area. An attack from a puncture bar more or less parallel to the package axis, contacting the edge of the damaged area from the secondary slapdown event, could either cause a local exposure of the top end structure of the cask, or possibly substantially dislodge the upper impact limiter due to partial or complete failure of the attachments.

BRR Package Safety Analysis Report

Significant puncture damage could also occur from an attack on the slapdown damage if the puncture bar is aimed at the massive cask end structure. The angle of the bar to the damaged surface will need to be a compromise between an angle that aims through the package c.g., without being so steep that it just bounces off. This test will also explore the maximum damage at the drain port.

2.12.2.3.3 NCT Free Drop

For the BRR package, which weighs just over 30,000 lb, the normal conditions of transport (NCT) free drop height required by 10 CFR §71.71(c)(7) is 2 feet. This represents only 6.7% of the energy of the HAC free drop height of 30 feet. The effect of the NCT free drop on the maximum impact and crush deformation can be found by increasing the free drop height from 30 feet to 32 feet. The governing impact (cold, 15° slapdown, secondary impact) increases by less than 4%, and the governing crush deformations (c.g.-over-corner, hot, and 15° slapdown, secondary, hot) increase by only 2%. These differences may be neglected, particularly considering that the bounding impact used in the finite element analysis is approximately 35% greater than that predicted by Appendix 2.12.5, *Impact Limiter Performance Evaluation*. Therefore, the NCT free drop does not need to be included in the certification test program.

2.12.2.4 Summary of Certification Tests

Based on the discussions in Section 2.12.2.3, *Identification of Worst-Case Test Orientations*, the planned certification tests for the BRR package are summarized below and in Table 2.12.2-1. Free drops are depicted in Figure 2.12.2-1 and puncture drops in Figure 2.12.2-2.

2.12.2.4.1 Test Sequence and Damage Accumulation

The order of free drops and punctures is given below. The order and sequence of free drop and puncture damage may be altered as long as the test objectives, as outlined above, are satisfied. If stated to be cold, the bulk average temperature of the foam must be per the discussion given in Section 2.12.2.2.1, *Temperature*. Interference of damage is expected to be negligible.

The test sequence envisions three separate prototypic impact limiter test articles. Package No. 1 consists of impact limiter nos. 1 and 2, and Package No. 2 consists of Impact Limiter nos. 2 and 3, each using the same dummy cask. The test series consists of three, 30-foot free drops, and five, 40-inch puncture drops.

Note that since all test articles are identical and include the thicker end plate, each end of the test package qualifies as the package "top", as necessary. No tests need to be performed on the package "bottom".

Test D1. Package No. 1, Limiter No. 1 will be tested in the end drop orientation at cold temperature. The purpose of this test is to quantify the maximum end drop impact acceleration, and to prepare a surface for the subsequent puncture on the thicker end plate (test P1).

Test P1. Package No. 1, Limiter No. 1 will be dropped on the puncture bar through the package c.g., onto the thicker end plate at cold temperature. The axis of the bar should pass approximately one bar diameter in from the plate edge. The axis of the bar should be oblique in order to enhance its ability to cut into the plate. The purpose of this test is to demonstrate that the thicker end plate does not perforate.

BRR Package Safety Analysis Report

Test D2. Package No. 2, Limiter Nos. 2 (primary) and 3 (secondary) will be tested in the 15° slapdown orientation at cold temperature. The purpose of this test is to quantify the maximum impact acceleration (secondary impact) and, using analysis, to quantify the maximum crush strain (secondary impact). An additional purpose is to prepare a surface for subsequent puncture testing.

Test D3. Package No. 2, Limiter No. 3 will be tested in the c.g.-over-corner orientation. The temperature does not need to be controlled, but it must be well characterized for later analysis. The purpose of this test is to quantify the maximum crush strain in the c.g.-over-corner orientation (analytically using properties at maximum temperature); also to ensure the thicker end plate does not cause unexpected results or failure of the weld joints; and to prepare a surface for the subsequent puncture test (test P4). The impact point should be opposite from the slapdown damage.

Test P2. Package No. 2, Limiter No. 2 will be dropped such that the puncture bar strikes the inside edge of the slapdown primary-end damage from test D2. The cask axis will be as vertical as possible, given that the secondary impact limiter must clear the puncture bar. The purpose of this puncture test is to either expose a region next to the cask top end structure which could soak in heat in the HAC fire, or possibly dislodge the limiter by failing some or all attachments. The puncture bar will need to have adequate length; bending of the bar would not be an unexpected outcome of this test.

Test P3. Package No. 2, Limiter No. 2 will be dropped onto the puncture bar with an impact point on the primary-end impact damage from test D2. The exact impact point and orientation of the package axis may be chosen by the Test Engineer in light of the damage which occurs in test D2, but the package axis should be nearly horizontal (0° to 15° from the horizontal), and the impact point approximately halfway between the cask end surface and the limiter outside end surface. Therefore, the bar axis is not through the package c.g., but could do significant damage before the package has time to rotate.

Test P4. Package No. 2, Limiter No. 3 will be dropped on the damage from the c.g.-over-corner free drop, with impact on the thinner conical shell material. The puncture bar edge will align with the joint between the thick end plate and the thinner conical plate, and be aimed to miss significant support from the cask end structure, i.e., with the package axis inclined approximately 75° from the horizontal. This will miss the package c.g. by only a few inches, and the energy loss will be insignificant. The purpose of this test is to quantify a possible worst-case configuration for the HAC fire thermal analysis.

Test P5. Package No. 2, Limiter No. 3 will be dropped such that the puncture bar strikes the approximate center of the slapdown secondary damage, in order to create the smallest remaining foam thickness adjacent to the cask end structure (location of the drain port). The cask axis should be approximately 30° to the horizontal. The bar axis should be aimed directly at the cask end structure, but it will not be directly through the c.g. To aim through the c.g. would mean that impact with the damaged limiter would be too oblique, and the cask would be expected to only bounce off of the bar.

2.12.2.4.2 Measurements

Measurements of the certification test results will be made in explicit support of the test objectives identified in Section 2.12.2.3, *Identification of Worst-Case Test Orientations*, and will consist of configuration (dimensional) measurements of the damage, and acceleration

BRR Package Safety Analysis Report

measurements of the free drops. Temperature measurements will be made on an ongoing basis to fully characterize the bulk average temperature of the foam.

Measurements of the free drop deformation damage will take springback of the limiter into account, and by use of crush gages or other techniques, attempt to obtain the maximum crush at the moment of impact. Puncture measurements should be made from the prevailing damage surface and record the depth and diameter, or other relevant information, of the puncture test damage. A conventional speed video and still photographic record of each drop and puncture should also be made.

Accelerometers should be redundant, and placed to adequately characterize the primary and secondary slapdown impacts. The data should be filtered to obtain the rigid body impact, using the guidance of a fast Fourier transform (FFT), or equivalent, of the time history data.

2.12.2.5 Acceptance Criteria

The following are the acceptance criteria for certification testing of the BRR package:

1. The impact limiter shells must retain their general integrity for all impacts and deformations. Ripped welds or other tears or fissures are acceptable as long as they are limited in extent and compatible with the HAC fire thermal analysis. Full puncture perforation of the impact limiter shells in regions of standard thickness is expected.
2. The impact limiter attachments must retain the limiters on the cask. A limited degree of distortion or dislodging of the limiters is acceptable, but must be compatible with the HAC fire thermal analysis.
3. The impact limiters must maintain package deceleration to acceptable levels. The safety analyses will utilize as inputs values which bound the results of the certification test.
4. The thicker end plate must not perforate in the puncture drop test.
5. The maximum damage to the limiter from the single worst-case free drop and puncture test sequence must fall within the bounding assumptions used in the HAC fire thermal analysis.

BRR Package Safety Analysis Report

Table 2.12.2-1 - Summary of Certification Tests

No.	Test Description	Test Limiter	Temperature	Purpose of Test & Expected Damage
D1	End drop	#1	Cold (see note 2)	Maximum end impact
D2	Slapdown oblique drop, 15°	#2 & #3	Cold (see note 2)	Maximum slapdown secondary impact, obtain data to permit calculation of maximum strain
D3	C.G. over corner drop	#3	Not controlled	Obtain data to permit calculation of maximum strain
P1	Oblique through c.g. on thicker end plate on test D1 damage	#1	Cold (see note 2)	Demonstrate perforation resistance of thicker end plate
P2	Approx. parallel to package axis, on test D2 primary-end damage	#2	Not controlled	Quantifies possible maximum accumulation of free drop and puncture damage – local severe damage or dislodge limiter
P3	Approx. perpendicular to package axis, on test D2 primary-end damage	#2	Not controlled	Quantifies possible maximum accumulation of free drop and puncture damage – chimney or other severe damage
P4	On test D3 damage, on thick/thin joint, near c.g.	#3	Not controlled	Quantifies possible maximum accumulation of free drop and puncture damage – minimum foam thickness at cask corner
P5	Oblique to package axis, on test D3 secondary-end damage	#3	Not controlled	Quantifies possible maximum accumulation of free drop and puncture damage – minimum foam thickness at cask side

Notes:

1. All free drops (Dx) are from 30 feet, and all punctures (Px) are from 40 inches.
2. See Section 2.12.2.2.1, *Temperature*.

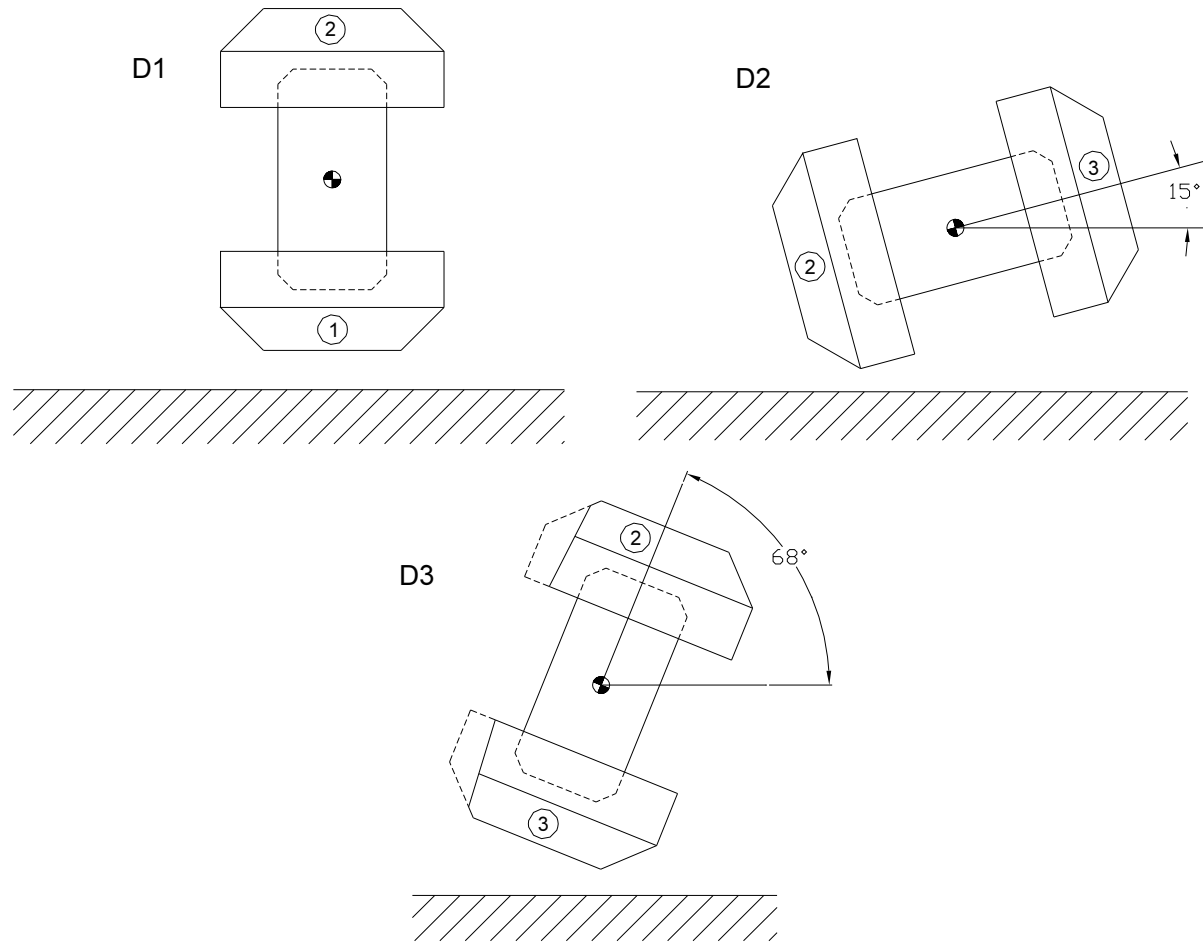


Figure 2.12.2-1 - BRR Package Free Drop Orientations

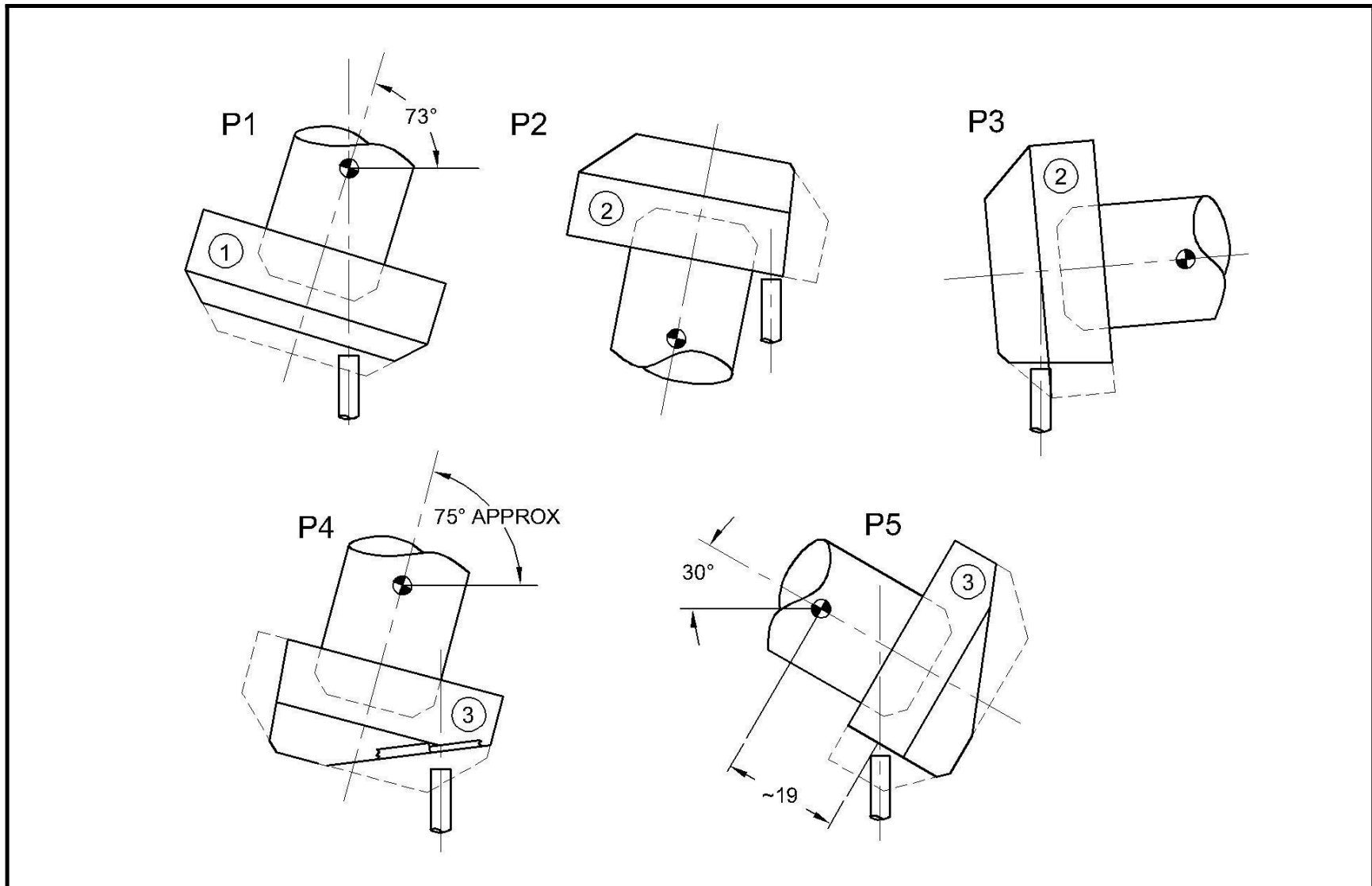


Figure 2.12.2-2 - BRR Package Puncture Drop Orientations

2.12.3 Certification Test Results

This appendix presents results of the certification tests that were performed on the BEA Research Reactor package impact limiters. The information contained in the certification test report is summarized.

2.12.3.1 Introduction

Demonstration of the compliance of the BRR package design with the requirements of 10 CFR §71.73 is achieved primarily by analysis. Certification testing is used to demonstrate the performance of the polyurethane foam-filled impact limiters. The tests reported in this appendix were performed using prototypic, half-scale test impact limiters and a dummy cask which had prototypically scaled weight. Both the impact limiters and the attachments (including the limiter attachment components and the cask attachment components) were of prototypic materials and construction. The impact limiter test specimens were in full compliance with the drawings in Section 1.3.3, *Packaging General Arrangement Drawings*, except for the scale factor of 1/2, and with the exceptions discussed below in Section 2.12.3.3, *Test Unit Configuration*.

The objectives of these tests were to demonstrate the general structural integrity of the impact limiters and attachments in free drop and puncture events, to confirm the maximum impact magnitudes, and to verify that the maximum damage to the impact limiters was bounded by the assumptions used in the thermal and criticality analyses. Further discussion of the tests, including a justification of the tests chosen, is provided in Appendix 2.12.2, *Certification Test Plan*. A comparison of the test results to the impact limiter calculations is given in Section 2.12.5.3, *Reconciliation with Certification Test Results*.

2.12.3.2 Test Facilities

Free drop and puncture testing was performed at Hiline Engineering in Richland, Washington. The drop pad had a total weight of approximately 50,000 lb. The embedded steel plate target had a thickness of 2½ inches. The pad therefore constituted an essentially unyielding surface for the test package, which weighed somewhat less than 4,000 lb.

In accordance with the requirements of 10 CFR §71.73(c)(3), the half-scale puncture bars were fabricated from solid, 3-inch diameter mild steel bars. Puncture bars of two lengths were used: 25 inches and 50 inches long, measured from the top of the baseplate. The length of each bar was designed to allow the puncture event to proceed to completion before the test package gained any support from the unyielding surface, but without excessive length. Each puncture bar was welded with gussets perpendicularly to a thick, mild steel plate. The top edge of each puncture bar was finished to a 1/8-inch maximum radius. Each puncture bar assembly was securely welded to the impact surface.

2.12.3.3 Test Unit Configuration

The certification test articles were essentially prototypic, half-scale models of the BRR package impact limiters. Three test articles were fabricated using drawings which were in compliance with the drawings in Section 1.3.3, *Packaging General Arrangement Drawings*, except for the differences enumerated and justified below.

BRR Package Safety Analysis Report

The dummy cask was a steel cylinder which represented the BRR cask in half-scale. It consisted of a thick-walled carbon steel outer cylinder, having an outer diameter of 19 inches and an inner diameter of 12.3 inches. The inner cavity was occupied by a lead-filled pipe. The cask impact limiter attachments were prototypic and made of Type 304 stainless steel. The cask attachments were welded to stainless steel plates which were embedded in the surface of the dummy cask, thus ensuring that the entire impact limiter attachment load path was fully prototypic. The weights of the dummy cask and impact limiters are given in Table 2.12.3-1.

The following list summarizes the differences between the test articles and the full-scale production impact limiters:

1. The half-scale impact limiters had no lifting features, which consist of threaded lifting bosses located in the end sheet of the upper limiter. This omission had no effect on the test results.
2. The half-scale impact limiters had no paint. This omission had no effect on the test results.
3. The dummy cask, which modeled the cask, shield plug, closure lid, and maximum contents, weighed 3,181 lb. In full-scale, that weight would be eight times larger, or 25,448 lb. This is approximately 7% less than the estimated upper bound weight of the full-scale cask body, less impact limiters, of 27,400 lb. This difference is not significant.
4. Subsequent to testing, the impact limiter corner joint between the top surface and the cylindrical outer shell has been revised. This change came about as a result of the tests documented in Section 2.12.3.5.4, *Repeated Oblique Slapdown Free Drop Test D2R* and Section 2.12.3.5.8, *Puncture Drop Test P5*. In the secondary slapdown impact of free drop D2R, and exacerbated in the subsequent puncture drop P5, the outer shell seam split open, exposing the polyurethane foam. To prevent this seam failure from recurring, the outer shell joint has been redesigned to include two lap joints on the corner angle. The 'from' and 'to' configuration of the outer shell joint is shown in Figure 2.12.3-3. Since the outer joint can no longer be used as a final closure joint of the impact limiter shell during fabrication, a new seam has been introduced near the inner shell, as shown in Figure 2.12.3-4. Since the redesigned corner joint is stronger than the tested design, the change is conservative.
5. Subsequent to testing, the full-scale inner diameter of the impact limiter was reduced from 38.5 inches to 38.25 inches, which reduces the diametral clearance between the impact limiter and the cask OD from 0.5 inches to 0.25 inches. This change has the effect of reducing the attachment loads, since it will more closely couple the impact limiter to the cask. Thus the change is conservative.
6. The impact limiter attachment ball-lock pins used in testing were made of carbon steel. The full-scale production pins will be made of stainless steel. Since the stainless steel pins have a higher rated load than the carbon steel pins, this difference is conservative.
7. Subsequent to testing, the impact limiter attachment to the cask has been increased in size. This change came about as a result of the tests documented in Section 2.12.3.5.3, *Oblique Slapdown Free Drop Test D2* and Section 2.12.3.5.4, *Repeated Oblique Slapdown Free Drop Test D2R*. In the oblique slapdown drops D2 and D2R, a majority of the attachments of the primary impact limiter failed. To prevent this failure from recurring, the attachments have been increased in size and in quantity. The detail of the change, and the result of a confirmatory retest, are documented in Section 2.12.3.6, *Confirmatory Test of Attachments*.

2.12.3.4 Instrumentation

2.12.3.4.1 Accelerometers

Accelerometers were used to record the impact of each free drop, except drop D2C, which was a confirmatory test for the revised impact limiter attachments. Accelerations of the puncture drops were not recorded. For axial or near-axial drop orientations (D1 – end drop, and D3 – c.g.-over-corner drop), the measurement axis of the accelerometers was axial. For the near-horizontal, 15° slapdown drops (D2 and D2R), the measurement axis was transverse to the cask axis.

Four axial and four transverse mounting positions were provided at each end of the cask. The measurement axes were as close to the cask surface as possible, and the mounting blocks were rigidly welded to the cask. The transverse measurement axis was located 8.68 inches from the flat end of the cask. The mounting location and orientation of each accelerometer is shown in Figure 2.12.3-5 and Figure 2.12.3-6. The transverse accelerometers at each end were all mounted on the same axial plane with their axes parallel.

The raw data was conditioned and low-pass filtered at a level of 1019 Hz. As shown in Section 2.12.3.7, *Accelerometer Plots*, the filtered accelerometer time histories retain a significant vibrational component, indicating that a lower filter cutoff frequency could have been used, which would have lowered the peak values. The rigid body peak accelerations (i.e., without a vibrational component) are estimated by observation of the accelerometer time histories and are shown in Table 2.12.3-6 in Section 2.12.3.7, *Accelerometer Plots*.

The (1019 Hz) filtered peak acceleration values are adjusted using the accelerometer calibration constants listed in Table 2.12.3-5 below. The calibration constants were not entered into the signal conditioner, and therefore are applied manually only to the peak value of the accelerometer output, as shown in Section 2.12.3.5, and not to the entire output. Thus, the filtered accelerometer plots, in Section 2.12.3.7, do not show the effect of this adjustment. Since the calibration constants are all between 0.89 and 0.97 mV/g, the adjusted peak acceleration value is approximately 10% higher than the peak value shown on the plots in Section 2.12.3.7. Individual results are discussed in Section 2.12.3.5.

2.12.3.4.2 Thermocouples

A refrigerated trailer was present onsite to chill the certification test articles prior to assembly onto the dummy cask for testing. Thermocouples were inserted in 1/8-inch diameter holes in each test article, five inches deep, and approximately 6.75 inches from the flat annulus side of the test article. Two thermocouples were used for each test article, located 180° apart. Since the minimum temperature which could be set on the chiller unit was -20 °F, the test articles were generally between -10 °F and -20 °F at the time of test. The temperature of the foam in tests D3, P2, P2C, P3, P4, and P5 was not required to be cold. Temperature of the foam was recorded just prior to the test for the impact limiter(s) experiencing impact or puncture.

2.12.3.5 Test Results

Results for the initial series of four, 30-ft free drop tests and five puncture drop tests are given in the sections below. (Results for the confirmatory test of the attachments (tests D2C and P2C) are given in Section 2.12.3.6, *Confirmatory Test of Attachments*.) The tests were performed in the order D1, P1, D2, D2R, P2, D3, P4, P5, P3. A description of the tests is given in Table 2.12.3-2.

Figures of the tests are shown in Figure 2.12.3-1 and Figure 2.12.3-2. Peak accelerations given in tables below are taken from column B, 'From Plots, Calibration Adjusted' of Table 2.12.3-6, in Section 2.12.3.7, *Accelerometer Plots*. The average of the peak values is then resolved to a value which is perpendicular to the ground, when necessary. Since the data was collected orthogonal to the cask axes, the resolution of the data in the oblique impact cases is as follows.

For test D1, which was a vertical end drop, the accelerometers were mounted with their measurement axes parallel to the dummy cask axis. Therefore, the accelerometer readings require no adjustment.

For tests D2 and D2R, which were identical, 15° slapdown free drops, the accelerometers were mounted with their measurement axes transverse to the dummy cask axis. For the secondary impact, in which the cask axis is essentially parallel to the ground, the accelerometer readings require no adjustment. For the primary impact at 15°, the average accelerometer reading is divided by the cosine of the recorded impact angle to obtain the impact which occurred perpendicular to the ground.

For test D3, which was the c.g.-over-corner free drop, the accelerometers were mounted with their measurement axes parallel to the dummy cask axis. The average accelerometer reading is divided by the cosine of 23°, which corresponds to the recorded angle between the cask axis in the c.g.-over-corner drop and the ground, to obtain the impact perpendicular to the ground.

All puncture drop tests were performed from a height of 40 inches above the top of the puncture bar. All puncture tests except P2 and P2C were performed using a 25-inch long puncture bar. Tests P2 and P2C utilized the 50-inch long bar. The puncture bars remained securely attached to the steel drop pad in all cases.

For each test, the recorded temperature of the polyurethane foam was taken as described in Section 2.12.3.4.2, *Thermocouples*. Note that all data reported in this appendix applies to the half-scale test unless stated otherwise. According to the laws of scaling, the full-scale linear measurements are twice those recorded here, and the full-scale accelerations are half of those recorded here. The tests are documented in the order in which they were performed.

2.12.3.5.1 Free Drop, Vertical (D1)

Test D1 was performed using a drop height of 30 feet, oriented with the cask axis vertical, as shown in Figure 2.12.3-1 and Figure 2.12.3-7. The lower impact limiter was serial number 1. The two polyurethane foam temperature readings were -16.4 °F and -15.6 °F. Four accelerometers were used. Results are shown in the table below.

Free Drop Test D1 (End)					
Channel	12	13	14	15	Avg.
Peak Value	110g	121g	113g	118g	116g

The impact deformation was a combination of outside-in and inside-out. The outside-in crush depth is calculated from the diameter of the scuff mark (contact area) on the bottom of the limiter. Two orthogonal diameter measurements showed a scuff diameter of 27-1/2 and 27-5/8 inches, or an average of 27.6 inches. Since the original diameter of the bottom of the impact

limiter was 24.0 inches, and the tapered portion had an angle of 45°, the outside-in crush distance is:

$$(D_{\text{scuff}} - D_{\text{orig}}) / 2 = 1.8 \text{ inches}$$

The inside-out crush distance is calculated from the dimension from the top of the dummy cask (with the upper impact limiter removed) to the outside rim of the lower impact limiter. Since the outside rim of the limiter is undeformed, this measurement will reveal how far the dummy cask has "sunk" into the lower impact limiter. Measurements of this distance, taken in four quadrants, were 29-7/8, 29-7/8, 30-1/2, and 30-7/16 inches. The average value is 30.2 inches. In an undeformed limiter, the top surface of the cask would stand $(38.6 - 6.8) = 31.8$ inches above the outer rim of the lower limiter, given that the cask is 38.6 inches long, and the center pocket of the limiter is 6.8 inches deep. The inside-out crush is therefore $(31.8 - 30.2) = 1.6$ inches. The sum of the outside-in and inside-out crush distances is therefore $1.8 + 1.6 = 3.4$ inches.

The impact limiter was securely attached following the test. Of the six impact limiter attachment pins, one failed by bending and shear, and others showed signs of bending without failure. At least two had no noticeable damage. The shells of the limiter deformed without any tearing or exposure of foam. The post-test configuration is depicted in Figure 2.12.3-8 and Figure 2.12.3-9.

2.12.3.5.2 Puncture Drop Test P1

Puncture test P1 was performed immediately after drop test D1. The test was a c.g.-over-corner impact on the thicker bottom plate of the impact limiter, near the outer edge of the thicker plate, as shown in Figure 2.12.3-2 and Figure 2.12.3-10. The impact took place on the crush damage from free drop test D1, on serial number 1. The angle of the cask axis was $73^\circ \pm 3^\circ$ to the horizontal. The two polyurethane foam temperature readings were -3.8°F and -5.0°F .

The bar impact was located approximately one inch from the outer edge of the thicker bottom plate (i.e., the center of the 3-inch bar was approximately 2-1/2 inches in from the edge). The impact created a dent approximately 1-3/4 inches deep. One or two rebound impacts having negligible deformation also occurred. There were no signs of cracking in the dent or in the nearby weld seam. The post-test configuration is depicted in Figure 2.12.3-11 and Figure 2.12.3-12.

2.12.3.5.3 Oblique Slapdown Free Drop Test D2

Test D2 was performed using a drop height of 30 feet, oriented with the cask axis at 16° to the horizontal, as shown in Figure 2.12.3-1 and Figure 2.12.3-13. The primary (lower) impact limiter was serial number 2, and the secondary (upper) impact limiter was serial number 3. The polyurethane foam temperature reading in the primary limiter was -15.6°F (only one thermocouple was functioning), and in the secondary limiter, the readings were -13.8°F and -16.4°F . Four accelerometers were used at each end. Results are shown in the table below.

The general post-test configuration is shown in Figure 2.12.3-14. Comparing the measurements of the undeformed and deformed impact limiters, as shown in Figure 2.12.3-15, the crush distance, perpendicular to the ground, was 3.9 inches for the primary impact limiter and 4.0 inches for the secondary impact limiter.

Free Drop Test D2 (15° Oblique)					
Channel	16	17	18	19	Avg., Primary End
Peak Value, g	Severed wire	133g	137g	135g	140g \perp to ground*
Channel	12	13	14	15	Avg., Secondary End
Peak Value, g	102g	108g	110g	108g	107g

*Equal to $(133 + 137 + 135)/3/\cos(16^\circ)$.

In the test, all of the attachment pins on the primary impact limiter sheared off. The limiter remained attached to the cask, although after coming to rest, it was displaced approximately 1-1/2 inches at the top, as shown in Figure 2.12.3-16. None of the pins failed on the secondary impact limiter. There was some incipient cracking of the weld seam on the secondary limiter, but the cracks were of insignificant size and no foam was exposed. The impact surfaces of the impact limiters are shown in Figure 2.12.3-17.

2.12.3.5.4 Repeated Oblique Slapdown Free Drop Test D2R

Test D2R was designed as a repeat of test D2, made after increasing the size of the attachment pins from the original diameter of 1/4 inches to 1/2 inches. To accommodate this increase, the hole through the cask attachment lugs was increased to 1/2 inches and the hole in the impact limiter blade was increased to 5/8 inches. The effect of increasing the blade hole size was to reduce the ligament width on both sides of the hole, but especially on the inner side (toward the cask body). These changes were made to all three impact limiter test articles. Due to the small size of these ligaments, the inner ligament width on serial numbers 1 and 3 were enhanced after drilling by application of a Type 308 weld overlay. Serial number 2 ligaments were not enhanced after drilling. The average ligament widths of the three impact limiters are as follows:

- S/N 001: 0.306 inches (weld overlay enhanced)
- S/N 002: 0.243 inches (not welded)
- S/N 003: 0.320 inches (weld overlay enhanced)

The attachment pins were Carr-Lane part no. CL-8-BLPT-2.00, 1/2-inch diameter carbon steel ball lock pins, having a rated load of 16,000 lb, or four times that of the 1/4-inch pins.

Test D2R was performed using a drop height of 30 feet, oriented with the cask axis at 17° to the horizontal, as shown in Figure 2.12.3-1 and Figure 2.12.3-18. The primary (lower) impact limiter was serial number 2, rotated 180° from its orientation in test D2. The secondary (upper) impact limiter was serial number 1. The polyurethane foam temperature readings in the primary limiter were -13.4 °F and -12.8 °F, and in the secondary limiter, the readings were -13.0 °F and -13.4 °F. Four accelerometers were used at each end. Results are shown in the table below.

Free Drop Test D2R (15° Oblique)					
Channel	16	17	18	19	Avg., Primary End
Peak Value, g	111g	116g	106g	106g	115g \perp to ground*
Channel	12	13	14	15	Avg., Secondary End
Peak Value, g	113g	111g	106g	124g	114g

*Equal to $(111 + 116 + 106 + 106)/4/\cos(17^\circ)$.

The general post-test configuration is shown in Figure 2.12.3-19. Comparing the measurements of the undeformed and deformed impact limiters, as shown in Figure 2.12.3-20, the crush distance, perpendicular to the ground, was 4.0 inches for the primary impact limiter and 3.9 inches for the secondary impact limiter. Note that the measurements of the crush in test D2 are very similar to these (3.9 inches primary and 4.0 inches secondary). This is to be expected since the tests are essentially identical. However, since test D2 showed the apparent anomaly of the primary impact being significantly higher than the secondary impact (the opposite would be expected), then test D2R will be taken as the official crush results for this orientation.

In the test, none of the attachment pins failed, but four out of six of the blades of the primary limiter failed by tensile failure of the inner ligaments, as shown in Figure 2.12.3-21. The limiter remained attached to the cask, although after coming to rest, it was displaced approximately 2 inches at the top, as shown in Figure 2.12.3-19. None of the pins or ligaments failed on the secondary impact limiter, although the holes were elongated up to 0.854 inches.

In addition, the corner joint between the top annular plate and the outer cylindrical shell of the secondary impact limiter (serial number 1) failed in the impact region, as shown in Figure 2.12.3-22. This limiter had been tested in the 30-foot end drop (D1) and the subsequent puncture (P1), and the torn joint may have been the result of over-testing. The tear had a maximum opening of 1/2 inches. It appeared to start at the outer edges of the impact zone and travel inward. The length of the torn joint on one side was 7-1/2 inches, and on the other side 10-1/4 inches, with approximately 4-3/4 inches of sound material in the center. The tear appeared in both the weld as well as in the leg of the corner angle located on the top surface. However, the tear did not occur in the outer cylindrical shell side of the joint, where the thickness is double by virtue of the lap joint used in that position.

2.12.3.5.5 Puncture Drop Test P2

Puncture test P2 was performed immediately after drop test D2R. The longer puncture bar was used to impact the top annular surface of the damaged primary impact limiter (serial number 2), as shown in Figure 2.12.3-2 and Figure 2.12.3-23. The orientation could not be over the center of gravity due to the desired impact location. The impact occurred just to the inside of the bulge, in approximately the radial center of the annular plate. The two polyurethane foam temperature readings were -0.2 °F and -3.0 °F.

The impact dent on the annular plate was negligible, but the impact limiter became significantly dislodged from the cask end due to the failure of the impact limiter attachment blades, as shown in Figure 2.12.3-24. By inspection of the conventional-speed video record, the impact limiter was displaced by a greater amount than is shown in the figure, before it was driven partially back on by a secondary impact with the safety wall.

2.12.3.5.6 CG-Over-Corner Free Drop Test D3

Test D3 was performed from a drop height of 30 feet, with the cask axis oriented at 67° to the horizontal, or essentially center of gravity over corner, as shown in Figure 2.12.3-1 and Figure 2.12.3-25. The lower impact limiter was serial number 3, rotated 180° from its orientation in test D2. The polyurethane foam temperature reading in the lower limiter was -2.2 °F (the other thermocouple was not functioning). Four accelerometers were used at each end, oriented parallel

to the cask axis. Results are shown in the table below. Note, since channels 16 – 17 exhibited excess noise, only channels 12 – 15 are used.

Free Drop Test D3 (CG Over Corner)					
Channel	12	13	14	15	Avg.
Peak Value, g	106g	111g	110g	103g	117g \pm to ground*

*Equal to $(106 + 111 + 110 + 103)/4/\cos(23^\circ)$.

The general post-test configuration is shown in Figure 2.12.3-26. Comparing the measurements of the undeformed and deformed impact limiters, as shown in Figure 2.12.3-27, the crush distance perpendicular to the ground was 5.5 inches.

None of the pins or ligaments failed the test, although the holes were elongated up to 0.725 inches. There were no shell failures and no exposure of foam.

2.12.3.5.7 Puncture Drop Test P4

Puncture test P4 was performed on the damage incurred in free drop test D3, on serial number 3. The bar impacted just outside the thicker bottom plate, on the 0.12-inch thick material which once constituted the tapered region of the shell. The orientation is shown in Figure 2.12.3-2 and Figure 2.12.3-28. The cask axis was oriented at 74° to the horizontal. The line of action was nearly, but not completely, c.g.-over-corner. The polyurethane foam temperature readings in the lower limiter were 17.6°F and 5.0°F .

As expected, the puncture bar penetrated the shell, and entered the foam to a depth of 2-1/4 inches. The width of the hole was 4 inches, and the length of the hole/torn flap was 5 inches. The impact limiter attachments were not affected. A close-up view of the damage is shown in Figure 2.12.3-29.

2.12.3.5.8 Puncture Drop Test P5

Puncture test P5 was performed on the damaged corner joint created in free drop test D2R on serial number 1 (the secondary impact end). The orientation is shown in Figure 2.12.3-2 and Figure 2.12.3-30. The puncture bar was oriented at approximately 45° to the package axis, and contacted a fold which was adjacent to the damaged corner joint. Since the test was carried out shortly after puncture test P4, the polyurethane foam temperature is considered to be essentially the same as that recorded for test P4.

The bar caught the fold and tore the damaged joint open as shown in Figure 2.12.3-31 and Figure 2.12.3-32. The total length of the damage, measured as a chord, was approximately 26 inches. At the location of the bar (i.e., the center of the damage), the width was 5 inches. On either side the width of the opening was approximately 2-1/2 inches, tapering to zero at the ends. Only negligible amounts of foam were lost from the shells as shown in Figure 2.12.3-32.

2.12.3.5.9 Puncture Drop Test P3

Puncture test P3 was performed on the secondary slapdown damage incurred by serial number 3 in free drop test D2. The orientation is shown in Figure 2.12.3-2 and Figure 2.12.3-33. The bar struck the damaged area approximately in the center. The cask axis was at a small angle to the

horizontal. Since the test was carried out shortly after puncture tests P4 and P5, the polyurethane foam temperature is considered to be essentially the same as that recorded for test P4.

The depth of the impact dent was approximately one inch. There was no sign of cracking or tearing of the impact limiter shell, as shown in Figure 2.12.3-34.

2.12.3.6 Confirmatory Test of Attachments

The confirmatory tests were performed on February 17, 2009 at Hiline, in order to demonstrate the adequacy of the redesigned impact limiter attachments. The test used the existing dummy cask and impact limiters, which had been altered to enhance the strength of the attachments. The revisions made to the test articles resulted in attachments which, in full-scale, were not stronger than the attachment design used on the production hardware.

None of the other tests will be invalidated by the increase in the strength of the attachments. In all of the other tests, the attachments did not fail, therefore, making the attachments stronger had no effect on the prior tests.

The tests that were selected to demonstrate the attachments were the D2 free drop and P2 puncture drop configurations. The D2 drop was chosen since that is the orientation in which the primary impact limiter attachments consistently failed. Attachment failures did not occur in any other impacts. The P2 puncture was chosen since a) a puncture subsequent to free drop is required by 10 CFR 71, and b) it is the puncture test that places the greatest load on the attachments. The test article having the greatest remaining capacity for an additional impact was serial no. 2, which was the primary limiter in tests D2 and D2R. The secondary limiter in the confirmatory tests was serial no. 3, which was less damaged than serial no. 1. The confirmatory tests were designated D2C and P2C.

Prior damage required that the CTU be rotated 90° about its axis. Since the attachment pattern has only one plane of symmetry, this meant that instead of one worst-case loaded attachment at 12 o'clock (relative to the impact at 6 o'clock), there were two attachments at approximately 11 and 1 o'clock, which were loaded somewhat less than in the prior drops. However, since the production redesign now features eight attachments, the load developed in each of the two maximum-loaded attachments in this test was greater than the maximum load which would develop in the production design.

2.12.3.6.1 Description of Design Changes

The configuration of the attachments was increased in capacity as much as possible given the limitations of the existing hardware. In no case did the revised test hardware have a greater strength than the revised full-scale design. A detailed comparison of the test configuration and the full-scale design is given in Section 2.7.1.7, *Impact Limiter Attachments*. The revised CTU attachment is depicted in Figure 2.12.3-35. The nominal thickness of the blades, made of ASTM Type 304 material, was 3/8 inches. The width of the blades was increased to 1.5 inches, and their inner edge was set at 1/8 inches from the inner diameter of the impact limiter. The new blades were attached to the original blade roots using a full penetration weld, and the region between the top surface of the limiter and the new blade (approximately 1/2-inches) was buttered with weld metal to approximately the dimensions of the new blade. The hole in the blade was match-drilled from the existing hole in the cask attachments, and drilled out to 9/16 inches in diameter. The thickness, width, hole diameter, and hole-to-inner edge dimension for each blade

before testing are given in Table 2.12.3-3. Serial no. 2 was mated with end A of the dummy cask, at the existing orientation marks.

Since the secondary impact limiter attachments did not fail in either prior slapdown drop, the refurbishment to serial no. 3 was minimal. The existing 3/16-inch thick blade was cut off and replaced with the same thickness material by a full penetration weld, match drilled to the existing holes on cask end B, and drilled out to 9/16-inch diameter. Both limiters were attached using 1/2 inch diameter carbon steel ball lock pins (the same specification as used in test D2R).

Since the test articles had both received two prior 30-ft drop impacts, and since good data was collected in the same orientation in tests D2 and D2R, test D2C was not instrumented with accelerometers. Both impact limiters were cold for the free drop test. Foam temperature was not recorded for the secondary limiter since the purpose of this test was not related to the secondary impact event.

2.12.3.6.2 Oblique Slapdown Free Drop Test D2C Results

Test D2C was performed using a drop height of 30 feet, oriented with the cask axis at 17° to the horizontal, as shown in Figure 2.12.3-1 and Figure 2.12.3-36. The primary (lower) impact limiter was serial no. 2, and the secondary (upper) impact limiter was serial no. 3. The polyurethane foam temperature readings in the primary limiter were -8.8 °F and -5.6 °F. The primary limiter was oriented so that blade nos. 5 and 6 were directly opposite the impact, where experience showed that the attachment loads are the highest.

The crush deformations were very similar to those obtained in tests D2 and D2R on the same limiter. All of the attachments, both primary and secondary, remained completely intact. Figure 2.12.3-37 and Figure 2.12.3-38 show the post-test configuration of the two most highly loaded attachments, at locations #5 and #6, respectively. All welds attaching the blades to the impact limiter appeared in good condition without failure. The attachments were examined in further detail following the puncture test.

2.12.3.6.3 Puncture Drop P2C Results

Puncture test P2C was performed immediately after drop test D2C. The longer puncture bar was used to impact the top annular surface of the damaged primary impact limiter (serial no. 2), as shown in Figure 2.12.3-2 and Figure 2.12.3-39. The orientation could not be over the center of gravity due to the desired impact location. The impact occurred adjacent to the outside edge of the limiter, halfway between attachment locations #5 and #6, thus maximizing the moment arm and loading of those attachments. The polyurethane foam temperature reading closest to the impact was lower than -3.0 °F.

The impact caused the long puncture bar to bend somewhat, but the attachment to the steel drop pad plate remained intact. The impact dent on the annular plate was negligible, without any cracking or tearing of the steel shell, and no exposure of foam. The attachments all appeared to be in good shape following the test. Figure 2.12.3-40 shows the impact dent and the attachment at location #5.

2.12.3.6.4 Examination of Attachments

After removal of the impact limiters from the dummy cask, the attachments were examined in detail. There was very little evidence of plastic deformation in the attachments, except that the holes of the most highly loaded blades were very slightly elongated. There was no evidence of bearing yielding in the hole, and no evidence of bending or cracking in the attachment pins. There was no evidence of weld cracking or deformation, except in one case, part of the weld between the blade and the annular sheet showed some shear. This was due to deformation of the annular plate in the puncture test, and this weld has no role in the impact limiter attachment load path. Table 2.12.3-4 shows the measurements of the blade after test. Comparing Table 2.12.3-3 and Table 2.12.3-4, the largest increase in the hole dimension (measured in-line with the attachment loading direction, parallel to the cask axis) was 0.034 inches for blade no. 5, which is negligible. A comparison of the hole-to-edge dimension indicates that this distance appeared to increase slightly in several cases (ranging between a 0.016-inch decrease in width to a 0.010-inch increase), but as this goes against reason, it is assumed to be caused by measuring error on the rough surfaces. Figure 2.12.3-41 shows the blade configuration at location #5, and Figure 2.12.3-42 shows location #6, after all testing. Figure 2.12.3-43 shows a view of all of the pins used to retain the primary impact limiter. These photographs demonstrate that the attachments were essentially unchanged by the test loads.

The cask receptacle plate holes were somewhat elongated from prior testing (they were not refurbished). After the tests, the holes did not appear to have deteriorated any further.

BRR Package Safety Analysis Report

Table 2.12.3-1 - CTU Weights

Component	Weight, lb
Dummy Cask	3,181
Impact Limiter Serial No. 1	278
Impact Limiter Serial No. 2	276
Impact Limiter Serial No. 3	276

Table 2.12.3-2 - Summary of Certification Tests

No.	Test Description	Test Limiter	Temperature
D1	End drop	#1	Cold per Section 4.3
D2	Slapdown oblique drop, 15°	#2 & #3	Cold per Section 4.3
D2R	Slapdown oblique drop, 15°	#2 & #1	Cold per Section 4.3
D2C	Slapdown oblique drop, 15°	#2 & #3	Cold per Section 4.3
D3	C.G.-over-corner drop	#3	Not controlled
P1	Oblique through c.g. on thicker end plate on test D1 damage	#1	Cold per Section 4.3
P2	Approx. parallel to package axis, on test D2 primary-end damage	#2	Not controlled
P2C	Approx. parallel to package axis, on test D2C primary-end damage	#2	Not controlled
P3	Approx. perpendicular to package axis, on test D2 primary-end damage	#2	Not controlled
P4	On test D3 damage, on thick/thin joint, near c.g.	#3	Not controlled
P5	Oblique to package axis, on test D3 secondary-end damage	#3	Not controlled

Notes:

1. All free drops (Dx) are from 30 feet, and all punctures (Px) are from 40 inches.
2. Figures of each orientation are provided in Figure 2.12.3-1 and Figure 2.12.3-2.
3. See Section 2.12.3.6, *Confirmatory Test of Attachments*, for a description of tests D2C and P2C.

Table 2.12.3-3 - Attachment Pretest Data (Serial No. 2 Before D2C), inches

No.	Blade Thick	Blade Width	Hole Dia.	Hole-to-Edge
1	0.376	1.515	0.565	0.376
2	0.375	1.517	0.565	0.353
3	0.375	1.520	0.563	0.375
4	0.377	1.519	0.565	0.471
5	0.376	1.519	0.565	0.420
6	0.377	1.519	0.565	0.396

Table 2.12.3-4 - Attachment Post-test Data (Serial No. 2 After D2C), inches

No.	Hole Axial* Diameter	Hole Lateral** Diameter	Hole-to-Edge
1	0.573	0.567	0.360
2	0.569	0.565	0.354
3	0.568	0.565	0.375
4	0.567	0.566	0.472
5	0.599	0.566	0.430
6	0.585	0.569	0.400

Note: Blade thickness and width were unchanged from the pre-test measurements.

*Parallel to cask axis

**Taken at right angle to axial diameter

Table 2.12.3-5 - Accelerometer Calibration Constants

Accelerometer Channel	Calibration Constant (mV/g)
12	0.935
13	0.926
14	0.930
15	0.941
16	0.916
17	0.889
18	0.905
19	0.973

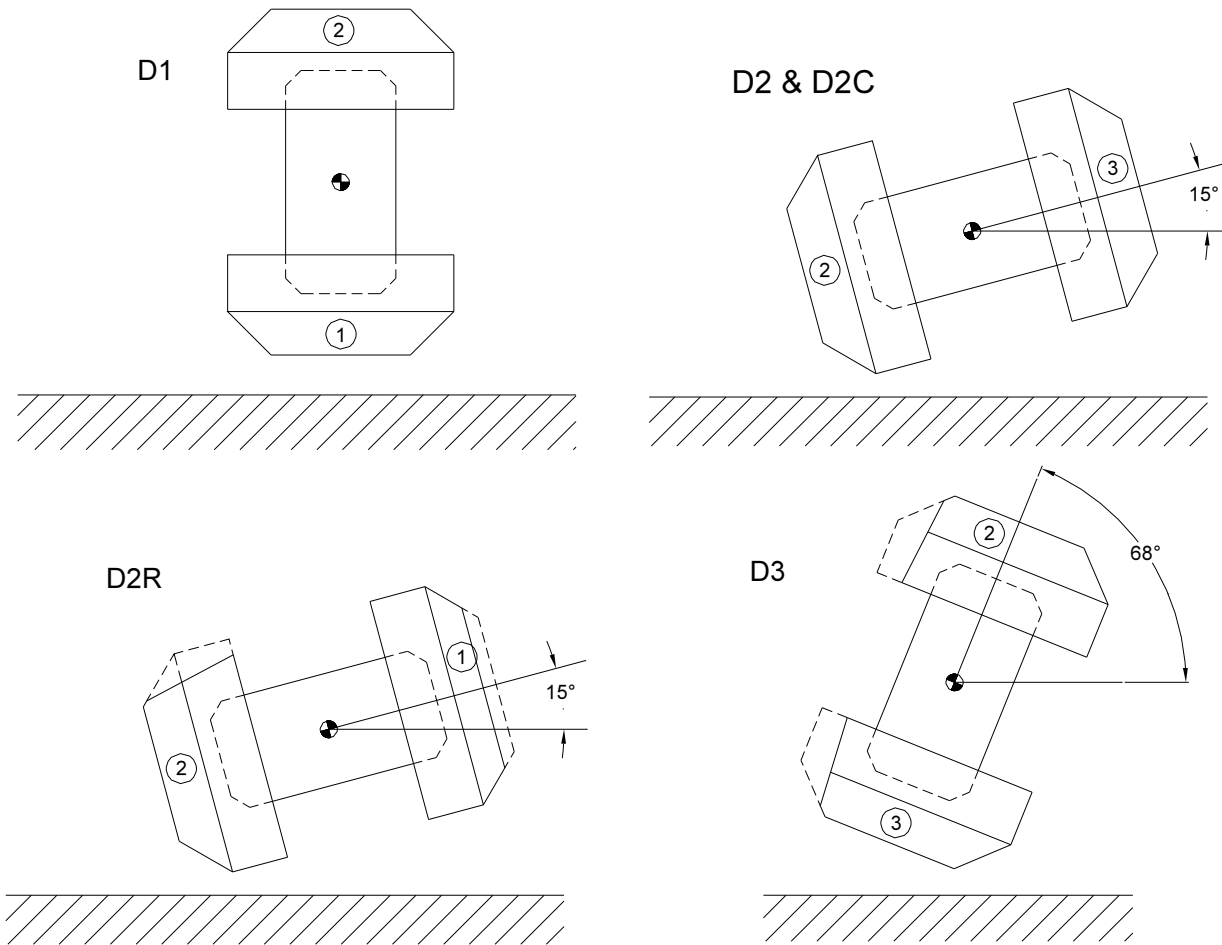


Figure 2.12.3-1 - BRR Package Free Drop Orientations

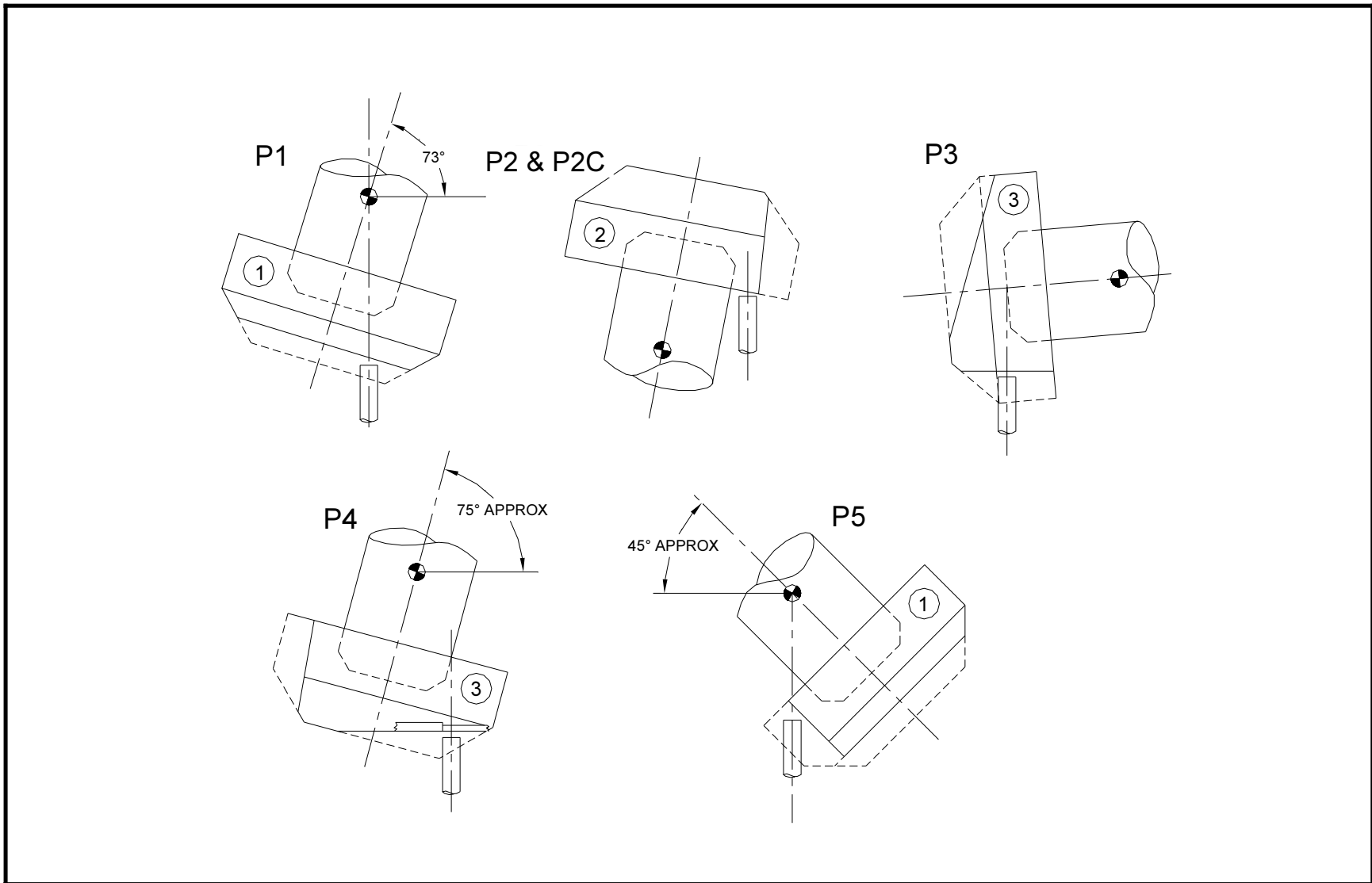


Figure 2.12.3-2 - BRR Package Puncture Drop Orientations

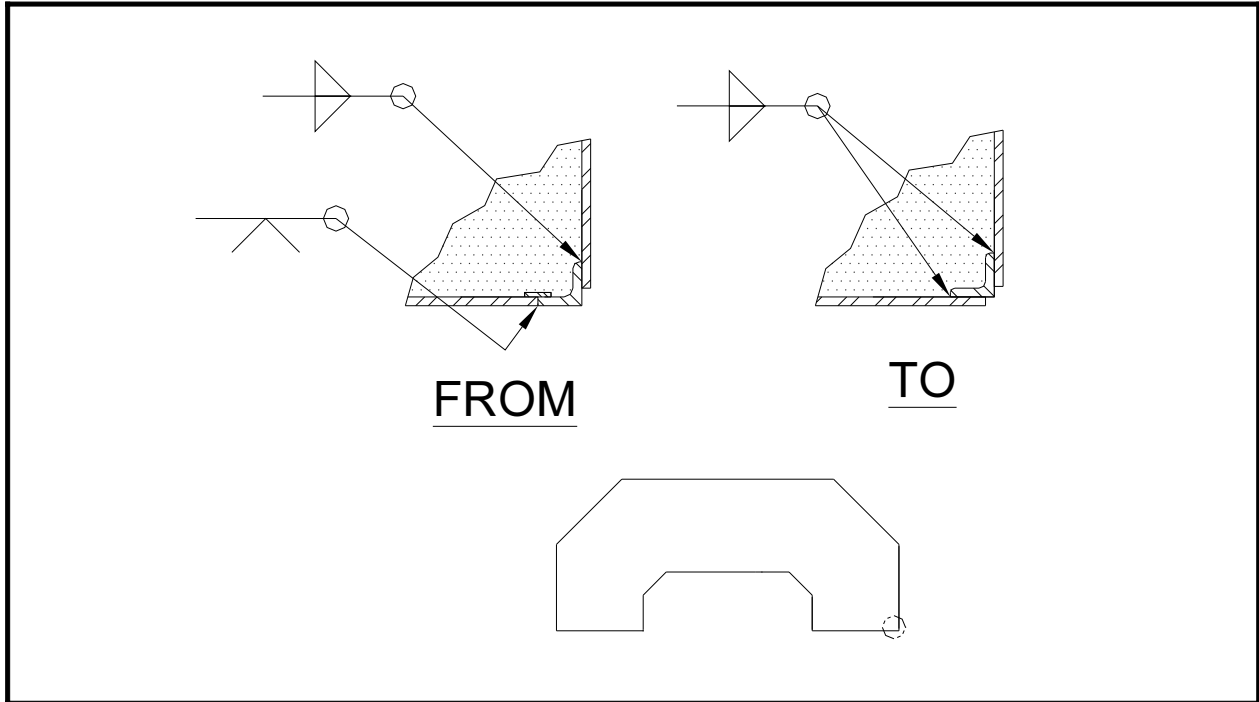


Figure 2.12.3-3 - Change to Outer Impact Limiter Joint

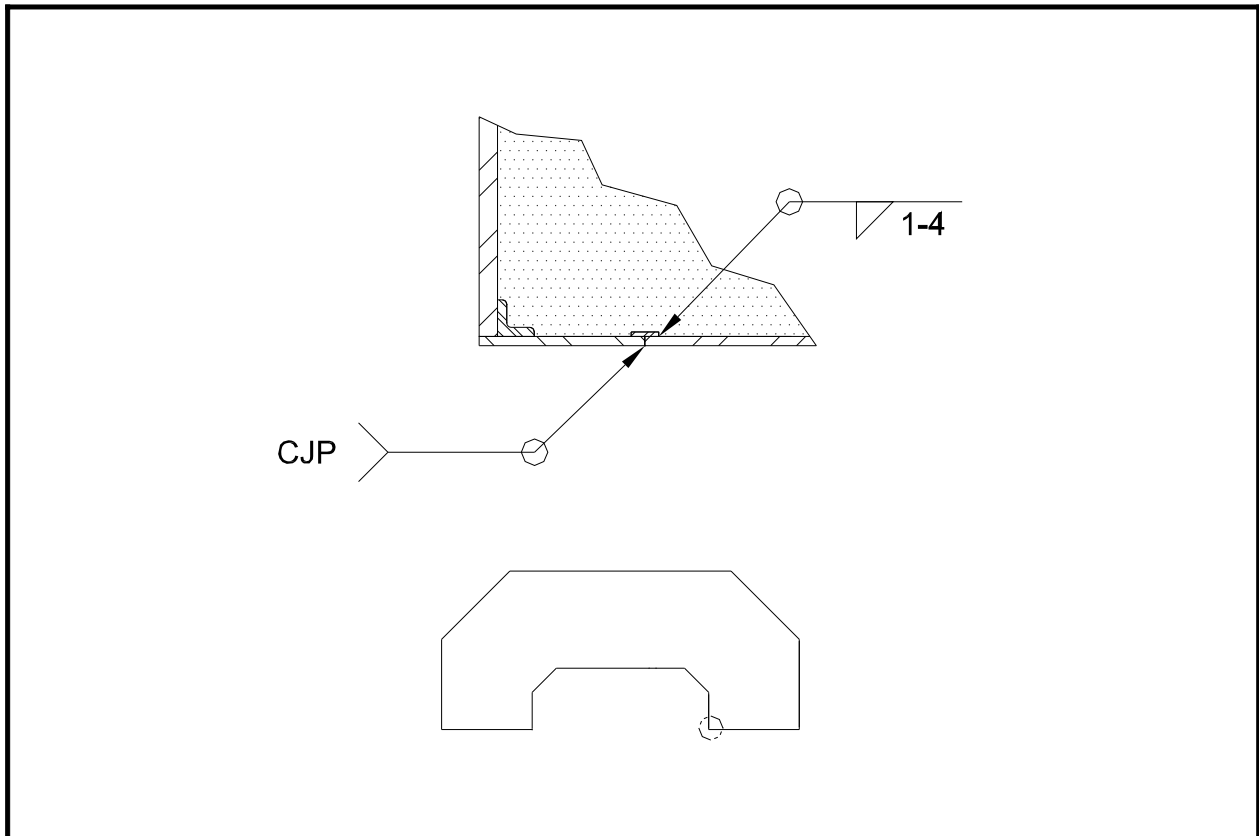


Figure 2.12.3-4 - Added Weld Seam Near Impact Limiter Inner Diameter

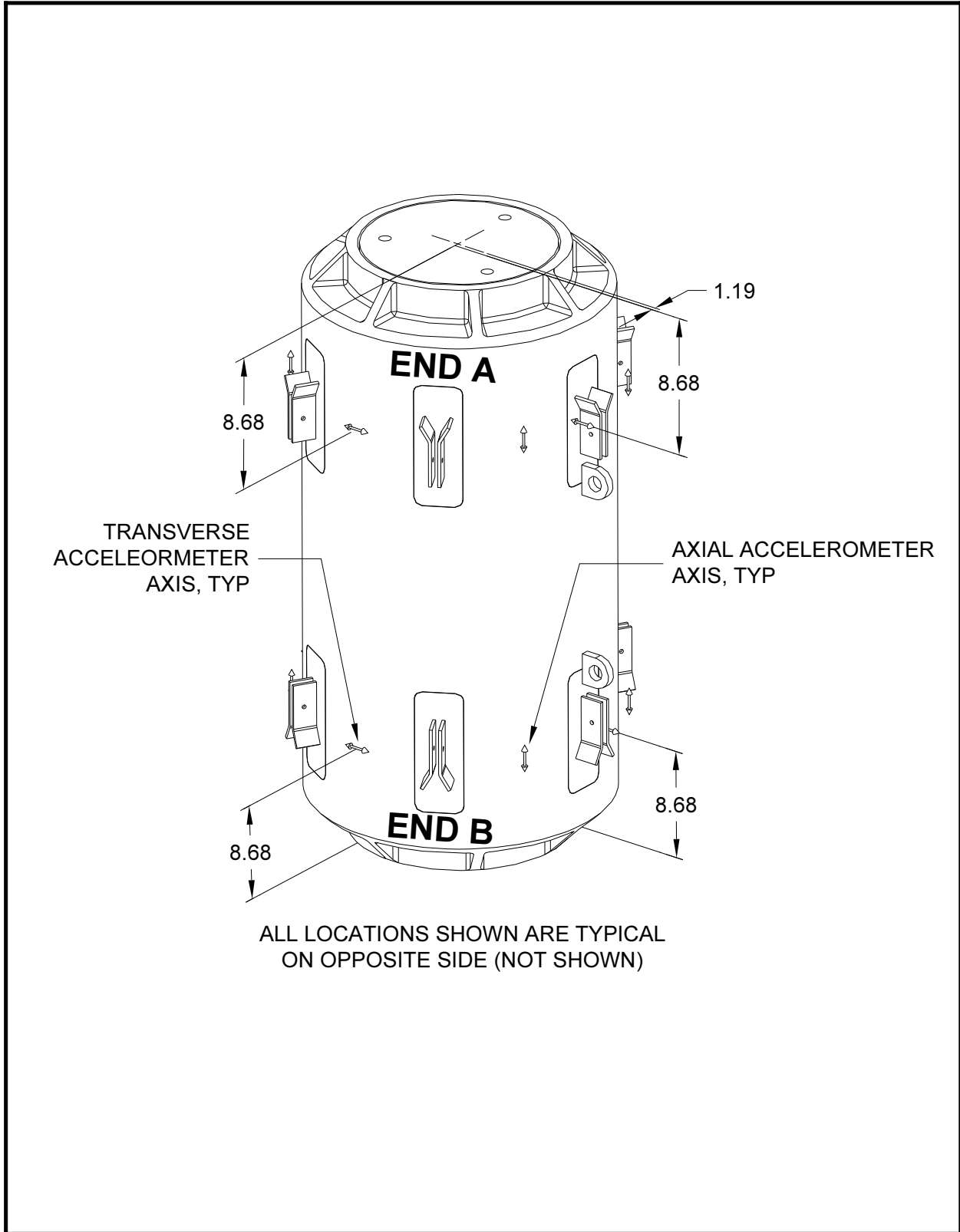


Figure 2.12.3-5 - Accelerometer Mounting

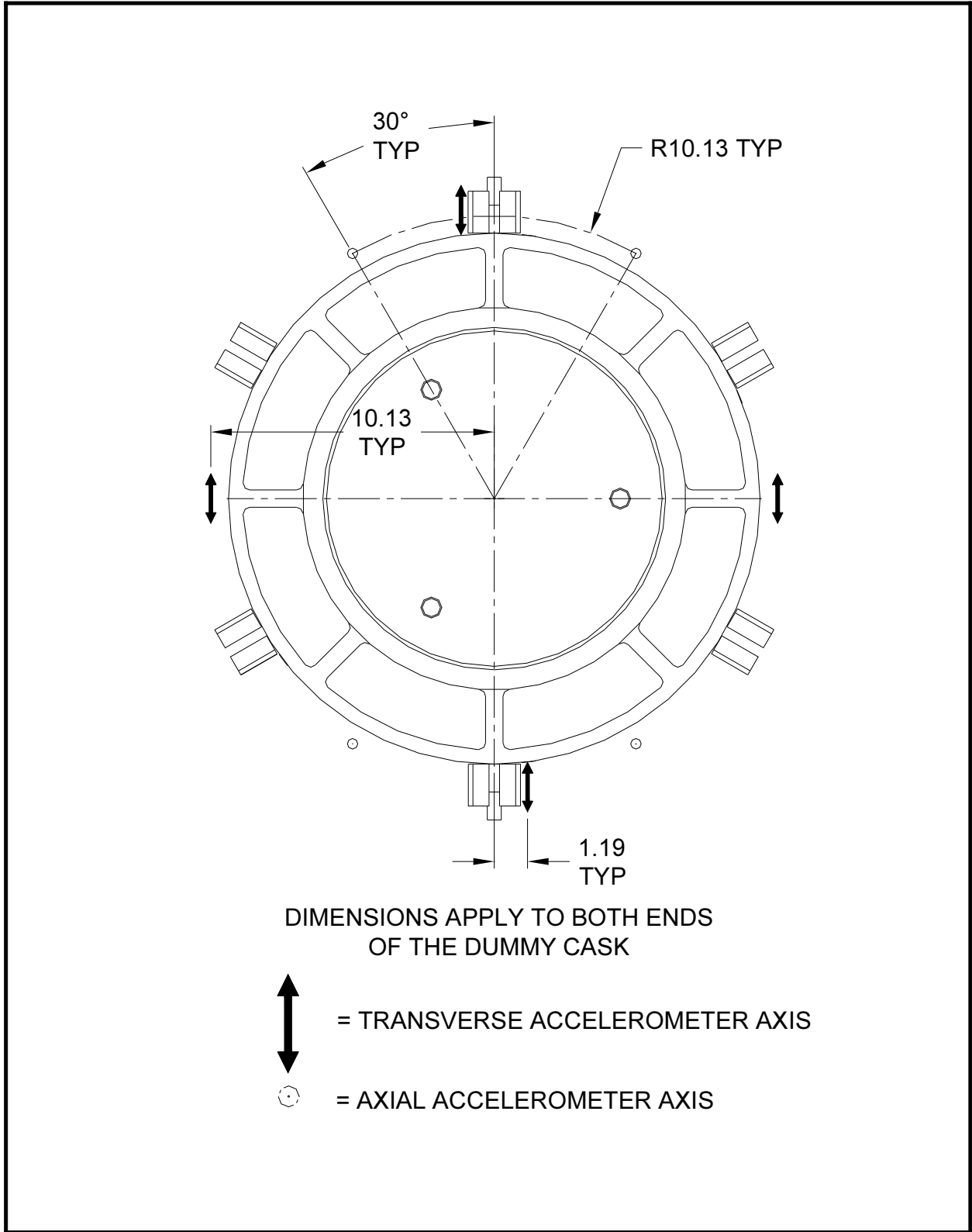


Figure 2.12.3-6 - Accelerometer Mounting, Top View



Figure 2.12.3-7 - Free Drop Test D1 Orientation



Figure 2.12.3-8 - Free Drop Test D1 Inside-Out Deformation



Figure 2.12.3-9 - Free Drop Test D1 Outside-In Deformation



Figure 2.12.3-10 - Puncture Test P1 Orientation



Figure 2.12.3-11 - Puncture Test P1 Deformation



Figure 2.12.3-12 - Puncture Test P1 Deformation – Close-up View



Figure 2.12.3-13 - Free Drop Test D2 Orientation



Figure 2.12.3-14 - Free Drop Test D2 Post-test Configuration

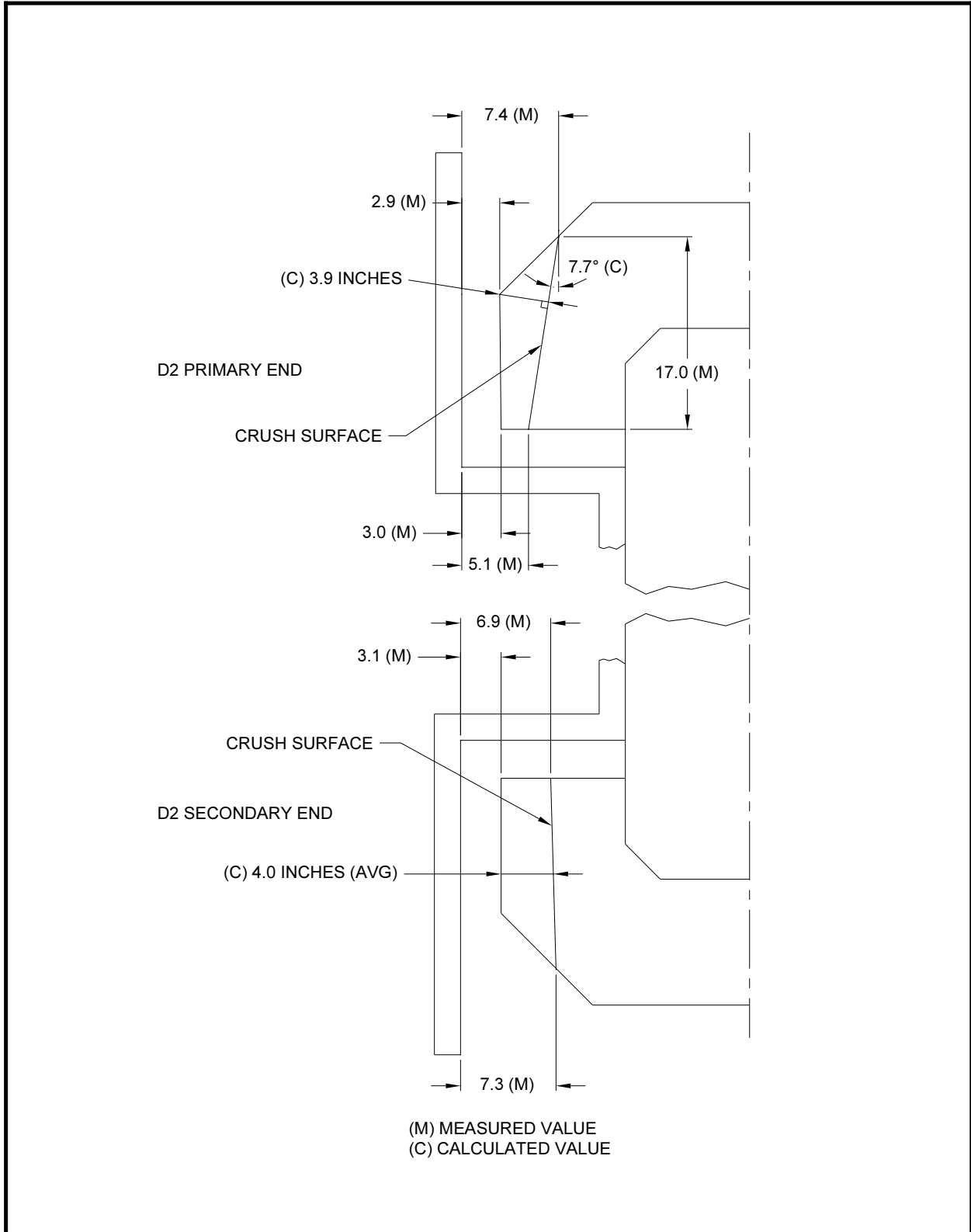


Figure 2.12.3-15 - Free Drop Test D2 Crush Measurements



Figure 2.12.3-16 - Free Drop Test D2, Close-up View of Failed Attachments



Figure 2.12.3-17 - Free Drop Test D2 Impact Deformation Surfaces



Figure 2.12.3-18 - Free Drop Test D2R Orientation



Figure 2.12.3-19 - Free Drop Test D2R Post-test Configuration

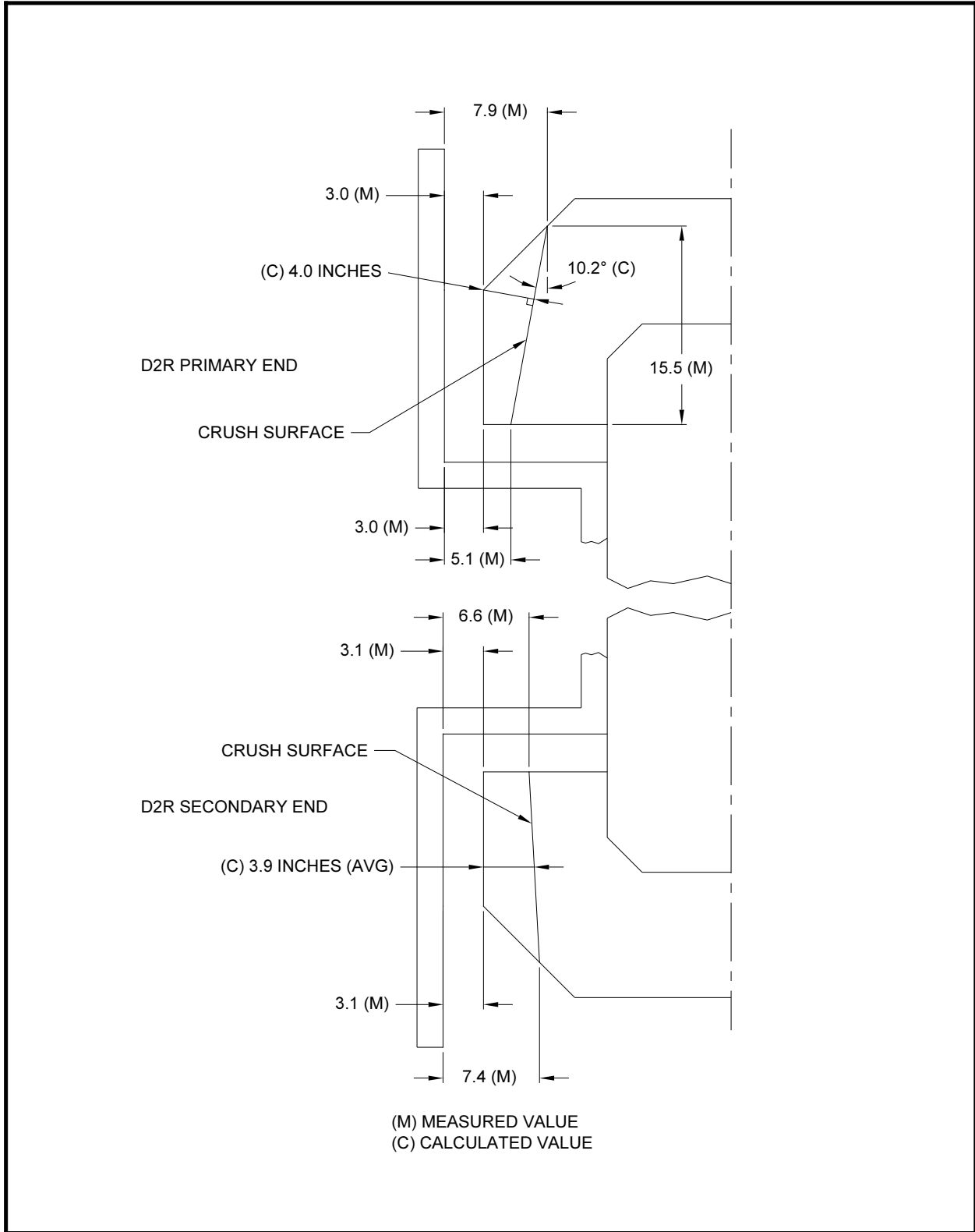


Figure 2.12.3-20 - Free Drop Test D2R Crush Measurements



Figure 2.12.3-21 - Free Drop Test D2R, Close-up View of Failed Attachments



Figure 2.12.3-22 - Free Drop Test D2R, View of Torn Corner Joint



Figure 2.12.3-23 - Puncture Test P2 Orientation



Figure 2.12.3-24 - Puncture Test P2 Result



Figure 2.12.3-25 - Free Drop Test D3 Orientation



Figure 2.12.3-26 - Free Drop Test D3 Deformation

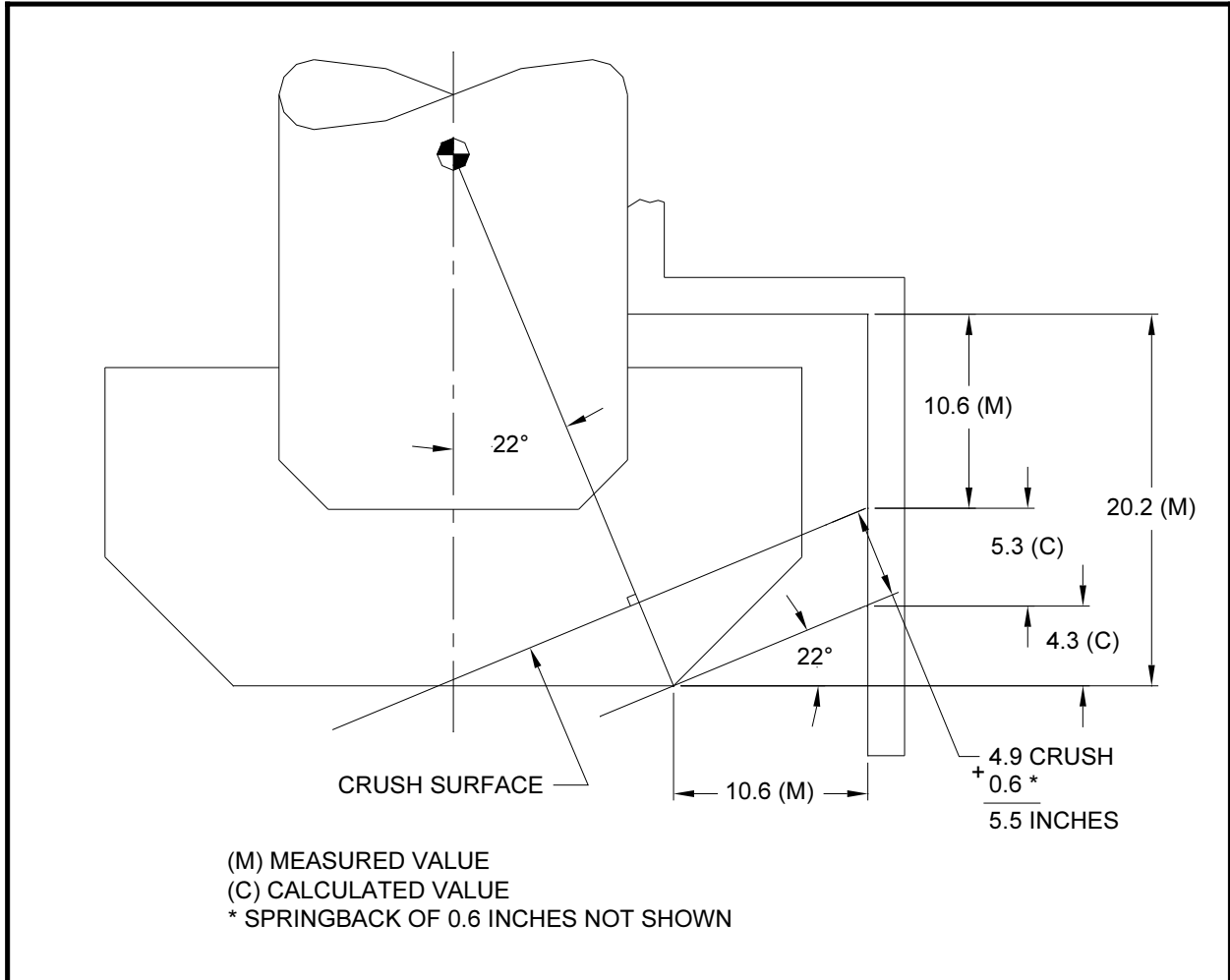


Figure 2.12.3-27 - Free Drop Test D3 Crush Measurements



Figure 2.12.3-28 - Puncture Test P4 Orientation



Figure 2.12.3-29 - Puncture Test P4 Damage



Figure 2.12.3-30 - Puncture Test P5 Orientation



Figure 2.12.3-31 - Puncture Test P5 Damage



Figure 2.12.3-32 - Puncture Test P5 Damage



Figure 2.12.3-33 - Puncture Test P3 Orientation



Figure 2.12.3-34 - Puncture Test P3 Damage

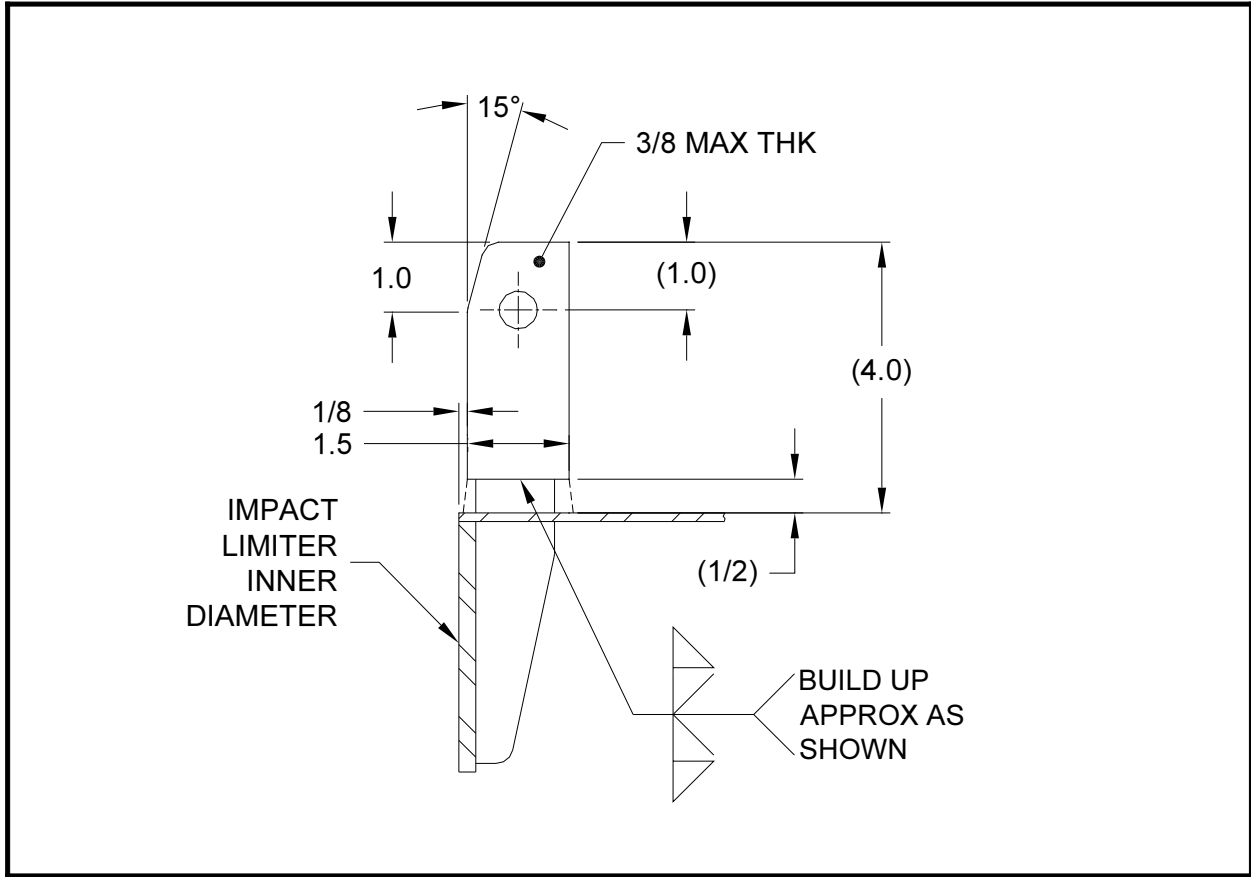


Figure 2.12.3-35 - Revised Half-Scale Attachment Configuration



Figure 2.12.3-36 - Free Drop Test D2C Orientation



Figure 2.12.3-37 - Attachment Location #5 After Free Drop D2C



Figure 2.12.3-38 - Attachment Location #6 After Free Drop D2C



Figure 2.12.3-39 - Puncture Test P2C Orientation



Figure 2.12.3-40 - Puncture Test P2C Result



Figure 2.12.3-41 - Blade Location #5 Post-test Configuration



Figure 2.12.3-42 - Blade Location #6 Post-test Configuration

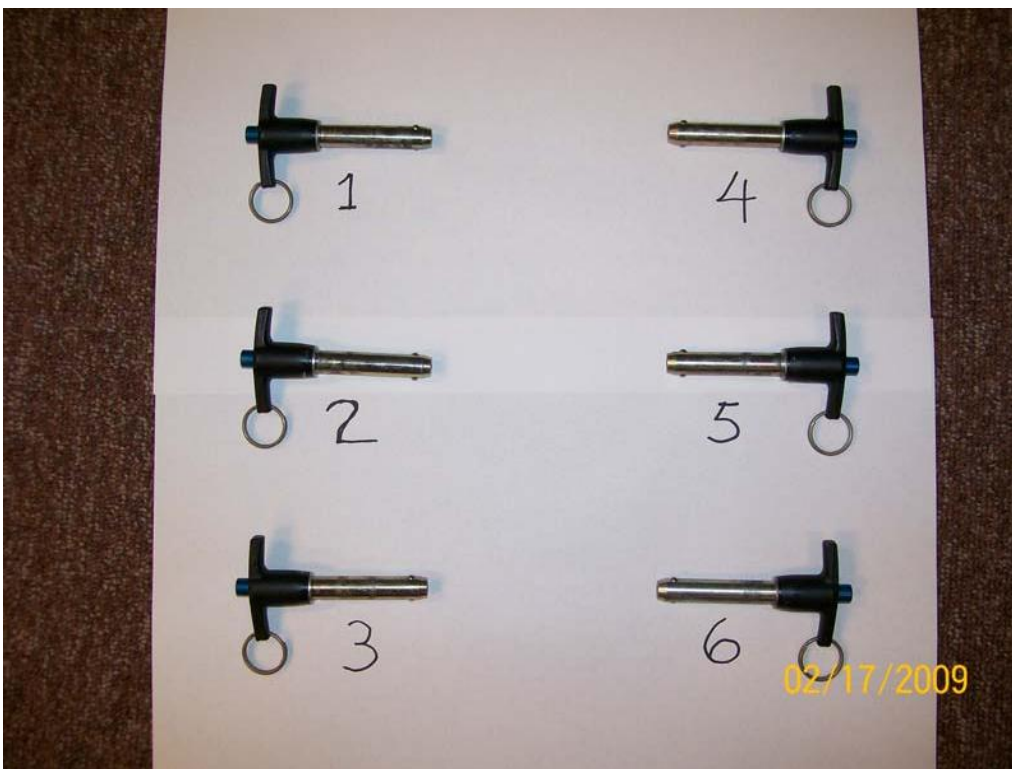


Figure 2.12.3-43 - Primary Impact Limiter Attachment Ball Lock Pins, Post-test

2.12.3.7 Accelerometer Plots

The following figures show the filtered time history accelerometer responses by channel number. Results for all instrumented tests (D1, D2, D2R, and D3) are given. Test D1 used two accelerometers at each end; all other tests used four at each end. For the slapdown cases (D2 and D2R), channels 12 – 15 were located at the secondary end, and channels 16 – 19 were located at the primary end. The time histories in these plots are the result of filtering the accelerometer outputs at 1019Hz. They are not adjusted for the accelerometer calibration constants.

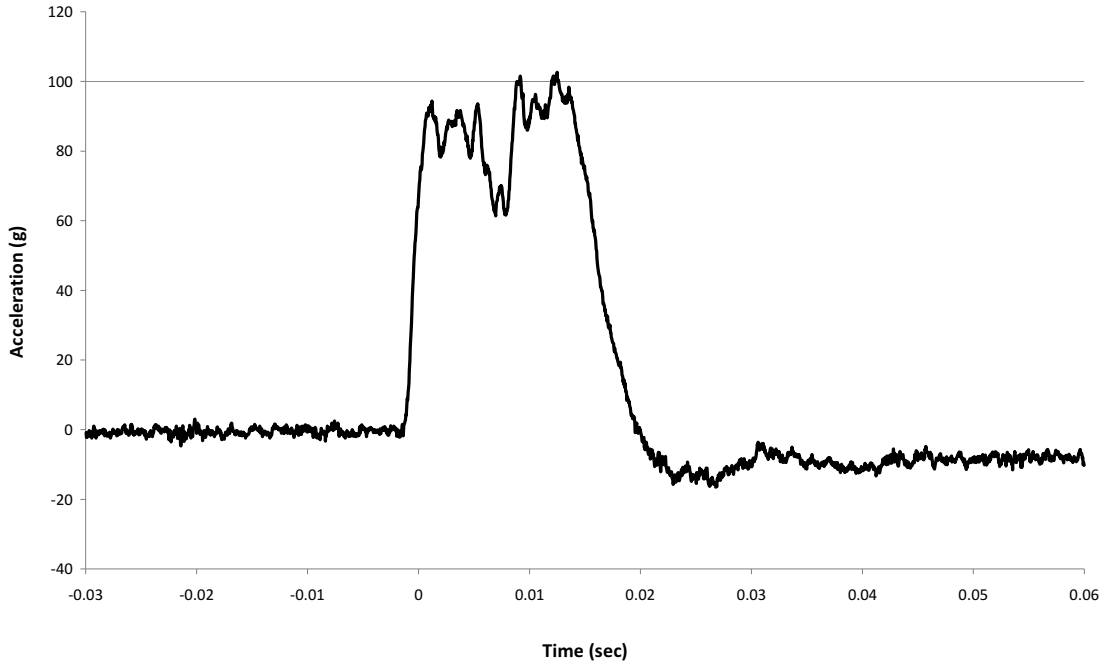
Table 2.12.3-6 (on the following page) lists the estimated rigid body peak accelerations obtained from the plots. Notes for Table 2.12.3-6:

1. The 'Peak From Plots' (column A) is the peak value taken directly off of the following acceleration time histories. For example, for test D1, channel 12, the peak value is 103g.
2. The 'From Plots, Calibration Adjusted' (column B) is found by dividing the 'Peak From Plots' data by the accelerometer calibration constant found in Table 2.12.3-5. For channel 12, the constant is 0.935. Therefore the adjusted peak value of the example is $103/0.935 = 110g$.
3. The 'Estimated Rigid Body Peak' (column C) is made by inspection of the corresponding accelerometer output plot. For the example case, the estimated rigid body peak is 95g.
4. The 'Rigid Body, Calibration Adjusted' (column D) is found by dividing the 'Estimated Rigid Body Peak' by the accelerometer calibration adjustment constant as described above. Following the example, $95/0.935 = 102g$.
5. The 'Reduction, ½ Scale' (column E) is the reduction in peak impact which could be credited if the estimated rigid body peak is used instead of the peak from the plot. For the example case, the reduction is 110 (column B) minus 102 (column D) = 8g in half-scale. The average reduction for each set of four accelerometers corresponding to each impact is also given in column E.

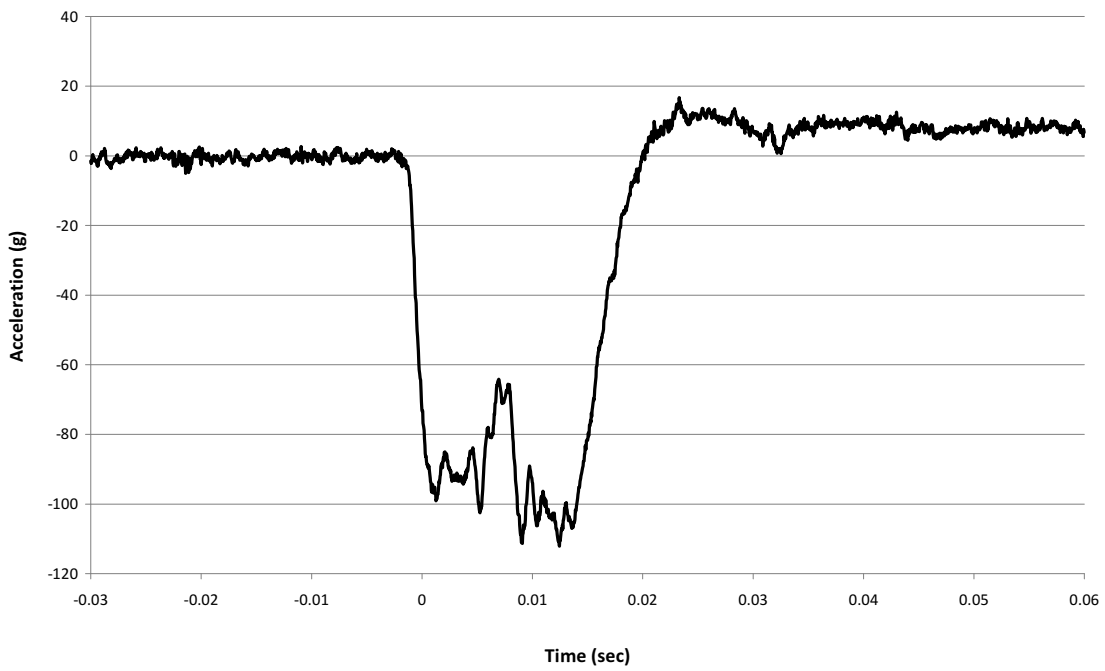
Table 2.12.3-6 – Rigid Body Results Estimates (see notes on previous page)

Test No.	Channel	Peak from Plots, g	From Plots, Calibration Adjusted, g	Estimated Rigid Body Peak, g	Rigid Body, Calibration Adjusted, g	Reduction, ½ Scale, g
		A	B	C	D	E
D1	12	103	110	95	102	8
(Primary)	13	112	121	104	112	9
	14	105	113	101	109	4
	15	111	118	105	112	6
Avg.						7
D2	12	95	102	91	97	5
(Secondary)	13	100	108	97	105	3
	14	102	110	100	108	2
	15	102	108	97	103	5
Avg.						4
D2	16	Severed wire	---	---	---	---
(Primary)	17	118	133	106	119	14
	18	124	137	110	122	15
	19	131	135	116	119	16
Avg.						15
D2R	12	105	113	96	103	10
(Secondary)	13	103	111	97	105	6
	14	99	106	93	100	6
	15	117	124	95	101	23
Avg.						11
D2R	16	102	111	92	100	11
(Primary)	17	103	116	97	109	7
	18	96	106	85	94	12
	19	103	106	90	92	14
Avg.						11
D3	12	99	106	85	91	15
(Primary)	13	103	111	87	94	17
	14	102	110	84	90	20
	15	97	103	85	90	13
Avg.						16

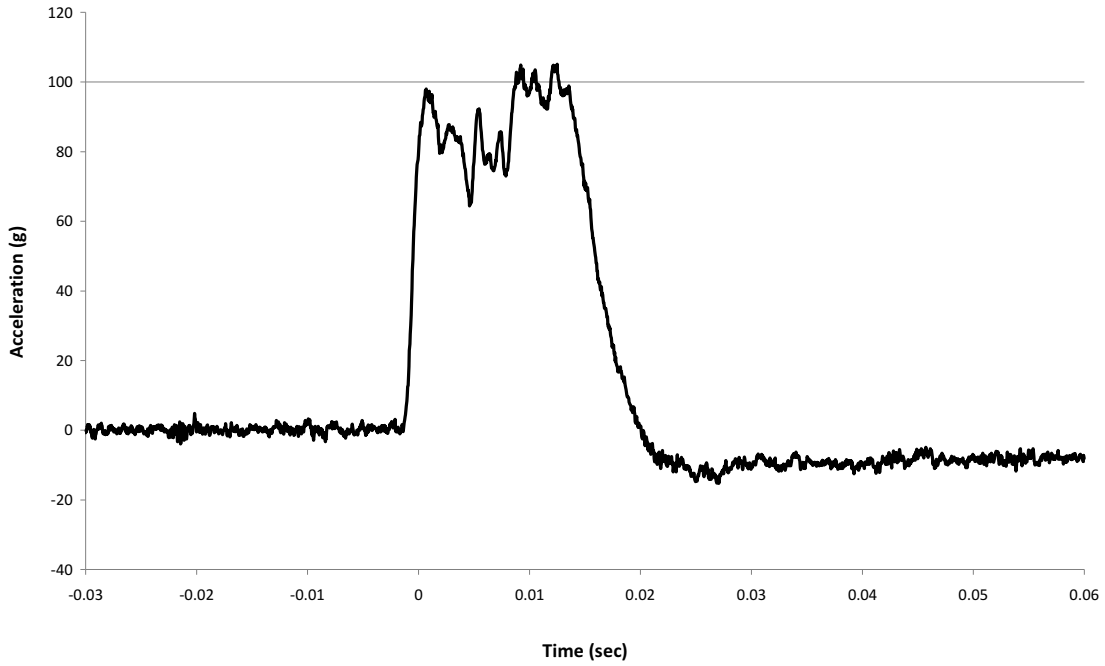
BEA Research Reactor Package Half-Scale Free Drop Test
Test D1 (End), Channel 12



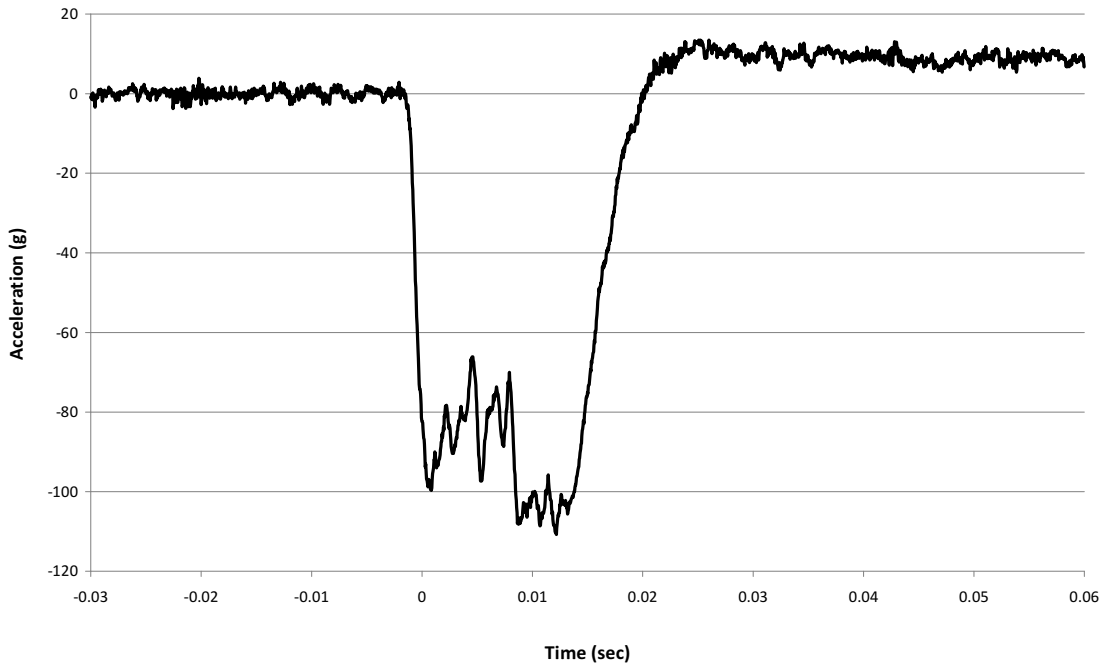
BEA Research Reactor Package Half-Scale Free Drop Test
Test D1 (End), Channel 13



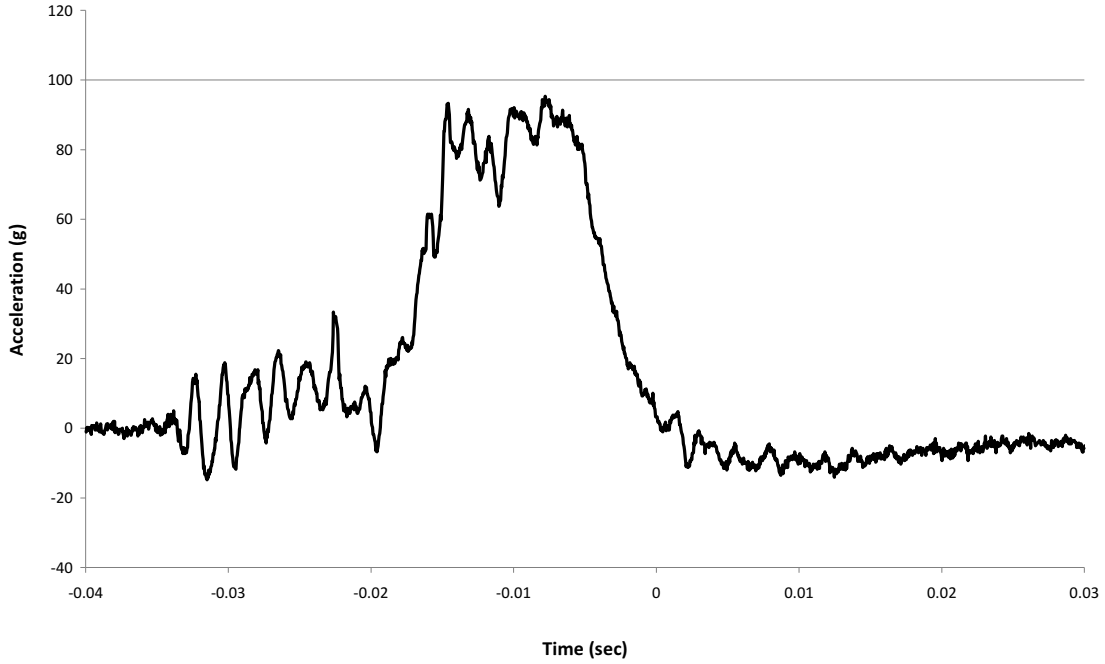
BEA Research Reactor Package Half-Scale Free Drop Test
Test D1 (End), Channel 14



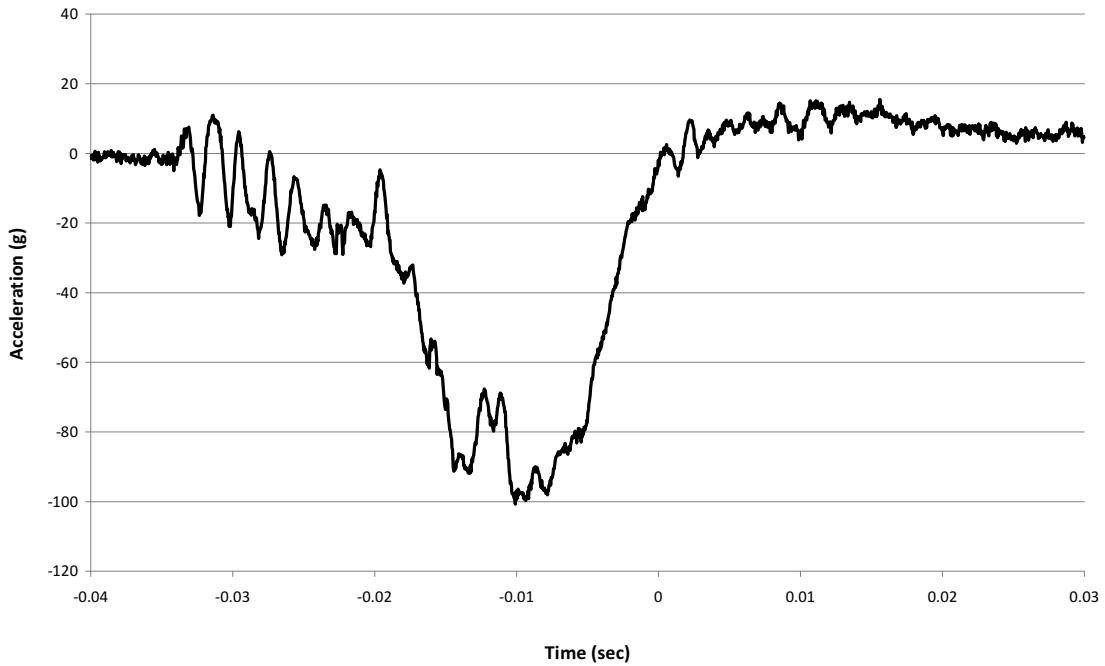
BEA Research Reactor Package Half-Scale Free Drop Test
Test D1 (End), Channel 15



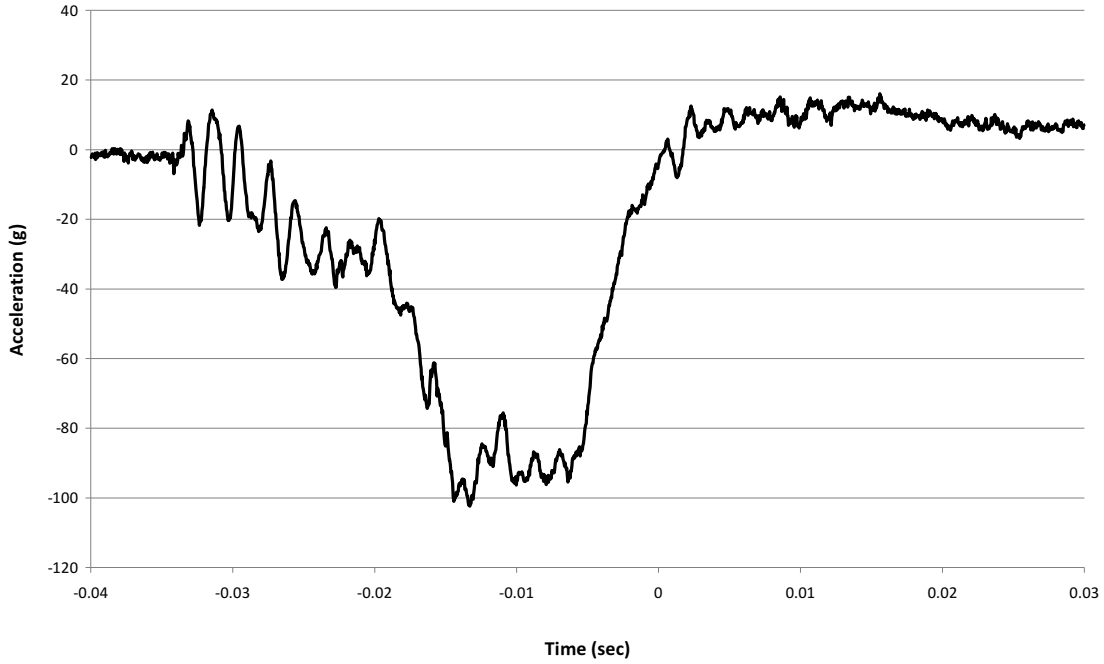
**BEA Research Reactor Package Half-Scale Free Drop Test
Test D2 (15° Oblique), Channel 12 (Secondary Impact)**



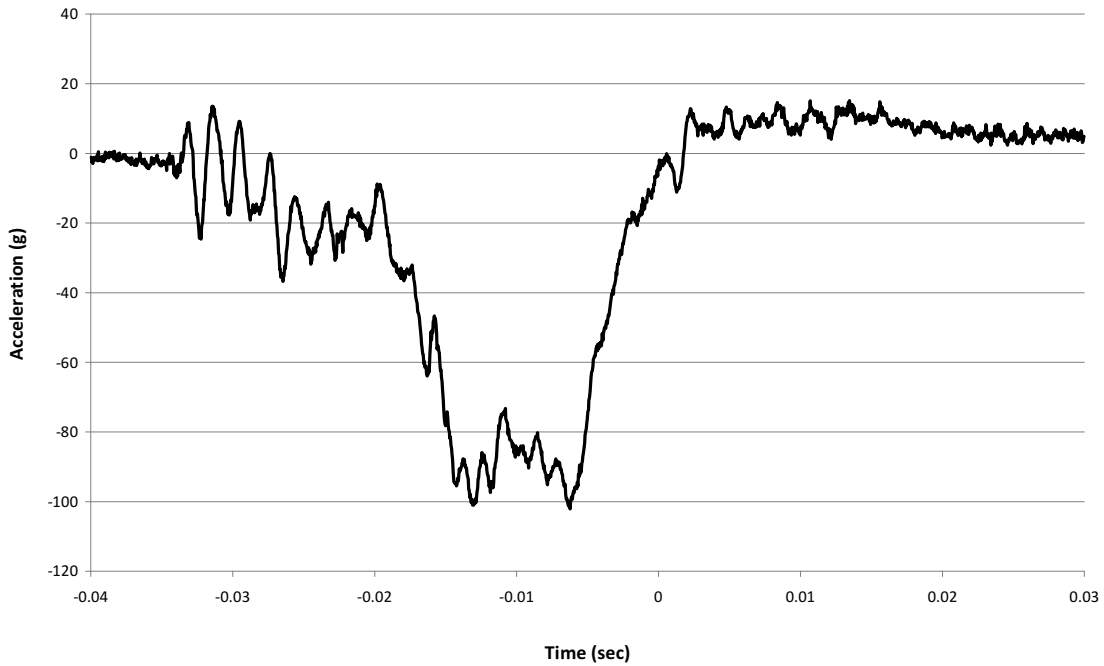
**BEA Research Reactor Package Half-Scale Free Drop Test
Test D2 (15° Oblique), Channel 13 (Secondary Impact)**



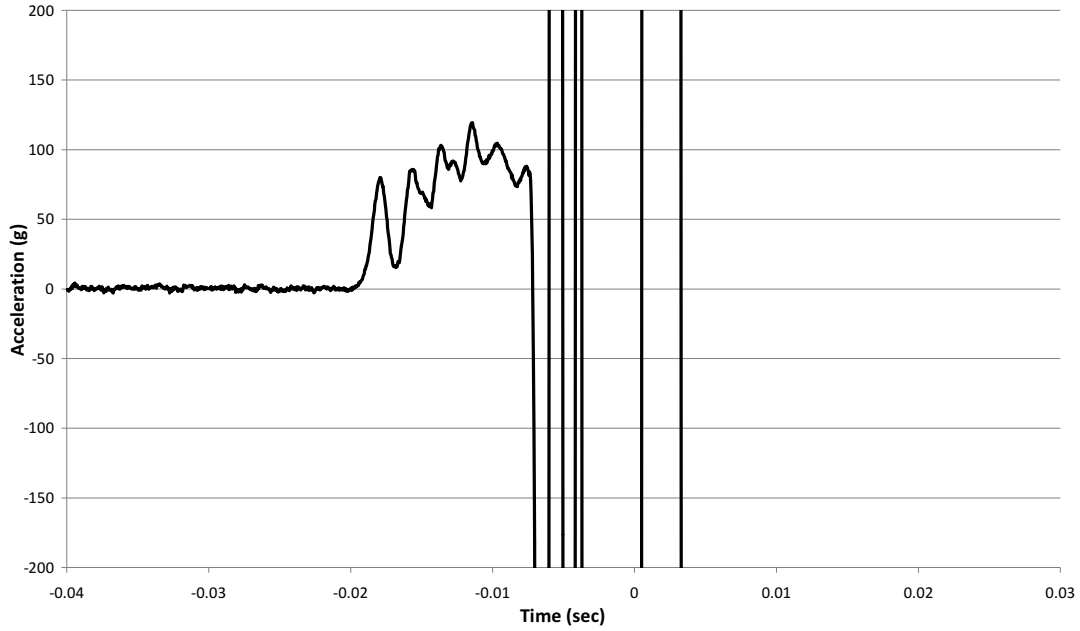
**BEA Research Reactor Package Half-Scale Free Drop Test
Test D2 (15° Oblique), Channel 14 (Secondary Impact)**



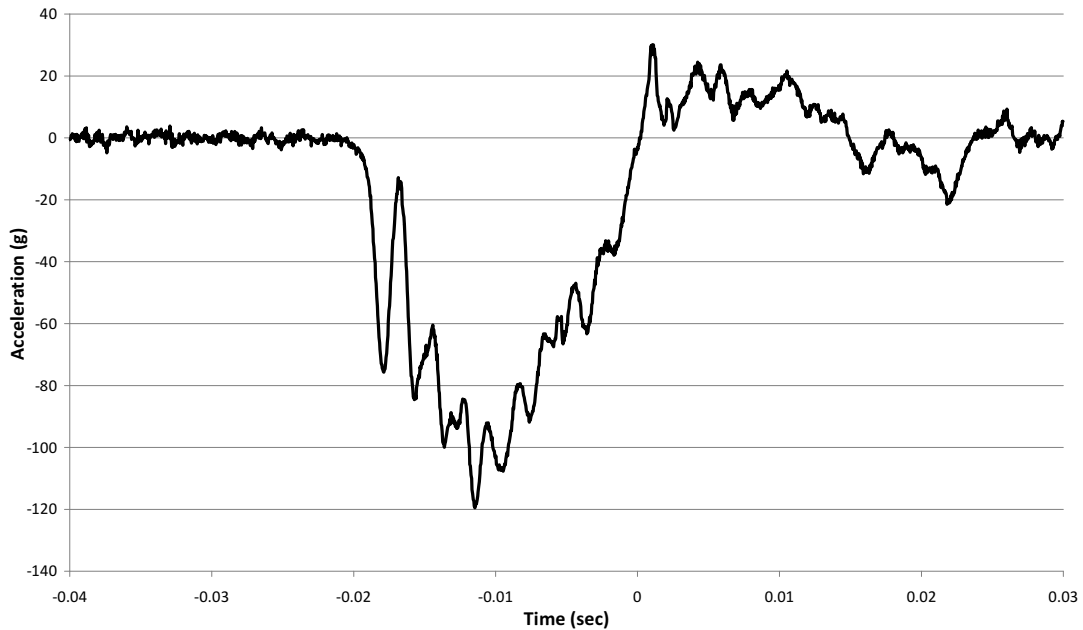
**BEA Research Reactor Package Half-Scale Free Drop Test
Test D2 (15° Oblique), Channel 15 (Secondary Impact)**



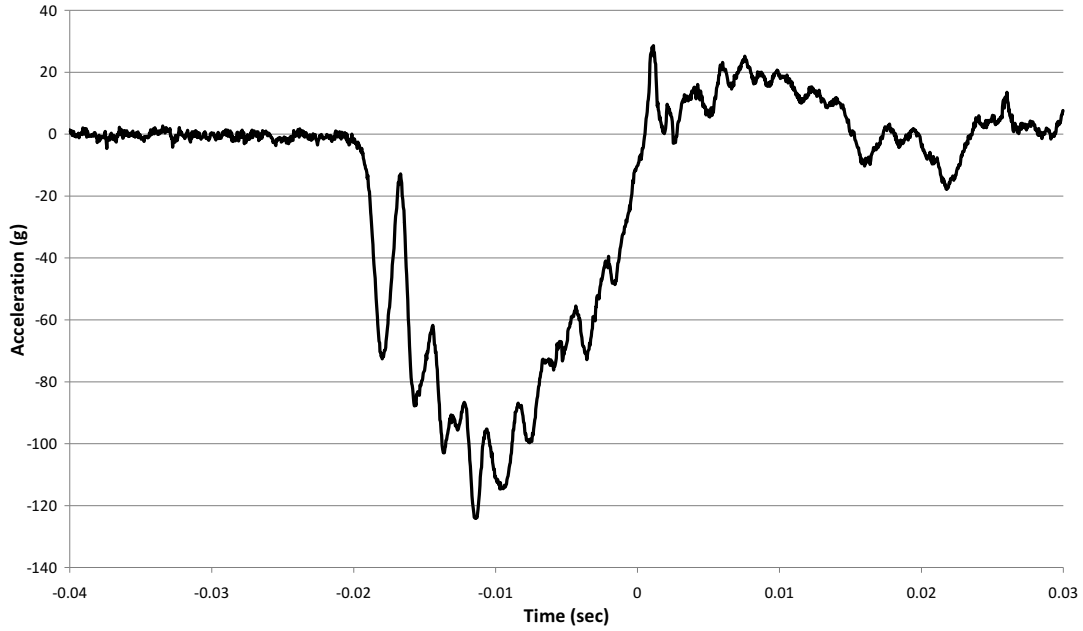
BEA Research Reactor Package Half-Scale Free Drop Test
Test D2 (15° Oblique), Channel 16 (Primary Impact)



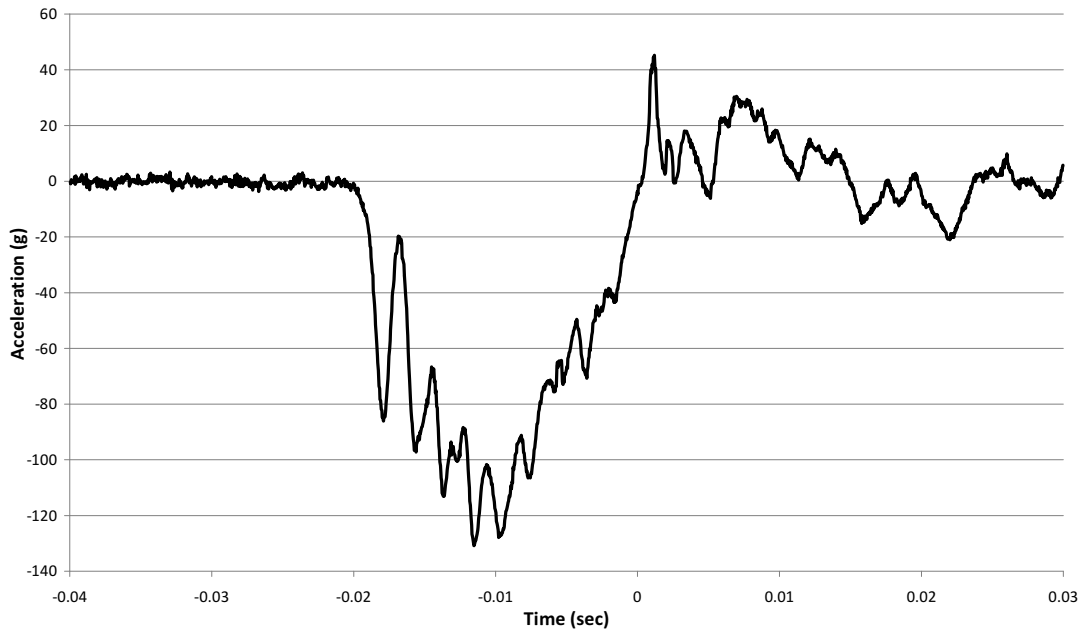
BEA Research Reactor Package Half-Scale Free Drop Test
Test D2 (15° Oblique), Channel 17 (Primary Impact)



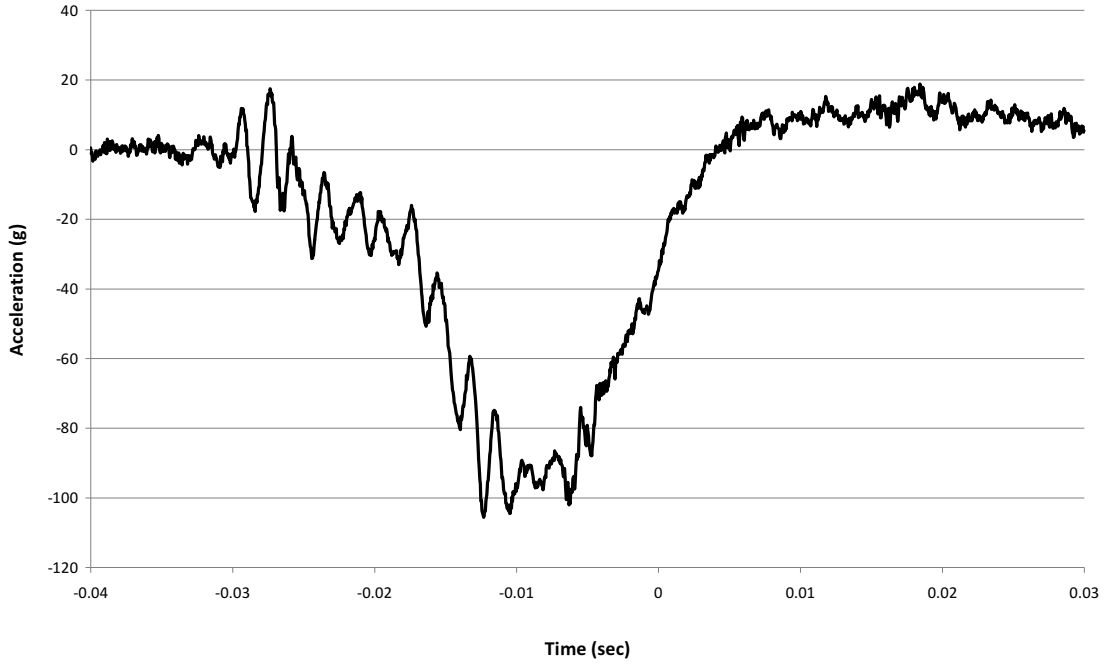
BEA Research Reactor Package Half-Scale Free Drop Test
Test D2 (15° Oblique), Channel 18 (Primary Impact)



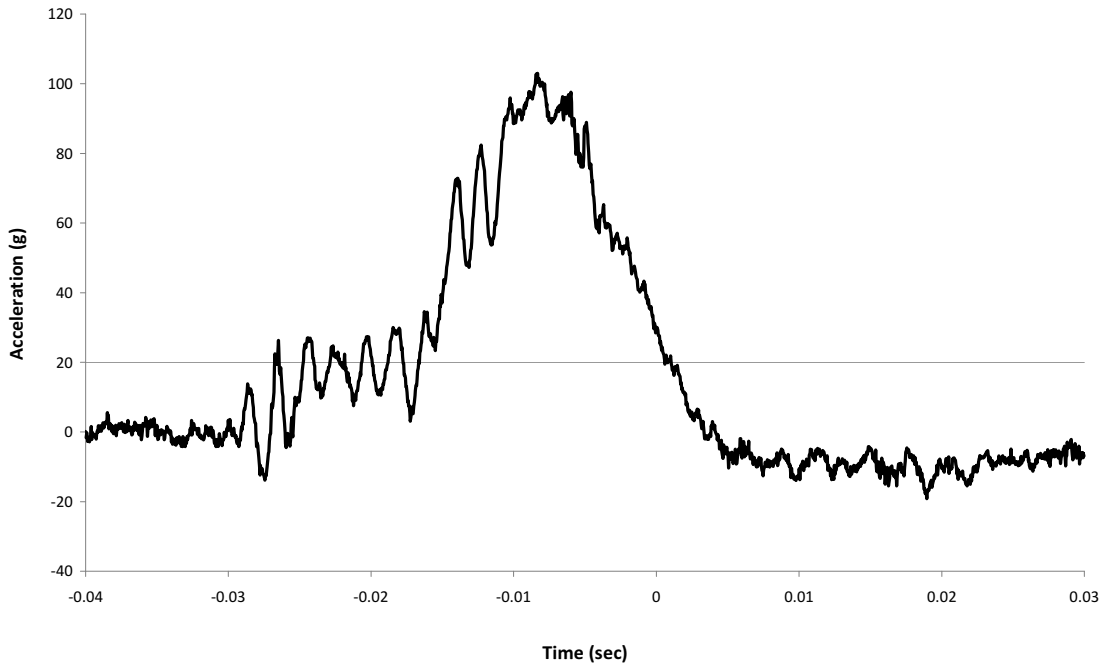
BEA Research Reactor Package Half-Scale Free Drop Test
Test D2 (15° Oblique), Channel 19 (Primary Impact)



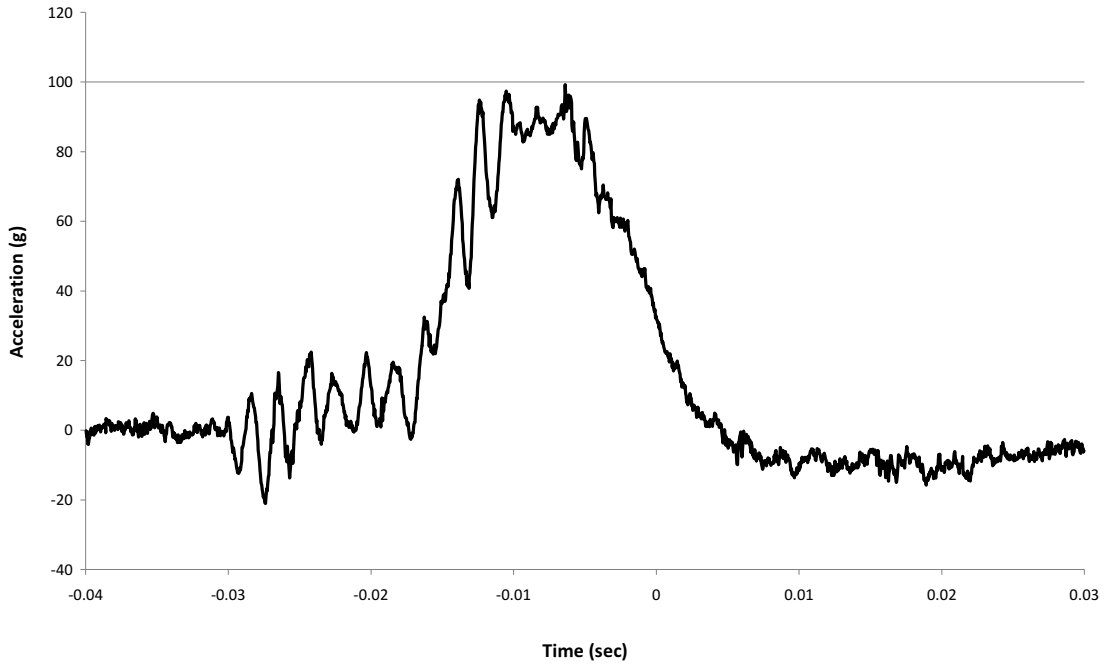
BEA Research Reactor Package Half-Scale Free Drop Test
Test D2R (15° Oblique), Channel 12 (Secondary Impact)



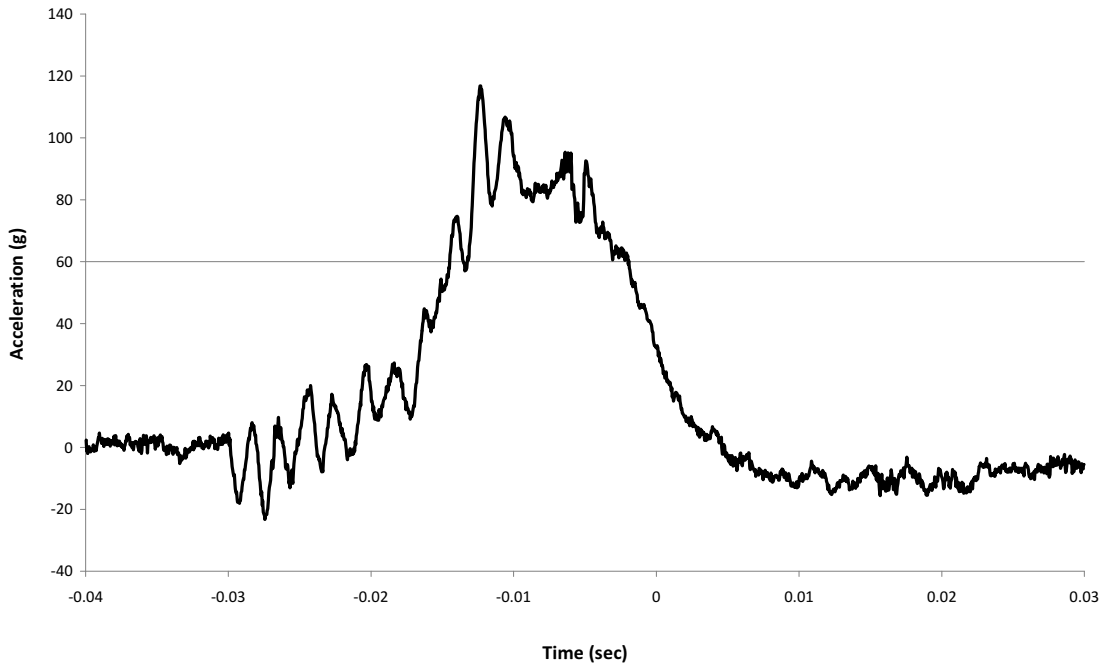
BEA Research Reactor Package Half-Scale Free Drop Test
Test D2R (15° Oblique), Channel 13 (Secondary Impact)



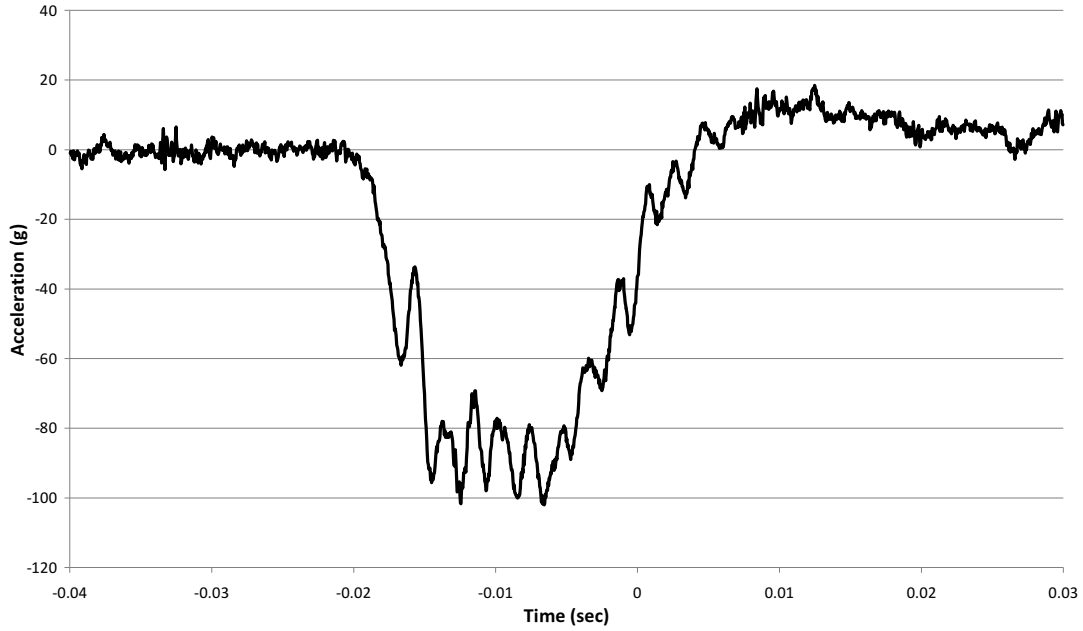
**BEA Research Reactor Package Half-Scale Free Drop Test
Test D2R (15° Oblique), Channel 14 (Secondary Impact)**



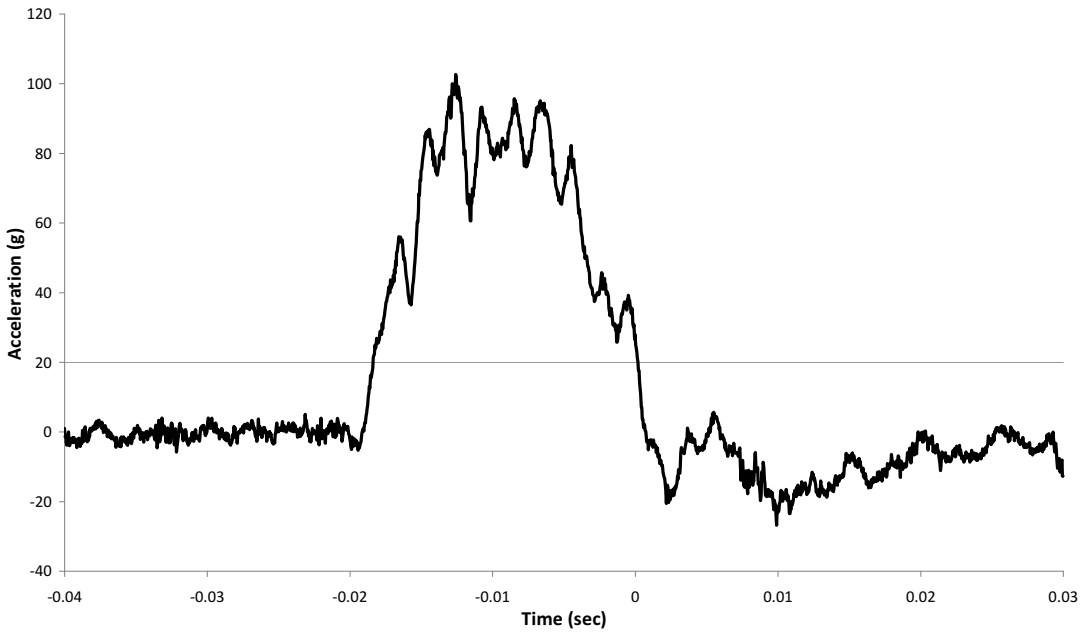
**BEA Research Reactor Package Half-Scale Free Drop Test
Test D2R (15° Oblique), Channel 15 (Secondary Impact)**



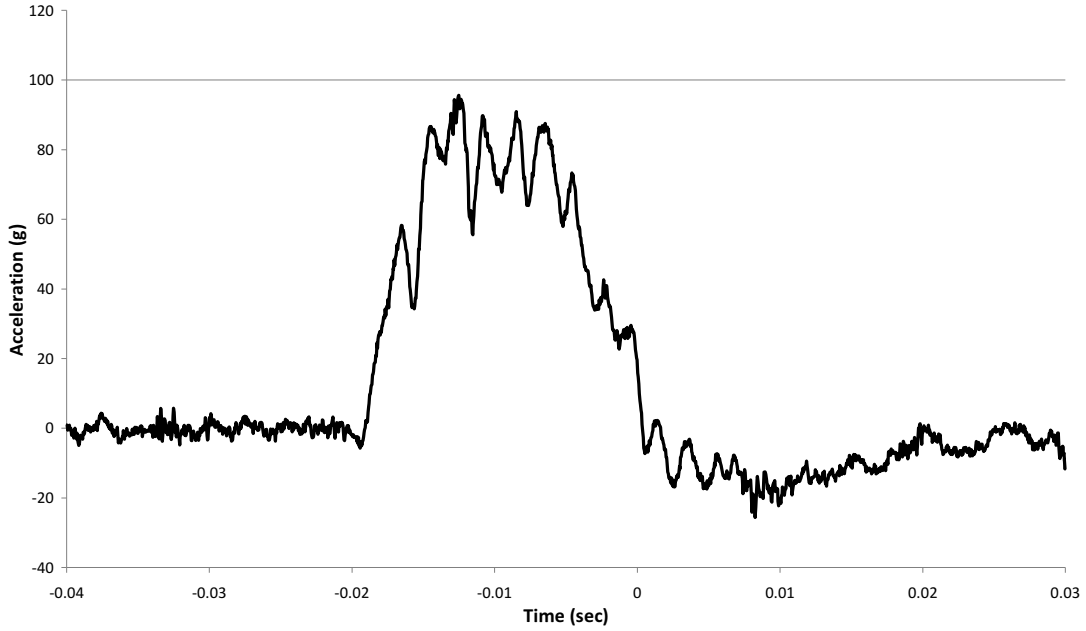
BEA Research Reactor Package Half-Scale Free Drop Test
Test D2R (15° Oblique), Channel 16 (Primary Impact)



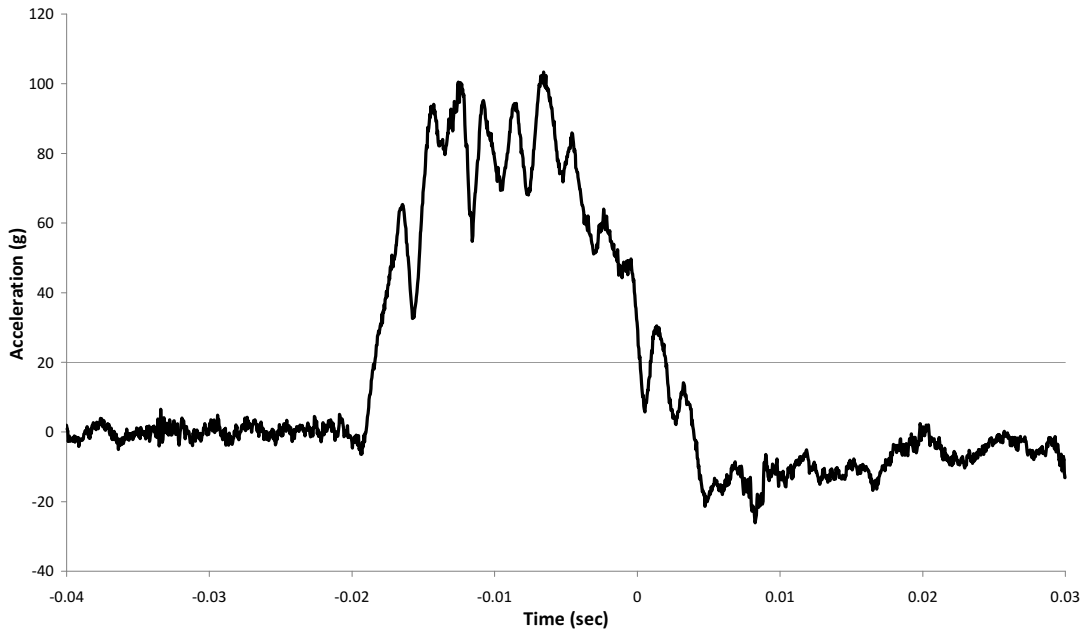
BEA Research Reactor Package Half-Scale Free Drop Test
Test D2R (15° Oblique), Channel 17 (Primary Impact)



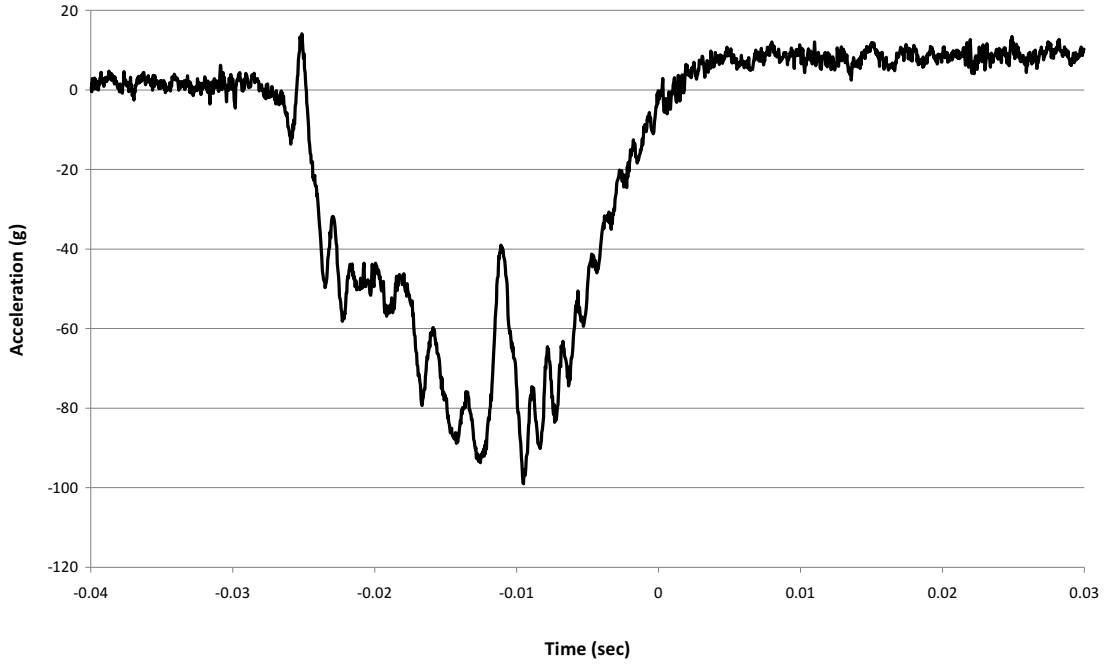
BEA Research Reactor Package Half-Scale Free Drop Test
Test D2R (15° Oblique), Channel 18 (Primary Impact)



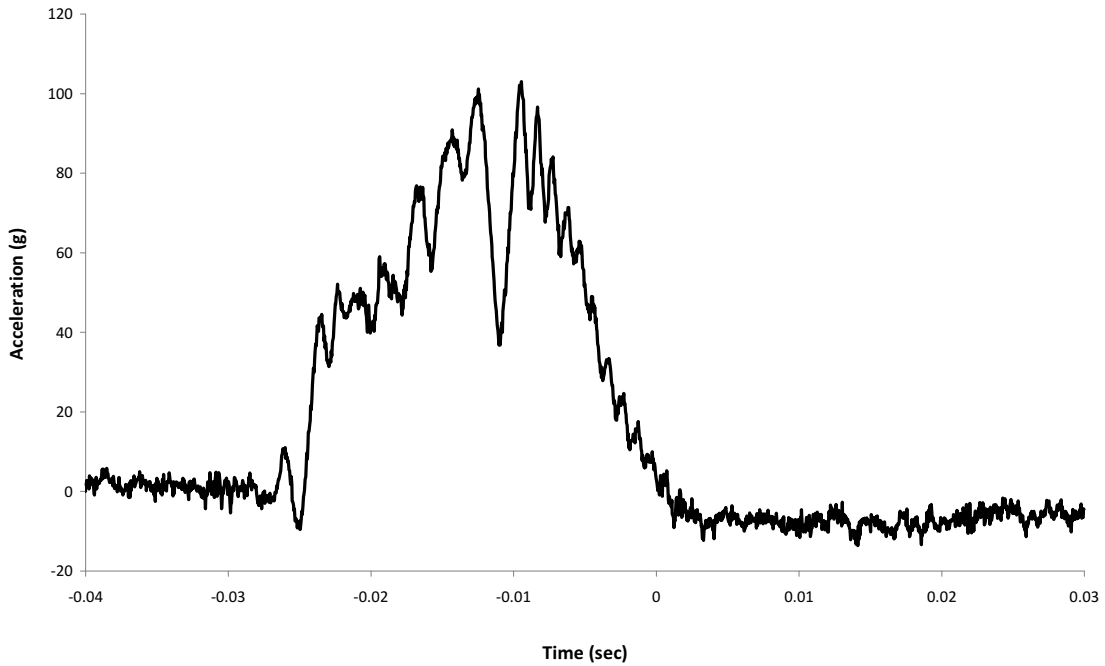
BEA Research Reactor Package Half-Scale Free Drop Test
Test D2R (15° Oblique), Channel 19 (Primary Impact)



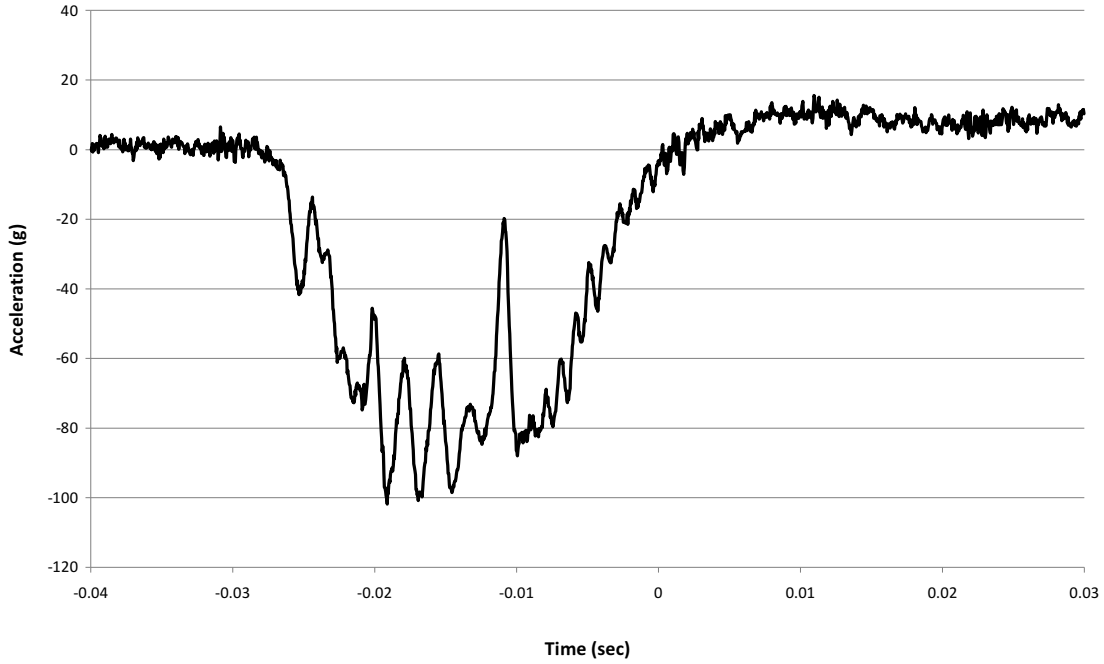
**BEA Research Reactor Package Half-Scale Free Drop Test
Test D3 (CG Over Corner), Channel 12**



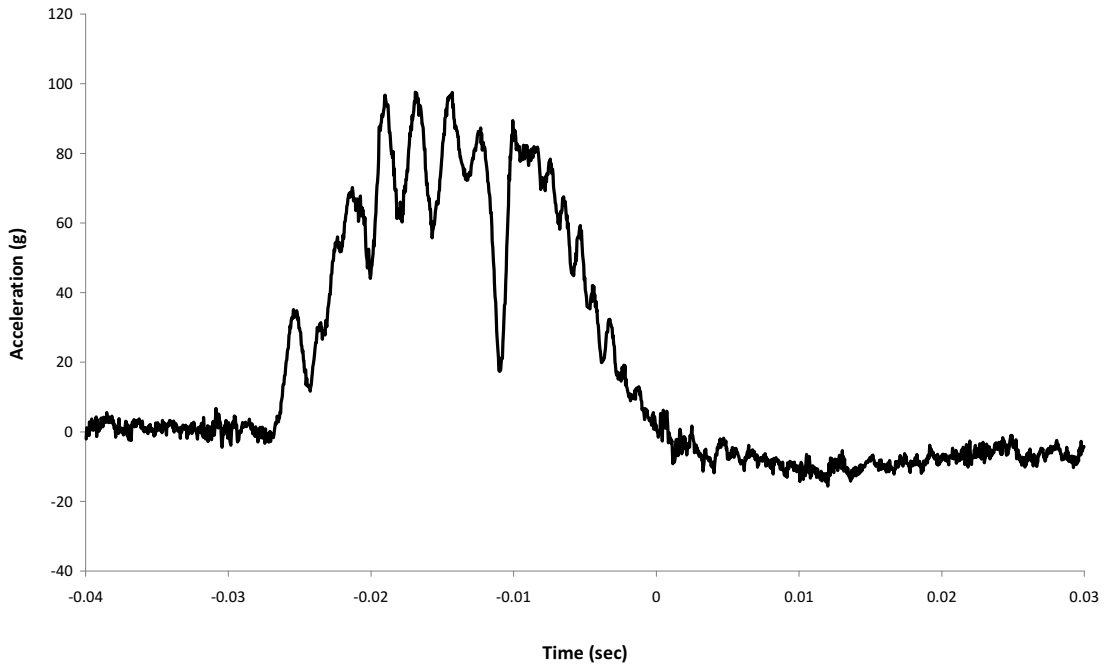
**BEA Research Reactor Package Half-Scale Free Drop Test
Test D3 (CG Over Corner), Channel 13**



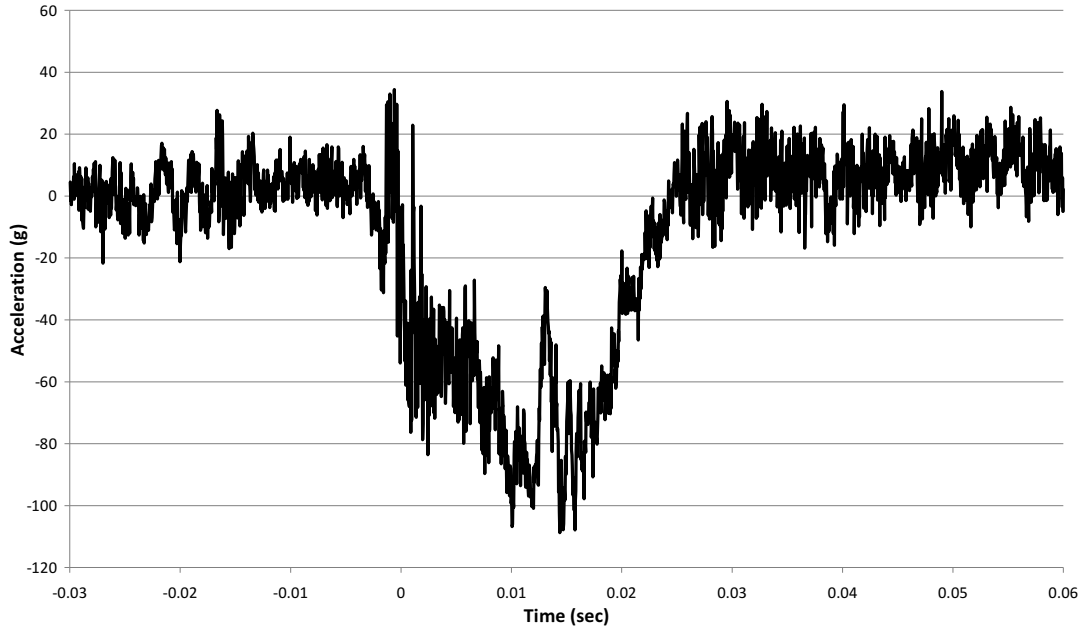
**BEA Research Reactor Package Half-Scale Free Drop Test
Test D3 (CG Over Corner), Channel 14**



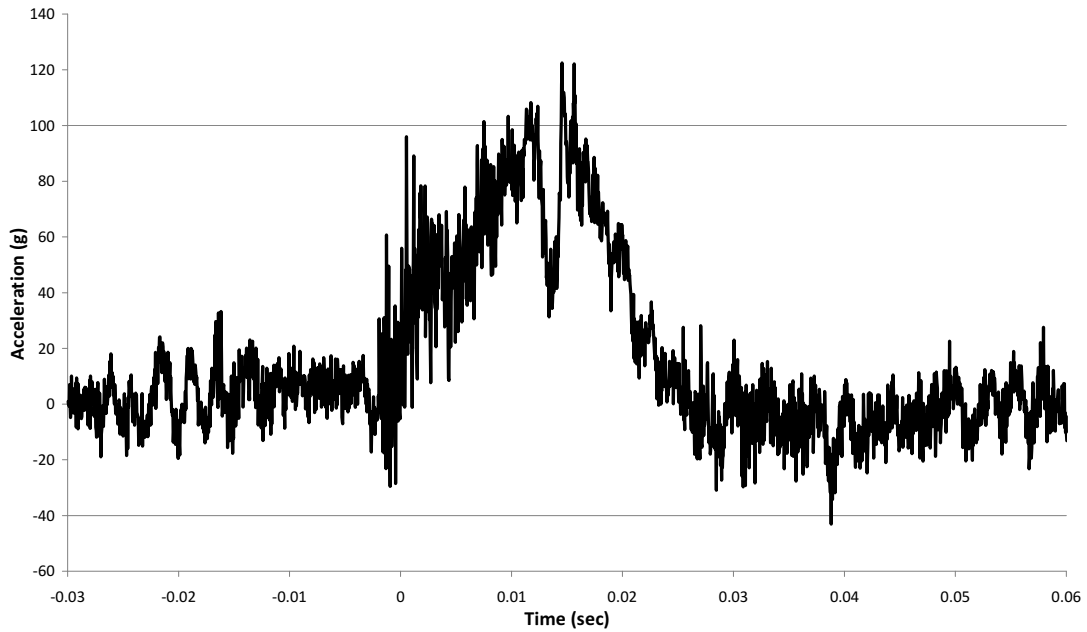
**BEA Research Reactor Package Half-Scale Free Drop Test
Test D3 (CG Over Corner), Channel 15**



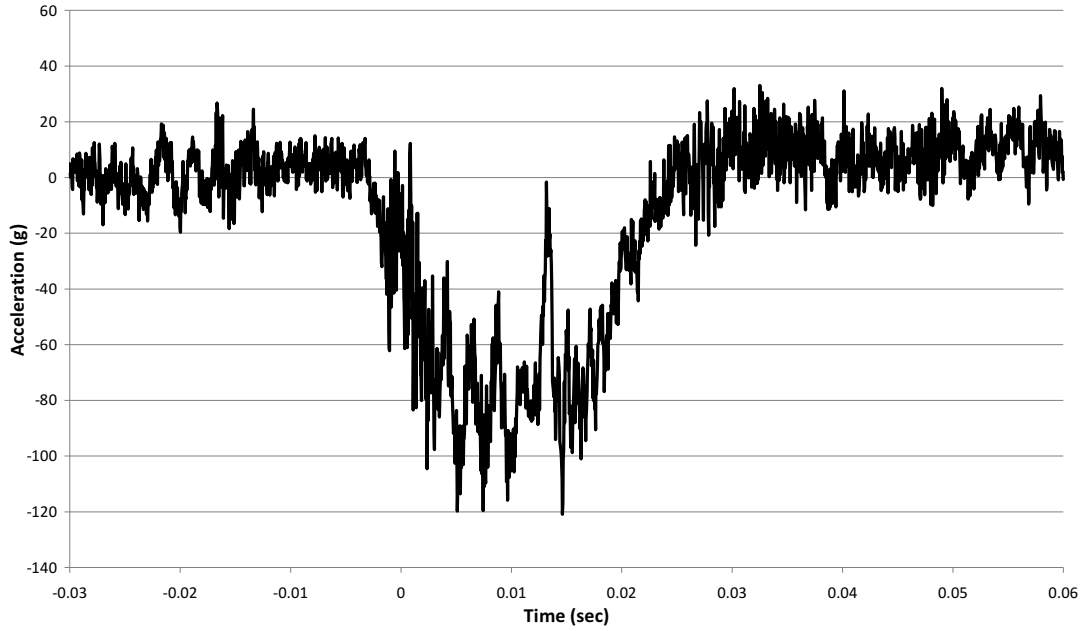
BEA Research Reactor Package Half-Scale Free Drop Test
Test D3 (CG Over Corner), Channel 16



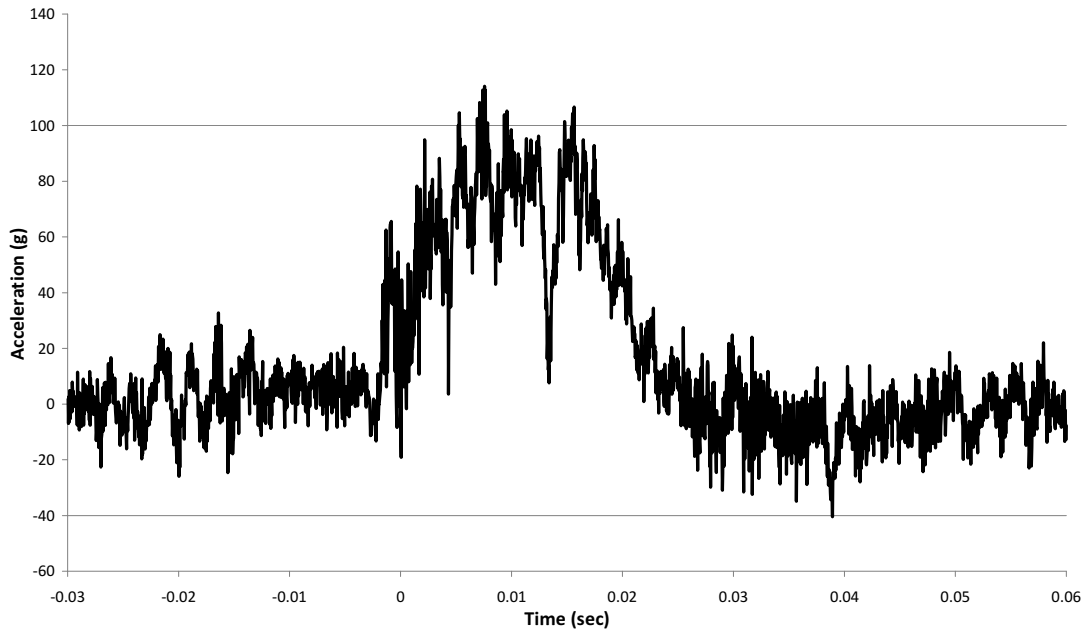
BEA Research Reactor Package Half-Scale Free Drop Test
Test D3 (CG Over Corner), Channel 17



BEA Research Reactor Package Half-Scale Free Drop Test
Test D3 (CG Over Corner), Channel 18



BEA Research Reactor Package Half-Scale Free Drop Test
Test D3 (CG Over Corner), Channel 19



2.12.4 Stress Analysis Finite Element Models

This appendix describes the finite element analysis of the BRR package body. The structural components considered are the upper and lower end structures, the inner shell, and the outer shell. The shield plug, closure lid, and fuel baskets are analyzed separately. Both Normal Conditions of Transport (NCT) and Hypothetical Accident Conditions (HAC) are considered. Loading types include design pressure, thermal, and free drop impact.

2.12.4.1 Analysis Model Description

The finite element model of the BRR package body is used to calculate stress under NCT and HAC in the structural members of the cask, which consist of the upper and lower massive end structures, the inner shell, and the outer shell. The impact limiters, the fuel baskets, the shield plug, the thermal shield, the impact limiter attachments, and the closure lid are not modeled structurally, but their mass is accounted for as discussed below. The lead shielding material in the sides and bottom of the cask body is also not explicitly modeled, and is further discussed below. The model is built in ANSYS Revision 11.0 using half symmetry along a vertical plane through the cask center. The structural elements are SOLID95, 20-node bricks, and the thermal elements are SOLID90, 20-noded bricks. A pressure of 25 psi, corresponding to the design pressure identified in Section 2.6.1.1, *Summary of Pressures and Temperatures*, is applied to the interior surface of the model in each case. The pressure is applied to all element interior surfaces which fall within the location of the inner (containment) O-ring. The pressure creates a small net force which is reacted by forces in the opposite direction applied at the bolt circle of the closure lid. For load cases which do not include inertia forces, the model is constrained by the symmetry plane and by fixed nodes at the edge of the cask outer bottom surface. When inertia loads are applied, the model constraint is individually discussed in the following sections. The finite element mesh is shown in Figure 2.12.4-1.

2.12.4.2 Loading of the Model

Besides the design pressure discussed above, the model is loaded by thermal loads and by free drop impact loads.

2.12.4.2.1 Thermal Loads

A detailed thermal analysis is performed in Chapter 3, *Thermal Evaluation*. The thermal analysis performed using the model described in this section is done only to transform the thermal results obtained in Chapter 3 into the form required by the stress analysis model. This is done by assigning selected key nodal temperatures taken from the Chapter 3 analysis, and running the thermal/stress model described in this section using thermal elements (SOLID90) to obtain temperatures at each node of the model. The location of the key nodes at which the Chapter 3 NCT temperatures were transferred directly to the thermal/stress model are shown in Figure 2.12.4-2. Convection and radiation are set to zero. Thermal conductivity is a required SOLID90 input but does not affect the result and is therefore set to an arbitrary value of 1. The resulting temperature distribution is essentially the same as that obtained in Chapter 3, and is shown in Figure 2.12.4-3. The nodal temperatures are used in the stress analysis along with

BRR Package Safety Analysis Report

temperature-dependent coefficients of thermal expansion taken from Table 2.2-1 and Table 2.2-2 to obtain thermal stress.

Another source of thermal loading is the lead gamma shield used in the annulus between the inner and outer shells. Due to different thermal expansion coefficients, the lead gamma shielding applies a radial pressure to the outer surface of the inner shell under NCT hot conditions. As shown in Section 2.6.1.2.3, *Lead*, this pressure can be assigned an upper bound value of 350 psi. For the NCT hot case, this pressure is applied to the inner shell outer surface over the entire length of the side lead cavity. The treatment of lead in load cases which include free drop impact loads is discussed below.

2.12.4.2.2 Free Drop Impact Loads

Stress is generated in the BRR cask body in a free drop impact through self weight of the components and the applied loads of components not modeled. The resulting forces are reacted over the interface areas of the impact limiter(s). A bounding impact deceleration field of 40g is applied for the NCT cases as discussed in Section 2.6.7, *Free Drop*, and 120g is applied for the HAC cases as discussed in Section 2.7.1, *Free Drop*. As shown in Section 2.7.1, the governing orientations for stress analysis are the end drop (top end down and bottom end down), and the side drop.

The weight of the shield plug, fuel basket, closure lid, and the impact limiter not in contact with the ground (e.g., the one on top in an end drop) are accounted for by applying pressure to the region of contact. The applied load is equal to the weight of the component multiplied by the appropriate impact g-load, divided by the contact area. Component weights are taken from Table 2.1-2, (half of these values are used for half symmetry) and the contact areas are calculated using the drawings in Appendix 1.3.3, *Packaging General Arrangement Drawings*. The density of stainless steel is 0.29 lb/in³. The weight of the thermal shield and impact limiter attachments is included in the cask body model by a slight adjustment of the material density.

The lead gamma shielding is not explicitly modeled. Instead, for simplicity and conservatism, it is treated as a liquid material, thus applying a hydrostatic pressure within the side and lower lead cavities. The magnitude of the pressure is:

$$p = \gamma gh$$

where the pressure at any point, p , is applied on the side and lower surfaces of the lead cavity, g is the acceleration of gravity, h is the depth of the lead, and γ is the density of lead, equal to 0.41 lb/in³. Due to the conservatism of this assumption, it is not necessary to additionally apply the lead thermal load of 350 psi (see Section 2.12.4.2.1, *Thermal Loads*) to any free drop load cases.

Once all of the impact loads have been applied, the model is constrained at a minimum number of nodes for stability. The impact limiter support loads are then adjusted until near-perfect balance is achieved between the applied loads (inertia loads of the cask structure, lead, and separate components) and the impact reaction (the impact limiter). In each case, the total reaction force is essentially equal to the total decelerated weight (i.e., total weight of the BRR package, less the weight of the limiter(s) contacting the ground) times 40 (NCT) or 120 (HAC). Greater detail on the application of the inertia loads, the lead hydrostatic pressure loads, and the displacement constraints is provided in the sections discussing each load case.

BRR Package Safety Analysis Report

These analyses do not include a dynamic load factor (DLF), since the impact acceleration used is nearly 50 % higher than the maximum test result (see Section 2.12.5.3, *Reconciliation with Certification Test Results*), and because the cask structures are relatively stiff, which would result in a DLF not significantly different from unity.

2.12.4.3 Material Properties

For load cases that do not evaluate thermal stress, the modulus of elasticity is evaluated at the bounding NCT hot temperature of 250 °F, or $E = 27.3 \times 10^6$ psi from Table 2.6-1. Poisson's ratio is equal to 0.3. For load cases in which thermal stress is included, both the modulus of elasticity and the thermal expansion coefficient are evaluated at the nodal temperatures determined in the thermal run, using data from Table 2.2-1 and Table 2.2-2. All allowable stresses are evaluated at the NCT hot temperature of 250 °F.

2.12.4.4 Load Cases and Allowable Stress

Load cases are identified which allow the evaluation of the model stresses using the allowable stresses defined in Table 2.1-1. For NCT, numerical values of allowable stress are taken from Table 2.6-1 for a temperature of 250 °F. The primary membrane (P_m) allowable stress is S_m , which is equal to 20,000 psi. The primary membrane plus bending ($P_m + P_b$) stress allowable is $1.5S_m$, or 30,000 psi, and the primary plus bending plus secondary ($P_m + P_b + Q$) stress allowable is $3.0S_m$, or 60,000 psi.

For HAC, the numerical values depend on the value of S_u , which is smaller for the forged or cast materials used for the upper and lower end structures and the inner shell (see Table 2.2-2). At a temperature of 250 °F, the minimum value of $S_u = 64,050$ psi. The primary membrane (P_m) allowable stress is the lesser of $2.4S_m$ or $0.7S_u$, or a minimum of 44,835 psi. The primary membrane plus bending ($P_m + P_b$) stress allowable is the lesser of $3.6S_m$ or S_u , or a minimum of 64,050 psi.

Because, in the NCT cases, the resulting stresses are relatively low and it is not necessary to separately identify the membrane stress. Therefore the margin of safety may be conservatively determined by applying the maximum stress intensity to the primary membrane stress allowable.

For the HAC cases, the maximum stress resulting from the model is evaluated by decoupling the primary stress from bending and secondary stress. Thus, in each HAC case, the stresses are linearized to distinguish between the decoupled stresses and separate allowables are applied.

The load cases and allowable stresses are listed in the following table. Note: the design pressure of 25 psig is present in all load cases.

Case No.	Section No.	Description	Stress Evaluated
1	2.12.4.4.1	Design pressure only	Primary
2	2.12.4.4.2	Lead shrinkage pressure with thermal	Secondary
3	2.12.4.4.3	NCT bottom-down end drop	Primary
4	2.12.4.4.4	NCT bottom-down end drop with thermal	Secondary
5	2.12.4.4.5	HAC bottom-down end drop	Primary
6	2.12.4.4.6	NCT top-down end drop	Primary
7	2.12.4.4.7	NCT top-down end drop with thermal	Secondary
8	2.12.4.4.8	HAC top-down end drop	Primary
9	2.12.4.4.9	NCT side drop	Primary
10	2.12.4.4.10	NCT side drop with thermal	Secondary
11	2.12.4.4.11	HAC side drop	Primary

2.12.4.4.1 Case No. 1, Design Pressure Only

In this case, the only applied load is the design pressure of 25 psig, applied to the interior of the cask body at a radius less than or equal to that of the inner (containment) O-ring. The design pressure loading is shown in Figure 2.12.4-4. The model is constrained by the symmetry plane and by nodes at the outer edge of the cask bottom surface.

Results are shown in Figure 2.12.4-5. The maximum stress intensity is 281 psi at the midpoint of the payload cavity bottom. Conservatively using the NCT membrane stress allowable of 20,000 psi, the margin of safety is:

$$MS = \frac{20,000}{281} - 1 = +70.2$$

2.12.4.4.2 Case No. 2, Lead Shrinkage Pressure With Thermal

Case No. 2 starts with the 25 psig pressure of Case No. 1 and adds the lead shrinkage pressure to the outside surface of the inner shell, all along the side lead cavity. In addition, thermal stress is calculated using the NCT hot case temperatures and temperature dependent coefficients of thermal expansion. Both of these loads are described in Section 2.12.4.2.1, *Thermal Loads*. The model is constrained by the symmetry plane and by nodes at the outer edge of the cask bottom surface.

Results are shown in Figure 2.12.4-6. The maximum stress intensity is 6,933 psi at the top of the inner shell cross section. Since this result includes secondary stress, the allowable is 60,000 psi. The margin of safety is:

$$MS = \frac{60,000}{6,933} - 1 = +7.65$$

2.12.4.4.3 Case No. 3, NCT Bottom-Down End Drop

In this case, the applied loads are the design pressure from Case No. 1 and the free drop weight of the shield plug, fuel basket, closure lid, and impact limiter. The free drop loads are described in Section 2.12.4.2.2, *Free Drop Impact Loads*. The cask body orientation is vertical, with the bottom end down. The weight of the side lead applies a hydrostatic pressure based on depth as described in Section 2.12.4.2.2. The weight of the lower lead is modeled as two separate hydrostatic loads based the inner and outer lead columns above the upper surface of the lower closure plate. The bottom-down end drop loading is shown in Figure 2.12.4-7. The model is constrained by the symmetry plane and by nodes at the outer edge of the cask bottom surface.

Results are shown in Figure 2.12.4-8. The maximum stress intensity is 15,202 psi at the outside surface of the bottom end structure. Conservatively using the NCT membrane stress allowable of 20,000 psi, the margin of safety is:

$$MS = \frac{20,000}{15,202} - 1 = +0.32$$

2.12.4.4.4 Case No. 4, NCT Bottom-Down End Drop With Thermal

Case No. 4 adds the thermal loading described in Section 2.12.4.2.1, *Thermal Loads*, to Case No. 3.

Results are shown in Figure 2.12.4-9. The maximum stress intensity is 14,586 psi at the top of the inner shell cross section. Since this result includes secondary stress, the allowable is 60,000 psi. The margin of safety is:

$$MS = \frac{60,000}{14,586} - 1 = +3.11$$

2.12.4.4.5 Case No. 5, HAC Bottom-Down End Drop

Case No. 5 is the same as Case No. 3, except with an HAC inertia field of 120g.

Results are shown in Figure 2.12.4-10. The maximum stress intensity is 45,681 psi at the outside surface of the bottom end structure. In the prior NCT load cases, the membrane allowable has been conservatively applied to the maximum stress intensity, which makes it unnecessary to differentiate the actual membrane stress from the membrane plus bending stress. Since this is an HAC case, the less conservative approach is applied; the stress is linearized through the lower massive end structure cross section. Results are shown in Figure 2.12.4-11. The maximum primary membrane stress is 22,680 psi. The HAC membrane stress allowable is 44,835 psi. The margin of safety is:

$$MS = \frac{44,835}{22,680} - 1 = +0.98$$

The maximum membrane plus bending stress is 43,080 psi. The HAC membrane plus bending stress allowable is 64,050. The margin of safety is:

$$MS = \frac{64,050}{43,080} - 1 = +0.49$$

2.12.4.4.6 Case No. 6, NCT Top-Down End Drop

In this case, the weight of the shield plug, fuel basket and closure lid are modeled as forces located at the lid bolt circle. The shield plug is modeled as a pressure distributed on the impact limiter contact area. Design pressure is applied as in Case No. 1. The cask body orientation is vertical, with the top end down. The weight of the side lead applies a hydrostatic pressure based on depth as described in Section 2.12.4.2.2, *Free Drop Impact Loads*. The weight of the lower lead is modeled as two separate hydrostatic loads based the inner and outer lead columns above the upper and lower shelves of the lower lead cavity. The top-down end drop loading is shown in Figure 2.12.4-12. The model is constrained by the symmetry plane and by nodes at the outer edge of the cask top surface.

Results are shown in Figure 2.12.4-13. The maximum stress intensity is 13,248 psi at the top of the inner shell. Conservatively using the NCT membrane stress allowable of 20,000 psi, the margin of safety is:

$$MS = \frac{20,000}{13,248} - 1 = +0.51$$

2.12.4.4.7 Case No. 7, NCT Top-Down End Drop With Thermal

Case No. 7 adds the thermal loading described in Section 2.12.4.2.1, *Thermal Loads*, to Case No. 6.

Results are shown in Figure 2.12.4-14. The maximum stress intensity is 13,258 psi at the top of the inner shell. Since this result includes secondary stress, the allowable is 60,000 psi. The margin of safety is:

$$MS = \frac{60,000}{13,258} - 1 = +3.53$$

2.12.4.4.8 Case No. 8, HAC Top-Down End Drop

Case No. 8 is the same as Case No. 6, except with an HAC inertia field of 120g.

Results are shown in Figure 2.12.4-15. The maximum stress intensity is 40,140 psi at the top of the inner shell. In this HAC case, the stress is linearized, through the line of highest stress intensity in the top inner shell cross section. The linearized results are shown in Figure 2.12.4-16. The maximum primary membrane stress is 22,720 psi. The HAC membrane stress allowable is 44,835 psi. The margin of safety is:

$$MS = \frac{44,835}{22,720} - 1 = +0.97$$

The maximum membrane plus bending stress is 33,400 psi. The HAC membrane plus bending stress allowable is 64,050. The margin of safety is:

$$MS = \frac{64,050}{33,400} - 1 = +0.92$$

2.12.4.4.9 Case No. 9, NCT Side Drop

In this case, the applied loads are the design pressure from Case No. 1 and the free drop weight of the shield plug, fuel basket, and closure lid. The applied loads and supporting pressures are applied as pressures over an included angle of 30°, which represents the circumferential extent of contact. The cask body orientation is horizontal. The weight of the side and bottom lead shields are modeled as a hydrostatic pressures as described in Section 2.12.4.2.2, *Free Drop Impact Loads*. The side drop loading is shown in Figure 2.12.4-17 and Figure 2.12.4-18. The model is constrained by the symmetry plane and by two nodes at the top and bottom of the cask and one node at the top to constrain radial and axial motion respectively.

Results are shown in Figure 2.12.4-19. The maximum stress intensity is 18,935 psi at the bottom outside edge of the lower lead cavity. Conservatively using the NCT membrane stress allowable of 20,000 psi, the margin of safety is:

$$MS = \frac{20,000}{18,935} - 1 = +0.06$$

2.12.4.4.10 Case No. 10, NCT Side Drop With Thermal

Case No. 10 adds the thermal loading described in Section 2.12.4.2.1, *Thermal Loads*, to Case No. 9.

Results are shown in Figure 2.12.4-20. The maximum stress intensity is 22,704 psi at the shield plug shelf. Since this result includes secondary stress, the allowable is 60,000 psi. The margin of safety is:

$$MS = \frac{60,000}{22,704} - 1 = +1.64$$

2.12.4.4.11 Case No. 11, HAC Side Drop

Case No. 11 is the same as Case No. 9, except with an HAC inertia field of 120g.

Results are shown in Figure 2.12.4-21. The maximum stress intensity is 56,810 psi at the bottom outside edge of the lower lead cavity. The stress, as in prior HAC cases, is linearized through the lower closure plate cross section. Results are shown in Figure 2.12.4-22. The maximum primary membrane stress is 16,330 psi. The HAC membrane stress allowable is 44,835 psi. The margin of safety is:

$$MS = \frac{44,835}{16,330} - 1 = +1.75$$

The maximum membrane plus bending stress is 51,990 psi. The HAC membrane plus bending stress allowable is 64,050. The margin of safety is:

$$MS = \frac{64,050}{51,990} - 1 = +0.23$$

2.12.4.5 Summary

Table 2.12.4-1 summarizes the margins of safety of the BRR package finite element analysis, as established in the sections above. Since all margins of safety are positive, the structural components considered (the upper and lower end structures, the inner shell, and the outer shell) are not of concern.

Table 2.12.2-1 – Finite Element Analysis Results

Analysis Description	Reference Section	Margin of Safety
Case No. 1, Design Pressure Only	2.12.4.4.1	+ 70.2
Case No. 2, Lead Shrinkage Pressure With Thermal	2.12.4.4.2	+ 7.65
Case No. 3, NCT Bottom-Down End Drop	2.12.4.4.3	+ 0.32
Case No. 4, NCT Bottom-Down End Drop With Thermal	2.12.4.4.4	+ 3.11
Case No. 5, HAC Bottom-Down End Drop	2.12.4.4.5	+ 0.49 ^①
Case No. 6, NCT Top-Down End Drop	2.12.4.4.6	+ 0.51
Case No. 7, NCT Top-Down End Drop With Thermal	2.12.4.4.7	+ 3.53
Case No. 8, HAC Top-Down End Drop	2.12.4.4.8	+ 0.92 ^①
Case No. 9, NCT Side Drop	2.12.4.4.9	+ 0.06
Case No. 10, NCT Side Drop With Thermal	2.12.4.4.10	+ 1.64
Case No. 11, HAC Side Drop	2.12.4.4.11	+ 0.23 ^①

Notes:

1. Minimum value shown.

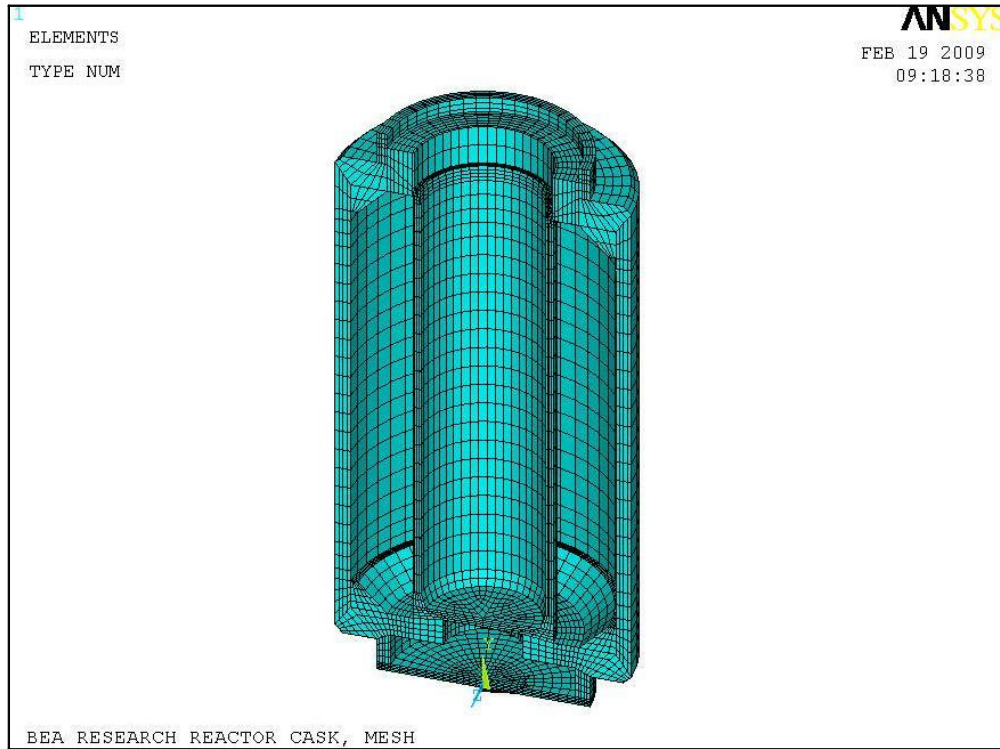


Figure 2.12.4-1 – Finite Element Mesh

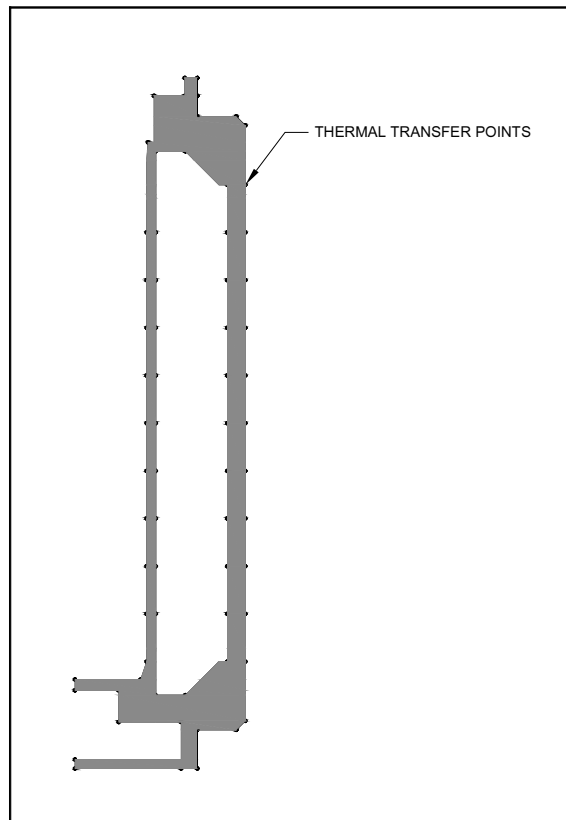


Figure 2.12.4-2 – Thermal Transfer Points

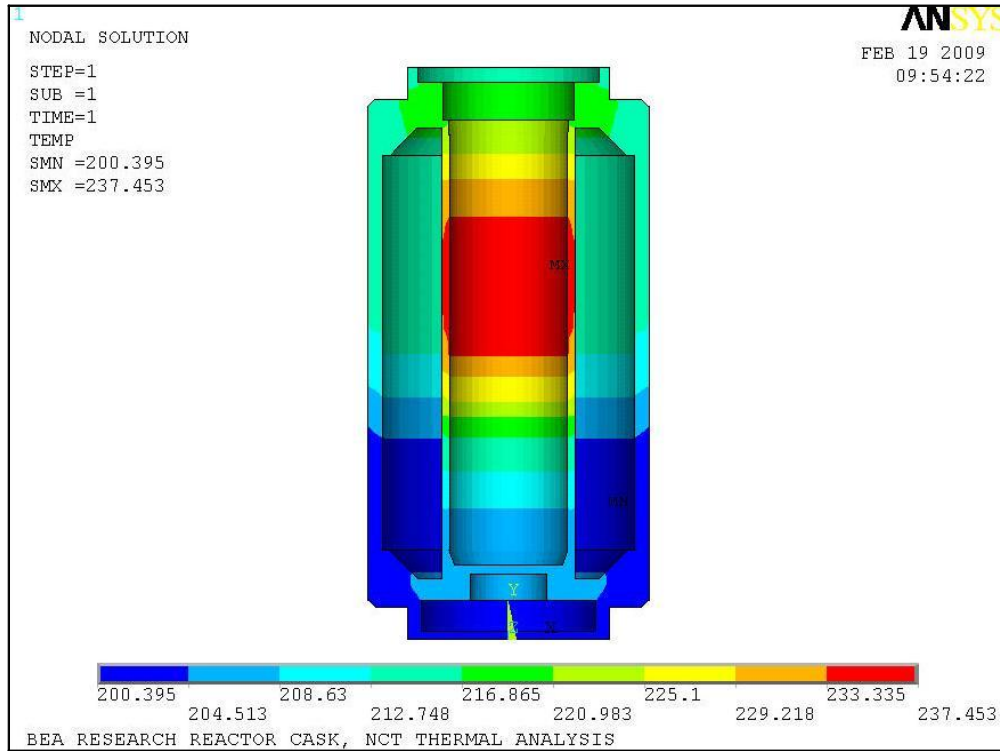


Figure 2.12.4-3 – Temperature Distribution

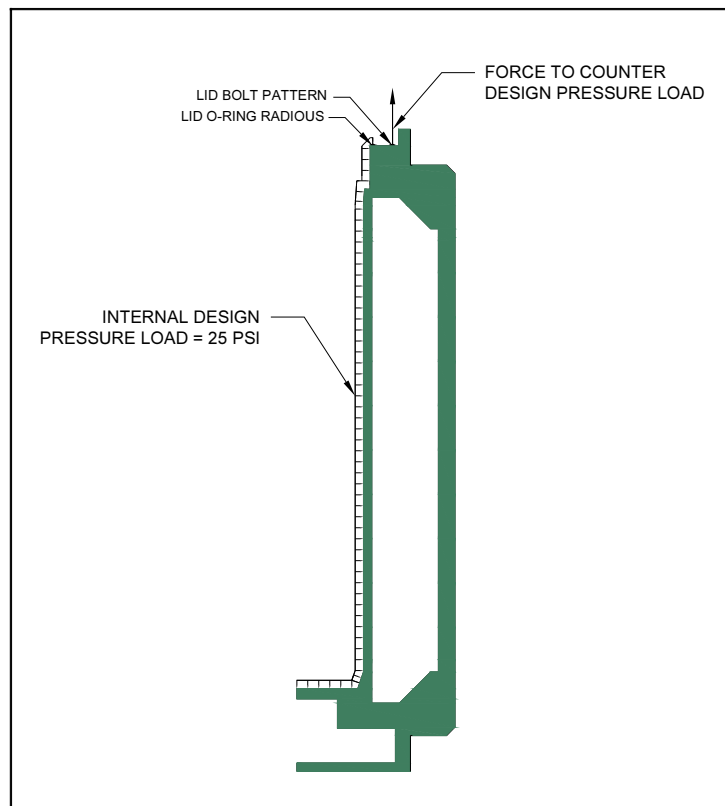


Figure 2.12.4-4 – Design Pressure Loading

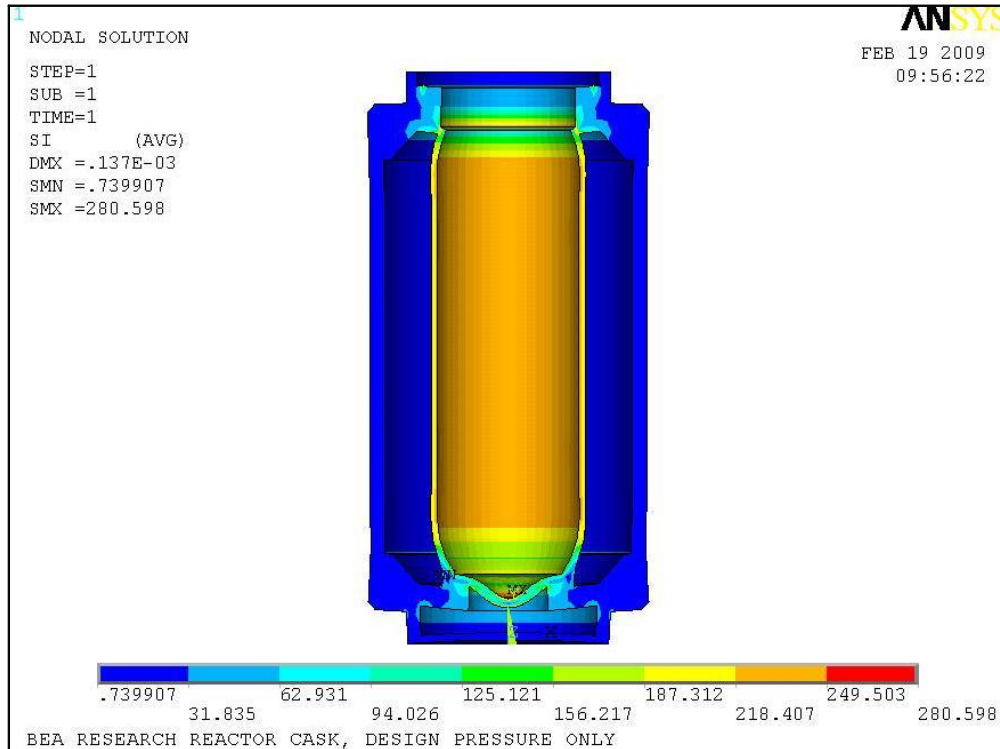


Figure 2.12.4-5 – Internal Pressure Only

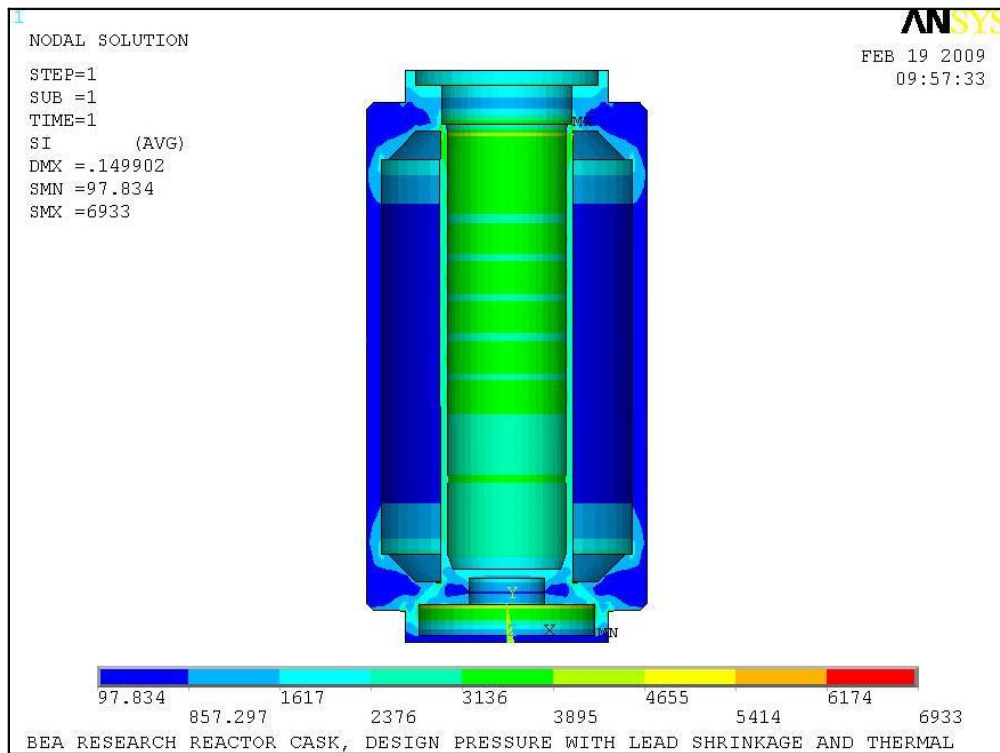


Figure 2.12.4-6 – Lead Shrinkage Pressure With Thermal

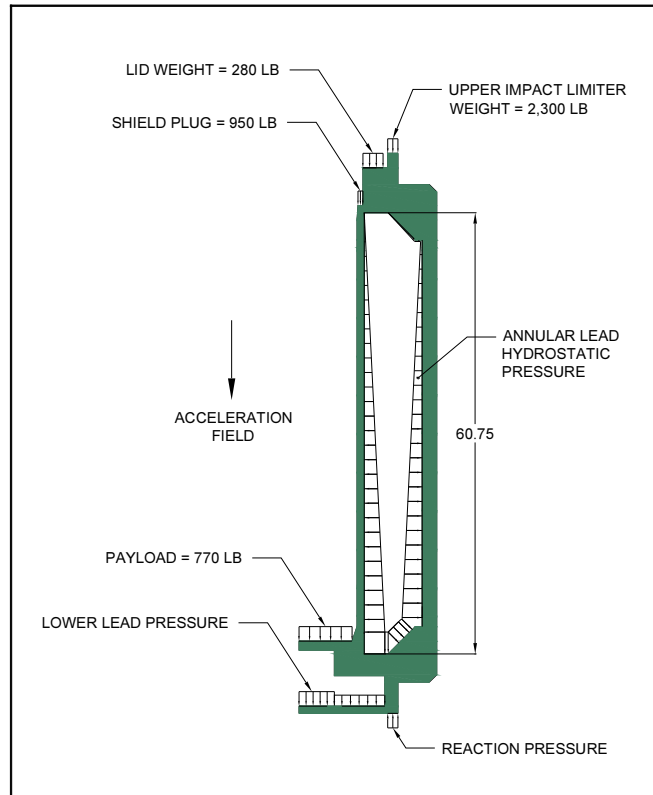


Figure 2.12.4-7 –Bottom-Down End Drop Loading

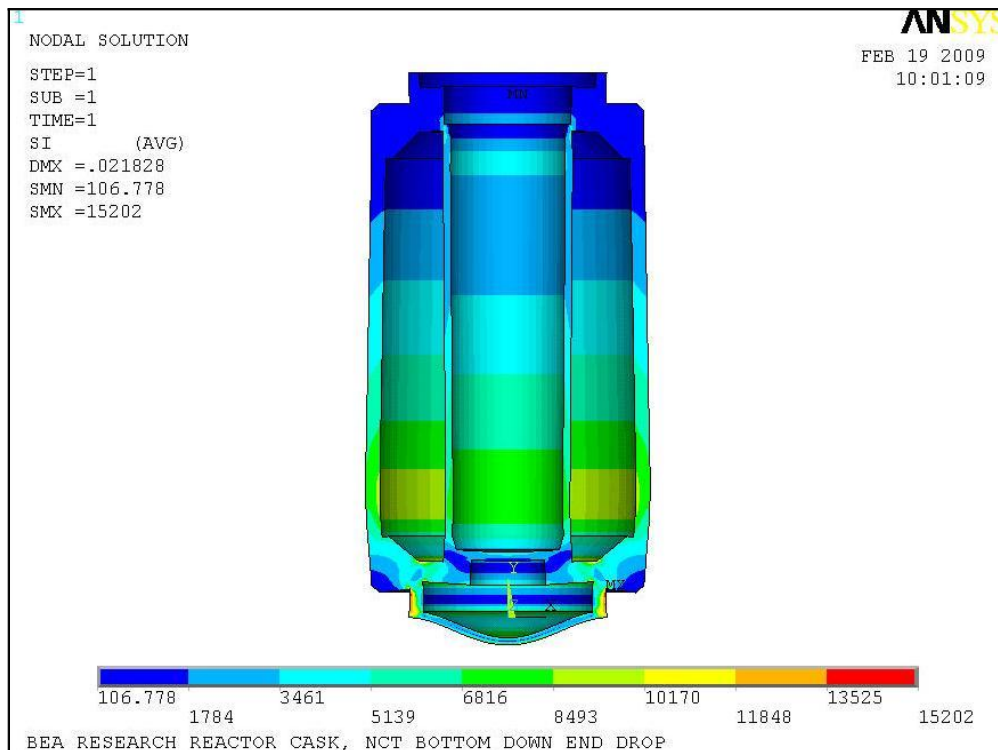


Figure 2.12.4-8 – NCT Bottom-Down End Drop

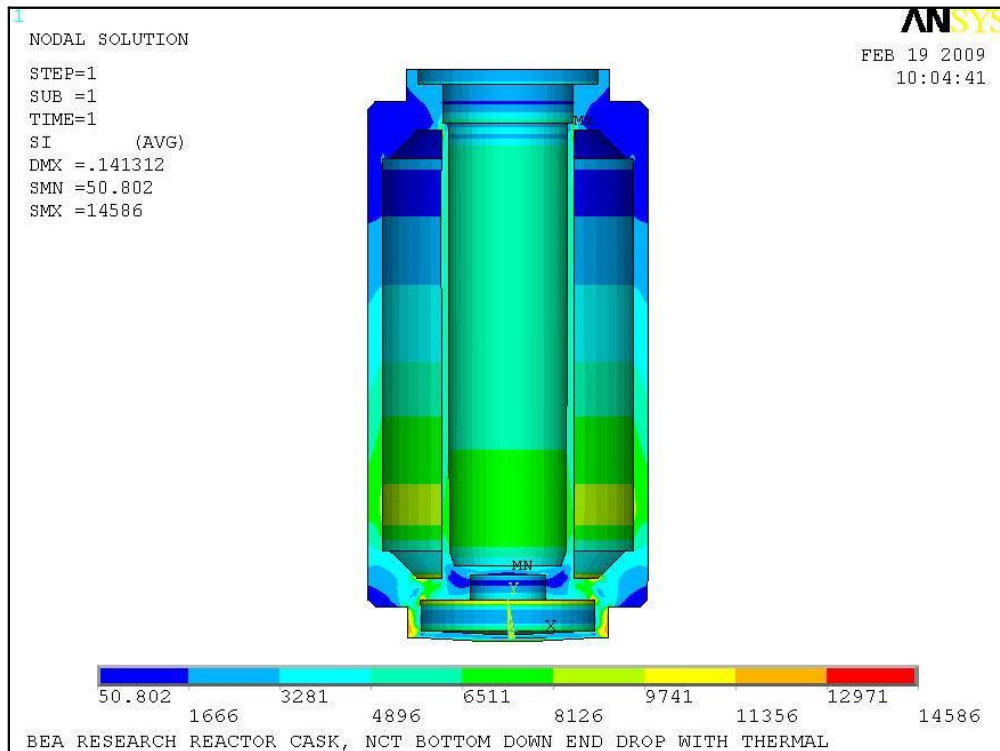


Figure 2.12.4-9 – NCT Bottom-Down End Drop With Thermal

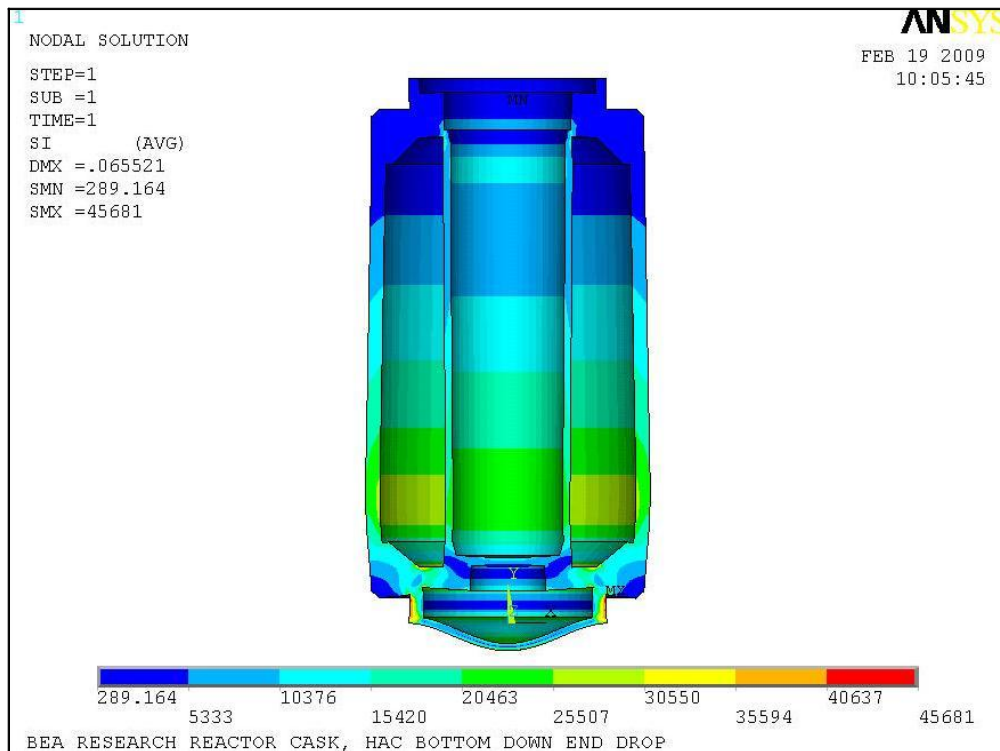


Figure 2.12.4-10 – HAC Bottom-Down End Drop

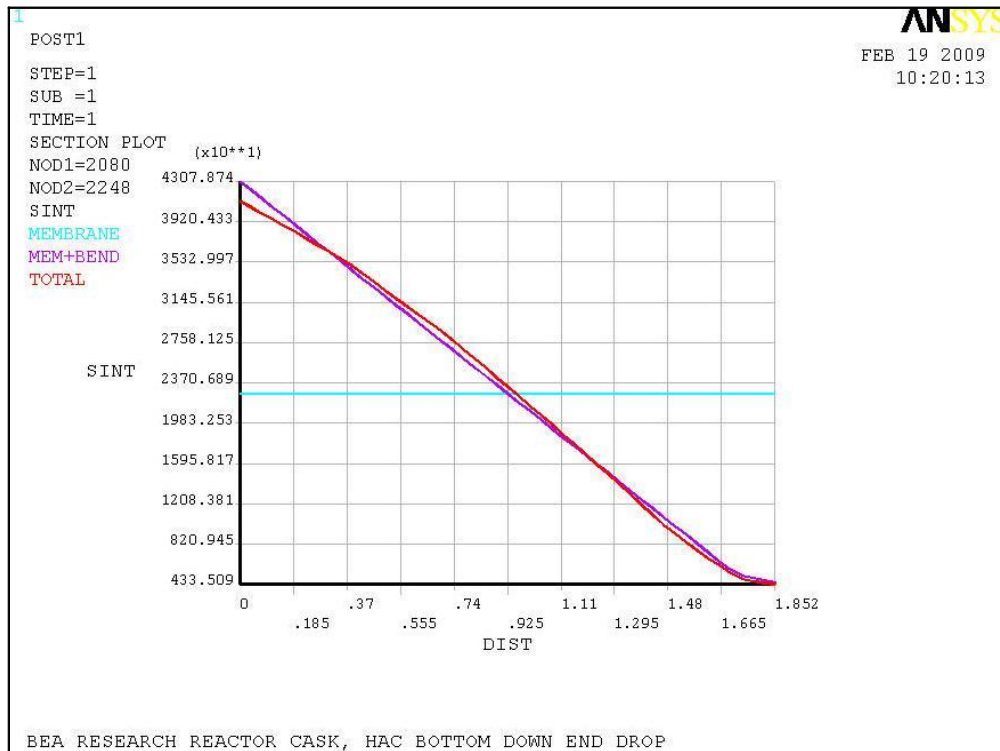


Figure 2.12.4-11 – HAC Bottom-Down End Drop Linearized Stress

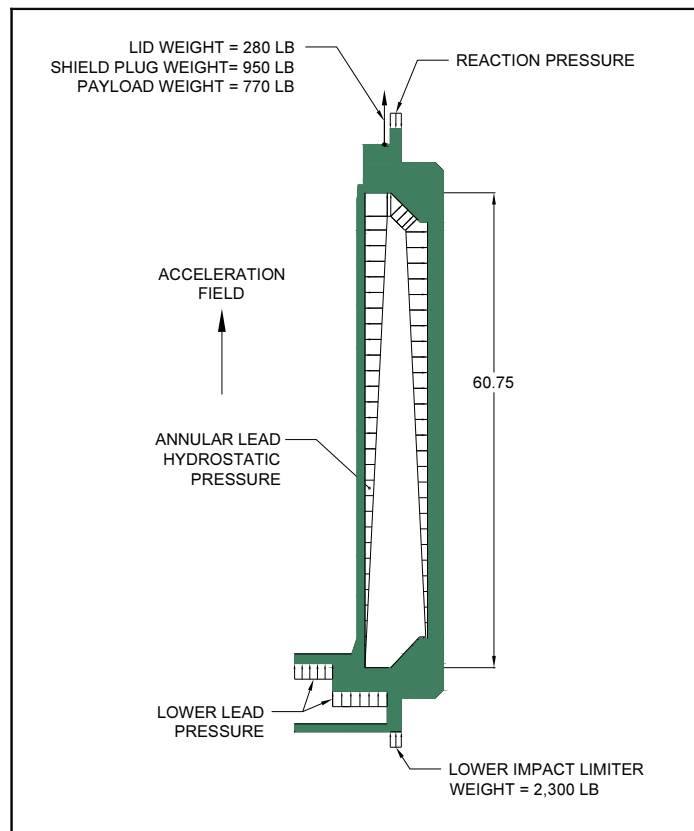


Figure 2.12.4-12 – Top-Down End Drop Loading

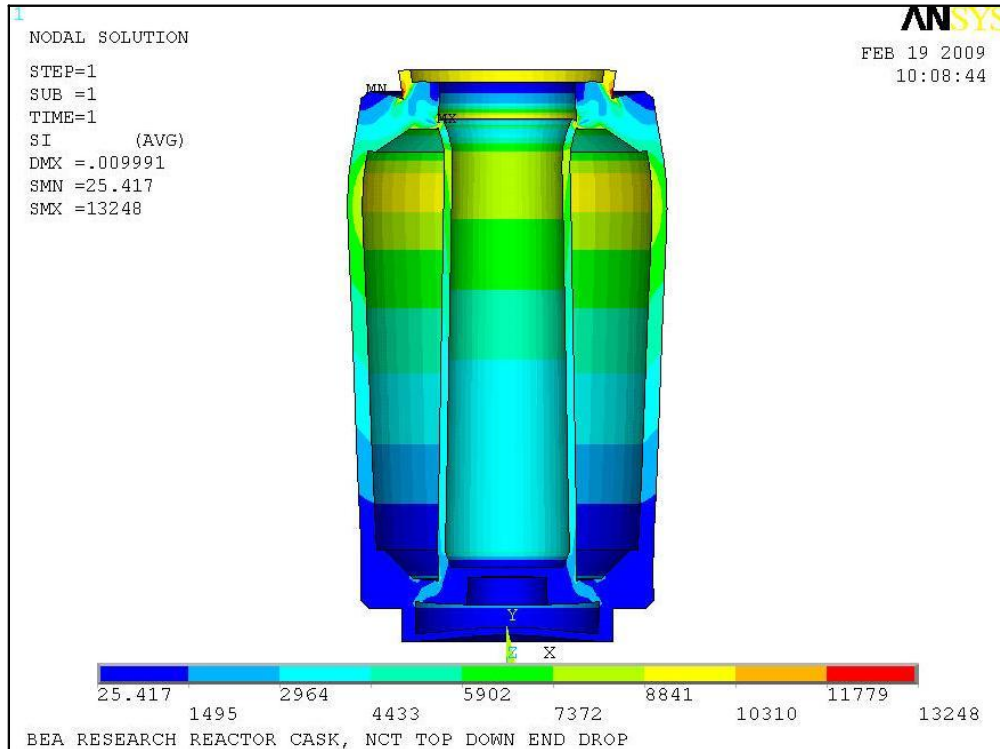


Figure 2.12.4-13 – NCT Top-Down End Drop

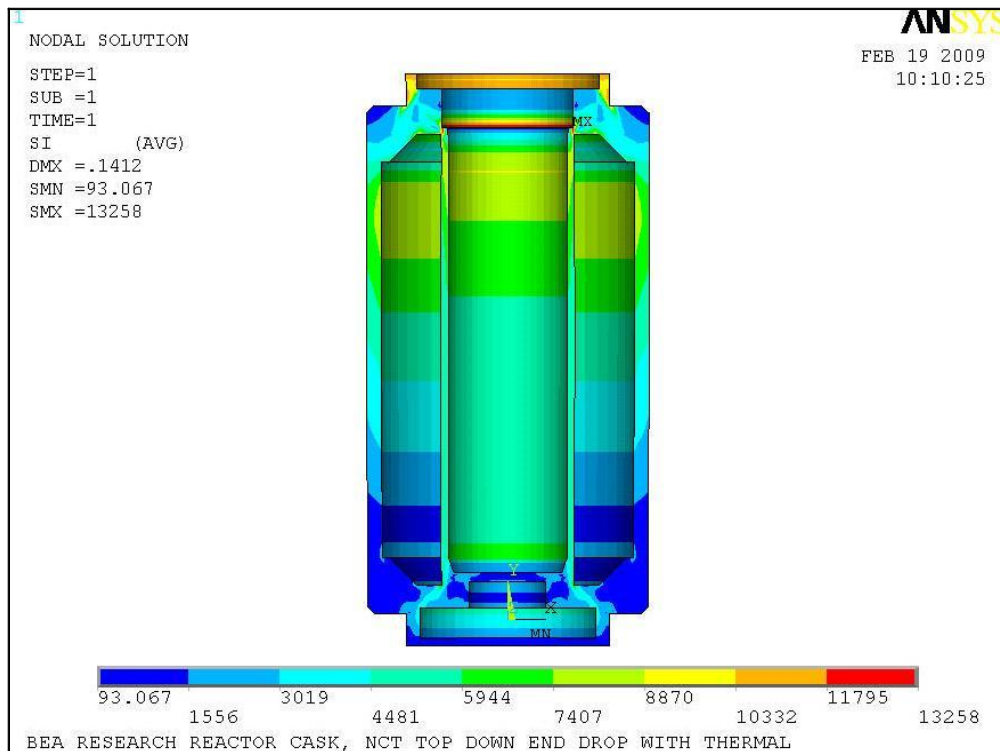


Figure 2.12.4-14 – NCT Top-Down End Drop With Thermal

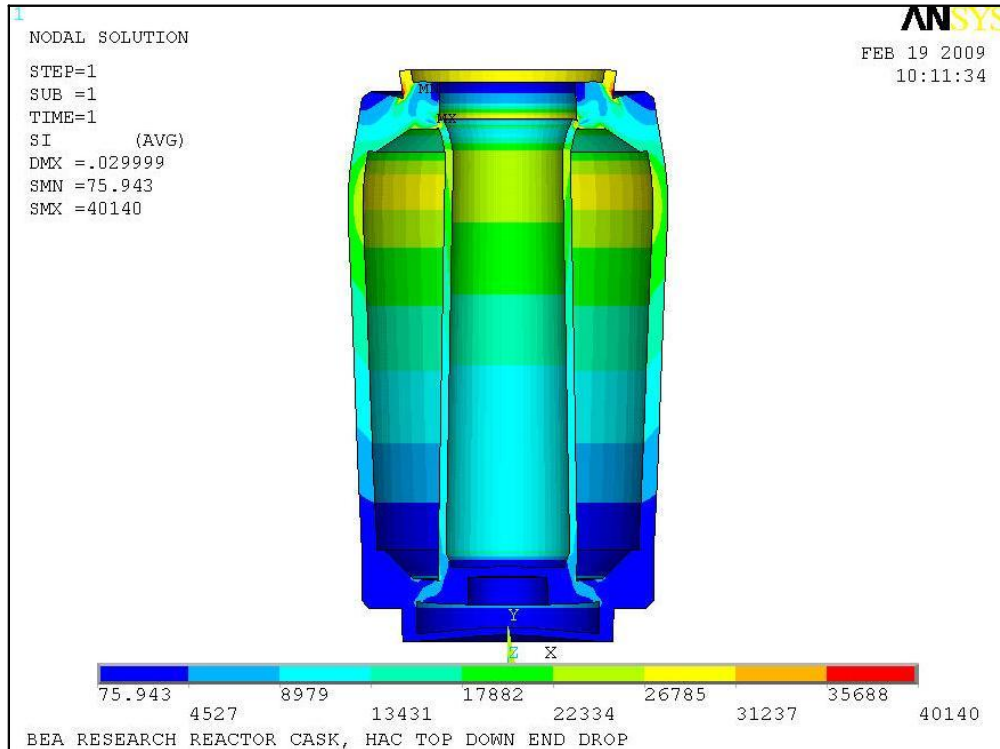


Figure 2.12.4-15 – HAC Top-Down End Drop

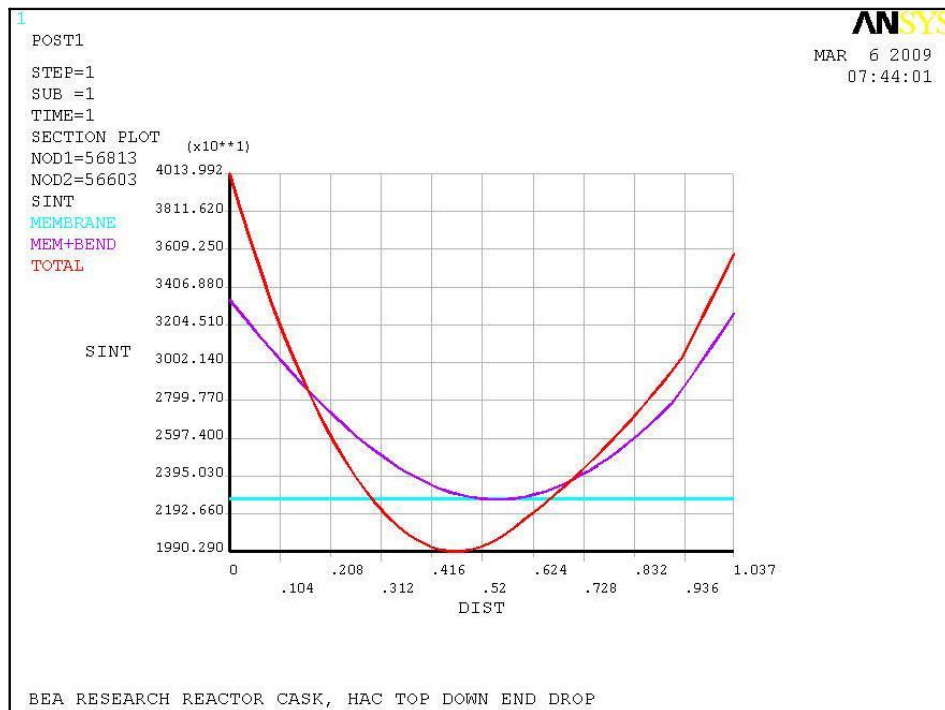


Figure 2.12.4-16 – HAC Top-Down End Drop Linearized Stress

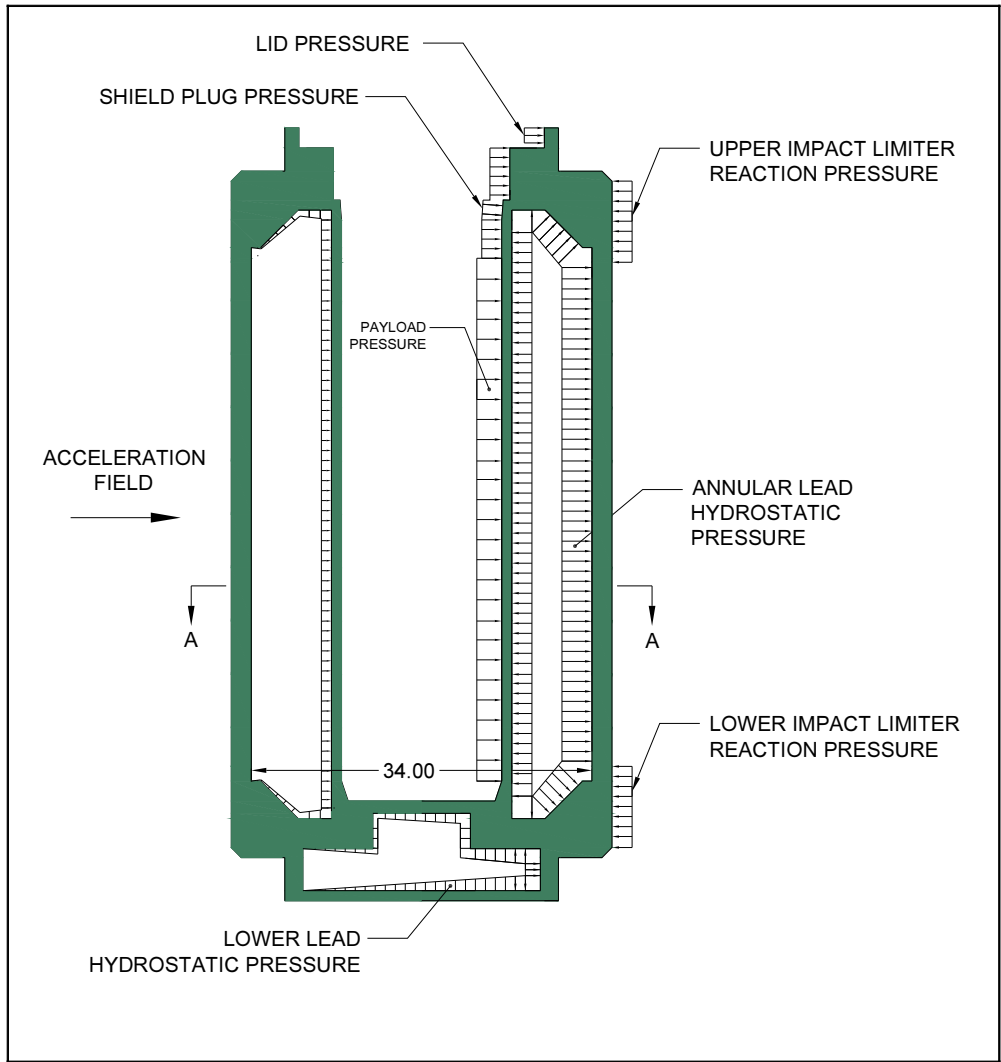


Figure 2.12.4-17 – NCT Side Drop Loading

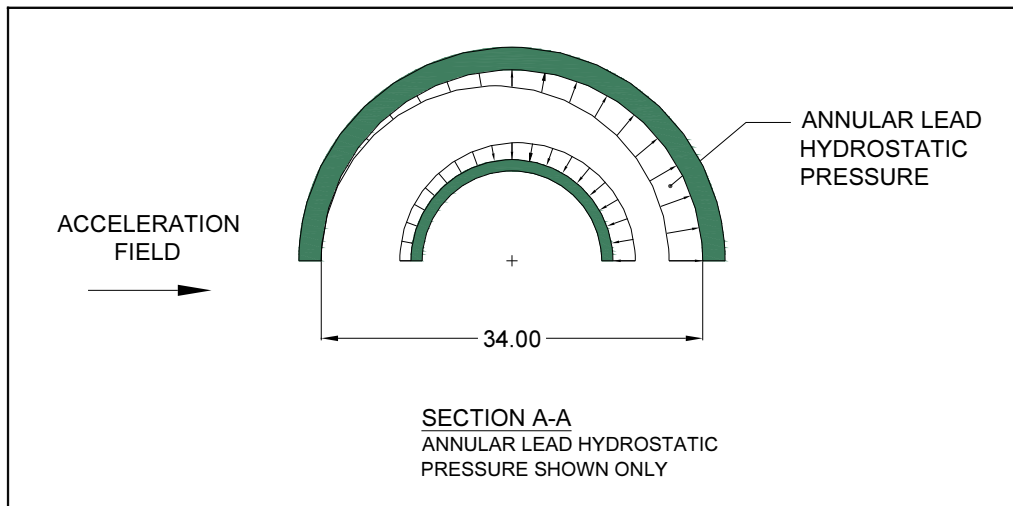


Figure 2.12.4-18 – NCT Side Drop Loading

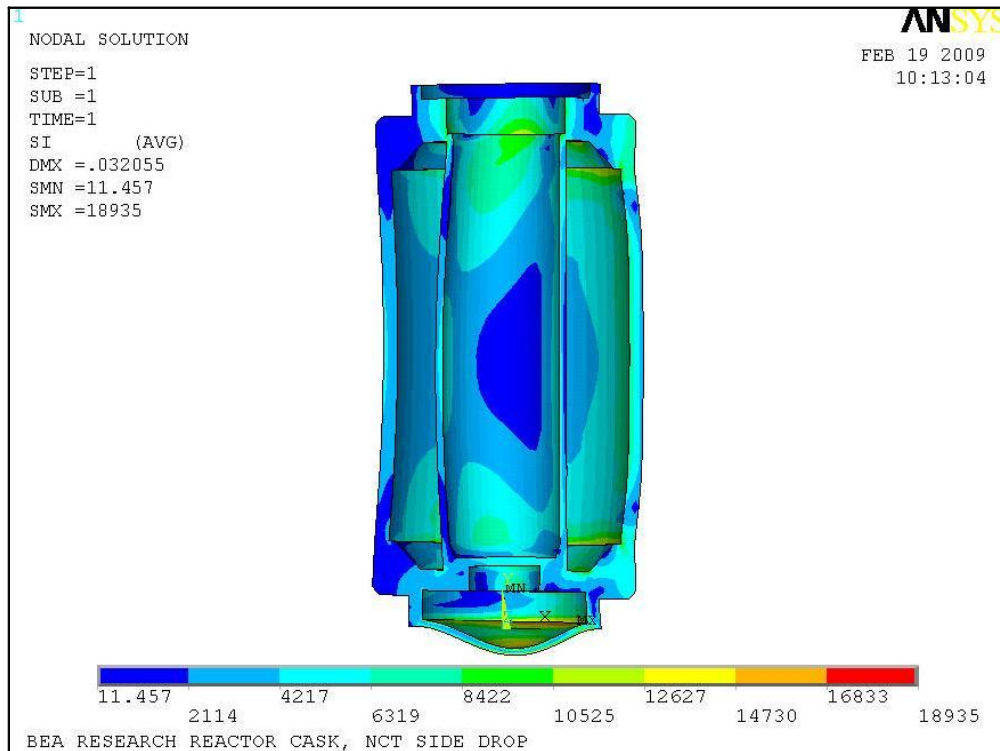


Figure 2.12.4-19 – NCT Side Drop

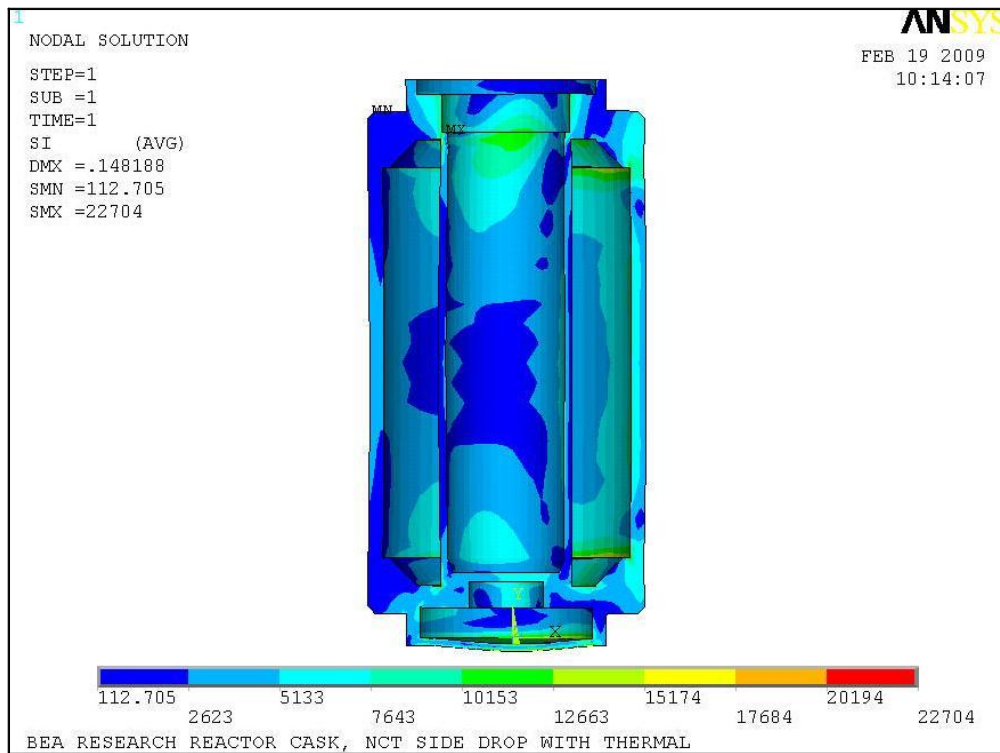


Figure 2.12.4-20 – NCT Side Drop With Thermal

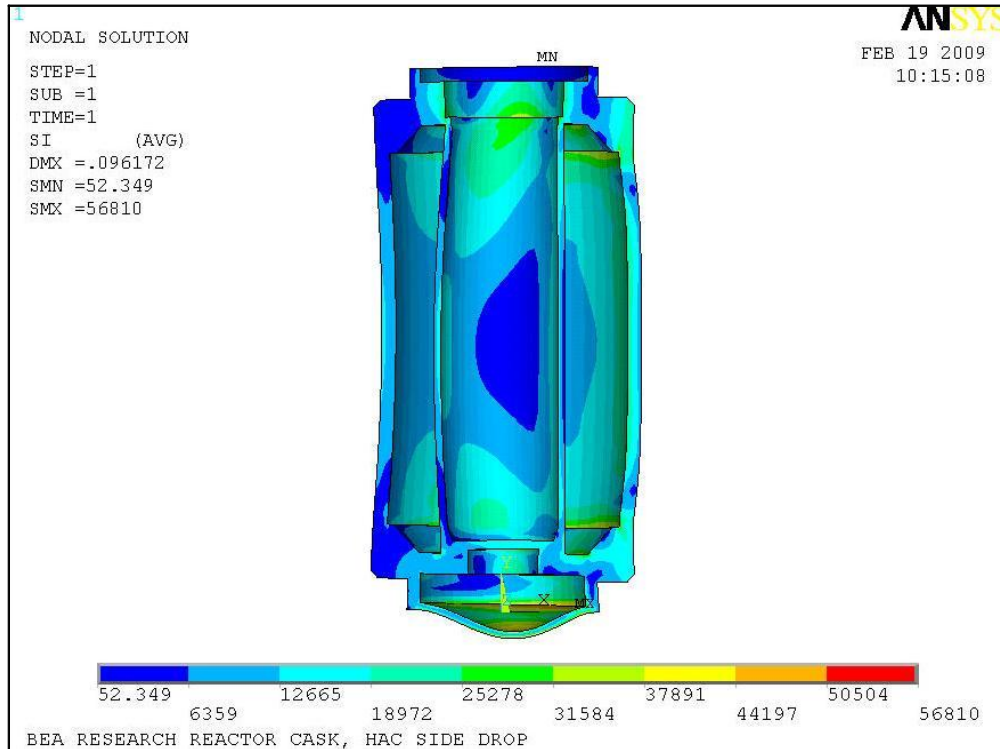


Figure 2.12.4-21 – HAC Side Drop

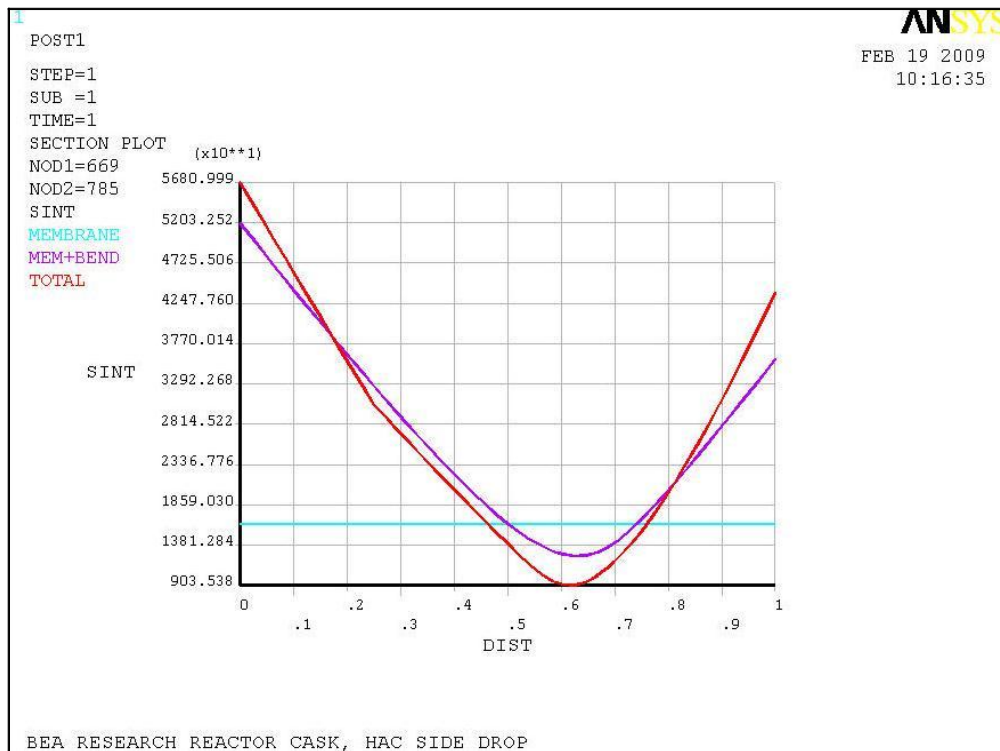


Figure 2.12.4-22 – HAC Side Drop Linearized Stress

2.12.5 Impact Limiter Performance Evaluation

This appendix presents the analytical evaluation of the impact and crush performance of the BRR package impact limiters. The impact magnitude and crush deformation of the limiters in several impact orientations, and at hot and cold bounding temperatures, is presented. Each step of the analysis is presented in detail, including the establishment of the crush properties of the polyurethane energy-absorbing foam, the calculation of the impact limiter force-deflection curves using the CASKDROP computer program, and the calculation of the impact response of the package using the SLAPDOWN computer program. A description of CASKDROP and SLAPDOWN are given in Appendix 2.12.6, *Analysis Software Descriptions*.

This appendix concludes with a reconciliation between the analysis results and test results, which shows that the analysis results are generally bounding. Of note, the impact magnitude used for stress analysis of 120g is nearly 50% greater than the highest test or analysis result.

2.12.5.1 Introduction

The analysis procedure of the impact limiter performance proceeds in three steps:

1. Calculate the effective stress-strain properties of the 9 lb/ft³ polyurethane foam used within the limiter to absorb energy. The analysis begins with the room temperature, quasi-static stress-strain curves obtained from the foam manufacturer, and then adjusts the curves for minimum (-20 °F) and maximum (150 °F) temperature, for manufacturing tolerance ($\pm 10\%$ on the bulk average strength property), for a dynamic (strain rate) effect, for the difference between the crush axis and the axes of material orthotropy, and for the effect of the outer steel shell.
2. Calculate the overall force-deflection relation for the limiter in each orientation, using the fully adjusted stress-strain curve established above and the geometry of the limiter. The result is a force-deflection curve for each orientation at each extreme temperature.
3. Calculate the overall response of the cask and impact limiters, modeling the cask as a rigid rod and the impact limiters as non-linear springs. The result is the impact magnitude and crush deformation of each impact limiter. If the impact orientation is not stable (i.e., a "slapdown"), calculate the acceleration at the end of the payload cavity farthest from the c.g. of the package.

These steps will now be presented in detail. The impact limiter geometry is found on drawing 1910-01-02-SAR in Appendix 1.3.3, *Packaging General Arrangement Drawings*. The basic, room temperature, quasi-static polyurethane foam stress-strain properties are taken from the database provided by the foam manufacturer, General Plastics Manufacturing Co. of Tacoma, WA. Pertinent pages from their web site are shown in Figure 2.12.5-1. Both limiters are taken to be identical, since the only actual difference is the presence of lifting bosses in the upper limiter. The maximum foam temperature of 150 °F is established in Section 2.6.1.1, *Summary of Pressures and Temperatures*. The minimum temperature is -20 °F as defined in [1].

The polyurethane foam is introduced into the impact limiter steel shells as a liquid, which then solidifies. During solidification, orthotropy of properties is established along an axis perpendicular to the ground ("parallel-to-rise") and on the orthogonal axis ("perpendicular-to-rise"). The parallel-to-rise direction is the same as the axis of the package.

2.12.5.1.1 Foam Stress-Strain Determination

The foam stress-strain curves are a function of the given strain, temperature, manufacturing tolerance, dynamic crush factor, drop orientation, and a steel shell adjustment. This procedure is illustrated by means of example calculations for 10% strain and a drop orientation of 15° from the horizontal. The static crush strength at ambient temperature (75 °F) for both perpendicular and parallel-to-foam rise are calculated using the method and formulas given in Tables 7 and 8 of the manufacturer's data sheet shown in Figure 2.12.5-1. The resulting static, room temperature crush strengths are shown in the left-hand columns of Table 2.12.5-1 (parallel-to-rise) and Table 2.12.5-2 (perpendicular-to-rise). The basic equation for static crush strength is:

$$\sigma = Y\rho^S$$

where σ is the crush strength in psi, ρ is the foam density in lb/ft³, and Y and S are constants which depend on the strain level. As an example, for 10% strain,

$$\sigma_{\text{Para}}(\varepsilon = 10\%) = Y\rho^S = (7.3058)(9)^{1.6590} = 280 \text{ psi}$$

$$\sigma_{\text{Perp}}(\varepsilon = 10\%) = Y\rho^S = (6.3841)(9)^{1.7182} = 278 \text{ psi}$$

The static crush strength is modified by a temperature coefficient and a manufacturing tolerance for both the hot (150 °F) and cold (-20 °F) conditions. The manufacturing tolerance is included by entering a $\pm 10\%$ variation in the crush strength. These two effects are conservatively combined such that the -10% manufacturing tolerance is applied to the hot temperature case (both tend to reduce crush strength) and the +10% manufacturing tolerance is applied to the cold temperature case (both tend to increase crush strength).

Static crush strength using the C_T values found in Tables 7 and 8 of Figure 2.12.5-1 combining the cold (-20 °F) temperature with the plus manufacturing tolerance is illustrated by the following example for 10% strain:

$$\sigma_{\text{Para}}(\varepsilon = 10\%) = C_T(\sigma_{\text{Para}})(1 + \text{Bias}) = 1.29(280)(1 + 0.1) = 397 \text{ psi}$$

$$\sigma_{\text{Perp}}(\varepsilon = 10\%) = C_T(\sigma_{\text{Perp}})(1 + \text{Bias}) = 1.32(278)(1 + 0.1) = 404 \text{ psi}$$

Similarly, static crush strength at the hot (150 °F) temperature with the minus manufacturing tolerance gives:

$$\sigma_{\text{Para}}(\varepsilon = 10\%) = C_T(\sigma_{\text{Para}})(1 - \text{Bias}) = 0.71(280)(1 - 0.1) = 179 \text{ psi}$$

$$\sigma_{\text{Perp}}(\varepsilon = 10\%) = C_T(\sigma_{\text{Perp}})(1 - \text{Bias}) = 0.72(278)(1 - 0.1) = 180 \text{ psi}$$

The manufacturer's data extends as far as a strain of 70%. In some drop orientations at the hot temperature, local strains are expected to exceed this value. In order to account for this, the manufacturer's data was extrapolated between 70% and 80% strain. To demonstrate the validity of this approach, the extrapolated curve is compared to data up to 80% strain that has been previously published [34] by the same manufacturer, in Figure 2.12.5-18¹. The curves shown in Figure 2.12.5-18 are for a temperature of 150 °F and parallel to rise. Note that between zero and

¹ Note from Figure 2.12.5-18 that polyurethane foam does not have a discrete "lock up" point. While the foam becomes much stiffer at high strains, this occurs relatively gradually compared to other materials such as aluminum honeycomb.

70% strain, the two curves are quite similar, which demonstrates that foam behavior has not changed significantly since the previous data was published. As shown in the figure, the lower curve (current data, extrapolated above 70%) has a slower rise in stress with increasing strain than the upper (previously published) data curve. Use of the extrapolated curve (according to the procedure used in this appendix) will result in a conservatively greater crush deformation prediction than the upper curve. Since the actual foam behavior may tend to be more in line with the upper stress-strain curve, a calculation of package impact acceleration was made using the upper curve, according to the procedure described in Section 2.12.5.1, *Introduction*. This calculation results in the largest impact acceleration that would be expected from the hot case utilizing foam stress-strain behavior like that previously published in the region beyond 70% strain. Since the largest impact was desired, the stress-strain curve was conservatively increased by 10% for manufacturing variability. The results are given in Table 2.12.5-25, which compare the results of the two curves utilizing the governing 15° slapdown orientation. The results, as expected, show less strain and higher impact for the previously published stress-strain data. Although the maximum impact of 89.6g is slightly higher than the cold case maximum value of 86.8g, it is still far below the bounding value used in stress calculations of 120g. Therefore, the method of extrapolating the hot case foam stress-strain values is acceptable. Note that in the one case where a strain of up to 83.2% is needed (see Table 2.12.5-14), the stress for 80% is used, adding further conservatism to the maximum impact limiter deformation strain result.

The resulting static crush strengths at the temperature extremes are shown in the right-hand columns of Table 2.12.5-1 (parallel-to-rise) and Table 2.12.5-2 (perpendicular-to-rise).

The static crush strength is further modified to account for the dynamic loading of the impact limiter. Table 9 in the manufacture's datasheet (reproduced in Figure 2.12.5-1) provides the method used to calculate the dynamic crush strength. The formula used is:

$$\sigma_{\text{Dynamic}} = Y_{\text{int}} (\sigma_{\text{Static}})^S$$

where Y_{int} and S are different values than those defined above, and σ_{Static} is the static crush strength given on the right-hand side of Table 2.12.5-1 and Table 2.12.5-2. Examples for 10% strain at room temperature and the two temperature extremes are given as follows:

Dynamic crush strength at room temperature:

$$\sigma_{\text{Para}}(\varepsilon = 10\%) = Y\sigma_{\text{Para}}^S = (1.2971)(280)^{1.0330} = 437 \text{ psi}$$

$$\sigma_{\text{Perp}}(\varepsilon = 10\%) = Y\sigma_{\text{Perp}}^S = (1.2971)(278)^{1.0330} = 434 \text{ psi}$$

Dynamic crush strength at the cold temperature:

$$\sigma_{\text{Para}}(\varepsilon = 10\%) = Y\sigma_{\text{Para}}^S = (1.2971)(397)^{1.0330} = 627 \text{ psi}$$

$$\sigma_{\text{Perp}}(\varepsilon = 10\%) = Y\sigma_{\text{Perp}}^S = (1.2971)(404)^{1.0330} = 639 \text{ psi}$$

Dynamic crush strength at the hot temperature:

$$\sigma_{\text{Para}}(\varepsilon = 10\%) = Y\sigma_{\text{Para}}^S = (1.2971)(179)^{1.0330} = 276 \text{ psi}$$

$$\sigma_{\text{Perp}}(\varepsilon = 10\%) = Y\sigma_{\text{Perp}}^S = (1.2971)(180)^{1.0330} = 277 \text{ psi}$$

BRR Package Safety Analysis Report

Table 9 does not provide values for the dynamic crush strength for strains above 70%. The values for S and Y for 70% strain are used to extend the curve up to 80% for the hot case (the room temperature case must also be extended in order to perform the adjustment for the steel shell as shown below). This keeps the dynamic crush strength dependence on the static crush strength similar to that of the highest strain in Table 9. If the value of either variable (S or Y) is modeled too high, the dynamic crush strength will be greatly increased resulting in much lower deformation. Since much of the energy from the crush will be dissipated in the initial 70% strain, small variations of the dynamic crush strength at the highest strains are negligible. The effect of this assumption will be compared against the test data. Table 2.12.5-3 and Table 2.12.5-4 show the result of the dynamic crush adjustment.

The variation in crush strength due to drop orientation is calculated based on the angle of the drop test with respect to the horizontal plane and the axis of the cask. The rise direction of the polyurethane foam is assumed to be parallel to the axis of the cask. An ellipse function is used to combine the parallel and perpendicular crush strength curves to obtain the crush curve for a particular drop orientation. The example for 10% strain and an impact orientation of 15° is carried out below.

Room temperature crush strength adjusted for orientation:

$$\sigma_{\text{Ambient}} = \frac{1}{\sqrt{\left(\frac{\sin \theta}{\sigma_{\text{Para}}}\right)^2 + \left(\frac{\cos \theta}{\sigma_{\text{Perp}}}\right)^2}} = \frac{1}{\sqrt{\left(\frac{\sin(15^\circ)}{437}\right)^2 + \left(\frac{\cos(15^\circ)}{434}\right)^2}} = 434 \text{ psi}$$

Cold crush strength adjusted for orientation:

$$\sigma_{\text{Cold}} = \frac{1}{\sqrt{\left(\frac{\sin \theta}{\sigma_{\text{Para}}}\right)^2 + \left(\frac{\cos \theta}{\sigma_{\text{Perp}}}\right)^2}} = \frac{1}{\sqrt{\left(\frac{\sin(15^\circ)}{627}\right)^2 + \left(\frac{\cos(15^\circ)}{639}\right)^2}} = 638 \text{ psi}$$

Hot crush strength adjusted for orientation:

$$\sigma_{\text{Hot}} = \frac{1}{\sqrt{\left(\frac{\sin \theta}{\sigma_{\text{Para}}}\right)^2 + \left(\frac{\cos \theta}{\sigma_{\text{Perp}}}\right)^2}} = \frac{1}{\sqrt{\left(\frac{\sin(15^\circ)}{276}\right)^2 + \left(\frac{\cos(15^\circ)}{277}\right)^2}} = 277 \text{ psi}$$

Table 2.12.5-5, Table 2.12.5-6, and Table 2.12.5-7 show the stress-strain values adjusted for dynamic loading.

Finally, the stress-strain curves generated by this method were biased upward to account for the steel shell of the impact limiter. A bias equivalent to a 47 percent strength increase was applied to the foam crush strength at ambient (75 °F) temperature. This bias is based on results obtained in engineering tests of the MOX Fresh Fuel Package (MFFP, NRC Docket 71-9295, Appendix 2.12.1). The bias was applied by adding 47% of the room temperature adjusted crush strength (see Table 2.12.5-5) to either the cold or hot adjusted crush strengths (Table 2.12.5-6 and Table 2.12.5-7, respectively). Following the example,

Crush strength biased for steel shell, cold (10% strain, 15° orientation):

BRR Package Safety Analysis Report

$$\sigma(\varepsilon) = 0.47(\sigma_{\text{Ambient}}) + \sigma_{\text{Cold}} = .47(434) + 638 = 842 \text{ psi}$$

Crush strength biased for steel shell, hot (10% strain, 15° orientation):

$$\sigma(\varepsilon) = 0.47(\sigma_{\text{Ambient}}) + \sigma_{\text{Hot}} = .47(434) + 277 = 481 \text{ psi}$$

Table 2.12.5-8 presents the complete set of stress-strain data that supports the calculation of impact limiter force-deflection curves. These values represent a summary of the adjustments to the static, room temperature data for temperature extremes, manufacturing tolerance, dynamic effect, impact orientation, and steel shell bias.

2.12.5.1.2 Force-Deflection Curves

The force-deflection curves are calculated using the computer program CASKDROP. Given an impact limiter external geometry, orientation to the impacting surface, and crush strength corresponding to that orientation, CASKDROP calculates the total crush force for each increment of deflection. The calculational technique is described in detail in Appendix 2.12.6, *Analysis Software Descriptions*. In summary, CASKDROP divides the crush area into small regions, and for each differential element, calculates the strain and, by means of the stress-strain table, the corresponding stress. Multiplying the stress times the differential area and summing all of the individual forces results in the total force at a given level of crush deformation. Repeating this process at a range of crush deformations results in the complete force-deflection curve.

The geometry shown in Figure 2.12.5-2 is utilized with CASKDROP. There are very small differences between the geometry shown and the drawings given in Appendix 1.3.3, *Packaging General Arrangement Drawings*, but the effect on the force-deflection curves is negligible.

The drop angle formed when the package center of gravity is directly over the conical diameter corner of the impact limiter is of particular interest. This angle is known as the center of gravity over corner, or cg-over-corner. At this angle, the impact limiter will absorb all of the drop kinetic energy on the primary impact. This angle is calculated as:

$$\theta_{\text{cg}} = \text{Tan}^{-1} \frac{L}{d_c} = \text{Tan}^{-1} \left[\frac{119.5}{48.1} \right] = 68^\circ$$

where L is the total height of the cask, and d_c is the conical diameter.

CASKDROP was used to generate force-deflection curves for drop orientations of 0°, 15°, 30°, 45°, 60°, 68° and 90° from a horizontal cask orientation. Since the cg-over-corner drop orientation is considered critical for the calculation, that angle was selected instead of 75° in the sequence. Table 2.12.5-9 summarizes the input data used with the CASKDROP program for this solution. Note: because CASKDROP actually solves for the total crush in stable orientations using an energy approach, the program requires inputs of package weight and drop height. However, since only the force-deflection output is relevant here, the weight and drop height are not listed in the table.

Force-deflection curves are taken directly from the CASKDROP output files, except for the case of the horizontal side drop. Since CASKDROP outputs a single force-deflection curve, the result must be divided by 2 in this case, since two limiters are in contact with the ground. The force-deflection curves for the stated orientations, for hot and cold conditions, are shown in Figure 2.12.5-3 through Figure 2.12.5-9.

2.12.5.1.3 Impact Acceleration and Crush Deformation

The SLAPDOWN program, as described in Appendix 2.12.6, *Analysis Software Descriptions*, was used to analyze the impact response of the BRR package with the unyielding surface. It is particularly useful when the center of gravity is not directly over the impact point. Under these circumstances, the package will generally hit, begin to rotate, and strike the ground a second time as a “slapdown” impact. SLAPDOWN conducts a time-integration analysis using a model of the package as a rigid rod, and of the impact limiters as non-linear springs. Given a drop height, the package has an initial velocity at impact. The energy is absorbed first by the primary spring/impact limiter ('nose'), which imparts a rotational force to the model, until the secondary spring/impact limiter ('tail') comes in contact. Most of the energy absorbed by the springs is lost, except the portion that is restored by springback. The position, angle, velocity, and acceleration in both linear and rotational modes are calculated for each time step.

The force-deflection curves calculated by CASKDROP were input into SLAPDOWN to produce the results listed in this analysis. The primary impact limiter non-linear spring data was equal to the force-deflection curve created for the corresponding impact orientation. The secondary impact limiter non-linear spring was equal to the force-deflection curve for the zero degree orientation (i.e., horizontal) in each case. Additional input variables used in SLAPDOWN are summarized in Table 2.12.5-10, and briefly described below.

Length, Nose-to-CG – the distance along the cask axis from the location of impact to the CG of the cask. The impact location is dependent on the drop angle and ranges from one-half the total span between impact limiter springs of $77.13/2 = 38.565$ inches for the side drop, to zero for the cg-over-corner drop (68°) and end drop (90°). Note that the discrete location of the impact limiter springs has been taken as coincident with the flat ends of the cask body.

Length, Tail-to-CG – the distance from the location of the secondary impact to the CG. This value remains the same as the secondary impact is considered to be a horizontal impact in all cases.

Radius, Nose Limiter – the radius of the primary impact limiter.

Radius, Tail Limiter – the radius of the secondary impact limiter.

Body Mass – the total mass of the cask and impact limiters expressed in $\text{lb}_m\text{-s}^2/\text{in}$, equivalent to the bounding package weight of 32,000 lb from Table 2.1-2.

Rotational Moment of Inertia – the rotational moment of inertia of the cask and assembly, calculated using the weight and geometry of the package.

Drop Height – the initial height of the cask prior to free drop measured in feet.

Impact Angle – the orientation of the primary impact, measured to the horizontal.

2.12.5.2 Results

The results of the analysis include the maximum crush and acceleration values for the given orientations. For unstable, i.e., slapdown orientations, the acceleration output is taken at a distance of 29.565 inches from the c.g. of the cask, which is conservatively further from the c.g. than either end of the payload cavity, and it is the maximum acceleration that the payload will experience.

The calculated impact limiter strain is determined as a percentage of the maximum allowable crush. The allowable crush is the distance between the point of impact on the limiter and the closest point of the internal shell of the limiter, and is calculated from the drawings for each orientation of primary impact. The allowable crush for secondary impact is the same for all cases, since the orientation is assumed to be horizontal in each case. The actual crush distance is the value provided as part of the SLAPDOWN output. The impact limiter strain is:

$$\varepsilon_{IL} = \frac{\text{Actual Crush}}{\text{Allowable Crush}}(100\%)$$

2.12.5.2.1 HAC Free Drop Results

Table 2.12.5-11 through Table 2.12.5-14 summarize the HAC free drop results. Note that maximum accelerations are governed by the cold case, and maximum impact limiter strain by the hot case. Figure 2.12.5-10 and Figure 2.12.5-11 show the maximum impact limiter strain developed for the primary and secondary impacts for the specified impact orientations. From a comparison of the two plots, the overall maximum impact limiter strain occurs in the secondary impact, hot case, for a primary impact orientation of 15°. Figure 2.12.5-12 and Figure 2.12.5-13 show the maximum acceleration of the cask for the specified drop orientations. The overall maximum impact acceleration occurs in the secondary impact, cold case, for a primary impact orientation of 15°.

2.12.5.2.2 NCT Free Drop Results

The NCT test requires the cask to be dropped from a height of two feet, per 10 CFR §71.71(c)(7). Table 2.12.5-15 through Table 2.12.5-18 summarize the NCT free drop results, using the same orientations and force-deflection curves as for the HAC cases.

Figure 2.12.5-14 and Figure 2.12.5-15 show the maximum impact limiter strain developed for the NCT primary and secondary impacts for the specified impact orientations. The maximum strain for the primary impact occurs at 68°, while the maximum strain for the secondary impact is seen to occur at a primary impact orientation of 15°. In both cases, the maximum strain is bounded by all the HAC strains for both primary and secondary impacts.

Figure 2.12.5-16 and Figure 2.12.5-17 show the maximum acceleration of the cask for the specified drop orientations. The maximum impact acceleration occurs in the 90° orientation. As expected, all NCT impact cases are bounded by the HAC cases. The NCT governing cases are different than the HAC governing cases, but this is to be expected due to the difference in impact velocity and energy absorbed.

2.12.5.2.3 Combined HAC and NCT Free Drop Results

Since 10 CFR 71 requires that the NCT free drop precede the HAC free drop, the effect of the combination of both drops is next considered. Since the impact acceleration is a function of the crush of the limiter, and the crush of the limiter is a function of the energy absorbed, a 2-foot free drop followed by a 30-foot free drop (taken in the same orientation on the same spot) may be modeled as a single 32-foot free drop. This is a conservative assumption, which neglects the effect of material springback which will occur after the initial NCT impact.

A sample of selected cold impact cases, where the acceleration was shown to be the highest, as shown in Table 2.12.5-19 and Table 2.12.5-20 demonstrates that the maximum increase in acceleration is less than 5 percent. A sample of selected hot impact cases, where the strain was shown to be greater than the cold impact cases, is shown in Table 2.12.5-21 and Table 2.12.5-22. From the results of the combined NCT and HAC drop, it is clear that the effect of the NCT free drop on the HAC free drop is negligible.

2.12.5.3 Reconciliation with Certification Test Results

To verify the BRR Package functions as intended, a half-scale CTU was tested in three drop orientations as described in Appendix 2.12.3, *Certification Test Results*. The results of the test indicate that the results predicted in this calculation are conservative. The test results for the HAC end, slapdown, and c.g.-over-corner orientations are shown in Table 2.12.5-23. To convert the half-scale results to full-scale, the acceleration is divided by 2, and the crush distance is multiplied by 2.

The transverse accelerometers were located 8.68 inches from the end of the cask, or 17.36 inches in the equivalent full-scale, whereas the SLAPDOWN calculations correspond to the end of the cask cavity at the bottom, bounded by a distance of 29.565 inches from the cask c.g. This difference does not affect the stable impact orientations such as the end (D1) and c.g. over corner (D3), but for the slapdown impact (D2R), an adjustment of the test results must be made before comparison to the SLAPDOWN calculations.

The acceleration at any point along the axis in an oblique impact can be found from:

$$a_i = a_{c.g.} + \alpha L$$

where $a_{c.g.}$ is the acceleration of the center of gravity (in/s^2), α is the rotational acceleration in rad/s^2 , and L is the distance of the point i from the c.g. in inches. Since $a_{c.g.}$ was not measured in the test, it must be calculated using the known location of the transverse accelerometers and the rotational acceleration calculated using SLAPDOWN. At the moment of maximum primary impact, the rotational acceleration is calculated by SLAPDOWN to be $\alpha_p = 534 \text{ rad/s}^2$. The full scale equivalent location of the accelerometers from the cask c.g. was:

$$L_{\text{accel}} = \frac{L_{\text{cask}}}{2} - 17.36 = 21.21 \text{ in}$$

where $L_{\text{cask}} = 77.13$ inches, and the full scale equivalent location of the accelerometers from the cask end was 17.36 inches. The full-scale acceleration of the cask c.g. for the primary event in the test therefore can be computed as:

$$a_{\text{test c.g.-P}} = a_{\text{accel-P}} - \alpha_p L_{\text{accel}} = 10,892 \text{ in/s}^2$$

where the full-scale measured acceleration from Table 2.12.5-23 for the primary impact of test D2R, $a_{\text{accel-P}} = 57.5g$ (i.e., $22,218 \text{ in/s}^2$), and the location of the accelerometers, $L_{\text{accel}} = 21.21$ inches from the cask c.g. The acceleration of the test cask at the location of used for the SLAPDOWN runs (i.e., the bottom end of the payload cavity) is therefore:

$$a_{\text{adj-P}} = a_{\text{test c.g.-P}} + \alpha_p L_{\text{adj}} = 26,680 \text{ in/s}^2 = 69.0g$$

where the distance from the cask c.g. to the location of the SLAPDOWN output is $L_{adj} = 29.565$ inches. The corresponding SLAPDOWN calculated output acceleration for the primary impact is equal to 71.0g from Table 2.12.5-11.

Similarly, at the moment of maximum secondary impact, the rotational acceleration is calculated by SLAPDOWN to be $\alpha_S = 687 \text{ rad/s}^2$. The full-scale acceleration of the cask c.g. for the secondary event in the test can be computed as:

$$a_{\text{test c.g.-S}} = a_{\text{accel-S}} - \alpha_S L_{\text{accel}} = 7,454 \text{ in/s}^2$$

where the full-scale measured acceleration from Table 2.12.5-23 for the secondary impact of test D2R, $a_{\text{accel-S}} = 57.0\text{g}$ (i.e., $20,025 \text{ in/s}^2$), and L_{accel} is the same as above. The acceleration of the test cask at the location used for the SLAPDOWN runs (i.e., the bottom end of the payload cavity) is therefore:

$$a_{\text{adj-S}} = a_{\text{test c.g.-S}} + \alpha_S L_{\text{adj}} = 27,765 \text{ in/s}^2 = 71.8\text{g}$$

The corresponding SLAPDOWN calculated output acceleration for the secondary impact is equal to 86.8g from Table 2.12.5-12.

The results show that the corrected test accelerations are still below the maximum acceleration used in stress analysis of 120g. The maximum secondary acceleration of 71.8g is lower than the calculated value of 86.8g. The corrected primary acceleration of 69.0g is also below the calculated value of 71.0g. This indicates that the calculation is essentially bounding for all cases. The principal conclusion, however, is that the actual accelerations of the BRR package are well below the bounding value of 120g used in the stress calculations.

As stated in Section 2.12.3.3, *Test Unit Configuration*, the weight of the test cask was 3,181 lb, or when properly adjusted for scale, approximately 7% below the maximum equivalent full-scale weight of 32,000 lb. This had the effect of conservatively increasing the recorded accelerations of the CTU. Correspondingly, the crush deformations were slightly underestimated in the test, since there was less kinetic energy in the drop.

The force-deflection curves discussed in Section 2.12.5.1.2, *Force-Deflection Curves*, show that the strain increases nonlinearly with an increase in applied load. Therefore, although an increase in weight will result in an increased deformation, each succeeding crush strain increment becomes smaller as a greater force is applied, particularly as the end of crush is neared. Thus the percent change in the crush distance will be smaller in magnitude than the percent change in weight. Since the increase in the crush distance will be less than the weight increase, and since the weight increase is small in magnitude, the crush distance is bounded by the values in the calculation. This holds true for both the cold and hot temperature conditions developed in this calculation. The bounding crush strain corresponds to the 15° secondary impact in the hot case. As shown in Table 2.12.5-14, the predicted crush is 15.9 inches. Since, as shown in Table 2.12.5-24, the cold secondary crush was measured to be 36% lower than the prediction, then the small increase in weight of 7% will not invalidate the hot case maximum predicted crush. Thus the predictions are conservative.

A comparison of the calculated ('Calc') and full-scale equivalent test ('Actual') impact limiter performance is given in Table 2.12.5-24. A negative sign in the '% Less' columns indicates that the test result was lower than the calculated value.

2.12.5.4 Conclusion

The impact limiter evaluation is used to establish a bounding impact magnitude for stress analysis in other sections of this SAR. The maximum impact occurs in the cold temperature case. For NCT, the maximum overall impact is equal to 32.9g in the 90° orientation, from which a bounding impact for all orientations of 40g is taken. For HAC, the maximum overall impact is 86.8g in the 15° secondary slapdown impact, and a very conservative value of 120g is used as a bounding impact for all orientations.

The maximum strain occurs under HAC in the hot temperature case, and equals 83.2% in the 15° secondary slapdown case.

Table 2.12.5-1 - Parallel-to-Rise Static Compressive Strength (psi)

Strain	Room Temperature (75 °F)				-20 °F		150 °F	
	Y, int	density	S	Crush Str	C _T	Crush Str	C _T	Crush Str
10%	7.3058	9	1.6590	280	1.29	397	0.71	179
20%	6.7276	9	1.7021	283	1.36	423	0.73	186
30%	6.4961	9	1.7350	294	1.32	427	0.74	196
40%	6.9137	9	1.7255	306	1.29	434	0.75	207
50%	5.6711	9	1.8877	359	1.26	498	0.76	246
60%	5.3279	9	2.0431	474	1.28	667	0.76	324
65%	5.9871	9	2.0870	587	1.29	833	0.76	402
70%	6.2085	9	2.1868	758	1.37	1142	0.81	553
75%				952				710
80%				1,204				928

Table 2.12.5-2 - Perpendicular-to-Rise Static Compressive Strength (psi)

Strain	Room Temperature (75 °F)				-20 °F		150 °F	
	Y, int	density	S	Crush Str	C _T	Crush Str	C _T	Crush Str
10%	6.3841	9	1.7182	278	1.32	404	0.72	180
20%	6.5943	9	1.6946	273	1.35	405	0.74	182
30%	6.1154	9	1.7403	280	1.34	413	0.79	199
40%	5.7722	9	1.8023	303	1.32	440	0.77	210
50%	5.3041	9	1.9054	349	1.32	507	0.77	242
60%	5.3181	9	2.0392	470	1.33	688	0.77	326
65%	5.7864	9	2.1002	584	1.34	861	0.77	405
70%	5.7701	9	2.2255	767	1.36	1,147	0.78	538
75%				971				683
80%				1,240				878

Table 2.12.5-3 - Parallel-to-Rise Dynamic Crush Strength

Strain	Dynamic Crush Strength Coefficients		Dynamic Crush Strength (psi)		
	Y, int	S	75 °F	-20 °F	150 °F
10%	1.2971	1.0330	437	627	276
20%	1.4397	1.0069	424	635	278
30%	1.5181	0.9941	432	625	288
40%	1.3887	1.0028	432	613	292
50%	1.4419	0.9912	492	680	338
60%	1.4275	0.9831	610	853	419
65%	1.3871	0.9910	769	1088	528
70%	1.4660	0.9586	844	1251	624
75%	1.4660	0.9586	1,051		793
80%	1.4660	0.9586	1,316		1,025

Table 2.12.5-4 - Perpendicular-to-Rise Dynamic Crush Strength

Strain	Dynamic Crush Strength Coefficients		Dynamic Crush Strength (psi)		
	Y, int	S	75 °F	-20 °F	150 °F
10%	1.2971	1.0330	434	639	277
20%	1.4397	1.0069	409	608	272
30%	1.5181	0.9941	411	605	293
40%	1.3887	1.0028	428	622	296
50%	1.4419	0.9912	478	692	332
60%	1.4275	0.9831	605	879	422
65%	1.3871	0.9910	765	1124	532
70%	1.4660	0.9586	854	1256	608
75%	1.4660	0.9586	1,071		764
80%	1.4660	0.9586	1,354		972

Table 2.12.5-5 - Dynamic Strength Adjusted for Impact Angle (75 °F)

Strain	Angle of Impact (degrees)						
	0	15	30	45	60	68	90
	Compressive Stress (psi)						
10%	434	434	435	435	436	437	437
20%	409	410	413	416	420	422	424
30%	411	412	416	421	426	429	432
40%	428	428	429	430	431	431	432
50%	478	479	481	485	488	490	492
60%	605	605	606	607	609	609	610
65%	765	765	766	767	768	768	769
70%	854	853	851	849	846	845	844
75%	1,071	1,070	1,066	1,061	1,056	1,054	1,051
80%	1,354	1,351	1,344	1,335	1,325	1,321	1,316

Table 2.12.5-6 - Dynamic Strength Adjusted for Impact Angle (-20 °F)

Strain	Angle of Impact (degrees)						
	0	15	30	45	60	68	90
	Compressive Stress (psi)						
10%	639	638	636	633	630	629	627
20%	608	610	614	621	628	631	635
30%	605	606	610	615	620	622	625
40%	622	621	620	617	615	614	613
50%	692	691	689	686	683	682	680
60%	879	877	872	866	859	857	853
65%	1,124	1,121	1,115	1,106	1,097	1,093	1,088
70%	1,256	1,256	1,255	1,253	1,252	1,252	1,251

Table 2.12.5-7 - Dynamic Strength Adjusted for Impact Angle (150 °F)

Strain	Angle of Impact (degrees)						
	0	15	30	45	60	68	90
	Compressive Stress (psi)						
10%	277	277	277	276	276	276	276
20%	272	272	273	275	276	277	278
30%	293	293	292	290	289	289	288
40%	296	296	295	294	293	293	292
50%	332	332	333	335	336	337	338
60%	422	422	421	420	420	419	419
65%	532	532	531	530	529	529	528
70%	608	609	612	616	620	622	624
75%	764	766	771	778	785	789	793
80%	972	975	984	997	1,011	1,017	1,025

Table 2.12.5-8 - Fully Adjusted Polyurethane Foam Stress-Strain Data

Strain	Angle of Impact (degrees)						
	0	15	30	45	60	68	90
-20 °F Stress (psi)							
10%	843	842	840	837	835	834	832
20%	800	803	808	817	825	829	834
30%	798	800	806	813	820	824	828
40%	823	822	822	819	818	817	816
50%	917	916	915	914	912	912	911
60%	1,163	1,161	1,157	1,151	1,145	1,143	1,140
65%	1,484	1,481	1,475	1,466	1,458	1,454	1,449
70%	1,657	1,657	1,655	1,652	1,650	1,649	1,648
150 °F Stress (psi)							
10%	481	481	481	480	481	481	481
20%	464	465	467	471	473	475	477
30%	486	487	488	488	489	491	491
40%	497	497	497	496	496	496	495
50%	557	557	559	563	565	567	569
60%	706	706	706	705	706	705	706
65%	892	892	891	890	890	890	889
70%	1,009	1,010	1,012	1,015	1,018	1,019	1,021
75%	1,267	1,269	1,272	1,277	1,281	1,284	1,287
80%	1,608	1,610	1,616	1,624	1,634	1,638	1,644

Table 2.12.5-9 - CASKDROP Input Data

Input Data	Value
Impact Limiter Outside Diameter, in.	78.0
Impact Limiter Overall Length, in.	34.6
Impact Limiter Conical Diameter, in.	48.1
Impact Limiter Conical length, in.	15.0
Impact Limiter End Thickness, in.	21.2
Impact Limiter Hole Diameter, in.	0
Impact Limiter Hole Length, in.	0
Body Outside Diameter, in.	38.0
Body Overall Length, in.	77.13
Frictional Coefficient	0

Table 2.12.5-10 - SLAPDOWN Input Data

Input data	Value
Length, Nose-to-C.G., in.	Variable
Length, Tail-to-C.G., in.	38.565
Radius, Nose Limiter, in.	39.0
Radius, Tail Limiter, in.	39.0
Body Mass, lb _m -s ² /in.	82.816
Rotational Moment of inertia, in-lb _m -s ²	63,246
HAC Drop Height, ft.	30
NCT Drop Height, ft	2
HAC + NCT Drop Height, ft	32
Impact Angle (with Horizontal)	Variable
Force Deflection Curves	Variable
Friction Coefficient	0

Table 2.12.5-11 - Cold Primary Impact Results, HAC

Primary Impact Angle	Acceleration	Crush	Allowable Crush	Crush Margin	Limiter Strain
(deg)	(g)	(in)	(in)	(in)	%
0	63.3	11.0	19.1	8.1	57.6
15	71.0	10.7	21.4	10.7	50.0
30	79.7	12.3	22.1	9.8	55.7
45	80.4	11.0	21.4	10.4	51.4
60	82.6	13.1	22.6	9.5	58.0
68	69.6	13.3	22.5	9.2	59.1
90	72.4	7.3	20.2	12.9	36.1

Table 2.12.5-12 - Cold Secondary Impact Results, HAC

Primary Impact Angle	Acceleration	Crush	Allowable Crush	Crush Margin	Limiter Strain
(deg)	(g)	(in)	(in)	(in)	%
0	63.3	11.0	19.1	8.1	57.6
15	86.8	12.1	19.1	7.0	63.4
30	66.2	9.3	19.1	9.8	48.7
45	56.0	7.7	19.1	11.4	40.3
60	40.1	5.1	19.1	14.0	26.7

Table 2.12.5-13 - Hot Primary Impact Results, HAC

Primary Impact Angle	Acceleration	Crush	Allowable Crush	Crush Margin	Limiter Strain
(deg)	(g)	(in)	(in)	(in)	%
0	55.1	14.5	19.1	4.6	75.9
15	53.4	13.6	21.4	7.8	63.6
30	60.8	15.8	22.1	6.3	71.5
45	66.6	14.4	21.4	7.0	67.3
60	67.9	16.5	22.6	6.1	73.0
68	55.4	16.6	22.5	5.9	73.8
90	54.8	10.5	20.2	9.7	52.0

Table 2.12.5-14 - Hot Secondary Impact Results, HAC

Primary Impact Angle	Acceleration	Crush	Allowable Crush	Crush Margin	Limiter Strain
(deg)	(g)	(in)	(in)	(in)	%
0	55.1	14.5	19.1	4.6	75.9
15	83.2	15.9	19.1	3.2	83.2
30	54.2	12.5	19.1	6.6	65.4
45	43.4	10.5	19.1	8.6	55.0
60	29.9	7.1	19.1	12.0	37.2

Table 2.12.5-15 - Cold Primary Impact Results, NCT

Primary Impact Angle	Acceleration	Crush	Allowable Crush	Crush Margin	Limiter Strain
(deg)	(g)	(in)	(in)	(in)	%
0	19.7	2.8	19.1	16.3	14.7
15	19.1	4.1	21.4	17.3	19.2
30	21.2	4.7	22.1	17.4	21.3
45	25.9	3.0	21.4	18.4	14.0
60	24.2	5.0	22.6	17.6	22.1
68	15.2	5.2	22.5	17.3	23.1
90	32.9	1.5	20.2	18.7	7.4

Table 2.12.5-16 - Cold Secondary Impact Results, NCT

Primary Impact Angle	Acceleration	Crush	Allowable Crush	Crush Margin	Limiter Strain
(deg)	(g)	(in)	(in)	(in)	%
0	19.7	2.8	19.1	16.3	14.7
15	29.6	3.7	19.1	15.4	19.4
30	29.5	3.4	19.1	15.7	17.8
45	30.1	3.5	19.1	15.6	18.3
60	28.2	3.2	19.1	15.9	16.8

Table 2.12.5-17 - Hot Primary Impact Results, NCT

Primary Impact Angle	Acceleration	Crush	Allowable Crush	Crush Margin	Limiter Strain
(deg)	(g)	(in)	(in)	(in)	%
0	13.9	3.7	19.1	15.4	19.4
15	15.7	4.9	21.4	16.5	22.9
30	16.8	5.8	22.1	16.3	26.2
45	20.0	3.9	21.4	17.5	18.2
60	19.0	6.1	22.6	16.5	27.0
68	12.4	6.4	22.5	16.1	28.4
90	23.9	2.0	20.2	18.2	9.9

Table 2.12.5-18 - Hot Secondary Impact Results, NCT

Primary Impact Angle	Acceleration	Crush	Allowable Crush	Crush Margin	Limiter Strain
(deg)	(g)	(in)	(in)	(in)	%
0	13.9	3.7	19.1	15.4	19.4
15	22.5	5.1	19.1	14.0	26.7
30	21.8	4.5	19.1	14.6	23.6
45	20.8	4.6	19.1	14.5	24.1
60	21.1	4.3	19.1	14.8	22.5

Table 2.12.5-19 - Cold Primary Impact Results, HAC + NCT

Primary Impact Angle	HAC Acceleration	HAC+NCT Acceleration	Acceleration Increase	Percent Increase
(deg)	(g)	(g)	(g)	%
15	71.0	73.2	2.2	3.1
68	69.6	71.9	2.3	3.3
90	72.4	73.9	1.5	2.1

Table 2.12.5-20 - Cold Secondary Impact Results, HAC + NCT

Primary Impact Angle	HAC Acceleration	HAC+NCT Acceleration	Acceleration Increase	Percent Increase
(deg)	(g)	(g)	(g)	%
15	86.8	90.1	3.3	3.8

Table 2.12.5-21 - Hot Primary Impact Results, HAC + NCT

Primary Impact Angle	HAC Crush	HAC+NCT Crush	Crush Increase	Percent Increase
(deg)	(in)	(in)	(in)	%
15	13.6	14.0	0.4	2.9
68	16.6	17.0	0.4	2.4
90	10.5	10.9	0.4	3.8

Table 2.12.5-22 - Hot Secondary Impact Results, HAC + NCT

Primary Impact Angle	HAC Crush	HAC+NCT Crush	Crush increase	Percent Increase
(deg)	(in)	(in)	(in)	%
15	15.9	16.3	0.4	2.5

Table 2.12.5-23 - CTU Test Results

Test #	Type	Location	Half-Scale*			Full-Scale**			
			Measured Accel. (g)		Crush Distance (in)	Measured Accel. (g)			Crush Distance (in)
			1019 Hz Cutoff	Rigid Body Estimate		1019 Hz Cutoff	Rigid Body Estimate	Δ	
D1	End Drop	Primary	116	109	3.4	58.0	54.5	3.5	6.8
D2R	Oblique Slapdown	Primary	115	104	4.0	57.5	52.0	5.5	8.0
		Secondary	114	103	3.9	57.0	51.5	5.5	7.8
D3	CG Over Corner	Primary	117	101	5.5	58.5	50.5	8.0	11.0

*Values in the '1019Hz Cutoff' and 'Crush Distance' columns are obtained from Section 2.12.3.5. The 'Rigid Body Estimate' in half-scale is formed by subtracting the average reduction value for the impact event (found in column 'E' of Table 2.12.3-6) from the 1019Hz cutoff accelerometer response. For example, for test D1, the average reduction value is 7g, and therefore the rigid body estimate is $116 - 7 = 109$ g.

**Full-scale accelerations are one-half of the half-scale results. The column labeled 'Δ' is equal to the difference between the 1019Hz cutoff result and the rigid body estimate in full scale. For example, for test D1, the rigid body estimate is $58.0 - 54.5 = 3.5$ g lower than the 1019Hz cutoff result. From this it can be seen that the 1019Hz cutoff results are reasonable, and moderately conservative.

Table 2.12.5-24 - CTU Percentage of Predicted Results (Full-Scale)

Test #	Location	Acceleration (g)*			Crush Distance (in)		
		Calc	Actual	% Less	Calc	Actual	% Less
D1	Primary	72.4	58.0/54.5	-19.9/-24.7	7.3	6.8	-6.8
D2R	Primary	71.0	69.0/63.5	-2.8/-10.6	10.7	8.0	-25
	Secondary	86.8	71.8/66.3	-17.3/-23.6	12.1	7.8	-36
D3	Primary	69.6	58.5/50.5	-15.9/-27.4	13.3	11.0	-17

* Calculated accelerations are taken from Table 2.12.5-11 and Table 2.12.5-12. Actual acceleration values are given as A/B, where A is the value derived from the 1019 Hz cutoff data, and B is the value for the rigid body estimate. The actual acceleration values for tests D1 and D3 are taken directly from Table 2.12.5-23. The actual acceleration values for test D2R are taken from the results of the adjustment procedure described in Section 2.12.5.3. The rigid body estimates for D2R are formed by subtracting the ' Δ ' value (see Table 2.12.5-23) from the adjusted values. For example, for the D2R primary case, the adjusted value derived from the 1019Hz cutoff data in Section 2.12.5.3 is 69.0g, and the ' Δ ' value from Table 2.12.5-23 is 5.5g, thus the rigid body estimate for D2R primary is $69.0 - 5.5 = 63.5$ g. The two values in the '% Less' column correspond to the two values in the 'Actual' column, and show the amount that the actual values are less than the calculated values.

Table 2.12.5-25 - Comparison of Results Using Previously Published Stress-Strain Data*

Dataset	Primary Impact		Secondary Impact	
	Deflection, in	Acceleration, g	Deflection, in	Acceleration, g
Current Data	13.6	53.4	15.9	83.2
Previous Data	13.0	57.3	15.2	89.6

* HAC, 15° slapdown, 150 °F. "Current Data" results correspond to Table 2.12.5-13 and Table 2.12.5-14.

Design Guide for use of LAST-A-FOAM FR-3700 for Crash and Fire Protection of Radioactive Material Shipping Containers

Table 7: Static Nominal Crush Strength, Parallel to Direction of Rise (see Table 8 for Perpendicular to Rise)

For 4 to 10 lb _m /ft ³									
Temp	Correlation Factors	Crush Strength, psi, Parallel to Direction of Rise							
		10%	20%	30%	40%	50%	60%	65%	70%
-20°F	C _T	1.29	1.36	1.32	1.29	1.26	1.28	1.29	1.37
75°F	Y _{int}	7.3058	6.7276	6.4961	6.9137	5.6711	5.3279	5.9871	6.2085
	S	1.6590	1.7021	1.7350	1.7255	1.8877	2.0431	2.0870	2.1868
100°F	C _T	0.87	0.88	0.89	0.89	0.90	0.91	0.91	0.96
140°F	C _T	0.73	0.75	0.76	0.77	0.78	0.78	0.79	0.84
180°F	C _T	0.65	0.66	0.67	0.68	0.69	0.68	0.68	0.71
220°F	C _T	0.61	0.60	0.60	0.61	0.61	0.59	0.59	0.61
260°F	C _T	0.45	0.44	0.46	0.47	0.48	0.49	0.49	0.52
For 11 to 40 lb _m /ft ³									
Temp	Correlation Factor	Crush Strength, psi, Parallel to Direction of Rise							
		10%	20%	30%	40%	50%	60%	65%	70%
-20°F	C _T	1.35	1.33	1.32	1.31	1.31	1.30	1.28	1.26
75°F	Y _{int}	4.3422	3.8755	3.5241	3.0307	3.0402	3.4889	5.8935	5.6055
	S	1.8809	1.9321	1.9872	2.0755	2.1451	2.2143	2.1041	2.2368
100°F	C _T	0.86	0.87	0.88	0.88	0.89	0.90	0.90	0.97
140°F	C _T	0.72	0.74	0.75	0.75	0.75	0.76	0.76	0.81
180°F	C _T	0.62	0.63	0.65	0.65	0.65	0.65	0.64	0.68
220°F	C _T	0.56	0.56	0.57	0.57	0.56	0.54	0.54	0.57
260°F	C _T	0.40	0.40	0.41	0.42	0.41	0.43	0.43	0.47

The room temperature (75°F) foam crush strength is calculated at each %-Crush and is a function of density; $\sigma = Y_{int}(\rho)^S$, where Y_{int} and S are defined above, ρ is the nominal foam density in lb/ft³, and σ is the resulting crush stress in psi at the indicated strain. The foam crush strength at temperatures other than 75°F is calculated at each %-Crush and is a function of the strength at 75°F; $\sigma = \sigma_{75°F} C_T$. General Plastics Mfg. Co. is re-investigating the correlations factors at temperatures above and below 75°F. Please contact us for more specific and detailed data, as needed.



Figure 2.12.5-1 - General Plastics Data (Page 1 of 3)

Design Guide for use of LAST-A-FOAM FR-3700 for Crash and Fire Protection of Radioactive Material Shipping Containers

Table 8: Static Nominal Crush Strength, *Perpendicular* to Direction of Rise (see Table 7 for *Parallel* to Rise)

For 4 to 10 lb _m /ft ³									
Temp	Correlation Factors (see below)	Crush Strength, psi, Perpendicular to Direction of Rise							
		10%	20%	30%	40%	50%	60%	65%	70%
-20°F	C _T	1.32	1.35	1.34	1.32	1.32	1.33	1.34	1.36
75°F	Y _{int}	6.3841	6.5943	6.1154	5.7722	5.3041	5.3181	5.7864	5.7701
	S	1.7182	1.6946	1.7403	1.8023	1.9054	2.0392	2.1002	2.2255
100°F	C _T	0.85	0.87	0.88	0.89	0.90	0.91	0.91	0.92
140°F	C _T	0.75	0.77	0.78	0.79	0.79	0.79	0.79	0.80
180°F	C _T	0.63	0.66	0.68	0.69	0.69	0.70	0.69	0.70
220°F	C _T	0.59	0.59	0.60	0.61	0.60	0.60	0.59	0.60
260°F	C _T	0.45	0.45	0.47	0.48	0.48	0.48	0.48	0.48
For 11 to 40 lb _m /ft ³									
Temp	Correlation Factors (see below)	Crush Strength, psi, Perpendicular to Direction of Rise							
		10%	20%	30%	40%	50%	60%	65%	70%
-20°F	C _T	1.34	1.33	1.32	1.33	1.30	1.28	1.24	1.17
75°F	Y _{int}	4.1342	3.5581	3.2664	2.8352	2.8988	3.3972	6.5439	5.6464
	S	1.8957	1.9593	2.0109	2.0955	2.1602	2.2242	2.0660	2.2321
100°F	C _T	0.84	0.85	0.86	0.88	0.87	0.88	0.88	0.90
140°F	C _T	0.72	0.73	0.74	0.76	0.75	0.76	0.76	0.79
180°F	C _T	0.62	0.63	0.64	0.65	0.65	0.65	0.65	0.67
220°F	C _T	0.53	0.53	0.54	0.55	0.54	0.54	0.54	0.56
260°F	C _T	0.39	0.39	0.40	0.41	0.41	0.40	0.40	0.42

The room temperature (75°F) foam crush strength is calculated at each %-Crush and is a function of density; $\sigma = Y_{int}(\rho)^S$, where Y_{int} and S are defined above, ρ is the nominal foam density in lb/ft³, and σ in the resulting crush stress in psi at the indicated strain. The foam crush strength at temperatures other than 75°F is calculated at each %-Crush and is a function of the strength at 75°F; $\sigma = \sigma_{75°F} C_T$. General Plastics Mfg. Co. is re-investigating the correlations factors at temperatures above and below 75°F. Please contact us for more specific and detailed data, as needed.



Figure 2.12.5-1 - General Plastics Data, continued (Page 2 of 3)

Design Guide for use of LAST-A-FOAM FR-3700 for Crash and Fire Protection of Radioactive Material Shipping Containers

Dynamic Crush Strength

The crush strength of LAST-A-FOAM[®], like many materials, is modestly sensitive to strain rate. The static to dynamic adjustment shown in Table 9 is based on a significant testing program and included strain rates in the range of 30 sec⁻¹ to 100 sec⁻¹. It is expected that the adjustment will provide good predictions of dynamic impact strength of FR-3700 for most Packaging design conditions. This information is intended to be a guide for designers of impact mitigating devices. The constitutive material models may be useful in targeting a foam density or rage for a particular application. However, each design should be thoroughly analyzed or tested to understand the implications of the complete design.

Table 9: Static to Dynamic Crush Strength Adjustment

Strain	10%	20%	30%	40%	50%	60%	65%	70%
Y _{int}	1.2971	1.4397	1.5181	1.3887	1.4419	1.4275	1.3871	1.4660
S	1.0330	1.0069	0.9941	1.0028	0.9912	0.9831	0.9910	0.9586

The dynamic crush strength is calculated at each %-strain and a function of the static crush strength at the same %-strain;

$$\sigma_{\text{Dynamic}} = y_{\text{int}} (\sigma_{\text{Static}})^S$$

CAUTION: Use only units of PSI for input σ_{Static} value.



General Plastics Manufacturing Company
4910 Burlington Way • P.O. box 9097
Tacoma, WA 98409

Telephone: (800) 806-6051 or (253) 473-5000
Facsimile: (253) 473-5104

See our World Wide Web Site at:
www.generalplastics.com
E-mail address: sales@generalplastics.com

GENERAL PLASTICS MANUFACTURING COMPANY



Figure 2.12.5-1 - General Plastics Data, continued (Page 3 of 3)

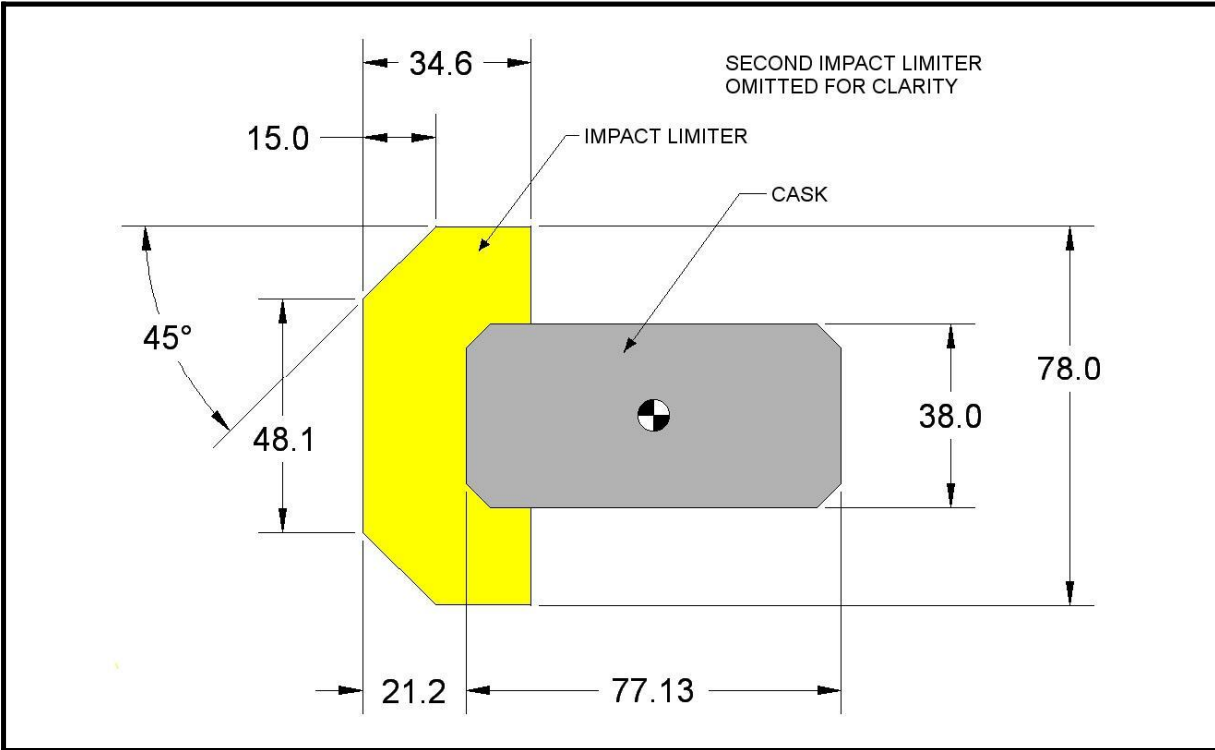


Figure 2.12.5-2 - Dimensions Used in CASKDROP

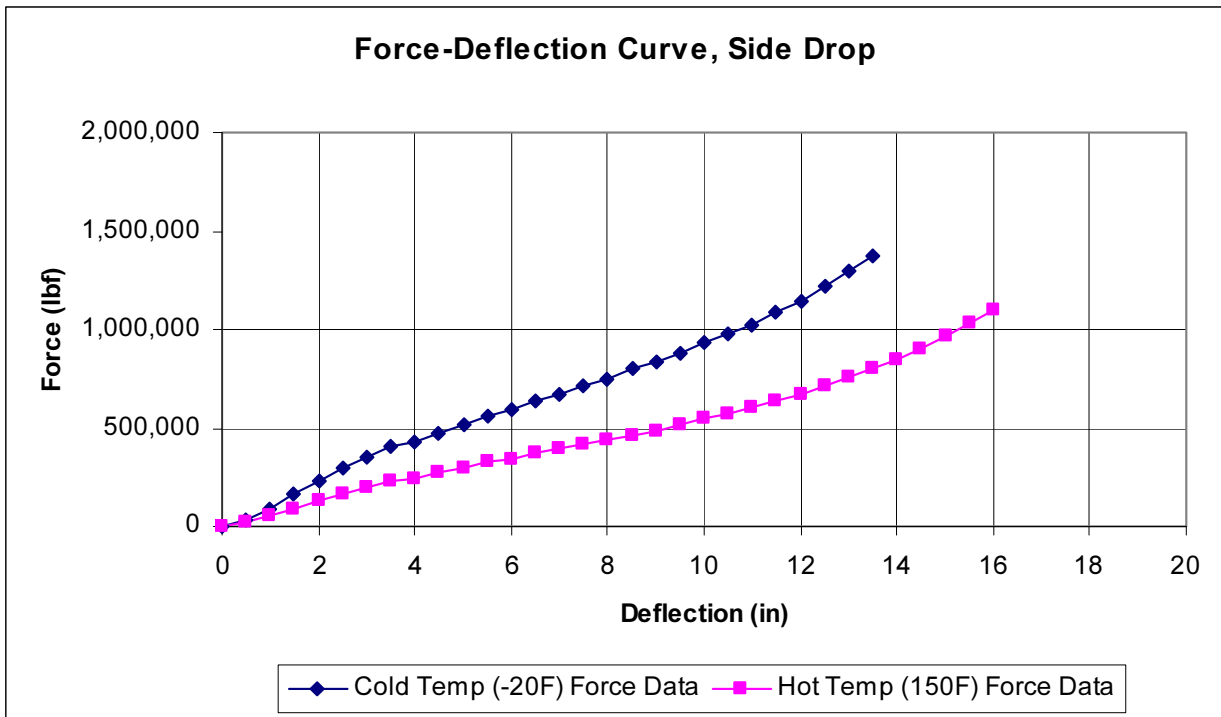


Figure 2.12.5-3 - Force-Deflection Curve, Side Orientation

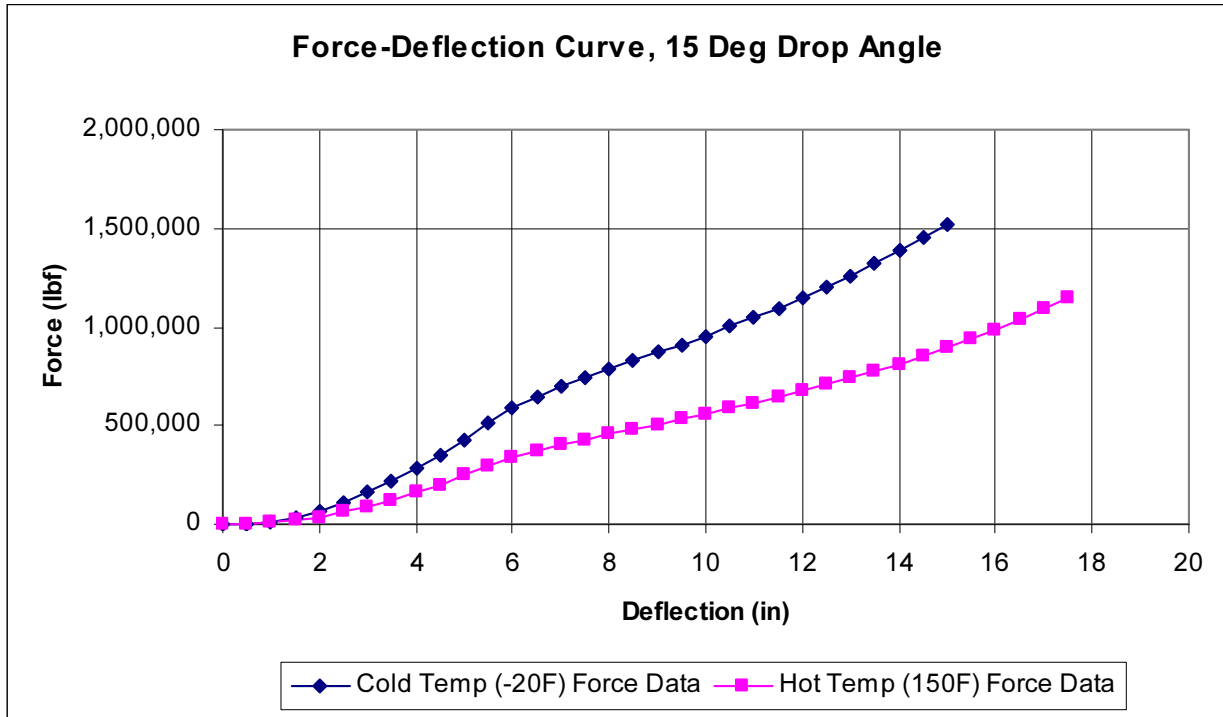


Figure 2.12.5-4 - Force-Deflection Curve, 15° Orientation

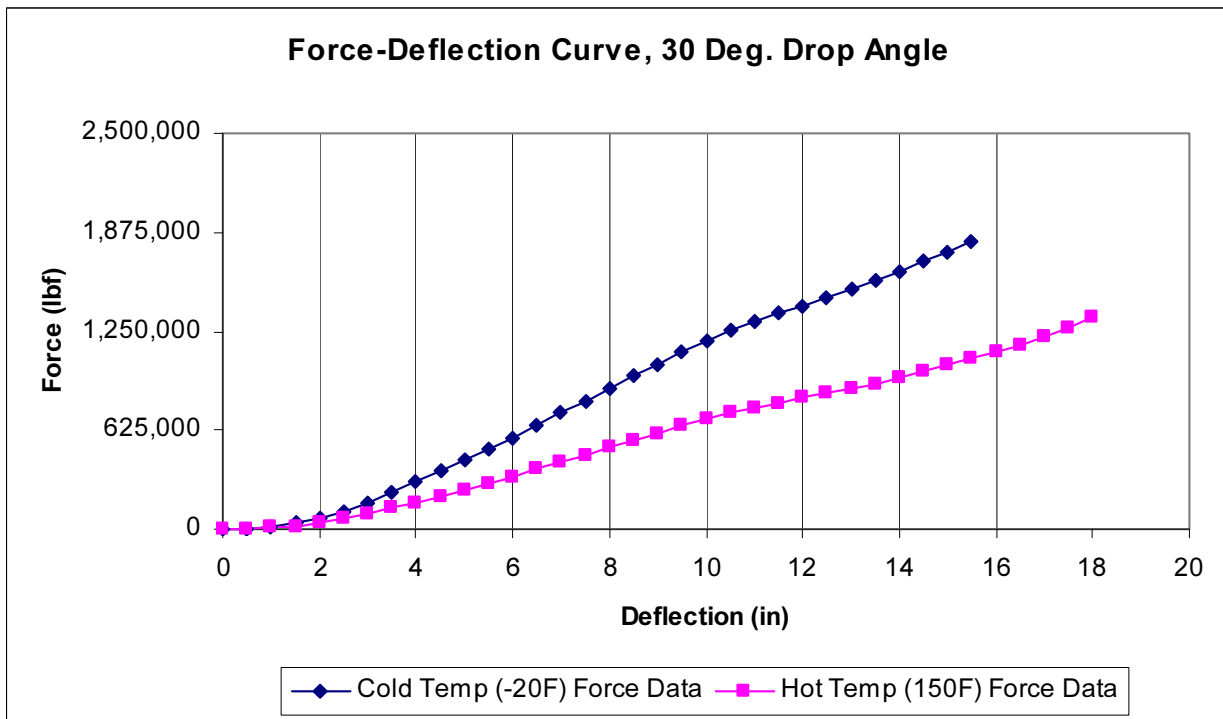


Figure 2.12.5-5 - Force-Deflection Curve, 30° Orientation

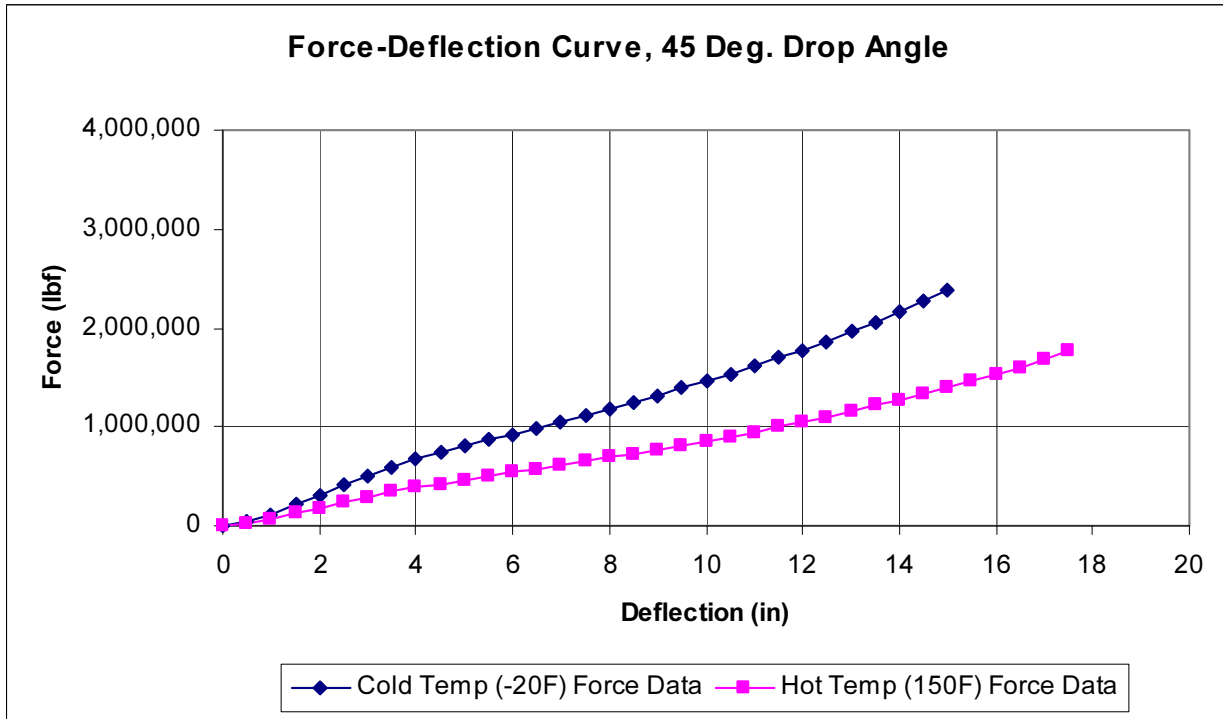


Figure 2.12.5-6 - Force-Deflection Curve, 45° Orientation

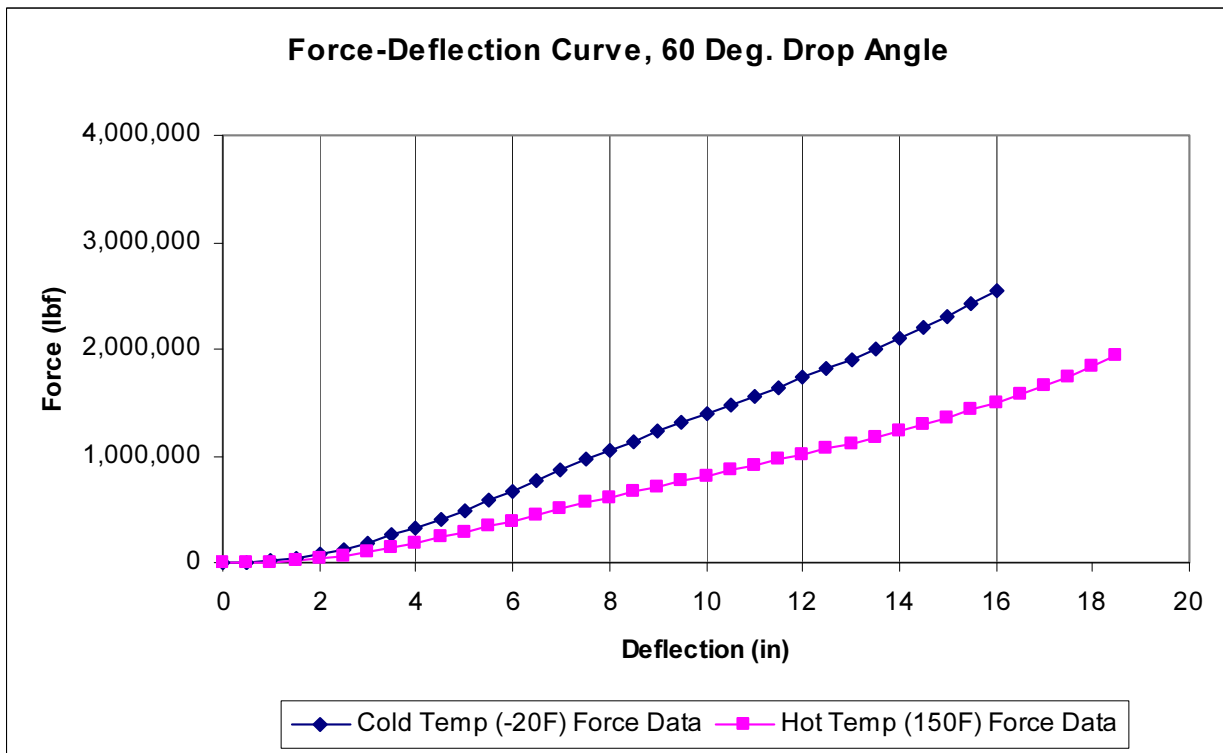


Figure 2.12.5-7 - Force-Deflection Curve, 60° Orientation

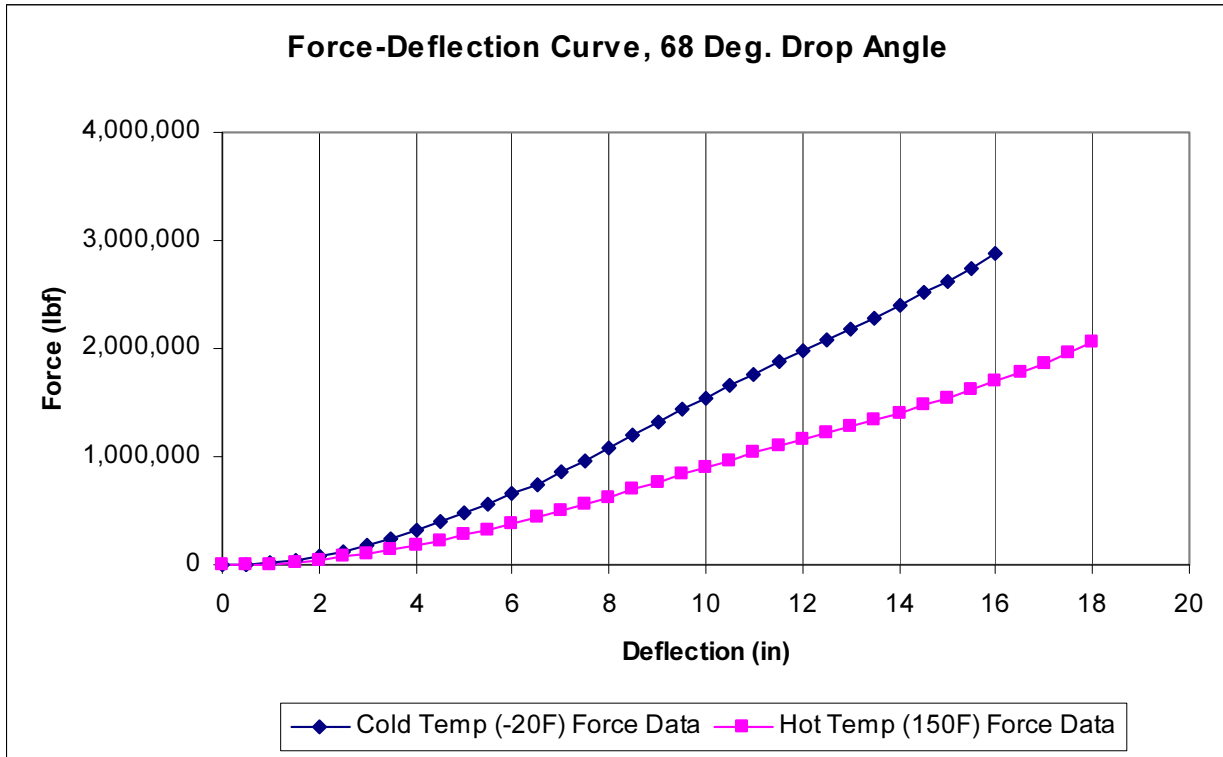


Figure 2.12.5-8 - Force-Deflection Curve, 68° Orientation

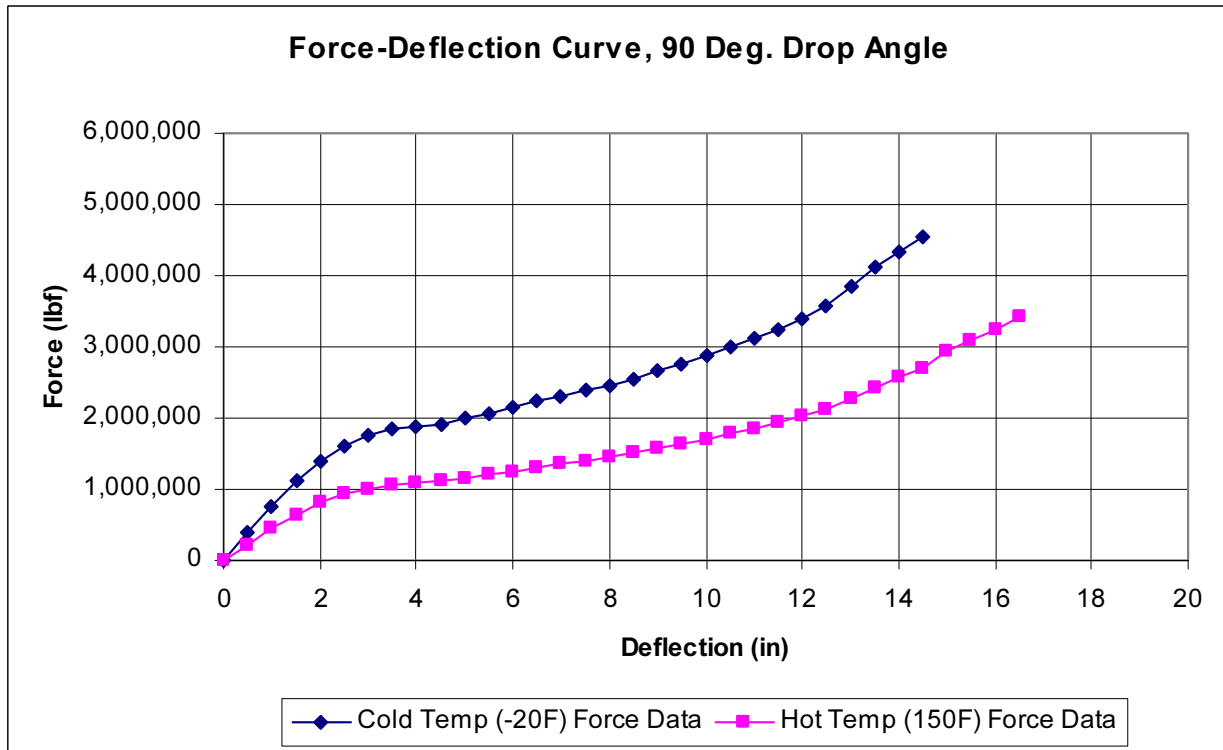


Figure 2.12.5-9 - Force-Deflection Curve, 90° Orientation

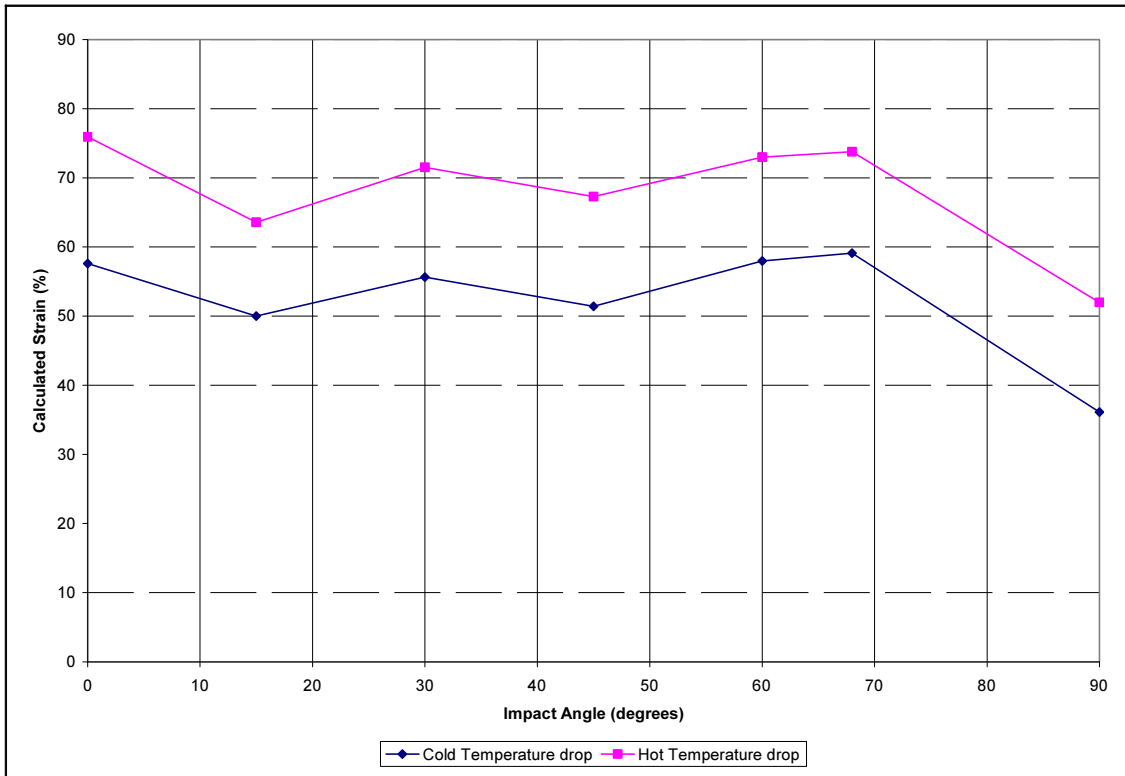


Figure 2.12.5-10 - Primary Impact Limiter Strain, HAC

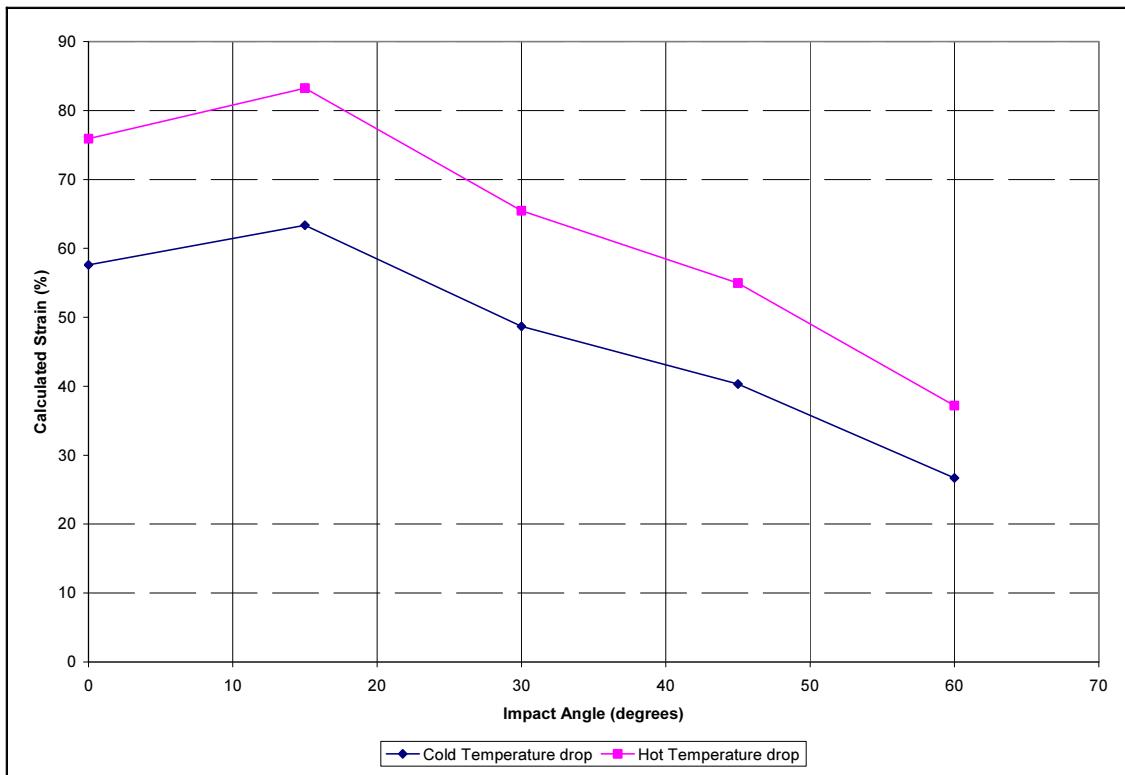


Figure 2.12.5-11 - Secondary Impact Limiter Strain, HAC

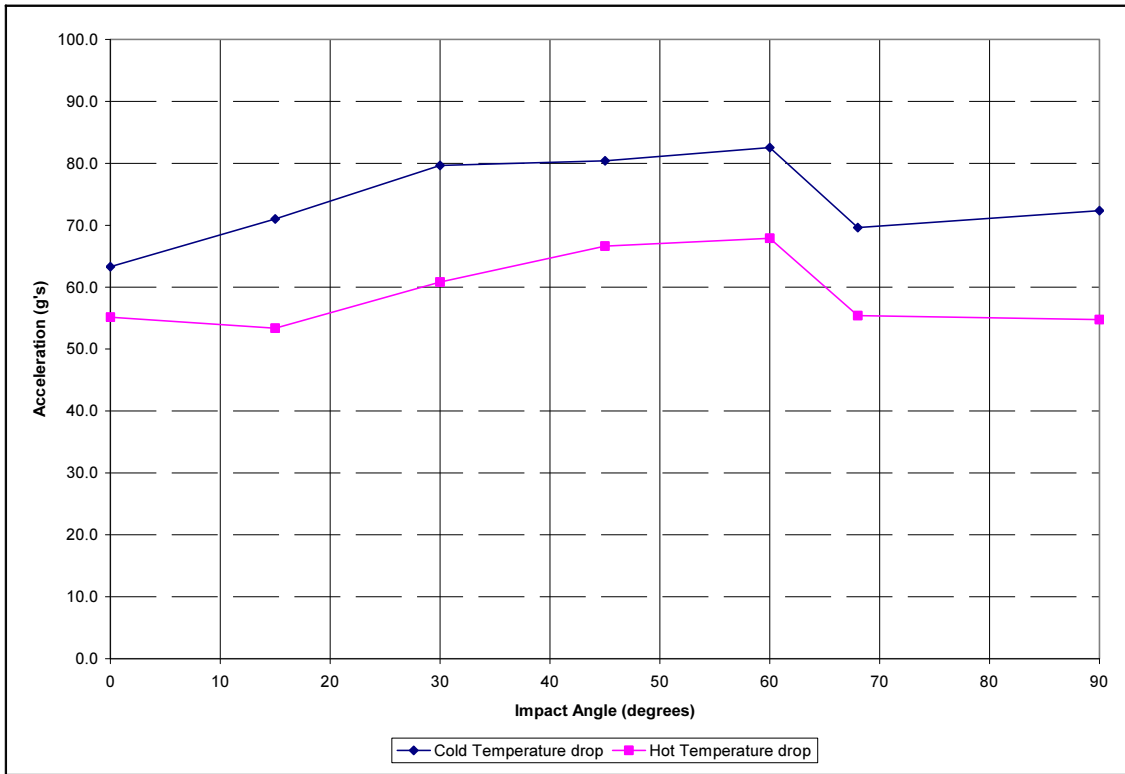


Figure 2.12.5-12 - Primary Impact Acceleration, HAC

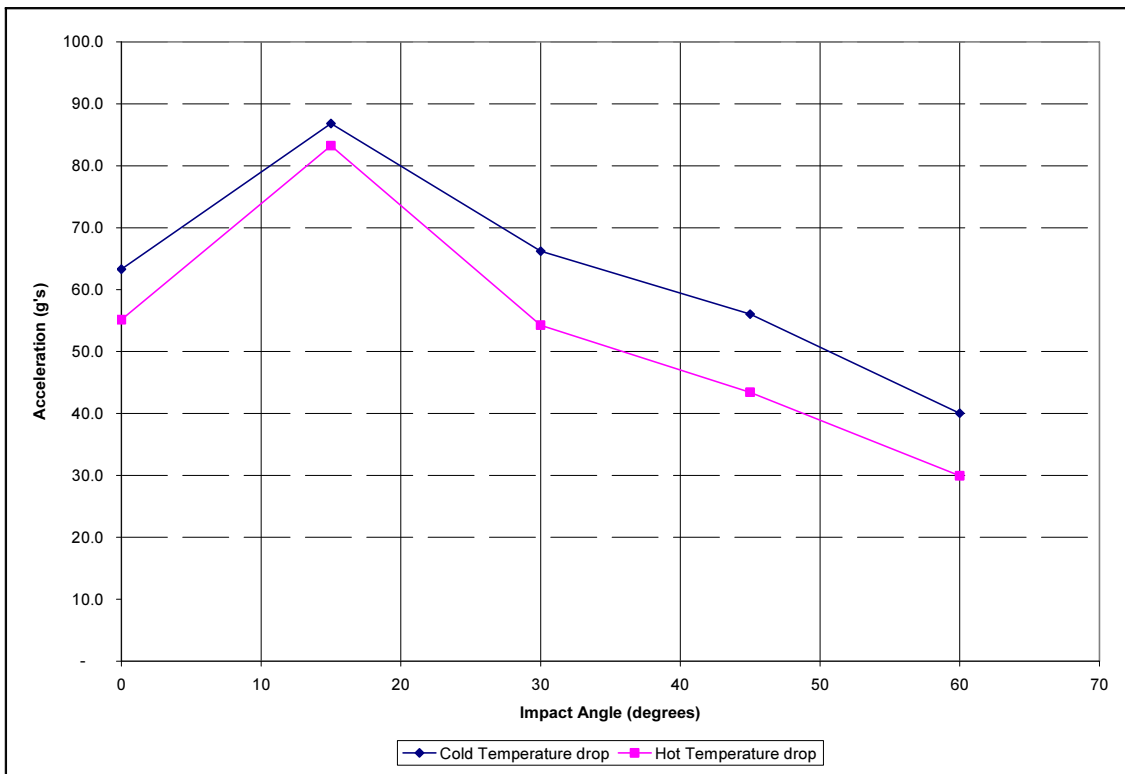


Figure 2.12.5-13 - Secondary Impact Acceleration, HAC

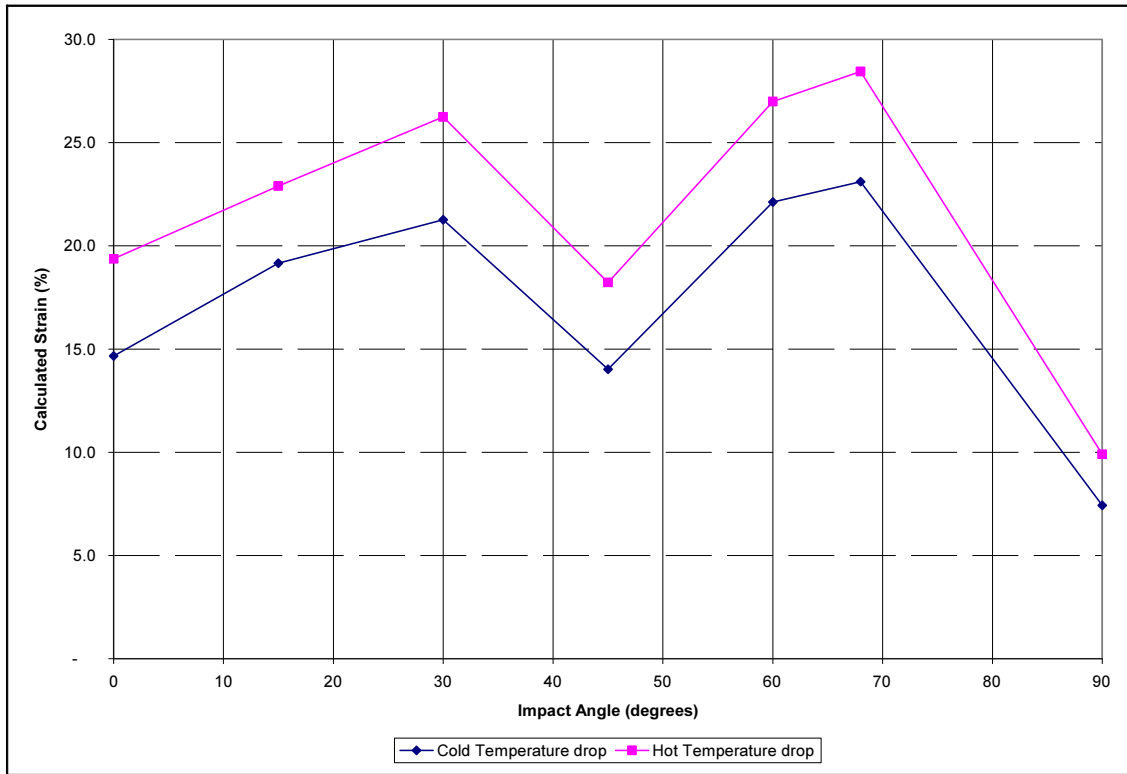


Figure 2.12.5-14 - Primary Impact Limiter Strain, NCT

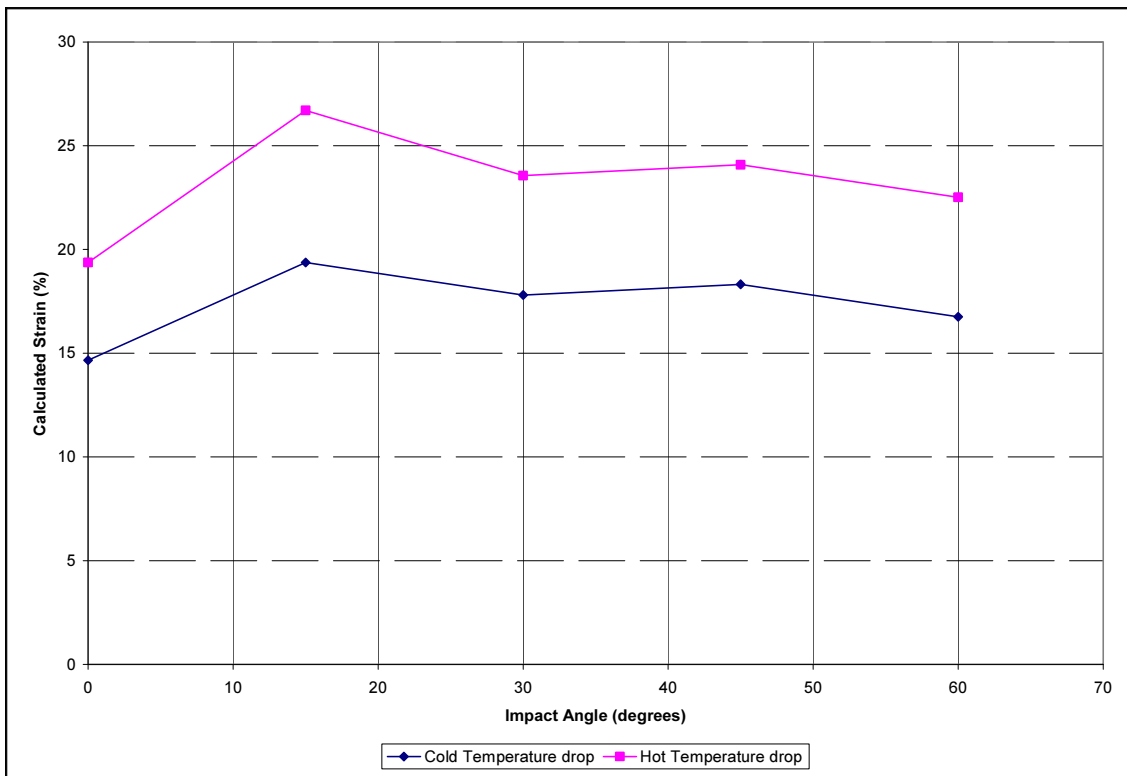


Figure 2.12.5-15 - Secondary Impact Limiter Strain, NCT

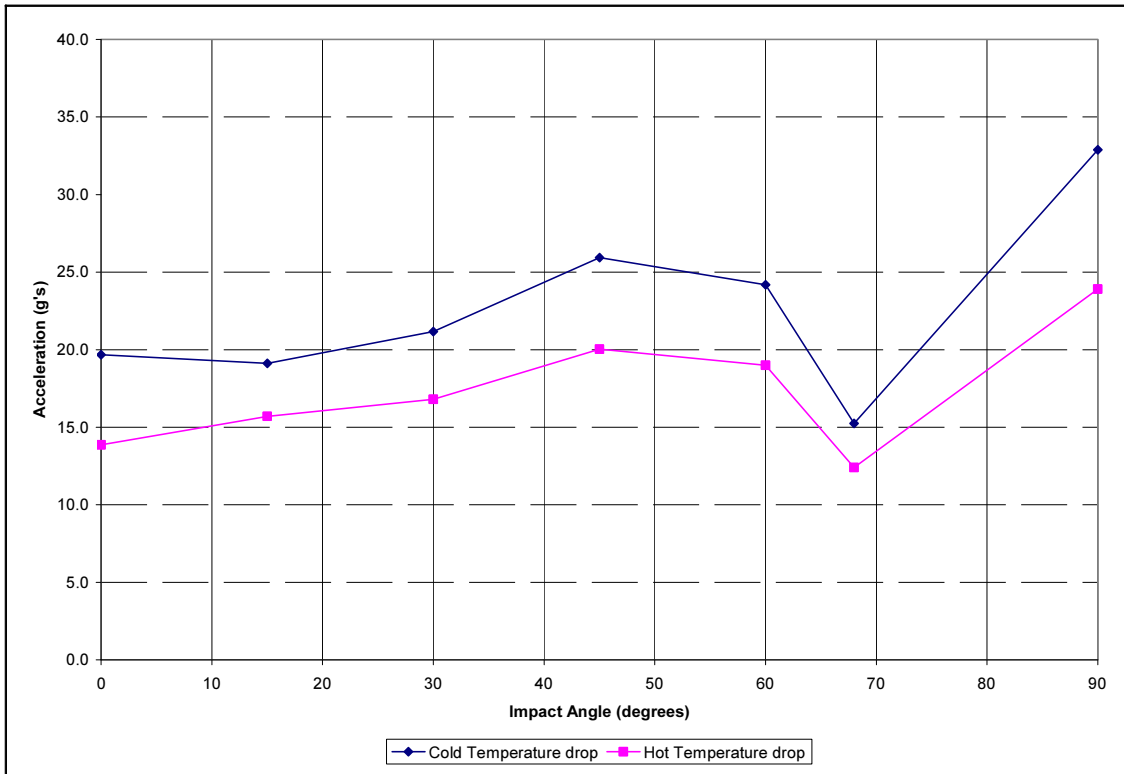


Figure 2.12.5-16 - Primary Impact Acceleration, NCT

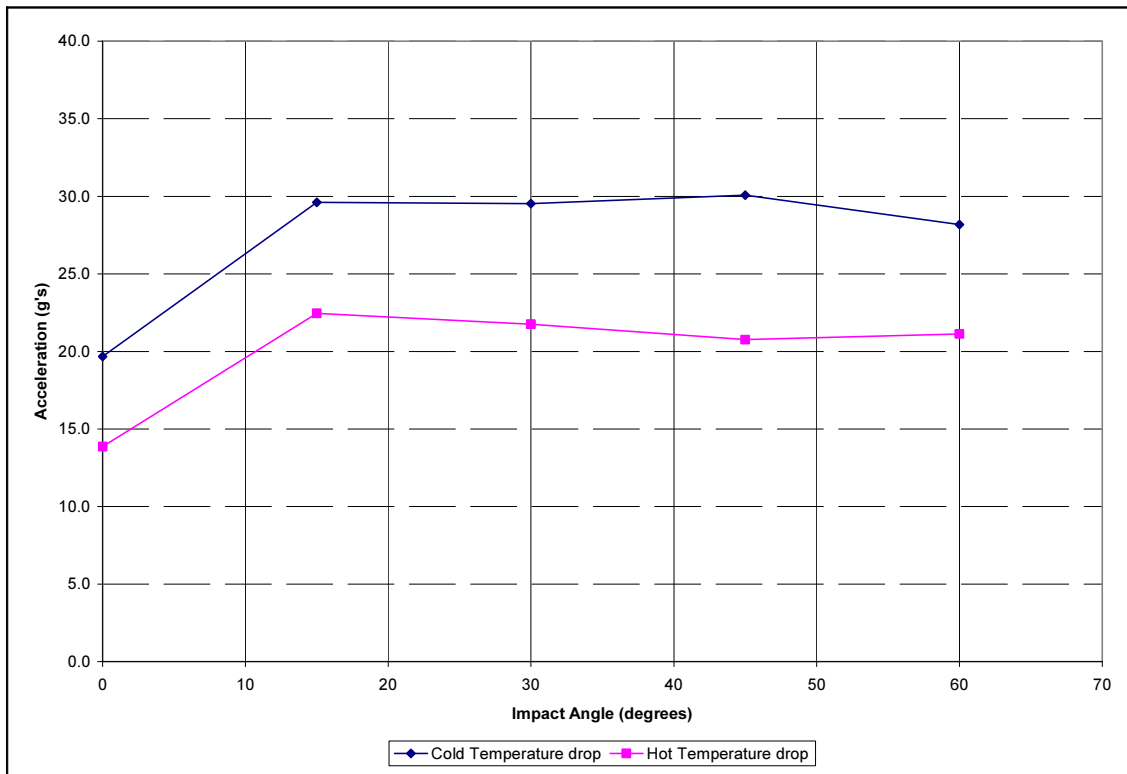


Figure 2.12.5-17 - Secondary Impact Acceleration, NCT

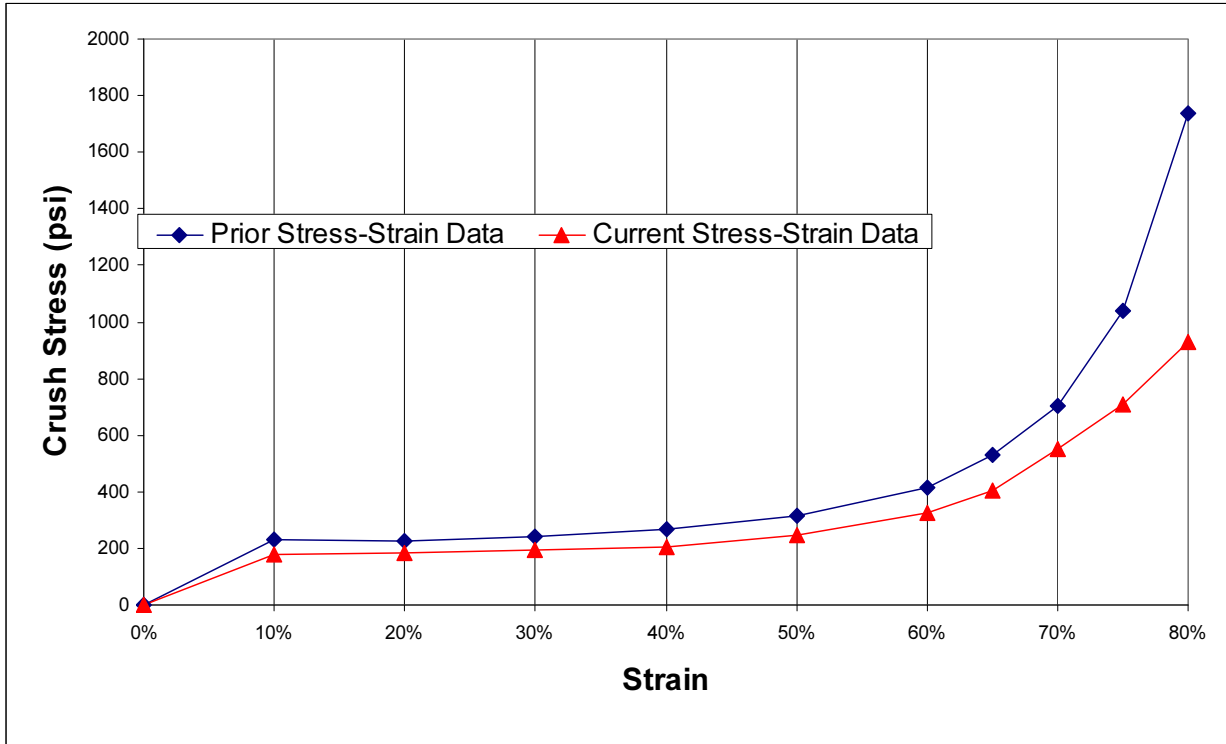


Figure 2.12.5-18 - Previously Published vs. Current Stress-Strain Data (150 °F)

2.12.6 Analysis Software Descriptions

This appendix contains descriptions of the computer codes CASKDROP and SLAPDOWN. Both of these programs are used in Appendix 2.12.5, *Impact Limiter Performance Evaluation*.

2.12.6.1 CASKDROP

This appendix briefly documents the methodology employed by the AREVA Federal Services proprietary computer program CASKDROP. Used in conjunction with an appropriate packaging dynamic analysis computer code (see Section 2.12.6.2, *SLAPDOWN*), the computer program CASKDROP is used to demonstrate compliance of the package with 10 CFR §71.71(c)(7) and 10 CFR §71.73(c)(1) for normal conditions of transport (NCT) and hypothetical accident conditions (HAC) of transport free drop analyses, respectively.

2.12.6.1.1 Using CASKDROP to Determine Impact Limiter Deformation Behavior

CASKDROP evaluates all angles of drop from 0° (horizontal) to 90° (vertical) by performing a quasi-static analysis that ignores rotational effects. At orientations where rotational effects are important, use of a dynamic analysis computer program such as SLAPDOWN is required utilizing the force-deflection data developed by CASKDROP. Note that although CASKDROP is capable of completely solving the impact analysis for orientations where rotation effects are not important (e.g., end, side, and c.g.-over-corner), the only program output which is utilized in the evaluation of the BRR Package free drop events is the formulation of the force-deflection relation for the impact limiters. The program SLAPDOWN, using the force-deflection input from CASKDROP, is utilized for the final evaluation of all orientations. The following material is a general documentation of CASKDROP, and is not limited to the features utilized for the BRR package.

CASKDROP assumes the package is protected by polyurethane foam-filled, energy absorbing impact limiters. Since the impact surface is unyielding, the impact limiters are assumed to absorb all of the potential energy of the drop event.

For all orientations of impact, the prediction of impact limiter deformation behavior can be approached from straightforward energy balance principles:

$$E = W(h + \delta) = \int_0^{\delta} F_x dx$$

where W is the package gross weight, h is the drop height, δ is the maximum impact limiter deformation, and F_x is the force imposed on the target at an impact limiter deformation of x . The left-hand term represents the potential energy of the free drop. The right-hand term represents the strain energy of the deformed impact limiter(s).

Given a specific drop angle, θ , and impact limiter deformation, δ , as illustrated in Figure 2.12.6-1, the result is an impact limiter crush plane “footprint.” Integration of the impact limiter crush plane yields a total crush force and centroidal distance of:

$$F = \iint \sigma\{\varepsilon\} dA \quad \text{and} \quad \bar{X} = \left(\frac{1}{F}\right) \iint \bar{x}\sigma\{\varepsilon\} dA$$

BRR Package Safety Analysis Report

respectively, where F is the total integrated force, $\sigma\{\varepsilon\}$ is the differential stress as a function of strain, dA is the differential area (i.e., dA is a function of the “x” and “y” directions, or dx and dy), \bar{X} is the total integrated centroidal distance from the package center of gravity, and \bar{x} is the differential centroidal distance from the package center of gravity.

With reference to Figure 2.12.6-1, the geometric calculations for the impact surface (crush plane) and the associated strains are carried out using a translating X'-Y'-Z' coordinate system, with the X'-Y' plane corresponding to the crush plane. Due to the cylindrical nature of the problem, the overall crush plane is comprised of a segment of an ellipse corresponding to the outside surface of the impact limiter. The optional end hole requires removal of its associated elliptical segment. Similarly, the optional conical surface is an elliptical, parabolic, or hyperbolic segment depending on both the drop angle, θ , and angle of the cone.

Calculation of the differential strain is somewhat more complex. As illustrated in Figure 2.12.6-2, the differential strain, $\varepsilon\{x,y\}$, is calculated at the center of the differential area, dA . The differential strain is determined by calculating the amount of vertical deformation at the (x, y) location on the crush plane. The vertical distance from point (x, y) on the impact surface to the package or upper impact limiter surface is found and denoted Z_{TOP} . Similarly, the vertical distance from point (x, y) on the impact surface to the undeformed lower impact limiter surface is found and denoted Z_{BOT} . In equation format the differential strain at location (x, y) is simply:

$$\varepsilon = \frac{Z_{BOT}}{Z_{BOT} + Z_{TOP}}$$

This strain is used to determine the corresponding crush stress from an implicit tabular definition of the crushable media stress-strain characteristics. For each differential area, dA , the differential force, dF , is found. The total force, F , is therefore the summation of the differential forces. Similarly, the centroidal distance, \bar{X} , is the summation of the moments, $\bar{x} \times dF$, divided by the total force.

Unbacked regions are defined as having an (x, y) location where Z_{TOP} is calculated to occur outside the package's “shadow” (i.e., or backing, occurring on the impact limiter surface). Unbacked regions usually utilize the nominal crush strength of the crushable media (typically 10% for polyurethane foam material) for integrated force purposes. The crush strength for unbacked regions is user-definable in the program CASKDROP.

For most drop angles, θ , and impact limiter deformations, δ , the impact limiter crush force, F , is transmitted to the package body in direct compression. Hence, the forces transmitted to the circumferential impact limiter attachments are essentially zero. However, for nearly vertical or horizontal orientations at small deformations where the crush force occurs beyond the edge of the package, the forces transmitted to the impact limiter attachments can be substantially large. It is important to note that only the nearly vertical or nearly horizontal orientations are required to produce the prying motion; all other orientations will always compress the impact limiter onto the package body. Figure 2.12.6-3 illustrates the near vertical and near horizontal orientations producing impact limiter separation forces.

For the near vertical orientation, the moment about point “a” determines whether a separation force exists at the impact limiter attachments. Assuming for this case that a counterclockwise moment is positive (i.e., will tend to “pry” the impact limiter off the package), the equation for the moment about point “a,” M_a , is:

$$M_a = Fx_F + F_{IL}x_{IL}$$

Similarly, for the near horizontal orientation, the moment about point “b” determines whether a separation force exists at the impact limiter attachments. Assuming for this case that a clockwise moment is positive (i.e., will tend to “pry” the impact limiter off the package), the equation for the moment about point “b,” M_b , is:

$$M_b = Fx_F - F_{IL}x_{IL}$$

If M_a or M_b are positive, a separation force will occur at the impact limiter attachments whereas if M_a or M_b are zero or negative, a separation force will not occur. Note that use of a conically shaped impact limiter typically eliminates the impact limiter separation force by causing the crush force, F , to almost always occur between points “a” and “b.”

2.12.6.1.2 An Example Problem for the CASKDROP Program

An example problem is illustrated in Figure 2.12.6-4. The CASKDROP program utilizes a variety of physical input data to determine package and impact limiter geometry. In all cases, the package and impact limiter are assumed axisymmetric. The package is cylindrical, as is the impact limiter. Two fundamental variations in the basic cylindrical shape of the impact limiter are an optional end hole and optional conical end. The end hole may extend part or all of the way from the outside surface of the impact limiter to the package end. The conical end may be a truncated or fully developed cone, defined by a cone diameter and a cone length at the outside surface of the impact limiter. By varying the impact limiter dimensions the result is a wide variety of possible impact limiter shapes, from a totally enclosing “overpack” to pointed end-only buffers.

The CASKDROP program was primarily developed as an impact limiter design tool. Geometry and analysis control input to the CASKDROP program is fully interactive allowing changes “on the fly.” Figure 2.12.6-5 illustrates the CASKDROP screen for data entry into the *Input Window*.

The CASKDROP program allows for three types of crushable media definition:

1. CONSTANT: a constant crush stress independent of calculated strain.
2. VARIABLE: a variable, user-defined stress-strain definition. The BRR package analysis uses this option by inputting the adjusted stress-strain curves as discussed in Appendix 2.12.5.
3. POLYFOAM: a built-in polyurethane foam database providing accurate stress-strain definition for 5 to 25 pound per cubic foot (pcf) density and temperatures of -20 °F to +300 °F based on extensive sample testing.

The example problem assumes 20 pcf polyurethane foam at a temperature of -20 °F. A +60% bias is applied to the temperature-corrected stress-strain data to account for dynamic strain rate effects for the example problem. Figure 2.12.6-6 illustrates the CASKDROP input screen for the polyurethane foam crush media for the example problem.

For the example problem, the CASKDROP program utilizes polyurethane foam where “parallel to rise” foam curing occurs in the axial direction and “perpendicular to rise” foam curing occurs in the radial direction, although the difference between these two directions is small. The user may optionally select the “parallel-to-rise” or “perpendicular-to-rise” properties to be reversed or global for all drop orientations. For orientations other than axial (end drop) and radial (side drop), the CASKDROP program interpolates foam properties using an ellipse function. For the case where

BRR Package Safety Analysis Report

crush stress “parallel-to-rise” is in the axial direction, σ_{PAR} , and crush stress “perpendicular-to-rise” is in the radial direction, σ_{PER} , the interpolation equation at drop angle, θ , is:

$$\sigma_{\theta} = \sqrt{\frac{1}{\left(\frac{\sin \theta}{\sigma_{PAR}}\right)^2 + \left(\frac{\cos \theta}{\sigma_{PER}}\right)^2}}$$

Similarly, for the case where crush stress “perpendicular-to-rise” is in the axial direction, σ_{PER} , and crush stress “parallel-to-rise” is in the radial direction, σ_{PAR} , the interpolation equation is:

$$\sigma_{\theta} = \sqrt{\frac{1}{\left(\frac{\sin \theta}{\sigma_{PER}}\right)^2 + \left(\frac{\cos \theta}{\sigma_{PAR}}\right)^2}}$$

The *Control Window* allows the user to specify various analysis and output controls. The *Control Window* is separated into *Analysis*, *Crush*, *Angle*, *Static*, *Dynamic*, *Print*, and *File*.

Three *Analysis* options are available: *dXY* defines the number of integration elements in the crush plane, 25 for the example problem; *SIn* defines the analysis methodology (Global versus Local Strain Theory), *Global* for the example problem; ϵ/σ defines the strain (or crush stress) value to be utilized in unbacked regions (e.g., if a value is specified between 0 and 1, it is assumed a strain value and the corresponding crush stress at that strain is used; if a value is specified greater than 1, it is assumed to be a crush stress), 0.1 for the example problem corresponding to a crush stress at 10% strain from the polyurethane foam database.

The *Crush* options define the incremental deformations to be analyzed. The example problem specifies analyzing for crush deformations from 0.25 inch to 20 inch in 0.25 inch increments. Specifying a *Max* value greater than the actual maximum available crush depth (as determined geometrically) flags the CASKDROP program to not exceed the maximum available crush depth.

Similarly, the *Angle* options define the incremental angular orientations to be analyzed. The example problem specifies analyzing for drop angles from 0° to 90° in 15° increments.

The *Static* options allow the user to specify quasi-static analyses providing *Full* display output, *Smry* (summary) output, or *Both*. The example problem specifies *Full* output to the display only. Similarly, the *Dynamic* options allow the user to specify dynamic analyses providing *Full* display output, *Smry* (summary) output, or *Both*. The example problem does not specify a dynamic analysis as that module is not completed in the CASKDROP program.

The *Print* and *File* options allow the user to specify *Full* display output, *Smry* (summary) output, or *Both* to the printer or a file. The example problem specifies *Full* output to an output file only.

The *Output Window* provides the location for *Static* and *Dynamic* display output. A quasi-static solution is achieved when the strain energy of the crushable media (*SE*) is equal to the free-falling kinetic energy of the package (*KE*), or $SE/KE = 1$. The following tables provide a sample file output at 0° (side drop), at 45°, and at 90° (end drop).

BRR Package Safety Analysis Report

Docket No. 71-9341

Rev. 0, March 2009

Side Drop
05-16-1995, 15:38:39

*** PACKAGING TECHNOLOGY ***

CASKDROP, v2.21
Jul 01, 1994

SAMPLE PROBLEM FOR QUALITY ASSURANCE CHECK (AREAS AND VOLUMES)			
Impact Limiter Weight (each) -	1,000 lbs	Cask and Payload Weight -	10,000 lbs
Impact Limiter Outside Diameter -	60.0000 in	Cask Outside Diameter -	40.0000 in
Impact Limiter Overall Length -	24.0000 in	Cask Overall Length -	48.0000 in
Impact Limiter Conical Diameter -	48.0000 in	Dynamic Unloading Modulus -	1.000E+07 lbs/in
Impact Limiter Conical Length -	10.0000 in	Rad Mass Moment of Inertia -	12,235 lb-in-s ²
Impact Limiter End Thickness -	12.0000 in	Frictional Coefficient -	0.0000
Impact Limiter Hole Diameter -	20.0000 in	Drop Height -	30.0000 ft
Impact Limiter Hole Length -	8.0000 in	Drop Angle from Horizontal -	0.0000°
Unbacked Area Threshold Strain -	0.1000 in/in	Crush Analysis Theory -	Global
Unbacked Area Crush Stress -	2,675 psi	Number of Integration Incs -	25

POLYFOAM CRUSH STRESS (Axial: " " to rise)	
Density = 20.000 pcf	
Temp = -20.000 F	
σ-yield = 2,552.3 psi	
Bias = 60.000%	
ε (in/in)	σ (psi)
0.000	0.0
0.100	2,552.3
0.200	2,687.0
0.300	2,868.8
0.400	3,302.9
0.500	4,115.1
0.600	6,074.3
0.650	7,942.0
0.700	10,925.0
0.750	15,001.8
0.800	26,829.5

POLYFOAM CRUSH STRESS (Radial: "⊥" to rise)	
Density = 20.000 pcf	
Temp = -20.000 F	
σ-yield = 2,675.0 psi	
Bias = 60.000%	
ε (in/in)	σ (psi)
0.000	0.0
0.100	2,675.0
0.200	2,785.4
0.300	2,959.9
0.400	3,345.9
0.500	4,147.7
0.600	6,062.8
0.650	7,868.8
0.700	10,180.0
0.750	15,554.4
0.800	29,704.8

POLYFOAM CRUSH STRESS (Actual Data @ 0.0°)	
Density = 20.000 pcf	
Temp = -20.000 F	
σ-yield = 2,675.0 psi	
Bias = 60.000%	
ε (in/in)	σ (psi)
0.000	0.0
0.100	2,675.0
0.200	2,785.4
0.300	2,959.9
0.400	3,345.9
0.500	4,147.7
0.600	6,062.8
0.650	7,868.8
0.700	10,180.0
0.750	15,554.4
0.800	29,704.8

DEFL (in)	MAX ε (%)	AREA (in ²)	VOLUME (in ³)	XBAR (in)	IMPACT FORCE (lbs)	ACCEL (g's)	I/L MOMENT (in-lbs)	STRAIN ENERGY (in-lbs)	KINETIC ENERGY (in-lbs)	SE/KE RATIO
0.250	2.50	221	37	0.00	106,881	8.9	0	13,360	4,323,000	0.00
0.500	5.00	318	105	0.00	289,508	24.1	0	62,909	4,326,000	0.01
0.750	7.50	396	194	0.00	518,875	43.2	0	163,957	4,329,000	0.04
1.000	10.00	465	302	0.00	733,200	61.1	0	320,466	4,332,000	0.07

BRR Package Safety Analysis Report

Docket No. 71-9341

Rev. 0, March 2009

Side Drop
05-16-1995, 15:38:39

*** PACKAGING TECHNOLOGY ***
(continued...)

CASKDROP, v2.21
Jul 01, 1994

DEFL (in)	MAX ϵ (%)	AREA (in ²)	VOLUME (in ³)	XBAR (in)	IMPACT FORCE (lbs)	ACCEL (g's)	I/L MOMENT (in-lbs)	STRAIN ENERGY (in-lbs)	KINETIC ENERGY (in-lbs)	SE/KE RATIO
1.250	12.49	528	425	0.00	955,009	79.6	0	531,492	4,335,000	0.12
1.500	14.99	587	565	0.00	1,107,366	92.3	0	789,289	4,338,000	0.18
1.750	17.49	644	719	0.00	1,270,225	105.9	0	1,086,488	4,341,000	0.25
2.000	19.99	699	886	0.00	1,371,441	114.3	0	1,416,697	4,344,000	0.33
2.250	22.49	752	1,068	0.00	1,509,207	125.8	0	1,776,778	4,347,000	0.41
2.500	24.99	804	1,262	0.00	1,668,937	139.1	0	2,174,046	4,350,000	0.50
2.750	27.49	855	1,469	0.00	1,761,221	146.8	0	2,602,815	4,353,000	0.60
3.000	29.99	906	1,690	0.00	1,946,101	162.2	0	3,066,230	4,356,000	0.70
3.250	32.49	955	1,921	0.00	2,044,813	170.4	0	3,565,095	4,359,000	0.82
3.500	34.98	1,005	2,167	0.00	2,249,052	187.4	0	4,101,828	4,362,000	0.94
3.614	36.13	1,027	2,285	0.00	2,326,676	193.9	0	4,363,372	4,363,372	1.00
3.750	37.48	1,053	2,424	0.00	2,419,003	201.6	0	4,956,582	4,365,000	1.14
4.000	39.98	1,101	2,692	0.00	2,640,297	220.0	0	5,588,994	4,368,000	1.28
4.250	42.48	1,149	2,975	0.00	2,759,520	230.0	0	6,263,971	4,371,000	1.43
4.500	44.98	1,197	3,267	0.00	2,956,003	246.3	0	6,978,412	4,374,000	1.60
4.750	47.48	1,244	3,571	0.00	3,208,534	267.4	0	7,748,979	4,377,000	1.77
5.000	49.98	1,292	3,889	0.00	3,357,376	279.8	0	8,569,718	4,380,000	1.96
5.250	52.48	1,339	4,219	0.00	3,603,141	300.3	0	9,439,782	4,383,000	2.15
5.500	54.97	1,385	4,556	0.00	3,906,997	325.6	0	10,378,550	4,386,000	2.37
5.750	57.47	1,432	4,909	0.00	4,215,273	351.3	0	11,393,833	4,389,000	2.60
6.000	59.97	1,479	5,275	0.00	4,573,066	381.1	0	12,492,376	4,392,000	2.84
6.250	62.47	1,520	5,650	0.00	4,961,100	413.4	0	13,684,147	4,395,000	3.11
6.500	64.97	1,559	6,035	0.00	5,404,072	450.3	0	14,979,793	4,398,000	3.41
6.750	67.47	1,597	6,430	0.00	5,893,283	491.1	0	16,391,963	4,401,000	3.72
7.000	69.97	1,632	6,834	0.00	6,440,254	536.7	0	17,933,655	4,404,000	4.07
7.250	72.47	1,666	7,246	0.00	7,087,717	590.6	0	19,624,651	4,407,000	4.45
7.500	74.96	1,698	7,667	0.00	8,001,352	666.8	0	21,510,785	4,410,000	4.88
7.750	77.46	1,730	8,095	0.00	9,446,226	787.2	0	23,691,732	4,413,000	5.37
8.000	79.96	1,760	8,532	0.00	11,484,412	957.0	0	26,308,062	4,416,000	5.96
8.250	82.46	1,790	8,976	0.00	13,964,555	1,163.7	0	29,489,183	4,419,000	6.67
8.500	84.96	1,818	9,427	0.00	16,801,077	1,400.1	0	33,334,887	4,422,000	7.54
8.750	87.46	1,846	9,885	0.00	19,931,256	1,660.9	0	37,926,428	4,425,000	8.57
9.000	89.96	1,873	10,350	0.00	23,276,639	1,939.7	0	43,327,415	4,428,000	9.78
9.250	92.45	1,899	10,822	0.00	26,896,391	2,241.4	0	49,599,044	4,431,000	11.19
9.500	94.95	1,925	11,300	0.00	30,724,250	2,560.4	0	56,801,624	4,434,000	12.81
9.750	97.45	1,950	11,784	0.00	34,740,688	2,895.1	0	64,984,741	4,437,000	14.65
10.000	99.95	1,974	12,275	0.00	38,887,797	3,240.6	0	74,188,302	4,440,000	16.71

BRR Package Safety Analysis Report

Docket No. 71-9341

Rev. 0, March 2009

Corner Drop
05-16-1995, 15:38:39

*** PACKAGING TECHNOLOGY ***

CASKDROP, v2.21
Jul 01, 1994

SAMPLE PROBLEM FOR QUALITY ASSURANCE CHECK (AREAS AND VOLUMES)			
Impact Limiter Weight (each) -	1,000 lbs	Cask and Payload Weight -	10,000 lbs
Impact Limiter Outside Diameter -	60.0000 in	Cask Outside Diameter -	40.0000 in
Impact Limiter Overall Length -	24.0000 in	Cask Overall Length -	48.0000 in
Impact Limiter Conical Diameter -	48.0000 in	Dynamic Unloading Modulus -	1.000E+07 lbs/in
Impact Limiter Conical Length -	10.0000 in	Rad Mass Moment of Inertia -	12,235 lb-in-s ²
Impact Limiter End Thickness -	12.0000 in	Frictional Coefficient -	0.0000
Impact Limiter Hole Diameter -	20.0000 in	Drop Height -	30.0000 ft
Impact Limiter Hole Length -	8.0000 in	Drop Angle from Horizontal -	45.0000°
Unbacked Area Threshold Strain -	0.1000 in/in	Crush Analysis Theory -	Global
Unbacked Area Crush Stress -	2,611 psi	Number of Integration Incs -	25

POLYFOAM CRUSH STRESS (Axial: " " to rise)	
Density =	20.000 pcf
Temp =	-20.000 F
σ-yield =	2,552.3 psi
Bias =	60.000%
ε (in/in)	σ (psi)
0.000	0.0
0.100	2,552.3
0.200	2,687.0
0.300	2,868.8
0.400	3,302.9
0.500	4,115.1
0.600	6,074.3
0.650	7,942.0
0.700	10,925.0
0.750	15,001.8
0.800	26,829.5

POLYFOAM CRUSH STRESS (Radial: "⊥" to rise)	
Density =	20.000 pcf
Temp =	-20.000 F
σ-yield =	2,675.0 psi
Bias =	60.000%
ε (in/in)	σ (psi)
0.000	0.0
0.100	2,675.0
0.200	2,785.4
0.300	2,959.9
0.400	3,345.9
0.500	4,147.7
0.600	6,062.8
0.650	7,868.8
0.700	10,180.0
0.750	15,554.4
0.800	29,704.8

POLYFOAM CRUSH STRESS (Actual Data @ 45.0°)	
Density =	20.000 pcf
Temp =	-20.000 F
σ-yield =	2,611.5 psi
Bias =	60.000%
ε (in/in)	σ (psi)
0.000	0.0
0.100	2,611.5
0.200	2,734.9
0.300	2,913.3
0.400	3,324.2
0.500	4,131.3
0.600	6,068.5
0.650	7,905.2
0.700	10,532.8
0.750	15,270.6
0.800	28,157.6

DEFL (in)	MAX ε (%)	AREA (in ²)	VOLUME (in ³)	XBAR (in)	IMPACT FORCE (lbs)	ACCEL (g's)	I/L MOMENT (in-lbs)	STRAIN ENERGY (in-lbs)	KINETIC ENERGY (in-lbs)	SE/KE RATIO
0.250	1.44	7	1	-8.30	1,351	0.1	0	169	4,323,000	0.00
0.500	2.88	20	4	-8.11	7,756	0.6	0	1,307	4,326,000	0.00
0.750	4.33	36	11	-7.90	21,631	1.8	0	4,981	4,329,000	0.00
1.000	5.79	55	22	-7.68	44,807	3.7	0	13,286	4,332,000	0.00
1.250	7.25	78	39	-7.44	78,737	6.6	0	28,729	4,335,000	0.01
1.500	8.71	102	61	-7.19	124,483	10.4	0	54,131	4,338,000	0.01
1.750	10.18	129	90	-6.92	182,320	15.2	0	92,481	4,341,000	0.02

BRR Package Safety Analysis Report

Corner Drop
05-16-1995, 15:38:39

*** PACKAGING TECHNOLOGY ***
(continued...)

CASKDROP, v2.21
Jul 01, 1994

DEFL (in)	MAX ε (%)	AREA (in ²)	VOLUME (in ³)	XBAR (in)	IMPACT FORCE (lbs)	ACCEL (g's)	I/L MOMENT (in-lbs)	STRAIN ENERGY (in-lbs)	KINETIC ENERGY (in-lbs)	SE/KE RATIO
2.000	11.66	158	126	-6.65	250,919	20.9	0	146,636	4,344,000	0.03
2.250	13.14	189	169	-6.39	327,791	27.3	0	218,975	4,347,000	0.05
2.500	14.63	222	221	-6.15	409,985	34.2	0	311,197	4,350,000	0.07
2.750	16.12	256	280	-5.92	495,229	41.3	0	424,349	4,353,000	0.10
3.000	17.64	290	349	-5.70	581,988	48.5	0	559,001	4,356,000	0.13
3.250	19.14	321	425	-5.53	666,955	55.6	0	715,119	4,359,000	0.16
3.500	21.04	350	509	-5.39	750,161	62.5	0	892,258	4,362,000	0.20
3.750	23.53	379	600	-5.30	832,241	69.4	0	1,090,058	4,365,000	0.25
4.000	26.04	407	698	-5.24	913,114	76.1	0	1,308,228	4,368,000	0.30
4.250	28.58	435	804	-5.21	993,967	82.8	0	1,546,613	4,371,000	0.35
4.500	31.14	462	916	-5.20	1,075,026	89.6	0	1,805,237	4,374,000	0.41
4.750	33.55	490	1,035	-5.22	1,157,389	96.4	0	2,084,289	4,377,000	0.48
5.000	35.86	517	1,161	-5.24	1,240,678	103.4	0	2,384,048	4,380,000	0.54
5.250	38.16	545	1,293	-5.27	1,325,202	110.4	0	2,704,783	4,383,000	0.62
5.500	40.44	573	1,433	-5.30	1,413,119	117.8	0	3,047,073	4,386,000	0.69
5.750	42.71	600	1,579	-5.33	1,503,231	125.3	0	3,411,616	4,389,000	0.78
6.000	44.96	628	1,733	-5.37	1,596,230	133.0	0	3,799,049	4,392,000	0.86
6.250	47.21	656	1,894	-5.40	1,692,397	141.0	0	4,210,127	4,395,000	0.96
6.359	48.17	668	1,966	-5.41	1,735,814	144.7	0	4,396,303	4,396,303	1.00
6.500	49.43	684	2,061	-5.42	1,792,981	149.4	0	4,837,403	4,398,000	1.10
6.750	51.75	711	2,236	-5.44	1,897,584	158.1	0	5,298,723	4,401,000	1.20
7.000	54.19	739	2,417	-5.46	2,009,560	167.5	0	5,787,116	4,404,000	1.31
7.250	56.65	767	2,605	-5.47	2,128,316	177.4	0	6,304,351	4,407,000	1.43
7.500	59.12	795	2,800	-5.48	2,255,709	188.0	0	6,852,354	4,410,000	1.55
7.750	61.60	824	3,002	-5.48	2,392,365	199.4	0	7,433,363	4,413,000	1.68
8.000	64.10	852	3,212	-5.47	2,538,941	211.6	0	8,049,776	4,416,000	1.82
8.250	66.60	881	3,429	-5.47	2,701,943	225.2	0	8,704,887	4,419,000	1.97
8.500	69.12	909	3,652	-5.45	2,882,629	240.2	0	9,402,959	4,422,000	2.13
8.750	71.65	938	3,883	-5.43	3,079,002	256.6	0	10,148,162	4,425,000	2.29
9.000	74.19	967	4,121	-5.38	3,300,885	275.1	0	10,945,648	4,428,000	2.47
9.250	76.75	995	4,367	-5.32	3,573,055	297.8	0	11,804,891	4,431,000	2.66
9.500	79.31	1,024	4,619	-5.26	3,901,592	325.1	0	12,739,222	4,434,000	2.87
9.750	81.89	1,053	4,879	-5.17	4,292,510	357.7	0	13,763,484	4,437,000	3.10
10.000	84.49	1,082	5,146	-5.06	4,763,070	396.9	0	14,895,432	4,440,000	3.35
10.250	87.09	1,109	5,419	-4.95	5,316,128	443.0	0	16,155,332	4,443,000	3.64
10.500	89.71	1,134	5,698	-4.83	5,947,562	495.6	0	17,563,293	4,446,000	3.95
10.750	92.34	1,161	5,985	-4.74	6,665,548	555.5	0	19,139,932	4,449,000	4.30
11.000	94.98	1,184	6,270	-4.63	7,465,195	622.1	0	20,906,275	4,452,000	4.70
11.250	97.64	1,206	6,563	-4.54	8,360,345	696.7	0	22,884,467	4,455,000	5.14

BRR Package Safety Analysis Report

Docket No. 71-9341

Rev. 0, March 2009

End Drop
05-16-1995, 15:38:39

*** PACKAGING TECHNOLOGY ***

CASKDROP, v2.21
Jul 01, 1994

SAMPLE PROBLEM FOR QUALITY ASSURANCE CHECK (AREAS AND VOLUMES)			
Impact Limiter Weight (each) -	1,000 lbs	Cask and Payload Weight -	10,000 lbs
Impact Limiter Outside Diameter -	60.0000 in	Cask Outside Diameter -	40.0000 in
Impact Limiter Overall Length -	24.0000 in	Cask Overall Length -	48.0000 in
Impact Limiter Conical Diameter -	48.0000 in	Dynamic Unloading Modulus -	1.000E+07 lbs/in
Impact Limiter Conical Length -	10.0000 in	Rad Mass Moment of Inertia -	12,235 lb-in-s ²
Impact Limiter End Thickness -	12.0000 in	Frictional Coefficient -	0.0000
Impact Limiter Hole Diameter -	20.0000 in	Drop Height -	30.0000 ft
Impact Limiter Hole Length -	8.0000 in	Drop Angle from Horizontal -	90.0000°
Unbacked Area Threshold Strain -	0.1000 in/in	Crush Analysis Theory -	Global
Unbacked Area Crush Stress -	2,552 psi	Number of Integration Incs -	25

POLYFOAM CRUSH STRESS (Axial: " " to rise)	
Density = 20.000 pcf	
Temp = -20.000 F	
σ-yield = 2,552.3 psi	
Bias = 60.000%	
ε (in/in)	σ (psi)
0.000	0.0
0.100	2,552.3
0.200	2,687.0
0.300	2,868.8
0.400	3,302.9
0.500	4,115.1
0.600	6,074.3
0.650	7,942.0
0.700	10,925.0
0.750	15,001.8
0.800	26,829.5

POLYFOAM CRUSH STRESS (Radial: "⊥" to rise)	
Density = 20.000 pcf	
Temp = -20.000 F	
σ-yield = 2,675.0 psi	
Bias = 60.000%	
ε (in/in)	σ (psi)
0.000	0.0
0.100	2,675.0
0.200	2,785.4
0.300	2,959.9
0.400	3,345.9
0.500	4,147.7
0.600	6,062.8
0.650	7,868.8
0.700	10,180.0
0.750	15,554.4
0.800	29,704.8

POLYFOAM CRUSH STRESS (Actual Data @ 90.0°)	
Density = 20.000 pcf	
Temp = -20.000 F	
σ-yield = 2,552.3 psi	
Bias = 60.000%	
ε (in/in)	σ (psi)
0.000	0.0
0.100	2,552.3
0.200	2,687.0
0.300	2,868.8
0.400	3,302.9
0.500	4,115.1
0.600	6,074.3
0.650	7,942.0
0.700	10,925.0
0.750	15,001.8
0.800	26,829.5

DEFL (in)	MAX ε (%)	AREA (in ²)	VOLUME (in ³)	XBAR (in)	IMPACT FORCE (lbs)	ACCEL (g's)	I/L MOMENT (in-lbs)	STRAIN ENERGY (in-lbs)	KINETIC ENERGY (in-lbs)	SE/KE RATIO
0.250	2.08	1,518	377	0.00	810,360	67.5	0	101,295	4,323,000	0.02
0.500	4.17	1,541	759	0.00	1,592,808	132.7	0	401,691	4,326,000	0.09
0.750	6.25	1,564	1,147	0.00	2,311,804	192.7	0	889,768	4,329,000	0.21
1.000	8.33	1,587	1,541	0.00	2,931,701	244.3	0	1,545,206	4,332,000	0.36
1.250	10.42	1,610	1,941	0.00	3,416,844	284.7	0	2,338,774	4,335,000	0.54
1.500	12.50	1,634	2,346	0.00	3,752,646	312.7	0	3,234,960	4,338,000	0.75
1.750	14.58	1,657	2,758	0.00	3,971,661	331.0	0	4,200,498	4,341,000	0.97

BRR Package Safety Analysis Report

End Drop
05-16-1995, 15:38:39

*** PACKAGING TECHNOLOGY ***
(continued...)

CASKDROP, v2.21
Jul 01, 1994

DEFL (in)	MAX ε (%)	AREA (in ²)	VOLUME (in ³)	XBAR (in)	IMPACT FORCE (lbs)	ACCEL (g's)	I/L MOMENT (in-lbs)	STRAIN ENERGY (in-lbs)	KINETIC ENERGY (in-lbs)	SE/KE RATIO
1.785	14.88	1,661	2,816	0.00	3,995,461	333.0	0	4,341,425	4,341,425	1.00
2.000	16.67	1,681	3,175	0.00	4,112,712	342.7	0	5,354,946	4,344,000	1.23
2.250	18.75	1,705	3,598	0.00	4,214,497	351.2	0	6,395,847	4,347,000	1.47
2.500	20.83	1,729	4,027	0.00	4,287,704	357.3	0	7,458,622	4,350,000	1.71
2.750	22.92	1,753	4,462	0.00	4,351,294	362.6	0	8,538,497	4,353,000	1.96
3.000	25.00	1,777	4,904	0.00	4,445,683	370.5	0	9,638,119	4,356,000	2.21
3.250	27.08	1,801	5,351	0.00	4,562,636	380.2	0	10,764,159	4,359,000	2.47
3.500	29.17	1,826	5,804	0.00	4,693,990	391.2	0	11,921,237	4,362,000	2.73
3.750	31.25	1,851	6,264	0.00	4,831,784	402.6	0	13,111,959	4,365,000	3.00
4.000	33.33	1,875	6,730	0.00	4,973,522	414.5	0	14,337,622	4,368,000	3.28
4.250	35.42	1,900	7,202	0.00	5,120,673	426.7	0	15,599,396	4,371,000	3.57
4.500	37.50	1,925	7,680	0.00	5,274,868	439.6	0	16,898,839	4,374,000	3.86
4.750	39.58	1,951	8,164	0.00	5,437,800	453.2	0	18,237,922	4,377,000	4.17
5.000	41.67	1,976	8,655	0.00	5,611,685	467.6	0	19,619,108	4,380,000	4.48
5.250	43.75	2,002	9,152	0.00	5,802,397	483.5	0	21,045,868	4,383,000	4.80
5.500	45.83	2,027	9,656	0.00	6,018,789	501.6	0	22,523,516	4,386,000	5.14
5.750	47.92	2,053	10,166	0.00	6,268,472	522.4	0	24,059,424	4,389,000	5.48
6.000	50.00	2,079	10,682	0.00	6,560,063	546.7	0	25,662,991	4,392,000	5.84
6.250	52.08	2,105	11,205	0.00	6,900,740	575.1	0	27,345,591	4,395,000	6.22
6.500	54.17	2,131	11,735	0.00	7,296,837	608.1	0	29,120,288	4,398,000	6.62
6.750	56.25	2,158	12,271	0.00	7,751,903	646.0	0	31,001,381	4,401,000	7.04
7.000	58.33	2,184	12,814	0.00	8,272,373	689.4	0	33,004,415	4,404,000	7.49
7.250	60.42	2,211	13,363	0.00	8,862,880	738.6	0	35,146,322	4,407,000	7.98
7.500	62.50	2,238	13,919	0.00	9,556,877	796.4	0	37,448,792	4,410,000	8.49
7.750	64.58	2,265	14,482	0.00	10,454,871	871.2	0	39,950,260	4,413,000	9.05
8.000	66.67	2,606	15,051	0.00	11,632,851	969.4	0	42,711,226	4,416,000	9.67
8.250	68.75	2,633	15,706	0.00	13,506,993	1,125.6	0	45,853,706	4,419,000	10.38
8.500	70.83	2,660	16,368	0.00	14,954,954	1,246.2	0	49,411,449	4,422,000	11.17
8.750	72.92	2,688	17,037	0.00	16,218,008	1,351.5	0	53,308,070	4,425,000	12.05
9.000	75.00	2,715	17,712	0.00	18,519,890	1,543.3	0	57,650,307	4,428,000	13.02
9.250	77.08	2,743	18,394	0.00	22,571,268	1,880.9	0	62,786,702	4,431,000	14.17
9.500	79.17	2,771	19,084	0.00	27,794,818	2,316.2	0	69,082,462	4,434,000	15.58
9.750	81.25	2,799	19,780	0.00	33,405,583	2,783.8	0	76,732,513	4,437,000	17.29
10.000	83.33	2,827	20,483	0.00	39,286,171	3,273.8	0	85,818,982	4,440,000	19.33
10.250	85.42	2,827	21,190	0.00	45,050,964	3,754.2	0	96,361,124	4,443,000	21.69
10.500	87.50	2,827	21,897	0.00	51,018,884	4,251.6	0	108,369,855	4,446,000	24.37
10.750	89.58	2,827	22,604	0.00	57,507,705	4,792.3	0	121,935,678	4,449,000	27.41
11.000	91.67	2,827	23,311	0.00	64,451,479	5,371.0	0	137,180,576	4,452,000	30.81
11.250	93.75	2,827	24,017	0.00	74,690,773	6,224.2	0	154,573,358	4,455,000	34.70
11.500	95.83	2,827	24,724	0.00	85,563,336	7,130.3	0	174,605,121	4,458,000	39.17
11.750	97.92	2,827	25,431	0.00	96,435,898	8,036.3	0	197,355,026	4,461,000	44.24
12.000	100.00	2,827	26,138	0.00	107,308,461	8,942.4	0	222,823,071	4,464,000	49.92

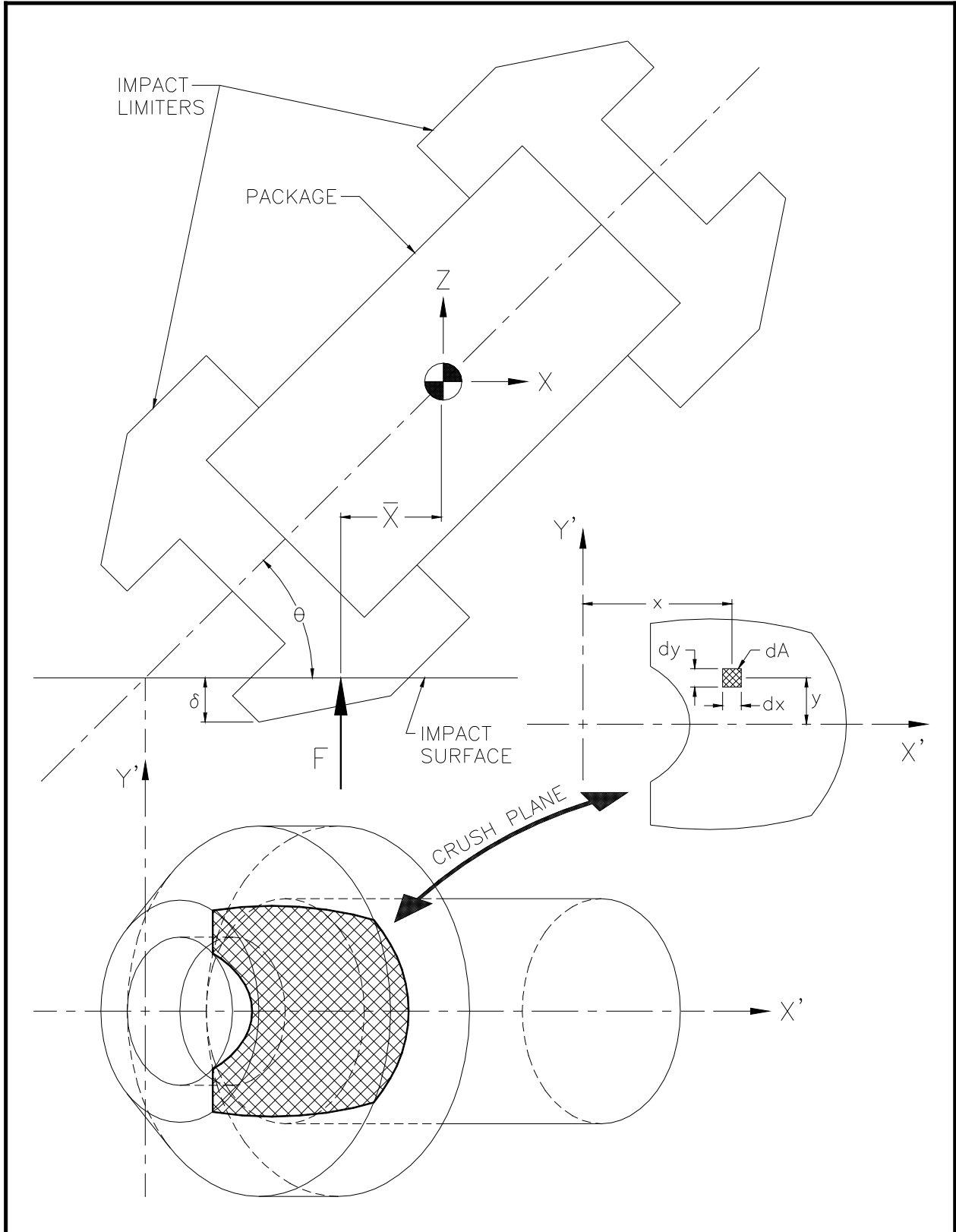


Figure 2.12.6-1 – Impact Limiter Force and Centroid Development

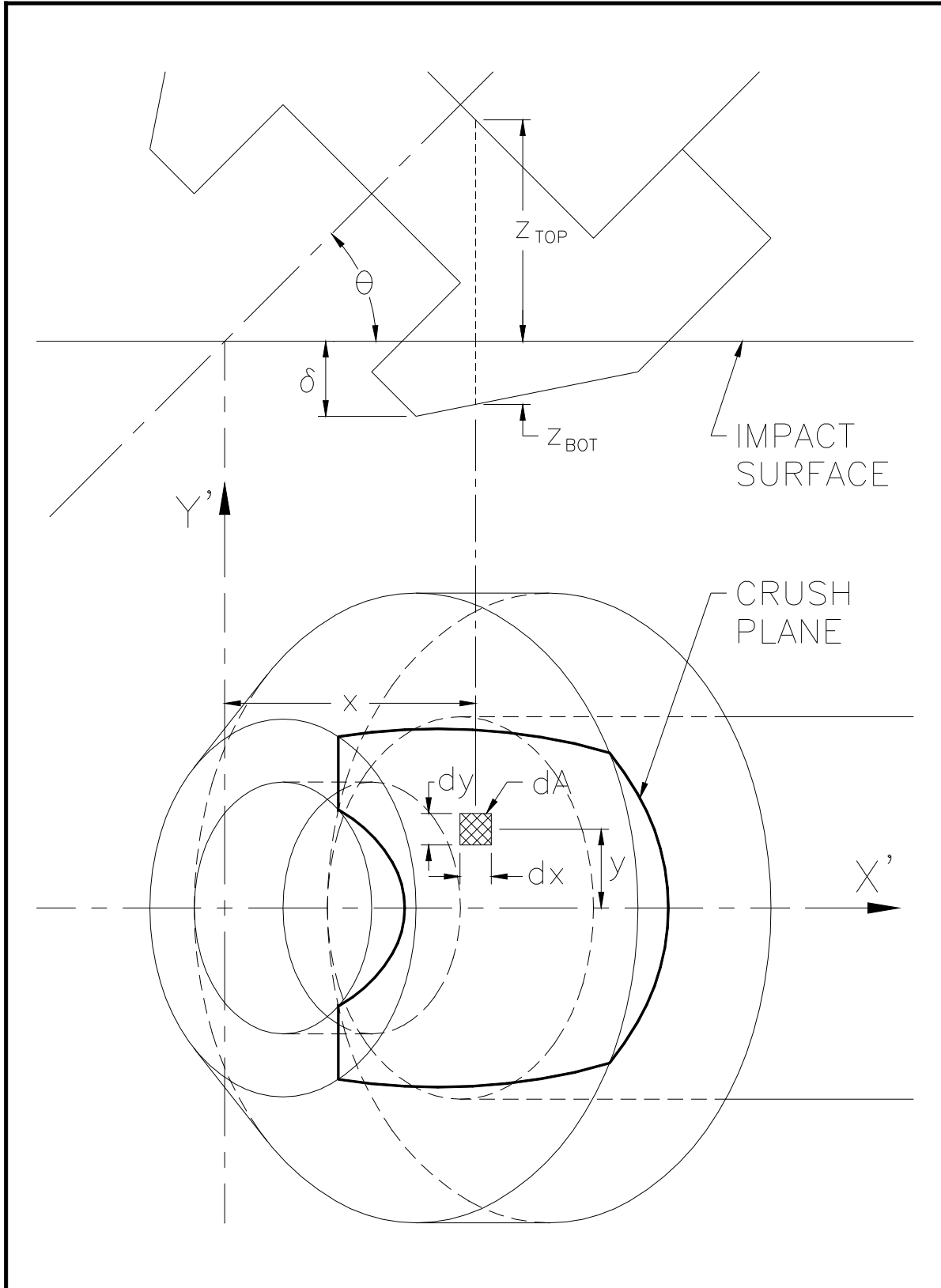


Figure 2.12.6-2 – Strain Determination

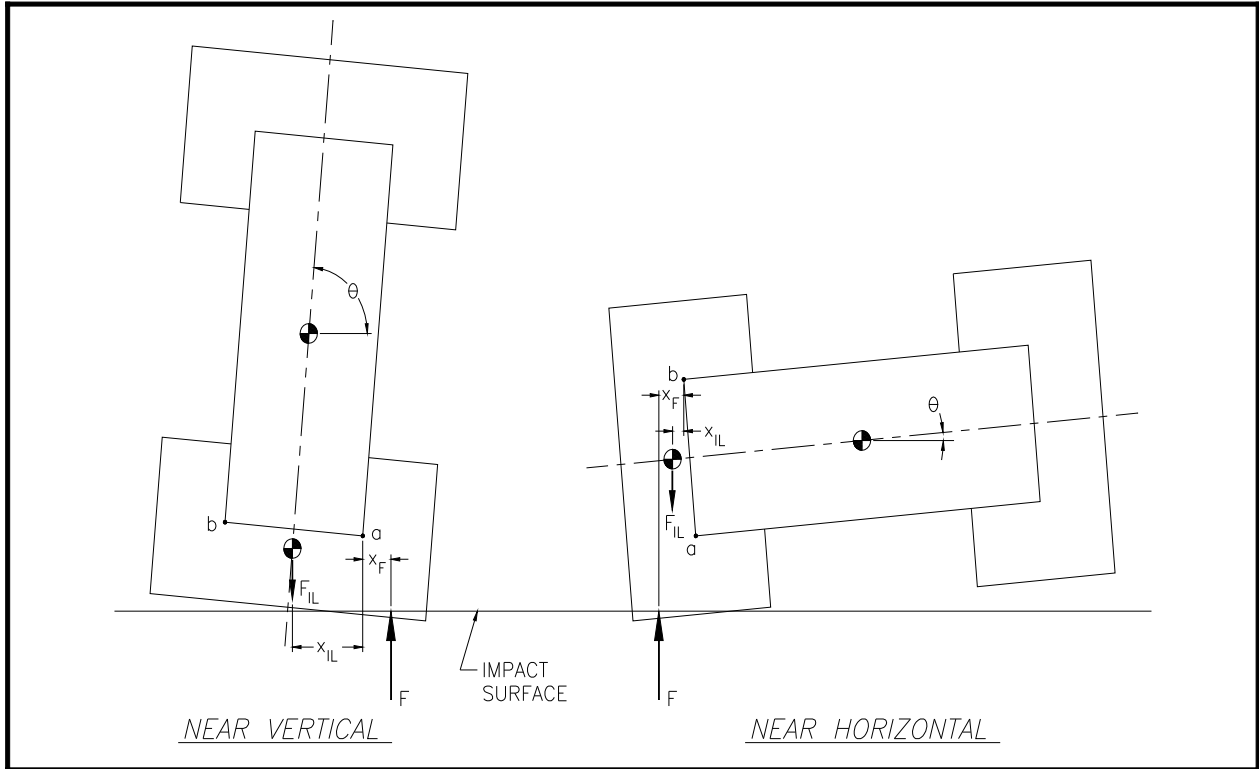


Figure 2.12.6-3 – Determination of Impact Limiter Separation Moments

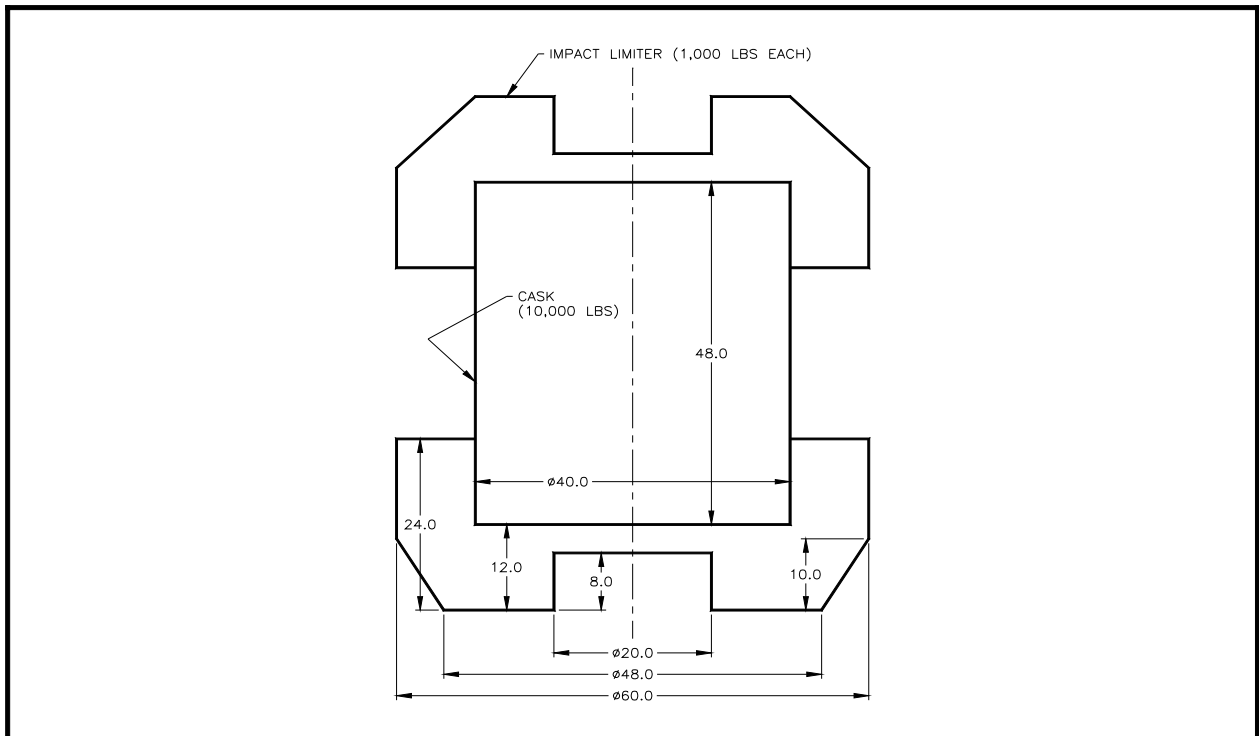


Figure 2.12.6-4 – Example Problem for CASKDROP

Packaging Technology's Cask Drop Analysis Program, v2.21
 Tuesday, May 16, 1995 3:38:19 pm

[Input Window]

Title: **SAMPLE PROBLEM FOR QUALITY ASSURANCE CHECK (AREAS AND VOLUMES)**

IL Weight (each, lbs): 1000	Cask/Payload Weight (lbs): 10000
IL Outside Diameter (in): 60	Cask Outside Diameter (in): 40
IL Overall Length (in): 24	Cask Overall Length (in): 48
IL Conical Diameter (in): 48	Free Drop Height (ft): 30
IL Conical Length (in): 10	Radial Mass MI (lb-in-s ²): 12235.16
IL End Thickness (in): 12	Frictional Coefficient (μ): 0
IL End Hole Diameter (in): 20	Unloading Modulus (lbs/in): 10000000
IL End Hole Length (in): 8	Crush Media Specification: PolyFoam

[Control Window]

Analysis	Crush (in)	Angle (°)	Static	Dynamic	Print	File
dXY: 25	Min: 0.25	Min: 0	Full <input checked="" type="checkbox"/>	Full <input type="checkbox"/>	Full <input type="checkbox"/>	Full <input checked="" type="checkbox"/>
Sln: Global	Max: 20	Max: 90	Smry <input type="checkbox"/>	Smry <input type="checkbox"/>	Smry <input type="checkbox"/>	Smry <input type="checkbox"/>
ϵ/σ : 0.1	Inc: 0.25	Inc: 45	Both <input type="checkbox"/>	Both <input type="checkbox"/>	Both <input type="checkbox"/>	Both <input type="checkbox"/>

[Output Window]

[PgUp]/[PgDn] keys toggle active window; [F10] exits program

Figure 2.12.6-5 – The CASKDROP Program *Input Window*

Packaging Technology's Cask Drop Analysis Program, v2.21
 Tuesday, May 16, 1995 3:38:29 pm

[Input Window]

Title: **SAMPLE PROBLEM FOR QUALITY ASSURANCE CHECK (AREAS AND VOLUMES)**

IL Weight (each, lbs): 1000	Cask/Payload Weight (lbs): 10000
IL Outside Di	r (in): 40
IL Overall	h (in): 48
IL Conical Di	t (ft): 30
IL Conical	in-s ²): 12235.16
IL End Thi	nt (μ): 0
IL End Hole Di	be/in): 10000000
IL End Hole	cation: PolyFoam

[Polyurethane Foam Database]

D (pcf): 20.0000 T (°F): -20.00
 σ (psi): 2552.3 Bias (%): 60

" " to rise		"⊥" to rise	
ϵ (in/in)	σ (psi)	ϵ (in/in)	σ (psi)
0.00	0.0	0.00	0.0
0.10	2,552.3	0.10	2,675.0
0.20	2,687.0	0.20	2,785.4
0.30	2,868.8	0.30	2,959.9
0.40	3,302.9	0.40	3,345.9
0.50	4,115.1	0.50	4,147.7
0.60	6,074.3	0.60	6,062.8
0.65	7,942.0	0.65	7,868.8
0.70	10,925.0	0.70	10,180.0
0.75	15,001.8	0.75	15,554.4
0.80	26,829.5	0.80	29,704.8

Orientation: Axial Orientation: Radial

[Control Window]

Analysis	Cr	Print	File
dXY: 25	Min	Full <input type="checkbox"/>	Full <input checked="" type="checkbox"/>
Sln: Global	Ma	Smry <input type="checkbox"/>	Smry <input type="checkbox"/>
ϵ/σ : 0.1	In	oth <input type="checkbox"/>	Both <input type="checkbox"/>

[Output Window]

[F2] calculates stress data and [F3] toggles orientation; [F10] exits...

Figure 2.12.6-6 – The CASKDROP Program *Polyurethane Foam Window*

2.12.6.2 SLAPDOWN

Impact limiter deflections and package accelerations are calculated using the Sandia National Laboratories-developed computer code SLAPDOWN [30]. This program solves the rigid-body equations of motion for a transportation package, given parameters such as weight, rotational moment of inertia, geometric relationships, and impact limiter force-deflection curves. The output consists of maximum impact limiter deformations and a time history of the parameters of motion (of principal interest, the acceleration at the center of gravity and angular acceleration). From these outputs, accelerations at any point on the package are found. Figure 2.12.6-7 shows the geometric parameters used, and Table 2.12.6-1 lists the required input parameters.

With respect to Figure 2.12.6-7, the line connecting points 1, 2, and 3 is the centerline axis of the cask. Points 4 and 5 represent the points of contact of the impact limiter with the impact surface. It is shown with the cask axis at an angle θ to the horizontal, but may impact the ground at any angle, up to and including vertical. The primary end is the end of the cask which strikes the ground first, and the secondary end (the slapdown end) is the end which strikes the ground second. The distances R1 and R2 are the outer radii, respectively, of each impact limiter. The impact limiter forces (which act along the lines of R1 and R2) are assumed to be always perpendicular to the impact surface, which is consistent with the assumption for each orientation that the force-deflection curve is defined perpendicular to the surface. The impact limiters are modeled as nonlinear, inelastic springs, and consist of the force-deflection relations developed in Section 2.12.6.1, *CASKDROP*. The elastic rebound stiffness determines how much of the energy absorbed by the limiter (the area under the force-deflection curve) is elastically recovered. Elastic rebound stiffness has a small effect on SLAPDOWN response, and is normally set at a value of 10^7 lb/in. The equations of motion are solved for all five nodes. The center of gravity (C.G.) is taken as the geometric center of the cask. Friction is assigned a value of zero, since this maximizes the impact forces and deflections for the secondary (slapdown) impact limiter.

Table 2.12.6-1 shows a listing of sample input for the SLAPDOWN program. Table 2.12.6-2 shows a listing of sample force-deflection data for the SLAPDOWN program. The force-deflection data for the primary impact limiter are obtained from *CASKDROP* for the stated primary impact orientation. The secondary impact limiter data is for a horizontal orientation. Table 2.12.6-3 shows a sample output of the SLAPDOWN program from the general output file. This is performed for a 15° primary oblique orientation. The angle of secondary contact with the ground surface is displayed at the end of the output list ("Tail Impact Angle"), and is nearly equal to zero, thus the horizontal orientation force-deflection data for the secondary impact is justified.

Table 2.12.6-4 shows a portion of the corresponding time history output file, showing the results only through the end of the primary impact. The time variable is given in the first column. In the second, third and fourth columns are given the results at the cask center of gravity (SLAPDOWN node 2): the vertical position is in the column headed POSY(2) (inches), the velocity is in the column headed VELY(2) (in/s), and the acceleration is in the column headed ACCY(2) (in/s²). The last three columns give the rotational parameters of angular position: the angle THETA (radians, horizontal is zero), the angular velocity OMEGA (r/s) and the angular acceleration ALPHA (r/s²).

BRR Package Safety Analysis Report

As verification of the SLAPDOWN code analysis methodology, the sample problem described above was compared to output from the public domain program SCANS [31]. The results compare well, as demonstrated in Table 2.12.6-5. Input data for the comparison is taken from Table 2.12.6-1.

Table 2.12.6-1 – Sample Inputs to the SLAPDOWN Program

Input Parameter	Description	Sample Value
Z1, Z2	Length from primary end to C.G., and from C.G. to secondary end, respectively (inch)*	90.38 (both sides)
R1, R2	Length from cask axis to impact limiter contact point, primary and secondary ends, respectively (inch)	63.0 (both ends)
μ_1, μ_2	Coefficient of friction, primary and secondary ends, respectively	0.0 (both ends)
m	Overall package mass (lb-s ² /inch)	611.0
I_{cg}	Radial mass moment of inertia about the package C.G. (in-lb-s ²)	$3.1(10)^6$
h	Drop height (ft)	30
θ	Angle with respect to horizontal of primary impact	Variable (15° used for example)
k	Elastic rebound stiffness of the impact limiter material (lb/inch)	10^7

*This dimension is measured from the cask C.G. to the center of the cylindrical portion of the impact limiter, which is the location of the line of action of side drop impact force.

Table 2.12.6-2 – Sample Force-Deflection to the SLAPDOWN Program

Primary Impact Limiter		Secondary Impact Limiter	
Deflection (in)	Force (lb)	Deflection (in)	Force (lb)
0	0	0	0
1	207,100	1	2,383,000
2	583,900	2	3,363,000
3	1,069,000	3	3,963,000
4	1,640,000	4	4,450,000
5	2,285,000	5	4,885,000
6	2,998,000	6	5,289,000
7	3,767,000	7	5,671,000
8	4,444,000	8	6,041,000
9	5,146,000	9	6,310,000
10	5,756,000	10	6,513,000
11	6,304,000	11	6,721,000
12	6,818,000	12	6,936,000
13	7,223,000	13	7,157,000
14	7,573,000	14	7,384,000
15	7,926,000	15	7,614,000

BRR Package Safety Analysis Report**Table 2.12.6-3 – Sample of SLAPDOWN General Output**

Sample Cask, 15 Degree Oblique

***** SEQUENCE OF EVENTS *****

```

** NOSE HIT      AT TIME 0.000E+0 VELOCITY = -5.275E+2  RATIO = 1.00E+0
** NOSE REBOUND AT TIME 3.311E-2 VELOCITY = 1.506E+1  RATIO = -2.86E-2
** NOSE UNLOAD  AT TIME 4.008E-2 VELOCITY = 1.346E+2  RATIO = -2.55E-1
** TAIL HIT      AT TIME 7.318E-2 VELOCITY = -7.061E+2  RATIO = 1.34E+0
** TAIL REBOUND AT TIME 1.037E-1 VELOCITY = 2.410E+1  RATIO = -4.57E-2
** TAIL UNLOAD  AT TIME 1.106E-1 VELOCITY = 1.422E+2  RATIO = -2.70E-1

```

```

Event over at time    0.11152      Time step size  0.00087
Time step multiplier  0.10          128 Plot times written to database

```

	DISPLACEMENT	VELOCITY	ACCELERATION	
NOSE	1.159E+1	1.346E+2	2.7317E+4	(MAX)
		-5.275E+2	-7.2971E+3	(MIN)
TAIL	1.206E+1	1.422E+2	2.9272E+4	(MAX)
		-7.061E+2	-6.4780E+3	(MIN)
CG		2.781E+1	1.0987E+4	(MAX)
		-5.277E+2	-3.8600E+2	(MIN)
ANGULAR		1.267E+0	2.0245E+2	(MAX)
		-4.623E+0	-1.8804E+2	(MIN)

```

MAXIMUM ENERGY:          3.4879E+7 (NOSE)
MAXIMUM ENERGY:          5.9471E+7 (TAIL)
IMPACT AT 80 IN FROM C.G. (x-n)      65.93 (g)
IMPACT AT 80 IN FROM C.G. (x-t)      70.35 (g)
TAIL IMPACT ANGLE =          1.91 DEG.

```

Table 2.12.6-4 – Sample of SLAPDOWN Time History Output

Title: Sample Cask, 15 Degree Oblique

9/29/2008 10:39:46 AM

Time, S	POSY (2)	VELY (2)	ACCY (2)	THETA	OMEGA	ALPHA
.0000E+0	.8639E+2	-.5275E+3	-.3860E+3	.2618E+0	.0000E+0	.0000E+0
.8712E-3	.8593E+2	-.5277E+3	-.2302E+3	.2618E+0	-.2335E-2	-.2680E+1
.1742E-2	.8547E+2	-.5277E+3	-.7449E+2	.2618E+0	-.7005E-2	-.5360E+1
.2614E-2	.8501E+2	-.5276E+3	.1862E+3	.2618E+0	-.1558E-1	-.9846E+1
.3485E-2	.8455E+2	-.5271E+3	.4689E+3	.2618E+0	-.2840E-1	-.1471E+2
.4356E-2	.8409E+2	-.5264E+3	.8029E+3	.2618E+0	-.4622E-1	-.2046E+2
.5227E-2	.8364E+2	-.5254E+3	.1164E+4	.2617E+0	-.6946E-1	-.2668E+2
.6098E-2	.8318E+2	-.5241E+3	.1552E+4	.2617E+0	-.9851E-1	-.3334E+2
.6970E-2	.8272E+2	-.5224E+3	.1972E+4	.2616E+0	-.1339E+0	-.4057E+2
.7841E-2	.8227E+2	-.5203E+3	.2399E+4	.2614E+0	-.1756E+0	-.4792E+2
.8712E-2	.8181E+2	-.5178E+3	.2863E+4	.2613E+0	-.2243E+0	-.5592E+2
.9583E-2	.8136E+2	-.5149E+3	.3321E+4	.2611E+0	-.2799E+0	-.6380E+2
.1045E-1	.8091E+2	-.5116E+3	.3817E+4	.2609E+0	-.3429E+0	-.7233E+2
.1133E-1	.8047E+2	-.5078E+3	.4306E+4	.2606E+0	-.4133E+0	-.8076E+2
.1220E-1	.8003E+2	-.5036E+3	.4807E+4	.2602E+0	-.4912E+0	-.8939E+2
.1307E-1	.7959E+2	-.4990E+3	.5312E+4	.2598E+0	-.5766E+0	-.9809E+2
.1394E-1	.7915E+2	-.4939E+3	.5801E+4	.2593E+0	-.6694E+0	-.1065E+3
.1481E-1	.7872E+2	-.4885E+3	.6221E+4	.2587E+0	-.7686E+0	-.1138E+3
.1568E-1	.7830E+2	-.4827E+3	.6628E+4	.2580E+0	-.8738E+0	-.1208E+3
.1655E-1	.7788E+2	-.4766E+3	.7025E+4	.2573E+0	-.9850E+0	-.1277E+3
.1742E-1	.7746E+2	-.4702E+3	.7416E+4	.2564E+0	-.1102E+1	-.1344E+3
.1830E-1	.7705E+2	-.4634E+3	.7790E+4	.2554E+0	-.1225E+1	-.1409E+3
.1917E-1	.7665E+2	-.4563E+3	.8132E+4	.2544E+0	-.1353E+1	-.1469E+3
.2004E-1	.7625E+2	-.4490E+3	.8426E+4	.2532E+0	-.1485E+1	-.1520E+3
.2091E-1	.7586E+2	-.4414E+3	.8704E+4	.2519E+0	-.1622E+1	-.1568E+3
.2178E-1	.7547E+2	-.4336E+3	.8964E+4	.2505E+0	-.1762E+1	-.1614E+3
.2265E-1	.7510E+2	-.4256E+3	.9189E+4	.2489E+0	-.1906E+1	-.1653E+3
.2352E-1	.7472E+2	-.4174E+3	.9391E+4	.2473E+0	-.2054E+1	-.1689E+3
.2439E-1	.7436E+2	-.4090E+3	.9577E+4	.2455E+0	-.2204E+1	-.1722E+3
.2527E-1	.7400E+2	-.4005E+3	.9746E+4	.2436E+0	-.2356E+1	-.1752E+3
.2614E-1	.7366E+2	-.3919E+3	.9897E+4	.2415E+0	-.2511E+1	-.1779E+3
.2701E-1	.7331E+2	-.3832E+3	.1002E+5	.2393E+0	-.2668E+1	-.1802E+3
.2788E-1	.7298E+2	-.3744E+3	.1013E+5	.2370E+0	-.2827E+1	-.1822E+3
.2875E-1	.7265E+2	-.3654E+3	.1023E+5	.2345E+0	-.2987E+1	-.1839E+3
.2962E-1	.7234E+2	-.3565E+3	.1030E+5	.2319E+0	-.3148E+1	-.1853E+3
.3049E-1	.7203E+2	-.3474E+3	.1036E+5	.2292E+0	-.3311E+1	-.1864E+3
.3136E-1	.7172E+2	-.3384E+3	.1040E+5	.2263E+0	-.3474E+1	-.1873E+3
.3223E-1	.7143E+2	-.3293E+3	.1042E+5	.2233E+0	-.3638E+1	-.1878E+3
.3311E-1	.7114E+2	-.3202E+3	.1043E+5	.2201E+0	-.3801E+1	-.1880E+3
.3398E-1	.7086E+2	-.3111E+3	.1042E+5	.2168E+0	-.3965E+1	-.1880E+3
.3485E-1	.7059E+2	-.3027E+3	.9658E+4	.2134E+0	-.4118E+1	-.1749E+3
.3572E-1	.7033E+2	-.2951E+3	.8787E+4	.2098E+0	-.4257E+1	-.1598E+3
.3659E-1	.7007E+2	-.2884E+3	.7627E+4	.2061E+0	-.4378E+1	-.1397E+3
.3746E-1	.6982E+2	-.2830E+3	.6214E+4	.2022E+0	-.4479E+1	-.1152E+3
.3833E-1	.6957E+2	-.2790E+3	.4593E+4	.1983E+0	-.4555E+1	-.8695E+2
.3920E-1	.6933E+2	-.2766E+3	.2814E+4	.1944E+0	-.4603E+1	-.5594E+2
.4008E-1	.6909E+2	-.2757E+3	.9348E+3	.1904E+0	-.4623E+1	-.2310E+2
.4095E-1	.6885E+2	-.2761E+3	-.3860E+3	.1863E+0	-.4623E+1	.0000E+0

Table 2.12.6-5 – Comparison of SLAPDOWN and SCANS Results

Parameter	SLAPDOWN Result	SCANS Result
Primary impact limiter deflection, inch	11.6	11.6
Secondary impact limiter deflection, inch	12.1	12.1
Primary vertical acceleration (e.g.), g	26.9	26.8
Secondary vertical acceleration (e.g.), g	28.5	28.5
Primary angular acceleration, radians/s ²	-188	-186
Secondary angular acceleration, radians/s ²	202	218

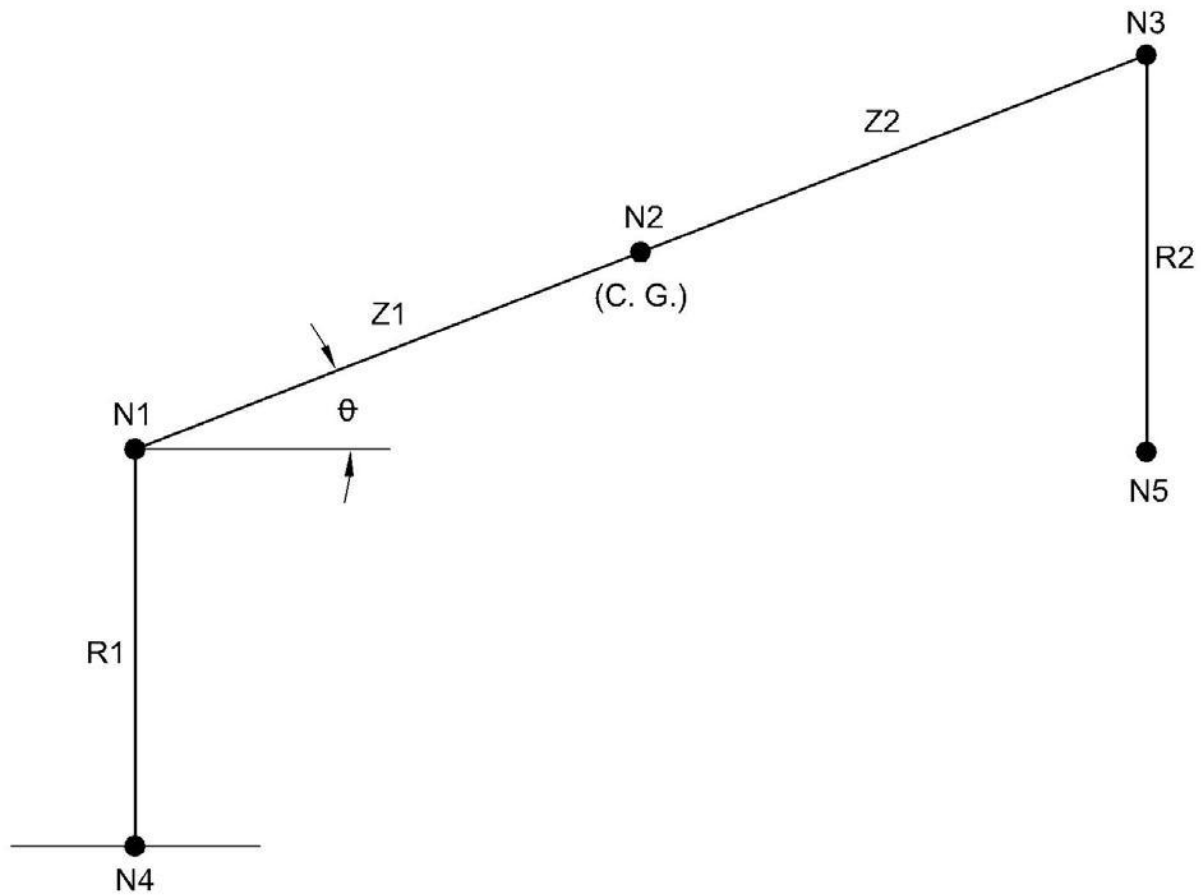


Figure 2.12.6-7 – SLAPDOWN Analytical Model

2.12.7 Seal Performance Tests

This appendix contains descriptions of the performance tests which have been run on the butyl rubber compound used for the containment O-ring seal and sealing washers used in the BRR package. The material is designated as Rainier Rubber R-0405-70. The performance tests which will be discussed have demonstrated the ability of this material to maintain a leaktight¹ containment boundary under minimum compression, minimum temperature, and maximum temperature conditions which are beyond those experienced in the BRR package.

2.12.7.1 Performance Tests Associated with the TRUPACT-II Package

Two sets of butyl rubber performance tests have been done in support of the TRUPACT-II package certification (NRC Docket 71-9218). All relevant tests have used a bore-type fixture which is consistent with the configuration of the O-ring seals in the TRUPACT-II.

The test configuration and procedure was similar between the two tests and will now be briefly described. More details are available in Section 2.10.7.4 and Section 2.10.7.4A of [2]. Only the small test fixture is considered, since it was used in both sets of tests. The test fixture consists of an inner ring containing two O-ring grooves on its outer diameter and an outer ring which fits over the inner ring and provides compression of the two test O-rings. The cross-sectional diameter of the test O-rings was nominally 0.400 inches, which is essentially equivalent to the 0.375 nominal dimension of the BRR package containment O-ring seal. To vary the O-ring compression in the test fixture, the radial position of the inner ring was controlled by jacking screws. When the inner ring was shifted to one side within the outer ring, a maximum compression was obtained on the side toward which the inner ring was shifted, and a minimum compression was obtained on the opposite side. The entire fixture could be placed in an environmental chamber and either cooled or heated for a set time. A helium leakage rate test was performed at various stages by testing the leakage rate between the outside of the fixture and the space between the two test O-rings.

The first set of tests was performed in 1989 and is documented in Section 2.10.7.4 of [2]. A typical test sequence consisted of the following steps:

1. Assemble the test fixture at ambient conditions.
2. Perform a leakage rate test with the inner ring centered in the outer ring.
3. Chill the fixture to -40 °F and perform a helium leakage rate test.
4. Allow the fixture to warm to -20 °F.
5. Shift the inner ring laterally within the outer ring to achieve maximum compression on one side and minimum compression on the other side.
6. Perform a helium leakage rate test with the fixture still at -20 °F.
7. Heat to an elevated temperature, maintaining the inner ring in the shifted position.

¹ Leaktight is defined as a maximum leakage rate of 1×10^{-7} ref-cc/sec, air, per [1].

8. Hold at temperature for 8 hours. Create a hard vacuum between the two test O-rings to confirm their integrity. A helium leakage rate test was not performed due to the tendency toward rapid saturation of the O-rings with helium at elevated temperature.
9. Chill the fixture to -20 °F, maintaining the inner ring in the shifted position.
10. Perform a final helium leakage rate test with the fixture still at -20 °F.

For each test, the maximum and minimum compressions were calculated using the dimensions of the fixture and of the test O-rings. The principal result of these tests was a demonstration that the subject rubber compound is capable of maintaining a leaktight condition at -20 °F with a minimum compression of 14.9% subsequent to an 8 hour soak at 400 °F. Details of the five small fixture tests are given in Table 2.12.7-1, adapted from Table 2.10.7-1 of [2]. Note that the term 'disk' in the table corresponds to the term 'inner ring' used in this description.

The second set of tests was performed in 1999, and are documented in Section 2.10.7.4A of [2]. These tests served to lower the minimum compression value at which a leaktight condition was demonstrated to be maintained. The tests used the same small test fixture, modified to allow it to achieve a lower minimum compression. The same test procedure was followed, except that all tests were run at a temperature of 400 °F. The principal result of these tests was a demonstration that the subject rubber compound is capable of maintaining a leaktight condition at -20 °F with a minimum compression of 12.9% subsequent to an 8 hour soak at 400 °F. Details of the three tests are given in Table 2.12.7-2, adapted from Table 2.10.7.4A-2 of [2].

2.12.7.2 Performance Tests Associated with the RTG Package

O-ring tests were also performed in support of the Radioisotope Thermoelectric Generator (RTG) package certification (DOE Docket 94-6-9904). The results are reported in Section 2.10.6 of [3]. In these tests, a face-type fixture was used which permitted four different compressions to be tested at once. Unlike the TRUPACT-II testing, and consistent with the conditions in a face-type configuration, the O-rings were not mechanically moved or disturbed throughout the test. The fixture consisted of an inner plate having three concentric grooves on each side. Each groove had a different depth and contained an O-ring made from butyl compound R-0405-70 as described above. The inner and outer O-rings on each side were the test specimens; the center O-rings were used only to support leakage rate testing of the test specimens. The O-rings were compressed by outer plates which were set off from the inner plate by shims which, along with the groove depths, controlled the amount of compression of each test O-ring. The nominal test O-ring cross-sectional diameter was 0.275 inches. The minimum compression created by the fixture was 10%, which was uniform around the entire circumference of the fixture. Compressions of 12%, 14%, and 15.5% were tested at the same time. The dimensions of the fixture and of the test specimens, and the resulting compression values, are shown in Table 2.12.7-3.

The time/temperature sequence was as follows:

1. Assemble the test fixture at ambient conditions and perform a helium leakage rate test.
2. Chill the fixture to -40 °F and perform a helium leakage rate test.
3. Heat the fixture to 380 °F, and hold for 24 hours. Confirm integrity of the test O-rings by placing a hard vacuum on the test cavity (less than 0.2 mbar).

BRR Package Safety Analysis Report

4. Allow the fixture to cool to 350 °F, and hold for 144 hours. The total time at elevated temperature is 168 hours, or one full week. Confirm integrity of the test O-rings by placing a hard vacuum on the test cavity (less than 0.2 mbar).
5. Cool the fixture to -20 °F and perform a final helium leakage rate test.

Each of the helium leakage rate tests demonstrated a leakage rate below the leaktight criterion of 1×10^{-7} ref-cc/sec, air, as defined by [1]. Of note, only the results from the outer O-ring tests (10% and 14% compression) were available at the time of publication of [3]. The successful completion of the inner O-ring tests (12% and 15.5% compression) was confirmed in [4].

2.12.7.3 Summary

The butyl rubber compound used for the BRR package containment seals was tested in both a bore-type and a face-type test fixture at low compression and elevated temperature. In the bore-type testing, the O-rings were demonstrated to be helium leaktight at a temperature of -20 °F after a soak at 400 °F for 8 hours at a minimum compression of 11.9%. In the face-type testing, the O-rings were demonstrated to be helium leaktight at a temperature of -20 °F after a soak at 380 °F for 24 hours followed by a soak at 350 °F for 144 hours at a minimum compression of 10%. These compression and temperature/time conditions exceed the severity of those experienced in the BRR package. The minimum compression of the BRR package containment seal O-ring is calculated in Section 4.1.3, *Seals*, and the maximum temperature under NCT and HAC is discussed in Chapter 3, *Thermal Evaluation*.

Table 2.12.7-1 – TRUPACT–II O-ring Seal Performance Test Results (1989)⑦

Test Number	O-ring Seal Cross-Sectional Diameter (inches)				Stretch (%)		Maximum Gap (inches)		Minimum Compression (%)				Soak Temperature and Helium Leakage Rate Test Results ④				
	O-ring Seal No. 1		O-ring Seal No. 2		Min	Max	Disk Center	Disk Offset	Disk Centered		Disk Offset		Disk Centered		Disk Offset		
	Min	Max	Min	Max					Min	Max	Min	Max	Min	Max	Ambient	-40 °F	-20 °F
1	0.387	0.397	0.387	0.396	2.0	4.1	0.026	③	22.1	25.6	14.9	20.0	Yes	Yes	Yes	350 °F	Yes
2	0.388	0.398	0.387	0.398	2.0	4.1	0.029	0.050	21.3	25.1	15.7	19.7	Yes	Yes	⑥	450 °F	No
3	0.387	0.397	0.387	0.399	2.0	4.1	0.027	0.052	21.9	25.8	15.2	19.4	Yes	Yes	Yes	400 °F	Yes
4	②	②	②	②	2.0	4.1	0.027	0.053	21.9	25.8	14.9	19.1	Yes	Yes	Yes	400 °F	Yes
5	②	②	②	②	2.0	4.1	0.026	0.050	22.1	26.0	15.7	19.9	Yes	Yes	Yes	400 °F	Yes

Notes:

- ① Material for all O-ring seal test specimens was butyl rubber compound R-0405-70, Rainier Rubber Co., Seattle, WA.
- ② Not measured; calculations assume the worst case range as taken from Tests Numbers 1 - 3 (i.e., Ø0.387 minimum to Ø0.399 maximum).
- ③ Range of values is 0.048 in. minimum to 0.053 in. maximum due to an indirect method of gap measurement (used for this test only).
- ④ A “Yes” response indicates that helium leakage rate testing demonstrated a leaktight condition as defined in [1], i.e., the leakage rate was less than or equal to 1×10^{-7} ref-cc/sec, air. In all cases, measured leak rates were less than or equal to 2.0×10^{-8} ref cc/s, helium, for tests with a “Yes” response.
- ⑤ No helium leakage rate tests were performed at elevated temperatures due to O-ring seal permeation and saturation by helium gas. The ability of the test fixture to establish a rapid, hard vacuum between the O-ring seals was used as the basis for leakage rate test acceptance at elevated temperatures. All tests rapidly developed a hard vacuum, with the exception of Test Number 2 at an elevated temperature of 450 °F, which slowly developed a vacuum.
- ⑥ Initial leakage rate of 1.0×10^{-5} ref cc/s, helium; became leaktight approximately one minute later.
- ⑦ Adapted from Table 2.10.7-1 of [2].

Table 2.12.7-2 – Supplementary TRUPACT–II O-ring Seal Performance Test Results (1999)④

Test No.	Disk Centered % Comp.		Disk Offset % Comp.		Helium Leak Tight②				
	O-ring #1	O-ring #2	O-ring #1	O-ring #2	Ambient Temp.	-40 °F	-20 °F (Disk Offset)	Hot Soak (Disk Offset)③	-20 °F (Disk Offset)
1	18.5	17.9	12.7	12.0	Yes	Yes	Yes	Held Vacuum	Yes
2	20.8	20.0	12.9	11.9	Yes	Yes	Yes	Held Vacuum	Yes
3	19.2	19.2	12.1	12.1	Yes	Yes	Yes	Held Vacuum	Yes

Notes:

- ① Material for all O-ring seal test specimens was butyl rubber compound R-0405-70, Rainier Rubber Co., Seattle, WA.
- ② Seal is considered to be leaktight if the actual leakage rate is less than or equal to 8×10^{-8} atm-cc/sec.
- ③ Hot soak was 8 hours at a uniform temperature of 400 °F.
- ④ Adapted from Table 2.10.7.4A-2 of [2].

Table 2.12.7-3 – RTG O-ring Seal Performance Test Parameters^③

Fixture Side	Outer groove depth, in.	Inner groove depth, in.	Shim Thickness, in.	Outer O-ring X- section, in.	Inner O-ring X- section, in.	Outer O-ring compression, %	Inner O-ring compression, %
Side A	0.2053	0.2000	0.044	0.2770	0.2773	10	12
Side B	0.2075	0.2033	0.031	0.2776	0.2774	14	15.5

Notes:

- ① Material for all O-ring seal test specimens was butyl rubber compound R-0405-70, Rainier Rubber Co., Seattle, WA.
- ② Each of the four test O-ring seals were leaktight per [1] when tested at a temperature of -20 °F following the time/temperature sequence of 380 °F for 24 hours followed by 350 °F for 144 hours.
- ③ Adapted from Table 4.1-1 and Table 4.1-2 of [3].

2.12.7.4 References

1. ANSI N14.5-1997, *American National Standard for Radioactive Materials – Leakage Tests on Packages for Shipment*, American National Standards Institute (ANSI), Inc.
2. *Safety Analysis Report for the TRUPACT-II Shipping Package*, USNRC Docket 71-9218, Revision 18, U.S. Department of Energy, Carlsbad Field Office, Carlsbad, New Mexico.
3. DOE Docket No. 94-6-9904, *Radioisotope Thermoelectric Generator Transportation System Safety Analysis Report for Packaging*, WHC-SD-RTG-SARP-001, prepared for the U.S. Department of Energy Office of Nuclear Energy under Contract No. DE-AC06-87RL10930 by Westinghouse Hanford Company, Richland, WA.
4. Westinghouse Hanford Company, *RTG Transportation System Packaging O-ring Material Thermal Validation Test Report for Face Seal Test Fixture*, WHC-SD-RTG-TRP-010, Rev 0.

2.12.8 Fuel Basket Stress Analysis

This appendix provides details of the stress analysis evaluations of the four fuel baskets used in the BRR package under HAC free drop conditions. One basket corresponds to each type of fuel, which includes the University of Missouri Research Reactor (MURR), the Massachusetts Institute of Technology Nuclear Research Reactor (MITR-II), Advanced Test Reactor (ATR), and Training, Research, Isotopes, General Atomics (TRIGA) reactors.

The evaluations consist of manual calculations and buckling evaluations using ASME B&PV Code Case N-284-2 [13]. An additional buckling evaluation technique for non-circular sections, used for the MITR-II basket, is referenced below. All buckling evaluations use a minimum factor of safety of 1.34, consistent with [13]. The bounding HAC impact acceleration of 120g is used for all analyses, which include free drops on the package end and on the package side. Basket and fuel weight is taken from Table 2.1-3. All of the material used in the fuel baskets is ASTM Type 304 stainless steel in various product forms including A240 (plate), A249 (tube), A269 (tube) A511 (tube), and A312 (pipe). Material properties are evaluated at the NCT maximum temperature of 400 °F, and taken from Table 2.2-1. Allowable stresses are taken from Table 2.1-1. The numeric values of allowable stress are given in Table 2.12.8-1. The analyses described in this appendix are based on the most critical load paths and demonstrate the structural integrity of the basket. Since each basket has a different design, the analyses which are most critical for each basket will be somewhat different.

Basket analyses do not include a dynamic load factor (DLF), since the impact acceleration used is nearly 50% higher than the maximum test result (see Section 2.12.5.3, *Reconciliation with Certification Test Results*), and because the basket structures are relatively stiff, which would result in a DLF not significantly different from unity.

2.12.8.1 MURR Basket

The MURR basket provides positioning and support for up to eight MURR fuel elements. The structure consists of an outer shell, an inner shell, eight radial separation plates, a support plate, and other stiffening components. From Table 2.1-3, the empty basket has a weight of 650 lb, and with eight fuel elements, the bounding weight is 770 lb. A cross sectional view of the basket is shown in Figure 2.12.8-1 and a view of the support plate is shown in Figure 2.12.8-2.

2.12.8.1.1 Fuel Support Plate Bending

The fuel support plate provides lower end support of the fuel elements. In the bottom-down vertical impact, the support plate is loaded by a maximum of eight fuel elements. Since each fuel element slot is supported by welds along three sides as shown in Figure 2.12.8-2, the loading of the plate can be analyzed for a single segment of the plate.

Stresses loading the plate can be modeled using [25], Table 24, Case 27. This is a conservative approach using the simply supported case. This method will ignore the in-plane moment reducing effects of the welds. The effective area of plate for the applied load is:

$$A_p = \frac{\pi}{4}(d_o^2 - d_i^2) - 8 \cdot \frac{\pi}{4}d_H^2 - 8 \cdot A_S = 106.3 \text{ in}^2$$

BRR Package Safety Analysis Report

where $d_o = 15.1$ inches is the outer diameter of the plate, $d_i = 7.0$ inches is the center hole diameter of the plate, $d_H = 0.8$ inches is the diameter of the eight drain holes, and $A_S = 3.781 \text{ in}^2$ is the area of the separator plates. For a density $\rho = 0.29 \text{ lb/in}^3$ and a plate thickness $t = 0.375$ inches, the weight of the plate is:

$$W_p = A_p t \rho = 11.6 \text{ lb}$$

For a single sector of the plate, the plate load is:

$$P_p = (nW_{FE} + W_p) \cdot a = 15,792 \text{ lb}$$

where the number of fuel elements, $n = 8$, the weight of individual MURR element, $W_{FE} = 15 \text{ lb}$, and the bounding acceleration is $a = 120g$. The distributed pressure load over each sector of the plate is equivalent to the total fuel load over the effective area of the plate.

$$q = \frac{P_p}{A_p} = 148.6 \text{ psi}$$

From Case 27 the maximum plate stress for each segment is:

$$\sigma_t = \beta_1 \frac{qa^2}{t^2} = 6,867 \text{ psi}$$

where $a = \frac{1}{2}d_o$ is the radius of the segment of plate, $t = 0.375$ inches is the thickness of the plate, and $\beta_1 = 0.114$ is a constant. The allowable combined membrane and bending stress is $S = 64,000 \text{ psi}$ from Table 2.12.8-1. The margin of safety is:

$$MS = \frac{S}{\sigma_t} - 1 = +8.32$$

Therefore the plate has sufficient capacity to support the applied load.

2.12.8.1.2 Outer Shell Slot Welds

The slot welds connect the outer shell to the inner components of the basket. In a bottom-down drop, the slot welds will take the full weight of the fuel, center shell, spacer plates, and fuel support plate. The $\frac{1}{4}$ inch fillet weld between the fuel support plate and the outer shell will be conservatively excluded from this calculation.

The combined slot weld area for the 32, 2.0 inch x 0.6 inch long slots with full radii is:

$$A_{SW} = 32 \left[\frac{\pi}{4} (0.6)^2 + 2.0(0.6) \right] = 47.4 \text{ in}^2$$

For this load case, the applied load is conservatively taken as the full weight of the loaded basket at an acceleration, $a = 120g$:

$$P_{SW} = (nW_{FE} + W_b) a = 92,400 \text{ lb}$$

where the weight of the fuel basket is $W_b = 650 \text{ lb}$. The shear stress due to the direct load is:

$$\tau_{SW} = \frac{P_{SW}}{A_{SW}} = 1,949 \text{ psi}$$

BRR Package Safety Analysis Report

From Table NG-3352-1 of [32] the allowable stress of the weld is multiplied by a weld quality factor of 0.35, which applies to an intermittent or plug weld with surface PT examination. From Table 2.12.8-1, the allowable stress for pure shear is $S = 22,320$ psi. The margin of safety is:

$$MS = \frac{(0.35)S}{\tau_{sw}} - 1 = +3.00$$

Therefore the slot welds have sufficient capacity to support the applied load.

2.12.8.1.3 Lower Shell Buckling

The lower section of shell is an unsupported column for a length of about 17.50 inches. The buckling load is analyzed using the method of ASME Code Case N284-2 [13]. Using the full weight of the basket as before will yield a conservative result. The loading on the lower shell from Section 2.12.8.1.2, *Outer Shell Slot Welds*, is $P_{sw} = 92,400$ lb. The cross sectional area of the shell is based on the inner diameter, d_i , of 15.1 inches and the wall thickness, t , of 0.25 inches.

$$A_{LS} = \pi(d_i + t)t = 12.1 \text{ in}^2$$

The axial stress is then:

$$\sigma_{\phi} = \frac{P_{sw}}{A_{LS}} = 7,636 \text{ psi}$$

An inner diameter of 15.1 inches, an outer diameter of 15.6 inches, and a length of 18.0 inches are used in the buckling analysis. A factor of safety of 1.34 is used, consistent with the requirements of [13]. The results, shown in Table 2.12.8-2, show that all the interaction parameters are less than unity, as required. Therefore, buckling of the lower shell of the MURR basket under the HAC end drop will not occur.

2.12.8.2 MITR-II Basket

The MITR-II basket provides support and positioning for up to eleven MITR-II fuel elements. The structure consists of eleven diamond-shaped support tubes, a reinforced base support shell, a fuel support plate, and other stiffening components. From Table 2.1-3, the empty basket has a weight of 290 lb, and with eleven fuel elements, the bounding weight is 400 lb. A cross sectional view of the basket is shown in Figure 2.12.8-3 and a cross section of a fuel support tube is shown in Figure 2.12.8-4.

2.12.8.2.1 Lower Shell Buckling

The lower section of shell is an unsupported column for a significant portion of its length. The buckling will be checked for an unbraced length of 26.3 inches. The buckling load is analyzed using the method of ASME Code Case N284-2 [13]. Using the full weight of the basket as before will yield a conservative result. The basket weight is $W = 400$ lb, the acceleration is $a = 120g$.

$$P = Wa = 48,000 \text{ lb}$$

BRR Package Safety Analysis Report

The cross sectional area of the shell is based on the inner diameter, d_i , of 13.5 inches and the wall thickness, t , of 0.25 inches.

$$A_{LS} = \pi(d_i + t)t = 10.8 \text{ in}^2$$

The axial stress is then:

$$\sigma_\phi = \frac{P}{A_{LS}} = 4,444 \text{ psi}$$

An inner diameter of 13.5 inches, an outer diameter of 14.0 inches, and a length of 26.3 inches are used in the buckling analysis. A factor of safety of 1.34 is used, consistent with the requirements of [13]. The results, shown in Table 2.12.8-2, show that all the interaction parameters are less than unity, as required. Therefore, buckling of the lower shell of the MITR-II basket under the HAC end drop will not occur.

2.12.8.2.2 Buckling of Fuel Tubes (Top Down Drop)

In a top-down impact, the individual fuel tubes support the weight of the lower shell and several other components. Since the method of N284-2 is only applicable to circular tube cross sections, the method of Appendix F [33] of the ASME code is used to check the stability of these elements. Conservatively, the full weight of the assembly, minus the fuel elements, is used.

The moment of inertia and cross sectional area of a single tube can be closely approximated using the geometry in Figure 2.12.8-4. The distance across the parallel sides is 2.94 inches. The minor angle is 60° . The length of each side is then:

$$h = \frac{2.94}{\cos(30^\circ)} = 3.39 \text{ inches}$$

The outer height and width of the tube cross-section is:

$$b = 2h \cos(60^\circ/2) = 5.87 \text{ inches}$$

$$d = 2h \sin(60^\circ/2) = 3.39 \text{ inches}$$

The inner height and width of the tube cross-section for a tube wall thickness of $t = 0.12$ inches are:

$$b_i = b - 2 \frac{t}{\sin(30^\circ)} = 5.39 \text{ inches}$$

$$d_i = d - 2 \frac{t}{\sin(60^\circ)} = 3.11 \text{ inches}$$

From [25] Table 1, Case 12, the area and moment of inertia are calculated as:

$$A_{ft} = \frac{1}{2}bd - \frac{1}{2}b_id_i = 1.57 \text{ in}^2$$

$$I_x = \frac{1}{48}bd^3 - \frac{1}{48}b_id_i^3 = 1.39 \text{ in}^4$$

BRR Package Safety Analysis Report

$$I_y = \frac{1}{48} db^3 - \frac{1}{48} d_i b_i^3 = 4.14 \text{ in}^4$$

The radius of gyration for the weaker bending direction of the tube is:

$$r_x = \sqrt{\frac{I_x}{A}} = 0.94 \text{ inches}$$

A method for calculating the allowable buckling stress in austenitic stainless steel is presented in Article NF-3322.1(c)(2) of the ASME B&PV Code [9]. Since the ends of the tubes are welded to the top and bottom plates, a value of $K = 0.5$ for embedded ends may be used. The length of the tube is $L = 26.88$ inches, and thus the ratio $KL/r_x = 14.30$. Therefore the allowable stress per paragraph NF-3322.1(c)(2)(a) is:

$$S = S_y \left(0.47 - \frac{KL/r}{444} \right) = 9,062 \text{ psi}$$

where the yield stress is $S_y = 20,700$ psi from Table 2.12.8-1. Since this allowable is calculated for normal loading it can be further modified for the HAC case. Per Paragraph F-1334 of [33], the allowable stress is:

$$S_a = 2S = 18,124 \text{ psi}$$

The load is bounded by the full weight of the empty basket, $W = 290$ lbs distributed over each of the 11 tubes, and the acceleration of $a = 120g$. The bounding load is:

$$\sigma_{ft} = \frac{Wa}{11A_{ft}} = 2,015 \text{ psi}$$

The Margin of Safety for the HAC case includes a safety factor of 1.34:

$$MS = \frac{S_a}{1.34\sigma_{ft}} - 1 = +5.71$$

Therefore the tubes have sufficient capacity to support the load developed by the top down end drop.

2.12.8.2.3 Side Drop Bending

For the side drop impact, each fuel tube in the MITR-II basket is modeled as a simply supported beam. Conservatively, the support offered by the center plate will be neglected. In addition, the moment of inertia of the individual tube will be calculated using the weak axis, resulting in a more conservative result than if the individual orientation for each tube were accounted for.

The applied load, assumed to be distributed along the beam, will be equal to the bounding weight of the fuel elements, $W_F = 10$ lbs, plus the self weight of the tube, and the acceleration of $a = 120g$. The load is:

$$P = (W_F + W_T)a = 2,640 \text{ lb}$$

Where the tube weight, W_T , is calculated below from the area and length above and the Type 304 density of $\rho = 0.29 \text{ lb/in}^3$.

$$W_T = A_{ft} L_t \rho = 12.2 \text{ lb}$$

BRR Package Safety Analysis Report

The bending moment for a tube length $L_t = 26.88$ inches is:

$$M = \frac{w \cdot L_t^2}{8} = \frac{PL_t}{8} = 8,870 \text{ in} \cdot \text{lb}$$

The bending stress is:

$$\sigma_b = \frac{Mc}{I_x} = 10,848 \text{ psi}$$

where $c = \frac{1}{2}d = 1.70$ in and the moment of inertia $I_x = 1.39 \text{ in}^4$ from Section 2.12.8.2.2, *Buckling of Fuel Tubes (Top Down Drop)*. From Table 2.12.8-1, the allowable stress is $S = 64,000$ psi for the combined membrane and bending stress. The margin of safety is:

$$MS = \frac{S}{\sigma_b} - 1 = +4.90$$

Therefore bending of the MITR-II fuel tubes will not occur on their weakest axis in the HAC side drop.

2.12.8.3 ATR Basket

The ATR basket provides support and positioning for up to eight ATR fuel elements. The structure consists of an outer shell, an inner shell, eight radial separation plates, a support plate, and other stiffening components. From Table 2.1-3, the empty basket has a weight of 450 lb, and with eight fuel elements, the bounding weight is 650 lb. A cross sectional view of the basket is shown in Figure 2.12.8-5 and a view of the support plate is shown in Figure 2.12.8-6.

2.12.8.3.1 Fuel Support Plate Bending

The fuel support plate provides lower end positioning of the fuel elements. In a bottom-down end drop, the support plate is loaded by a maximum of eight fuel elements. Each fuel element section of the plate is supported by welds along three sides as shown in Figure 2.12.8-5.

The plate is modeled using [25] Table 24, Case 27. This is the same conservative approach used in Section 2.12.8.1.1, *Fuel Support Plate Bending*. The load applied by eight fuel elements is averaged over the entire plate. The effective area of plate for the applied load is:

$$A_p = \frac{\pi}{4}(d_o^2 - d_i^2) - 8\frac{\pi}{4}d_H^2 - 8A_s = 86.3 \text{ in}^2$$

where $d_o = 13.0$ inches is the outer diameter of the plate, $d_i = 6.5$ inches is the center hole diameter of the plate, $d_H = 0.8$ inches is the diameter of the eight drain holes, and $A_s = 1.15 \text{ in}^2$ is the area of the separator plates. For a density $\rho = 0.29 \text{ lb/in}^3$, and a plate thickness $t = 0.5$ inches, the weight of the plate is:

$$W_p = A_p t \rho = 12.5 \text{ lb}$$

For a single sector of the plate, the plate load is:

$$P_p = (nW_{FE} + W_p)a = 25,512 \text{ lb}$$

BRR Package Safety Analysis Report

where the number of fuel elements, $n = 8$, the weight of an individual element, $W_{FE} = 25$ lb, and the acceleration, $a = 120g$. The distributed pressure load of the plate is:

$$q = \frac{P_p}{A_p} = 296 \text{ psi}$$

From [25] Table 24, Case 27, the maximum plate stress for each plate is:

$$\sigma_p = \beta_1 \frac{qa^2}{t^2} = 5,703 \text{ psi}$$

Where $a = \frac{1}{2}d_o$ is the radius of the segment of plate, $t = 0.5$ inches is the thickness of the plate, and $\beta_1 = 0.114$ is a constant. The allowable combined membrane and bending stress is $S = 64,000$ psi from Table 2.12.8-1. The margin of safety is:

$$MS = \frac{S}{\sigma_p} - 1 = +10.2$$

Therefore the plate has sufficient capacity to support the applied load.

2.12.8.3.2 Outer Shell Slot Welds

The slot welds connect the outer shell to the inner components of the basket. In a bottom-down drop, the slot welds are assumed to take the full load of the fuel, center shell, spacer plates, and fuel support plate. Conservatively, the full basket weight $W = 650$ lb will be applied. The combined slot weld area for the 72, 0.8 inch x 0.3 inch long slots with full radii is:

$$A_{sw} = 72 \left[\frac{\pi}{4} (0.3)^2 + 0.8(0.3) \right] = 20.2 \text{ in}^2$$

The applied load is the full weight at an acceleration of $a = 120g$.

$$P_{sw} = Wa = 78,000 \text{ lb}$$

The shear stress due to the direct load is:

$$\tau_{sw} = \frac{P}{A_{sw}} = 3,861 \text{ psi}$$

From Table NG-3352-1 of [32], the allowable stress of the weld is multiplied by a weld quality factor of 0.35, which applies to an intermittent or plug weld with surface PT examination. From Table 2.12.8-1, the allowable stress for pure shear is $S = 22,320$ psi. The margin of safety is:

$$MS = \frac{(0.35)S}{\tau_{sw}} - 1 = +1.02$$

Therefore the slot welds have sufficient capacity to support the applied load.

2.12.8.3.3 Side Drop Bending

For the side drop impact, the ATR basket can be modeled as a simply supported beam, supported on the end plates. Conservatively, the support plates at intermediate spacings will be neglected. The applied load, assumed to be distributed along the beam, is equal to the bounding weight of

BRR Package Safety Analysis Report

650 lb and the acceleration of $a = 120g$. The full basket load from Section 2.12.8.3.2, *Outer Shell Slot Welds*, is $P_{SW} = 78,000$ lb. The bending moment is:

$$M = \frac{wL_s^2}{8} = \frac{P_{SW}L_s}{8} = 500,955 \text{ in-lb}$$

where $L_s = 51.38$ inches, which is the full length of the inner shell. The moment of inertia from the combination of the two shells, (neglecting the contribution of any other components) is:

$$I = \frac{\pi}{64} [d_{1o}^4 - d_{1i}^4] + \frac{\pi}{64} [d_{2o}^4 - d_{2i}^4] = 272.7 \text{ in}^4$$

Where $d_{1o} = 13.5$ inches and $d_{1i} = 13.0$ inches are the inner and outer diameters of the outer shell, and $d_{2o} = 7.2$ inches and $d_{2i} = 6.5$ inches are the inner and outer diameters of the inner shell after machining. The highest bending stress is located at the outer radius of the outer shell, $c = 6.75$ inches. The bending stress is:

$$\sigma_b = \frac{Mc}{I} = 12,400 \text{ psi}$$

The allowable combined membrane and bending stress is $S = 64,000$ psi from Table 2.12.8-1. The margin of safety is:

$$MS = \frac{S}{\sigma_b} - 1 = +4.16$$

Therefore bending of the ATR basket in the side drop will not occur.

2.12.8.4 TRIGA Basket

The TRIGA basket provides support and positioning for up to nineteen TRIGA fuel elements. The structure consists of nineteen support tubes arranged in two concentric circles, a base plate, a center stiffener, and a top plate. The base plate is supported by two concentric circular shells. Fuel spacers are used with shorter versions of TRIGA fuel. From Table 2.1-3, the empty basket has a weight of 290 lb, and with nineteen fuel elements, the bounding weight is 480 lb. A cross sectional view of the basket is shown in Figure 2.12.8-7 and a view of the support plate is shown in Figure 2.12.8-8.

2.12.8.4.1 Fuel Support Plate Bending

The fuel support plate provides lower end support of the fuel elements. In the bottom-down vertical impact, the support plate is loaded by a maximum of nineteen fuel elements, the top plate, center plate, and the fuel tubes and fuel spacers. Conservatively, the full weight of the basket will be taken as a distributed load across the plate. This load is distributed evenly over the plate and is reacted by the outer and inner shells which support the plate.

The loaded surface area of the plate consists of the basic plate surface between the outer support shell outer diameter, $d_p = 13.0$ inches, and the inner support shell inner diameter of $d_i = 3.5$ inches. This area is further reduced by the 19 drain holes with a diameter of $d_h = 0.8$ inches.

$$A_p = \frac{\pi}{4} (d_p^2 - d_i^2 - 19d_h^2) = 113.6 \text{ in}^2$$

BRR Package Safety Analysis Report

The load per unit area on the plate is:

$$q = \frac{Wa}{A_p} = 507 \text{ psi}$$

where the weight on the plate is $W = 480 \text{ lb}$, and the acceleration, $a = 120g$.

The maximum plate stress can be calculated from [25] Table 24, Case 2c. The distributed load is applied over the area between the outer edge (radius $a = d_p/2$) of the outer base shell to the inner edge (radius $b = d_i/2$) of the schedule 40 pipe inner base shell. The interpolated values from case 2c of $K_{Mrmax} = 0.0575$ and $K_{Mtb} = -0.0754$ are based on the ratio of the outer and inner plate radii $b/a = 0.27$. The maximum moment in the plate is based on the maximum absolute value of these two factors, $K_{Max} = 0.0754$. The maximum bending moments is:

$$M_{Max} = K_{Max} qa^2 = 1,615 \text{ lb}$$

The maximum bending stress using the material thickness of the plate, $t = 0.5 \text{ in}$, is:

$$\sigma_b = -\frac{6M_{Max}}{t^2} = 38,760 \text{ psi}$$

The allowable combined membrane and bending stress is $S = 64,000 \text{ psi}$ from Table 2.12.8-1. The margin of safety is:

$$MS = \frac{S}{\sigma_b} - 1 = +0.65$$

Therefore the plate has sufficient capacity to support the applied load.

2.12.8.4.2 Shear Load on Pedestal Spacer Screw

Once adjusted, the length of the pedestal assembly is held in one of three positions by a single 1/4-20 UNC screw (minimum diameter, $d_n = 0.196 \text{ inches}$). The load on this screw will be in double shear and consist of the weight of one fuel element plus the weight of the spacer cap.

The weight of a single maximum length TRIGA fuel element is $W_L = 10 \text{ lbs}$. Conservatively using the weight of the heaviest element, even though the pedestals are only used with short fuel elements, the maximum shear load on the screw is:

$$P_{SS} = W_L (120) = 1,200 \text{ lb}$$

The shear area of the screw (double shear) is:

$$A_s = 2 \frac{\pi}{4} (d_n^2) = 0.0603 \text{ in}^2$$

The shear stress is:

$$\tau_s = \frac{P_{SS}}{A_s} = 19,900 \text{ psi}$$

From Table 2.12.8-1, the allowable for pure shear is $S = 22,320 \text{ psi}$. The margin of safety for HAC is:

BRR Package Safety Analysis Report

$$MS_{HAC} = \frac{S}{\tau_s} - 1 = +0.12$$

Therefore the screw has sufficient capacity to sustain the applied load.

2.12.8.4.3 Buckling of Fuel Tubes (Top Down Drop)

The TRIGA assembly may be supported by the 19 fuel tubes during a top down drop orientation. For consistency, this buckling case will be evaluated using the full weight of the assembly, $W = 290$ lb distributed over the 19 tubes. The buckling load is analyzed using the method of ASME Code Case N284-2 [13]. The complete length of the tube will be used as if it was not braced at the middle of its span. The applied load for each tube is:

$$P_{ft} = \frac{W_a}{19} = 1,832 \text{ lb}$$

The area of each tube is:

$$A_{ft} = \pi(d_i + t)t = 0.71 \text{ in}^2$$

where the inner diameter of each tube is $d_i = 1.76$ inches and the wall thickness is 0.12 inches. Based on this area the axial stress is:

$$\sigma_{ft} = \frac{P_{ft}}{A_{ft}} = 2,580 \text{ psi}$$

An inner diameter of 1.76 inches, an outer diameter of 2.0 inches, and a length of 48.00 inches are used. A factor of safety of 1.34 is used, consistent with the requirements of [13]. The results, shown in Table 2.12.8-2, show that all the interaction parameters are less than unity, as required. Therefore, buckling of the TRIGA basket fuel tubes under the HAC end drop will not occur.

2.12.8.4.4 Side Drop Bending

For the side drop impact, each fuel tube in the TRIGA basket is modeled as a simply supported beam. For an inner and outer diameter of the tube $d_i = 1.76$ inches, $d_o = 2.0$ inches, a length $L_t = 48.00$ inches, and a density $\rho = 0.29 \text{ lb/in}^3$, the weight of the tube is:

$$V_b = \frac{\pi}{4}(d_o^2 - d_i^2)L_t = 34.0 \text{ in}^3$$

$$W_T = V_b\rho = 9.86 \text{ lb}$$

The applied load, assumed to be distributed along the beam, will be equal to the bounding weight of the largest fuel element $W_F = 10$ lbs. For the combined weight the load is:

$$P = 120(W_F + W_T) = 2,383 \text{ lb}$$

The bending moment is:

$$M = \frac{wL_t^2}{8} = \frac{PL_t}{8} = 7,149 \text{ in-lb}$$

BRR Package Safety Analysis Report

where the reaction point separation is the unbraced length of the tube, $L_t = 24.0$ inches. The moment of inertia and area of a single tube is:

$$I = \frac{\pi}{64} [d_o^4 - d_i^4] = 0.314 \text{ in}^4$$

The bending stress is

$$\sigma_b = \frac{Mc}{I} = 22,767 \text{ psi}$$

where $c = \frac{1}{2}d_o$. From Table 2.12.8-1, the allowable stress is $S = 64,000$ psi for the combined membrane and bending stress. The margin of safety is:

$$MS = \frac{S}{\sigma_b} - 1 = +1.81$$

Therefore bending of the TRIGA fuel tubes will not occur.

2.12.8.5 Summary

Table 2.12.8-3 summarizes the margins of safety of the BRR package fuel baskets, as established in the sections above. Since all margins of safety are positive, and all Code Case N-284-2 interaction checks are less than unity, the BRR package fuel baskets are not of concern.

Table 2.12.8-1 – Material Properties and Allowable Stress

Parameter	(ASTM, Type 304) ^{①④}
NCT Hot Bounding Temperature, °F	400
Elastic Modulus, psi	26.4×10^6
Design Stress, S_m , psi	18,600
Yield Stress, S_y , psi	20,700
Ultimate Stress, S_u , psi	64,000
HAC Allowable Stresses	
Primary Membrane Stress Intensity (P_m), psi	Lesser of: $2.4S_m = 44,640$ $0.7S_u = 44,800$
Primary Membrane + Bending Stress Intensity ($P_m + P_b$), psi	Lesser of: $S_u = 64,000$ $3.6S_m = 66,960$
Pure Shear Stress Intensity, psi	Lesser of: $0.42S_u = 26,880$ ^② $1.2S_m = 22,320$ ^③

Notes:

1. ASTM A240, A249, A269, A276, A511, and A312.
2. ASME Code, Section III, Appendix F, Paragraph F-1334.2.
3. ASME Code, Section III, Subsection NG, Article NG-3225.
4. Governing values of allowable stress are in bold type.

Table 2.12.8-2 - Code Case N-284-2 Results Summary

Parameter	MURR	MITR-II	TRIGA	Remarks
Capacity Reduction Factors (-1511)				
$\alpha_{\phi L} =$	0.2070	0.2070	0.2070	
$\alpha_{\theta L} =$	0.8000	0.8000	0.8000	
$\alpha_{\phi\theta L} =$	0.8000	0.8000	0.8000	
Plasticity Reduction Factors (-1610)				
$\eta_{\phi} =$	0.1876	0.1706	0.0490	
$\eta_{\theta} =$	0.3655	0.4924	0.2187	
$\eta_{\phi\theta} =$	0.0865	0.0970	0.0510	
Theoretical Buckling Values (-1712.1.1)				
$C_{\phi} =$	0.6050	0.6050	0.6050	
$\sigma_{\phi eL} =$	520,261 psi	580,800 psi	2,038,979 psi	
$C_{\theta r} =$	0.0778	0.0487	0.0351	
$\sigma_{\theta eL} = \sigma_{r eL} =$	66,906 psi	46,753 psi	118,324 psi	
$C_h =$	0.0744	0.0474	0.0351	
$\sigma_{\theta eL} = \sigma_{h eL} =$	64,015 psi	45,468 psi	118,324 psi	
$C_{\phi\theta} =$	0.2087	0.1668	0.0904	
$\sigma_{\phi\theta eL} =$	179,445 psi	160,127 psi	304,652psi	
Elastic Interaction Equations (-1713.1.1)				
$\sigma_{xa} =$	80,369 psi	89,721 psi	314,977 psi	
$\sigma_{ha} =$	38,218 psi	27,145 psi	70,641 psi	
$\sigma_{ra} =$	39,944 psi	27,912 psi	70,641 psi	
$\sigma_{ta} =$	107,131 psi	95,598 psi	181,882 psi	
Axial + Hoop \Rightarrow Check (a):	N/A	N/A	N/A	<1 ∴ OK
Axial + Hoop \Rightarrow Check (b):	N/A	N/A	N/A	<1 ∴ OK
Axial + Shear \Rightarrow Check (c):	0.0950	0.0495	0.0082	<1 ∴ OK
Hoop + Shear \Rightarrow Check (d):	0.0000	0.0000	0.0000	<1 ∴ OK
Axial + Hoop + Shear \Rightarrow Check (e,a):	N/A	N/A	N/A	<1 ∴ OK
Axial + Hoop + Shear \Rightarrow Check (e,b):	N/A	N/A	N/A	<1 ∴ OK
Inelastic Interaction Equations (-1714.2.1)				
$\sigma_{xc} =$	15,077 psi	15,305 psi	15,448 psi	
$\sigma_{rc} =$	14,601 psi	13,745 psi	15,448 psi	
$\sigma_{tc} =$	9,269 psi	9,269 psi	9,269 psi	
Max(Axial, Hoop) \Rightarrow Check (a):	0.5065	0.2904	0.1670	<1 ∴ OK
Axial + Shear \Rightarrow Check (b):	0.5065	0.2904	0.1670	<1 ∴ OK
Hoop + Shear \Rightarrow Check (c):	0.0000	0.0000	0.0000	<1 ∴ OK

Table 2.12.8-3 – Fuel Basket Stress Analysis Results

Analysis Description	Reference Section	Margin of Safety
MURR Basket		
Fuel Support Plate Bending	2.12.8.1.1	+8.32
Outer Shell Slot Welds	2.12.8.1.2	+3.00
Lower Shell Buckling	2.12.8.1.3	Pass*
MITR-II Basket		
Lower Shell Buckling	2.12.8.2.1	Pass*
Fuel Tube Buckling	2.12.8.2.2	+5.71
Side Drop Bending	2.12.8.2.3	+4.90
ATR Basket		
Fuel Support Plate Bending	2.12.8.3.1	+10.2
Outer Shell Slot Welds	2.12.8.3.2	+1.02
Side Drop Bending	2.12.8.3.3	+4.16
TRIGA Basket		
Fuel Support Plate Bending	2.12.8.4.1	+0.65
Spacer Screw Shear Load	2.12.8.4.2	+0.12
Fuel Tube Buckling	2.12.8.4.3	Pass*
Side Drop Bending	2.12.8.4.4	+1.81

*Interaction equation checks are less than unity, as required by [13].

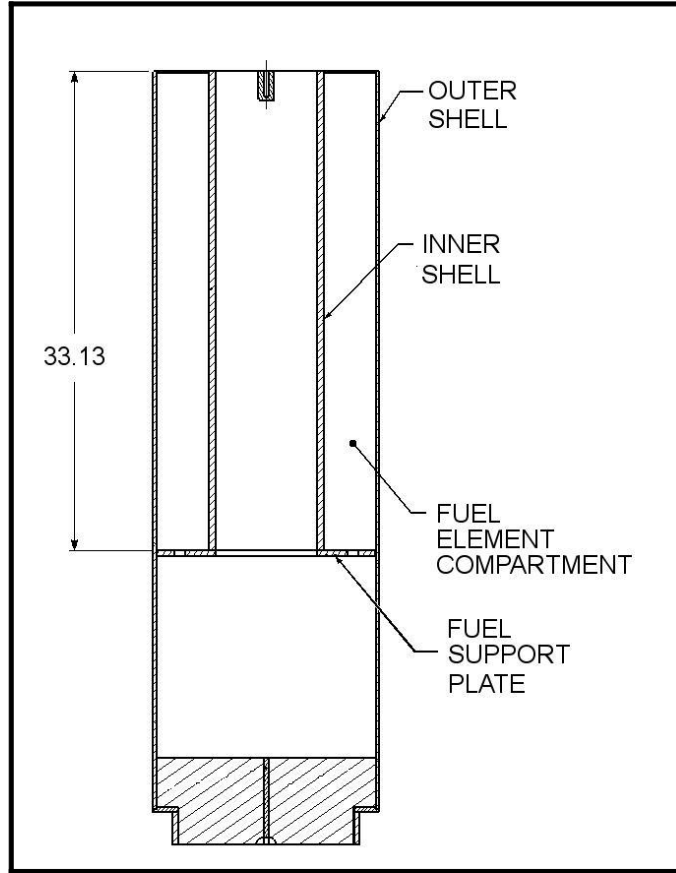


Figure 2.12.8-1 - MURR Fuel Basket Cross Section

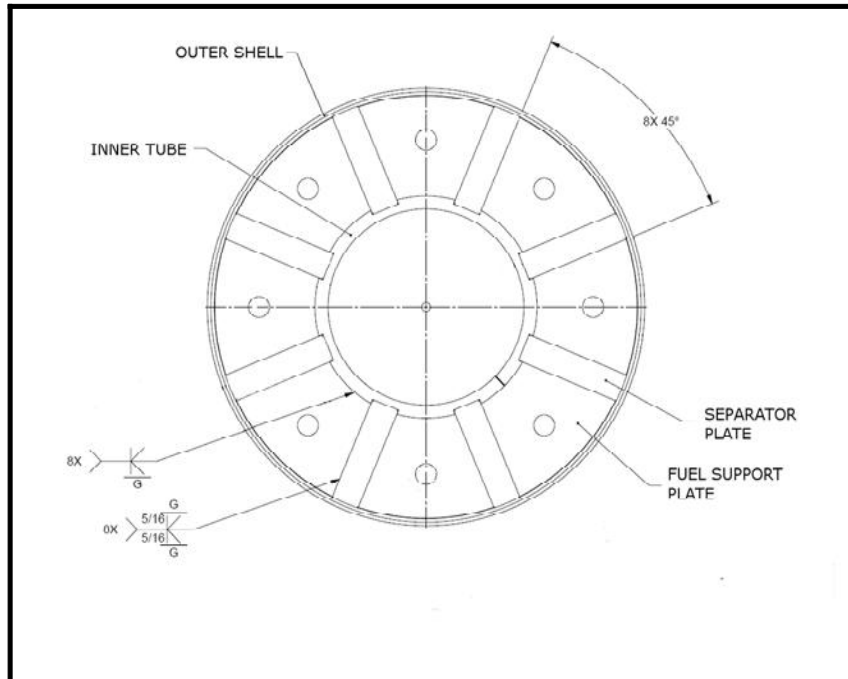


Figure 2.12.8-2 - MURR Fuel Basket View of Support Plate

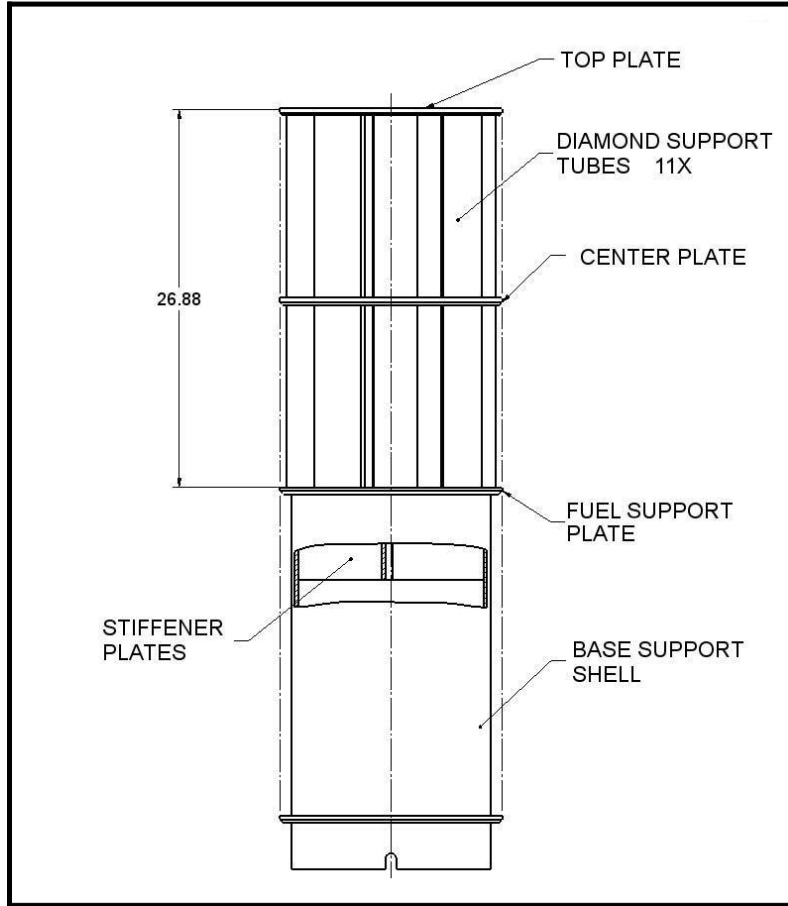


Figure 2.12.8-3 - MITR-II Fuel Basket Cross Section

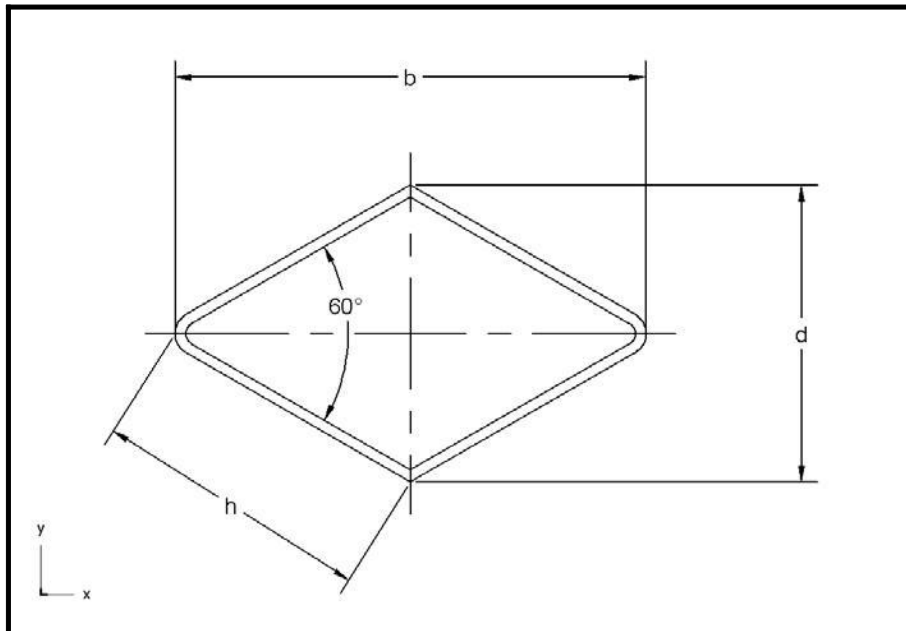


Figure 2.12.8-4 - MITR-II Support Tube Cross Section

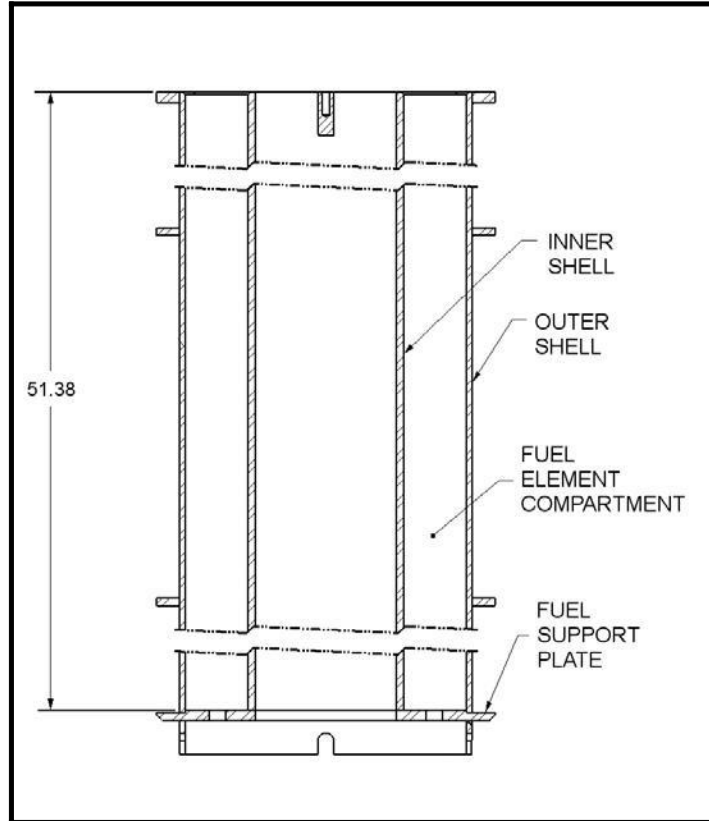


Figure 2.12.8-5 - ATR Fuel Basket Cross Section

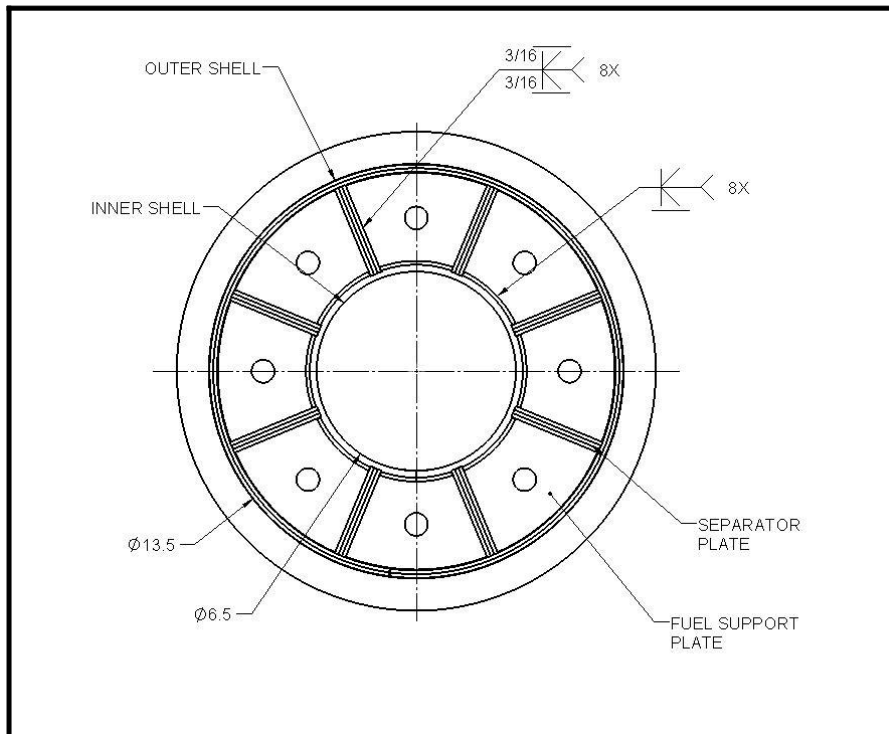


Figure 2.12.8-6 - ATR Fuel Basket View of Support Plate

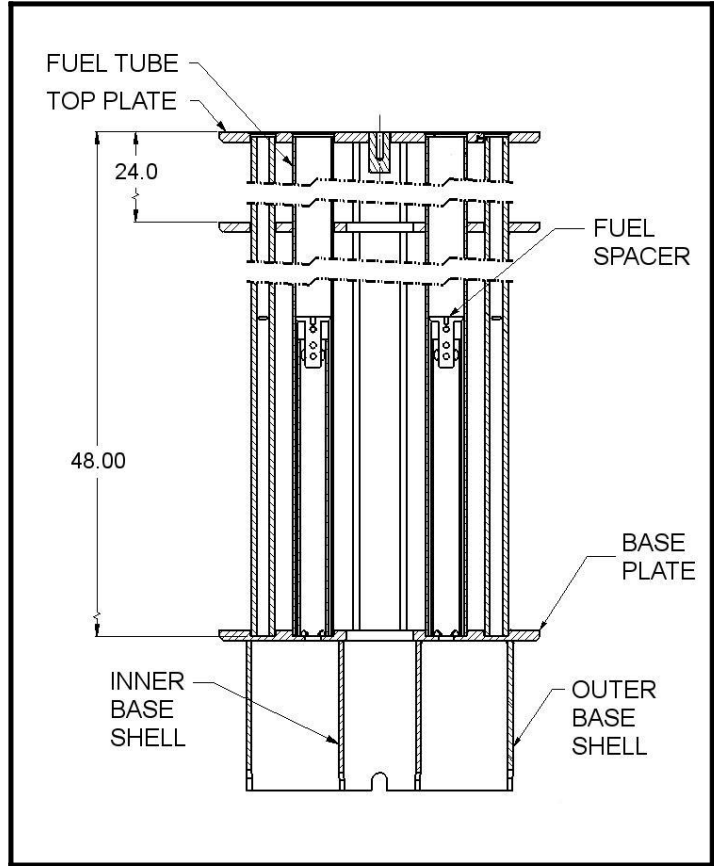


Figure 2.12.8-7 - TRIGA Fuel Basket Cross Section

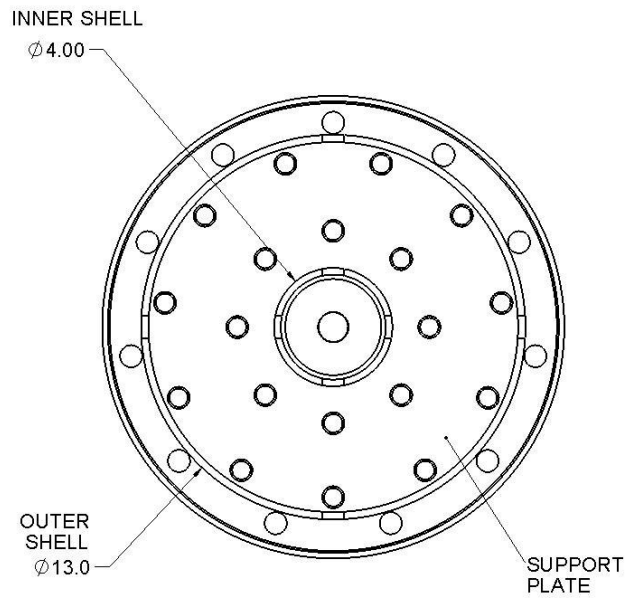


Figure 2.12.8-8 - TRIGA Fuel Basket View of Support Plate

3.0 THERMAL EVALUATION

This chapter identifies and describes the principal thermal design aspects of the BEA Research Reactor (BRR) package. The evaluations presented in this chapter demonstrate the compliance of the BRR package¹ as a Type B(U)F-96 shipping container with the thermal requirements of Title 10, Part 71 of the Code of Federal Regulations [1] when transporting a payload of irradiated fuel assemblies from various test and research reactors. These reactors include the Missouri University Research Reactor (MURR), the Massachusetts Institute of Technology Nuclear Research Reactor (MITR-II), Advanced Test Reactor (ATR), and Training, Research, Isotopes, General Atomics (TRIGA) reactors.

Specifically, all package components are shown to remain within their respective temperature limits under the normal conditions of transport (NCT). Further, per 10 CFR §71.43(g), the maximum temperature of the accessible package surfaces is demonstrated to be less than 185 °F for the maximum decay heat loading, an ambient temperature of 100 °F, and no insolation. Finally, the BRR package is shown to retain sufficient thermal protection following the HAC free and puncture drop scenarios to maintain all package component temperatures within their respective short term limits during the regulatory fire event and subsequent package cool-down.

3.1 Description of Thermal Design

The principal components of the BRR package are illustrated in Figure 1.2-1 through Figure 1.2-3 of Section 1.0, *General Information*. The principal components are: 1) a lead-shielded cask body, 2) a separate, removable upper shield plug, 3) a bolted closure lid, 4) upper and lower impact limiters containing polyurethane foam, and 5) a payload basket specific to the type of fuel being transported. Except for the closure bolts, the lead shielding, and the impact limiter attachment pins, the package is primarily of welded construction, using Type 304 austenitic stainless steel.

3.1.1 Design Features

The primary heat transfer mechanisms within the BRR packaging are conduction and radiation. The principal heat transfer from the exterior of the packaging is via convection and radiation to the ambient environment. The upper and lower impact limiter assemblies serve as the primary impact protection for the BRR package and its enclosed payload. The impact limiters also provide the principal thermal protection to the ends of the packaging, while a thermal shield is used to protect the portion of the packaging between the limiters from the high heat flux generated during the transient HAC fire event.

There is no pressure relief system included in the BRR packaging design. The thermal design features of the principal package components are described in the following paragraphs. See Section 1.0, *General Information*, for more detail.

¹ In the remainder of this chapter, the term ‘packaging’ refers to the assembly of components necessary to ensure compliance with the regulatory requirements, but does not include the payload. The term ‘package’ includes both the packaging components and the payload.

3.1.1.1 BRR Cask Body

The BRR cask body is a right circular cylinder approximately 77.1 inches long and 38 inches in diameter (not including the impact limiter attachments and the thermal shield). It is composed of upper and lower end structures that connect circular inner and outer shells. Lead located between the two circular shells, in the lower end closure structure, and in the shield plug provides radiological shielding for the package. This design results in a large thermal mass to surface area ratio capable of absorbing the high heat flux generated during the HAC fire event and limiting the temperature rise within the interior of the package. The payload cavity has a diameter of 16 inches and a length of 54 inches. Figure 1.2-3 provides an overview of the packaging dimensions.

The inner and outer shells and the end structures may be cast or forged from Type F304 stainless steel. Since the BRR package is designed to permit loading and unloading under water, the lower end structure contains a drain to allow removal of water from the payload cavity. The drain is sealed using a brass plug, butyl rubber seal, and a dust cap.

A thermal shield, composed of an outer sheet of 12 gauge (0.105-inch thick) Type 304 stainless steel and offset from the outer shell by small strips of the same 12 gauge material, covers the region of the outer shell not covered by the impact limiters. The shield serves to protect the outer shell from direct exposure to the high heat fluxes associated with the HAC fire accident event.

The lead shielding is made from ASTM B29, chemical lead, or optionally, from lead per Federal Specification QQ-L-171E, Grade A or C. The 8 inches thick lead shield in the side of the cask body is cast-in-place through openings in the upper end structure, thus eliminating/minimizing gaps between the lead and the steel shells. The shield at the bottom is made from lead sheet material which is packed firmly into place to yield a nominal thickness of 7.7 inches.

3.1.1.2 Removable Shield Plug

The removable shield plug rests on a shoulder located approximately half way along the length of the plug. The plug has a total thickness of 11.2 inches and a lead thickness of 9.7 inches. The outer shell is made from Type 304 plate material of various thicknesses and the cavity is filled with lead sheet material packed firmly into place. A ¾-inch diameter tube passes diagonally through the plug to ensure proper draining and drying of the cask while preventing a harmful shine path. Besides providing radiological shielding, the shield plug ensures a thermally significant separation distance between the basket's decay heat and the temperature sensitive closure seals.

3.1.1.3 BRR Cask Closure

The closure lid is made from 2-inch thick Type 304 stainless steel plate. It is attached to the cask using 12, 1-8 UNC electroless nickel plated bolts made of ASTM A320, Grade L43 material. The closure lid includes two O-ring seals made from butyl rubber of 3/8-inch cross sectional diameter. The inner O-ring is the containment seal, and the outer is the test seal. The seals are retained in dovetail grooves in the lid.

BRR Package Safety Analysis Report

The BRR package features two ports which are also part of the containment boundary: a vent port in the closure lid, and a drain port in the lower end structure. Both ports are closed with threaded brass plugs and sealed with butyl rubber washers. A brass dust cover protects the port plugs. The seal test port is not part of the containment boundary.

3.1.1.4 Impact Limiters

The impact limiters attached to ends of the BRR packaging, each with essentially identical designs, provide a significant level of thermal protection to the package. Each limiter is 78 inches in diameter and 34.6 inches long overall, with a conical section 15 inches long towards the outer end. The impact limiters are filled with rigid, closed-cell polyurethane foam with a nominal 9 lb/ft³ density that is poured in place. As described in Appendix 3.5.4, '*Last-A-Foam*' Response under HAC Conditions, the thermal decomposition of the closed-cell polyurethane foam during the HAC event absorbs a majority of the heat energy entering the impact limiters.

The foam is encased in a stainless steel shell for structural protection. The external shells (except for the outer end plates) are ¼ inches thick, while the internal shells which interface with the cask body are ½ inches thick. The outer end plates of the impact limiters are ½-inches thick. Plastic melt-out plugs are incorporated into the exterior shells of the limiters. The plugs are designed to soften and be expelled during the HAC fire event, thus relieving any pressure buildup in the limiters due to foam decomposition under elevated temperatures. The external surfaces of the impact limiter shell are covered with a white acrylic polyurethane coating to control solar absorptivity and raise thermal emissivity.

Each impact limiter is attached to the cask body via a set of eight (8) bayonet type connectors. The connectors consist of eight sets of two closely spaced plates, 1/2 inch thick, which go through the thermal shield and are welded to the outer shell of the cask. Mating with these plates are eight 3/4 inch thick plates attached to each limiter and which pass between the receptacle plates on the cask body. Each connection is completed by a stainless steel ball lock pin that passes through the three plates (two receptacle plates and one impact limiter plate).

3.1.1.5 Fuel Baskets

Four fuel baskets will be used with the BRR packaging, one for each type of fuel to be transported. Section 1.0, *General Information*, presents a description and illustration of each basket and fuel type to be loaded in the package. The baskets are made from welded construction using Type 304 stainless steel in plate, bar, pipe, and tubular forms. Each basket has a maximum diameter of 15.63 inches and a maximum length of 53.45 inches. The fuel cavities incorporated into each basket are sized and shaped to minimize free play between each fuel type and the basket, while ensuring the free insertion and removal of the elements. The baskets are open on the top with the basket designed to hold the fuel elements within approximately 3/8-inches of the basket's top end, nearest the shield plug. The baskets are designed to freely drain water when the cask is lifted out of the spent fuel pool.

3.1.2 Content's Decay Heat

The design basis decay heat loading for the irradiated fuel to be transported within the BRR packaging is a function of the irradiation history and the cooling time since discharge. Section

1.2.2, *Contents*, provides details of the fuel elements to be transported. For the purposes of this evaluation, the design basis decay heat loadings are as follows:

- MURR fuel: 158 W maximum per element, 1,264 W per basket
- MITR-II fuel: 30 W maximum per element, 330 W per basket
- ATR fuel: 30 W maximum per element, 240 W per basket
- TRIGA fuel: 20 W maximum per element, 380 W per basket

3.1.3 Summary Tables of Temperatures

Table 3.1-1 provides a summary of the package component temperatures under normal and accident conditions. The temperatures for normal conditions are based on an analytical model of the BRR package for steady-state operation with an ambient temperature of 100 °F and the 10 CFR §71.71(c)(1) prescribed insolation averaged over 24 hours. The temperatures for accident conditions are based on a transient simulation using an analytical model of a damaged BRR package. The damage conditions represent the worst-case hypothetical pre-fire damage predicted from a combination of physical drop testing using a half-scale certification test unit (CTU) and analytical structural evaluations.

The results for NCT conditions demonstrate that significant thermal margin exists for all package components. Further, the NCT evaluations demonstrate that the accessible surface temperatures will be below the maximum temperature of 185 °F permitted by 10 CFR §71.43(g) in an exclusive use shipment when transported in a 100 °F environment with no insolation. The results for HAC conditions also demonstrate that the design of the BRR package provides sufficient thermal protection to yield component temperatures that are significantly below the acceptable limits defined for each component. See Sections 3.2.2, *Technical Specifications of Components*, Section 3.3.1.1, *Maximum Temperatures*, and Section 3.4.3, *Maximum Temperatures and Pressure*, for more discussion.

Table 3.1-3 summarizes the permitted fuel basket loadings determined by this safety evaluation.

3.1.4 Summary Tables of Maximum Pressures

Table 3.1-2 presents a summary of the maximum pressures predicted under NCT and HAC conditions. The BRR package has a design maximum pressure of 25 psig (39.7 psia). Since the release of fission generated gases from uranium-aluminide and uranium-zirconium hydride based fuels is diffusion-limited as opposed to the direct release mechanism for commercial spent nuclear fuel, the pressurization of the cask cavity due to gaseous release from breached fuel elements will be insignificant [30, 31]. Based on an assumed fill gas temperature of 70 °F, the maximum pressure rise under NCT will be less than 6 psig, while the pressure rise under HAC conditions will be less than 9 psig. Based on the NCT pressure, the maximum normal operating pressure (MNOP) is set at a bounding level of 10 psig.

Table 3.1-1 – Maximum Temperatures for NCT and HAC Conditions

Location / Component ^①	NCT Hot Conditions, °F	Accident Conditions, °F	Maximum Allowable	
			Normal	Accident
Fuel Element Plate	350	451	400	1,100
Fuel Element Side Plate	348	449	400	1,100
Fuel Basket	334	437	800	800
Inner Shell	237	393	800	800
Lead	233	482	620	620
Outer Shell	216	704	800	2,700
Thermal Shield	185	1,256	800	2,700
Lower End Structure	205	335	800	800
Upper End Structure	220	485	800	800
Shield Plug	225	317	620 ^②	620 ^②
Cask Lid	216	306	800	800
Closure/Vent Port Seals	216	306	250	400
Drain Port Seal	202	373	250	400
Upper Impact Limiter				
- Max. Foam	215	-	300	N/A
- Avg. Foam	146	-	300	N/A
- Shell	215	1,475	250 ^③	2,700 ^④
Lower Impact Limiter				
- Max. Foam	200	-	300	N/A
- Avg. Foam	142	-	300	N/A
- Shell	200	1,475	250 ^③	2,700 ^④
Max. Accessible Surface without Insolation	185 ^⑤	-	185	N/A
Cask Cavity Bulk Gas	259	388	N/A	N/A

Notes: ① Results assume a payload of eight (8) MURR fuel elements dissipating 158 W each and helium as the backfill gas.

② Temperature criterion based on melting point of the enclosed lead shielding.

③ Temperature criterion based on long term temperature limit for shell coating.

④ Temperature criterion based on melting point for the shell. No criteria for the polyurethane foam since its thermal decomposition serves as its principal means of providing thermal protection during the HAC event.

⑤ Maximum temperature occurs at the root of the upper cask impact limiter attachment lugs.

Table 3.1-2 – Summary of Maximum Pressures

Condition	Cask Cavity Pressure
NCT Hot	5.2 psi gauge
HAC Hot	8.8 psi gauge

Table 3.1-3 – Summary of Permissible BRR Package Fuel Basket Loadings

Payload	Backfill Gas for Transport	Max. Decay Heat Per Element	Max. Package Decay Heat
MURR Fuel	Helium	158	1,264
MITR-II Fuel	Helium	30	330
ATR Fuel	Helium	30	240
TRIGA Fuel	Helium	20	380

3.2 Material Properties and Component Specifications

The BRR packaging is fabricated primarily of a variety of Type 304 stainless steel product forms, lead, and polyurethane foam. The payload materials include 6061-T6 and/or 6061-0 aluminum, uranium-aluminide (UALx), and uranium-zirconium hydride (UZrH).

3.2.1 Material Properties

While a variety of Type 304 stainless steel specifications apply to the various components of the BRR packaging, each type exhibits the same thermal properties. Table 3.2-1 presents the thermal properties used to simulate the various Type 304 stainless steels used in the packaging. The thermal properties are taken from the ASME material properties database [2] and the density is taken from an on-line database [6]. Properties for temperatures between the tabulated values are calculated via linear interpolation within the heat transfer code.

Table 3.2-1 also presents the thermal properties for ASTM B29 chemical lead, as taken from reference [4]. The density value is taken from an on-line database [6].

The 9 lb_m/ft³ (pcf) polyurethane foam used in the package impact limiters is based on a proprietary formulation that provides predictable impact-absorption performance under dynamic loading, while also providing an intumescent char layer that insulates and protects the underlying materials when exposed to HAC fire conditions. The thermal properties under NCT conditions are obtained from the manufacturer's on-line website [18]. Since the thermal conductivity of the material is tied to its density and the manufacturing process can yield densities that are $\pm 15\%$ of the targeted value, this safety evaluation addresses the properties associated with both the low and high tolerance density foam (see Table 3.2-1). Since the low tolerance foam yields a lower thermal conductivity, it is assumed for NCT operations, while the higher thermal conductivity of the high tolerance density foam is used for HAC evaluation to conservatively bound the heat flow into the package.

Table 3.2-2 presents the thermal properties for the reactor fuel element material. The MURR, MITR-II, and ATR fuel elements are uranium-aluminide (UALx) based fuels, while the TRIGA fuel element is a uranium-zirconium hydride (UZrH) based fuel. The thermophysical properties for the MURR, MITR-II, and ATR fuel elements are based on information provided in reference [5]. While the reference was developed specifically for the ATR fuel element, the thermal properties are also applicable to the MURR and MITR-II fuel elements (after adjustment for fuel plate geometry and composition) for the purposes of this safety evaluation given the similarity in the base materials for all three fuel elements. For analysis purposes, the material used for the side plates, covers, and fuel cladding are assumed to be 6061-0 aluminum. The thermal properties for the fuel plates are determined as a composite of the cladding and the fuel core materials based on the fuel design drawings [12, 13, and 14] and the thermal properties for the materials of fabrication [5].

The details of the computed values for the MURR, MITR-II, and ATR fuel elements are presented in Appendix 3.5.3.9, *Determination of Composite Thermal Properties for Fuel Plates*. For simplicity, the thermal properties are assumed to be constant with temperature based on the use of conservatively high thermal conductivity and conservatively low specific heat values.

This approach maximizes the heat transfer into the fuel components during the HAC event, while under estimating the ability of the components to store the heat.

The TRIGA fuel element uses uranium-zirconium hydride metal (UZrH) as its active fuel component, graphite as a spacer material, and aluminum or stainless steel for the end fixtures and for the fuel cladding. While a variety of TRIGA fuel designs exist, the active fuel length is either 14 or 15 inches. Table 3.2-2 presents representative thermal properties for the simulated TRIGA fuel element. The properties for graphite are based on representative values for KK-8 graphite [16], while the thermal properties for UZrH are based on [17]. The properties for the end fixtures and fuel cladding are assumed to be stainless steel (Type 304) for the purposes of this safety evaluation since this conservatively limits the axial heat spreading within the fuel element given its lower conductivity versus that of aluminum.

The thermal properties for air and helium, presented in Table 3.2-3 and Table 3.2-4, respectively, are derived from curve fits provided in [19]. Because the gas thermal conductivity varies significantly with temperature, the computer model calculates the thermal conductivity across the gas filled spaces and between the package and the ambient as a function of the mean film temperature. All void spaces within the BRR cask cavity are assumed to be filled with helium at a pressure of one atmosphere following draining and drying.

The emissivity of 'as-received' Type 304 stainless steel has been measured as 0.25 to 0.28 [7], while the emissivity of weathered Type 304 stainless steel has been measured as being between 0.46 to 0.50 [8]. For the purpose of this analysis, an emissivity of 0.25 is assumed for the emittance from all radiating stainless steel surfaces of the cask cavity to account for the surface finish required for decontamination considerations. The exterior surfaces of the upper and lower end structures of the cask body assume a slightly higher emissivity of 0.30 assuming a lower level of surface finish and greater wear and tear.

The exterior surface of the outer shell covered by the thermal shield is assumed to have an emissivity of 0.587 [9] to account for its elevated surface oxidation following the lead pour procedure. Since this surface will not be directly exposed to the pool, it will receive only limited surface finishing following fabrication. The emissivity for the exterior surfaces of the package thermal shield is assumed to be 0.45 to account for weathering, while an emissivity of 0.40 is used for the inner surface of the thermal shield to account for its lower level of weathering. The solar absorptivity of Type 304 stainless steel is approximately 0.52 [9].

The surfaces of the fuel baskets are assumed to have an emissivity of 0.30 to account for the degree of polishing, etc. required for these surfaces due to decontamination considerations. This is slightly higher than the 0.25 value assumed for the cask cavity interior surfaces due to the greater wear and tear on these surfaces and the higher operating temperatures.

Exposed surfaces of lead are expected to oxidize rapidly and exhibit an emissivity of 0.6 [9].

The 6061-0 aluminum used for the MURR, MITR-II, and ATR fuel cladding, end fittings, and side plates is assumed to have a surface coating of boehmite ($\text{Al}_2\text{O}_3\text{H}_2\text{O}$). Per [10], a 25 μm boehmite film will exhibit a surface emissivity of approximately 0.92.

The exterior surfaces of the impact limiters will be finished with a white color coating system [11]. This coating system is expected to yield an emissivity in excess of 0.9 and a solar

absorptivity of approximately 0.20. For conservatism, an emissivity of 0.9 and a solar absorptivity of 0.30 are assumed by this evaluation.

The char layer associated with the decomposed polyurethane foam has a conservative surface emissivity of approximately 0.95 based on a combination of the material type, color, and surface roughness. No free surfaces will exist for the 'poured in place' foam under NCT conditions.

Under HAC conditions, all exterior surfaces of the package are assumed to attain an emissivity of 0.9. This assumption exceeds the minimum requirements of 10 CFR §71.73(c)(4) [1].

3.2.2 Technical Specifications of Components

The materials used in the BRR packaging that are considered temperature sensitive are the lead used for the radiological shielding, the polyurethane foam used in the impact limiters, the epoxy coating used on the impact limiter exterior surfaces, the butyl rubber compound used for the containment boundary seals, and the aluminum cladding and UAl_x fuel matrix used for the enclosed fuel assemblies. The other materials either have temperature limits above the maximum expected temperatures or are not considered essential to the function of the package.

Type 304 stainless steel has a melting point above 2,700 °F [6], but in compliance with the ASME B&PV Code [3], its allowable temperature is limited to 800 °F if the component serves a structural purpose (e.g., the material's structural properties are relied on for loads postulated to occur in the respective operating mode or accidental free drop condition). As such, the appropriate upper temperature limit under normal conditions is 800 °F for stainless steel components that form the containment boundary or are used in the fuel baskets. The upper limit for all other stainless steel components is 2,700 °F for both normal and accident conditions.

The applicable temperature criterion for the ASTM B29 lead is its melting point of approximately 620 °F [6].

Below 250 °F the variation in the thermal properties of the proprietary polyurethane foam with temperature are slight and reversible. While small variations in the foam properties will occur between 250 and 500 °F as water vapor and non-condensable gases are driven out of the foam, the observed changes are very slight. For conservatism, a long-term limit of 300 °F is assumed for the foam. There is no short term temperature limit for the foam as its decomposition under exposure to high temperatures is part of its mechanism for providing thermal protection during the HAC fire event. A detailed description of the foam's behavior under elevated temperatures is presented in Appendix 3.5.4, *'Last-A-Foam' Response under HAC Conditions*.

The exterior surfaces of the impact limiter shells are to be coated in a two step process consisting of a primer coat of polyamide epoxy, followed by an acrylic polyurethane top coat [11]. The color is white. The coating system is resistant to long term temperature exposure up to 250 °F and for intermittent exposure up to 275 °F.

The butyl rubber compound used for the containment seals is fabricated from Rainier Rubber compound R-0405-70 [20]. Butyl rubber has a long term temperature range of -75 °F to 250 °F [21]. Per Appendix 2.12.7, *Seal Performance Tests*, an acceptable short duration limit for this compound is 400 °F for 8 hours, 380 °F for 24 hours, and 350 °F for 144 hours. For conservatism, a long-term limit of 250 °F, a short-term limit of 400 °F for 8 hours, and a low temperature limit of -40 °F are assumed for this analysis.

Aluminum has a melting point of approximately 1,100 °F [6]; however for strength purposes the normal operational temperature of the fuel cladding and the UAl_x fuel matrix are limited to 400°F based on structural strength considerations for aluminum [3]. The limit under HAC conditions is 1,100°F. The same allowable temperature limits are conservatively used for the TRIGA fuel elements as well.

The minimum allowable service temperature for all BRR package components is below -40 °F.

Table 3.2-1 – Thermal Properties of Packaging Materials

Material	Temperature (°F)	Thermal Conductivity (Btu/hr-ft-°F)	Specific Heat (Btu/lb _m -°F)	Density (lb _m /in ³)
Stainless Steel ^① Type 304	-40	8.2	0.112	0.289
	70	8.6	0.114	
	100	8.7	0.115	
	200	9.3	0.119	
	300	9.8	0.123	
	400	10.4	0.126	
	500	10.9	0.129	
	600	11.3	0.130	
	700	11.8	0.132	
	800	12.3	0.134	
	1000	13.1	0.135	
	1200	14.0	0.138	
	1400	14.9	0.141	
	1500	15.3	0.142	
Lead ^② ASTM B29, chemical lead	-58	21.67	0.030	0.4097
	32	20.4	0.030	
	80.6	19.99	0.030	
	158	19.88	0.031	
	260.6	19.36	0.032	
	428	18.43	0.033	
	608	16.49	0.033	
	620.6	16.35	0.036	
Polyurethane Foam	-	0.01872 ^③	0.353	0.00599 ^③
	-	0.01728 ^④	0.353	0.00443 ^④

Notes:

① Reference [2], Material Group J. Properties valid for ASTM A351, Grade CF8A, ASTM A182, Type F304, ASTM A451, Grade CPF8A, and ASTM A240, Type 304 stainless steels.

② Reference [4].

③ Based on FR3709 'Last-a-Foam' high tolerance foam density (i.e., 9 pcf + 15%) properties [18].

④ Based on FR3709 'Last-a-Foam' low tolerance foam density (i.e., 9 pcf - 15%) properties [18].

Table 3.2-2 – Thermal Properties of Fuel Element Materials

Material	Temperature (°F)	Thermal Conductivity (Btu/hr-ft-°F)	Specific Heat (Btu/lb _m -°F)	Density (lb _m /in ³)
Aluminum ^① Type 6061-0	32	102.3	-	0.0976
	62	-	0.214	
	80	104.0	-	
	170	107.5	-	
	260	109.2	0.225	
	350	109.8	-	
	440	110.4	0.236	
	530	110.4	-	
	620	109.8	0.247	
	710	108.6	-	
	800	106.9	0.258	
	890	105.2	-	
	980	103.4	0.269	
	1080	101.1	0.275	
MURR Fuel Plate ^②	-	49.2	0.195	0.119
MITR-II Fuel Plate ^②	-	66.6	0.208	0.113
ATR Fuel Plate 1 ^②	-	46.6	0.193	0.120
ATR Fuel Plates 2 to 18 ^②	-	69.6	0.210	0.112
ATR Fuel Plate 19 ^②	-	38.9	0.188	0.122
TRIGA Graphite ^③	-	46.2	0.250	0.060
TRIGA Fuel ^④	-	10.40	0.191	0.134

Notes:

- ① Reference [5]
- ② Values determined based on composite value of aluminum cladding and fuel core material (see Appendix 3.5.3.9, *Determination of Composite Thermal Properties for Fuel Plates*). Thermal conductivity value valid for axial and circumferential heat transfer within fuel plates.
- ③ Representative value, based on Reference [16].
- ④ Representative value, based on Reference [17].

Table 3.2-3 – Thermal Properties of Air

Temperature (°F)	Density lb _m /in ³ ①	Specific Heat (Btu/lb _m -°F)	Dynamic Viscosity (lb _m /ft-hr)	Thermal Conductivity (Btu/hr-ft-°F)	Prandtl Number ②	Coef. Of Thermal Exp. (°R ⁻¹) ③
-40	Use Ideal Gas Law w/ Molecular wt = 28.966	0.240	0.03673	0.0121	Compute as Pr = c _p μ / k	Compute as β = 1/(°F+459.67)
0		0.240	0.03953	0.0131		
50		0.240	0.04288	0.0143		
100		0.241	0.04607	0.0155		
200		0.242	0.05207	0.0178		
300		0.243	0.05764	0.0199		
400		0.245	0.06286	0.0220		
500		0.248	0.06778	0.0240		
600		0.251	0.07242	0.0259		
700		0.253	0.07680	0.0278		
800		0.256	0.08098	0.0297		
900		0.259	0.08500	0.0315		
1000		0.262	0.08887	0.0333		
1200		0.269	0.09620	0.0366		
1400		0.274	0.10306	0.0398		
1500		0.277	0.10633	0.0412		

Table Notes:

- ① Density computed from ideal gas law as $\rho = PM/RT$, where R= 1545.35 ft-lbf/lb-mole-R, T= temperature in °R, P= pressure in lbf/ft², and M= molecular weight of air. For example, at 100 °F and atmospheric pressure of 14.69lbf/in², $\rho = (14.69*144 \text{ in}^2/\text{ft}^2*28.966 \text{ lbm/lb-mole})/1545.35*(100+459.67) = 0.071 \text{ lbm/ft}^3 = 4.099 \times 10^{-5} \text{ lbm/in}^3$.
- ② Prandtl number computed as $Pr = c_p\mu / k$, where c_p= specific heat, μ = dynamic viscosity, and k = thermal conductivity. For example, at 100 °F, $Pr = 0.241*0.04607/0.0155 = 0.72$.
- ③ Coefficient of thermal expansion is computed as the inverse of the absolute temperature. For example, at 100 °F, $\beta = 1/(100+459.67) = 0.00179$.

Table 3.2-4 – Thermal Properties of Helium

Temperature (°F)	Density lb _m /in ³ ①	Specific Heat (Btu/lb _m -°F)	Dynamic Viscosity (lb _m /ft-hr)	Thermal Conductivity (Btu/hr-ft-°F)	Prandtl Number ②	Coef. Of Thermal Exp. (°R ⁻¹) ③
-40	Use Ideal Gas Law w/ Molecular wt = 4.0026 g/mole	1.240	0.04032	0.0738	Compute as Pr = c _p μ / k	Compute as β = 1/(°F+459.67)
0		1.240	0.04306	0.0784		
50		1.240	0.04634	0.0837		
100		1.240	0.04944	0.0886		
200		1.240	0.05520	0.0981		
300		1.240	0.06088	0.1075		
400		1.240	0.06643	0.1177		
500		1.240	0.07153	0.1291		
600		1.240	0.07640	0.1403		
700		1.240	0.08116	0.1508		
800		1.240	0.08580	0.1607		
900		1.240	0.09033	0.1702		
1000		1.240	0.09475	0.1793		
1200		1.240	0.10327	0.1971		
1400		1.240	0.11139	0.2144		
1500	1.240	0.11531	0.2231			

Table Notes:

- ① Density computed from ideal gas law as $\rho = PM/RT$, where R= 1545.35 ft-lbf/lb-mole-R, T= temperature in °R, P= pressure in lbf/ft², and M= molecular weight of helium.
- ② Prandtl number computed as $Pr = c_p\mu / k$, where c_p= specific heat, μ = dynamic viscosity, and k = thermal conductivity.
- ③ Coefficient of thermal expansion is computed as the inverse of the absolute temperature.

3.3 Thermal Evaluation for Normal Conditions of Transport

This section presents the thermal evaluation of the BRR for normal conditions of transport (NCT). Under NCT, the package will be transported in a vertical orientation. This establishes the orientation of the exterior surfaces of the package for determining the free convection heat transfer coefficients and insolation loading. The package support system is configured to mate with the lower impact limiter such that the conical and base surfaces of the limiter are fully enclosed. As such, the NCT evaluations conservatively assume an adiabatic condition for these surfaces (i.e. there is no heat transfer to or from the ambient).

3.3.1 Heat and Cold

The NCT thermal performance is determined using a three-dimensional thermal model of the BRR packaging and its enclosed payloads. The models provide a full height, half symmetry representation of the packaging and payload components. The modeling approach permits simulation of the varying insolation loads along the length of the package, captures the various degrees of symmetry within the fuel baskets, and allows the non-symmetry conditions of the HAC free drop damage to be simulated. A separate thermal model is used to evaluate the NCT thermal performance for each of the four potential fuel payloads. The details of the NCT thermal modeling are provided in Appendix 3.5.3, *Analytical Thermal Model*.

The safety evaluation for the BRR packaging components is based on a payload of eight (8) MURR fuel elements since its maximum decay heat loading of 1,264 W exceeds by a factor of over 3 the maximum package decay heat loading of 380 W for the TRIGA fuel payload and by even larger margins the 330 W for the MITR-II fuel payload and the 240 W for the ATR fuel payload. The peak temperatures achieved by the packaging components for the transport of the MITR-II, ATR, and TRIGA payloads are bounded by those predicted for the MURR fuel payload.

3.3.1.1 Maximum Temperatures

MURR Fuel Basket

Table 3.3-1 presents the predicted BRR package temperatures under NCT conditions for the transportation of a fully loaded MURR fuel basket dissipating 1,264 W of decay heat. The analysis assumes a helium gas backfill in order to limit the peak temperature of the MURR fuel plates to 400 °F or less, based on structural considerations.

The results demonstrate that large thermal margins exist for essentially all of the packaging and payload components. The minimum thermal margin of 34 °F (i.e., 250 - 216 °F), occurs for the cask closure seals. A similar thermal margin of 35 °F occurs for the coating used on the external surfaces of the impact limiters. These margins are adequate given the conservative assumptions used in the modeling, including neglecting the beneficial contribution of the stand-off strips when computing the temperature rise between the thermal shield and the outer shell and the assumption of a small, but uniform gap between the lead and the outer shell. Removing these conservatisms will decrease the cask body surface temperatures and increase the thermal margins for the seals and the impact limiter coating by an estimated 9 °F.

Figure 3.3-1 to Figure 3.3-4 present the predicted temperature distribution within the BRR package for the NCT Hot condition. The elevation of the MURR fuel payload within the cask cavity is clearly evident from the temperature distribution seen in Figure 3.3-1 and Figure 3.3-3. The temperature distribution within the impact limiters illustrated in Figure 3.3-2 also reflects the elevation of the payload, plus the upright orientation of the package for NCT conditions in that the inside face of the lower impact limiter experiences the solar loading for a flat horizontal surface, while the same face for the upper impact limiter has a zero solar loading because of its downward orientation.

Figure 3.3-3 illustrates the temperature distribution in the structural shell of the cask. The presence of the impact limiter attachment lugs can be seen by the localized 'cool' spots in the temperature distribution of the outer shell. As noted in the description of the NCT thermal model provided in Appendix 3.5.3, *Analytical Thermal Model*, the NCT Hot results are based on an earlier cask design that used 6 instead of the current 8 attachment lugs per limiter, cask lug plates that are 0.38-inches thick by 2.75-inches wide vs. the current 0.5-inches thick by 3.63-inches wide, and a 0.25-inch vs. 0.125-inch radial gap between the limiter and the cask shell. Since the earlier design version provides slightly conservative results for NCT due to its lower surface area for heat dissipation to the ambient, it is appropriate for predicting the peak NCT temperatures.

Figure 3.3-4 presents the predicted temperature distribution within the MURR fuel basket under the NCT Hot condition.

Evaluation of the package for an ambient air temperature of 100 °F without insolation loads demonstrates that the temperatures of all exterior surfaces of the packaging are below the maximum temperature of 185 °F permitted by 10 CFR §71.43(g) for accessible surface temperature in an exclusive use shipment. The peak accessible surface temperature occurs at the root of the upper impact limiter attachment lugs. A sensitivity analysis, based on the revised lug design, as described in Appendix 3.5.3, *Analytical Thermal Model*, confirms that the peak accessible surface temperature in the vicinity of the upper impact limiter attachment lugs (see temperature distribution in Figure 3.3-5) is 185 °F or less.

MITR-II Fuel Basket

Table 3.3-2 presents the predicted maximum temperature achieved within the MITR-II fuel basket under the NCT Hot condition with a helium gas backfill. The peak temperatures for the BRR packaging components are bounded by those presented in Table 3.3-1. The design basis maximum decay heat loading for the MITR-II fuel elements to be transported is 30 W per element, or 330 W for a payload of eleven (11) fuel elements. The results demonstrate that the design criterion of a maximum fuel plate temperature of 400 °F is met if helium is used as the backfill gas. Figure 3.3-6 presents the predicted temperature distribution within the MITR-II fuel basket under the NCT Hot condition.

ATR Fuel Basket

Table 3.3-3 presents the predicted maximum temperature achieved within the ATR fuel basket under the NCT Hot condition with a helium gas backfill. The peak temperatures for the BRR packaging are again bounded by those presented in Table 3.3-1. The design basis maximum decay heat loading for the ATR fuel elements to be transported is 30 W per element, or 240 W

for a payload of eight (8) fuel elements. Although this level of decay heat loading could be accommodated using air as the backfill gas, a helium gas backfill is to be used to maintain consistency with the loading procedures for the other payloads. Figure 3.3-7 presents the predicted bounding temperature distribution within the ATR fuel basket under the NCT Hot condition.

TRIGA Fuel Basket

Table 3.3-4 presents the predicted maximum temperature achieved within the TRIGA fuel basket under the NCT Hot condition with a helium backfill. The design basis maximum decay heat loading for the TRIGA fuel elements to be transported is 20 W per element, or 380 W for a payload of nineteen (19) fuel elements. As seen from Table 3.3-4, the results demonstrate that the design criterion of a maximum fuel element temperature of 400 °F is met. Figure 3.3-8 presents the predicted bounding temperature distribution within the TRIGA fuel basket under the NCT Hot condition.

3.3.1.2 Minimum Temperatures

The minimum temperature achieved within each of the fuel baskets would be achieved with a zero decay heat load and an ambient air temperature of -40 °F per 10 CFR §71.71(c)(2). The evaluation of this thermal condition requires no thermal calculation. Instead, all package components will eventually achieve the -40 °F temperature under steady-state conditions. As discussed in Section 3.2.2, *Technical Specifications of Components*, the -40 °F temperature is within the allowable operating temperature range for all package components.

3.3.2 Maximum Normal Operating Pressure

The cask cavity is to be filled with helium at atmospheric pressure following the draining and drying process. Since the release of fission generated gases from uranium-aluminide and uranium-zirconium hydride based fuel is diffusion-limited as opposed to the direct release mechanism for commercial spent nuclear fuel, the pressurization of the cask cavity due to gaseous release from breached fuel elements will be insignificant [30, 31] and is ignored for this safety evaluation.

The peak pressure developed within the cask cavity under NCT conditions can be conservatively estimated by assuming that the cavity gas reaches a bulk average temperature that is equal to the mean of the average inner shell temperature and the average fuel basket temperature. Under the NCT Hot condition with the MURR fuel payload the average temperature of the inner shell is 225 °F. Combining this temperature with the average fuel basket temperature of 293 °F yields a predicted bulk average backfill gas temperature of 259 °F.

Assuming the backfill gas has an initial temperature of 70 °F at the time of filling and that a fill pressure of one atmosphere is used, the predicted maximum operating pressure within the cask cavity for the transport of the MURR payload can be estimated via:

$$\text{Cavity Pressure} = 14.7 \text{ psia} \frac{(259^\circ \text{F} + 460^\circ \text{F})}{(70^\circ \text{F} + 460^\circ \text{F})} - 14.7 \text{ psia}$$

$$\text{Cavity Pressure} = 5.2 \text{ psig}$$

The equivalent peak bulk average fill gas temperatures for the MITR-II, ATR, and TRIGA baskets are 170, 164, and 174 °F, respectively. As such, the associated peak cask cavity pressures under NCT conditions are 2.8, 2.6, and 2.9 psig, respectively. Based on these NCT pressures, the maximum normal operating pressure (MNOP) within the cask cavity is set at a bounding level of 10 psig.

3.3.3 Vacuum Drying Operations

An evaluation of the proposed vacuum drying operation was conducted to ensure that the component temperatures will remain within their normal temperature limits. The vacuum drying operations consist of the following general steps:

- 1) the cask body, without the impact limiters, bottom drain plug, cask lid, and cask shield plug are placed in the reactor pool.
- 2) the fuel elements to be transported are placed in the fuel basket within the cask,
- 3) the shield plug is placed into the cask,
- 4) the loaded cask is lifted above the pool and the enclosed water allowed to drain back into the pool. At this point, the cask cavity is filled with air.
- 5) following decon operations, the loaded cask is moved to the facility work area where the drain port and cask lid is installed. The vent port tool is installed and vacuum drying is initiated.
- 6) the minimum pressure achieved under vacuum drying is 1 to 3 torr.

The transient evaluation of these operations used a modification of the NCT thermal model described in Appendix 3.5.3, *Analytical Thermal Model*. The modifications made for this evaluation consisted of assuming air as the backfill gas. While the impact limiters will not be installed during vacuum drying operations, and the cask lid will not be installed until just before vacuum drying begins, leaving these components in the thermal model greatly simplified the model modifications required and is seen as having no significant impact on the transient temperatures. The effect of being submerged in the reactor pool is addressed by assuming all cask components are at equilibrium with a maximum temperature of 80 °F.

At time = 0, the loaded cask is assumed to be lifted from the pool, the water drained and the cask cavity filled with air, the ambient conditions are conservatively assumed to be 100 °F without insolation. The transient analysis is conducted for a period of 8 hours and followed by a steady-state evaluation to establish the peak temperatures that would occur if the helium backfill is not established. The MURR fuel element payload is selected as a basis for the vacuum drying evaluation since its decay heat loading is over 3 times greater than any of the other potential payloads.

The thermal analysis of vacuum drying assumes that the thermal conductivity of the gas filling the voids of the packaging and the payload remain unchanged from its base value at atmospheric pressure conditions for vacuum pressures of 1 torr or greater. There are two states that define the process by which heat is transferred by a gas [32]:

viscous state, in which the totality of molecules is responsible for the heat transfer. The viscous state occurs as long as the pressure is higher than the range in which the

molecular state occurs. Within the viscous state the thermal conductivity of a gas is independent of pressure.

molecular state, heat conductivity in the molecular state is when the gas pressure is so low that the molecular mean free path is about equal or greater than the distance between the plates. The thermal conductivity of the gas is no longer characterized by the viscous state for conductivity and therefore the conductivity is dependent on pressure. The heat transfer process under these conditions is called free molecular conduction.

The pressure at which the molecular mean free path is equal to the minimum distance between the surfaces within the packaging is determined below for air as the fill gas. Per [33], the mean free path of the fill gas molecules is computed via:

$$L = \frac{k \times T}{\pi \times \sqrt{2} \times P \times d^2}$$

where:

$k = 1.380658 \times 10^{-23}$ J/K, the Boltzmann constant

P = pressure in Pa

T = temperature in K

d = molecule diameter, in m

At the lowest practical vacuum pressure of 1 torr (133 Pa) used for vacuum drying and a conservatively high gas temperature of 525 °F (547K) based on the hottest fuel element (as determined from the steady-state analysis), the mean free path for air with a molecule diameter of about 3×10^{-10} m (based on oxygen, [33]) is:

$$L = \frac{1.380658 \times 10^{-23} \times 547}{\pi \times \sqrt{2} \times 133 \times (3 \times 10^{-10})^2}$$

$$L = 1.42 \times 10^{-4} \text{ m} = 0.006 \text{ inches}$$

Since this mean free path is much smaller than the smallest significant gap in the model (i.e., the gap between fuel plates), the gas heat transfer everywhere within the model can be characterized as being in the viscous state and independent of the gas pressure.

Figure 3.3-9 illustrates the predicted package heat up following removal from the fuel pool. The illustrated thermal transient conservatively ignores the cooling effect provided by the water remaining in the cask cavity as it evaporates and the increased thermal conductivity provided by moist air over the dry air conductivity assumed by the thermal modeling. As seen by the transient curves presented in Figure 3.3-9, a minimum of 8 hours exists before the peak fuel plate temperature reaches the NCT limit of 400 °F. Since this temperature limit is set by structural considerations for the accident drop events and since no credible drop event exists between the time the cask is placed in the facility work area and the vacuum drying is completed and the cask

is prepared for transportation, the actual temperature limit for the fuel elements under vacuum drying can be higher.

Oxidization of aluminum fuel has been studied for long term exposure to moist air and saturated water vapor at temperatures up to 400 °F (200 °C) [34, 35]. The results show no significant oxidization and no damage to the fuel cladding as a result of the exposure. As such, no fuel damage is expected for the limited time and exposure temperatures seen under vacuum drying.

In conclusion, the transient results in Figure 3.3-9 demonstrate that adequate time and thermal margin exists to allow the necessary vacuum drying operations to be completed without exceeding the maximum allowable component temperature limits. While even the steady-state temperatures with air as the backfill gas will not result in any damage to the fuel elements, the vacuum drying operations will include a provision to backfill the cask cavity with helium gas if the vacuum drying has not been completed within 8 hours. Once filled with the helium gas, the package temperatures are bounded by those presented in Section 3.3.1.1, *Maximum Temperatures*, for NCT conditions.

Table 3.3-1 – NCT Temperatures for BRR Packaging with MURR Fuel

Component	Temperature (°F) ^①		
	NCT Hot ^④	NCT Hot without Solar	Max. Allowable
MURR Fuel Plate	350	331	400
MURR Side Plate	348	329	400
MURR Fuel Basket	334	315	800
Inner Shell	237	216	800
Lead	233	213	620
Outer Shell	216	195	800
Thermal Shield	185	182	800
Lower End Structure	205	184	800
Upper End Structure	220	200	800
Shield Plug	225	205	620 ^②
Cask Lid	216	197	800
Closure/Vent Port Seals	216	197	250
Drain Port Seal	202	181	250
Upper Impact Limiter			
- Max. Foam	215	196	300
- Avg. Foam	146	132	300
- Shell	215	196	250 ^③
Lower Impact Limiter			
- Max. Foam	200	179	300
- Avg. Foam	142	127	300
- Shell	200	179	250 ^③
Max. Accessible Surface	-	185 ^⑤	185
Cask Cavity Bulk Gas	259	239	N/A

Notes: ① Results assume a payload of eight (8) MURR fuel elements dissipating 158 W each and helium as the backfill gas.

② Temperature criterion based on melting point of the enclosed lead shielding.

③ Temperature criterion based on long term temperature limit for shell coating.

④ Results conservatively based on an earlier design for the cask and impact limiter attachment lugs. See Appendix 3.5.3 for a description of the design change and the conservative impact of ignoring the design change for NCT Hot modeling.

⑤ Maximum temperature occurs at the root of the upper cask impact limiter attachment lugs.

Table 3.3-2 – NCT Hot Temperatures for BRR Packaging with MITR-II Fuel

Component [ⓐ]	Temperature (°F)	
	11 Elements @ 30 W Each	Max. Allowable
MITR-II Fuel Plate	263	400
MITR-II Side Plate	262	400
MITR-II Fuel Basket	244	800
Cask Cavity Bulk Gas	170	N/A

Note: [ⓐ] Temperatures for packaging components bounded by values in Table 3.3-1.

Table 3.3-3 – NCT Hot Temperatures for BRR Packaging with ATR Fuel

Component [ⓐ]	Temperature (°F)	
	8 Elements @ 30 W Each	Max. Allowable
ATR Fuel Plate	197	400
ATR Side Plate	197	400
ATR Fuel Basket	195	800
Cask Cavity Bulk Gas	164	NA

Note: [ⓐ] Temperatures for packaging components bounded by values in Table 3.3-1.

Table 3.3-4 – NCT Hot Temperatures for BRR Packaging with TRIGA Fuel

Component [ⓐ]	Temperature (°F)	
	19 Elements @ 20 W Each	Max. Allowable
TRIGA Fuel Element	355	400
TRIGA End Fitting	308	400
TRIGA Fuel Basket	287	800
Cask Cavity Bulk Gas	174	NA

Note: [ⓐ] Temperatures for packaging components bounded by values in Table 3.3-1.

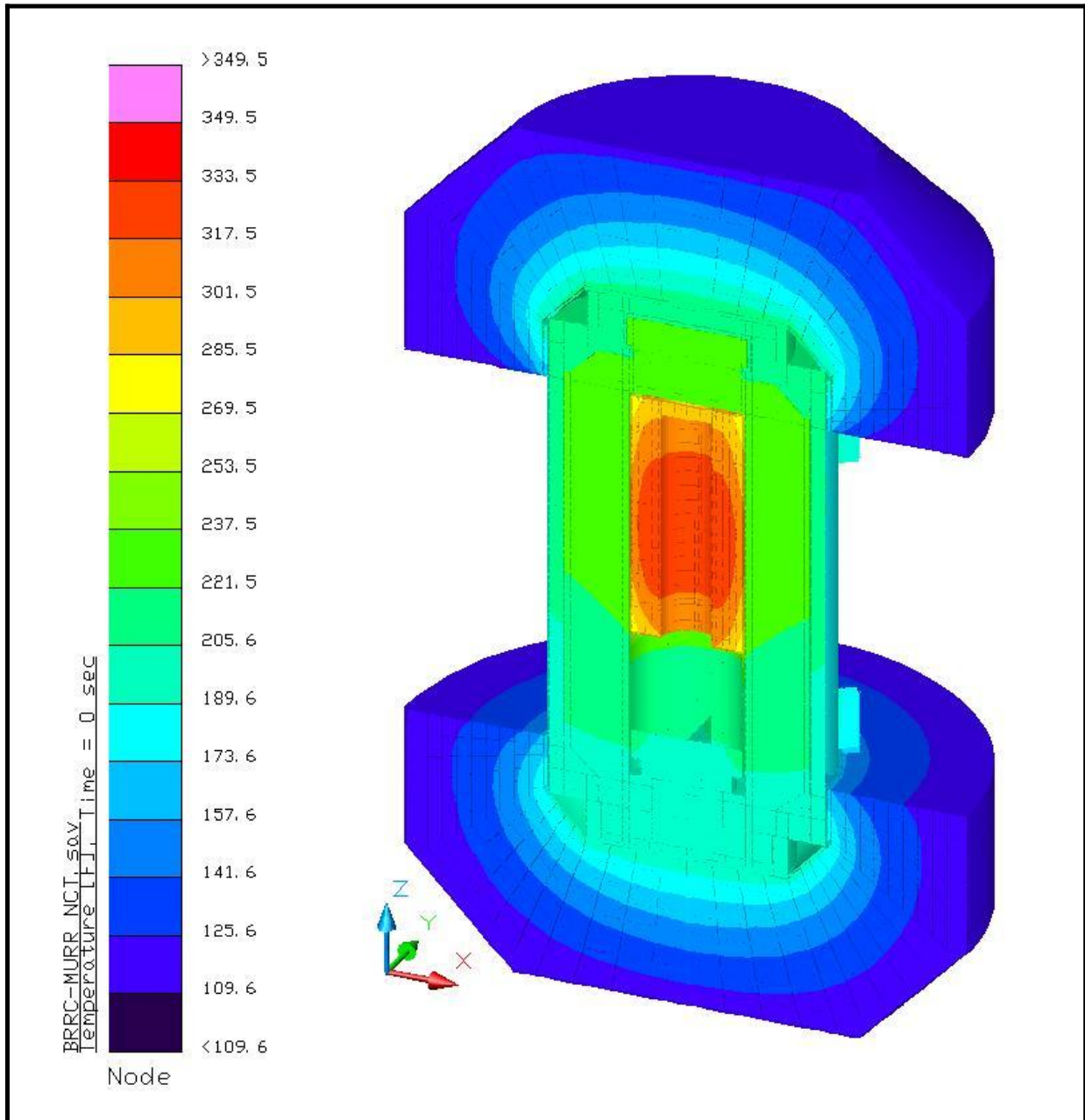
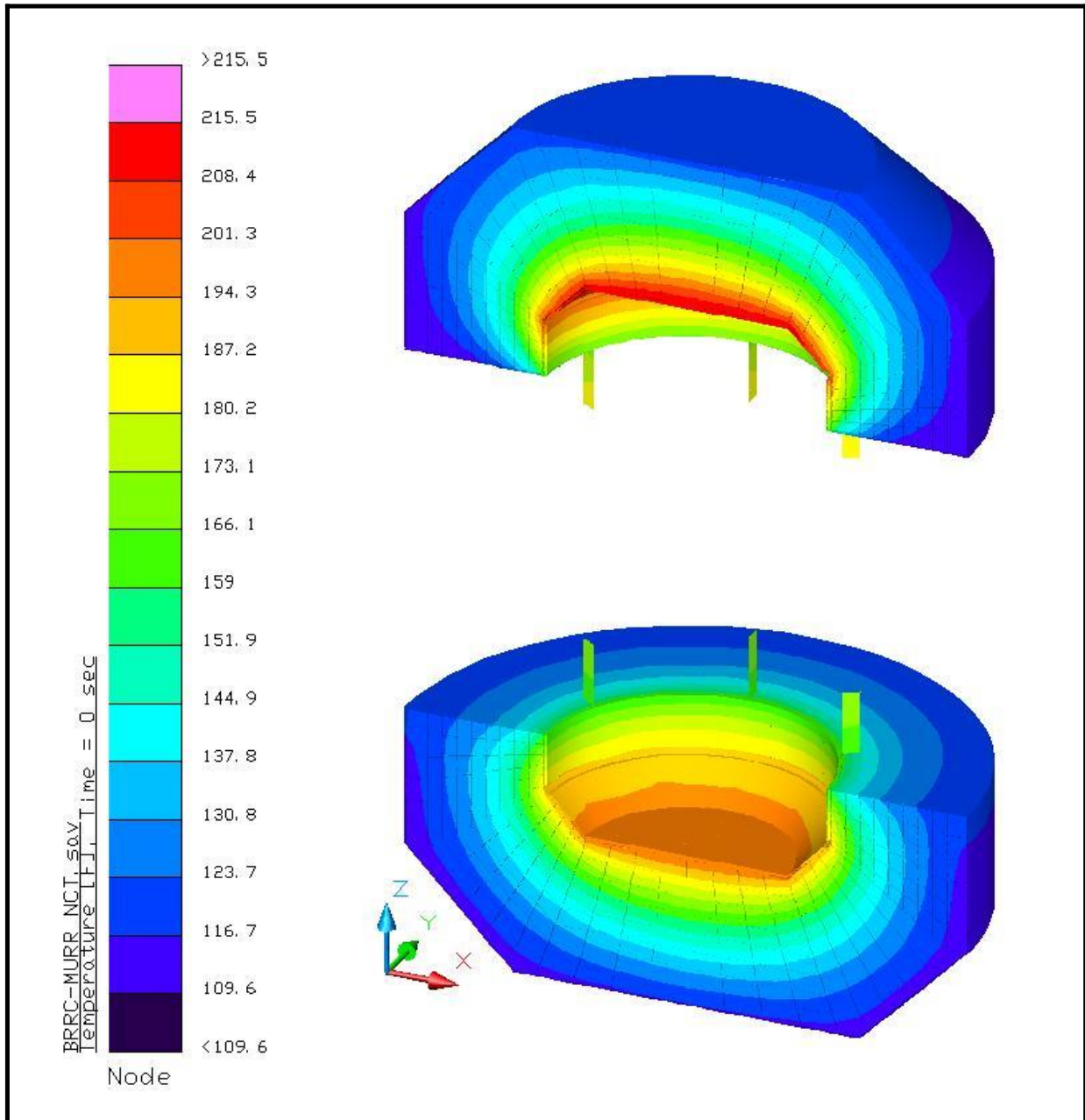


Figure 3.3-1 – BRR Package Temperature Distribution for NCT Hot Condition with MURR Fuel Basket



Note: Earlier design of 6 vs. 8 attachment lugs per limiter depicted. Results bound the revised design under NCT

Figure 3.3-2 – Impact Limiter Temperature Distribution for NCT Hot Condition with MURR Fuel Basket

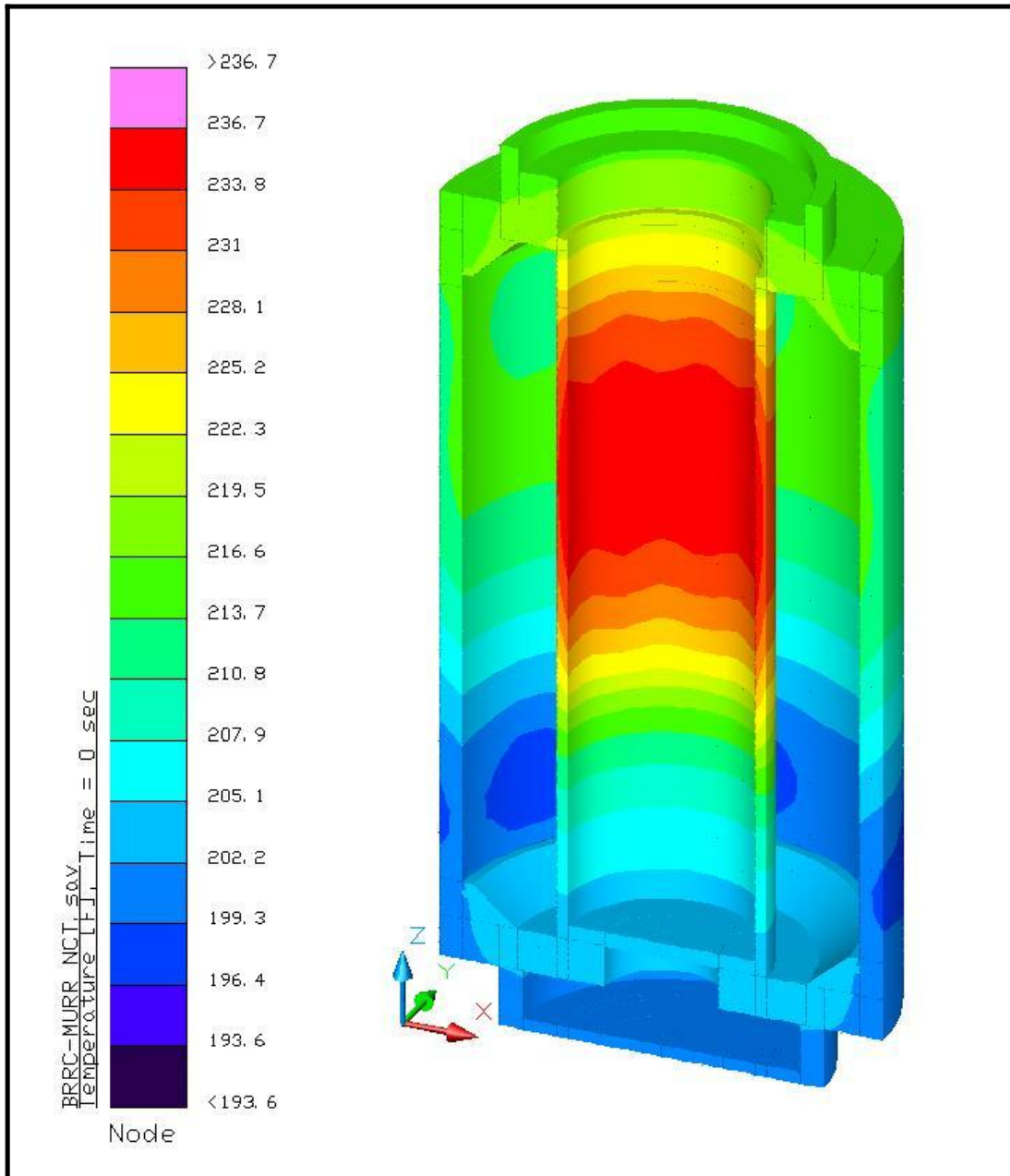


Figure 3.3-3 – Structural Shell Temperature Distribution for NCT Hot Condition with MURR Fuel Basket

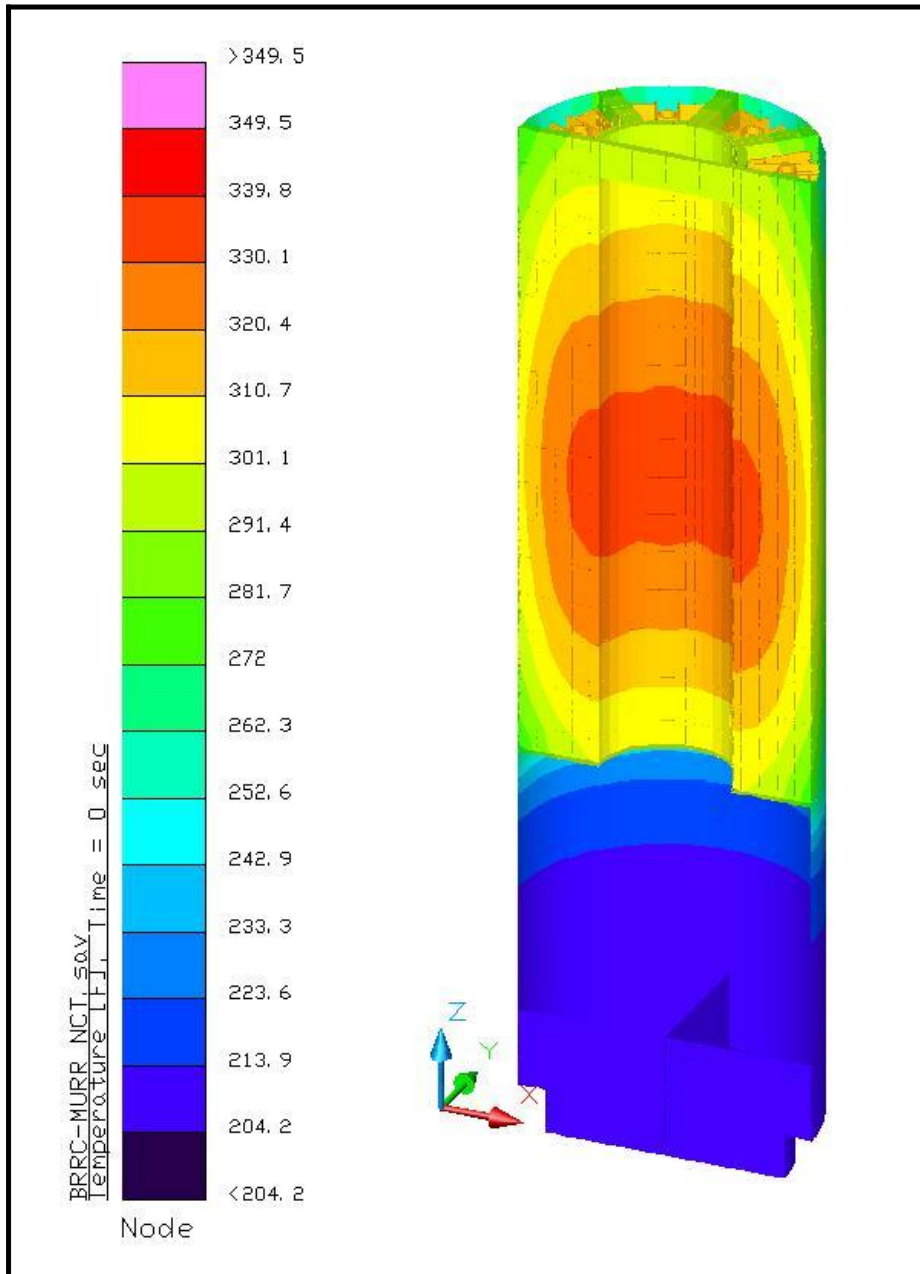
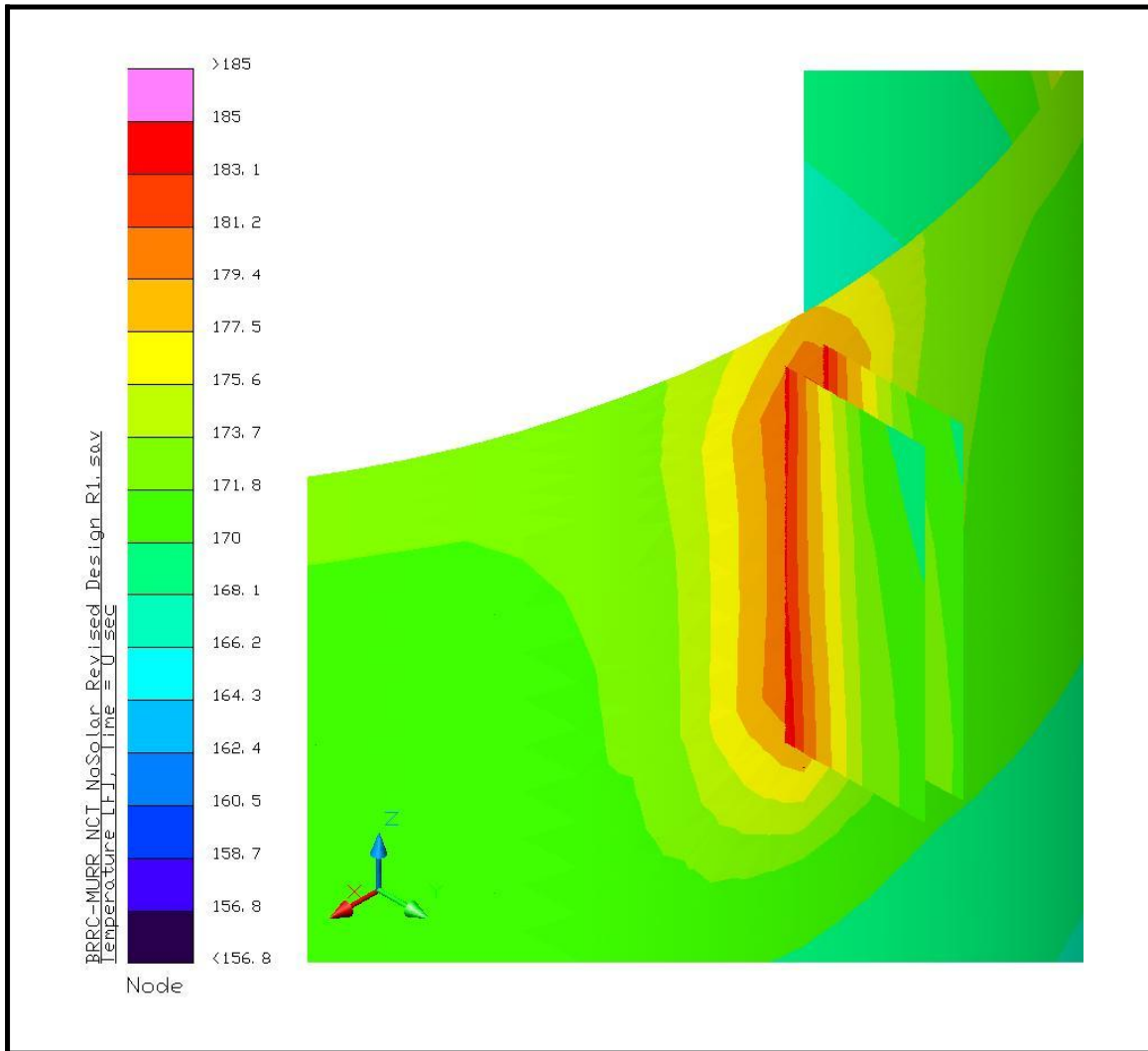
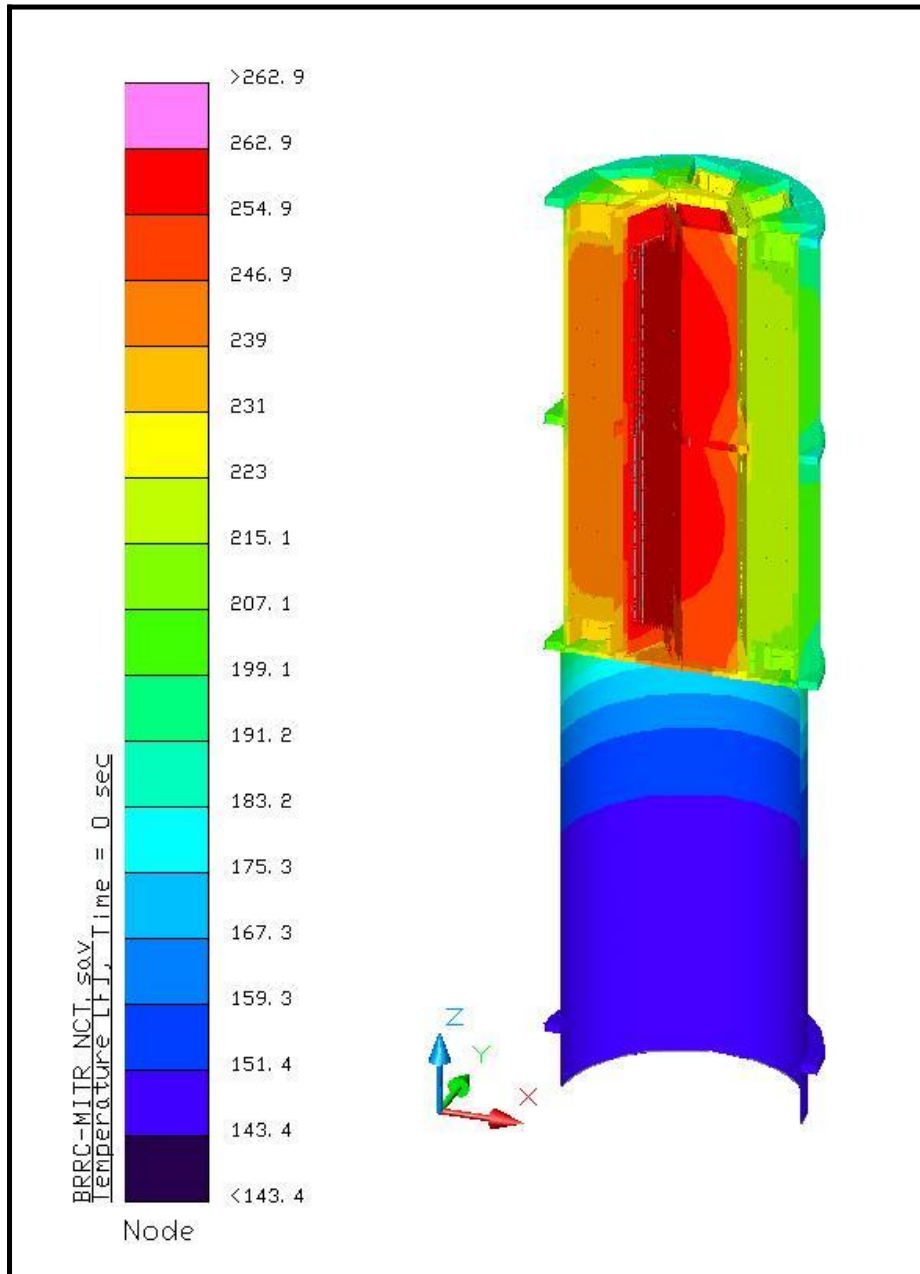


Figure 3.3-4 – MURR Fuel Basket Temperature Distribution for NCT Hot Condition



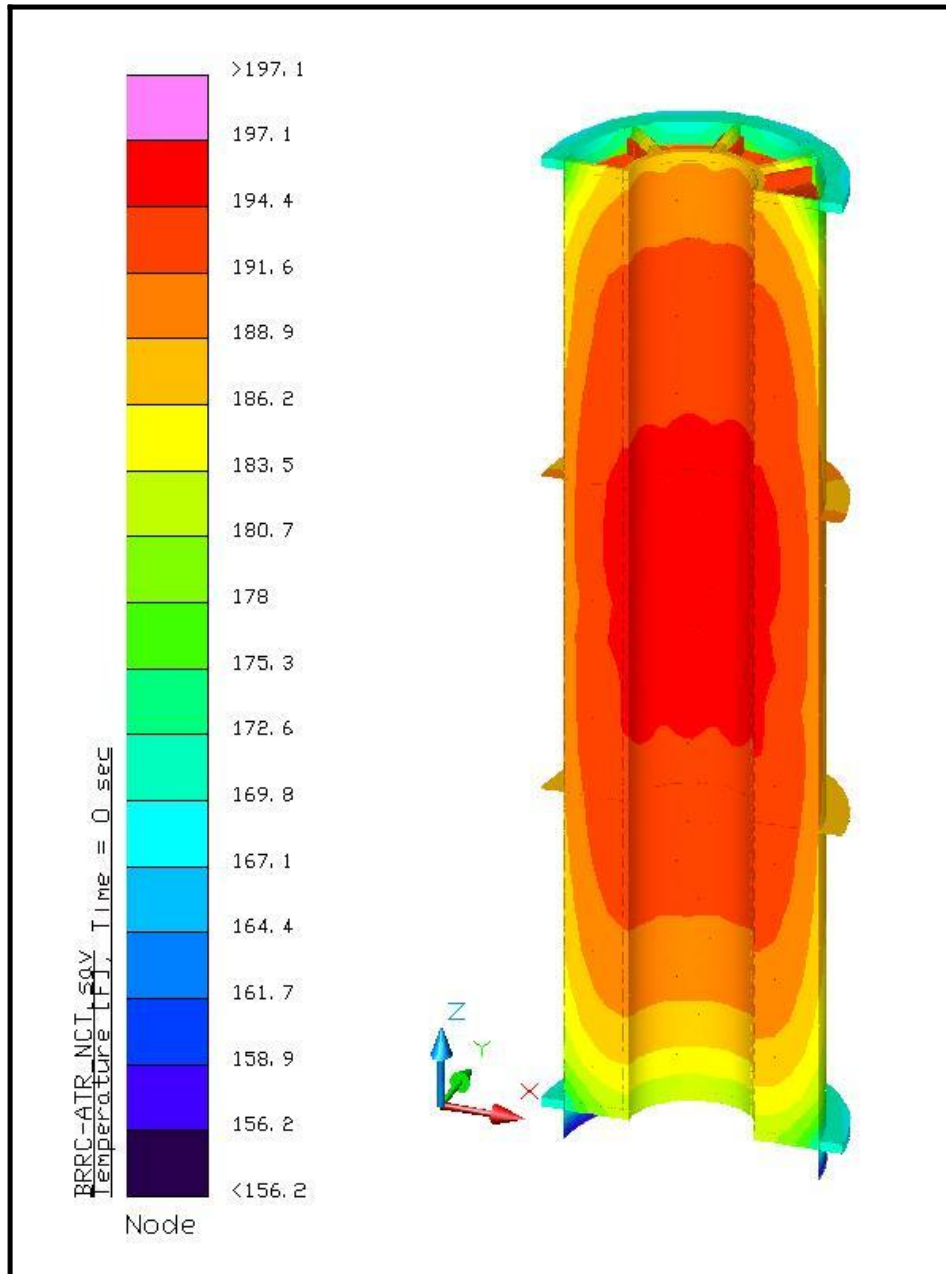
Surface Temperature Distribution in Vicinity of Impact Limiter Attachment Lugs

Figure 3.3-5 – Peak Accessible Surface Temperature for NCT No Solar



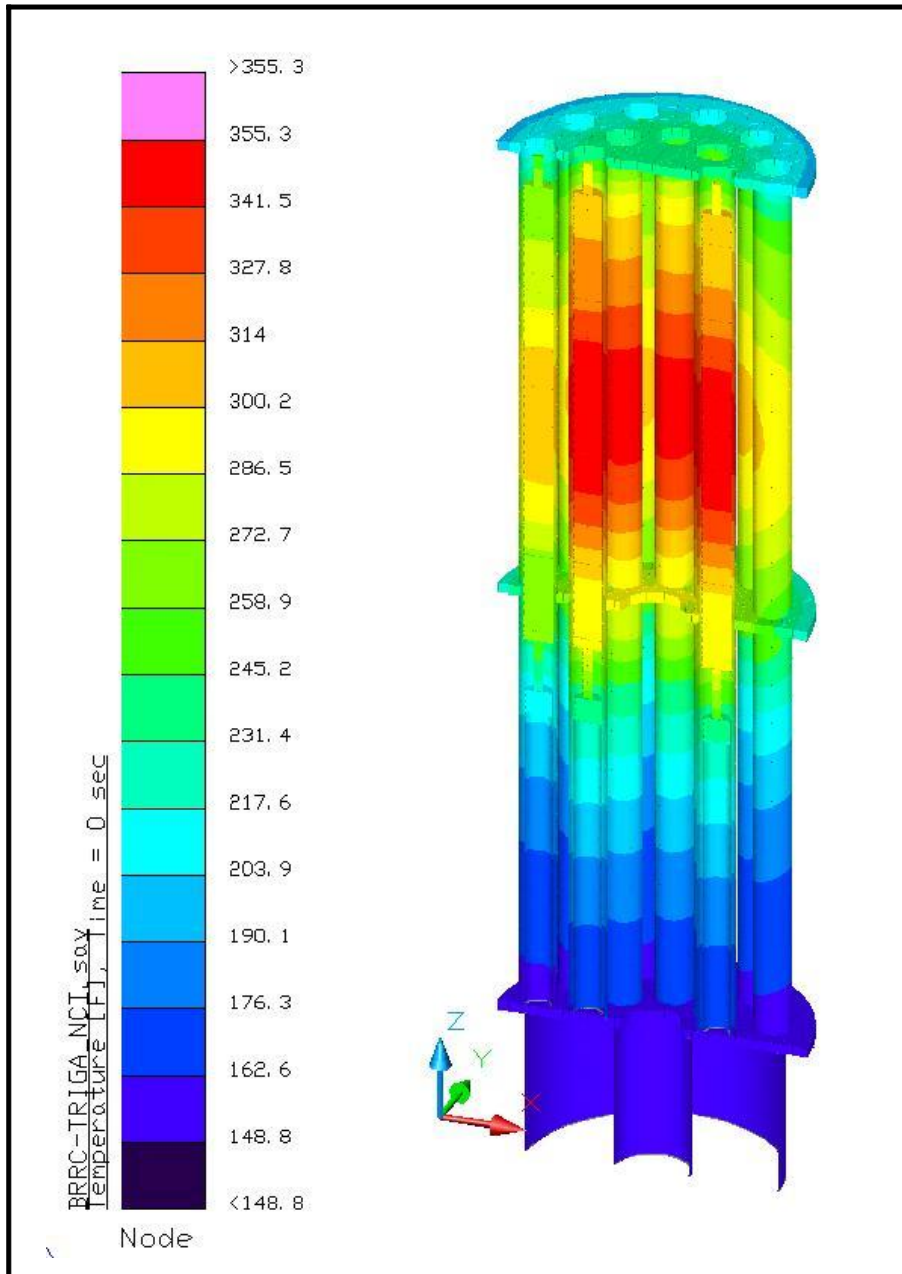
Note: Results are for basket decay heat loading of 330 W

Figure 3.3-6 – MITR-II Fuel Basket Temperature Distribution for NCT Hot Condition



Note: Results are for basket decay heat loading of 240 W

Figure 3.3-7 – ATR Fuel Basket Temperature Distribution for NCT Hot Condition



Note: Results are for basket decay heat loading of 380 W

Figure 3.3-8 – TRIGA Fuel Basket Temperature Distribution for NCT Hot Condition

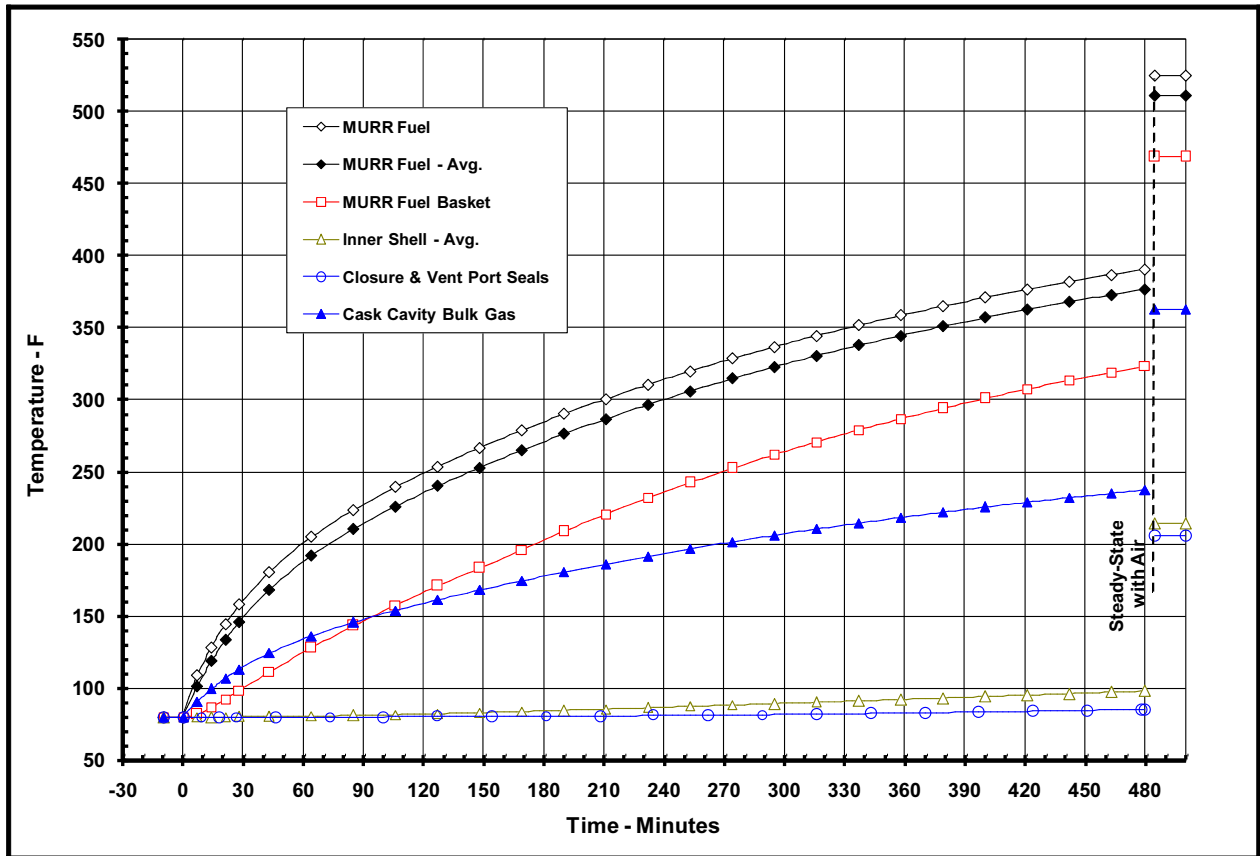


Figure 3.3-9 – Bounding Transient Heat Up During Vacuum Drying

3.4 Thermal Evaluation for Hypothetical Accident Conditions

This section presents the thermal evaluation of the BRR package under the hypothetical accident condition (HAC) specified in 10 CFR §71.73(c)(4) based on an analytical thermal model of the BRR. The analytical model for HAC is a modified version of the half symmetry NCT model described in Appendix 3.5.3.1, *Description of BRR Packaging Thermal Model for NCT Conditions*, with the MURR fuel element payload. The MURR payload is selected as a basis for the HAC evaluation since its decay heat loading is more than 3 times greater than any of the other potential payloads.

The principal model modifications made to convert the NCT thermal model to the HAC model consists of modifying the impact limiter attachment thermal model to reflect the design modifications following the drop testing, simulating the expected package damage resulting from the HAC defined drop events, capturing the thermal decomposition of the polyurethane foam under HAC conditions, changing the package surface emissivities to reflect the assumed presence of soot and/or surface oxidization, assumed contact between the thermal shield and the outer shell and zero lead gap to maximize the heat flow into the package, and changing the package orientation from upright to horizontal to reflect its probable orientation following the HAC drop event.

Physical testing using a half scale certified test unit (CTU) is used to establish the expected level of damage sustained by the BRR package from the 10 CFR 71.73 prescribed free and puncture drops that are assumed to precede the HAC fire event. Appendix 2.12.3, *Certification Test Results*, provides the configuration and initial conditions of the test articles, the test facilities and instrumentation used, and the test results. Appendix 3.5.3.7, *Description of Thermal Model for HAC Conditions*, provides an overview of the test results, the rationale for selecting the worst-case damage scenario, and the details of the thermal modeling used to simulate the package conditions during the HAC fire event.

3.4.1 Initial Conditions

The initial conditions assumed for the package prior to the HAC event are described below in terms of the modifications made to the NCT thermal model to simulate the assumed package conditions prior to and during the HAC event. These modifications are:

- Simulated the worst-case damage arising from the postulated HAC free and puncture drops as described in Appendix 3.5.3.7, *Description of Thermal Model for HAC Conditions*,
- Changed the package orientation from upright to horizontal to reflect the assumed position of the package following an HAC accident event,
- Increased the emissivity of all external surfaces to 0.9 and the solar absorptivity to 0.9 to account for possible oxidation and/or soot accumulation on the surfaces,
- Increased the emissivity of the interior surface of the thermal shield from 0.4 to 0.6 to account for oxidization during the HAC event,
- Added heat transfer via radiation within the impact limiter enclosures with an emissivity of 0.95 to account for the potential loss of polyurethane foam from thermal decomposition,

- Assumed an initial temperature distribution equivalent to the package at steady-state conditions with a 100 °F ambient and no insolation. This assumption complies with the requirement of 10 CFR §71.73(b).

Following the free and puncture bar drop events, the BRR package is assumed come to rest in a horizontal position prior to the initiation of the fire event. The MURR basket and the fuel element are predicted to remain intact and experience no significant re-positioning as a result of the drop events. Since the package geometry is essentially axi-symmetrical, the thermal performance under HAC conditions is independent of the rotational orientation of the package.

3.4.2 Fire Test Conditions

The fire test conditions analyzed to address the 10 CFR §71.73(c) requirements are as follows:

- The initial ambient conditions are assumed to be 100 °F ambient with no insolation,
- At time = 0, a fully engulfing fire environment consisting of a 1,475 °F ambient with an effective emissivity of 1.0 is used to simulate the average flame temperature of the hydrocarbon fuel/air fire event. The assumption of an average flame emissivity coefficient of 1.0 conservatively bounds the minimum 0.9 flame emissivity specified by 10 CFR Part §71.73(c)(4).
- The convection heat transfer coefficients between the package and the ambient during the 30-minute fire event are based on an average gas velocity of 10 m/sec [29]. Following the 30-minute fire event the convection coefficients are based on still air.
- The ambient condition of 100 °F with insolation is assumed following the 30-minute fire event. A solar absorptivity of 0.9 is assumed for the exterior surfaces to account for potential soot accumulation on the package surfaces.

The transient analysis is continued for 4.5 hours after the end of the 30-minute fire to capture the peak package temperatures.

3.4.3 Maximum Temperatures and Pressure

3.4.3.1 Maximum HAC Temperatures

Table 3.4-1 presents the predicted peak temperature for the BRR package with the MURR fuel payload under HAC conditions. Given that the MURR payload dissipates a significantly higher decay heat than the other potential payloads, the presented temperatures are bounding for all payloads. As seen from the table, significant thermal margins exist for all components. The closure and vent/drain port seals remain below their maximum allowable temperature due to a combination of their location, the amount of foam remaining, even after the conservative damage assumptions, and the surrounding thermal mass of the upper and lower end structures. For example, the peak temperature predicted for the vent/drain port seals arises for the improbable condition of the worst case damage described in Appendix 3.5.3.7, *Description of Thermal Model for HAC Conditions*, for the impact limiter aligning directly opposite of the drain port location. Without that conservative assumption, the peak vent/drain port temperature would be approximately 300 °F.

Figure 3.4-1 illustrates the temperature profile within the BRR package at the end of the 30-minute hypothetical fire. The illustrated profile demonstrates the thermal protection afforded to the package by the thermal shield and the polyurethane filled impact limiters since the high temperatures are limited to narrow regions on the exterior of the packaging. This thermal protection occurs despite the conservative level of damage assumed for the impact limiters.

Figure 3.4-2 and Figure 3.4-3 illustrate the temperature response profiles for selected package components. The relatively low temperature rise seen for the fuel elements and the fuel basket over the HAC event further demonstrates the thermal protection afforded by the BRR package design.

3.4.3.2 Maximum HAC Pressures

The peak cask cavity pressure under HAC conditions is conservatively estimated in the same manner as for NCT conditions (i.e., the bulk average cavity gas temperature is assumed to be equal to the mean of the average inner shell temperature and the average fuel basket temperature). The potential pressurization of the cask cavity due to failed cladding on the uranium-aluminide and uranium-zirconium hydride based fuel elements is ignored for this safety evaluation since the release of fission generated gases from these fuel types is diffusion-limited as opposed to the direct release mechanism for commercial spent nuclear fuel. At the conditions seen within the BRR package, the pressurization of the cask cavity due to gaseous release from breached fuel elements will be insignificant [30, 31] and is ignored for this safety evaluation.

Under the HAC condition with the MURR fuel payload, the peak bulk average gas temperature achieved during the HAC transient is 388 °F. Based on an assumed backfill gas temperature of 70 °F, the predicted maximum pressure within the cask cavity is computed via:

$$\text{Cavity Pressure} = 14.7 \text{ psia} \frac{(388^\circ \text{F} + 460^\circ \text{F})}{(70^\circ \text{F} + 460^\circ \text{F})} - 14.7 \text{ psia}$$

$$\text{Cavity Pressure} = 8.8 \text{ psig}$$

Given the significantly greater decay heat of the MURR fuel element payload, the computed peak HAC pressure will bound those achieved for the MITR-II, ATR, and TRIGA baskets.

3.4.4 Maximum Thermal Stresses

The maximum thermal stresses under the HAC condition are addressed in Section 2.7.4, *Thermal*.

Table 3.4-1 – HAC Temperatures

Component	Temperature (°F) ^①			
	End of Fire	Peak	Post-fire Steady State	Max. Allowable
MURR Fuel Plate	344	451	326	1,100
MURR Side Plate	341	449	324	1,100
MURR Fuel Basket	326	437	310	800
Inner Shell	301	393	211	800
Lead	471	482	207	620
Outer Shell	704	704	200	2,700
Thermal Shield	1,256	1,256	180	2,700
Lower End Structure	318	335	182	800
Upper End Structure	485	485	198	800
Shield Plug	234	317	201	620 ^②
Cask Lid	215	306	196	800
Closure/Vent Port Seals	212	306	196	400
Drain Port Seal	365	373	195	400
Upper Impact Limiter				
- Max. Foam	-	-	-	N/A ^③
- Avg. Foam	-	-	-	N/A ^③
- Shell	1,475	1,475	195	2,700 ^③
Lower Impact Limiter				
- Max. Foam	-	-	-	N/A ^③
- Avg. Foam	-	-	-	N/A ^③
- Shell	1,475	1,475	190	2,700 ^③
Cask Cavity Bulk Gas	305	388	257	N/A

Notes: ^① Results assume a payload of eight (8) MURR fuel elements dissipating 158 W each and helium as the backfill gas.

^② Temperature criterion based on melting point of the enclosed lead shielding.

^③ Temperature criterion based on melting point for the shell. No criteria for the polyurethane foam since its thermal decomposition serves as its principal means of providing thermal protection during the HAC event.

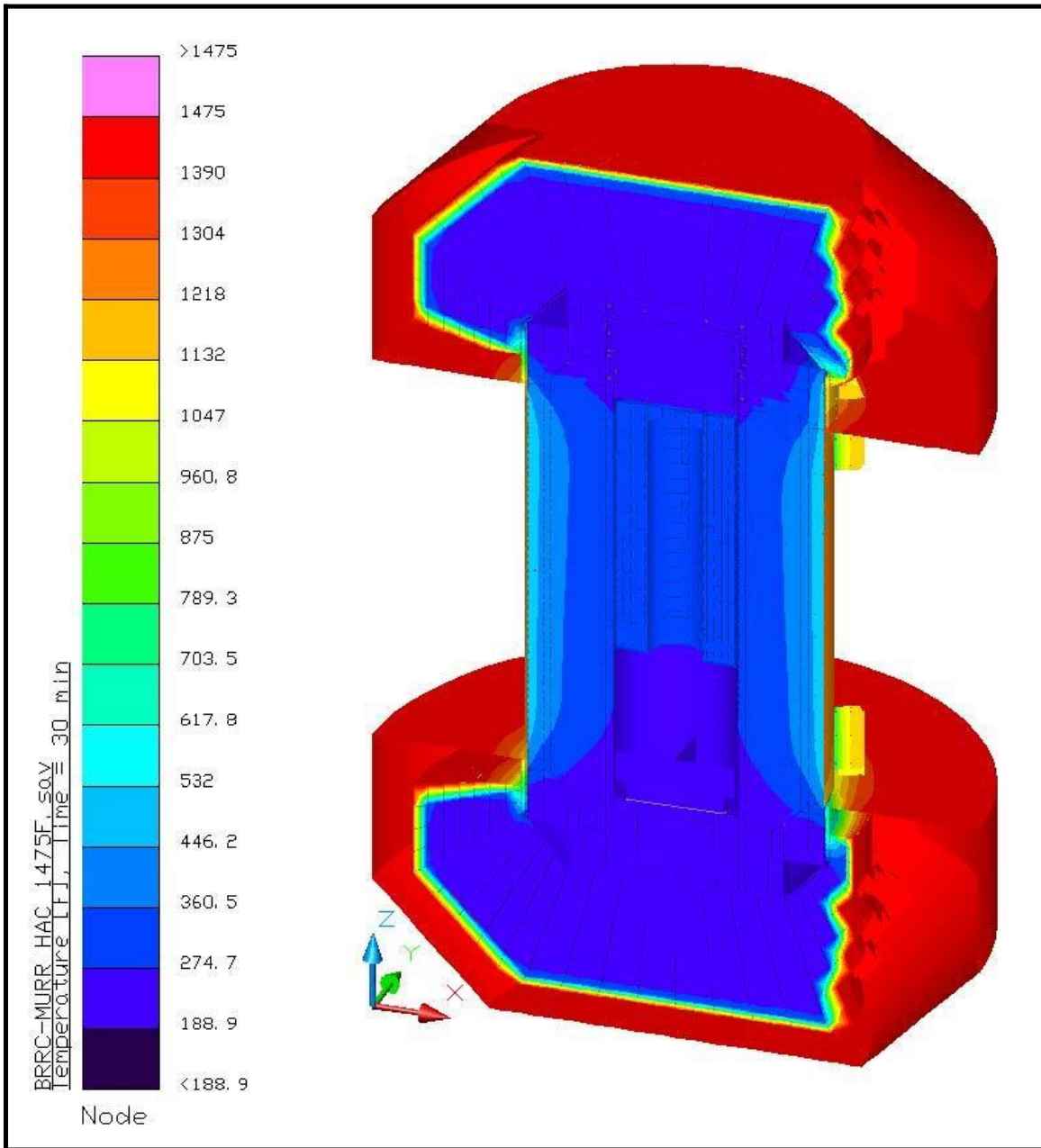


Figure 3.4-1 – BRR Package HAC Temperature Distribution at End of 30 Minute Fire

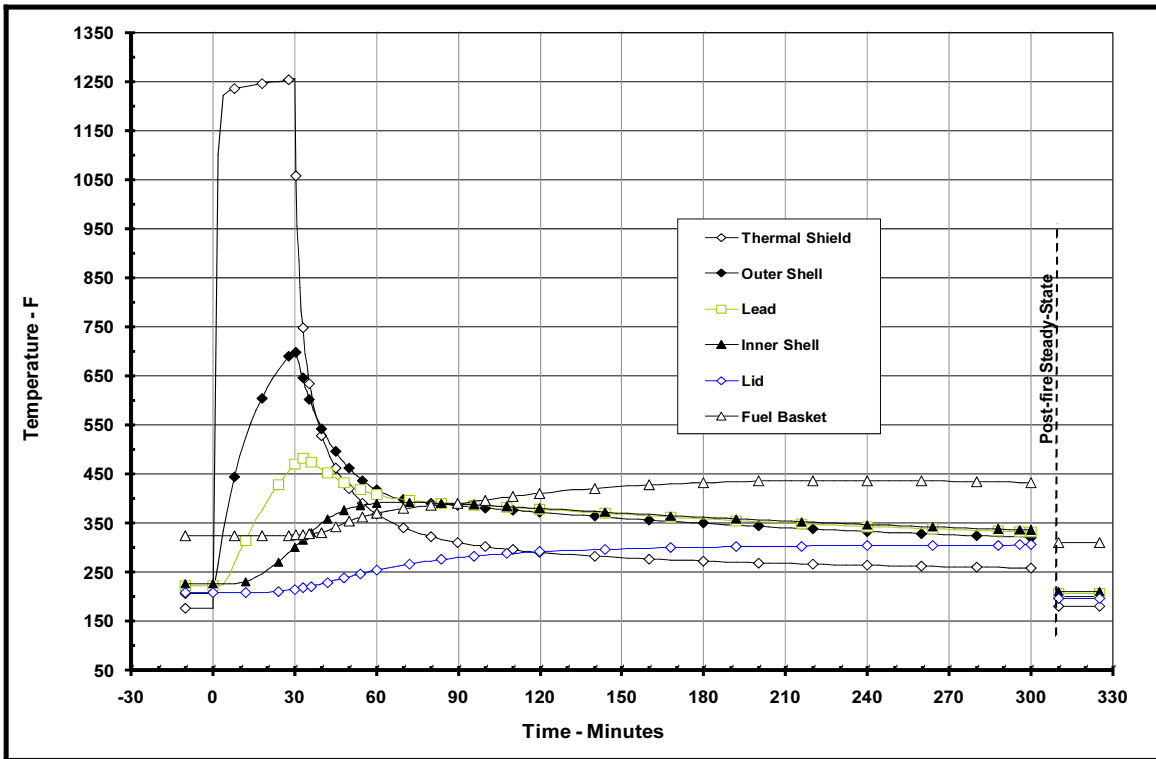


Figure 3.4-2 –Thermal Response to HAC Event, Package Components

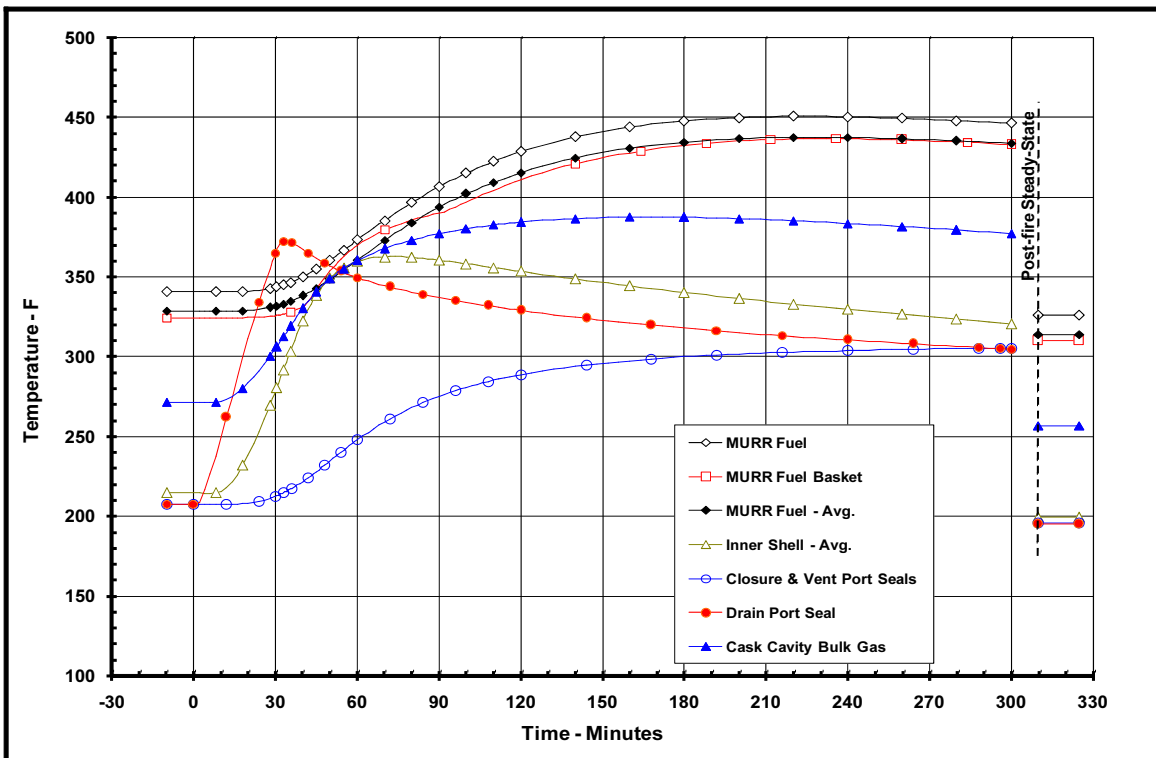


Figure 3.4-3 – Thermal Response to HAC Event, Payload, Seals, and Bulk Gas

3.5 Appendices

- 3.5.1 References
- 3.5.2 Computer Analysis Results
- 3.5.3 Analytical Thermal Model
- 3.5.4 'Last-A-Foam' Response under HAC Conditions

3.5.1 References

1. Title 10, Code of Federal Regulations, Part 71 (10 CFR 71), *Packaging and Transportation of Radioactive Materials*, United States Nuclear Regulatory Commission (USNRC), 01-01-08 Edition.
2. American Society of Mechanical Engineers (ASME) Boiler and Pressure Vessel (B&PV) Code, Section II, Part D, 2007.
3. American Society of Mechanical Engineers (ASME) Boiler & Pressure Vessel Code, Section III, Rules for Construction of Nuclear Facility Components, Division 1, Subsection NB, Class 1 Components, & Subsection NG, Core Support Structures, 2007 Edition.
4. Y.S. Touloukian, *Thermophysical Properties of Matter*, the TPRC Data Series, Plenum Publishing Corp., New York, NY, 1970.
5. Polkinghorne, S. and Lacy, J., *Thermophysical And Mechanical Properties Of ATR Core Materials*, Report No. PG-T-91-031, August 1991, EG&G Idaho, Inc.
6. Matweb, Online Material Data Sheets, www.matweb.com.
7. Frank, R., and Plagemann, W., *Emissivity Testing of Metal Specimens*, Boeing Analytical Engineering coordination sheet No. 2-3623-2-RF-C86-349, August 21, 1986. Testing accomplished in support of the TRUPACT-II design program.
8. Azzazy, M., *Emissivity Measurements of 304 Stainless Steel*, prepared for Southern California Edison, September 6, 2000, Transnuclear File No. SCE-01.0100.
9. Gubareff, G., Janssen, J., and Torborg, R., *Thermal Radiation Properties Survey*, 2nd Edition, Honeywell Research Center, 1960.
10. Gustavsen, Arild, *Heat Transfer in Window Frames with Internal Cavities*, PhD Thesis, Norwegian University of Science and Technology, Trondheim, Norway, September 2001.
11. Series 66 and 73 Product Data Sheets, Tnemec Company, Inc. 6800 Corporate Drive Kansas City, MO, www.tnemec.com.
12. MURR Fuel Drawings, EG&G Drawings No. 409406, Rev E and 409407, Rev N.
13. MITR-II Fuel Drawings, EG&G Drawings No. 410368, Rev A, 410369, Rev C, and 419486, Rev A.
14. ATR Mark VII Fuel Element Assembly, INEEL Drawing No. DWG-405400, Rev-19.
15. TRIGA Fuel Element Description, University of Utah Class Notes, Nuclear Engineering, CVEEN 5700/6700.
16. *KK-8 Graphite High Temperature Thermal Characteristics with Supporting Data*, letter from Harold E. Cook (Carbon/Graphite Group, Inc.) to Corwin Robinson (EG&G Mound Applied Technologies), dated March 13, 1992.
17. Greenspan, E., *Hydride Fuel for Improving the Design and Performance of LWRs*, Presentation to 233rd ACS National Meeting, Chicago, IL, 2007.
18. Last-A-Foam™ On-line Data Sheet, www.generalplastics.com.

19. Rohsenow, Hartnett, and Choi, Handbook of Heat Transfer, 3rd edition, McGraw-Hill, 1998.
20. Rainier Rubber Company, Seattle, WA, www.rainierrubber.com.
21. *Parker O-Ring Material Offering Guide*, ORD 5712, August 2002, www.parkerorings.com.
22. Thermal Desktop[®], Version 5.1, Cullimore & Ring Technologies, Inc., Littleton, CO, 2007.
23. SINDA/FLUINT, *Systems Improved Numerical Differencing Analyzer and Fluid Integrator*, Version 5.1, Cullimore & Ring Technologies, Inc., Littleton, CO, 2007.
24. AFS Report TR-VV-06-001, Rev. 0, *Thermal Desktop[®] and SINDA/FLUINT Testing and Acceptance Report*, Version 5.1, Areva Federal Services, LLC, 2008.
25. Kreith, Frank, Principles of Heat Transfer, 3rd edition, Harper & Row, 1973.
26. Guyer, Eric, Handbook of Applied Thermal Design, McGraw-Hill, Inc., 1989.
27. Williamson, C., and Iams, Z., *Thermal Assault and Polyurethane Foam - Evaluating Protective Mechanisms for Transport Containers*, General Plastics Manufacturing Company, Tacoma, WA, Waste Management '05 Symposium, Tucson, AZ, 2005.
28. Williamson, C., and Iams, Z., *Thermal Assault and Polyurethane Foam - Evaluating Protective Mechanisms*, General Plastics Manufacturing Company, Tacoma, WA, presented at PATRAM International Symposium, Berlin, Germany, 2004.
29. Schneider, M.E and Kent, L.A., *Measurements of Gas Velocities and Temperatures in a Large Open Pool Fire*, Heat and Mass Transfer in Fire - HTD Vol. 73, 1987, ASME, New York, NY.
30. Vinson, D., Sindelar, R., and Iyer, N., *Containment Evaluation of Breached AL-SNF For Cask Transport*, Savannah River National Laboratory - Materials Science & Technology, Aiken, SC 29808.
31. TRIGA[®] Fuel Description, General Atomics website, <http://triga.ga.com>.
32. Roth A, Vacuum Technology, 2nd Edition, Elsevier Science, 1982.
33. Lide, D., Handbook of Chemistry and Physics, 83rd Edition, The Chemical Rubber Co., 2002-2003.
34. Peacock Jr., H. B., et. al., *Evaluation of Corrosion of Aluminum Based Reactor Fuel Cladding Materials During Dry Storage*, WSRC-TR-95-0345, Westinghouse Savannah River Company.
35. Lam, P, Sindelar, R, and Barrett, K., *Corrosion of Aluminum-Uranium Alloys in Water Vapor at 200°C*, WSRC-MS-98-00858, Westinghouse Savannah River Company.

3.5.2 Computer Analysis Results

Due to the size and number of the output files associated with each analyzed condition, results from the computer analysis are provided on a CD-ROM.

3.5.3 Analytical Thermal Model

The analytical thermal model of the BRR package was developed for use with the Thermal Desktop[®] [22] and SINDA/FLUINT [23] computer programs. These programs are designed to function together to build, exercise, and post-process a thermal model. The Thermal Desktop[®] computer program is used to provide graphical input and output display function, as well as computing the radiation exchange conductors for the defined geometry and optical properties. Thermal Desktop[®] is designed to run as an AutoCAD[®] application. As such, all of the CAD tools available for generating geometry within AutoCAD[®] can be used for generating a thermal model. In addition, the use of the AutoCAD[®] layers tool presents a convenient means of segregating the thermal model into its various elements.

The SINDA/FLUINT computer program is a general purpose code that handles problems defined in finite difference (i.e., lumped parameter) and/or finite element terms and can be used to compute the steady-state and transient behavior of the modeled system. Although the code can be used to solve any physical problem governed by diffusion-type equations, specialized functions used to address the physics of heat transfer and fluid flow make the code primarily a thermal code.

The SINDA/FLUINT and Thermal Desktop[®] computer programs have been validated for safety basis evaluations for nuclear related projects [24].

Together, the Thermal Desktop[®] and SINDA/FLUINT codes provide the capability to simulate steady-state and transient temperatures using temperature dependent material properties and heat transfer via conduction, convection, and radiation. Complex algorithms may be programmed into the solution process for the purposes of computing heat transfer coefficients as a function of the local geometry, gas thermal properties as a function of species content, temperature, and pressure, or, for example, to estimate the effects of buoyancy driven heat transfer as a function of density differences and flow geometry.

3.5.3.1 Description of BRR Packaging Thermal Model for NCT Conditions

The BRR packaging is represented by a 3-dimensional, half symmetry thermal model for the NCT evaluations. This modeling choice captures the full height of the packaging components and allows the incorporation of the varying insolation loads that will occur along the length of the package, the various degrees of symmetry within the fuel baskets, and the non-symmetry of the HAC free drop damage. The various packaging components are defined using a combination of planar and solid elements. Program features within the Thermal Desktop[®] computer program automatically compute the various areas, lengths, thermal conductors, and view factors involved in determining the individual elements that make up the thermal model of the complete assembly.

It should be noted that the NCT thermal model described below is based on an earlier design that used 6 instead of the current 8 attachment lugs per limiter, lug plates that are 0.38-inches thick by 2.75-inches wide vs. the current 0.5-inches thick by 3.63-inches wide, and a 0.25-inch vs. 0.125-inch radial gap between the limiter and the cask shell. Since these variations from the current design result in a lower surface area for heat dissipation to the ambient, the predicted NCT temperatures will be slightly higher than those expected for the current design. Because of this conservatism, the results are valid for the safety evaluations under NCT conditions. The design variations are incorporated for the HAC evaluations.

Figure 3.5-1 to Figure 3.5-5 illustrates 'solid' views of the BRR packaging thermal model. The model is composed of solid and plate type elements representing the various packaging components. Thermal communication between the various components is via conduction, radiation, and surface-to-surface contact. A total of approximately 20,500 nodes, 110 planar elements, and 4,900 solid elements are used to simulate the modeled components. Nearly 80 of the solid elements are finite difference solids (i.e., FD solids), a Thermal Desktop[®] computer program feature that permits a group of solid elements to be represented by a single entity. As such, the number of individual solid 'bricks' utilized in the modeling is actually significantly larger than the 4,900 value indicated above. In addition, one boundary node is used to represent the ambient environment for convection purposes and two boundary nodes is used to represent the ambient temperature for the purpose of radiation heat transfer. The use of separate boundary nodes for radiation heat transfer allows the model to capture the effective emissivity of the ambient environment.

As seen from Figure 3.5-1, the modeling accurately captures the geometry of the various components of the packaging, including the impact limiters, the inner and outer shells, the upper and lower end structures, the closure lid and shield plug, and lead sections. Also captured, but not easily seen in the figure due to the scale of the figures, is the thermal shield and the impact limiter attachment lugs. The minimal spatial resolution provided by the thermal modeling for the cask body components is approximately 1.75 inches in the radial direction, 2 inches in the axial direction, and every 10° in the circumferential direction. Greater spatial resolution (i.e., smaller radial and axial distances) is provided near the cask ends where larger thermal gradients are expected. A slightly lower spatial resolution is provided for the exterior portions of the impact limiters since the relatively low thermal conductivity of the polyurethane foam will yield correspondingly low heat flows.

Figure 3.5-2 illustrates the thermal modeling used for the various stainless steel components of the BRR cask body, while Figure 3.5-3 illustrates the thermal modeling of the lead structures within the cask body. The figures demonstrate that the geometry of the cask components is accurately captured by the thermal modeling.

Figure 3.5-4 illustrates the modeling used for the shell of the shield plug. While the height, radius, and shell thickness of the shield plug are accurately captured, the diagonal pipe and 4° taper are not included for modeling simplicity and because these details have no significant effect on the thermal performance of the packaging. Although the lead sheets used to fill the shield plug cavity are to be oversized and then hammered into place, the thermal modeling conservatively assumes a small (i.e., 0.0625-inch) uniform gap exists between the lead sheets and the shield plug shell.

The thermal modeling of the impact limiters, as illustrated in Figure 3.5-5, accurately captures the compound shape of the limiter's inner shell and the placement of the attachment lugs. Since the fabrication tolerance of the polyurethane foam used to fill the impact limiters can yield foam densities that are $\pm 15\%$ of the targeted $9 \text{ lb}_m/\text{ft}^3$ (pcf) foam density and since the foam's conductivity is a function of its density, the thermal modeling conservatively assumes a low tolerance foam density (i.e., 9 pcf less $15\% \approx 7.65$ pcf) for NCT evaluations and a high tolerance foam density (i.e., 9 pcf plus $15\% \approx 10.35$ pcf) for HAC evaluations.

3.5.3.2 Description of MURR Fuel and Basket Thermal Model

Figure 3.5-6 illustrates the thermal modeling of the MURR fuel basket and fuel element used for this evaluation. Approximately 2,600 nodes, 160 planar elements, and 1,000 solid elements are used to simulate the modeled components of the fuel basket, while approximately 3,300 nodes, 340 planar elements, and 550 solid elements are used to simulate the modeled components of each MURR fuel element.

The fuel basket modeling captures the inner and outer shells, the plates used to section off or divide the basket into compartments to house the individual fuel elements, and the base. While the inner shell and the divider plates are simulated using solid elements, the 0.25-inch thick outer shell and the base plates are represented by planar elements since the temperature difference though their thickness will be small. All of the basket components are assumed to be Type 304 stainless steel. The fuel elements are assumed to be essentially centered within in each compartment with the heat transfer between the fuel elements and the basket assumed to be via conduction and radiation across the separation gap and via contact with the plate supporting the fuel elements.

The fuel element simulation includes separate representation of the twenty-four (24) curved composite fuel plates, the side plates, and the upper and lower end box castings. Heat transfer between the individual fuel plates is simulated via conduction and radiation, while the heat transfer between the fuel plates and the side plates is via radiation and conduction through the crimped edges. The size, curvature, distance between the fuel plates, and the composite thermal properties of the plates are based on the information presented in Appendix 3.5.3.9, *Determination of Composite Thermal Properties for Fuel Plates*. The decay heat loading for the fuel elements is applied as a surface heat flux over the active fuel length of the plates.

Heat transfer between the fuel basket and the BRR packaging is assumed to be via conduction and radiation across the assumed uniform gap between the basket and the inner shell of the packaging. Direct contact is assumed between the base of the fuel basket and the base of the cask cavity. Because of the combination of decay heat and the criterion to limit the maximum fuel plate temperature to $400 \text{ }^\circ\text{F}$ or less (see Section 3.2.2), the BRR cask cavity is to be filled with helium gas at a pressure of one atmosphere following the draining and drying process.

3.5.3.3 Description of MITR-II Fuel and Basket Thermal Model

Figure 3.5-7 illustrates the thermal modeling of the MITR-II fuel basket and fuel element used for this evaluation, while Figure 3.5-8 illustrates the solids modeling used to represent the void spaces between the fuel tubes. Approximately 2,650 nodes, 170 planar elements, and 400 solid elements are used to simulate the modeled components of the fuel basket, while approximately 1,480

nodes, 75 planar elements, and 230 solid elements are used to simulate the modeled components of each MITR-II fuel element.

The fuel basket modeling captures the thin shell tubes used to house the fuel elements, the stiffening ribs/plates, and the base shell. All of the basket components are assumed to be Type 304 stainless steel. The fuel elements are assumed to be essentially centered within in each compartment with the heat transfer between the fuel elements and the basket assumed to be via conduction and radiation across the separation gap and via contact with the plate supporting the fuel elements.

The fuel element simulation includes separate representation of the fifteen (15) composite fuel plates, the side plates, and the upper and lower end box castings. Heat transfer between the individual fuel plates is simulated via conduction and radiation, while the heat transfer between the fuel plates and the side plates is via radiation and conduction through the crimped edges. The size, distance between the fuel plates, and the composite thermal properties of the plates are based on the information presented in Appendix 3.5.3.9, *Determination of Composite Thermal Properties for Fuel Plates*. The decay heat loading for the fuel elements is applied as a uniform surface heat flux over the active fuel length of the plates.

Heat transfer between the fuel basket and the BRR packaging is assumed to be via a combination of conduction and radiation across the gaps between the various basket surfaces and the inner shell of the packaging. The cask cavity is to be filled with helium gas to limit the maximum fuel plate temperature to 400 °F or less (see Section 3.2.2).

3.5.3.4 Description of ATR Fuel and Basket Thermal Model

Figure 3.5-9 illustrates the thermal modeling of the ATR fuel basket and fuel element used for this evaluation. Approximately 3,000 nodes, 50 planar elements, and 90 FD solid elements are used to simulate the modeled components of the fuel basket, while approximately 3,300 nodes, 95 planar elements, and 325 solid elements are used to simulate the modeled components of each ATR fuel element. As previously explained, an FD solid is a Thermal Desktop[®] computer program feature that permits a group of solid elements to be represented by a single entity. As such, the number of individual solid ‘bricks’ utilized in the modeling of the ATR fuel basket is actually significantly larger than 90.

The fuel basket modeling captures the inner and outer shells, the plates used to section off or divide the basket into compartments to house the individual fuel elements, the stiffening ribs, and the base. All of the basket components are assumed to be Type 304 stainless steel. The fuel elements are assumed to be essentially centered within in each compartment with the heat transfer between the fuel elements and the basket assumed to be via conduction and radiation across the separation gap.

The fuel element simulation includes separate representation of the nineteen (19) curved composite fuel plates and the side plates (including the cutouts). The upper and lower end boxes are to be removed prior to loading of the fuel assemblies within the basket. Heat transfer between the individual fuel plates is simulated via conduction and radiation, while the heat transfer between the fuel plates and the side plates is via radiation and conduction through the crimped edges. The size, curvature, distance between the fuel plates, and the composite thermal properties of the plates are based on the information presented in Appendix 3.5.3.9,

Determination of Composite Thermal Properties for Fuel Plates The decay heat loading for the fuel elements is applied as a uniform surface heat flux over the active fuel length of the plates.

Heat transfer between the fuel basket and the BRR packaging is assumed to be via a combination of conduction and radiation across the gaps between the various basket surfaces and the inner shell of the packaging. The thermal evaluations assume the cask cavity is filled with helium gas.

3.5.3.5 Description of TRIGA Fuel and Basket Thermal Model

Figure 3.5-10 illustrates the thermal modeling of the TRIGA fuel basket and fuel element used for this evaluation, while Figure 3.5-11 illustrates the solids modeling used to represent the void spaces between the fuel tubes. Approximately 7,500 nodes, 60 planar elements, and 1,000 solid elements are used to simulate the modeled components of the fuel basket, while approximately 1,030 nodes and 7 FD solid elements are used to simulate the modeled components of each TRIGA fuel element. As previously explained, an FD solid is a Thermal Desktop[®] computer program feature that permits a group of solid elements to be represented by a single entity. As such, the number of individual solid ‘bricks’ utilized in the modeling of each TRIGA fuel element is actually significantly larger than 7.

The fuel basket modeling captures the individual tubes used to house each fuel element, stiffening ribs, and the spacers used to position the shorter length fuel elements within the basket. All of the basket components are assumed to be fabricated of Type 304 stainless steel. The fuel elements are assumed to be essentially centered within in each compartment with the heat transfer between the fuel elements and the basket assumed to be via conduction and radiation across the separation gap and via contact with the plate supporting the fuel elements.

The fuel element simulation includes separate representation of the uranium zirconium hydride metal section, the graphite section, and the upper and lower end fittings. Since the temperature difference across the fuel cladding is small for the decay heats involved, the cladding is not modeled separately. The TRIGA fuel has two design active fuel lengths; 14 and 15 inches. The decay heat loading for the fuel elements is applied as a uniform volumetric heat flux over the active fuel length. The modeling assumes the shorter length to conservatively bound the maximum volumetric heat generation.

Heat transfer between the fuel basket and the BRR packaging is assumed to be via a combination of conduction and radiation across the gaps between the various basket surfaces and the inner shell of the packaging. The thermal evaluations assume the cask cavity is filled with helium.

3.5.3.6 Insolation Loads

The insolation loading on the BRR package is based on the 10CFR71.71(c)(1) specified insolation values over a 24-hour period. Since the BRR packaging is characterized by thermally massive shells and large foam filled impact limiters, the interior temperatures of the packaging will be effectively ‘decoupled’ from the diurnal changes in insolation loading. As such, a steady-state thermal model based on the application of the 10CFR71.71(c)(1) specified insolation values averaged over 24 hours is used to evaluate the design basis package temperatures under NCT conditions.

3.5.3.7 Description of Thermal Model for HAC Conditions

The thermal evaluations for the hypothetical accident condition (HAC) are conducted using an analytical thermal model of the BRR package. The HAC thermal model is a modified version of the half symmetry NCT model described above. The principal model modifications consist of simulating the expected package damage resulting from the drop events that are assumed to precede the HAC fire, changing the package surface emissivities to reflect the assumed presence of soot and/or surface oxidization, and simulating the thermal performance of the polyurethane foam used in the impact limiters.

Physical testing using a half scale certification test unit (CTU) is used to establish the expected level of damage sustained by the BRR packaging as a result of the 10 CFR 71.73 prescribed free and puncture drops that are assumed to precede the HAC fire event. The configuration and initial conditions of the test article, a description of the test facility, test article instrumentation, and the test results are documented Section 2.12.3, *Certification Test Results*. The drop tests covered a range of hypothetical free drop orientations and puncture bar drops. An overview of the results of the drop tests is provided below. For full details, including photographs and figures, see Section 2.12.3, *Certification Test Results*. It should be noted that all of the noted dimensions in this discussion are for the half scale model and need to be doubled to yield the equivalent full scale results.

- 1) The worst case physical damage to the exterior of the package occurs from an oblique slap down free drop. Overall, the resulting damage is thermally insignificant: an inward crush of approximately 4 inches and two small breaches in the joint along the outer diameter of the limiter. However, a subsequent drop on a puncture bar caught the fold in the limiter shell created by the oblique slap down drop and tore the damaged joint open. The total chord length of the damaged area measured approximately 26 inches. The width of the opening at the center was 5 inches and tapering to nearly zero at the ends. The chord length of the flap opening is approximately 22.6 inches. Negligible amounts of foam were lost from the limiter from the opening.
- 2) The CG over corner drop resulted in a crush distance of 5.5 inches. A subsequent puncture bar drop on the damage area resulted in the partial penetration of the shell. The puncture bar penetrated the underlying foam to a depth of 2-1/4 inches. The width of the breach/torn flap in the limiter shell was 4 inches and its length was 5 inches.
- 3) The vertical end drop resulted in impact limiter deformation that was a combination of outside-in and inside-out. The drop resulted in no tearing of the limiter shell and no exposure of the underlying foam. The crush distance was 3.4 inches. A subsequent puncture bar drop on the damaged area created a dent approximately 1-3/4 inches deep. One or two rebound impacts also occurred with negligible deformation. There were no signs of cracking in the dent or in the nearby weld seam.
- 4) The drop testing showed the original impact limiter attachment design was not adequate to fully retain the impact limiters on the package for the slapdown free drop event. The attachments were redesigned and retested to ensure complete attachment of the limiters. See Section 2.12.3, *Certification Test Results*, for further discussion.
- 5) No deformation of the impact limiter inner shell was noted.

Subsequent to the drop test, the impact limiter design was modified to improve its performance. These modifications increased the number of attachment lugs from 6 to 8 per limiter, increased the size and thickness of each lug from 0.38-inches thick by 2.75-inches wide to 0.5-inches thick by 3.63-inches wide, increased the size of the attachment pins, reduced the gap between the cask and the impact limiter inner shell from 0.25 to 0.125 inches, and a re-design of the limiter joint that cracked under the side/slap down drop (see Item 1 above).

Besides scaling the noted crush dimensions to the full scale design, the projected damage also needs to reflect the effect of temperature on the polyurethane foam's structural properties since the drop test was conducted under cold conditions and the worst case crush will arise under warm conditions. Figure 3.5-12 depicts the predicted crush depths under hot conditions for the vertical end, C.G. over corner, and side/slap down drop orientations based on an evaluation presented in Section 2.12.5, *Impact Limiter Performance Evaluation*. As seen from the figure, the side/slap down drop orientation is predicted to result in both the greatest crush depth and the closest approach to the inner shell of the limiter. Per Appendix 3.5.4, *'Last-A-Foam' Response under HAC Conditions*, approximately 3.5 to 3.8 inches of the nominally 9 pcf polyurethane foam will decompose during a 30 minute HAC fire event. This foam loss (or recession depth) will be even less for foam in the vicinity of crush damage since its effective density will have increased as a result of the crush damage. Any foam depths greater than 4 inches remaining after the HAC drop events will result in the underlying temperatures rising only marginally during the HAC fire event. Examination of Figure 3.5-12 demonstrates that the vertical end drop and C.G. over corner drops will leave more than 4 inches of foam everywhere, even without credit for increased foam density due to crush. As such, the side/slap down drop event is selected as the controlling scenario for impact limiter damage for the HAC evaluations.

The controlling puncture bar damage is determined from the half-scale drop results described in Section 2.12.3, *Certification Test Results*. Since the polyurethane foam forms an intumescent char that swells and tends to fill voids or gaps created by the puncture bar damage, the level of damage incurred by direct attack to the impact limiter's exterior shell would be thermally insignificant. An untested puncture bar scenario consisting of an impact to the thermal shield of the cask is also considered. This type of impact can be expected to cause a local depression in the thermal shield and potentially a small tear. However, overall, the thermal shield would retain its functionality with the region of elevated temperatures being localized to the size of the puncture bar and similar in temperature level to that seen at the impact limiter attachment lug locations. Therefore, the controlling puncture bar damage is assumed to be an attack on the impact limiter skin joint that tears a flap type opening in the limiter skin (see Item 1 above). While the re-design of the impact limiters following the drop tests is expected to eliminate this type of damage, it is assumed for the HAC evaluation to conservatively bound all other potential puncture bar damage scenarios.

Based on the above observations and the general assumptions for the package condition for the HAC evaluations, the NCT thermal model described above was modified for the HAC evaluations via the following steps:

- 1) Assume the package has been ejected from its support stand and is lying on its side. As such, the convective heat transfer from the package's exterior surfaces is based on a horizontal orientation. In addition, the adiabatic boundary condition assumed for selected surfaces of the lower impact limiter under NCT conditions are switched to active heat transfer surfaces.
- 2) The surface emissivity for all exterior surfaces is assumed to be 0.9 to account for potential oxidation and/or soot accumulation. The emissivity of all inside surfaces of the impact limiter exposed as the result of foam decomposition is assumed to be 0.95 to account for adherence of foam char.
- 3) The small, uniform gap conservatively assumed between the lead and the outer shell under NCT conditions is eliminated to maximize the heat flow into package.
- 4) Thermal conductance via the stand-off strips under the thermal shield is assumed for the HAC condition. Thermal credit for the stand-off strips was conservatively ignored for the NCT evaluations.
- 5) The number and size of the impact limiter attachments are increased for the HAC evaluation to reflect the re-design of the impact limiter following the drop testing. The NCT evaluations ignored this change since neglecting the added surface area yields conservative results.
- 6) A minimum of 3.8 inches of foam is removed from around the perimeter of the impact limiters at the start of the HAC evaluation. This change conservatively bounds the impact of the gradual decomposition of the foam over the 30 minute fire event. The conductivity of the remaining foam is set to that associated with foam fabricated at the high end of the density tolerance range (i.e., 9 pcf + 15%) in order to conservatively bound the heat transfer into the package.
- 7) Simulate the sideways crushing of the upper and lower impact limiters under hot drop conditions. This consisted of removing approximately 15.8 inches from one side of the impact limiters.
- 8) Simulate the conservative assumption that a puncture bar attack tears a flap in the upper impact limiter. This consisted of removing a total of 6.1 inches of foam over a 60° segment of the impact limiter to conservatively capture the additional recession depth over 3.8 inches that may occur due to the direct exposure of the foam surfaces to the flame (see Appendix 3.5.4, *'Last-A-Foam' Response under HAC Conditions*). Added radiation and convection conductors to the exposed region of the impact limiter's inner shell to reflect the conservative assumption that a flap opening has occurred in the upper impact limiter.
- 9) Simulated the possible shifting of the impact limiter by replacing the 0.125 inch nominal gap between the inner shell of the limiters and the cask shell with a direct contact conductance over an approximate 1 inch x 7.2 inch area (i.e., the modeled height of the cylindrical portion of the limiter's inner shell). The contact is placed in the center of the side drop foam crush damage and conservatively bounds the line-contact expected between two cylindrical bodies with no deformation.

Figure 3.5-13 illustrates the revised thermal model of the impact limiters used for the HAC evaluations. All other aspects of the BRR packaging remain the same as used for the NCT thermal evaluations.

3.5.3.8 Convection Coefficient Calculation

The BRR package thermal model uses semi-empirical relationships to determine the level of convection heat transfer from the exterior package surfaces under both the regulatory NCT and HAC conditions. The convective heat transfer coefficient, h_c , has a form of:

$$h_c = Nu \frac{k}{L}$$

where k is the thermal conductivity of the gas at the mean film temperature and L is the characteristic length of the vertical or horizontal surface. The convection coefficient is correlated via semi-empirical relationships against the local Rayleigh number and the characteristic length. The Rayleigh number is defined as:

where
$$Ra_L = \frac{\rho^2 g_c \beta L^3 \Delta T}{\mu^2} \times Pr$$

- g_c = gravitational acceleration, 32.174 ft/s²
- β = coefficient of thermal expansion, °R⁻¹
- ΔT = temperature difference, °F
- ρ = density of air at the film temperature, lb_m/ft³
- μ = dynamic viscosity, lb_m/ft-s
- Pr = Prandtl number = ($c_p \mu$) / k
- L = characteristic length, ft
- k = thermal conductivity at film temp., Btu/ft-hr-°F
- c_p = specific heat, Btu/ lb_m -°F
- Ra_L = Rayleigh #, based on length ‘L’

Note that k , c_p , and μ are each a function of air temperature as taken from Table 3.2-3. Values for ρ are computed using the ideal gas law, β for an ideal gas is simply the inverse of the absolute temperature of the gas, and Pr is computed using the values for k , c_p , and μ from Table 3.2-3. Unit conversion factors are used as required to reconcile the units for the various properties used.

The natural convection from a discrete vertical surface is computed using Equations 4-13, 4-24, 4-31, and 4-33 of reference [19], which is applicable over the range $1 < \text{Rayleigh number (Ra)} < 10^{12}$:

$$Nu^T = \bar{C}_L Ra^{1/4}$$

$$\bar{C}_L = \frac{0.671}{\left(1 + (0.492/Pr)^{9/16}\right)^{4/9}}$$

$$Nu_L = \frac{2.0}{\ln(1 + 2.0/Nu^T)}$$

$$Nu_t = C_t^V Ra^{1/3} / \left(1 + 1.4 \times 10^9 Pr/Ra\right)$$

$$C_t^V = \frac{0.13 \text{Pr}^{0.22}}{(1 + 0.61 \text{Pr}^{0.81})^{0.42}}$$

$$\text{Nu} = \frac{h_c L}{k} = [(\text{Nu}_L)^6 + (\text{Nu}_t)^6]^{1/6}$$

The natural convection from a vertical cylindrical surface is computed by applying a correction factor to the laminar Nusselt number (Nu_L) determined using the same methodology and Nu_t for a vertical plate (see above). The characteristic dimension, L , is the height of the vertical cylinder and D is the cylinder's diameter. The correction factor as defined by Equations 4-44 of reference [19] is:

$$\text{Nu}_{L\text{-Cylinder}} = \frac{\delta}{\ln(1 + \delta)} \text{Nu}_{L\text{-Plate}}$$

$$\delta = \frac{1.8 \times L/D}{\text{Nu}_{\text{Plate}}^T}$$

$$\text{Nu}_{\text{Vert. Cylinder}} = \frac{h_c L}{k} = [(\text{Nu}_{L\text{-Cylinder}})^6 + (\text{Nu}_{t\text{-Plate}})^6]^{1/6}$$

Natural convection from horizontal surfaces is computed from Equations 4-13, 4-25, 4-39, and 4-40 of reference [19], where the characteristic dimension (L) is equal to the plate surface area divided by the plate perimeter. For a heated surface facing upwards or a cooled surface facing downwards and $\text{Ra} > 1$:

$$\text{Nu} = \frac{h_c L}{k} = [(\text{Nu}_L)^{10} + (\text{Nu}_t)^{10}]^{1/10}$$

$$\text{Nu}_L = \frac{1.4}{\ln\left(1 + 1.4 / \left(0.835 \times \bar{C}_L \text{Ra}^{1/4}\right)\right)}$$

$$\bar{C}_L = \frac{0.671}{\left(1 + (0.492/\text{Pr})^{9/16}\right)^{4/9}}$$

$$\text{Nu}_t = 0.14 \times \left(\frac{1 + 0.0107 \times \text{Pr}}{1 + 0.01 \times \text{Pr}}\right) \times \text{Ra}^{1/3}$$

For a heated surface facing downwards or a cooled surface facing upwards and $10^3 < \text{Ra} < 10^{10}$, the correlation is as follows:

$$\text{Nu} = \text{Nu}_L = \frac{2.5}{\ln(1 + 2.5/\text{Nu}^T)}$$

$$\text{Nu}^T = \frac{0.527}{\left(1 + (1.9/\text{Pr})^{9/10}\right)^{2/9}} \text{Ra}^{1/5}$$

Calculation of the convection coefficient from a horizontal cylindrical surface is computed using Equation 3-43, Chapter 1, from [26], where the characteristic length, D , is the outer diameter of the cylinder. This equation, applicable for $10^{-5} < Ra < 10^{12}$, is as follows:

$$Nu = \frac{h_c D}{k} = \left\{ 0.60 + \frac{0.387 Ra_D^{1/6}}{\left[1 + (0.559/Pr)^{9/16} \right]^{8/27}} \right\}^2$$

The forced convection coefficients applied during the HAC fire event are computed using the relationships in Table 6-5 of reference [25] for a flat surface, where the characteristic dimension (L) is equal to the length along the surface and the free stream flow velocity is V . The heat transfer coefficient is computed based on the local Reynolds number, where the Reynolds number is defined as:

$$Re_L = \frac{V \times \rho \times L}{\mu}$$

$$\text{For } Re < 5 \times 10^5 \text{ and } Pr > 0.1: Nu = 0.664 \times Re_L^{0.5} \times Pr^{0.33}$$

$$\text{For } Re > 5 \times 10^5 \text{ and } Pr > 0.5: Nu = 0.036 \times Pr^{0.33} \times [Re_L^{0.8} - 23,200]$$

Given the turbulent nature of the 30-minute fire event, a characteristic length of 0.25 feet is used for all surfaces to define the probable limited distance for boundary growth. Figure 3.5-14 presents an illustration of the level of convective heat transfer coefficient predicted by the above equation during the HAC transient.

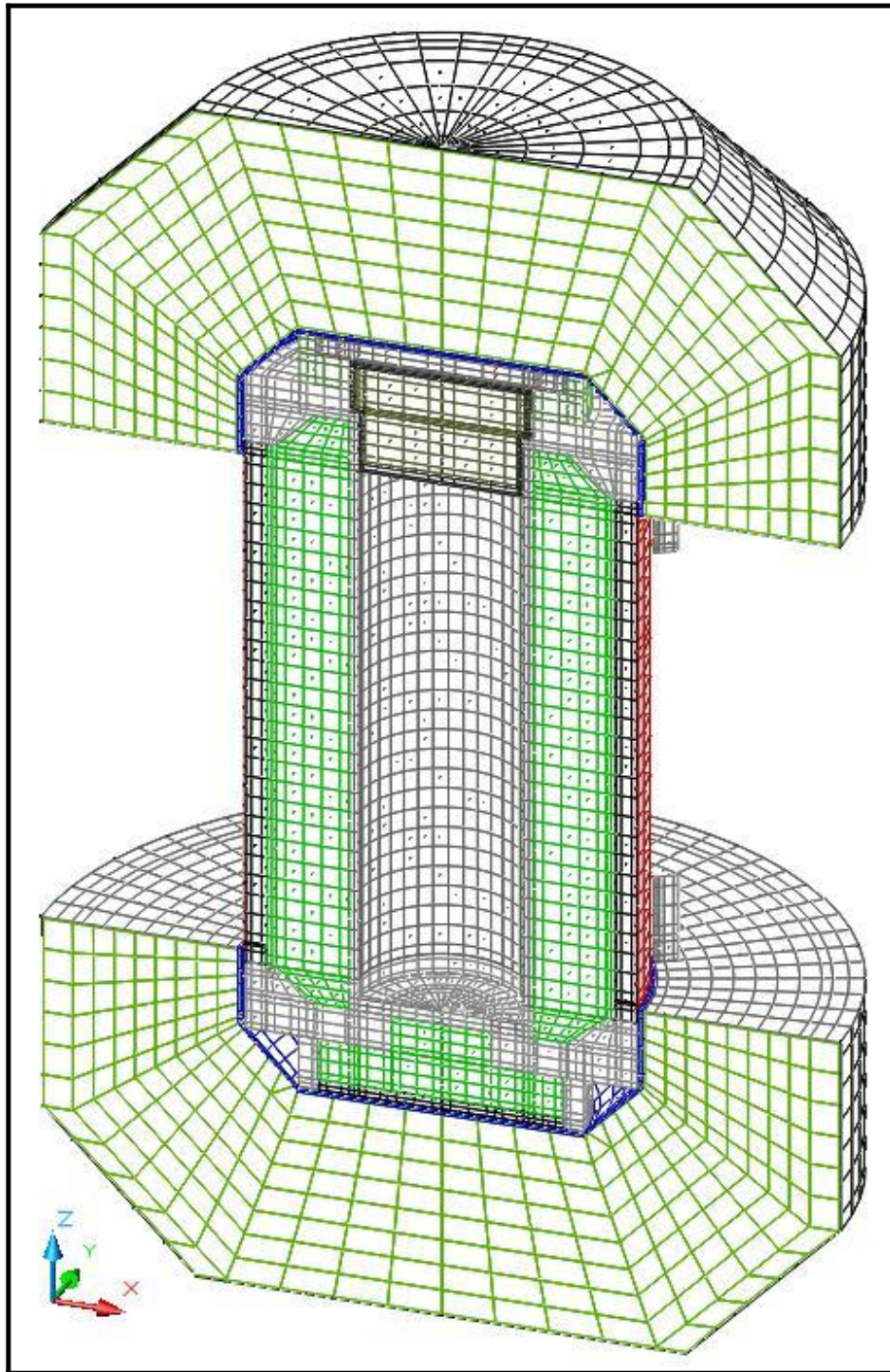


Figure 3.5-1 – Isometric View of ‘Solids’ Thermal Model for BRR Packaging

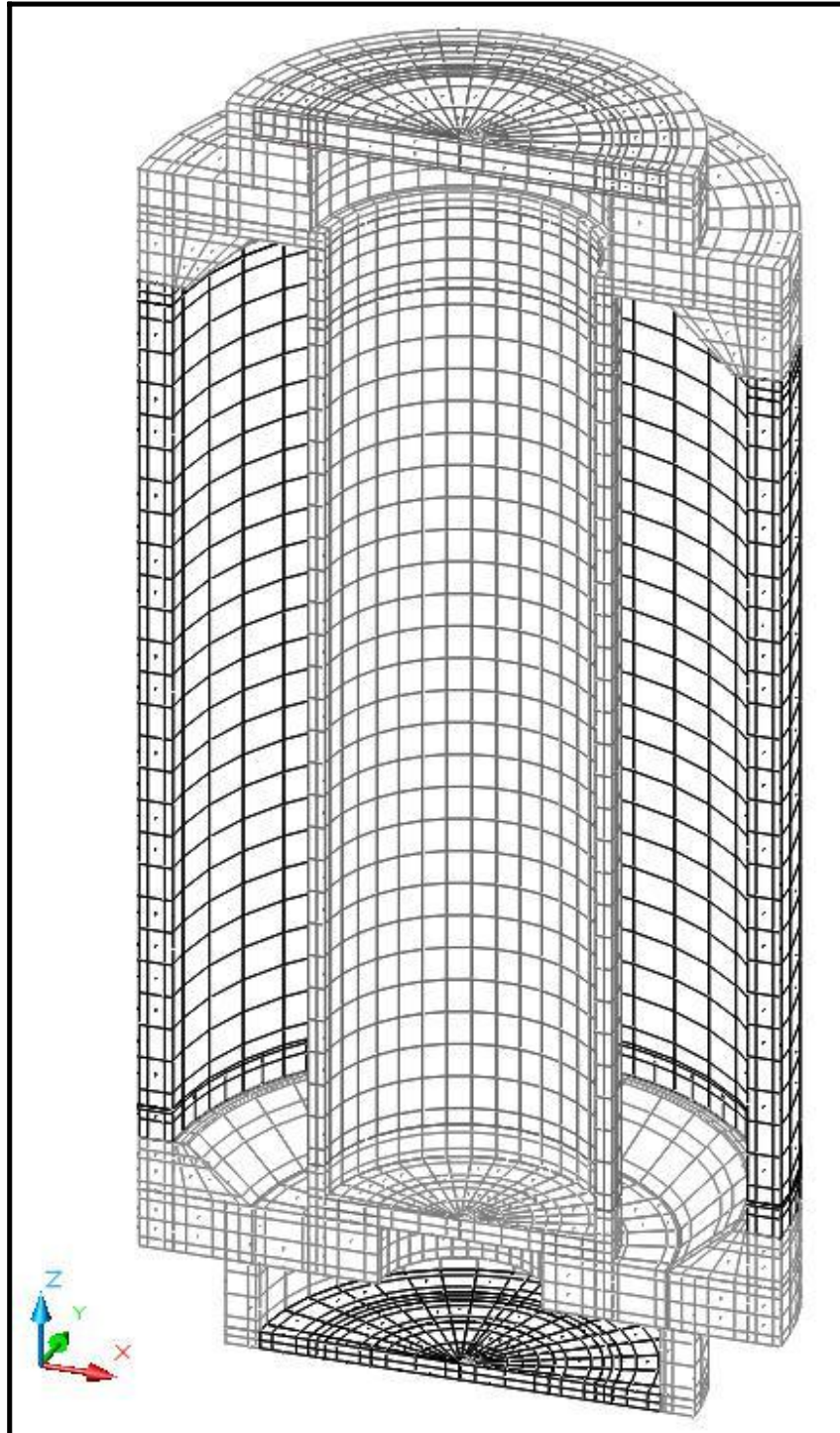


Figure 3.5-2 – Isometric View of ‘Solids’ Thermal Model for Inner/Outer Shells and Upper/Lower Structures

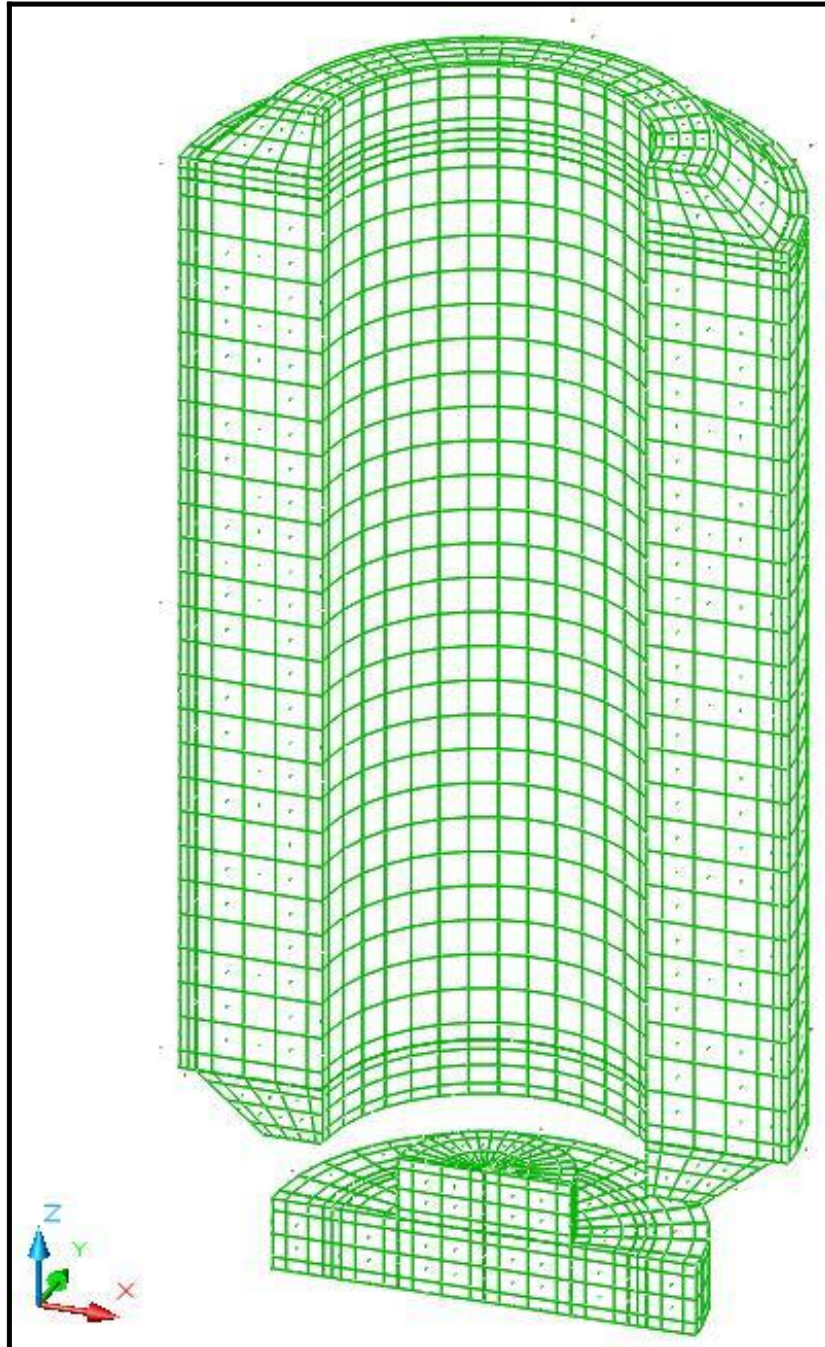


Figure 3.5-3 – Isometric View of ‘Solids’ Thermal Model for Cask Lead Sections

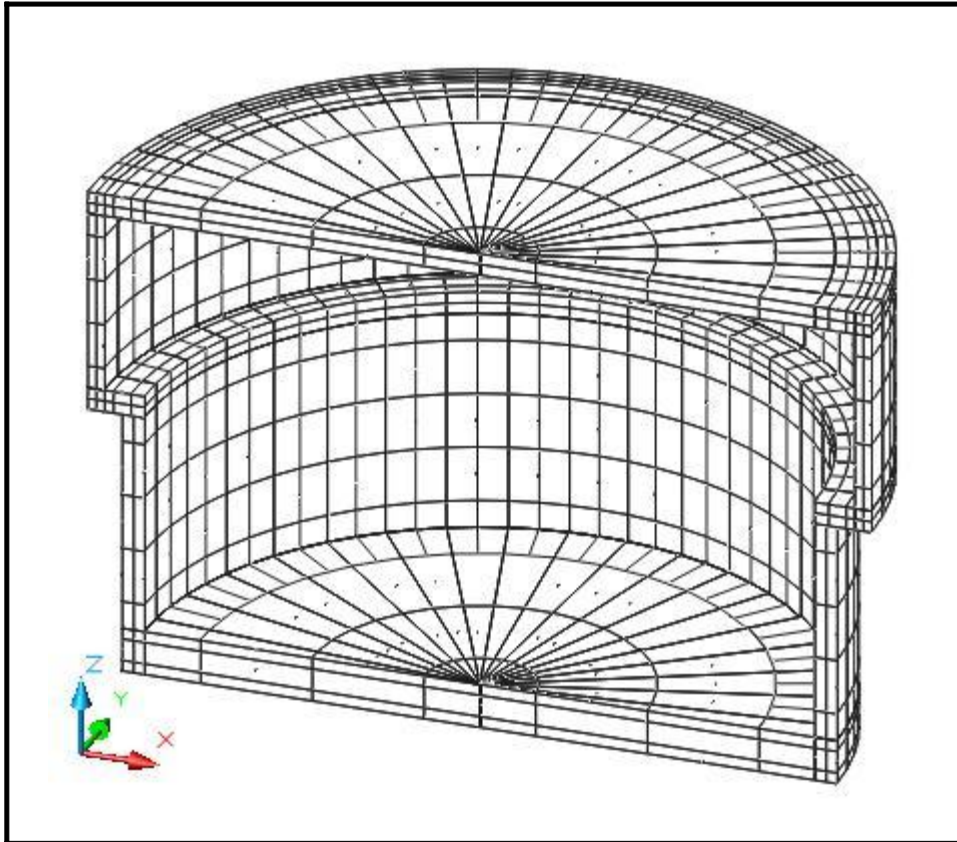


Figure 3.5-4 – Isometric View of ‘Solids’ Thermal Model for Shield Plug Shell

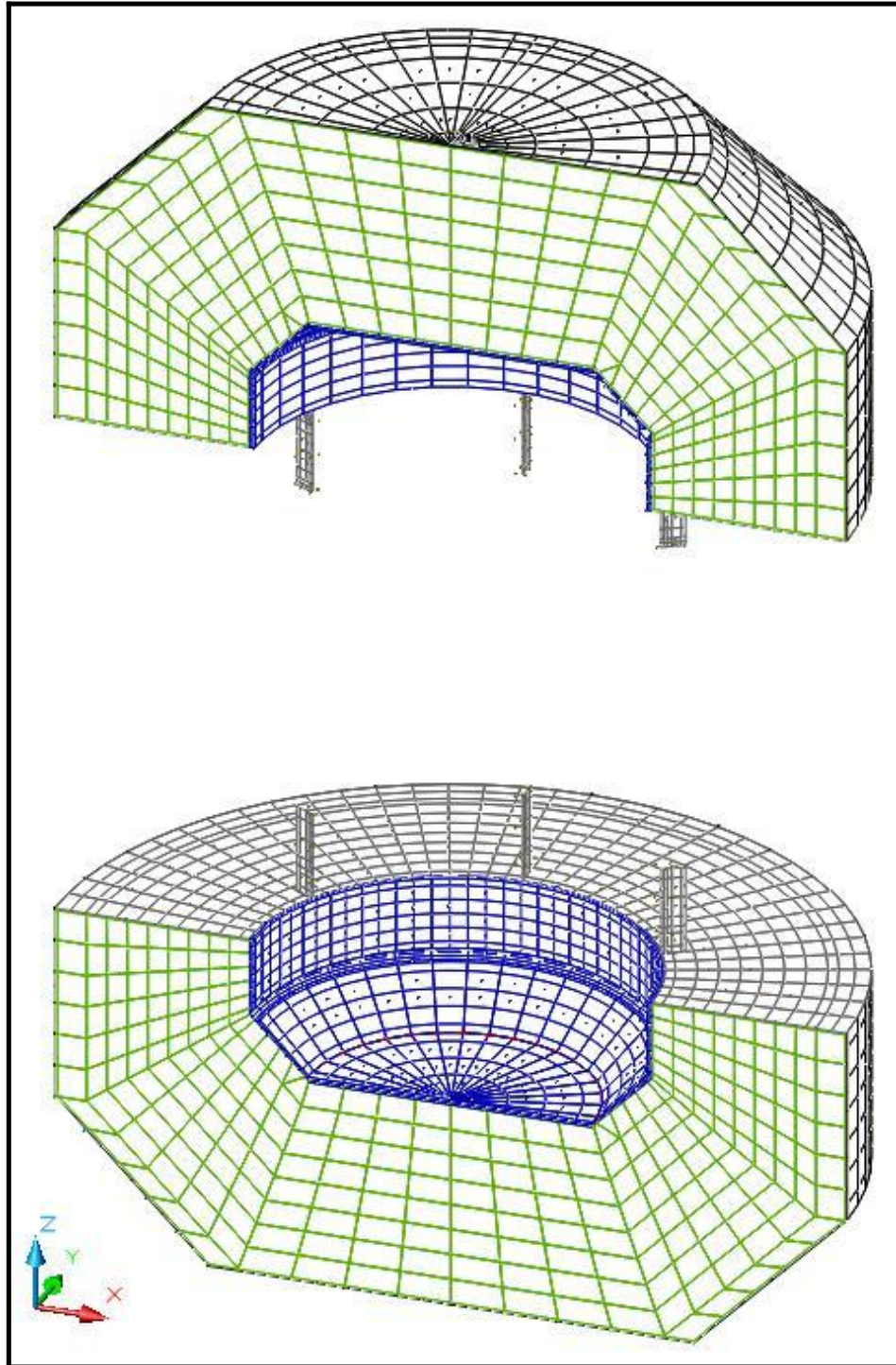


Figure 3.5-5 – Isometric View of ‘Solids’ Thermal Model for Impact Limiters

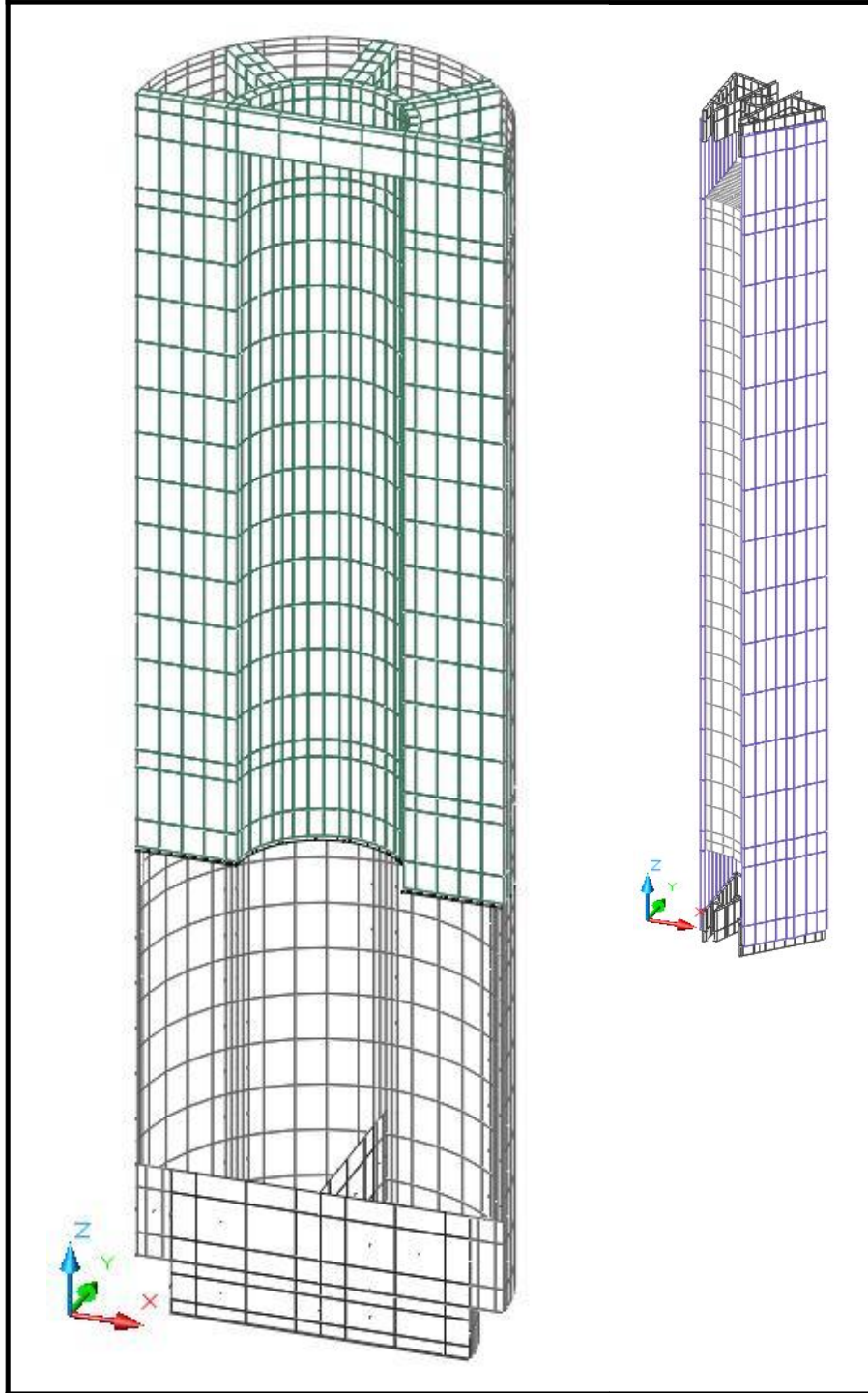


Figure 3.5-6 – Isometric View of ‘Solids’ Thermal Model for MURR Fuel Basket and Element

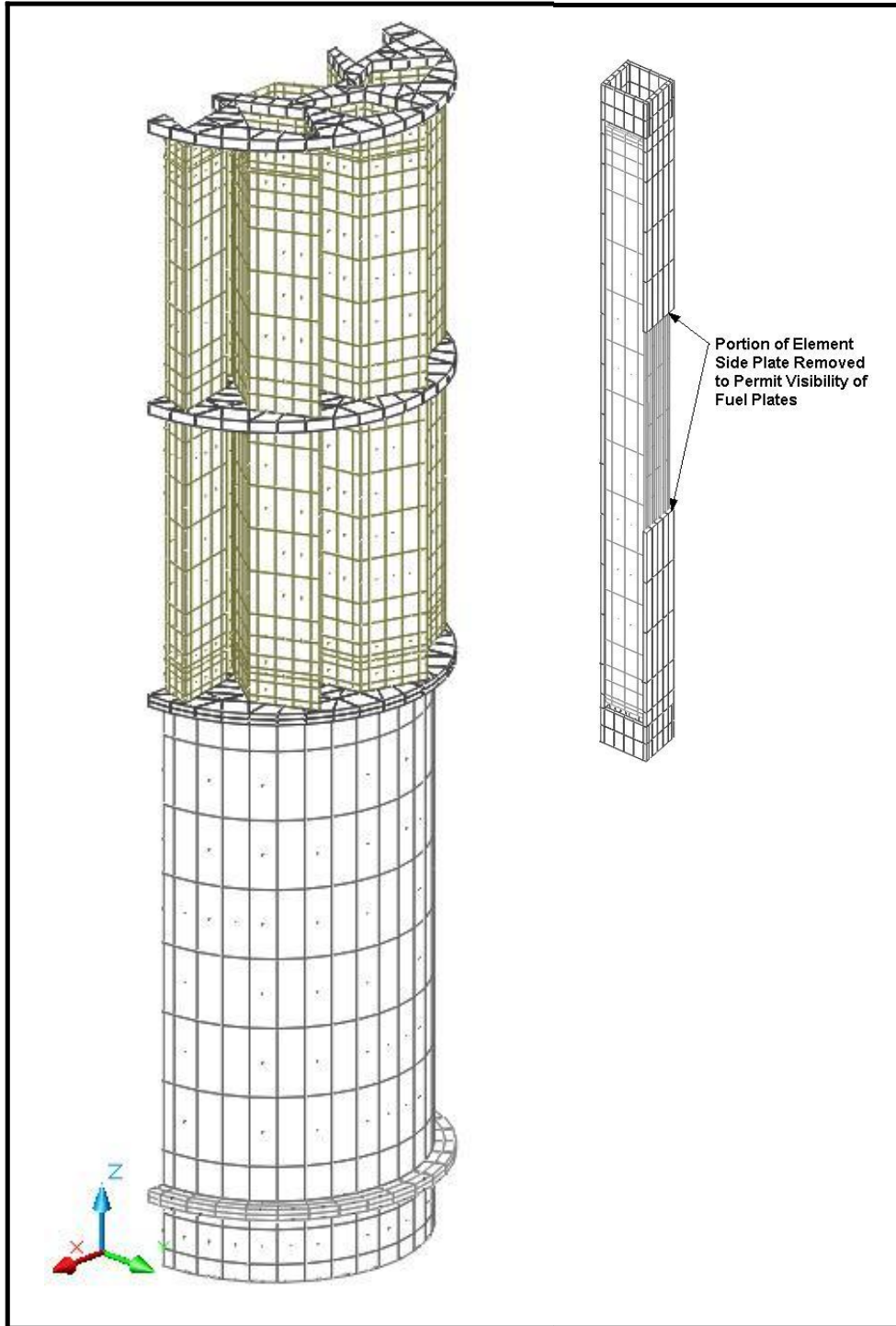


Figure 3.5-7 – Isometric View of ‘Solids’ Thermal Model for MITR-II Fuel Basket and Element

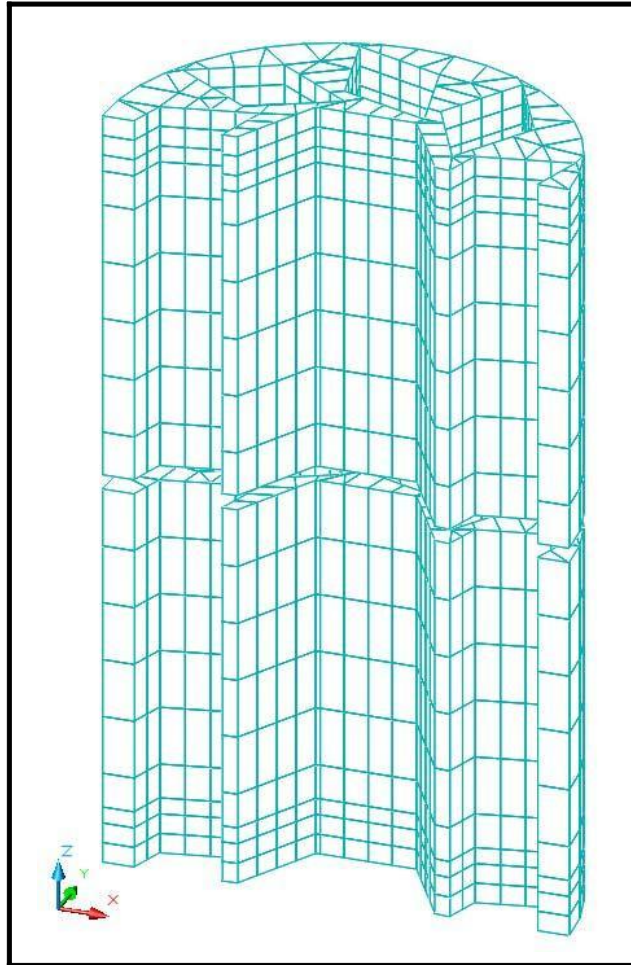


Figure 3.5-8 – Isometric View of ‘Void Space’ Modeling Between MITR-II Fuel Tubes

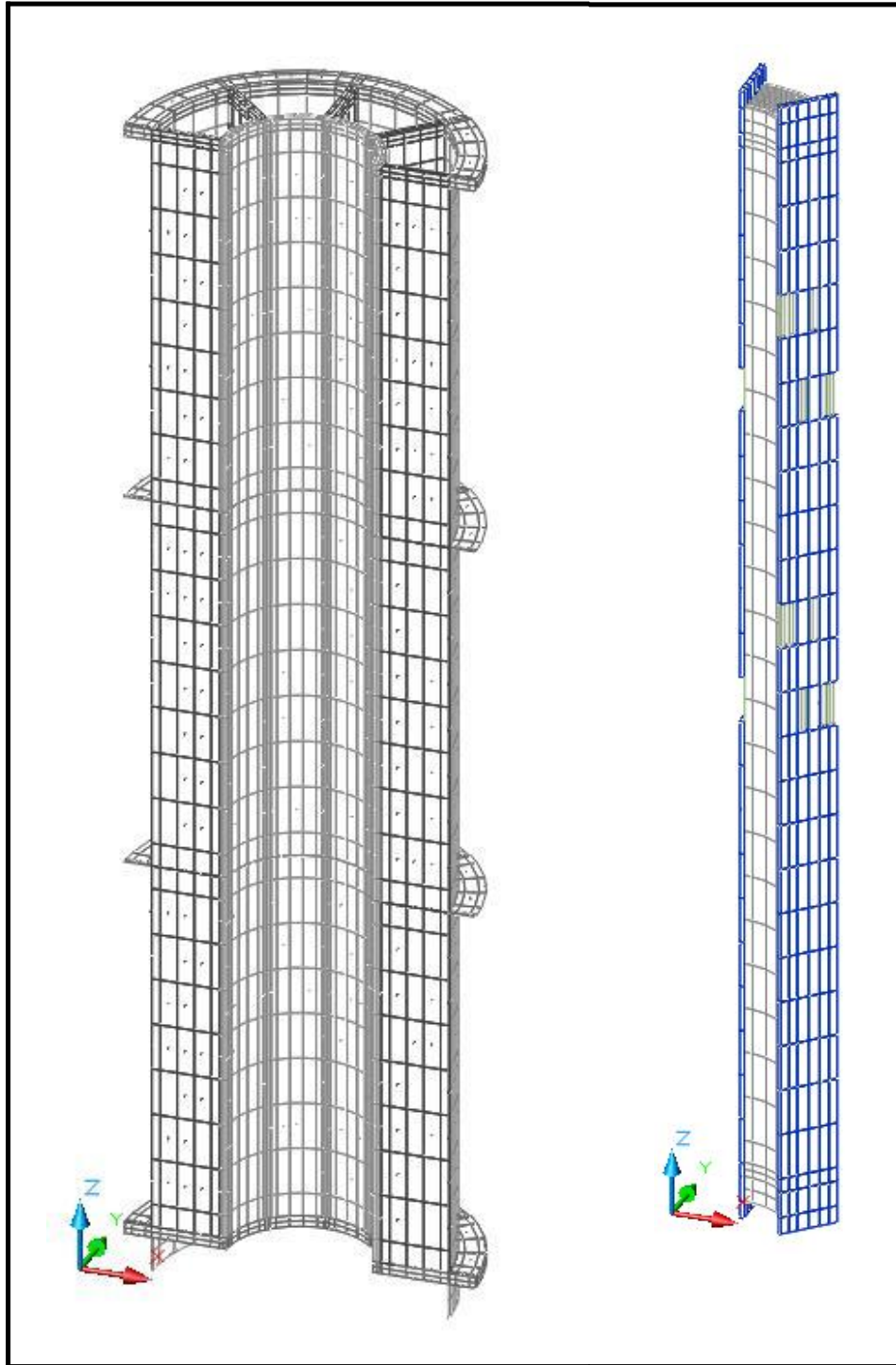


Figure 3.5-9 – Isometric View of ‘Solids’ Thermal Model for ATR Fuel Basket and Element

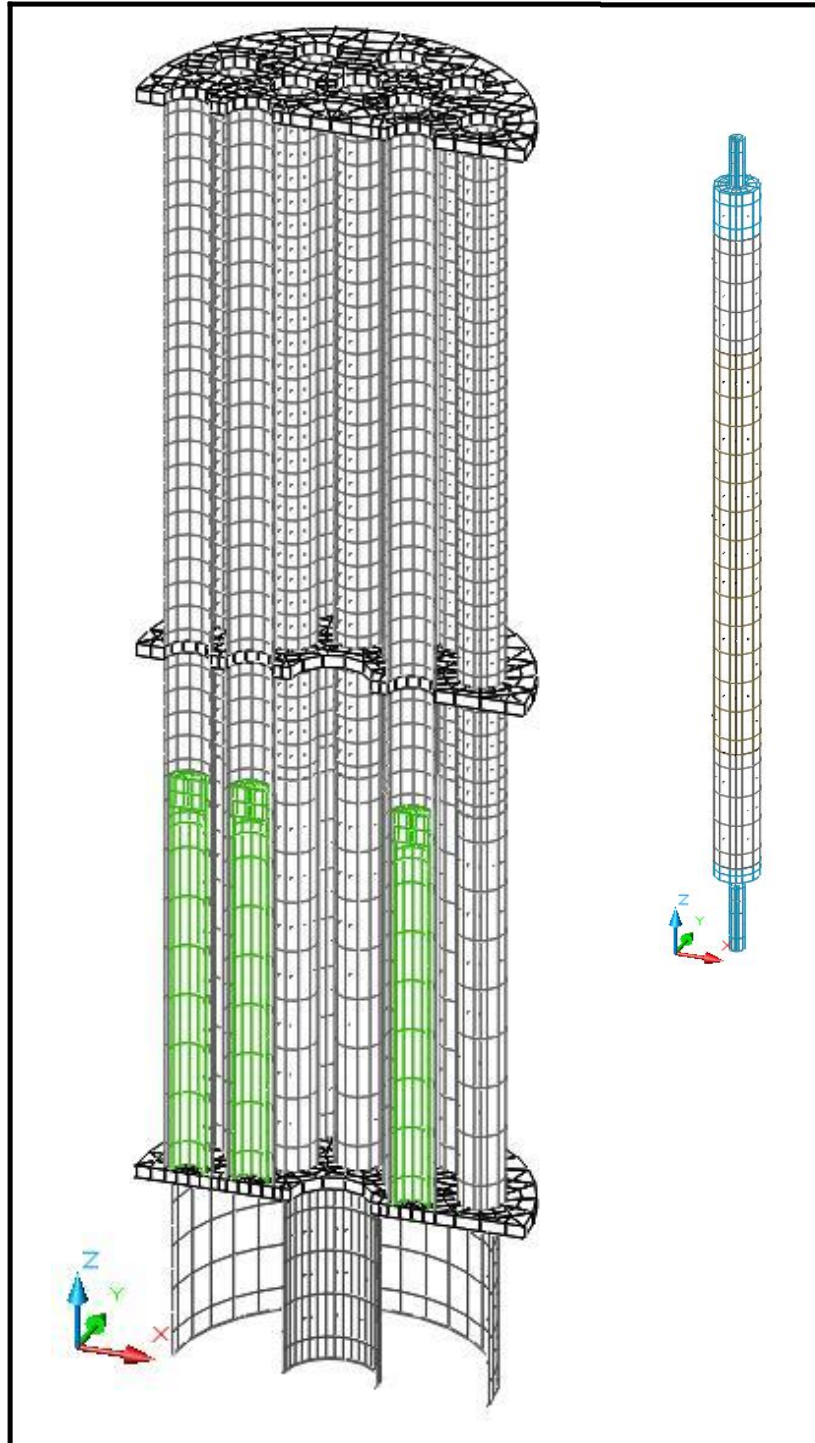


Figure 3.5-10 – Isometric View of ‘Solids’ Thermal Model for TRIGA Fuel Basket and Element

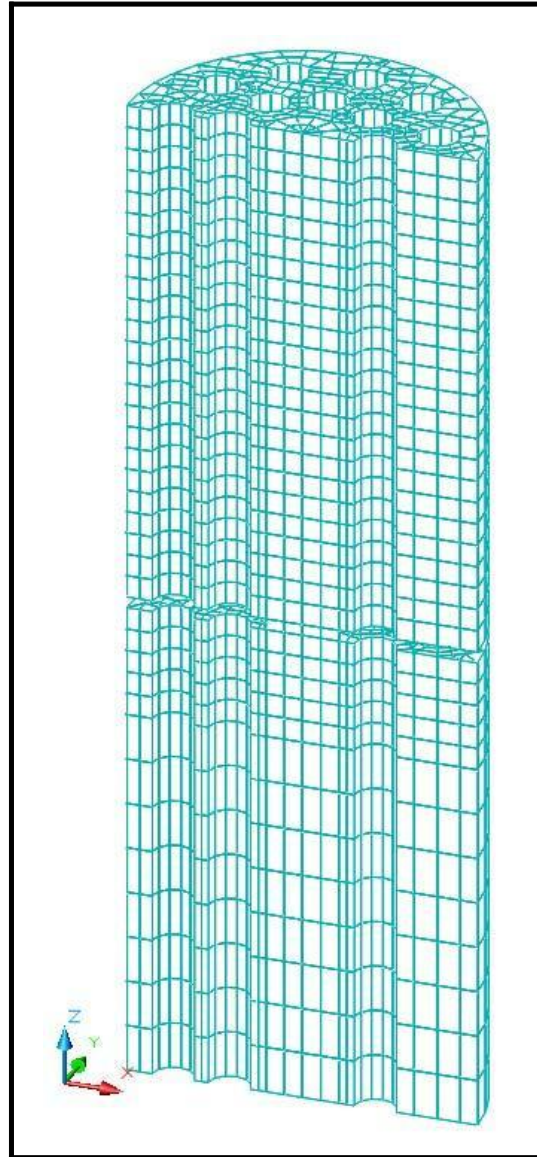


Figure 3.5-11 – Isometric View of ‘Void Space’ Modeling for TRIGA Basket

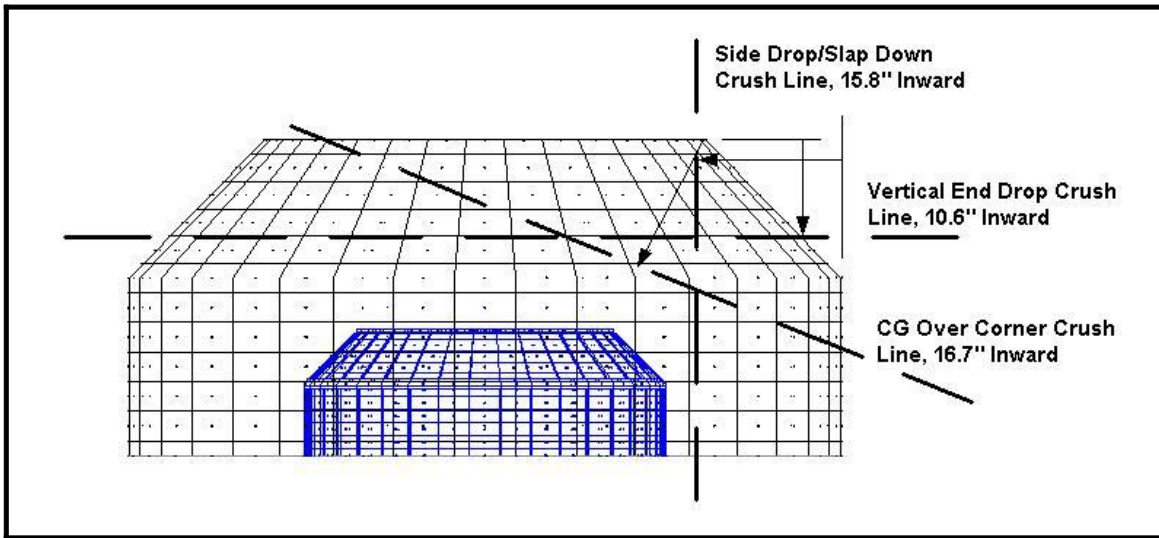


Figure 3.5-12 – Impact Limiter HAC Drop Crush Distances

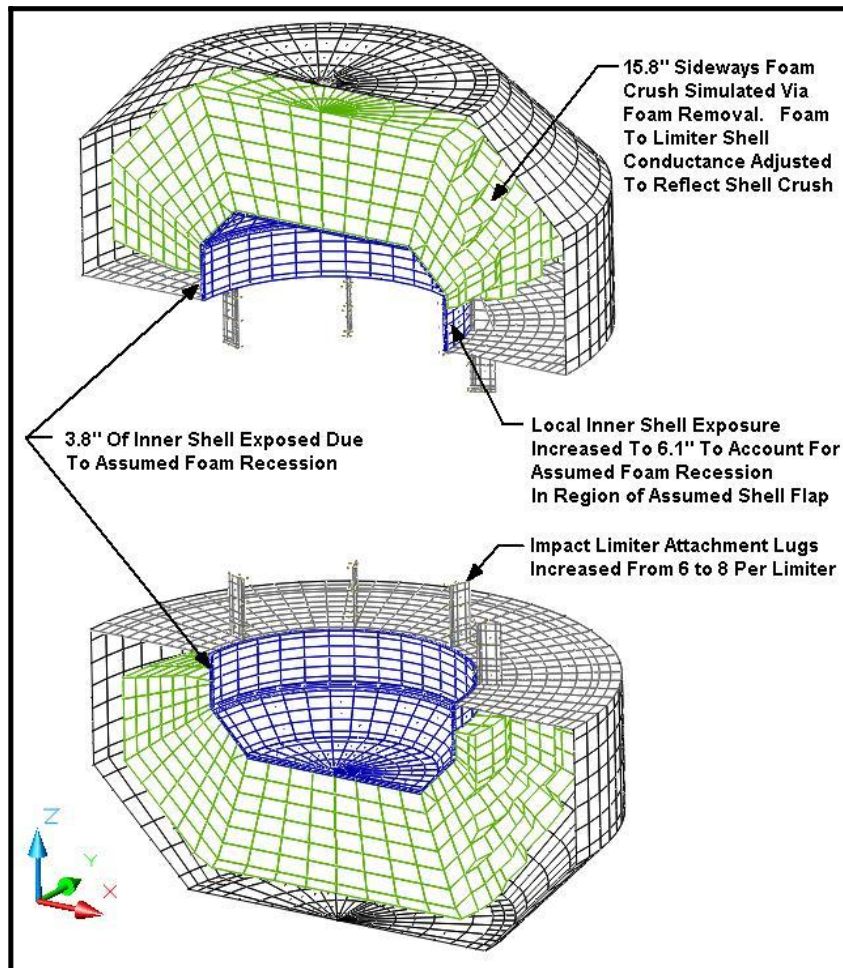


Figure 3.5-13 – Simulated HAC Damage to Impact Limiters

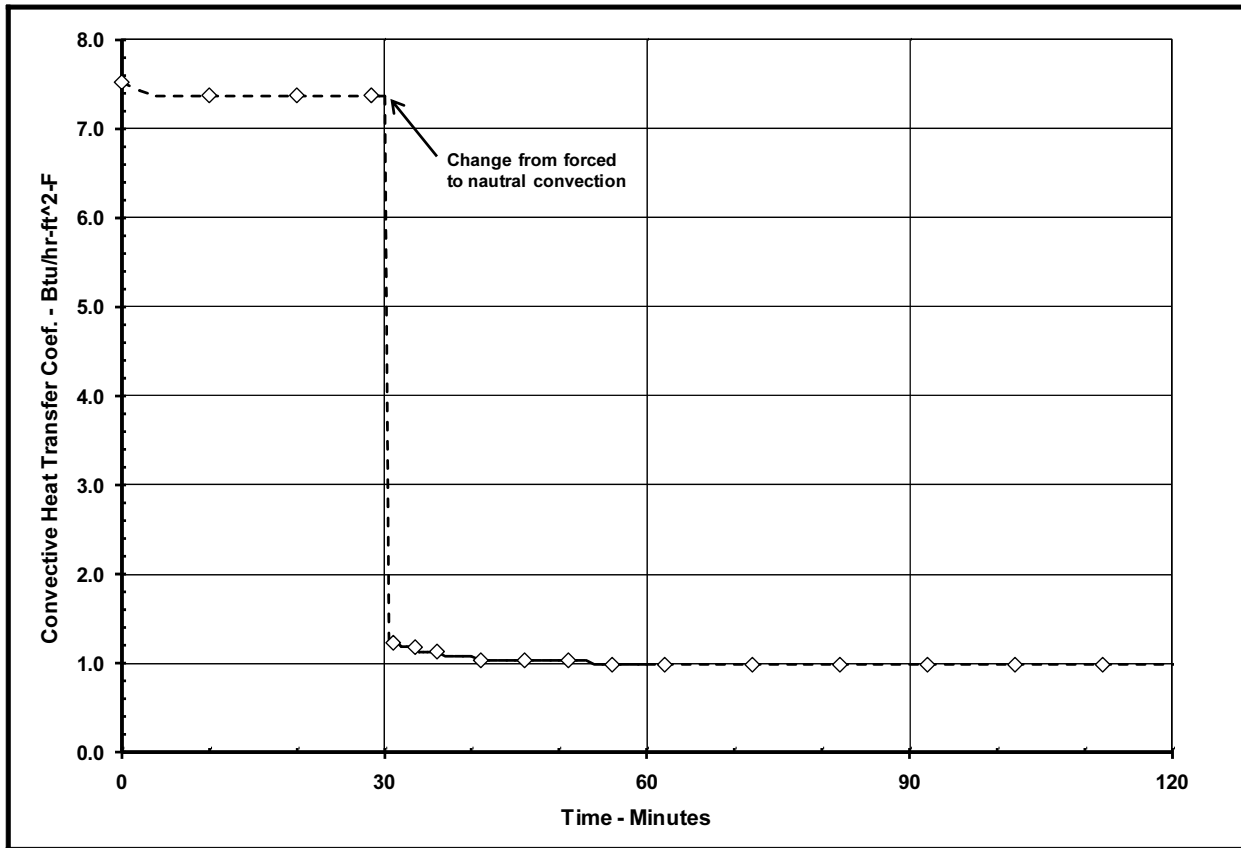
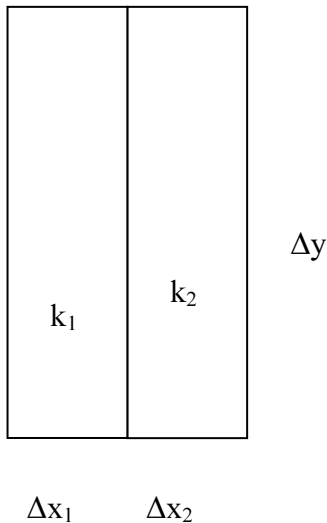


Figure 3.5-14 – Convection Coefficient Variation During HAC Transient

3.5.3.9 Determination of Composite Thermal Properties for Fuel Plates

Thermal Properties for ATR Fuel Plates

The ATR fuel plates are a composite material consisting of a fissile fuel matrix sandwiched within aluminum cladding. For the purposes of this calculation, the fuel composite is treated as a homogenous material with lumped thermal properties as defined below. This modeling approach is justified since the thermal gradient within the fuel element will be very low given that the un-irradiated fuel has essentially no decay heat.



Because of the thinness of the plates, the average conductivity is required only for the axial and circumferential direction. Conductivity through the plates is not required as this analysis assumes a zero temperature gradient in that direction. Mean density and specific heat values are also defined below.

Circumferential and Axial Conductivity

Ignoring the affect of curvature, the heat flow can be written as,

$$q = -\Delta x \Delta z \bar{k} \frac{\Delta T}{\Delta y} = -\Delta x_1 \Delta z k_1 \frac{\Delta T}{\Delta y} - \Delta x_2 \Delta z k_2 \frac{\Delta T}{\Delta y}$$

where $\Delta x = \sum_i \Delta x_i$

From which, $\bar{k} = \frac{\Delta x_1 k_1 + \Delta x_2 k_2}{\Delta x}$

Mean Density

The mean density of the fuel plates is computed from:

$$Mass = \Delta x \Delta y \Delta z \bar{\rho} = \Delta x_1 \Delta y \Delta z \rho_1 + \Delta x_2 \Delta y \Delta z \rho_2, \text{ from which } \bar{\rho} = \frac{\Delta x_1 \rho_1 + \Delta x_2 \rho_2}{\Delta x}$$

Mean Specific Heat

In the same manner used to define the mean density, the mean specific heat for the fuel plates is computed as;

$$\bar{\rho} \bar{c}_p \Delta x \Delta y \Delta z = \rho_1 c_{p_1} \Delta x_1 \Delta y \Delta z + \rho_2 c_{p_2} \Delta x_2 \Delta y \Delta z, \text{ from which, } \bar{c}_p = \frac{\rho_1 c_{p_1} \Delta x_1 + \rho_2 c_{p_2} \Delta x_2}{\bar{\rho} \Delta x}$$

The thermal properties for the individual plates making up the ATR fuel element are computed using the above approach and thermophysical [5] and geometric data [14] for the ATR fuel element.

Based on these data sources, the radius of the inner plate is 3.015 inches, while the radius of the outer plate is 5.44 inches. The gap between the plates is 0.078 inches. The thickness of the aluminum cladding is 0.015 inches.

While the thermal properties for the aluminum cladding and the fissile fuel matrix material will vary with temperature, for the purposes of this evaluation, fixed material properties are assumed in order to simplify the calculation. To provide conservatism for this modeling approach, conservatively low value is assumed for the specific heat for each component, while a conservatively high thermal conductivity value is used. This methodology will result in over-predicting the temperature rise within the composite material during the HAC fire event.

The thermal properties used in this calculation are:

- 1) Aluminum cladding thermal conductivity = 191 W/m-K, conservatively high value from [5], page 18
- 2) Fissile fuel matrix (UAl_x) = 14.47 W/m-K, conservatively high based on equation 2.3 from [5], at 300K
- 3) Aluminum cladding density = 2702 kg/m³, from [5], page 16
- 4) Fissile fuel matrix (UAl_x) density = 3680 kg/m³, from [5], Table 2.5, average density
- 5) Aluminum cladding specific heat = 1034 J/kg-K, from [5], Table 3.2, mean value at 600K
- 6) Fissile fuel matrix (UAl_x) specific heat = 708 J/kg-K, from [5], Table 2.4, average value at 600K

Table 3.5-1 presents the composite thermal conductivity, specific heat, and density values for each of the nineteen (19) fuel plates making up the ATR fuel element. These composite values are based on the thermal property values given above and the geometry depicted in Figure 3.5-15.

Thermal Properties for MIT Fuel Plates

Like the ATR fuel, the MIT fuel plates are a composite material consisting of a fissile fuel matrix sandwiched within an aluminum cladding. The thermal properties for the plates making up the MIT fuel element are computed using the same approach described above for the ATR fuel and the data contained in [5] and [13]. The plates have a thickness of 0.08 inches and a width of 2.526 inches. The nominal gap between the plates is 0.078 inches. Since the aluminum cladding contains 110 grooves on each side of the plate, the effective thickness of the cladding is reduced from 0.025 inches to 0.02 inches.

Table 3.5-2 presents the composite thermal conductivity, specific heat, and density values for the fifteen (15) fuel plates making up the MIT fuel element. These composite values are based on the thermal property values provided above for the ATR fuel element and the geometry described in Table 3.5-2 and depicted in Figure 3.5-16.

Thermal Properties for MURR Fuel Plates

The MURR fuel plates are also a composite of a fissile fuel matrix sandwiched within an aluminum cladding. The thermal properties for the MURR fuel element are computed using the

same approach described above for the ATR fuel and the data contained in [5] and [12]. The inner plate has an inner radius of 2.77 inches and an arc length of 1.993 inches, while the outer plate has an inner radius of 5.76 inches and an arc length of 4.342 inches. The nominal gap between the plates is 0.08 inches. The thickness of the aluminum cladding is 0.01 inches.

Table 3.5-3 presents the composite thermal conductivity, specific heat, and density values for the twenty four (24) fuel plates making up the MURR fuel element. These composite values are based on the thermal property values provided above for the ATR fuel element and the geometry described in Table 3.5-3 and depicted in Figure 3.5-17.

Thermal Properties for TRIGA Fuel Element

The cladding thickness for the TRIGA fuel is relatively thin and the fuel's thermal properties are dominated by the homogenous properties for the uranium-zirconium hydride fuel and the graphite materials. As such, composite properties are not required. Instead, the thermal properties listed in Table 3.2-2 for the uranium-zirconium hydride fuel and the graphite are used directly in the thermal model.

Table 3.5-1 – Composite ATR Fuel Plate Thermal Properties

Plate	Plate Thickness, in	UAlx Thickness, in	Axial & Circumferential Conductivity (W/m-K)	Inner radius, in	Outer radius, in	Mean radius, in	Mean density, kg/m ³	Mean specific heat, J/(kg K)
1	0.08	0.05	80.7	3.015	3.095	3.055	3313.3	807.7
2	0.05	0.02	120.4	3.173	3.223	3.198	3093.2	878.9
3	0.05	0.02	120.4	3.301	3.351	3.326	3093.2	878.9
4	0.05	0.02	120.4	3.429	3.479	3.454	3093.2	878.9
5	0.05	0.02	120.4	3.557	3.607	3.582	3093.2	878.9
6	0.05	0.02	120.4	3.685	3.735	3.710	3093.2	878.9
7	0.05	0.02	120.4	3.813	3.863	3.838	3093.2	878.9
8	0.05	0.02	120.4	3.941	3.991	3.966	3093.2	878.9
9	0.05	0.02	120.4	4.069	4.119	4.094	3093.2	878.9
10	0.05	0.02	120.4	4.197	4.247	4.222	3093.2	878.9
11	0.05	0.02	120.4	4.325	4.375	4.350	3093.2	878.9
12	0.05	0.02	120.4	4.453	4.503	4.478	3093.2	878.9
13	0.05	0.02	120.4	4.581	4.631	4.606	3093.2	878.9
14	0.05	0.02	120.4	4.709	4.759	4.734	3093.2	878.9
15	0.05	0.02	120.4	4.837	4.887	4.862	3093.2	878.9
16	0.05	0.02	120.4	4.965	5.015	4.990	3093.2	878.9
17	0.05	0.02	120.4	5.093	5.143	5.118	3093.2	878.9
18	0.05	0.02	120.4	5.221	5.271	5.246	3093.2	878.9
19	0.1	0.07	67.4	5.349	5.449	5.399	3386.6	786.0

Table 3.5-2 – Composite MIT Fuel Plate Thermal Properties

Plate	Plate Thickness, in	UAlx Thickness, in	Axial and Circumferential Conductivity (W/m-K)	Plate Width, in	Mean density, kg/m ³	Mean specific heat, J/(kg K)
1 to 15	0.08*	0.03	115.3	2.314	3121.1	869.3

* - mean plate thickness estimated at 0.07 inches after allowance for ribbing

Table 3.5-3 – Composite MURR Fuel Plate Thermal Properties

Plate	Plate Thickness, in	UAlx Thickness, in	Axial and Circumferential Conductivity (W/m-K)	Inner radius, in	Outer radius, in	Plate Arc Length, in	Mean density, kg/m ³	Mean specific heat, J/(kg K)
1	0.05	0.03	85.1	2.77	2.82	1.993	3288.8	815.1
2	0.05	0.03	85.1	2.9	2.95	2.095	3288.8	815.1
3	0.05	0.03	85.1	3.03	3.08	2.197	3288.8	815.1
4	0.05	0.03	85.1	3.16	3.21	2.300	3288.8	815.1
5	0.05	0.03	85.1	3.29	3.34	2.402	3288.8	815.1
6	0.05	0.03	85.1	3.42	3.47	2.504	3288.8	815.1
7	0.05	0.03	85.1	3.55	3.6	2.606	3288.8	815.1
8	0.05	0.03	85.1	3.68	3.73	2.708	3288.8	815.1
9	0.05	0.03	85.1	3.81	3.86	2.810	3288.8	815.1
10	0.05	0.03	85.1	3.94	3.99	2.912	3288.8	815.1
11	0.05	0.03	85.1	4.07	4.12	3.014	3288.8	815.1
12	0.05	0.03	85.1	4.2	4.25	3.116	3288.8	815.1
13	0.05	0.03	85.1	4.33	4.38	3.218	3288.8	815.1
14	0.05	0.03	85.1	4.46	4.51	3.321	3288.8	815.1
15	0.05	0.03	85.1	4.59	4.64	3.423	3288.8	815.1
16	0.05	0.03	85.1	4.72	4.77	3.525	3288.8	815.1
17	0.05	0.03	85.1	4.85	4.9	3.627	3288.8	815.1
18	0.05	0.03	85.1	4.98	5.03	3.729	3288.8	815.1
19	0.05	0.03	85.1	5.11	5.16	3.831	3288.8	815.1
20	0.05	0.03	85.1	5.24	5.29	3.933	3288.8	815.1
21	0.05	0.03	85.1	5.37	5.42	4.035	3288.8	815.1
22	0.05	0.03	85.1	5.5	5.55	4.137	3288.8	815.1
23	0.05	0.03	85.1	5.63	5.68	4.239	3288.8	815.1
24	0.05	0.03	85.1	5.76	5.81	4.342	3288.8	815.1

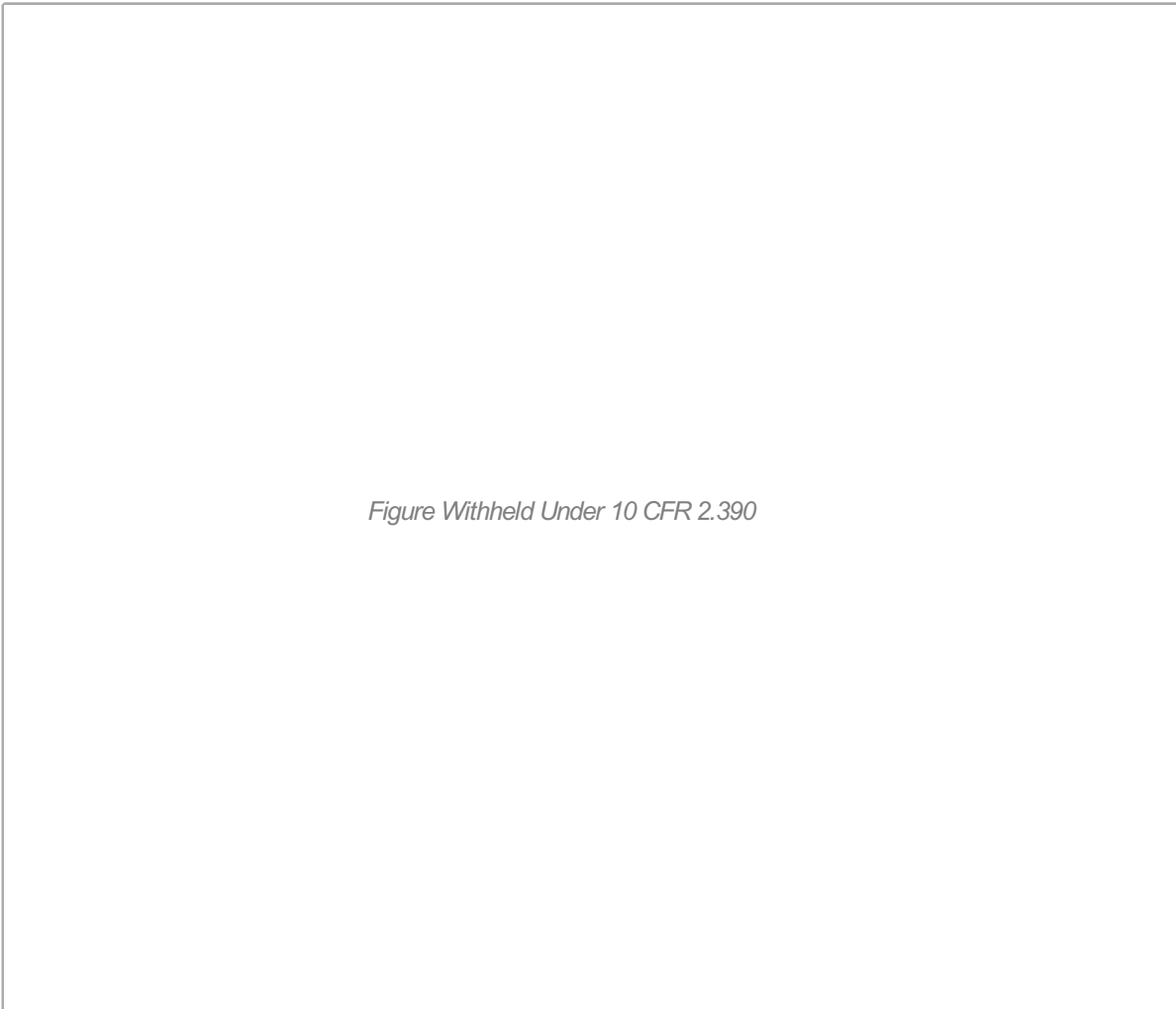


Figure Withheld Under 10 CFR 2.390

Figure 3.5-15 – ATR Fuel Element Cross Section

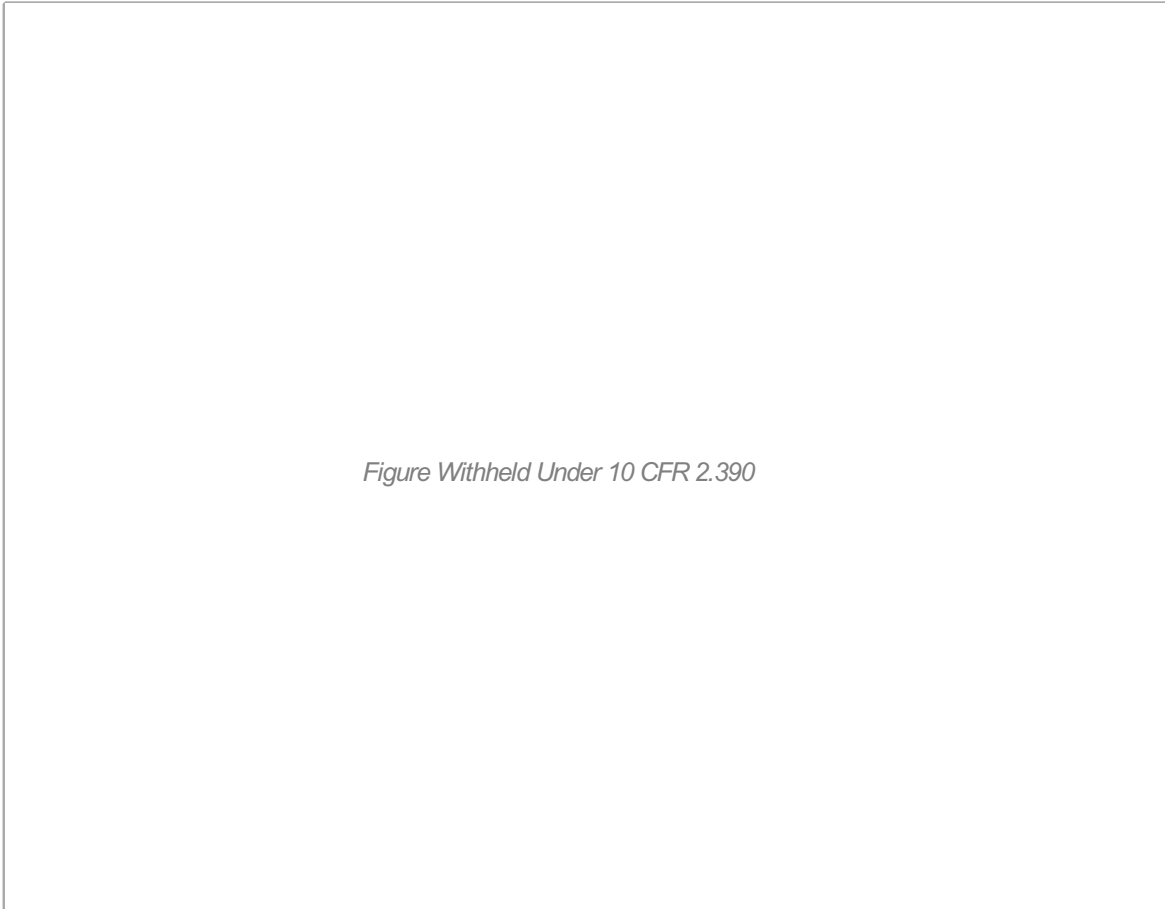


Figure 3.5-16 – MIT Fuel Element Cross Section



Figure 3.5-17 – MURR Fuel Element Cross Section

3.5.4 'Last-A-Foam' Response under HAC Conditions

The General Plastics LAST-A-FOAM® FR-3700 rigid polyurethane foam [18] used in the impact limiters has been used for numerous transportation packages. The FR-3700 formulation is specially designed to allow predictable impact-absorption performance under dynamic loading, while also providing a significant level of thermal protection under the HAC conditions. Upon exposure to fire temperatures, this proprietary foam decomposes into an intumescent char that swells and tends to fill voids or gaps created by free drop or puncture bar damage. This thermal decomposition absorbs a significant amount of the heat transferred into the foam, which is then expelled from the impact limiters as a high temperature gas. Because the char has no appreciable structural capacity and will not develop unless there is space available, the char will not generate stresses within the adjacent package components. Without available space the pyrolysis gases developed as a result of the charring process will move excess char mass out through the vent ports and prevent its buildup. Only as the charring process continues and space becomes available will the char be retained, filling the available space and plugging holes at the surface of the impact limiters. The thermal decomposition process does not alter or cause a chemical reaction within the adjacent materials.

The mechanisms behind the observed variations in the thermal properties and behavior of the FR-3700 foam at elevated temperatures are varied and complex. A series of fire tests [27 and 28] conducted on 5-gallon cans filled with FR-3700 foam at densities from 6.7 to 25.8 lb/ft³ helped define the expected performance of the foam under fire accident conditions. Under the referenced fire tests, one end of the test article was subjected to an open diesel fueled burner flame at temperatures of 980 to 1,200°C (1,800 to 2,200 °F) for more than 30 minutes. A thermal shield prevented direct exposure to the burner flame on any surface of the test article other than the hot face. Each test article was instrumented with thermocouples located at various depths in the foam. In addition, samples of the foam were subjected to thermogravimetric analysis (TGA) to determine the thermal decomposition vs. temperature. The exposure temperatures for the TGA tests varied from 70 to 1,500 °F, and were conducted in both air and nitrogen atmospheres. The result for the nitrogen environment (see Figure 3.5-18) is more representative of the low oxygen environment existing within the impact limiter shells encasing the foam. These test results indicate that the following steps occur in the thermal breakdown of the foam under the level of elevated temperatures reached during the HAC fire event:

- Below 250 °F, the variation in foam thermal properties with temperature is slight and reversible. As such, fixed values for specific heat and thermal conductivity are appropriate.
- Between 250 and 500 °F, small variations in foam thermal properties occur as water vapor and non-condensable gases are driven out of the foam. As such, fixed values for specific heat and thermal conductivity are also appropriate for this temperature range. Further, the observed changes are so slight that the same thermal properties used for temperatures below 250 °F may also be used to characterize the thermal performance of the foam between 250 and 500 °F.
- Irreversible thermal decomposition of the foam begins as the temperature rises above 500 °F and increases non-linearly with temperature. Based on the TGA testing (see

Figure 3.5-18), approximately 2/3's of this decomposition occurs over a narrow temperature range centered about 670 °F.

- The decomposition is accompanied by vigorous out-gassing from the foam and an indeterminate amount of internal heat generation. The internal heat generation arises from the gases generated by the decomposition process that are combustible under piloted conditions. However, since the decomposition process is endothermic, the foam will not support combustion indefinitely. Further, the out-gassing process removes a significant amount of heat from the package via mass transport.
- The weight loss due to out-gassing not only has direct affect on the heat flux into the remaining virgin foam, but changes the composition of the resulting foam char since the foam constituents are lost at different rates. This change in composition affects both the specific heat and the thermal conductivity of the foam char layer.
- As temperature continues to rise, the developing char layer begins to take on the characteristics of a gas-filled cellular structure where radiative interchange from one cell surface to another becomes the dominant portion of the overall heat transfer mechanism. This change in heat transfer mechanisms causes the apparent heat conductivity to take on a highly non-linear relationship with temperature.
- Finally, at temperatures above 1,250 °F, the thermal breakdown of the foam is essentially completed and only about 5 to 10% of the original mass is left. In the absence of direct exposure to a flame or erosion by the channeling of the outgas products through the foam, the char layer will be the same or slightly thicker than the original foam depth. This char layer will continue to provide radiative shielding to the underlying foam material.

Since the thermal decomposition of the foam is an endothermic process, the foam is self-extinguishing and will not support a flame once the external flame source is removed. However, the gases generated by the decomposition process are combustible and will burn under piloted conditions. A portion of these generated gases can remain trapped within the charred layer of the foam after the cessation of the HAC fire event and continue to support further combustion, although at a much reduced level, until a sufficient time has passed for their depletion from the cell structure. This extended time period is typically from 15 to 45 minutes.

The sharp transition in the state of the foam noted in Figure 3.5-18 at or about 670 °F can be used to correlate the observed depth of the foam char following a burn test with the occurrence of this temperature level within the foam. The correlation between the foam recession depth and the foam density, as compiled from a series of tests, is expressed by the relation:

$$y = -0.94581 - 11.64 \times \log_{10}(x)$$

where, y = the recession depth, cm

x = foam density (g/cm^3)

Based on this correlation, the recession depth expected for the nominal 9 pcf density foam used in the packaging is estimated to be 3.5 inches. The loss of foam could increase to a depth of approximately 3.8 inches for foam fabricated at the low end of the density tolerance (i.e., 7.65 pcf).

It should be noted that these results assume that the foam is enclosed within a steel shell with surface openings that are approximately 0.3 ft² or smaller. The presence of the steel enclosure helps shield the foam from the heat flux of a HAC fire event and helps contain the foam char that is generated. Test results with and without a steel interface between the foam and the heat source indicates that the foam loss could be an additional 1.5 inches for the 7.65 pcf foam if larger face areas are exposed directly to the fire.

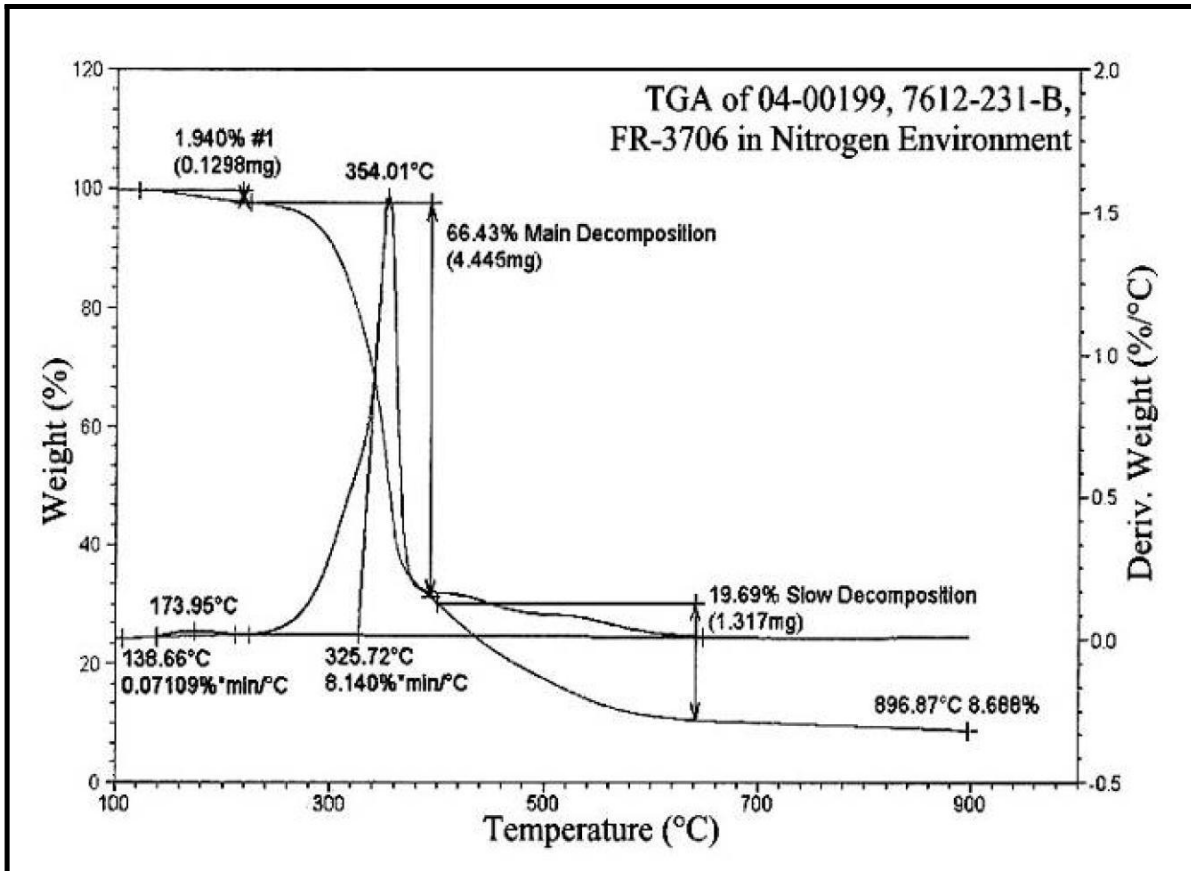


Figure 3.5-18 – TGA Analysis of Foam Decomposition in Nitrogen Environment

4.0 CONTAINMENT

4.1 Description of the Containment System

4.1.1 Containment Boundary

The BRR package provides a single level of leaktight containment, defined as a leakage rate of less than 1×10^{-7} reference cubic centimeters per second (ref-cm³/s), air, per ANSI N14.5 [1]. The containment boundary of the BRR package consists of the following elements. Unless noted, all elements are made of ASTM Type 304 stainless steel in various product forms. A full description of the packaging is given in Section 1.2.1, *Packaging*.

- The lower massive end structure (including the passage to the drain port)
- The inner cylindrical shell
- The upper massive end structure
- The containment O-ring seal (the inner seal in the closure lid; face-type seal made of butyl elastomer)
- The closure lid
- The vent port in the closure lid (closed using a brass port plug, sealed with a butyl sealing washer)
- The drain port in the lower end structure (closed using a brass port plug, sealed with a butyl sealing washer)

The containment boundary is shown in Figure 4.1-1.

4.1.2 Containment Penetrations

Besides the bolted closure lid, there are two containment penetrations: the vent port, located in the closure lid, and the drain port, located in the lower end structure, as described above. Each penetration is designed and tested to ensure leaktight sealing integrity, i.e., a leakage rate not exceeding 1×10^{-7} ref-cm³/s, per ANSI N14.5.

4.1.3 Seals

The elastomeric portion of the containment boundary is comprised of a nominally 3/8-inch diameter, O-ring face seal located in the inner groove in the closure lid, and seal washer sealing elements (an O-ring integrated with a stainless steel washer) for the vent and drain ports. The seals are made using a butyl elastomer compound suitable for continuous use between the temperatures of -65 °F and 225 °F [2], and capable of much higher temperatures during the HAC fire case transient. Further discussion of the thermal performance capabilities of the butyl rubber seals is provided in Appendix 2.12.7, *Containment Seal Performance Tests*.

Two O-ring seals are provided in the closure lid: the inner seal is containment, and the outer forms an annular space for leakage rate testing of the containment seal. The leakage rate tests used for various purposes are summarized in Section 4.4, *Leakage Rate Tests for Type B Packages*, and described in detail in Chapter 8, *Acceptance Tests and Maintenance Program*.

The O-ring containment seal is retained in the closure lid using a dovetail groove having a depth of 0.284 ± 0.003 inches, or $0.281 - 0.287$ inches. The O-ring has a cross sectional diameter of 0.375 ± 0.007 inches, or $0.368 - 0.382$ inches. The minimum compression corresponds to the maximum groove depth and the minimum O-ring cross-sectional diameter:

$$C_{\text{Min}} = 100 \times \left(1 - \frac{G_{\text{Max}}}{D_{\text{Min}}} \right) = 22\%$$

where $G_{\text{Max}} = 0.287$ inches and $D_{\text{Min}} = 0.368$ inches. The maximum compression corresponds to the minimum groove depth and the maximum O-ring cross-sectional diameter:

$$C_{\text{Max}} = 100 \times \left(1 - \frac{G_{\text{Min}}}{D_{\text{Max}}} \right) = 26\%$$

where $G_{\text{Min}} = 0.281$ inches and $D_{\text{Max}} = 0.382$ inches. The Parker O-ring Handbook [7] recommends a minimum compression of 16%. The limit for maximum compression is when the O-ring cross-section, adjusted for maximum temperature, fills the cross sectional area of the dovetail groove. This condition occurs for the BRR package closure O-ring at a compression of 31.2%. The compression range of 22% to 26% will therefore provide satisfactory performance of the O-ring during all NCT and HAC.

4.1.4 Welds

All welds used in the containment boundary are full penetration and volumetrically inspected to ensure structural and containment integrity. The welds joining the inner shell to either end structure are ultrasonically inspected in accordance with the ASME Code, Subsection NB, Article NB-5000, and Section V, Article 4 [4]. The weld joining the inner shell and the lower end structure may be optionally radiograph inspected in accordance with the ASME Code, Subsection NB, Article NB-5000, and Section V, Article 2 [3]. All containment boundary welds are inspected by liquid penetrant inspection on the final pass in accordance with the ASME Code, Subsection NB, Article NB-5000, and Section V, Article 6 [5]. All containment boundary welds are confirmed to be leaktight as discussed in Section 8.1.4, *Fabrication Leakage Rate Tests*.

4.1.5 Closure

The closure lid completes the containment boundary, and is attached to the cask body using (12) 1-8 UNC socket head cap screws tightened to 220 ± 20 ft-lb. As shown in Chapter 2, *Structural Evaluation*, the closure lid cannot become detached by any internal pressure, NCT, or HAC events. The closure lid, including the vent port, is completely covered by the upper impact limiter, which is attached to the cask using eight (8) 1-inch diameter ball lock pins. Similarly, the drain port is covered by the lower impact limiter. Thus, the containment openings cannot be inadvertently opened.

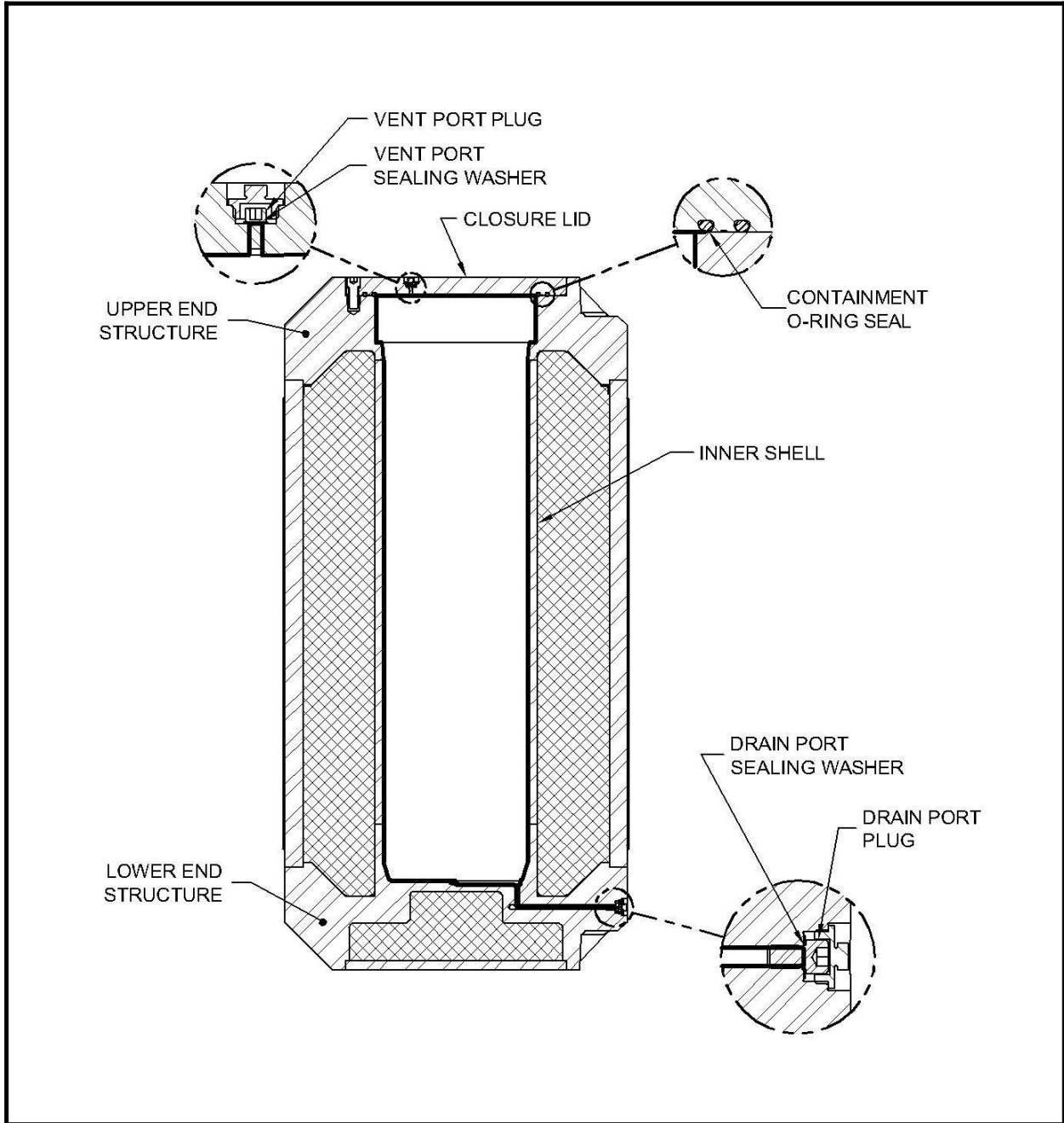


Figure 4.1-1 – BRR Package Containment Boundary

4.2 Containment Under Normal Conditions of Transport

The results of the NCT structural and thermal evaluations presented in Sections 2.6, *Normal Conditions of Transport*, and 3.3, *Thermal Evaluation Under Normal Conditions of Transport*, respectively, demonstrate that there is no release of radioactive materials per the “leaktight” definition of ANSI N14.5 under any of the NCT tests described in 10 CFR §71.71 [6].

4.3 Containment Under Hypothetical Accident Conditions

The results of the HAC structural and thermal evaluations performed in Sections 2.7, *Hypothetical Accident Conditions*, and 3.4, *Thermal Evaluation Under Hypothetical Accident Conditions*, respectively, demonstrate that there is no release of radioactive materials per the “leaktight” definition of ANSI N14.5 under any of the hypothetical accident condition tests described in 10 CFR §71.73.

4.4 Leakage Rate Tests for Type B Packages

4.4.1 Fabrication Leakage Rate Tests

During fabrication, the containment boundary is leakage rate tested as described in Section 8.1.4, *Fabrication Leakage Rate Tests*. The fabrication leakage rate tests are consistent with the guidelines of Section 7.3 of ANSI N14.5. This leakage rate test verifies the containment integrity of the BRR packaging to a leakage rate not to exceed 1×10^{-7} ref-cm³/s, air.

4.4.2 Maintenance/Periodic Leakage Rate Tests

Annually, or at the time of damaged containment seal replacement or sealing surface repair, the containment O-ring seal and the vent port and drain port sealing washers are leakage rate tested as described in Section 8.2.2, *Maintenance/Periodic Leakage Rate Tests*. The maintenance/periodic leakage rate tests are consistent with the guidelines of Section 7.4 of ANSI N14.5. This test verifies the sealing integrity of the containment seals to a leakage rate not to exceed 1×10^{-7} ref-cm³/s, air.

4.4.3 Preshipment Leakage Rate Tests

Prior to shipment of the loaded BRR package, the containment O-ring seal and the vent port and drain port sealing washers are leakage rate tested per Section 7.4, *Preshipment Leakage Rate Test*. The preshipment leakage rate tests are consistent with the guidelines of Section 7.6 of ANSI N14.5. This test verifies the sealing integrity of the containment seals to a leakage rate sensitivity of 1×10^{-3} ref-cm³/s, air.

The maintenance/periodic leakage rate tests, described in Section 8.2.2, *Maintenance/Periodic Leakage Rate Tests*, may be performed as an option, in lieu of the preshipment leakage rate tests.

4.5 Appendix

4.5.1 References

1. ANSI N14.5-1997, *American National Standard for Radioactive Materials – Leakage Tests on Packages for Shipment*, American National Standards Institute (ANSI), Inc.
2. Rainier Rubber Company, Seattle, WA.
3. American Society of Mechanical Engineers (ASME) Boiler and Pressure Vessel Code, Section III, *Rules for Construction of Nuclear Facility Components*, Division 1 – Subsection NB, *Class 1 Components*, and Section V, *Nondestructive Examination*, Article 2, *Radiographic Examination*, 2007 Edition.
4. American Society of Mechanical Engineers (ASME) Boiler and Pressure Vessel Code, Section III, *Rules for Construction of Nuclear Facility Components*, Division 1 – Subsection NB, *Class 1 Components*, and Section V, *Nondestructive Examination*, Article 4, *Ultrasonic Examination Methods for Welds*, 2007 Edition.
5. American Society of Mechanical Engineers (ASME) Boiler and Pressure Vessel Code, Section III, *Rules for Construction of Nuclear Facility Components*, Division 1 – Subsection NB, *Class 1 Components*, and Section V, *Nondestructive Examination*, Article 6, *Liquid Penetrant Examination*, 2007 Edition.
6. Title 10, Code of Federal Regulations, Part 71 (10 CFR 71), *Packaging and Transportation of Radioactive Material*, 01-01-08 Edition.
7. Parker O-ring Handbook, ORD-5700, Parker-Hannifin Corporation, Cleveland, OH, © 2007.

5.0 SHIELDING EVALUATION

The Battelle Energy Alliance (BEA) Research Reactor (BRR) Package is used to transport spent fuel from a variety of research reactors, including the University of Missouri Research Reactor (MURR), Massachusetts Institute of Technology Research Reactor (MITR-II), Advanced Test Reactor (ATR), and various types of Training, Research, Isotope General Atomics (TRIGA) reactors. The following analyses demonstrate that the BRR Package complies with the external radiation requirements of 10 CFR §71.47 [1]. MCNP5 v1.30 [2] is used to compute the dose rates.

5.1 Description of Shielding Design

5.1.1 Design Features

The principal design features are a lead-filled shield plug, lead-filled side wall, and lead-filled bottom. The top plug consists of approximately 9.5-in lead, with a 1-in stainless steel bottom plate, and 0.5-in stainless steel top plate. The lid is constructed of stainless steel 2-in thick. The lead in the side wall of the cask is 8-in thick. The inner steel shell is 1-in thick, and the outer stainless steel shell is 2-in thick. The cask bottom consists of 7.7-in of lead through the centerline, with a 1-in stainless steel bottom cover plate, and approximately 1.2-in stainless steel inner forging.

The fuel is positioned within one of four custom-designed baskets. The baskets maintain their geometry under normal conditions of transport (NCT) and hypothetical accident conditions (HAC), as demonstrated in Section 2.7.1.5, *Fuel Basket Stress Analysis*, thereby maintaining the location of the source.

5.1.2 Summary Table of Maximum Radiation Levels

Although the dose rates are relatively low and non-exclusive use transportation could be justified, because the cask is heavy and only one cask will be transported per vehicle, exclusive use dose rate limits are applied.

Maximum NCT and HAC dose rates are reported in Table 5.1-1. The fuel type associated with each dose rate is provided in the table. Because the geometry of the source, basket design, and source strength vary widely between the fuel types, no one fuel type may be considered bounding at all dose rate locations.

The cask is transported in a vertical orientation in an open vehicle. Because the transport vehicle is open, the dose rate limit is 200 mrem/hr at both the package and vehicle surfaces. The vehicle is assumed to be 8 feet wide, and the vehicle side surface is the projection at this distance. The top and bottom vehicle surfaces are assumed to correspond to the top and bottom of the impact limiters, although the vehicle does not have a top because it is open. The 2 m dose rate is computed 2 m from the vehicle side, while the occupied location (i.e., the driver) is computed 25 feet from the centerline of the cask.

BRR Package Safety Analysis Report

Dose rates are very low. Under NCT, the maximum package surface dose rate is 13.4 mrem/hr, the maximum dose rate 2 m from the vehicle surface is 0.3 mrem/hr, and the dose rate in the occupied location is 0.05 mrem/hr. Under HAC, the maximum dose rate at 1 m from the package is 2.3 mrem/hr.

Table 5.1-1 – Summary of Maximum Total Dose Rates (Exclusive Use)

NCT	Package Surface (mrem/hr)			Vehicle Surface (mrem/hr)		
	Fuel→	TRIGA	MITR-II	MURR	TRIGA	TRIGA
Radiation	Top	Side	Bottom	Top	Side	Bottom
Gamma	7.0	3.2	3.63	7.0	2.8	3.63
Neutron	0.2	10.2	0.02	0.2	0.1	0.02
Total	7.2	13.4	3.7	7.2	2.9	3.7
Limit	200	200	200	200	200	200

NCT	2 m from Vehicle Surface (mrem/hr)			Occupied Location (mrem/hr)
	Fuel→	NA	MITR-II	NA
Radiation	Top	Side	Bottom	Side
Gamma	NA	0.1	NA	0.02
Neutron	NA	0.2	NA	0.03
Total	NA	0.3	NA	0.05
Limit	10	10	10	2

HAC	1 m from Package Surface (mrem/hr)		
	Fuel→	TRIGA	TRIGA
Radiation	Top	Side	Bottom
Gamma	2.2	1.6	1.5
Neutron	0.1	0.1	0.01
Total	2.3	1.7	1.5
Limit	1000	1000	1000

5.2 Source Specification

A neutron and gamma source term is developed for each of the four fuel types. The source terms for MURR, MITR-II, and ATR are developed using the TRITON sequence of SCALE6 [3]. The TRIGA source is derived from nuclide activities obtained from INEL-96/0482 [4].

5.2.1 Gamma Source

5.2.1.1 MURR Fuel

The MURR gamma source term is generated by the TRITON sequence of SCALE6. TRITON is a control module that coordinates program flow between the SCALE6 modules involved in the depletion sequence, primarily NEWT and ORIGEN-S.

The TRITON sequence uses a predictor-corrector approach. The two-dimensional discrete ordinates module NEWT calculates the burnup-dependent flux distribution across the fuel element, which is collapsed to three groups for input to the ORIGEN-S depletion module. The first NEWT calculation is performed using the 238-group ENDF/B-VII cross-section library. This flux distribution is then used to collapse the 238-group cross-section library to 49 groups to accelerate subsequent NEWT calculations. Therefore, the 49-group library is problem-dependent. The fuel is depleted over a specified time interval, and the depleted mixture is then used as input to the subsequent NEWT flux calculation. The number of time steps is determined by the user-defined input. One library generation per fuel cycle is the default, although more steps may be requested to improve accuracy. A more detailed discussion of the predictor-corrector approach of the TRITON sequence may be found in Section T.1.2.3 of the TRITON user's manual [3]. An annotated TRITON input file is included in Section 5.5.3.1, *TRITON Input File*. A discussion of this input file follows.

The two-dimensional NEWT model of the MURR fuel element has been simplified compared to the actual fuel element geometry. The MURR fuel element has 24 curved plates, although these plates are modeled as flat in NEWT. Only half of the fuel element is modeled, taking credit for symmetry. In the actual fuel element, the arc length of the fuel meat is different for each plate. To simplify the NEWT model, one-half the average fuel meat arc length is modeled for all 24 plates. Therefore, it is necessary to define only one fuel plate, and then repeat this fuel plate in a 1x24 array. All relevant data used to develop the TRITON model is shown in Table 5.2-1. The NEWT model geometry is shown in Figure 5.2-1.

The nominal fuel meat arc length for each plate is provided in Table 6.9-3 of Chapter 6, *Criticality Evaluation*. Based on these nominal arc lengths, the average fuel meat arc length is 2.882-in. The nominal fuel meat thickness is 0.02-in, and the nominal plate thickness is 0.05-in. The nominal channel thickness between plates is 0.08-in, so the nominal pitch is $0.05+0.08 = 0.13$ -in. These parameters are used as input both in the NEWT model and the LATTICECELL card.

Three materials are modeled; fuel, cladding, and moderator. The number densities of the fuel are computed based on the fuel loading and fuel meat volume. The density of the fuel meat is estimated using the equation listed in Table 6.2-5 of Chapter 6, *Criticality Evaluation*, using the

known density of U-235. Aluminum and water are modeled as pure. Temperatures for the fuel, cladding, and water during reactor operation are typical values for this reactor.

The MURR fuel element has a fuel loading of 775.0 ± 7.8 g U-235. Two TRITON models are developed, one for the minimum fuel loading (767.2 g U-235), and a second for the maximum fuel loading (782.8 g U-235). The U-235 enrichment is 93%. The balance of uranium is modeled as U-238. The fuel is burned in 21 cycles. The first 20 cycles are 7 days in duration, and the final cycle is 4 days in duration, giving a total irradiation time of 144 days. The total core power is 10.0 MW, with 8 fuel elements, so the average element power is 1.25 MW. A peak fuel element could have a power greater than 1.25 MW for any particular cycle, but because no fuel element is ever maintained at the peak power throughout its entire life, modeling an average value of 1.25 MW is conservative. For an element power of 1.25 MW, the total burnup is 180 MWD. Power is input to TRITON in units of MW/MTU. Two weeks of cooling is assumed between each cycle. The source is allowed to cool 180 days after reactor shutdown.

The fuel cycle is modeled as an extreme case of the MURR fuel cycle. Unlike many other research reactors, MURR does not use a once-through fuel cycle. Each fuel element is cycled in and out of the core several times before reaching the final discharge burnup. Typically, a given fuel element is irradiated in several 6.2 to 6.5-day periods with varying cooling (non-irradiation) times in between the irradiation periods. For this calculation, the fuel assembly is irradiated in 7.0-day periods in a one-week-in and two-week-out pattern until the fuel is discharged. This overestimates the source term since MURR fuel elements generally remain outside the core for several weeks at a time during their active life and are never cycled in and out of the core continuously until discharge. Therefore, the irradiation parameters utilized result in a source term that bounds any expected MURR fuel element.

The OPUS module of SCALE6 is used to extract key data from the output, including decay heat, U-235 mass, plutonium activity, and the source term. Note that all TRITON output uses a basis of 1 MTU because the specific power must be input in units of MW/MTU. Therefore, the results must be multiplied by the fuel loading (in MTU) of the fuel element to obtain the desired results for a single fuel element.

The gamma source term for both the maximum and minimum fuel loadings are nearly identical (within 0.02%), although the source term computed for the minimum fuel loading is slightly higher. The MURR gamma source computed with the minimum fuel loading is summarized in Table 5.2-3. Note that the MURR basket may transport up to eight fuel elements.

A representative axial burnup distribution is provided in Table 5.2-4. This distribution is the ratio of the burnup in each segment to the average burnup.

Key output data are summarized in Table 5.2-2. The fuel depletion may be computed based on the initial and final U-235 mass. The initial U-235 mass is 767.2 g, and the final U-235 mass is 530.4 g, or a depletion of 30.9%. The decay heat at a decay time of 180 days is 147.6 W.

5.2.1.2 MITR-II Fuel

The MITR-II gamma source term is generated by the TRITON sequence in the same manner as MURR fuel. Data used to develop the TRITON model is summarized in Table 5.2-1, and the NEWT model for MITR-II is shown in Figure 5.2-2. An actual MITR-II fuel element has a trapezoidal design, although the fuel is modeled in NEWT as a simple rectangle for simplicity.

The MITR-II fuel element has a loading of 510.0 ± 10 g U-235. Two TRITON models are developed, one for the minimum fuel loading (500.0 g U-235), and a second for the maximum fuel loading (513.0 g U-235). The U-235 enrichment is 93%. The balance of uranium is modeled as U-238.

The fuel is burned in one 900 day cycle. The average fuel element power is 0.25 MW for a 6.0 MW reactor with 24 fuel elements. A peak fuel element could have a power greater than 0.25 MW for any particular cycle, but because no fuel element is ever maintained at the peak power throughout its entire life, modeling an average value of 0.25 MW is conservative. Therefore, for an element power of 0.25 MW, the burnup is 225 MWD. The irradiation time is highly conservative because the MITR-II reactor typically operates on a monthly cycle, and operates only 300 days per year. The source is allowed to cool 930 days after reactor shutdown.

The MITR-II gamma source is summarized in Table 5.2-3. Consistent with the MURR gamma source, the source is slightly larger using the minimum fuel loading. Note that the MITR-II basket may transport up to 11 fuel elements.

The axial burnup distribution is provided in Table 5.2-5. This distribution is the ratio of the burnup in each segment to the average burnup. A symmetric distribution is utilized. Because the widths of the distribution are not constant (the end segments are half the width of the remaining segments), the distribution input to MCNP must be divided by 2 for the end regions, as indicated in the last column in the table.

Key output data are summarized in Table 5.2-2. The fuel depletion may be computed based on the initial and final U-235 mass. The initial U-235 mass is 500.0 g, and the final U-235 mass is 203.3 g, or a depletion of 59.3%. The decay heat at a decay time of 930 days is 23.7 W.

5.2.1.3 ATR Fuel

The ATR gamma source term is generated by the TRITON sequence in the same manner as MURR and MITR-II fuel. Data used to develop the TRITON model is summarized in Table 5.2-1, and the NEWT model for ATR is shown in Figure 5.2-3. An ATR fuel element is similar in geometry to a MURR fuel element, although an ATR fuel element has 19 fuel plates instead of 24. The NEWT model uses the same base assumption as the MURR model that the plates may be modeled as flat using the average half-width of the fuel meat. The average fuel meat arc length is 2.65-in (see Table 6.9-1 in Chapter 6, *Criticality Evaluation*).

There are two general classes of ATR fuel element, XA and YA. The XA fuel element has a fresh fuel loading of $1,075 \pm 10$ g U-235. The XA fuel element is further subdivided into fuel element types 7F, 7NB, 7NBH. In the 7F fuel element, all 19 fuel plates are loaded with enriched uranium in an aluminum matrix with the eight outer plates (1 through 4 and 16 through 19) containing boron as a burnable poison. The fuel element 7NB contains no burnable poison. The 7NBH fuel element is similar to the 7NB fuel element except that it contains one or two borated plates. The YA fuel element is identical to the 7F fuel element except that plate 19 of the YA fuel element is an aluminum alloy plate containing neither uranium fuel nor boron burnable poison. The YA fuel element has a fresh fuel loading of $1,022.4 \pm 10$ g U-235.

ATR fuel has an additional complexity that each fuel plate has different uranium number densities. The U-235 number densities in plates 5 through 15 are approximately constant, although the U-235 number densities in plates 1 through 4 and 16 through 19 are reduced. In the NEWT models, all 19 plates are assigned the same number densities for simplicity, although the total fuel loading is preserved. This level of detail is sufficient to generate a source term for shielding applications, especially since that the ATR fuel element is homogenized in the MCNP shielding model.

Both the XA type 7NB and 7F fuel elements are modeled in TRITON. The B-10 loading of the type 7F element is 660 mg (which has been conservatively rounded up to 700 mg), and for simplicity is distributed evenly throughout all 19 plates rather than only on the eight outer plates. The 7NBH element is bounded by the 7F element. The XA element bounds the YA element because the fission density (fissions/cm³) limit is the same for both fuel types, and the type XA element has a larger fuel volume than the type YA element.

Fuel plate 1 is nominally 0.080-in thick, fuel plates 2 through 18 are nominally 0.050-in thick, and fuel plate 19 is nominally 0.100-in thick. In the TRITON models, 0.050-in is used for all plates for simplicity. The fuel meat is nominally 0.02-in thick for all 19 plates. Channels 2 through 10 have a nominal width of 0.078-in, while channels 11 through 19 have a nominal width of 0.077-in. The channel width is modeled at 0.078-in between all plates for simplicity. Therefore, the pitch is $0.05+0.078 = 0.128$ -in.

Three TRITON models are developed:

- Type 7NB, minimum fuel loading (1065.0 g U-235),
- Type 7NB, maximum fuel loading (1085.0 g U-235),
- Type 7F, minimum fuel loading (1065.0 g U-235),

The U-235 enrichment is 93%. The balance of uranium is modeled as U-238.

The burnup parameters are selected to bound the highest burned ATR fuel element ever generated. This element had a starting U-235 loading of 1075 g, and a final U-235 loading of 457 g, or a depletion of 57.5%. The fuel is burned in one continuous cycle for 48 days to achieve approximately the same level of depletion of the highest burned ATR element. A bounding element power of 10 MW is utilized, for a total burnup of 480 MWD². The source is allowed to cool 1670 days after reactor shutdown.

The fuel cycle modeled is an extreme case of the ATR fuel cycle. The ATR reactor consists of 5 lobes of 8 fuel elements each, and the maximum lobe power is 60 MW (total reactor power is limited to 250 MW). Therefore, the average power in a maximum power lobe is 7.5 MW, although the maximum fuel element power may be in the range from 8 to 9 MW. A fuel element power of 10 MW is conservatively modeled. Likewise, a typical cycle length is in the range from 49 to 56 days, while 48 days is modeled. To completely burn a fuel element would typically require a minimum of three cycles, and any down time between cycles has been conservatively ignored in the calculation.

² The element burnup of 480 MWD should not be a limit for licensing purposes because the element burnup is typically not known in units of MWD. ATR staff compute and report the final U-235 mass within an element.

The ATR gamma source is summarized in Table 5.2-3. Note that the ATR basket may transport up to eight fuel elements.

The axial burnup distribution provided in Table 5.2-6 is simply assumed based upon a peak of 1.45 at the axial center. This distribution is the ratio of the burnup in each segment to the average burnup. The distribution is divided over 10 segments of equal width over the fuel length of 48-in (121.92 cm).

Key output data are summarized in Table 5.2-2. The fuel depletion may be computed based on the initial and final U-235 mass. The initial U-235 mass is 1065.0 g, and the final U-235 mass is 440.5 g, or a depletion of 58.6%. The decay heat at a decay time of 1670 days is 29.8 W.

5.2.1.4 TRIGA Fuel

The TRIGA fuel gamma source term is derived from information in INEL-96/0482 [4]. This report provides detailed activity values for 145 key isotopes as a function of burnup and decay time for four different TRIGA fuel types. These four fuel types are included in Section 1.2.2, *Contents*:

- Type 101 = aluminum-clad standard
- Type 103 = stainless steel-clad standard
- Type 109 = High-enrichment Fuel Life Improvement Program (FLIP)
- Type 117 = Low-enrichment Fuel Life Improvement Program (FLIP-LEU-I)

Key parameters for the four fuel types are summarized in Table 5.2-7. Decay times range from discharge to 20 years. Note that the minimum decay time reported in this table has been selected to be the minimum for transportation purposes.

The models used to generate the source are described in [4]. The TRIGA fuel is modeled with an irradiation time of 4 years. TRIGA reactors tend to run only sporadically rather than continuously, and TRIGA fuel elements often have residence times exceeding 10 years. Therefore, the source is conservative.

For shielding calculations, a bounding source term is selected. The Type 109 fuel has by far the largest burnup of the four candidate TRIGA fuels and hence results in the largest source. It is desired to set a minimum decay time of 1 year for the two higher-burnup fuels (Type 109 and 117) to allow many of the short-lived daughters to decay. For the two standard fuels, a much shorter 28 day decay time is stipulated. It may be demonstrated that the Type 109 fuel is bounding simply by comparing key isotopes (e.g., Co-60, Sr-90, Cm-244, etc.) in the activity tables provided in [4].

A fifth fuel type is included in Section 1.2.2, *Contents*, Type 203 (8.5 wt.% instrumented, stainless steel clad), which is simply a longer, instrumented version of Type 103. The source term for this fuel type is not specifically provided in [4]. However, the source for a Type 203 fuel element would be comparable to a Type 103 element, and the Type 103 element is well-bounded by the high-burnup Type 109 fuel element utilized in the shielding calculations.

However, source term data that could be utilized directly in MCNP are not provided in [4]. Rather, these activities are input into SCALE6 (ORIGEN-S) [3] to generate a suitable source

term that may be used in shielding computations. The source information from Table F.14 of [4] at discharge is input to ORIGEN-S, and then decayed to 1 year. The gamma source for TRIGA fuel is summarized in Table 5.2-3 **Error! Reference source not found.** Note that the TRIGA basket holds 19 fuel elements.

No axial burnup profile is provided for TRIGA fuel, and a flat distribution is utilized.

5.2.2 Neutron Source

The neutron sources are extracted from the same output files that define the gamma sources, as described in Section 5.2.1, *Gamma Source*. The neutron source for MURR, MITR-II, ATR, and TRIGA are presented in Table 5.2-8 **Error! Reference source not found.** The neutron sources presented are the combined spontaneous fission and (α ,n) components. Aluminum in the fuel matrix is used as the target nucleus to generate the (α ,n) source for the MURR, MITR-II, and ATR fuels. For the TRIGA fuels, no (α ,n) target nuclides are present in the fuel matrix. By default, ORIGEN-S utilizes oxygen as a target nucleus if no other target nuclides are present. To be conservative, the (α ,n) source with an oxygen target is included in the total for TRIGA, although the actual (α ,n) source would be effectively zero because there is no applicable target nuclide in the fuel matrix. This assumption results in an additional conservatism of 9% in the neutron source for the TRIGA fuels.

The neutron sources for MURR, MITR-II, and ATR are extracted from the minimum fuel loading models, consistent with the gamma sources. However, while the fuel loading had essentially no effect on the gamma source, the neutron source is noticeably larger when the minimum fuel loading is utilized. For these fuels, the increase in neutron source strength when using the minimum fuel loading rather than maximum fuel loading is approximately 1 to 3%.

The neutron sources for MURR, MITR-II, ATR, and TRIGA fuel are input with the same axial distribution provided in Section 5.2.1, *Gamma Source*.

Table 5.2-1 – TRITON Input and Supporting Data (MURR, MITR-II, ATR)

Parameter	MURR(-)	MURR(+)	MITR-II(-)	MITR-II(+)	ATR(-)①	ATR(+)
U-235 loading (g)	767.2	782.8	500.0	513.0	1065.0	1085.0
Fuel meat temperature (K)	358.0	358.0	341.0	341.0	378.0	378.0
Fuel cladding temp. (K)	355.2	355.2	338.0	338.0	372.4	372.4
Water temp. (K)	327.4	327.4	323.0	323.0	340.8	340.8
Water density (g/cm ³)	0.983	0.983	0.9968	0.9968	0.9786	0.9786
Fuel meat width (in)	2.88	2.88	2.08	2.08	2.65	2.65
Fuel meat thickness (in)	0.02	0.02	0.03	0.03	0.02	0.02
Fuel plate thickness (in)	0.05	0.05	0.08②	0.08	0.05	0.05
Fuel plate pitch (in)	0.13	0.13	0.158	0.158	0.128	0.128
Active fuel length (in)	24.0	24.0	22.375	22.375	48.0	48.0
Number of fuel plates	24	24	15	15	19	19
Fuel Meat Volume (cm ³)	544.1	544.1	342.5	342.5	792.6	792.6
U density (g/cm ³)	1.52	1.55	1.57	1.61	1.44	1.47
U-235 density (g/cm ³)	1.41	1.44	1.46	1.50	1.34	1.37
U-238 density (g/cm ³)	0.1061	0.1083	0.1099	0.1127	0.1011	0.1030
Al density (g/cm ³)	2.25	2.25	2.24	2.23	2.26	2.26
UAlx+Al density (g/cm ³)	3.77	3.79	3.81	3.84	3.71	3.73
N U-235 (atom/b-cm)	3.6124E-03	3.6859E-03	3.7399E-03	3.8371E-03	3.4426E-03	3.5072E-03
N U-238 (atom/b-cm)	2.6847E-04	2.7393E-04	2.7794E-04	2.8517E-04	2.5584E-04	2.6065E-04
N Al (atom/b-cm)	5.0239E-02	5.0110E-02	5.0015E-02	4.9844E-02	5.0538E-02	5.0425E-02
U mass (g)	824.9	841.7	537.6	551.6	1145.2	1166.7
U mass (MTU)	8.2495E-04	8.4172E-04	5.3763E-04	5.5161E-04	1.1452E-03	1.1667E-03
Element power (MW)	1.25	1.25	0.25	0.25	10.0	10.0
Sp. Power (MW/MTU)	1515.3	1485.1	465.0	453.2	8732.4	8571.4
Irradiation time (D)	144.0	144.0	900.0	900.0	48.0	48.0
Cycles (#)	21	21	1	1	1	1
Decay time (D)	180	180	930	930	1670	1670
Burnup (MWD)	180.0	180.0	225.0	225.0	480.0	480.0
Burnup (MWD/MTU)	218,196	213,848	418,500	407,895	419,155	411,429

①Data in this column is for the model without B-10. For the model including B-10, the B-10 number density is 5.3115E-05 atoms/b-cm. The nominal B-10 loading in an ATR Type 7F assembly is 660 mg. This value has been conservatively rounded up to 700 mg.

②The grooves present in MITR-II cladding have been neglected.

Table 5.2-2 – TRITON Output Data (MURR, MITR-II, ATR)

Parameter	MURR(-)Ⓣ	MURR(+)	MITR-II(-)	MITR-II(+)
Initial U-235 (g)	767.2	782.8	500.0	513.0
Final U-235 (g)	530.4	545.8	203.3	215.8
Depleted mass (g)	236.8	237.0	296.7	297.2
Depletion (%)	30.9%	30.3%	59.3%	57.9%
Element decay heat (W)	147.6	147.6	23.7	23.6
Parameter	ATR(-)	ATR(+)	ATR(-) with B-10	--
Initial U-235 (g)	1065.0	1085.0	1065.0	--
Final U-235 (g)	440.8	460.1	440.5	--
Depleted mass (g)	624.2	624.9	624.5	--
Depletion (%)	58.6%	57.6%	58.6%	--
Element decay heat (W)	29.8	29.8	29.8	--

ⓉBounding analysis values in boldface.

Table 5.2-3 – Gamma Source Terms

	MURR	MITR-II	ATR	TRIGA
Upper Energy Bin (MeV)	Gamma Source (γ/s)			
4.50E-02 [ⓐ]	2.576E+14	4.379E+13	5.575E+13	2.573E+13
1.00E-01	9.423E+13	1.584E+13	1.973E+13	9.352E+12
2.00E-01	9.441E+13	1.370E+13	1.527E+13	8.658E+12
3.00E-01	1.976E+13	3.229E+12	3.897E+12	1.952E+12
4.00E-01	1.478E+13	2.426E+12	2.881E+12	1.498E+12
6.00E-01	4.237E+13	1.798E+13	1.445E+13	7.684E+12
8.00E-01	4.328E+14	3.918E+13	5.736E+13	1.928E+13
1.00E+00	7.534E+12	7.774E+12	5.941E+12	3.454E+12
1.33E+00	3.040E+12	1.398E+12	1.387E+12	8.832E+12
1.66E+00	1.786E+12	7.108E+11	5.689E+11	2.637E+12
2.00E+00	2.304E+11	3.700E+10	3.490E+10	2.716E+10
2.50E+00	2.171E+12	2.874E+11	2.387E+11	2.099E+11
3.00E+00	8.765E+09	1.392E+09	1.346E+09	1.065E+09
4.00E+00	4.661E+08	1.061E+08	1.061E+08	8.208E+07
5.00E+00	9.414E+01	1.355E+03	7.644E+02	2.045E+03
6.50E+00	3.740E+01	5.414E+02	3.051E+02	8.196E+02
8.00E+00	7.270E+00	1.058E+02	5.955E+01	1.606E+02
1.00E+01	1.582E+00	2.311E+01	1.300E+01	3.407E+01
Total	9.707E+14	1.463E+14	1.775E+14	8.932E+13
Number of Fuel Elements in Basket	8	11	8	19
Basket Total	7.766E+15	1.610E+15	1.420E+15	1.697E+15

[ⓐ]The lower energy bound for this group is 0.01 MeV.

Table 5.2-4 – Axial Burnup Distribution, MURR

Distance from Bottom of Fuel Element (cm)	Axial Burnup Distribution
5	0.872
10	0.939
15	1.132
20	1.233
25	1.367
30	1.358
35	1.308
40	1.233
45	1.023
50	0.679
55	0.486
60	0.369

Table 5.2-5 – Axial Burnup Distribution, MITR-II

Distance from Bottom of Fuel Element (cm)	Axial Burnup Distribution	MCNP Input
2.368	0.999	0.500
4.736	0.788	0.394
9.472	0.788	0.788
14.208	0.901	0.901
18.944	1.042	1.042
23.680	1.140	1.140
28.416	1.253	1.253
33.152	1.267	1.267
37.888	1.112	1.112
42.624	1.028	1.028
47.360	0.901	0.901
52.096	0.774	0.774
54.464	0.802	0.401
56.833	0.999	0.500

Table 5.2-6 – Axial Burnup Distribution, ATR

Distance from Bottom of Fuel Element (cm)	Axial Burnup Distribution
12.19	0.50
24.38	0.70
36.58	1.00
48.77	1.30
60.96	1.45
73.15	1.45
85.34	1.30
97.54	1.00
109.73	0.70
121.92	0.50

Table 5.2-7 – TRIGA Fuel Parameters

Fuel Type	Enrichment (%)	Maximum U-235 depletion (%)	Maximum Burnup (MWD/MTU)	Minimum Decay Time
Type 101 (Aluminum-clad standard)	20.0	22.42	36,953	28 days
Type 103/203 (Stainless steel-clad standard)	20.0	20.72	34,111	28 days
Type 109 (FLIP)	70.0	59.74	339,368	1 year
Type 117 (FLIP-LEU-I)	20.0	43.81	75,415	1 year

Table 5.2-8 – Neutron Source Term

	MURR	MITR-II	ATR	TRIGA
Upper Energy Bin (MeV)	Neutron Source (n/s)	Neutron Source (n/s)	Neutron Source (n/s)	Neutron Source (n/s)
1.000E-08 [ⓐ]	6.449E-09	2.486E-08	1.201E-08	7.233E-08
3.000E-08	7.938E-09	6.731E-08	3.617E-08	1.283E-07
5.000E-08	8.240E-09	9.002E-08	4.933E-08	1.547E-07
1.000E-07	2.361E-08	2.987E-07	1.652E-07	4.866E-07
2.250E-07	7.635E-08	1.077E-06	5.993E-07	1.703E-06
3.250E-07	7.588E-08	1.119E-06	6.239E-07	1.748E-06
4.140E-07	7.688E-08	1.152E-06	6.430E-07	1.802E-06
8.000E-07	4.171E-07	6.366E-06	3.556E-06	9.942E-06
1.000E-06	2.611E-07	4.026E-06	2.254E-06	6.247E-06
1.125E-06	1.772E-07	2.740E-06	1.534E-06	4.233E-06
1.300E-06	2.632E-07	4.080E-06	2.284E-06	6.318E-06
1.855E-06	1.351E-05	2.345E-05	8.317E-06	2.276E-05
3.059E-06	3.703E-05	6.370E-05	2.319E-05	6.128E-05
1.068E-05	2.487E-04	5.868E-04	2.809E-04	6.377E-04
2.902E-05	2.430E-03	1.530E-02	1.047E-02	2.622E-03
1.013E-04	1.556E-02	9.885E-02	6.686E-02	1.909E-02
5.830E-04	1.850E-01	1.192E+00	8.143E-01	2.893E-01
3.035E-03	2.194E+00	1.450E+01	9.925E+00	3.385E+00
1.503E-02	2.700E+01	1.756E+02	1.204E+02	3.705E+01
1.111E-01	8.508E+02	5.440E+03	3.766E+03	7.566E+02
4.076E-01	5.625E+03	3.378E+04	2.328E+04	4.304E+03
9.072E-01	1.323E+04	7.709E+04	5.285E+04	9.353E+03
1.423E+00	1.235E+04	7.524E+04	5.203E+04	9.709E+03
1.827E+00	8.372E+03	5.188E+04	3.576E+04	6.981E+03
3.012E+00	7.363E+03	4.241E+04	2.753E+04	1.626E+04
6.376E+00	5.001E+02	7.811E+03	4.327E+03	1.357E+04
2.000E+01	4.587E+01	7.907E+02	4.356E+02	1.207E+03
Total	4.837E+04	2.946E+05	2.001E+05	6.218E+04
Number of Fuel Elements in Basket	8	11	8	19
Basket Total	3.869E+05	3.241E+06	1.601E+06	1.181E+06

[ⓐ]The lower energy bound for this group is 1.0E-11 MeV.

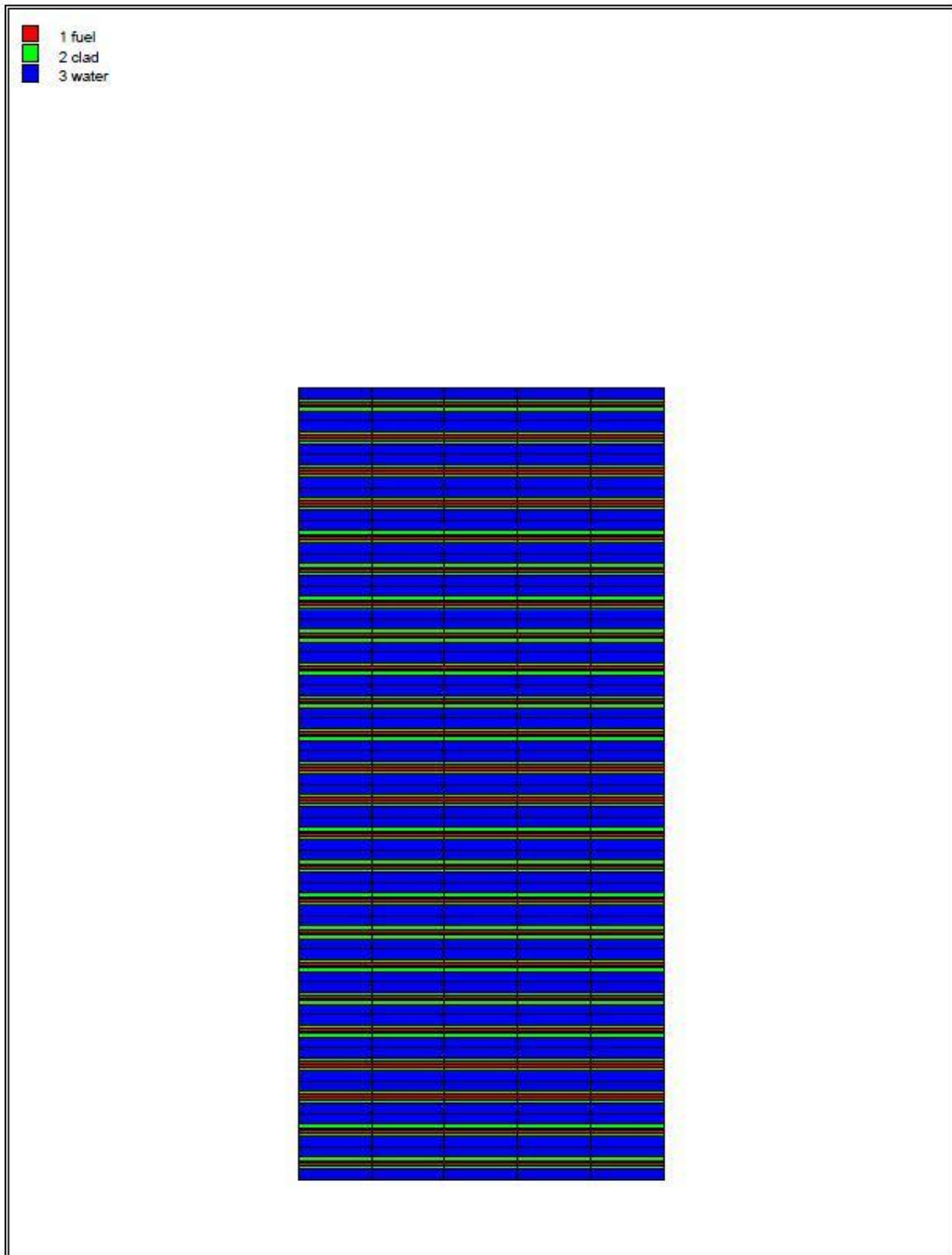


Figure 5.2-1 – NEWT Model for MURR

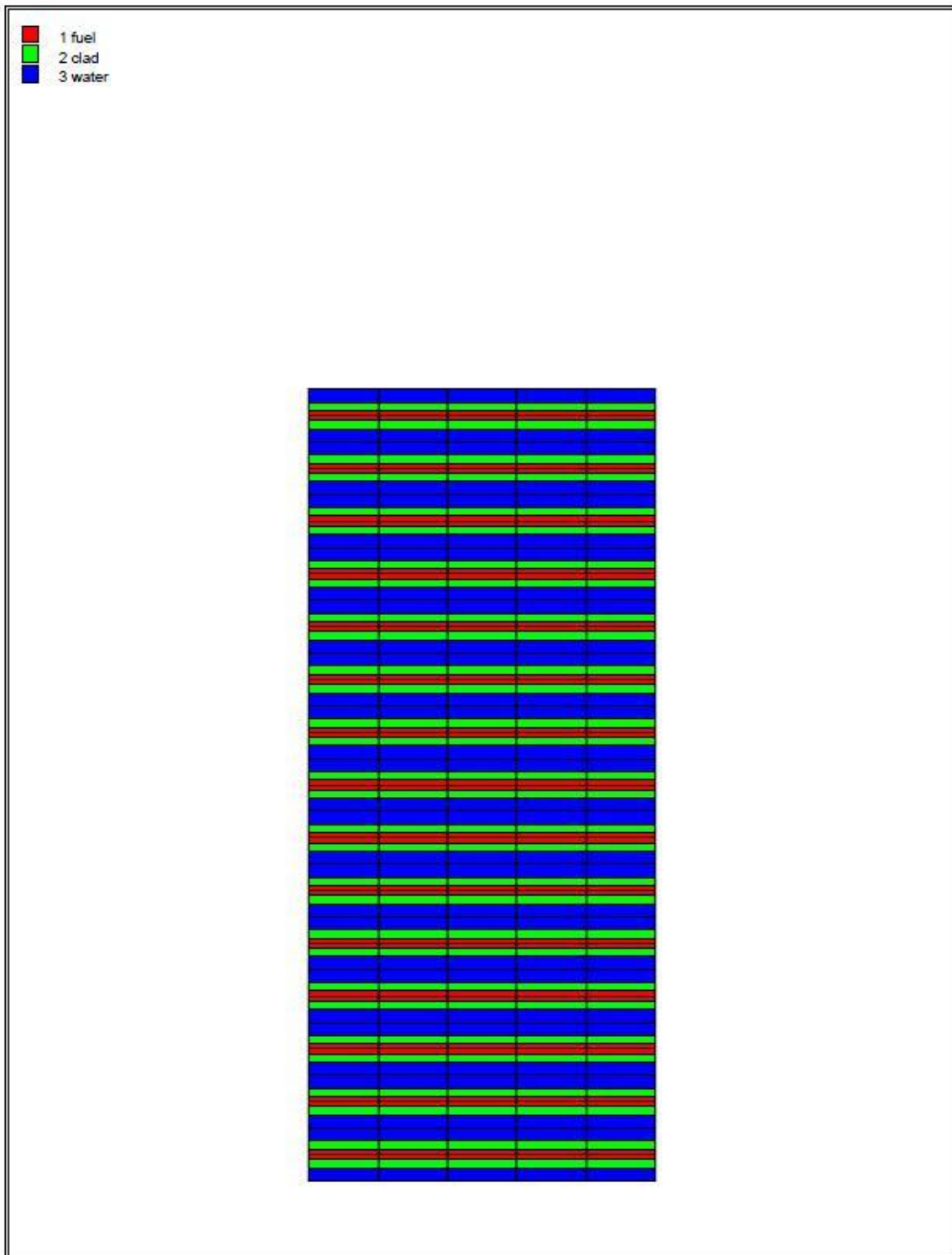


Figure 5.2-2 – NEWT Model for MITR-II

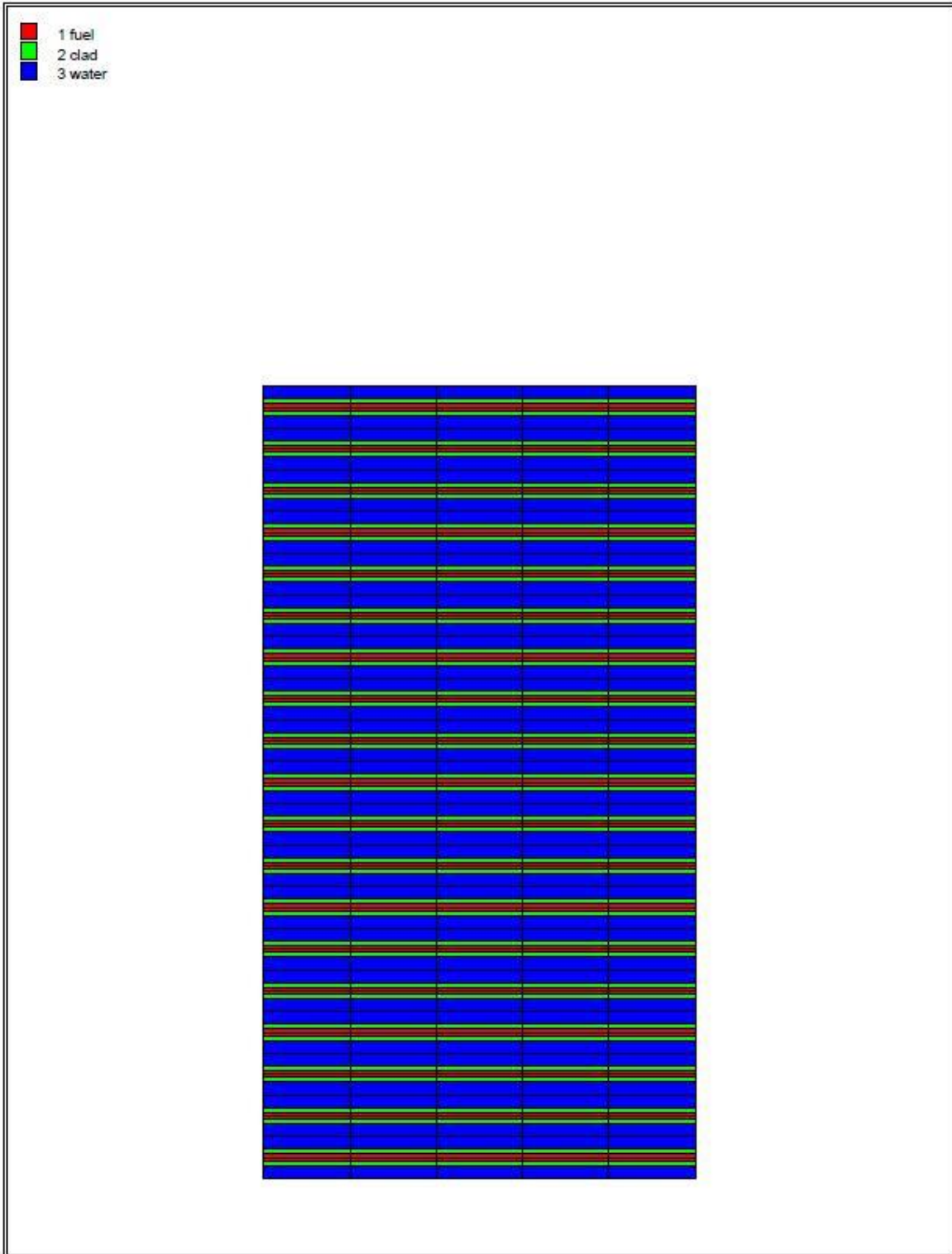


Figure 5.2-3 – NEWT Model for ATR

5.3 Shielding Model

5.3.1 Configuration of Source and Shielding

All relevant design features of the BRR Package are modeled in three-dimensions in MCNP, as shown in Figure 5.3-1. The key dimensions relevant to the MCNP model are summarized in Table 5.3-1 and are obtained from Section 1.3.3, *Packaging General Arrangement Drawings*. Minor details are not included in this table but may be inferred from the drawings.

Some differences exist between the as-modeled and packaging general arrangement drawing dimensions, as shown in Table 5.3-1. Most differences are small and may be neglected. The only notable differences are the outer diameter of the impact limiters, and the diameter of lead at the bottom of the cask. The outer diameter of the impact limiters is modeled at a reduced diameter of 72.0-in, which is conservative because the dose rate tally location is brought closer to the source. Also, the lead diameter in the cask bottom is modeled at 9.75-in rather than 10.3-in, which is conservative for shielding.

To simplify model preparation and add conservatism, the impact limiters are modeled simply as air, neglecting the impact limiter foam and outer steel shell. The “impact limiter air” is modeled with a different material number than the other air regions to more clearly illustrate the location of the impact limiters (see Figure 5.3-1), although the composition is unchanged. Credit is taken for the distance provided by the impact limiters, although the impact limiters are modeled simply as cylinders without the conical regions.

An axial lead slump of 1.18-in (see Section 2.7.1.2, *End Drop*) is modeled at the top of the cask. This slump represents the maximum expected slump due to lead shrinkage and a drop event. Also, an additional 0.0625-in radial lead shrinkage is assumed.

Each fuel element type is transported in its own unique basket. Key geometrical parameters for the four basket designs are summarized in Table 5.3-2. As with the cask, this table shows both the actual and as-modeled dimensions. Most differences are within round-off and may be neglected. For the TRIGA basket, the final cavity length is longer than the as-modeled dimension, although this has no effect on the results because the fuel elements are modeled shifted upward to the bottom of the shield plug. The baskets and source are also shown graphically in Figure 5.3-2 and Figure 5.3-3.

Because the MURR, MITR-II, and ATR fuels are geometrically complex, the fuel elements are homogenized over the active length of the fuel and distributed across the width of each basket compartment. Fuel element homogenization is a standard practice utilized to simplify complex source geometry and has little effect on the final results. Basic fuel dimensions used in the homogenization calculation are summarized in Table 5.3-3. These fuel dimensions are not modeled explicitly in MCNP.

For the TRIGA fuel, the fuel is a simple cylindrical design. Therefore, the TRIGA fuel elements are modeled explicitly, and the source is distributed over the fuel pellets. Basic geometrical data for the modeled TRIGA fuel is summarized in Table 5.3-3. For the TRIGA fuel, the Type 109 fuel is modeled, as this fuel type results in the largest source.

Because each basket is custom designed for each fuel type, there is little space for axial shifting of the fuel elements. Of course, because the cask is transported in a vertical orientation, the fuel elements would simply rest on the bottom of the basket support plate during NCT. However, because it is desired to use the same MCNP models for both NCT and HAC, the fuel is modeled near the top of the cavity in each model. Modeling the fuel near the lid places the source in the closest proximity to the interface between the lid and cask side, where the lead concentration is at a minimum. Note that in actual practice, the active fuel region will never be up against the cask lid because of the offset due to the fuel element support structures (end caps, nozzles, etc.).

Table 5.3-3 provides both the active fuel length and total overall length of each fuel element. If it is assumed that the active fuel is centered within the fuel element, the minimum distance between the active fuel and cask lid may be estimated. In all models, the distance between the top of the active fuel and bottom of the cask lid is less than or equal to this minimum distance. The minimum estimated and modeled distances from the top of the active fuel to the bottom of the lid are listed below.

- MURR: 4.25-in estimated, 4.00-in modeled
- MITR-II: 1.945-in estimated, 0.54-in modeled
- ATR: 1.5-in estimated, 0.54-in modeled
- TRIGA: 6.95-in estimated, 2.6-in modeled

NCT dose rates are tallied at the package surface (i.e., surface of cask body and impact limiters), surface of the vehicle (the vehicle is assumed to be 8 feet wide), 2 m from the surface of the vehicle, and in the occupied location of the vehicle driver (assumed to be 25 feet from the cask centerline.) Details of the tally locations, with figures, are provided with the results in Section 5.4.4, *External Radiation Levels*.

Because the impact limiters are modeled as air, both NCT and HAC dose rates may be computed from a single MCNP model. Under HAC, tallies are measured 1 m from the surface of the package. In the radial direction, this distance is measured from the surface of the cask, so any radial impact limiter crush does not impact the dose rate location. In the axial direction, because an end drop results in a maximum crush of 10.5-in, as shown in Appendix 2.12.5, *Impact Limiter Performance Evaluation*, Table 2.12.5-13, a bounding crush of 12-in is applied at each end. The 1 m tally surface is measured from the hypothetical crushed end of the impact limiter, although the impact limiter crush is not modeled explicitly (since the impact limiter is modeled simply as air). It is demonstrated in Section 2.7.1.5, *Fuel Basket Stress Analysis* that the baskets remain intact after a drop event, and therefore the baskets may be modeled as undamaged for both NCT and HAC.

5.3.2 Material Properties

As indicated in Section 5.3.1, *Configuration of Source and Shielding*, homogenized fuel number densities are utilized in the MURR, MITR-II, and ATR fuel models. For nominal fuel meat and cladding thicknesses, the total mass of U-235, U-238, and aluminum is estimated for each fuel element. For this computation, all structural aluminum is ignored, and the width of the plates is treated as equal to the width of the fuel matrix for simplicity. These assumptions result in a conservative underestimate of the aluminum mass. These masses are distributed over the

BRR Package Safety Analysis Report

volume of each basket over the active fuel length. The basket compartment volumes are computed based on the dimensions provided in Table 5.3-2. The homogenized data are summarized in Table 5.3-4, and homogenized number densities are provided in Table 5.3-5. Note that the number densities of all three fuel types are quite similar, as all three fuel types are aluminum plate fuel.

The TRIGA fuel composition is provided in Table 5.3-6 and is based on 196 g uranium, 2,060 g zirconium, H/Zr ratio of 1.6, and U-235 enrichment of 70%. The composition of stainless steel cladding utilized is taken from the SCALE material library [5] and is provided in Table 5.3-7. The zirconium rod in the center of the active fuel is modeled as pure with a density of 6.5 g/cm³ [1]. The graphite reflectors in the TRIGA fuel elements are modeled as air.

The baskets are manufactured out of stainless steel, and the cask is constructed of stainless steel and lead. The stainless steel composition and density utilized in the MCNP models are provided in Table 5.3-7. Lead is modeled as pure with a density of 11.35 g/cm³ [1].

Void spaces are filled with dry air. The composition is obtained from SCALE material library [5] and is provided in Table 5.3-8.

Table 5.3-1 – Key Cask Model Dimensions

Item	Dimension (in)
Cask Radial	
Cask inner diameter	16.0
Cask inner steel thickness	1.0
Cask lead thickness	8.0, modeled as 7.9375
Cask lead radial shrinkage gap (assumed)	0.0625
Cask outer steel thickness	2.0
Cask outer diameter (w/o heat shield)	38.0
Cask to heat shield gap	0.105
Heat shield thickness	0.105
Upper and lower impact limiter diameter	78.0, modeled as 72.0
Cask Axial Top	
Shield plug bottom plate thickness	1.0
Shield plug lead thickness	9.7, modeled as 9.58
Shield plug top plate thickness	0.5
Shield plug overall height	11.2, modeled as 11.08
Shield plug vent pipe inner diameter (schedule 40S)	0.824
Lid thickness	2.0
Upper impact limiter thickness at centerline	21.2
Overall height (including impact limiters)	119.5
Cask Axial Bottom	
Bottom outer plate thickness	1.0
Bottom lead thickness at centerline	7.7, modeled as 7.72
Bottom casting inner thickness (after machining)	1.1, modeled as 1.22
Bottom lead major diameter	23.7
Bottom lead minor diameter	10.3, modeled as 9.75
Drain hole diameter	0.5
Lower impact limiter thickness at centerline	21.2

Table 5.3-2 – Key Basket Model Dimensions

Item	Dimension (in)
MURR Basket	
Overall height	53.45
Cavity length	33.13
Support plate thickness	0.375
Compartment separator width	1.0
Shell outer diameter	15.63
Shell thickness	0.25
Inner tube outer diameter	7.9, modeled as 7.938
Inner tube inner diameter	7.0
MITR-II Basket	
Overall height	53.45
Cavity length	26.88, modeled as 26.87
Support plate thickness (after machining)	0.3, modeled as 0.25
Compartment thickness	0.12
Compartment perpendicular width	2.7
Outer row position diameter	10.6, modeled as 10.56
ATR Basket	
Overall height	53.45
Cavity length	51.38, modeled as 51.37
Support plate thickness	0.5
Compartment separator width	0.375
Shell outer diameter	13.5
Shell thickness	0.25
Inner tube outer diameter	7.2
Inner tube inner diameter	6.5
TRIGA Basket	
Overall height	53.45
Cavity length	48.0, modeled as 46.42
Support plate thickness (after machining)	0.3, modeled as 0.25
Tube outer diameter	2.0
Tube wall thickness	0.12, modeled as 0.11
Inner row position diameter	6.5
Outer row position diameter	11.5

Table 5.3-3 – Key Fuel Dimensions

Item	Dimension (in)
MURR^①	
Nominal active fuel length	24
Overall length	32.5
Nominal cladding thickness	0.015
Nominal fuel matrix thickness	0.02
Nominal fuel matrix width	variable
MITR-II^①	
Nominal active fuel length	22.375
Overall length	26.265
Nominal cladding thickness	0.025
Nominal fuel matrix thickness	0.03
Nominal fuel matrix width	2.076
ATR^①	
Nominal active fuel length	48
Overall length	51
Nominal cladding thickness (plate 1 / plates 2 – 18, plate 19)	0.03 / 0.015 / 0.04
Nominal fuel matrix thickness	0.02
Nominal fuel matrix width	variable
TRIGA (Type 109)	
Active fuel length	15
Overall length	28.9
Fuel pellet outer diameter	1.44
Fuel pellet inner diameter	0.25
Cladding outer diameter	1.48
Cladding thickness	0.02
Top reflector length	2.6
Top bottom reflector length	3.7
Zirconium rod diameter	0.225

^①The fuel dimensions for MURR, MITR-II, and ATR are used in the homogenization calculations, but are not modeled explicitly.

Table 5.3-4 – Homogenized Fuel Data

Parameter	MURR	MITR-II	ATR
U-235 (g)	785	515	1200
U-238 (g)	50.1	32.9	76.6
Al (g)	3353.1	2311.9	5414.5
Compartment volume (cm ³)	4884.2	3000.2	8192.0

Table 5.3-5 – Homogenized Fuel Number Densities (atom/b-cm)

Isotope	MURR	MITR-II	ATR
U-235	4.1178E-04	4.3979E-04	3.7531E-04
U-238	2.5952E-05	2.7717E-05	2.3653E-05
Al	1.5322E-02	1.7198E-02	1.4752E-02
Total	1.5760E-02	1.7666E-02	1.5151E-02

Table 5.3-6 – TRIGA Fuel Number Densities (atom/b-cm)

Isotope	TRIGA
H	5.6041E-02
Zr	3.5025E-02
U-235	9.0406E-04
U-238	3.8442E-04
Total	9.2354E-02

Table 5.3-7 – SS304 Composition

Component	Wt.%
C	0.08
Si	1.0
P	0.045
Cr	19.0
Mn	2.0
Fe	68.375
Ni	9.5
Density (g/cm ³)	7.94

Table 5.3-8 – Air Composition

Component	Wt.%
N	76.508
O	23.4793
C	0.0126
Density (g/cm ³)	0.0012

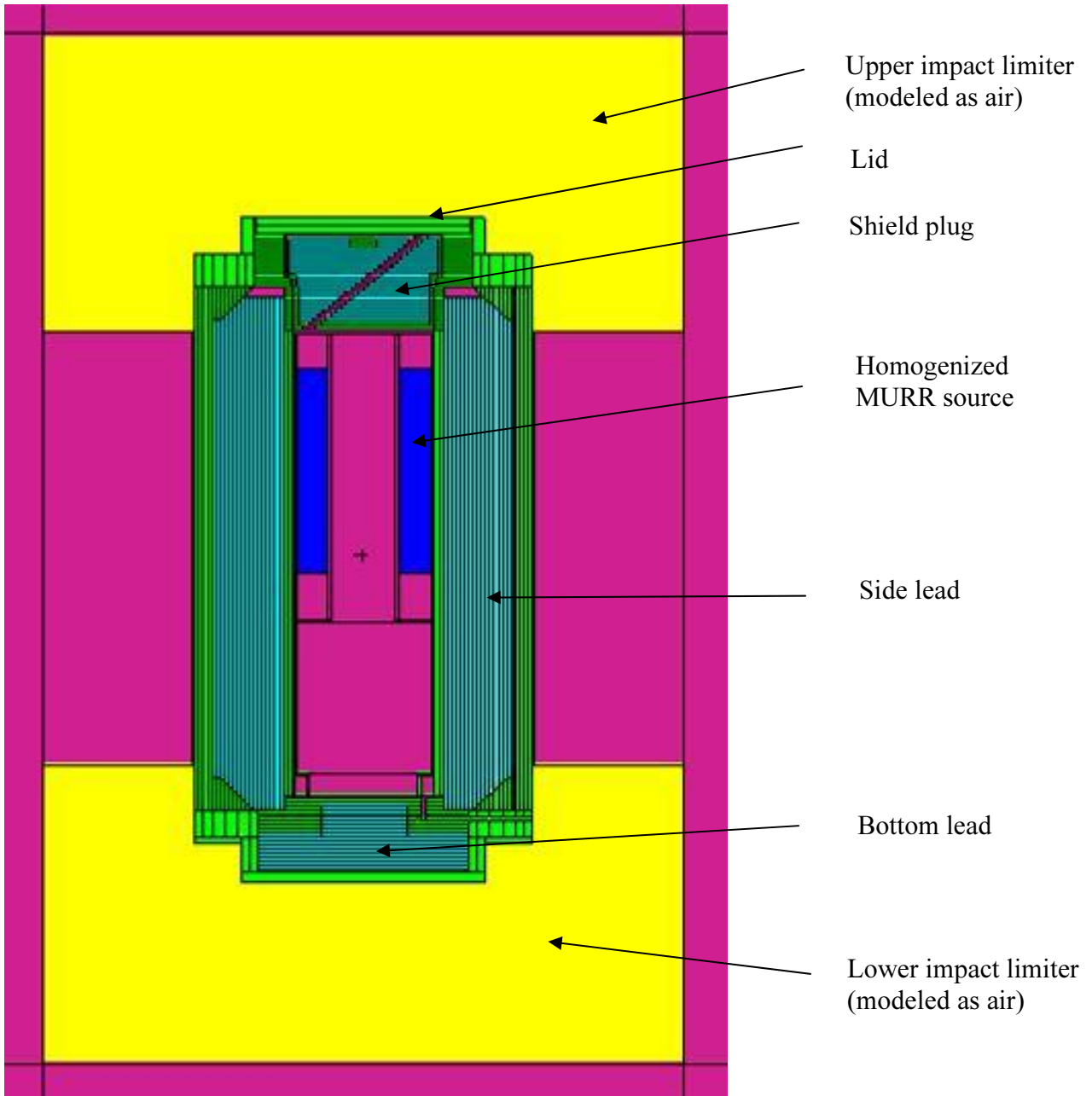
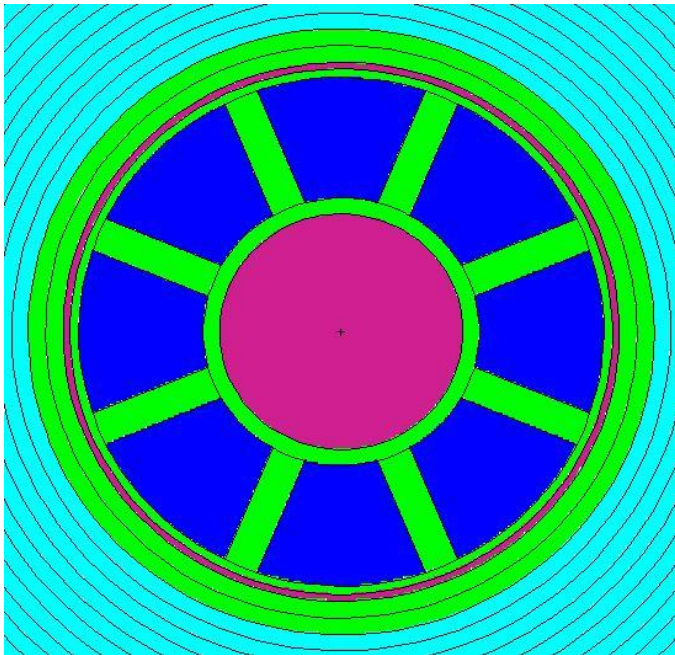
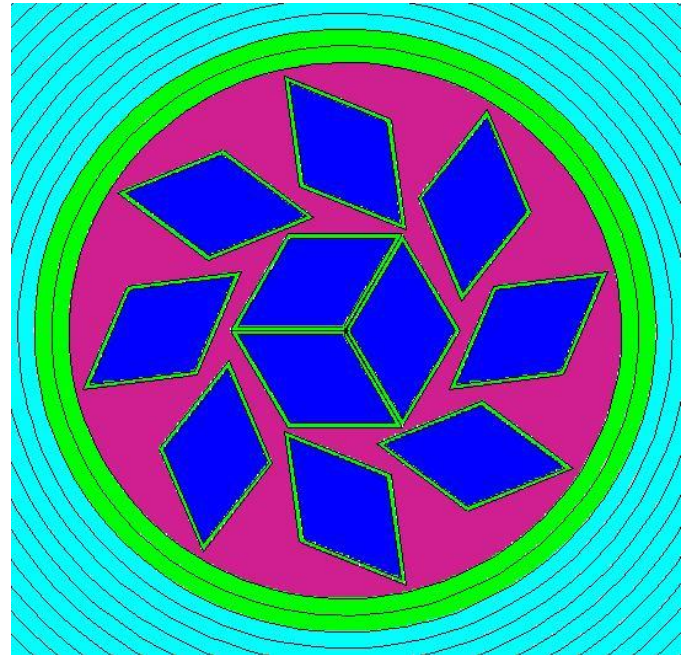


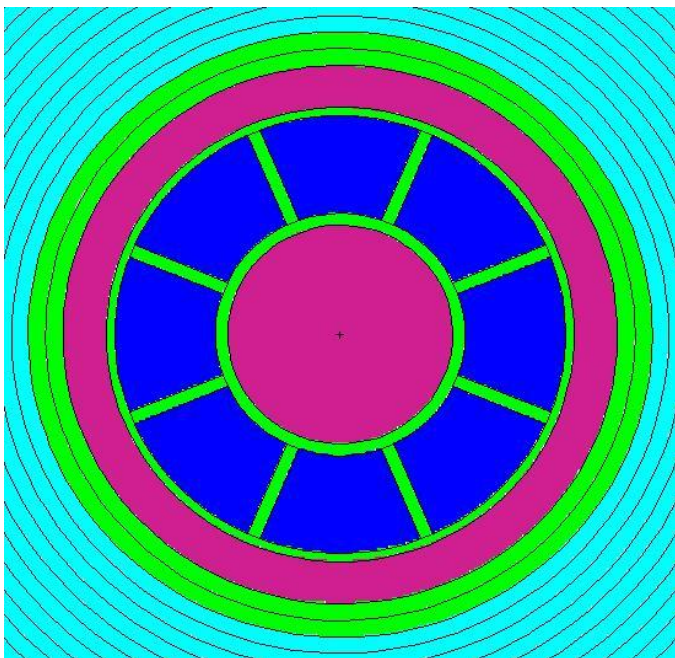
Figure 5.3-1 – Shielding Model



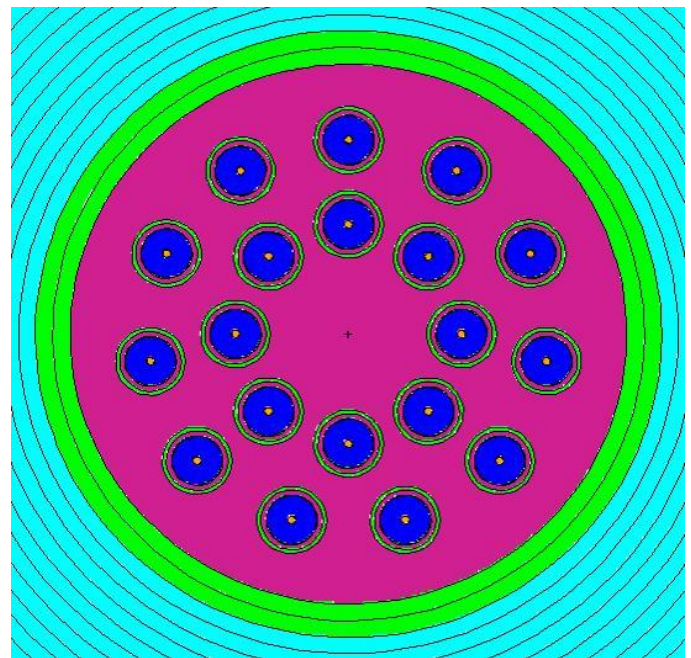
MURR



MITR-II



ATR



TRIGA

Figure 5.3-2 – Basket Models (cross section)

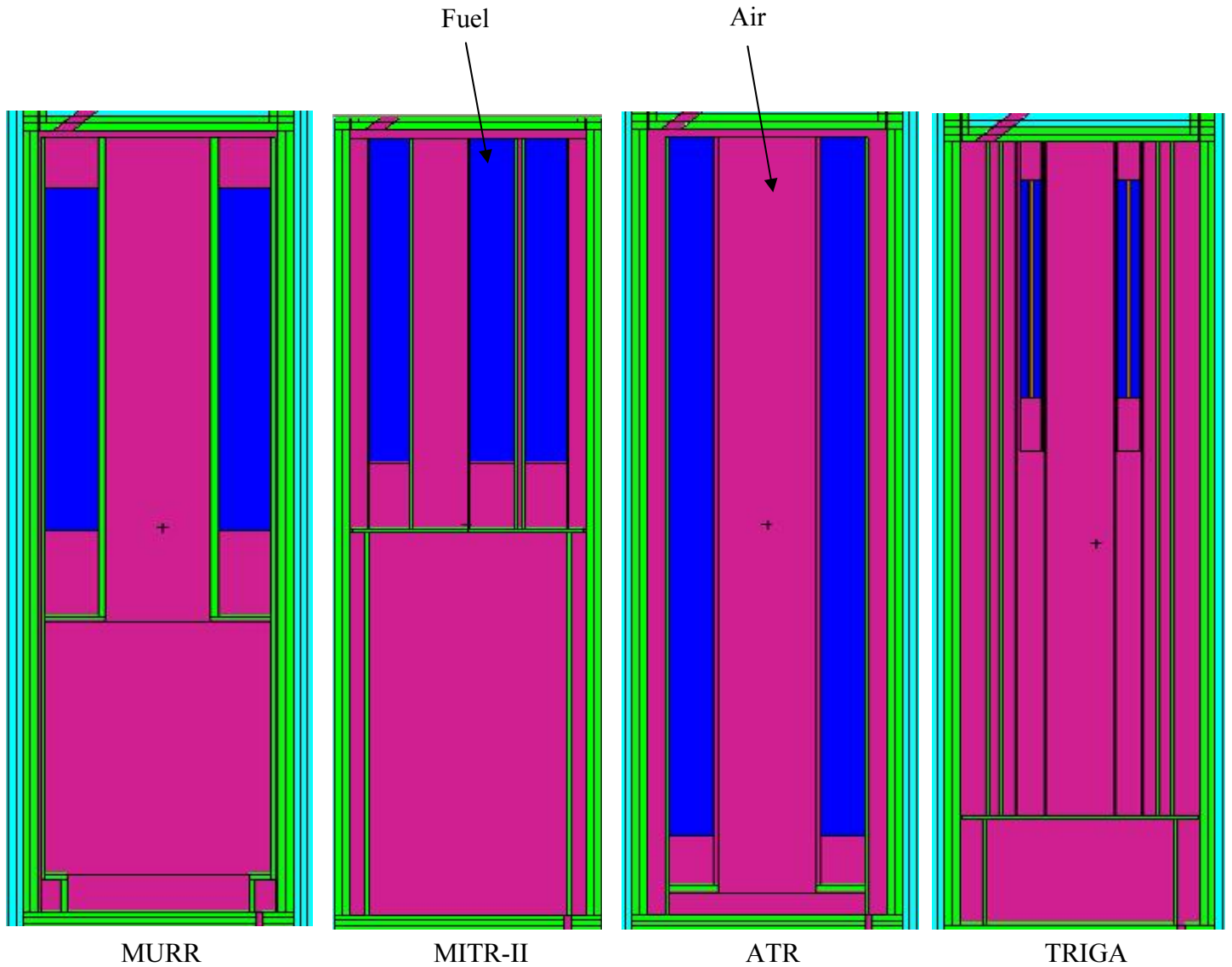


Figure 5.3-3 – Basket Models (axial)

5.4 Shielding Evaluation

5.4.1 Methods

The dose rates are computed using the MCNP5 v1.30 computer program [2]. All relevant package features are modeled in three-dimensions. For simplicity, the impact limiters are modeled simply as air, although the outer surfaces of the impact limiters are treated as the outer surfaces of the package when computing surface dose rates at the ends of the package. It is assumed that under HAC the impact limiters remain attached and suffer 12-in axial crush on each end, and the same MCNP model is used to compute both NCT and HAC dose rates. This approach is reasonable, because no shielding credit is taken for the impact limiters, other than distance.

Separate models are developed for neutron and gamma radiation. For MURR, MITR-II, and ATR fuel, the fuel plates are homogenized and fill the basket cavities. Homogenization is performed to simplify the source description. For the TRIGA fuel, because the fuel is a simple cylinder, the fuel is modeled explicitly, and the source is distributed over the fuel matrix. Note that subcritical neutron multiplication is handled automatically by MCNP.

Little clearance is available in any of the designs for axial shifting of the fuel. Because the fuel is positioned by the baskets closer to the lid end, to maximize the dose rates at the impact limiter surface, the fuel is modeled as shifted to the top of the cavity. Distance credit is taken for non-fuel structural material, such as the graphite reflectors in the TRIGA fuel.

In general, secondary gammas generated by neutron capture are not computed, as there is no hydrogenous neutron shielding material. Secondary gamma dose rates are computed only for the TRIGA fuel because hydrogen is included in the fuel matrix. However, even for the TRIGA fuel, the secondary gamma dose rate is essentially zero, because the secondary gammas are generated inside the cask, and are then attenuated in the shield.

In all cases, dose rates are computed on segmented surfaces so that the maximum dose rates may be located. Neutron and gamma surface fluxes are computed by MCNP, and converted to dose rates using flux-to-dose rate conversion factors (see Section 5.4.3, *Flux-to-Dose Rate Conversion*). Side dose rates are averaged over the circumference of the cylindrical tallies.

5.4.2 Input and Output Data

A sample input file (gamma source, MITR-II fuel) is included in Section 5.5.3.2, *MCNP Input File*. The input file may be compared against the gamma sources in table Table 5.2-3 and gamma axial distribution in Table 5.2-5 to verify proper model setup. Model geometry and material descriptions may be verified by inspection of the supplied input file.

The results are highly converged for all dose rate locations of interest. In the models with a gamma source, the materials are split into thin layers, and the importance of each layer is increased away from the source. In the models with a neutron source, the importances are all set to the same value, as there is no neutron shield. Statistical uncertainties are typically in the range of 2-3%.

5.4.3 Flux-to-Dose Rate Conversion

ANSI/ANS-6.1.1-1977 flux-to-dose rate conversion factors are used in this analysis. These are obtained from the MCNP User's Manual [2], Tables H.1 and H.2, although these values have been converted to provide results in mrem/hr rather than rem/hr. These conversion factors are provided in Table 5.4-1.

5.4.4 External Radiation Levels

A total of eight input files are developed to compute the NCT and HAC dose rates. A gamma and neutron model is developed for each of the four sources. The files are itemized as follows, where N refers to neutron modeling and G refers to gamma modeling:

- MURR fuel: MURR_N2, MURR_G2
- MITR-II fuel: MIT_N2, MIT_G2
- ATR fuel: ATR_N2, ATR_G2
- TRIGA fuel: TRIGA_NG2, TRIGA_G2

For exclusive use transport, the following 10 CFR 71.47 dose rates must be met:

- Maximum NCT cask surface dose rate of 200 mrem/hr. The higher 1000 mrem/hr limit is not claimed because the vehicle will be open. The dose rate limit applies at the outer surface of the heat shield, and the outer surface of the impact limiters. These results are summarized in Table 5.4-2 and Table 5.4-3. See also Figure 5.4-1 and Figure 5.4-2 for a graphical depiction of the tally locations.
- Maximum NCT vehicle surface dose rate of 200 mrem/hr. This limit is somewhat redundant because it is the same as the cask surface limit, and the cask surface dose rates are always higher than the vehicle surface dose rates. In this case, the vehicle surface is projected, because the actual vehicle will be open. It is assumed the vehicle is 8 ft wide, and the cask is laterally centered on the vehicle. These results are summarized in Table 5.4-4. See also Figure 5.4-3 and Figure 5.4-4 for a graphical depiction of the tally locations.
- Maximum NCT dose rate 2 m from the vehicle surface of 10 mrem/hr. These results are summarized in Table 5.4-4. See also Figure 5.4-3 and Figure 5.4-4 for a graphical depiction of the tally locations.
- Maximum NCT dose rate in any occupied location of 2 mrem/hr. The only occupied location is the driver of the vehicle, which is assumed to be 25 ft from the centerline of the cask. These results are summarized in Table 5.4-5. See also Figure 5.4-3 and Figure 5.4-4 for a graphical depiction of the tally location.
- Maximum HAC dose rate of 1000 mrem/hr 1 m from the surface of the cask. As the impact limiters will remain attached under HAC, the end dose rates are computed 1 m from the ends of the impact limiters, assuming 12-in crush on each end. In the radial direction, the dose rates are computed 1 m from the heat shield. These results are summarized in Table 5.4-6 and Table 5.4-7. See also Figure 5.4-3, Figure 5.4-4, and Figure 5.4-5 for a graphical depiction of the tally locations.

Dose rates are not constant along the side of the cask. The dose rate is typically at a maximum next to the active fuel, and becomes lower away from this region. Therefore, it is customary to segment the tallies into small regions in order to capture the maximum dose rate. On the side surface of the cask, the tally is divided into 12 equal segments 10.7 cm wide (see Figure 5.4-1). On the cylindrical sides of the impact limiters, the tally is divided into 5 equal segments 17.6 cm wide (see Figure 5.4-2). On the upper and lower impact limiter surfaces, the tally is divided into 9 concentric rings of width 10.2 cm (see Figure 5.4-2).

For the four side tallies (vehicle surface, 2 m from vehicle surface, occupied location, and 1 m HAC), the tallies are segmented into 15 segments 20.3 cm wide (see Figure 5.4-3 and Figure 5.4-4). In addition, the side dose rates above and below the impact limiter surfaces are also reported, although these tallies are approximately 70 cm wide.

The HAC 1 m tallies from the top and bottom of the impact limiters are divided into 11 segments, up to 1 m radially from the surface of the thermal shield (see Figure 5.4-5).

The dose rates reported in the following tables are the summed gamma and neutron dose rates. Dose rates are presented for each of the four fuel types. The maximum cask surface dose rate is 13.4 mrem/hr (limit = 200 mrem/hr). The maximum vehicle surface dose rate is 2.9 mrem/hr (limit = 200 mrem/hr). The maximum dose rate 2 m from the surface of the vehicle is 0.3 mrem/hr (limit = 10 mrem/hr), and the maximum dose rate at the occupied location is 0.05 mrem/hr (limit = 2 mrem/hr). Therefore, all of the NCT dose rates are met with large margins.

Note that the maximum dose rate on the vehicle surface occurs at location 1 (see Figure 5.4-4), which is actually above the upper impact limiter. The dose rate is peaking in this region rather than beside the source because the gamma shielding is greatly reduced in the "corners" of the cask. Also, the modeled lead slump in this region could be contributing to this effect.

The maximum HAC dose rate 1 m from the cask is 2.3 mrem/hr (limit = 1000 mrem/hr), and occurs at measured from the top at location 11, for the reasons cited in the previous paragraph. Clearly, the HAC dose rate limit is met with a large margin.

The detailed results from the MITR-II fuel, including statistical uncertainties, are reported in Section 5.5.2, *Detailed MITR-II Results*. MITR-II is selected for this detailed presentation because it results in the largest cask surface dose rate.

Table 5.4-1 – Flux-to-Dose Rate Conversion Factors

E (MeV)	Neutron Factors (mrem/hr)/(n/cm²/s)	E (MeV)	Neutron Factors (mrem/hr)/(n/cm²/s)
2.50E-08	3.67E-03	0.5	9.26E-02
1.00E-07	3.67E-03	1.0	1.32E-01
1.00E-06	4.46E-03	2.5	1.25E-01
1.00E-05	4.54E-03	5.0	1.56E-01
1.00E-04	4.18E-03	7.0	1.47E-01
0.001	3.76E-03	10.0	1.47E-01
0.01	3.56E-03	14.0	2.08E-01
0.1	2.17E-02	20.0	2.27E-01
E (MeV)	Gamma Factors (mrem/hr)/(γ/cm²/s)	E (MeV)	Gamma Factors (mrem/hr)/(γ/cm²/s)
0.01	3.96E-03	1.4	2.51E-03
0.03	5.82E-04	1.8	2.99E-03
0.05	2.90E-04	2.2	3.42E-03
0.07	2.58E-04	2.6	3.82E-03
0.1	2.83E-04	2.8	4.01E-03
0.15	3.79E-04	3.25	4.41E-03
0.2	5.01E-04	3.75	4.83E-03
0.25	6.31E-04	4.25	5.23E-03
0.3	7.59E-04	4.75	5.60E-03
0.35	8.78E-04	5.0	5.80E-03
0.4	9.85E-04	5.25	6.01E-03
0.45	1.08E-03	5.75	6.37E-03
0.5	1.17E-03	6.25	6.74E-03
0.55	1.27E-03	6.75	7.11E-03
0.6	1.36E-03	7.5	7.66E-03
0.65	1.44E-03	9.0	8.77E-03
0.7	1.52E-03	11.0	1.03E-02
0.8	1.68E-03	13.0	1.18E-02
1.0	1.98E-03	15.0	1.33E-02

Table 5.4-2 – NCT Cask Side Total Dose Rates (mrem/hr)

Location	MURR	MITR-II	ATR	TRIGA
1	2.2	9.5	2.1	6.7
2	5.0	12.2	2.9	9.9
3	8.5	13.4	3.6	10.7
4	10.9	12.9	4.2	9.1
5	11.1	10.9	4.7	5.8
6	9.0	8.1	4.9	3.1
7	5.2	5.4	4.8	1.8
8	2.1	3.6	4.5	1.1
9	0.7	2.4	4.0	0.7
10	0.3	1.7	3.3	0.5
11	0.2	1.2	2.5	0.4
12	0.1	0.9	1.8	0.3
Max	11.1	13.4	4.9	10.7
Limit = 200 mrem/hr				

Table 5.4-3 – NCT Impact Limiter Total Dose Rates (mrem/hr)

	Upper Impact Limiter Side				Lower Impact Limiter Side			
Location	MURR	MITR-II	ATR	TRIGA	MURR	MITR-II	ATR	TRIGA
1	2.0	2.9	0.5	6.1	0.2	0.5	0.6	0.2
2	1.4	2.3	0.5	4.4	0.1	0.3	0.4	0.1
3	0.9	1.8	0.4	2.7	0.2	0.3	0.5	0.1
4	0.7	1.8	0.5	1.8	0.3	0.2	0.6	0.1
5	1.0	2.3	0.6	1.8	0.3	0.2	0.6	0.1
Max	2.0	2.9	0.6	6.1	0.3	0.5	0.6	0.2
	Upper Impact Limiter Horizontal				Lower Impact Limiter Horizontal			
Location	MURR	MITR-II	ATR	TRIGA	MURR	MITR-II	ATR	TRIGA
1	1.4	1.8	0.3	2.1	3.5	1.0	0.7	0.3
2	1.5	1.8	0.3	2.3	3.7	1.0	0.7	0.4
3	2.0	2.0	0.4	2.8	2.8	0.9	0.6	0.3
4	2.1	2.1	0.4	3.1	1.8	0.6	0.5	0.2
5	1.7	2.0	0.4	3.5	1.1	0.3	0.4	0.1
6	1.6	2.1	0.4	3.9	0.6	0.2	0.4	0.1
7	1.8	2.4	0.5	4.8	0.4	0.2	0.4	0.1
8	2.3	3.1	0.6	6.8	0.3	0.2	0.5	0.1
9	2.3	3.2	0.6	7.2	0.3	0.2	0.5	0.1
Max	2.3	3.2	0.6	7.2	3.7	1.0	0.7	0.4
Limit = 200 mrem/hr								

Table 5.4-4 – NCT Vehicle Side and 2 m Total Dose Rates (mrem/hr)

Location	Vehicle Side				2 m from Vehicle Side			
	MURR	MITR-II	ATR	TRIGA	MURR	MITR-II	ATR	TRIGA
1	1.0	1.4	0.3	2.9	0.1	0.2	0.1	0.2
2	0.7	1.2	0.3	2.0	0.2	0.2	0.1	0.2
3	0.6	1.1	0.3	1.5	0.2	0.2	0.1	0.2
4	0.6	1.2	0.3	1.2	0.2	0.3	0.1	0.2
5	0.7	1.4	0.4	1.2	0.2	0.3	0.1	0.2
6	1.2	1.7	0.6	1.4	0.2	0.3	0.1	0.2
7	1.7	1.9	0.7	1.5	0.3	0.3	0.1	0.2
8	1.9	1.9	0.9	1.4	0.3	0.3	0.1	0.2
9	1.6	1.6	0.9	1.0	0.3	0.3	0.1	0.2
10	1.1	1.3	0.8	0.7	0.2	0.2	0.1	0.2
11	0.6	0.9	0.7	0.4	0.2	0.2	0.1	0.2
12	0.3	0.6	0.6	0.3	0.2	0.2	0.1	0.1
13	0.2	0.4	0.4	0.2	0.2	0.2	0.1	0.1
14	0.1	0.3	0.3	0.1	0.1	0.2	0.1	0.1
15	0.2	0.2	0.3	0.1	0.1	0.2	0.1	0.1
16	0.2	0.2	0.4	0.1	0.1	0.1	0.1	0.1
17	0.2	0.1	0.3	0.05	0.1	0.1	0.1	0.1
Max	1.9	1.9	0.9	2.9	0.3	0.3	0.1	0.2
	Limit = 200 mrem/hr				Limit = 10 mrem/hr			

Table 5.4-5 – NCT Occupied Location Total Dose Rates (mrem/hr)

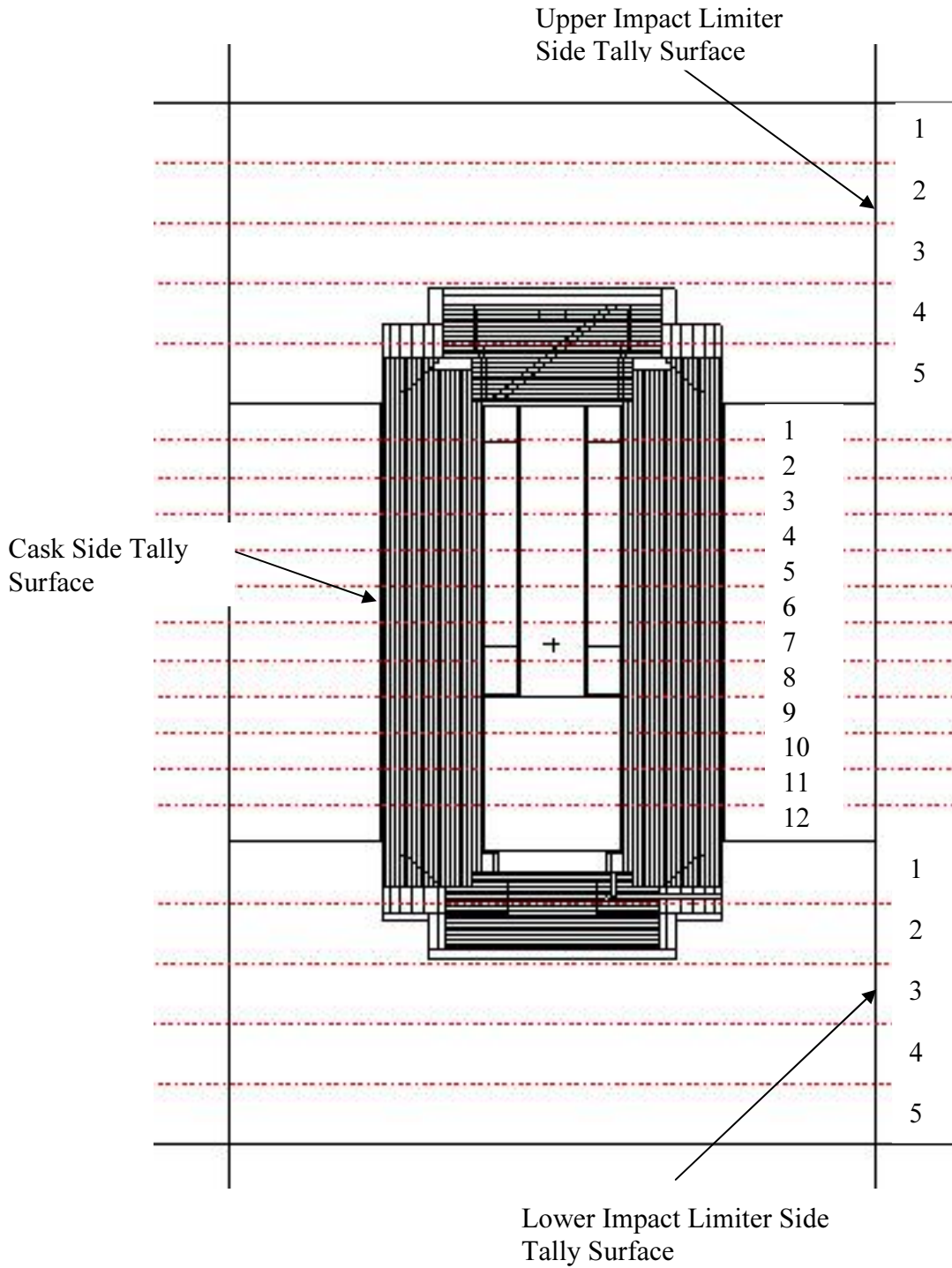
Location	MURR	MITR-II	ATR	TRIGA
1	0.04	0.05	0.02	0.04
2	0.04	0.05	0.02	0.04
3	0.04	0.05	0.02	0.04
4	0.04	0.05	0.02	0.04
5	0.04	0.05	0.02	0.04
6	0.05	0.05	0.02	0.04
7	0.05	0.05	0.02	0.04
8	0.04	0.05	0.02	0.04
9	0.04	0.05	0.02	0.04
10	0.04	0.05	0.02	0.04
11	0.04	0.05	0.02	0.04
12	0.04	0.04	0.02	0.03
13	0.04	0.04	0.02	0.03
14	0.04	0.04	0.02	0.03
15	0.04	0.04	0.02	0.03
16	0.04	0.04	0.02	0.03
17	0.03	0.04	0.02	0.03
Max	0.05	0.05	0.02	0.04
Limit = 2 mrem/hr				

Table 5.4-6 – HAC 1 m Side Total Dose Rates (mrem/hr)

Location	MURR	MITR-II	ATR	TRIGA
1	0.6	0.9	0.2	1.7
2	0.4	0.8	0.2	1.1
3	0.4	0.8	0.2	0.9
4	0.5	0.9	0.3	0.9
5	0.6	1.0	0.4	0.9
6	0.9	1.2	0.4	1.0
7	1.2	1.3	0.5	1.0
8	1.3	1.3	0.6	1.0
9	1.1	1.1	0.6	0.8
10	0.9	0.9	0.6	0.6
11	0.6	0.7	0.5	0.4
12	0.4	0.6	0.4	0.3
13	0.2	0.4	0.3	0.2
14	0.2	0.3	0.3	0.1
15	0.1	0.2	0.2	0.1
16	0.1	0.2	0.2	0.1
17	0.1	0.1	0.2	0.1
Max	1.3	1.3	0.6	1.7
Limit = 1000 mrem/hr				

Table 5.4-7 – HAC 1 m End Total Dose Rates (mrem/hr)

Location	Upper Impact Limiter				Lower Impact Limiter			
	MURR	MITR-II	ATR	TRIGA	MURR	MITR-II	ATR	TRIGA
1	0.6	0.7	0.1	1.0	1.4	0.4	0.3	0.1
2	0.7	0.7	0.1	1.0	1.5	0.4	0.3	0.1
3	0.8	0.8	0.1	1.2	1.3	0.4	0.2	0.1
4	0.8	0.8	0.1	1.2	1.0	0.3	0.2	0.1
5	0.8	0.8	0.1	1.2	0.8	0.3	0.2	0.1
6	0.7	0.8	0.1	1.3	0.6	0.2	0.2	0.1
7	0.7	0.8	0.1	1.3	0.5	0.2	0.2	0.1
8	0.6	0.8	0.1	1.3	0.3	0.1	0.1	0.05
9	0.6	0.8	0.1	1.4	0.3	0.1	0.1	0.04
10	0.6	0.9	0.2	1.7	0.2	0.1	0.1	0.03
11	0.8	1.0	0.2	2.3	0.1	0.1	0.2	0.04
Max	0.8	1.0	0.2	2.3	1.5	0.4	0.3	0.1
Limit = 1000 mrem/hr								



Note: All tallies are circumferential.

Figure 5.4-1 – Cask/Impact Limiter Side Tally Segmentations

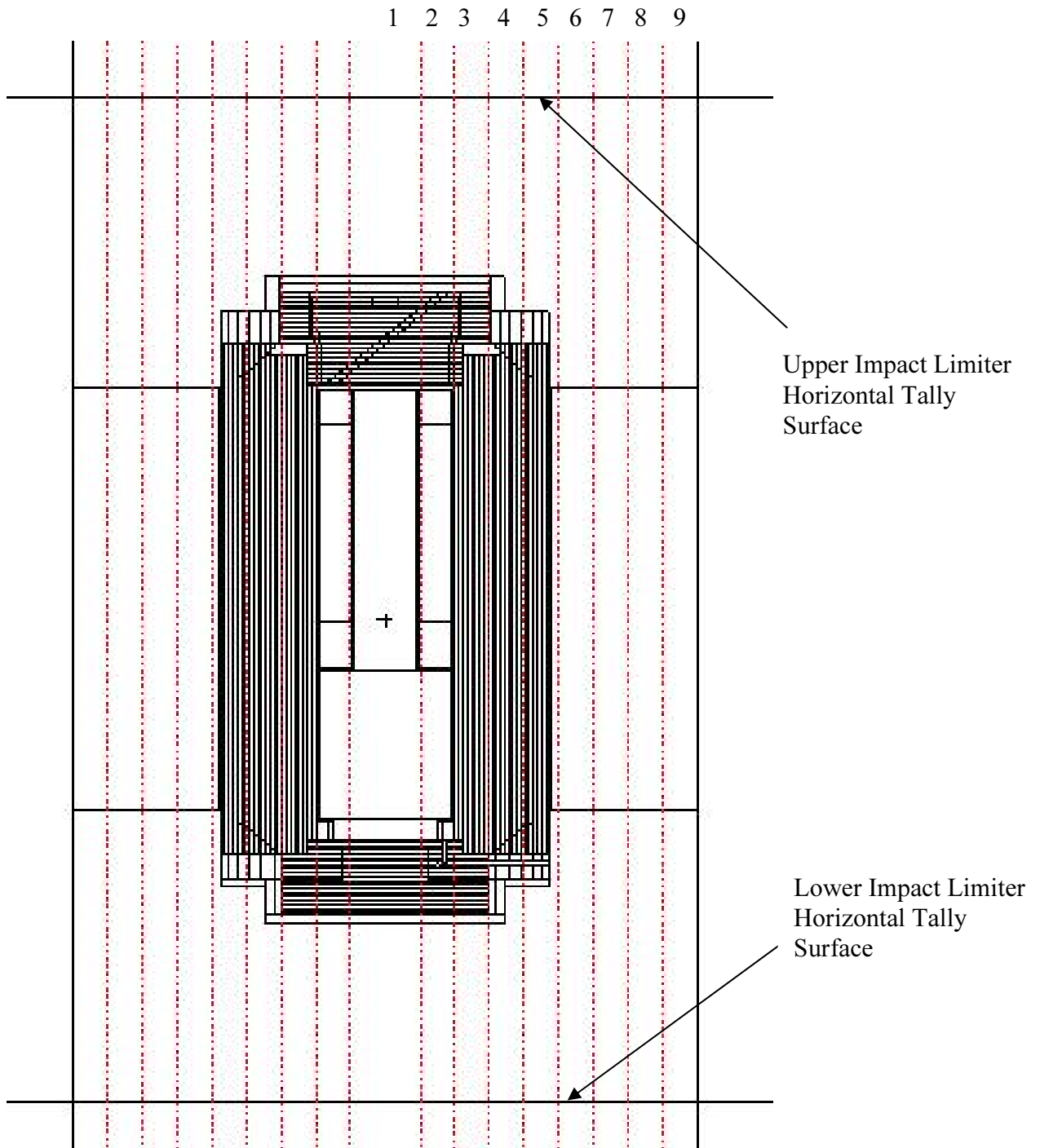
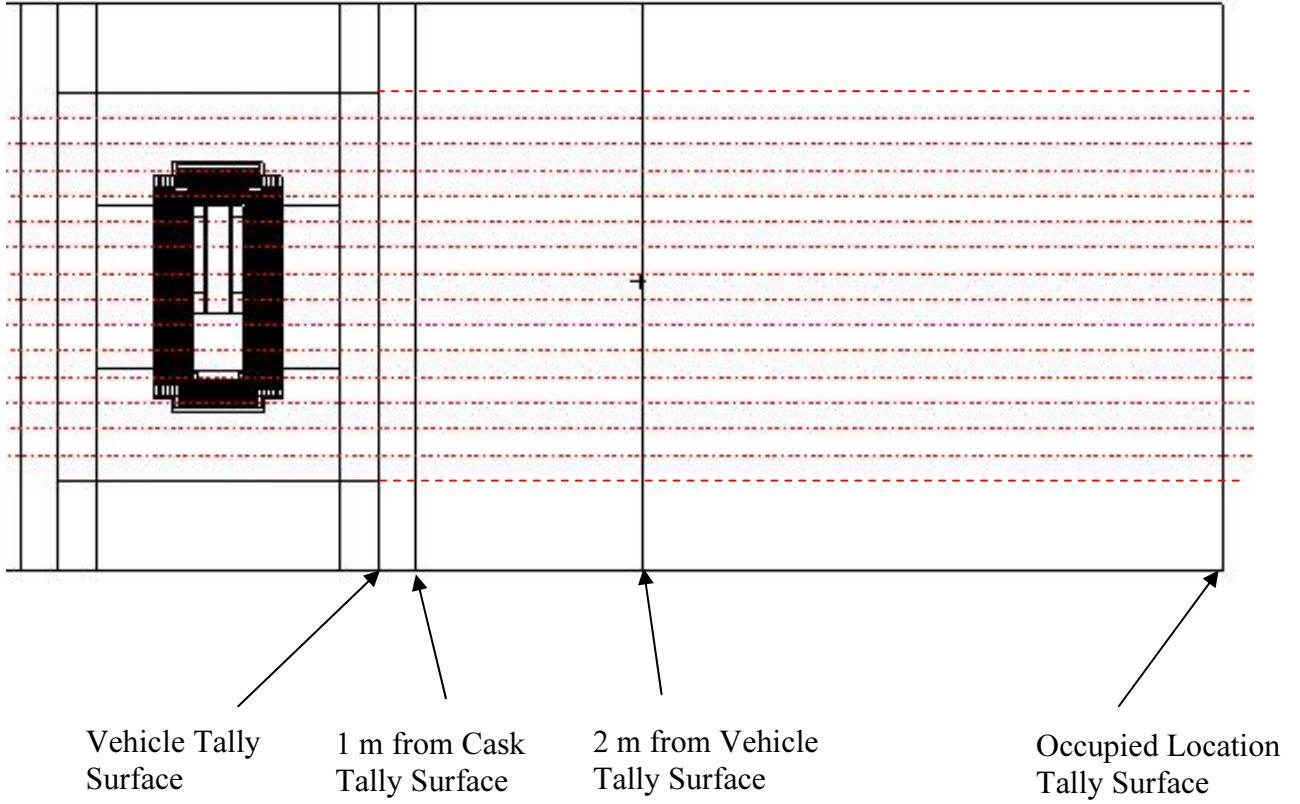
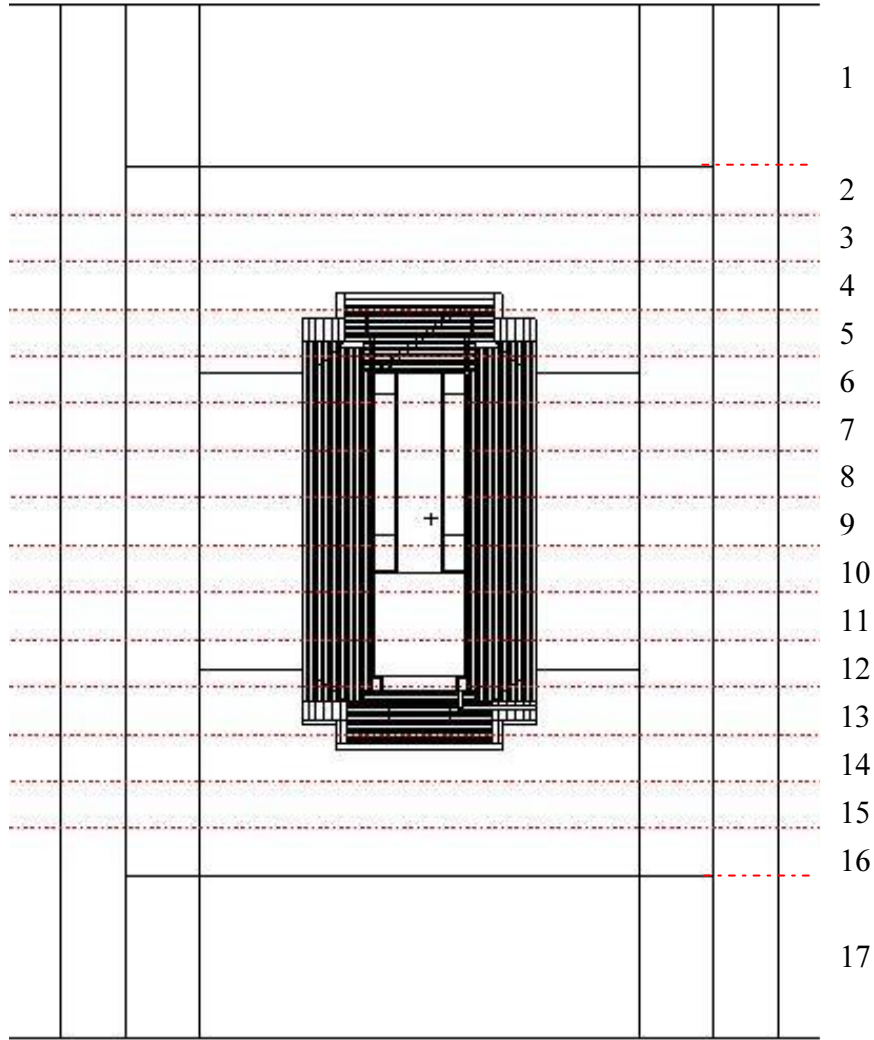


Figure 5.4-2 – Impact Limiter Horizontal Tally Segmentations



Note: All tallies are circumferential.

Figure 5.4-3 – Side Tally Locations



Note: All tallies are circumferential.

Figure 5.4-4 – Side Tally Segmentations (excluding cask surface)

1 m from Cask Impact
Limiter Tally Surface

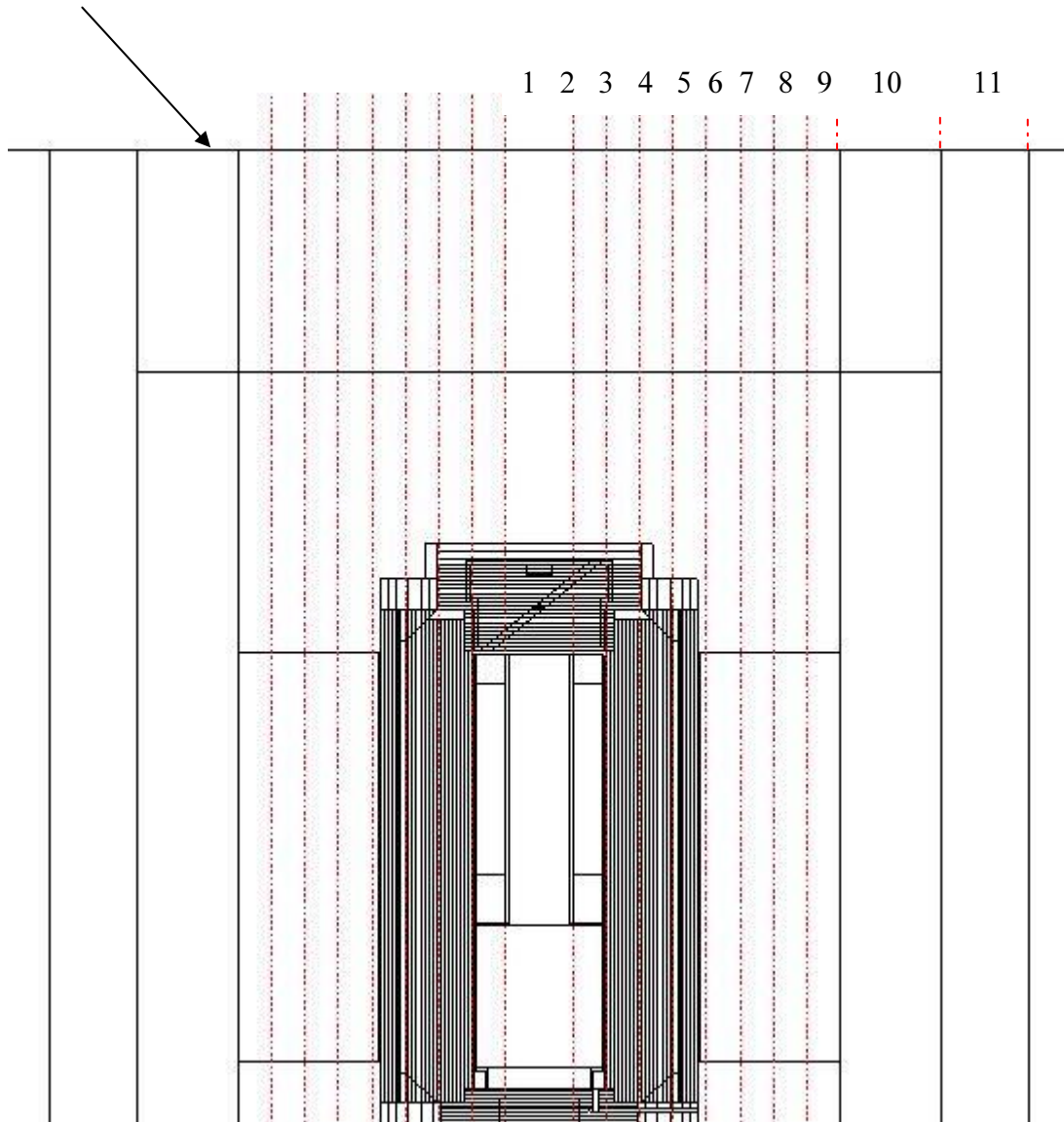


Figure 5.4-5 – HAC 1 m End Tally Segmentations

5.5 Appendices

5.5.1 References

1. Title 10, Code of Federal Regulations, Part 71 (10 CFR 71), Packaging and Transportation of Radioactive Material, 1-1-09 Edition.
2. MCNP5, "MCNP – A General Monte Carlo N-Particle Transport Code, Version 5; Volume II: User's Guide," LA-CP-03-0245, Los Alamos National Laboratory, April 2003. MCNP5 is distributed by the Radiation Safety Information Computational Center (www-rsicc.ornl.gov), Release C00710MNYCP02 (Windows PC).
3. SCALE: A Modular Code System for Performing Standardized Computer Analyses for Licensing Evaluations, ORNL/TM-2005/39, Version 6, Vols. I-III, January 2009.
4. JW Sterbentz, *Radionuclide Mass Inventory, Activity, Decay Heat, and Dose Rate Parametric Data for TRIGA Spent Nuclear Fuels*, INEL-96/0482, Idaho National Engineering Laboratory, March 1997.
5. *Standard Composition Library*, ORNL/TM-2005/39, Version 6, Vol. III, Section M8, January 2009.
6. *Nuclides and Isotopes, Chart of the Nuclides, Fifteenth Edition*, General Electric Co. and KAPL, Inc., 1996.

5.5.2 Detailed MITR-II Results

The following tables provide the detailed results for MITR-II fuel, because this fuel is limiting on the side of the cask.

Table 5.5-1 – MITR-II NCT Cask Side Dose Rates (mrem/hr)

Location	Gamma	σ	Neutron	σ	Total	σ
1	1.9	0.9%	7.6	0.1%	9.5	0.2%
2	2.7	0.7%	9.4	0.1%	12.2	0.2%
3	3.2	0.7%	10.2	0.1%	13.4	0.2%
4	3.0	0.7%	9.9	0.1%	12.9	0.2%
5	2.3	0.8%	8.6	0.1%	10.9	0.2%
6	1.4	1.0%	6.8	0.1%	8.1	0.2%
7	0.5	1.4%	4.9	0.2%	5.4	0.2%
8	0.1	2.3%	3.4	0.2%	3.6	0.2%
9	0.0	4.1%	2.4	0.2%	2.4	0.2%
10	0.0	8.1%	1.7	0.3%	1.7	0.3%
11	0.0	10.1%	1.2	0.3%	1.2	0.3%
12	0.0	8.8%	0.9	0.4%	0.9	0.4%

Table 5.5-2 – MITR-II NCT Impact Limiter Dose Rates (mrem/hr)

Location	Gamma	σ	Neutron	σ	Total	σ
Upper Impact Limiter Side						
1	2.4	2.2%	0.5	0.2%	2.9	1.8%
2	1.6	1.6%	0.6	0.2%	2.3	1.2%
3	0.9	1.2%	0.8	0.2%	1.8	0.7%
4	0.6	0.8%	1.2	0.1%	1.8	0.3%
5	0.6	0.5%	1.7	0.1%	2.3	0.2%
Lower Impact Limiter Side						
1	0.02	1.0%	0.5	0.2%	0.5	0.2%
2	0.02	3.2%	0.3	0.3%	0.3	0.3%
3	0.03	5.4%	0.2	0.4%	0.3	0.8%
4	0.1	6.5%	0.2	0.5%	0.2	1.7%
5	0.1	5.9%	0.1	0.6%	0.2	1.8%
Upper Impact Limiter Horizontal						
1	0.9	3.0%	0.9	0.8%	1.8	1.6%
2	1.0	2.9%	0.8	0.5%	1.8	1.6%
3	1.3	2.5%	0.8	0.4%	2.0	1.6%
4	1.4	2.2%	0.7	0.3%	2.1	1.4%
5	1.4	1.9%	0.6	0.3%	2.0	1.3%
6	1.6	1.7%	0.5	0.3%	2.1	1.3%
7	1.9	1.8%	0.5	0.3%	2.4	1.5%
8	2.7	2.5%	0.5	0.3%	3.1	2.1%
9	2.7	2.7%	0.4	0.3%	3.2	2.3%
Lower Impact Limiter Horizontal						
1	0.8	2.8%	0.2	1.8%	1.0	2.3%
2	0.8	2.8%	0.2	1.0%	1.0	2.3%
3	0.7	2.8%	0.2	0.8%	0.9	2.3%
4	0.4	2.6%	0.1	0.8%	0.6	2.0%
5	0.2	2.6%	0.1	0.8%	0.3	1.7%
6	0.1	2.5%	0.1	0.7%	0.2	1.4%
7	0.1	3.9%	0.1	0.7%	0.2	1.8%
8	0.1	3.9%	0.1	0.7%	0.2	1.5%
9	0.1	14.9%	0.1	0.6%	0.2	5.6%

Table 5.5-3 – MITR-II NCT Vehicle Surface Dose Rates (mrem/hr)

Location	Gamma	σ	Neutron	σ	Total	σ
1	1.1	2.0%	0.3	0.1%	1.4	1.6%
2	0.8	1.5%	0.4	0.2%	1.2	0.9%
3	0.5	1.2%	0.6	0.2%	1.1	0.6%
4	0.4	0.8%	0.8	0.1%	1.2	0.3%
5	0.4	0.5%	1.0	0.1%	1.4	0.2%
6	0.5	0.5%	1.2	0.1%	1.7	0.1%
7	0.6	0.5%	1.4	0.1%	1.9	0.1%
8	0.5	0.5%	1.4	0.1%	1.9	0.1%
9	0.4	0.5%	1.2	0.1%	1.6	0.1%
10	0.2	0.5%	1.0	0.1%	1.3	0.1%
11	0.1	0.6%	0.8	0.1%	0.9	0.1%
12	0.1	0.6%	0.6	0.2%	0.6	0.2%
13	0.03	0.8%	0.4	0.2%	0.4	0.2%
14	0.02	1.9%	0.3	0.2%	0.3	0.3%
15	0.03	3.7%	0.2	0.3%	0.2	0.5%
16	0.03	5.1%	0.2	0.4%	0.2	0.9%
17	0.03	6.1%	0.1	0.3%	0.1	1.6%

Table 5.5-4 – MITR-II NCT 2 m Vehicle Surface Dose Rates (mrem/hr)

Location	Gamma	σ	Neutron	σ	Total	σ
1	0.1	0.9%	0.1	0.1%	0.2	0.3%
2	0.1	0.6%	0.2	0.2%	0.2	0.2%
3	0.1	0.6%	0.2	0.2%	0.2	0.2%
4	0.1	0.5%	0.2	0.2%	0.3	0.2%
5	0.1	0.5%	0.2	0.2%	0.3	0.2%
6	0.1	0.5%	0.2	0.2%	0.3	0.2%
7	0.1	0.5%	0.2	0.2%	0.3	0.2%
8	0.1	0.5%	0.2	0.2%	0.3	0.2%
9	0.1	0.5%	0.2	0.2%	0.3	0.2%
10	0.1	0.5%	0.2	0.2%	0.2	0.2%
11	0.1	0.5%	0.2	0.2%	0.2	0.2%
12	0.1	0.5%	0.2	0.2%	0.2	0.2%
13	0.04	0.5%	0.1	0.2%	0.2	0.2%
14	0.04	0.6%	0.1	0.2%	0.2	0.2%
15	0.03	0.6%	0.1	0.2%	0.2	0.2%
16	0.02	0.6%	0.1	0.2%	0.1	0.2%
17	0.02	0.8%	0.1	0.1%	0.1	0.2%

Table 5.5-5 – MITR-II NCT Occupied Location Dose Rates (mrem/hr)

Location	Gamma	σ	Neutron	σ	Total	σ
1	0.02	0.5%	0.03	0.1%	0.05	0.2%
2	0.02	0.6%	0.03	0.3%	0.05	0.3%
3	0.02	0.6%	0.03	0.3%	0.05	0.3%
4	0.02	0.6%	0.03	0.2%	0.05	0.3%
5	0.02	0.6%	0.03	0.3%	0.05	0.3%
6	0.02	0.6%	0.03	0.2%	0.05	0.3%
7	0.02	0.6%	0.03	0.2%	0.05	0.3%
8	0.02	0.6%	0.03	0.2%	0.05	0.3%
9	0.01	0.6%	0.03	0.2%	0.05	0.3%
10	0.01	0.6%	0.03	0.3%	0.05	0.3%
11	0.01	0.6%	0.03	0.3%	0.05	0.3%
12	0.01	0.7%	0.03	0.3%	0.04	0.3%
13	0.01	0.7%	0.03	0.3%	0.04	0.3%
14	0.01	0.7%	0.03	0.3%	0.04	0.3%
15	0.01	0.7%	0.03	0.3%	0.04	0.3%
16	0.01	0.7%	0.03	0.3%	0.04	0.3%
17	0.01	0.5%	0.03	0.1%	0.04	0.2%

Table 5.5-6 – MITR-II HAC 1 m Side Dose Rates (mrem/hr)

Location	Gamma	σ	Neutron	σ	Total	σ
1	0.7	1.9%	0.3	0.1%	0.9	1.4%
2	0.4	1.2%	0.4	0.2%	0.8	0.6%
3	0.3	1.0%	0.5	0.2%	0.8	0.4%
4	0.3	0.7%	0.6	0.1%	0.9	0.2%
5	0.3	0.5%	0.7	0.1%	1.0	0.2%
6	0.4	0.5%	0.8	0.1%	1.2	0.2%
7	0.4	0.5%	0.9	0.1%	1.3	0.2%
8	0.4	0.5%	0.9	0.1%	1.3	0.2%
9	0.3	0.5%	0.8	0.1%	1.1	0.1%
10	0.2	0.5%	0.7	0.1%	0.9	0.1%
11	0.1	0.5%	0.6	0.1%	0.7	0.1%
12	0.1	0.5%	0.5	0.2%	0.6	0.1%
13	0.04	0.6%	0.4	0.2%	0.4	0.2%
14	0.03	1.0%	0.3	0.2%	0.3	0.2%
15	0.02	2.1%	0.2	0.3%	0.2	0.3%
16	0.02	3.2%	0.2	0.3%	0.2	0.5%
17	0.02	4.2%	0.1	0.2%	0.1	0.8%

Table 5.5-7 – MITR-II HAC Impact Limiter 1m End Dose Rates (mrem/hr)

Location	Gamma	σ	Neutron	σ	Total	σ
1 m from Upper Impact Limiter						
1	0.4	2.2%	0.3	1.3%	0.7	1.4%
2	0.4	2.1%	0.3	0.8%	0.7	1.4%
3	0.5	2.5%	0.3	0.6%	0.8	1.7%
4	0.5	2.1%	0.3	0.5%	0.8	1.4%
5	0.5	1.9%	0.2	0.5%	0.8	1.3%
6	0.5	1.9%	0.2	0.5%	0.8	1.3%
7	0.5	1.7%	0.2	0.4%	0.8	1.2%
8	0.5	1.7%	0.2	0.4%	0.8	1.3%
9	0.6	1.7%	0.2	0.4%	0.8	1.2%
10	0.7	2.0%	0.2	0.2%	0.9	1.5%
11	0.8	2.4%	0.2	0.2%	1.0	1.9%
1 m from Lower Impact Limiter						
1	0.3	4.1%	0.1	3.0%	0.4	3.5%
2	0.3	3.4%	0.1	1.9%	0.4	2.9%
3	0.3	3.1%	0.1	1.3%	0.4	2.6%
4	0.3	3.1%	0.1	1.2%	0.3	2.6%
5	0.2	2.9%	0.0	1.2%	0.3	2.3%
6	0.1	2.7%	0.0	1.1%	0.2	2.1%
7	0.1	2.7%	0.0	1.0%	0.2	1.9%
8	0.1	2.4%	0.0	0.9%	0.1	1.5%
9	0.1	2.4%	0.1	0.9%	0.1	1.3%
10	0.03	2.8%	0.1	0.4%	0.1	1.1%
11	0.03	9.1%	0.1	0.4%	0.1	2.5%

5.5.3 Sample Input Files

5.5.3.1 TRITON Input File

A sample TRITON input file for MURR is included. The file is annotated to aid in understanding the input.

Adding parm=weight instructs TRITON to collapse the 238-group ENDF/B-VII data library to a 49-group library for use in the NEWT calculations. The first NEWT calculation is performed with 238 groups, but all subsequent NEWT calculations use the collapsed library to accelerate the run time.

```
=t-depl          parm=weight
MURR Fuel Model
```

BRR Package Safety Analysis Report

```
v7-238
read comp
'Fuel
u-235 1 0 3.6124e-3      358.0 end
u-238 1 0 2.6847e-4      358.0 end
al    1 0 5.0239e-2      358.0 end
'Cladding
al    2                1.0 355.2 end
'Water
h2o   3 den=0.983      1.0 327.4 end
end comp
```

The pitch, fuel meat thickness, and cladding thickness are specified.

```
read celldata
latticecell symmslabcell pitch=0.3302 3 fueld=0.0508 1 cladd=0.127 2 end
end celldata
```

Depletion is to be carried out only in material 1 (aluminum cladding has negligible depletion and is neglected). The negative sign means that the total power is to be normalized to the fuel mixture region only. If a positive sign were entered, the power would be normalized across the entire fuel element model (including cladding and water). Due to small amounts of power generated by the cladding and water as a result of (n, γ) reactions, normalizing the power over the entire assembly results in less than the specified power in the fuel itself.

The power is specified in units of MW/MTU. BURN is the number of days at power, while DOWN is the number of days between cycles. NLIB is the number of data libraries to be generated for each burnup specification. Increasing the value of NLIB increases the accuracy (and length) of the calculation, although in this case the days at power are relatively short and one library per cycle is sufficient.

```
read depletion -1 end depletion
read burndata
power=1515.3 burn=7  down=14      nlib=1 end
power=1515.3 burn=4  down=180     nlib=1 end
end burndata
```


BRR Package Safety Analysis Report

```
end model
' End of NEWT model
end
```

5.5.3.2 MCNP Input File

A sample input file is provided for the MITR-II fuel with a gamma source.

```
BRRC
c
c lateral cask wall including Pb shield
c
10 4 -7.94 100 -157 1 -2 imp:p=1 $ SS inner shell split
11 4 -7.94 100 -157 2 -3 imp:p=2 $ SS inner shell split
12 8 -11.35 103 -133 3 -4 imp:p=4 $ Pb gamma shield split
13 8 -11.35 103 -133 4 -5 imp:p=8 $ Pb gamma shield split
14 8 -11.35 103 -133 5 -6 imp:p=16 $ Pb gamma shield split
15 8 -11.35 103 -133 6 -7 imp:p=32 $ Pb gamma shield split
16 8 -11.35 103 -133 7 -8 imp:p=64 $ Pb gamma shield split
17 8 -11.35 103 -133 8 -801 imp:p=128 $ Pb gamma shield split
18 8 -11.35 103 -133 801 -9 imp:p=200 $ Pb gamma shield split
19 4 -7.94 103 300 9 -10 imp:p=256 $ SS
20 4 -7.94 301 -132 9 -10 imp:p=256 $ SS
21 8 -11.35 -300 -301 -133 9 -10 imp:p=256 $ Pb gamma shield split
22 4 -7.94 103 300 10 -11 imp:p=512 $ SS
23 4 -7.94 301 -132 10 -11 imp:p=512 $ SS
24 8 -11.35 -300 -133 10 -11 imp:p=512 $ Pb gamma shield split
25 4 -7.94 103 300 11 -12 imp:p=1024 $ SS
26 4 -7.94 301 -132 11 -12 imp:p=1024 $ SS
27 8 -11.35 -300 -133 -301 11 -12 imp:p=1024 $ Pb gamma shield split
28 4 -7.94 103 300 12 -13 imp:p=2048 $ SS
29 4 -7.94 301 -132 12 -13 imp:p=2048 $ SS
30 8 -11.35 -300 -301 12 -13 imp:p=2048 $ Pb gamma shield split
31 4 -7.94 103 300 13 -14 imp:p=4096 $ SS
32 4 -7.94 301 -132 13 -14 imp:p=4096 $ SS
33 8 -11.35 -300 -301 13 -14 imp:p=4096 $ Pb gamma shield split
34 4 -7.94 103 300 14 -15 imp:p=8192 $ SS
35 4 -7.94 301 -132 14 -15 imp:p=8192 $ SS
36 8 -11.35 -300 -301 14 -15 imp:p=8192 $ Pb gamma shield split
37 4 -7.94 103 300 15 -16 imp:p=1.6e4 $ SS
38 4 -7.94 301 -132 15 -16 imp:p=1.6e4 $ SS
39 8 -11.35 -300 -301 15 -16 imp:p=1.6e4 $ Pb gamma shield split
40 4 -7.94 103 300 16 -17 imp:p=3.2e4 $ SS
41 4 -7.94 301 -132 16 -17 imp:p=3.2e4 $ SS
42 8 -11.35 -300 -301 16 -17 imp:p=3.2e4 $ Pb gamma shield split
43 4 -7.94 103 -101 17 -18 imp:p=6.4e4 $ SS
44 4 -7.94 102 -132 17 -18 imp:p=6.4e4 $ SS
45 8 -11.35 101 -102 17 -18 imp:p=6.4e4 $ Pb gamma shield split
46 4 -7.94 103 -101 18 -19 imp:p=1.3e5 $ SS
47 4 -7.94 102 -132 18 -19 imp:p=1.3e5 $ SS
48 8 -11.35 101 -102 18 -19 imp:p=1.3e5 $ Pb gamma shield split
49 4 -7.94 103 -101 19 -20 imp:p=2.6e5 $ SS
50 4 -7.94 102 -132 19 -20 imp:p=2.6e5 $ SS
51 1 -0.0012 101 -102 19 -20 imp:p=1.3e5 $ radial gap (Pb shrinkage
1/16")
52 1 -0.0012 133 -132 3 -301 imp:p=256 $ top axial gap (Pb shrinkage
1/4")
53 4 -7.94 3 -36 132 -152 imp:p=512
54 4 -7.94 103 -132 20 -21 imp:p=2.6e5 $ SS outer shell split
55 4 -7.94 103 -132 21 -22 imp:p=5.2e5 $ SS outer shell split
56 4 -7.94 103 -132 22 -23 imp:p=1.0e6 $ SS outer shell split
57 4 -7.94 103 -132 23 -24 imp:p=2.1e6 $ SS outer shell split
58 1 -0.0012 201 -200 24 -25 imp:p=2.1e6 $ air gap thermal shield
59 4 -7.94 201 -200 25 -26 imp:p=2.1e6 $ SS shell over thermal gap
c
c cask body bottom including Pb shield
c
```

BRR Package Safety Analysis Report

Rev. 2, November 2009

100	4	-7.94	104	-100	-3	#174	imp:p=1	\$ SS axial split bottom cask
101	4	-7.94	-104	105	-3	#174	imp:p=2	\$ SS axial split bottom cask
102	4	-7.94	-105	106	-3	#174	imp:p=4	\$ SS axial split bottom cask
104	8	-11.35	-106	103	-27		imp:p=8	\$ Bottom cask Pb split
105	4	-7.94	-106	103	-3	27 #174	imp:p=8	\$ SS split bottom cask
106	8	-11.35	-103	108	-27		imp:p=16	\$ bottom cask Pb split
107	8	-11.35	-108	109	-27		imp:p=32	\$ bottom cask Pb split
108	8	-11.35	-109	110	-27		imp:p=64	\$ bottom cask Pb split
109	8	-11.35	-110	111	-27		imp:p=128	\$ bottom cask Pb split
110	8	-11.35	-111	112	-27		imp:p=256	\$ bottom cask Pb split
111	8	-11.35	-112	113	-27		imp:p=512	\$ bottom cask Pb split
112	8	-11.35	-113	115	-27		imp:p=1024	\$ bottom cask Pb split
113	8	-11.35	115	-114	27	-33	imp:p=1024	\$ radius of first gap (Pb shrinkage)
c								
120	4	-7.94	108	-103	27	-801 #174	imp:p=16	\$ SS split bottom cask
121	4	-7.94	109	-108	27	-801 #174	imp:p=32	\$ SS split bottom cask
122	4	-7.94	110	-109	27	-801 #174	imp:p=64	\$ SS split bottom cask
123	4	-7.94	111	-110	27	-801 #175	imp:p=128	\$ SS split bottom cask
124	4	-7.94	112	-111	27	-801	imp:p=256	\$ SS split bottom cask
125	4	-7.94	113	-112	27	-801	imp:p=512	\$ SS split bottom cask
126	4	-7.94	114	-113	27	-801	imp:p=1024	\$ SS split bottom cask
128	4	-7.94	-103	114	801	-10 #175	imp:p=1024	\$ SS radial split bottom cask
129	4	-7.94	-103	114	10	-13 #175	imp:p=2048	\$ SS radial split bottom cask
130	4	-7.94	-103	114	13	-16 #175	imp:p=1.6e4	\$ SS radial split bottom cask
131	4	-7.94	-103	114	16	-20 #175	imp:p=1.3e4	\$ SS radial split bottom cask
132	4	-7.94	-103	114	20	-22 #175	imp:p=5.2e4	\$ SS radial split bottom cask
133	4	-7.94	-103	114	22	-24 #175	imp:p=2.1e6	\$ SS radial split bottom cask
c								
141	8	-11.35	-115	116	-33		imp:p=2048	\$ bottom cask Pb split
142	8	-11.35	-116	117	-33		imp:p=4096	\$ bottom cask Pb split
143	8	-11.35	-117	118	-33		imp:p=8192	\$ bottom cask Pb split
144	8	-11.35	-118	119	-33		imp:p=1.6e4	\$ bottom cask Pb split
145	8	-11.35	-119	120	-33		imp:p=3.3e4	\$ bottom cask Pb split
146	8	-11.35	-120	121	-33		imp:p=6.6e4	\$ bottom cask Pb split
147	8	-11.35	-121	122	-33		imp:p=1.3e5	\$ bottom cask Pb split
148	8	-11.35	-122	123	-33		imp:p=2.6e5	\$ bottom cask Pb split
149	8	-11.35	-123	125	-33		imp:p=5.2e5	\$ bottom cask Pb split
c								
170	4	-7.94	-114	125	33	-10	imp:p=5.2e5	\$ SS radial split bottom cask
171	4	-7.94	-114	125	10	-35	imp:p=1e6	\$ SS radial split bottom cask
172	4	-7.94	-114	126	35	-24	imp:p=2.1e6	\$ SS shoulder
173	4	-7.94	-125	127	-35		imp:p=1e6	\$ SS bottom plate (1")
174	1	-0.0012	309	-100	-306		imp:p=32	\$ vertical drain hole 95
175	1	-0.0012	-307	308	-24	#174	imp:p=1024	\$ horizontal drain hole 96
c								
c cask body top								
c								
201	4	-7.94	-134	145	41	-36	imp:p=1.3e5	\$ SS tapered interface with shield plug
202	4	-7.94	-145	146	41	-36	imp:p=6.6e4	\$ SS tapered interface with shield plug
203	4	-7.94	-146	147	41	-36	imp:p=3.3e4	\$ SS tapered interface with shield plug
204	4	-7.94	-147	148	41	-36	imp:p=1.6e4	\$ SS tapered interface with shield plug
205	4	-7.94	-148	149	41	-36	imp:p=8192	\$ SS tapered interface with shield plug
206	4	-7.94	-149	150	41	-36	imp:p=4096	\$ SS tapered interface with shield plug

207	4	-7.94	-150 151	302 -36	imp:p=2048	\$ SS tapered interface with shield plug
208	4	-7.94	-151 152	302 -36	imp:p=1024	\$ SS tapered interface with shield plug
209	4	-7.94	-152 153	302 -3	imp:p=512	\$ SS tapered interface with shield plug
210	4	-7.94	-153 154	302 -3	imp:p=256	\$ SS tapered interface with shield plug
211	4	-7.94	155 -154	1 -3	imp:p=128	\$ SS interface with shield plug
212	4	-7.94	1551 -155	1 -3	imp:p=64	\$ SS interface with shield plug
213	4	-7.94	1552 -1551	1 -3	imp:p=32	\$ SS interface with shield plug
214	4	-7.94	1553 -1552	1 -3	imp:p=16	\$ SS interface with shield plug
215	4	-7.94	1554 -1553	1 -3	imp:p=8	\$ SS interface with shield plug
216	4	-7.94	1555 -1554	1 -3	imp:p=4	\$ SS interface with shield plug
217	4	-7.94	156 -1555	1 -3	imp:p=2	\$ SS interface with shield plug
218	4	-7.94	157 -156	1 -3	imp:p=1	\$ SS interface with shield plug
c						
223	4	-7.94	-138 132	36 -11	imp:p=2.6e5	\$ SS radial split
224	4	-7.94	-138 132	11 -13	imp:p=5.2e5	\$ SS radial split
225	4	-7.94	-138 132	13 -16	imp:p=1.04e6	\$ SS radial split
226	4	-7.94	-138 132	16 -20	imp:p=2.1e6	\$ SS radial split
227	4	-7.94	-138 132	20 -22	imp:p=4.2e6	\$ SS radial split
228	4	-7.94	-138 132	22 -24	imp:p=8.4e6	\$ SS radial split
c						
230	4	-7.94	137 -136	-37	imp:p=4.2e6	\$ SS top closure lid split
231	4	-7.94	-135 136	-37	imp:p=8.4e6	\$ SS top closure lid split
232	1	-0.0012	-135 137	37 -36	imp:p=8.4e6	\$ radial gap at lid
233	4	-7.94	138 -135	36 -35	imp:p=4.2e6	\$ cask body
c						
240	4	-7.94	134 -143	-36 41	imp:p=2.6e5	\$ cask body top
241	4	-7.94	143 -142	-36 41	imp:p=5.2e5	\$ cask body top
242	4	-7.94	142 -140	-36 41	imp:p=1e6	\$ cask body top
243	4	-7.94	140 -137	-36 41	imp:p=2.1e6	\$ cask body top
c						
c shield plug						
c						
300	4	-7.94	140 -141 -40 161		imp:p=2.1e6	\$ SS top shield plug
301	1	-0.0012	-137 141 -41		imp:p=2.1e6	\$ axial gap at top of shield plug
302	1	-0.0012	140 -141 40 -41		imp:p=2.1e6	\$ radial gap at top of shield plug
303	8	-11.35	-140 142 -43 46 161		imp:p=1e6	\$ shield plug Pb split (no radial gap)
304	4	-7.94	-140 142 43 -40		imp:p=1e6	\$ SS top shield plug
305	1	-0.0012	-140 142 40 -41		imp:p=1e6	\$ gap split
306	4	-7.94	-140 142 -46		imp:p=1e6	\$ SS rod center
307	8	-11.35	-142 143 -43 46 161		imp:p=5.2e5	\$ shield plug Pb split
308	4	-7.94	-142 143 43 -40		imp:p=5.2e5	\$ SS top shield plug
309	1	-0.0012	-142 143 40 -41		imp:p=5.2e5	\$ gap split
310	4	-7.94	-142 143 -46		imp:p=5.2e5	\$ SS rod center
311	4	-7.94	-143 1431 -46		imp:p=2.6e5	\$ SS rod center
312	8	-11.35	-143 134 -43 #311 161		imp:p=2.6e5	\$ shield plug Pb split
313	4	-7.94	-143 134 43 -40		imp:p=2.6e5	\$ SS top shield plug
314	1	-0.0012	-143 134 40 -41		imp:p=2.6e5	\$ gap split
315	8	-11.35	-134 145 -43 161		imp:p=1.3e5	\$ shield plug Pb split
316	4	-7.94	-134 145 43 -40		imp:p=1.3e5	\$ SS top shield plug
317	1	-0.0012	-134 145 40 -41		imp:p=1.3e5	\$ gap split
318	8	-11.35	-145 146 -43 161		imp:p=6.6e4	\$ shield plug Pb split

319	4	-7.94	-145 146 43 -40	imp:p=6.6e4	\$ SS top shield plug
320	1	-0.0012	-145 146 40 -41	imp:p=6.6e4	\$ gap split
321	8	-11.35	-146 147 -43 161	imp:p=3.3e4	\$ shield plug Pb split
322	4	-7.94	-146 147 43 -40	imp:p=3.3e4	\$ SS top shield plug
323	1	-0.0012	-146 147 40 -41	imp:p=3.3e4	\$ gap split
324	8	-11.35	-147 148 -43 161	imp:p=1.6e4	\$ shield plug Pb split
325	4	-7.94	-147 148 43 -40	imp:p=1.6e4	\$ SS top shield plug
326	1	-0.0012	-147 148 40 -41	imp:p=1.6e4	\$ gap split
327	8	-11.35	-148 149 -43 161	imp:p=8192	\$ shield plug Pb split
328	4	-7.94	-148 149 43 -40	imp:p=8192	\$ SS top shield plug
329	1	-0.0012	-148 149 40 -41	imp:p=8192	\$ gap split
330	8	-11.35	(-149 150 -45 161):(160 -149 45 -43)	imp:p=4096	\$ shield plug Pb split
331	4	-7.94	-149 150 43 -40	imp:p=4096	\$ SS top shield plug
332	1	-0.0012	-149 150 40 -41	imp:p=4096	\$ gap split
333	4	-7.94	-160 150 45 -43	imp:p=4096	\$ SS ring at seating surface
334	8	-11.35	-150 151 -45 161	imp:p=2048	\$ shield plug Pb split
335	4	-7.94	-150 151 45 -303	imp:p=2048	\$ SS top shield plug
336	1	-0.0012	-150 151 303 -302	imp:p=2048	\$ gap split
337	8	-11.35	-151 152 -45 161	imp:p=1024	\$ shield plug Pb split
338	4	-7.94	-151 152 45 -303	imp:p=1024	\$ SS top shield plug
339	1	-0.0012	-151 152 303 -302	imp:p=1024	\$ gap split
340	8	-11.35	-152 153 -45 161	imp:p=512	\$ shield plug Pb split
341	4	-7.94	-152 153 45 -303	imp:p=512	\$ SS top shield plug
342	1	-0.0012	-152 153 303 -302	imp:p=512	\$ gap split
343	8	-11.35	-153 154 -45 161	imp:p=256	\$ shield plug Pb split
344	4	-7.94	-153 154 45 -303	imp:p=256	\$ SS top shield plug
345	1	-0.0012	-153 154 303 -302	imp:p=256	\$ gap split
346	8	-11.35	-154 155 -45 161	imp:p=128	\$ shield plug Pb split
347	4	-7.94	-154 155 45 -44	imp:p=128	\$ SS
348	1	-0.0012	-154 155 44 -1	imp:p=128	\$ gap split
350	8	-11.35	-155 1551 -45 161	imp:p=64	\$ shield plug Pb split
351	4	-7.94	-155 1551 45 -44	imp:p=64	\$ SS
352	1	-0.0012	-155 1551 44 -1	imp:p=64	\$ gap split
353	8	-11.35	-1551 1552 -45 161	imp:p=32	\$ shield plug Pb split
354	4	-7.94	-1551 1552 45 -44	imp:p=32	\$ SS
355	1	-0.0012	-1551 1552 44 -1	imp:p=32	\$ gap split
356	8	-11.35	-1552 1553 -45 161	imp:p=16	\$ shield plug Pb split
357	4	-7.94	-1552 1553 45 -44	imp:p=16	\$ SS
358	1	-0.0012	-1552 1553 44 -1	imp:p=16	\$ gap split
359	8	-11.35	-1553 1554 -45 161	imp:p=8	\$ shield plug Pb split
360	4	-7.94	-1553 1554 45 -44	imp:p=8	\$ SS
361	1	-0.0012	-1553 1554 44 -1	imp:p=8	\$ gap split
362	8	-11.35	-1554 1555 -45 161	imp:p=4	\$ shield plug Pb split
363	4	-7.94	-1554 1555 45 -44	imp:p=4	\$ SS
364	1	-0.0012	-1554 1555 44 -1	imp:p=4	\$ gap split
365	4	-7.94	-1555 156 -45 161	imp:p=2	\$ shield plug ss
366	4	-7.94	-1555 156 45 -44	imp:p=2	\$ SS
367	1	-0.0012	-1555 156 44 -1	imp:p=2	\$ gap split
368	4	-7.94	-156 157 -44 161	imp:p=1	\$ SS bottom shield plug
369	1	-0.0012	-156 157 44 -1	imp:p=1	\$ gap split
370	1	-0.0012	157 -156 -161	imp:p=1	\$ plug drain
371	1	-0.0012	156 -1555 -161	imp:p=2	\$ plug drain
372	1	-0.0012	1555 -1554 -161	imp:p=4	\$ plug drain
373	1	-0.0012	1554 -1553 -161	imp:p=8	\$ plug drain
374	1	-0.0012	1553 -1552 -161	imp:p=16	\$ plug drain
375	1	-0.0012	1552 -1551 -161	imp:p=32	\$ plug drain
376	1	-0.0012	1551 -155 -161	imp:p=64	\$ plug drain
377	1	-0.0012	155 -154 -161	imp:p=128	\$ plug drain
378	1	-0.0012	154 -153 -161	imp:p=256	\$ plug drain
379	1	-0.0012	153 -152 -161	imp:p=512	\$ plug drain
380	1	-0.0012	152 -151 -161	imp:p=1024	\$ plug drain
381	1	-0.0012	151 -150 -161	imp:p=2048	\$ plug drain
382	1	-0.0012	150 -149 -161	imp:p=4096	\$ plug drain
383	1	-0.0012	149 -148 -161	imp:p=8192	\$ plug drain
384	1	-0.0012	148 -147 -161	imp:p=1.6e4	\$ plug drain
385	1	-0.0012	147 -146 -161	imp:p=3.3e4	\$ plug drain

```

386 1 -0.0012 146 -145 -161          imp:p=6.6e4  $ plug drain
387 1 -0.0012 145 -134 -161          imp:p=1.3e5  $ plug drain
388 1 -0.0012 134 -143 -161          imp:p=2.6e5  $ plug drain
389 1 -0.0012 143 -142 -161          imp:p=5.2e5  $ plug drain
390 1 -0.0012 142 -140 -161          imp:p=1e6    $ plug drain
391 1 -0.0012 140 -141 -161          imp:p=2.1e6  $ plug drain
c
999 0      -1 100 -157      fill=1(22) imp:p=1 $ insert basket
c
c placeholders for IL and outside air volumes
c
400 3 -0.0012      (200 24 -50 -202):
      (138 -202 -24 35) :(-202 135 -35)  imp:p=8.4e6  $ placeholder for
upper IL
401 3 -0.0012      (-201 24 203 -50):
      (-24 -126 203 35):(-127 203 -24)  imp:p=4.2e6  $ placeholder for
lower IL
c
402 1 -0.0012 201 -200 -50 26          imp:p=4.2e6  $ lateral cask outer
air
403 1 -0.0012 50 -540 203 -202        imp:p=4.2e6  $ outer air
404 1 -0.0012 -203 211 -50            imp:p=4.2e6  $ bottom outer air
405 1 -0.0012 -203 211 50 -540        imp:p=4.2e6  $ bottom outer air
406 1 -0.0012 202 -210 -50           imp:p=8.4e6  $ outer air
407 1 -0.0012 202 -210 50 -540        imp:p=8.4e6  $ outer air
408 1 -0.0012 211 -210 540 -543       imp:p=4.2e6  $ outer air
409 1 -0.0012 211 -210 543 -541       imp:p=4.2e6  $ outer air
410 1 -0.0012 211 -210 541 -542       imp:p=4.2e6  $ outer air
c
1000 1 -0.0012      (542:-211:210) -999          imp:p=4.2e6
1001 0      999          imp:p=0
c
c Universe 1: Basket
c
600 0      620 -621 623 -622 680 -681 fill=5 u=1 imp:p=1 $ basket location
1
601 like 600 but trcl=2                u=1 imp:p=1 $ basket location
2
602 like 600 but trcl=3                u=1 imp:p=1 $ basket location
3
603 like 600 but trcl=4                u=1 imp:p=1 $ basket location
4
604 like 600 but trcl=5                u=1 imp:p=1 $ basket location
5
605 like 600 but trcl=6                u=1 imp:p=1 $ basket location
6
606 like 600 but trcl=7                u=1 imp:p=1 $ basket location
7
607 like 600 but trcl=8                u=1 imp:p=1 $ basket location
8
610 0      640 -641 643 -642 680 -681 fill=6 u=1 imp:p=1 $ inner location
1
611 like 610 but trcl=16                u=1 imp:p=1 $ inner location
2
612 like 610 but trcl=15                u=1 imp:p=1 $ inner location
3
620 1 -0.0012      680 -681 #600 #601 #602 #603 #604
      #605 #606 #607 #610 #611 #612 u=1 imp:p=1 $ inside basket
630 1 -0.0012      681          u=1 imp:p=1 $ above basket
631 4 -7.94      682 -680 -683        u=1 imp:p=1 $ support plate
632 4 -7.94      684 -685 -682        u=1 imp:p=1 $ basket bottom
633 1 -0.0012      -684 -682          u=1 imp:p=1
634 1 -0.0012      682 -680 683        u=1 imp:p=1
635 1 -0.0012      685 -682          u=1 imp:p=1
c
c Universe 2: Fuel
c

```

BRR Package Safety Analysis Report

```

700      2  1.7666e-02   686 -681      u=2      imp:p=1   $ fuel
701      1  -0.0012      -686:681     u=2      imp:p=1   $ air around fuel
c
c      Universe 5: Wedge 1 location outer
c
500      0           630 -631 633 -632 fill=2(0 13.8 0) u=5 imp:p=1
501      4 -7.94      -630:631:-633:632      u=5 imp:p=1
c
c      Universe 6: Wedge 1 location inner
c
510      0           650 -651 653 -652 fill=2(-2 -3.8 0) u=6 imp:p=1
511      4 -7.94      -650:651:-653:652      u=6 imp:p=1

c
c ***** cylindrical cask surfaces
c
1      cz  20.32      $ cask inner surface cavity wall radius
2      cz  21.59      $ split of cavity wall (1/2")
3      cz  22.86      $ outside inner shell radius
4      cz  24.06      $ gamma shield split
5      cz  25.26      $ gamma shield split
6      cz  26.46      $ gamma shield split
7      cz  27.66      $ gamma shield split
8      cz  28.86      $ gamma shield split
801    cz  30.06      $ gamma shield split
9      cz  31.2801     $ gamma shield split ***
10     cz  32.4725     $ gamma shield split
11     cz  33.6725     $ gamma shield split
12     cz  34.8725     $ gamma shield split
13     cz  36.0725     $ gamma shield split
14     cz  37.2725     $ gamma shield split
15     cz  38.4725     $ gamma shield split
16     cz  39.6725     $ gamma shield split
17     cz  40.8051     $ gamma shield split ***
18     cz  41.9975     $ gamma shield split
19     cz  43.02125    $ outer gamma shield (Pb shrinkage surface - 1/16")
20     cz  43.18      $ cask inner surface outer wall
21     cz  44.45      $ split outer wall (1/2")
22     cz  45.72      $ split outer wall (1/2")
23     cz  46.99      $ split outer wall (1/2")
24     cz  48.26      $ cask outer surface outer wall
25     cz  48.5267    $ air gap ( 0.105 ")
26     cz  48.7934    $ thermal shield outer surface
27     cz  12.3825    $ bottom lead sheet cavity (small)
c 28    cz  12.1285    $ radial gap due to lead shrinkage (1/10")
c
c 29    cz  14.0825    $ SS split bottom cask
c 30    cz  15.7825    $ SS split bottom cask
c 31    cz  17.4825    $ SS split bottom cask
c
c 33    cz  30.099     $ bottom lead sheet cavity (large)
c 34    cz  30.32125   $ bottom cask second radial gap surface due to lead
shrinkage
35     cz  34.6837    $ bottom and top cask SS outer surface
36     cz  31.115     $ top cask inner cavity for closure lid
37     cz  30.7975    $ closure lid radius
c
40     cz  22.1361    $ shield plug - SS outer radius(upper cylindrical region)
41     cz  22.3901    $ shield plug cavity
c 42    cz  19.15      $ shield plug SS inner radius at seating (item 7)
43     cz  21.1836    $ shield plug- SS inner radius (upper cylindrical region)
44     cz  20.066     $ shield plug - SS outer radius (lower cylindrical region)
45     cz  18.796     $ shield plug - SS inner radius (lower cylindrical region)
46     cz  3.81      $ SS bar at center of shield plug
c
50     cz  91.44     $ outer radius of impact limiter
c

```

```

c tally surfaces
c
c 51    cz    800          $ problem radial delimiter
c
c **** Horizontal planes
c
100    pz   -0.6426      $ bottom of cask inner cavity
101    pz    4.445       $ horizontal surface for lateral gamma shield
102    pz   139.7        $ horizontal surface at top of lateral gamma shield +3"
103    pz   -5.08       $ horizontal surface at bottom of lateral gamma shield
c
104    pz   -1.5        $ SS bottom cask split
105    pz   -2.54       $ SS bottom cask split
106    pz   -3.7338     $ bottom cask interface of SS - shrinkage gap
c 107    pz   -3.9878   $ bottom cask - lower horizontal surface of lead shrinkage
gap (1/10")
108    pz    -6         $ bottom cask - Pb split
109    pz   -6.845     $ bottom cask - Pb split
110    pz   -8.045     $ bottom cask - Pb split
111    pz   -9.245     $ bottom cask - Pb split
112    pz  -10.445     $ bottom cask - Pb split
113    pz  -11.645     $ bottom cask - Pb split
114    pz  -12.7       $ bottom cask - Pb split
115    pz  -12.954     $ bottom cask - lower horizontal surface of lead shrinkage gap
(1/10")
116    pz  -14.154     $ bottom cask - Pb split
117    pz  -15.354     $ bottom cask - Pb split
118    pz  -16.554     $ bottom cask - Pb split
119    pz  -17.754     $ bottom cask - Pb split
120    pz  -18.954     $ bottom cask - Pb split
121    pz  -20.154     $ bottom cask - Pb split
122    pz  -21.354     $ bottom cask - Pb split
123    pz  -22.554     $ bottom cask - Pb split
125    pz  -23.3426    $ bottom cask - lower Pb surface
126    pz  -14.9352    $ bottom cask - SS outer surface (shoulder)
127    pz  -25.8826    $ bottom cask - SS outer surface
c
c 131    pz  144.3736   $ horizontal surface at cask body top
132    pz  149.225     $ horizontal surface at top of lateral Pb shield cavity
133    pz  146.2278    $ top surface of lateral Pb shield after drop (1.12")
134    pz  159.7152    $ cask body top outer surface (shoulder)
135    pz  170.0276    $ top surface of closure lid
136    pz  167.4876    $ SS split in top lid
137    pz  164.9476    $ seating surface for top lid
138    pz  159.0802
c
140    pz  163.3728    $ shield plug Pb top surface
141    pz  164.6428    $ shield plug top surface
142    pz  162.1536    $ shield plug Pb split surface
143    pz  160.8836    $ shield plug Pb split surface
1431   pz  160.6296    $ surface for SS rod (surface 141- 1.5")
c 144    pz  159.6136   $ shield plug Pb split surface
145    pz  158.3436    $ shield plug Pb split surface
146    pz  157.0736    $ shield plug Pb split surface
147    pz  155.8036    $ shield plug Pb split surface
148    pz  154.5336    $ shield plug Pb split surface
149    pz  153.2636    $ shield plug Pb split surface
150    pz  151.7396    $ shield plug Pb split surface - modified
151    pz  150.7236    $ shield plug Pb split surface
152    pz  149.4536    $ shield plug Pb split surface
153    pz  148.1836    $ shield plug Pb split surface
154    pz  146.7104    $ shield plug Pb split surface - modified
155    pz  145.3896    $ new Pb split
1551   pz  144.1196    $ new Pb split
1552   pz  142.8496    $ new Pb split
1553   pz  141.5796    $ new Pb split
1554   pz  140.3096    $ new Pb split

```

BRR Package Safety Analysis Report

Rev. 2, November 2009

```

1555 pz 139.0396 $ bottom plug steel
156 pz 137.7696 $ SS surface at shield plug bottom -modified
157 pz 136.4996 $ bottom surface of shield plug -modified
160 pz 153.0096 $ upper SS surface at seating ring -new
161 20 cz 1.04648 $ pipe in shield plug
c
c surfaces for IL
c
200 pz 135.9916 $ upper interface IL with thermal shield
201 pz 8.1534 $ lower interface IL with thermal shield
202 pz 223.8756 $ upper surface of top impact limiter
203 pz -79.7306 $ bottom surface of bottom impact limiter
c
210 pz 293.3956 $ HAC upper surface
211 pz -149.2506 $ HAC lower surface
c
c various conical surfaces
c
300 kz -36.3601 1 1 $ tapered surface at bottom of lateral gamma shield
301 kz 180.5051 1 -1 $ tapered surface at top of lateral gamma shield
302 kz -143.9353 0.00489 1 $ tapered surface at cask top tapered cavity
303 kz -140.2468 0.00489 1 $ tapered surface at shield plug (SS)
c 304 kz -220.38 0.00275 1 $ tapered surface at shield plug (gap)
c 305 kz -122.0849 0.00489 1 $ tapered surface at shield plug (lead surface)
c
c bottom drain
c
306 c/z 17.145 0 0.635 $ vertical cylinder for bottom drain
307 c/x 0 -7.5184 0.635 $ horizontal cylinder for bottom drain
308 px 15.24 $ start of horizontal bottom drain
309 pz -7.94 $ depth of vertical drain
c
540 cz 121.92 $ surface of vehicle (4 ft=121.92 cm from BRRC centerline)
541 cz 321.92 $ 2 m from vehicle surface
542 cz 762.0 $ driver (25 ft=7.62m) from BRRC centerline)
543 cz 148.7934 $ 1m for HAC
c
c basket surfaces
c
620 1 py -3.6855 $ outer nine
621 1 py 3.6855
622 1 p -1.7321 -1 0 7.3711 $ left basket outer bound
623 1 p -1.7321 -1 0 -7.3711 $ right basket outer bound
c
630 1 py -3.3807
631 1 py 3.3807
632 1 p -1.7321 -1 0 6.7615 $ left basket inner bound
633 1 p -1.7321 -1 0 -6.7615 $ right basket inner bound
c
640 13 py -3.6855 $ inner three
641 13 py 3.6855
642 13 p -1.7321 -1 0 7.3711 $ left basket outer bound
643 13 p -1.7321 -1 0 -7.3711 $ right basket outer bound
c
650 13 py -3.3807
651 13 py 3.3807
652 13 p -1.7321 -1 0 6.7615 $ left basket inner bound
653 13 p -1.7321 -1 0 -6.7615 $ right basket inner bound
c
680 pz 67.5132 $ top of plate
681 pz 135.763 $ top of fuel (22.375")
682 pz 66.8782 $ bottom of plate
683 cz 19.8501
684 cz 17.145
685 cz 17.78
686 pz 78.9305
c

```

BRR Package Safety Analysis Report

```
c horizontal surfaces for segmentation
c
701 pz 18.8
702 pz 29.5
703 pz 40.1
704 pz 50.8
705 pz 61.4
706 pz 72.1
707 pz 82.7
708 pz 93.4
709 pz 104.0
710 pz 114.7
711 pz 125.3
c
720 pz 153.6 $ top IL
721 pz 171.1
722 pz 188.7
723 pz 206.3
c
740 pz -62.2 $ bottom IL
741 pz -44.6
742 pz -27.0
743 pz -9.4
c
c cylindrical surfaces for segmentation
c
760 cz 10.2
761 cz 20.3
762 cz 30.5
763 cz 40.6
764 cz 50.8
765 cz 61.0
766 cz 71.1
767 cz 81.3
c
770 pz -59.5
771 pz -39.2
772 pz -19.0
773 pz 1.2
774 pz 21.5
775 pz 41.7
776 pz 62.0
777 pz 82.2
778 pz 102.4
779 pz 122.7
780 pz 142.9
781 pz 163.2
782 pz 183.4
783 pz 203.6
c
999 sz 100 1000

c *****
c Dry air; density = 0.0012 g/cm^3
c *****
c
m1 7014 -76.508
8016 -23.4793
6000 -0.0126
c *****
c Homogenized fuel; atomic density = 1.7666e-02 atoms/(barn*cm)
c *****
c
m2 92235 4.3979e-4
92238 2.7717e-5
13027 1.7198e-2
c *****
```

BRR Package Safety Analysis Report

```
c      Dry air; density = 0.0012 g/cm^3
c
c      *****
m3     7014  -76.508
       8016  -23.4793
       6000  -0.0126
c      *****
c      SS304; Density = 7.94 g/cm^3
c      *****
m4     6012  -0.08
       14000 -1.0
       15000 -0.045
       24000 -19
       25000 -2
       26000 -68.375
       28000 -9.5
c      *****
c      Lead; Density = 11.35 g/cm^3
c      *****
m8     82000  1.0  $ lead
c
mode p
sdef cel=d1 rad=d2 ext=d3 erg=d10 axs=0 0 1 pos=0 0 78.9305 wgt=1.610E+15
si1    L  999:600:500:700 999:601:500:700 999:602:500:700
        999:603:500:700 999:604:500:700 999:605:500:700
        999:606:500:700 999:607:500:700
        999:610:510:700 999:611:510:700 999:612:510:700
sp1    1 1 1 1 1 1 1 1 1 1
si2    7.0
#      si3      sp3      $ fuel axial dist
       0        0
       2.368    0.500
       4.736    0.394
       9.472    0.788
       14.208   0.901
       18.944   1.042
       23.680   1.140
       28.416   1.253
       33.152   1.267
       37.888   1.112
       42.624   1.028
       47.360   0.901
       52.096   0.774
       54.464   0.401
       56.833   0.500
#      si10     sp10
       H        D
       0        0
       1.00E-02 0
       4.50E-02 4.379E+13
       1.00E-01 1.584E+13
       2.00E-01 1.370E+13
       3.00E-01 3.229E+12
       4.00E-01 2.426E+12
       6.00E-01 1.798E+13
       8.00E-01 3.918E+13
       1.00E+00 7.774E+12
       1.33E+00 1.398E+12
       1.66E+00 7.108E+11
       2.00E+00 3.700E+10
       2.50E+00 2.874E+11
       3.00E+00 1.392E+09
       4.00E+00 1.061E+08
       5.00E+00 1.355E+03
       6.50E+00 5.414E+02
       8.00E+00 1.058E+02
       1.00E+01 2.311E+01
```

BRR Package Safety Analysis Report

```

c      Total 1.463E+14
c      Total*11 1.610E+15
c
c      ansi/ans-6.1.1-1977 flux-to-dose, photons (mrem/hr)/(p/cm**2/s)
de0    0.01  0.03  0.05  0.07  0.10  0.15  0.20  0.25  0.30
        0.35  0.40  0.45  0.50  0.55  0.60  0.65  0.70  0.80
        1.00  1.40  1.80  2.20  2.60  2.80  3.25  3.75  4.25
        4.75  5.00  5.25  5.75  6.25  6.75  7.50  9.00  11.0
        13.0  15.0
df0    3.96-3 5.82-4 2.90-4 2.58-4 2.83-4 3.79-4 5.01-4 6.31-4 7.59-4
        8.78-4 9.85-4 1.08-3 1.17-3 1.27-3 1.36-3 1.44-3 1.52-3 1.68-3
        1.98-3 2.51-3 2.99-3 3.42-3 3.82-3 4.01-3 4.41-3 4.83-3 5.23-3
        5.60-3 5.80-3 6.01-3 6.37-3 6.74-3 7.11-3 7.66-3 8.77-3 1.03-2
        1.18-2 1.33-2
c
c      Tallies
c
c      FC2      Radial doses at contact (between IL on heat shield)
F2:p    26
FS2     -701 -702 -703 -704 -705 -706 -707 -708 -709 -710 -711
c
c      FC12     Radial doses at top side IL surface
F12:p   50
FS12    -200 -720 -721 -722 -723 -202
c
c      FC22     Radial doses at bottom side IL surface
F22:p   50
FS22    -203 -740 -741 -742 -743 -201
c
c      FC32     Doses at top limiter horizontal surface
F32:p   202
FS32    -760 -761 -762 -763 -764 -765 -766 -767 -50
c
c      FC42     Doses at bottom limiter horizontal surface
F42:p   203
FS42    -760 -761 -762 -763 -764 -765 -766 -767 -50
c
c      FC52     Doses at vehicle surface (4 ft from BRRC centerline)
F52:p   540
FS52    -203 -770 -771 -772 -773 -774 -775 -776 -777 -778
        -779 -780 -781 -782 -783 -202
c
c      FC62     Doses at 2m from vehicle surface
F62:p   541
FS62    -203 -770 -771 -772 -773 -774 -775 -776 -777 -778
        -779 -780 -781 -782 -783 -202
c
c      FC72     Doses at driver seat (25 ft from BRRC centerline)
F72:p   542
FS72    -203 -770 -771 -772 -773 -774 -775 -776 -777 -778
        -779 -780 -781 -782 -783 -202
c
c      FC82     HAC Doses at 1 m side
F82:p   543
FS82    -203 -770 -771 -772 -773 -774 -775 -776 -777 -778
        -779 -780 -781 -782 -783 -202
c
c      FC92     HAC Doses at 1m top
F92:p   210
FS92    -760 -761 -762 -763 -764 -765 -766 -767 -50 -540 -543
c
c      FC102    HAC Doses at 1m bottom
F102:p  211
FS102   -760 -761 -762 -763 -764 -765 -766 -767 -50 -540 -543
c
c      TRCL definitions
c

```

BRR Package Safety Analysis Report

```
*tr1    0 13.4112 0 22.5 112.5 90 67.5 22.5 90 $ wedge 1
*tr2    0 0 0      45 135 90 45 45 90      $ wedge 2(8)
*tr3    0 0 0      90 180 90 0 90 90      $ wedge 3(7)
*tr4    0 0 0     135 225 90 45 135 90     $ wedge 4(6)
*tr5    0 0 0     180 90 90 90 180 90     $ wedge 5
*tr6    0 0 0     135 45 90 225 135 90    $ wedge 6
*tr7    0 0 0     90 0 90 180 90 90      $ wedge 7
*tr8    0 0 0     45 45 90 135 45 90      $ wedge 8
*tr13   -2.1279 -3.6856 0                $ inner wedge
*tr15    0 0 0     120 210 90 30 120 90    $ inner wedge
*tr16    0 0 0     120 30 90 210 120 90    $ inner wedge
*tr20    0 0 150.022 50 90 140 90 0 90 40 90 50 $ pipe
*tr22    0 0 -0.6426

c
prdmp   j j 1 2
ctme    800
phys:p  4j 1
```

6.0 CRITICALITY EVALUATION

The Battelle Energy Alliance (BEA) Research Reactor (BRR) package is used to transport spent fuel from a variety of research reactors, including the University of Missouri Research Reactor (MURR), Massachusetts Institute of Technology Research Reactor (MITR-II), Advanced Test Reactor (ATR), and various types of Training, Research, Isotope General Atomics (TRIGA) reactors. The following analyses demonstrate that the BRR package complies with the requirements of 10 CFR 71.55 and 71.59. Based on the analysis, the Criticality Safety Index (CSI), per 10 CFR 71.59, is 0.

6.1 Description of Criticality Design

6.1.1 Design Features

Each fuel type has a unique basket that is used to properly position the fuel within the cask cavity. These baskets limit the number of fuel elements that may be shipped at a given time, and also control the spacing between the fuel elements. No poisons are utilized in the package. The separation provided by the packaging is sufficient to maintain criticality safety.

6.1.2 Summary Table of Criticality Evaluation

The upper subcritical limit (USL) for ensuring that the package is acceptably subcritical, as determined in Section 6.8, *Benchmark Evaluations*, is:

$$USL = 0.9209$$

The package is considered to be acceptably subcritical if the computed k_{safe} (k_s), which is defined as $k_{effective}$ (k_{eff}) plus twice the statistical uncertainty (σ), is less than or equal to the USL, or:

$$k_s = k_{eff} + 2\sigma \leq USL$$

The USL is determined on the basis of a benchmark analysis and incorporates the combined effects of code computational bias, the uncertainty in the bias based on both benchmark-model and computational uncertainties, and an administrative margin. The results of the benchmark analysis indicate that the USL is adequate to ensure subcriticality of the package.

The packaging design is shown to meet the requirements of 10 CFR 71.55(b). No credit is taken for fuel element burnup in any models. In the single package normal conditions of transport (NCT) models, credit is taken for the leaktight performance of the cask, while in the single package hypothetical accident condition (HAC) models, water is modeled in all cavities at the density in which reactivity is maximized. For the aluminum plate fuels (MURR, MITR-II, ATR), the most reactive credible configuration is utilized by maximizing the gap between the fuel plates. Maximizing this gap maximizes the moderation and hence the reactivity because the system is undermoderated. In all single package models, 12-in of water reflection is utilized.

Infinite reflection is utilized in both NCT and HAC array models. In the HAC array cases, internal and external water moderation is selected to optimize the reactivity.

The maximum results of the criticality calculations for each of the four fuel element types are summarized in Table 6.1-1. The maximum calculated k_s is 0.890, which occurs for the HAC array case for MITR-II fuel. The maximum reactivity is less than the USL of 0.9209. The MITR-II fuel results in the most reactive configuration because the MITR-II basket allows fuel elements to be placed in the center of the basket, while the center of the basket is empty for both MURR and ATR. The most reactive MURR, ATR, and TRIGA cases are well below the USL.

Note that the TRIGA fuel is significantly more reactive than the aluminum plate fuel types under NCT. This is because hydrogen is included in the TRIGA fuel matrix, providing some moderation. However, the reactivity of the NCT TRIGA cases is still very low.

6.1.3 Criticality Safety Index

An infinite number of packages is used in the array calculations for both NCT and HAC. Therefore, the criticality safety index per 10 CFR 71.59 is 0.

Table 6.1-1 – Summary of Criticality Evaluation

Normal Conditions of Transport (NCT)				
	MURR	MITR-II	ATR	TRIGA
Case	k_s	k_s	k_s	k_s
Single Unit Maximum	0.085	0.075	0.088	0.417
Infinite Array Maximum	0.197	0.187	0.234	0.539
Hypothetical Accident Conditions (HAC)				
	MURR	MITR-II	ATR	TRIGA
Case	k_s	k_s	k_s	k_s
Single Unit Maximum	0.761	0.875	0.685	0.709
Infinite Array Maximum	0.807	0.890	0.697	0.720
USL = 0.9209				

6.2 Fissile Material Contents

Four different spent fuel types are allowed contents: MURR, MITR-II, ATR, and TRIGA. For criticality control purposes, all fuel is modeled as fresh, and the information provided in this section pertains to fresh fuel.

6.2.1 MURR Fuel Element

The package can accommodate up to eight MURR fuel elements. Each MURR element contains up to 782.8 g U-235, enriched up to 93 wt.%. This fuel loading and enrichment is bounded by modeling 785 g U-235 and 94% enrichment. The weight percents of the remaining uranium isotopes are 1.2 wt.% U-234, 0.7 wt.% U-236, and 5.0-7.0 wt.% U-238. Each fuel element contains 24 curved fuel plates. Fuel plate 1 has the smallest radius, while fuel plate 24 has the largest radius, as shown in Figure 6.2-1. The fuel “meat” is a mixture of uranium metal and aluminum, while the cladding and structural materials are an aluminum alloy.

The relevant fuel element information is summarized in Figure 6.2-2. Each fuel plate is nominally 0.05-in thick, with a thickness tolerance of ± 0.002 -in. The fuel meat is nominally 0.02-in thick, and the cladding is nominally 0.015-in thick. The plate cladding material is aluminum. Fuel element side plates are fabricated of ASTM B 209, aluminum alloy 6061-T6 or 6061-T651. These fuel element side plates have a minimum thickness of 0.145-in. The channel width between the plates is 0.080 ± 0.008 -in. These tolerances represent average and not localized channel width. For an actual fuel element, the channel width may exceed these tolerances in localized areas.

The midpoint radii of the fuel plates are treated as fixed quantities, and are computed based on nominal dimensions. However, the channel width is modeled at the maximum value of 0.088-in between all plates in all final (i.e., non-parametric) fuel element models. To achieve this channel width between all fuel plates, the cladding is modeled with a reduced thickness of 0.011-in, or a total plate thickness of 0.042-in. This plate thickness is impossible to achieve in actual practice because it is below the allowable minimum plate thickness of 0.048-in.

The arc length of the fuel meat changes from plate to plate. Reference minimum fuel meat arc length and inner radius dimensions for each plate are provided on Figure 6.2-2. The active fuel length ranges from 23.25-in to 24.75-in.

It is necessary to determine the number densities of the fuel meat, which are the same for all fuel plates. To determine the number densities of the fuel meat, it is first necessary to compute the volume of the fuel meat. The volume of the fuel meat for each plate is the maximum arc length of the meat (nominal + 0.065-in) multiplied by the nominal active fuel length (24.0-in) and meat thickness (0.02-in). The active fuel length and meat thickness are modeled at nominal values in all final (i.e., non-parametric) fuel element models, and the use of these dimensions is justified in Section 6.9.2, *Parametric Evaluations to Determine the Most Reactive Fuel Geometries*. It is demonstrated in Section 6.9.2.2, *MURR Fuel Parametric Evaluation*, that reactivity increases with increasing meat arc length. The results of the fuel meat volume computations for all 24 plates are provided in Table 6.2-1 for maximum fuel arc length.

The U-235 gram density for each fuel plate is computed by dividing the U-235 mass by the total volume, or $785 \text{ g}/556.4 \text{ cm}^3 = 1.41 \text{ g/cm}^3$. The fuel itself is a mixture of UAl_x and aluminum. An equation that relates the U-235 density to the overall fuel meat density for ATR fuel is presented in Table 6.2-5. Because ATR and MURR fuel are of the same type, the fuel density equation shown in Table 6.2-5 is also used to develop the MURR fuel matrix density. Using this equation, the total density of the fuel matrix is computed to be approximately 3.77 g/cm^3 .

From the fuel volumes, U-235 gram densities, and total mixture densities provided, the number densities for the fuel region may be computed. These number densities are provided in Table 6.2-2. The U-235 weight percent is modeled at 94%. Representative weight percents of 0.6% and 0.35% are utilized for U-234 and U-236, respectively, and the balance (5.05%) is modeled as U-238.

6.2.2 MITR-II Fuel Element

The package can accommodate up to 11 MITR-II fuel elements. Each MITR-II element contains up to 513 g U-235, enriched up to 93 wt.%. This fuel loading and enrichment is bounded by modeling 515 g U-235 and 94% enrichment. The weight percents of the remaining uranium isotopes are 1.2 wt.% U-234, 0.7 wt.% U-236, and 5.0-7.0 wt.% U-238. Each fuel element contains 15 flat fuel plates, as shown in Figure 6.2-3. The fuel “meat” is a mixture of uranium metal and aluminum, while the cladding and structural materials are an aluminum alloy.

The relevant fuel element information is summarized in Figure 6.2-4. Each fuel plate is nominally 0.08-in thick, with a thickness tolerance of ± 0.003 -in. The fuel meat is nominally 0.03-in thick, and the cladding is nominally 0.025-in thick. The plate cladding material is aluminum. Fuel element side plates are fabricated of ASTM B 209, aluminum alloy 6061-T6. These fuel element side plates have a nominal thickness of 0.188-in. The channel width between the plates is 0.078 ± 0.004 -in. These tolerances represent average and not localized channel width. For an actual fuel element, the channel width may exceed these tolerances in localized areas.

The maximum and minimum active fuel lengths and maximum and minimum active fuel widths may be computed based the dimensions on Figure 6.2-4:

- Maximum active fuel length = $(23.0+0.01)-2(0.125) = 22.76$ -in
- Minimum active fuel length = $(23.0-0.01)-2(0.5) = 21.99$ -in
- Maximum active fuel width = $2.531 - 2(0.18) = 2.171$ -in
- Minimum active fuel width = $2.521 - 2(0.27) = 1.981$ -in.

The nominal active fuel length may be estimated as the average of the maximum and minimum values, or 22.375-in.

It is necessary to determine the number densities of the fuel meat, which are the same for all fuel plates. To determine the number densities of the fuel meat, it is first necessary to compute the volume of the fuel meat. The volume of the fuel meat for each plate is the maximum width of the meat (2.171-in) multiplied by the active fuel length (22.375-in) and meat thickness (0.03-in). The active fuel length and meat thickness are modeled at nominal values in all final (i.e., non-parametric) fuel element models, and the use of these dimensions is justified in Section 6.9.2,

Parametric Evaluations to Determine the Most Reactive Fuel Geometries. It is demonstrated in Section 6.9.2.3, *MITR-II Fuel Parametric Evaluation*, that reactivity increases with increasing meat width. The total meat volume is therefore $(15)(0.03)(22.375)(2.171)(2.54^3) = 358.2 \text{ cm}^3$.

The centerlines of the fuel plates are treated as fixed quantities, and are computed based on nominal dimensions. However, the channel width is modeled at the maximum value between all plates in all final (i.e., non-parametric) fuel element models. The maximum channel width is 0.082-in. The fuel plates also have grooves a maximum of 0.012-in deep cut into the surface of the fuel plates to increase heat transfer. Because the grooves cover approximately half the surface area of the cladding, half of the groove depth (i.e., 0.006-in) is removed from each cladding plate, increasing the effective channel width to 0.094-in. To achieve this channel width between all fuel plates, the cladding is artificially reduced to a thickness of 0.017-in, or a total plate thickness of 0.064-in.

The U-235 gram density for each fuel plate is computed by dividing the U-235 mass by the total volume, or $515 \text{ g}/358.2 \text{ cm}^3 = 1.44 \text{ g/cm}^3$. The fuel itself is a mixture of UAl_x and aluminum. An equation that relates the U-235 density to the overall fuel meat density for ATR fuel is presented in Table 6.2-5. Because ATR and MITR-II fuel are of the same type, the fuel density equation shown in Table 6.2-5 is also used to develop the MITR-II fuel matrix density. Therefore, using this equation, the total density of the fuel matrix is computed to be approximately 3.79 g/cm^3 .

From the fuel volumes, U-235 gram densities, and total mixture densities provided, the number densities for the fuel region may be computed. These number densities are provided in Table 6.2-3. The U-235 weight percent is modeled at 94%. Representative weight percents of 0.6% and 0.35% are utilized for U-234 and U-236, respectively, and the balance (5.05%) is modeled as U-238.

6.2.3 ATR Fuel Element

The package can accommodate up to eight ATR fuel elements. Each element contains up to 1085 g U-235, enriched up to 93 wt.%. This fuel loading and enrichment is bounded by modeling 1200 g U-235 and 94% enrichment. The weight percents of the remaining uranium isotopes are 1.2 wt.% U-234 (max), 0.7 wt.% U-236 (max), and 5.0-7.0 wt.% U-238. Each fuel element contains 19 curved fuel plates. Fuel plate 1 has the smallest radius, while fuel plate 19 has the largest radius, as shown in Figure 6.2-5. The fuel “meat” is a mixture of uranium metal and aluminum, while the cladding and structural material are an aluminum alloy.

The relevant fuel element details are summarized on Figure 6.2-6. Fuel plate 1 is nominally 0.080-in thick, fuel plates 2 through 18 are nominally 0.050-in thick, and fuel plate 19 is nominally 0.100-in thick. The plate thickness tolerance is +0.000/-0.002-in for all plates. The fuel meat is nominally 0.02-in thick for all 19 plates. The plate cladding material is aluminum ASTM B 209, 6061-0. Fuel element side plates are fabricated of ASTM B 209, aluminum alloy 6061-T6 or 6061-T651. These fuel element side plates have a minimum thickness of 0.182-in. Channels 2 through 10 have a width of 0.078 ± 0.007 -in, while channels 11 through 19 have a width of $0.077 +0.008/-0.006$ -in. These tolerances represent average and not localized channel width. For an actual fuel element, the channel width may exceed these tolerances in localized areas.

The midpoint radii of the fuel plates are treated as fixed quantities, and are computed based on nominal dimensions. However, the channel width is modeled at the maximum value of 0.085-in between all plates in all final (i.e., non-parametric) fuel element models. To achieve this channel width between all fuel plates, the cladding thickness is artificially reduced by 0.0035-in. Such a scenario is impossible to achieve in actual practice because it would result in overall plate thicknesses below the allowed minimum value.

The arc length of the fuel meat changes from plate to plate. This arc length varies based on the distance from the edge of the fuel meat to the fuel element side plate, as defined for each plate on Figure 6.2-6. This dimension is 0.245-in (max)/0.145-in (min) for fuel plates 1 and 19, 0.145-in (max)/0.045-in (min) for fuel plates 2 through 17, and 0.165-in (max)/0.065-in (min) for fuel plate 18. The smaller this dimension, the larger the arc length of the fuel meat.

The active fuel length varies between a minimum of 47.245-in ($= 49.485 - 2*1.12$) and a maximum of 48.775-in ($= 49.515 - 2*0.37$) for all fuel plates.

It is demonstrated in Section 6.9.2.1, *ATR Fuel Parametric Evaluation*, that reactivity increases with increasing meat arc length. Therefore, the arc length is modeled at the maximum value. To determine the number densities of the fuel meat, it is first necessary to compute the volume of the fuel meat. The volume of the fuel meat for each plate is the maximum arc length of the meat multiplied by the fuel length (48-in) and meat thickness (0.02-in). The fuel length and meat thickness are treated as fixed quantities in all fuel element models, and the use of these dimensions is justified in Section 6.9.2.1.

The fuel meat volume for each of the 19 fuel plates is provided in Table 6.2-4. The mass of U-235 per plate utilized in the analysis is also provided in Table 6.2-4. The U-235 gram density for each fuel plate is also computed. Note that the U-235 gram density is higher in the inner plates compared to the outer plates.

The fuel itself is a mixture of UAl_x and aluminum. The density of this mixture is proportional to the U-235 gram density, as shown in Table 6.2-5. These data are perfectly linear, and a linear fit of the data is $\rho_2 = 0.8733\rho_1 + 2.5357$, where ρ_2 is the total gram density of the mixture, and ρ_1 is the gram density of the U-235 in the mixture. This equation is used to compute the total mixture gram density provided as the last column in Table 6.2-4.

From the fuel volumes, U-235 gram densities, and total mixture densities provided, the number densities for the fuel region of each fuel plate may be computed. These number densities are provided in Table 6.2-6. The U-235 weight percent is modeled at 94%. Representative weight percents of 0.6% and 0.35% are utilized for U-234 and U-236, respectively, and the balance (5.05%) is modeled as U-238.

6.2.4 TRIGA Fuel Element

The package can accommodate up to 19 TRIGA fuel elements. While many different types of TRIGA fuel elements have been fabricated over the past 40 years, only five specific TRIGA fuel element types are considered in this analysis:

1. 8 wt.% uranium, aluminum clad (General Atomics catalog number 101)
2. 8.5 wt.% uranium, stainless steel clad (General Atomics catalog number 103)

3. 8.5 wt.% uranium, stainless steel clad, high enriched uranium (General Atomics catalog number 109)
4. 20 wt.% uranium, stainless steel clad (General Atomics catalog number 117)
5. 8.5 wt.% uranium, instrumented, stainless steel clad (General Atomics catalog number 203)

The fuel matrix of a TRIGA fuel element consists of a mixture of uranium and zirconium hydride. Therefore, the TRIGA elements contain hydrogen moderator material. Detailed fuel characteristics for the five TRIGA fuel element types are summarized in Table 6.2-7. A schematic of a typical stainless steel clad fuel element is shown in Figure 6.2-8.

TRIGA fuel elements consist of a central active fuel region with graphite axial reflectors above and below the active fuel. Type 101 and 103 TRIGA fuel manufactured prior to 1964 utilizes thin samarium trioxide discs between the active fuel and graphite reflectors. Type 109, 117, and 203 TRIGA fuel utilizes a thin molybdenum disc between the active fuel and lower reflector rather than samarium trioxide. The samarium trioxide discs act as a burnable poison and are conservatively omitted from the models. The molybdenum disc is only 0.031-in thick and has essentially no effect on the reactivity, as demonstrated in Section 6.9.2.4, *TRIGA Fuel Parametric Evaluation*. For this reason, the molybdenum disc is also omitted from the models.

For all TRIGA fuel elements with the exception of Type 101, a solid zirconium rod with an outer diameter of 0.225-in is placed along the active fuel length in the center of the fuel pellet. It is assumed that the inner diameter of the fuel pellet is 0.25-in to allow a small clearance between the rod and the fuel.

The fuel elements are modeled in detail from the bottom of the bottom reflector to the top of the top reflector. The end cap regions are neglected for simplicity. The graphite reflectors are modeled at the same diameter as the fuel pellets for simplicity, although the actual graphite reflectors have a slightly smaller diameter, as shown in Table 6.2-7. The Type 109 and 117 fuel elements contain erbium poison, although this poison is conservatively ignored in the criticality models.

The number densities within the TRIGA fuel elements are computed based upon the information in Table 6.2-7. Because the masses of U-235 and uranium are provided, the uranium number densities in the fuel may be computed based on the known volumes. The uranium is treated as a mix of only U-235 and U-238 for simplicity. The zirconium number density is computed based on the zirconium mass provided, and the hydrogen number density is computed based upon the H/Zr ratio. The fuel number densities for the five fuel types are summarized in Table 6.2-8.

Table 6.2-1 – MURR Fuel Volume Computation (maximum arc length)

Plate	Midpoint Radius (cm)	Fuel Arc (cm)	Volume ^① (cm ³)
1	7.0993	4.5034	13.9460
2	7.4295	4.7625	14.7484
3	7.7597	5.0216	15.5507
4	8.0899	5.2832	16.3608
5	8.4201	5.5423	17.1632
6	8.7503	5.8014	17.9655
7	9.0805	6.0604	18.7678
8	9.4107	6.3195	19.5701
9	9.7409	6.5786	20.3724
10	10.0711	6.8377	21.1747
11	10.4013	7.0968	21.9770
12	10.7315	7.3558	22.7793
13	11.0617	7.6149	23.5816
14	11.3919	7.8765	24.3918
15	11.7221	8.1356	25.1941
16	12.0523	8.3947	25.9964
17	12.3825	8.6538	26.7987
18	12.7127	8.9129	27.6011
19	13.0429	9.1719	28.4034
20	13.3731	9.4310	29.2057
21	13.7033	9.6901	30.0080
22	14.0335	9.9492	30.8103
23	14.3637	10.2083	31.6126
24	14.6939	10.4699	32.4228
Total			556.4024

① Volume is computed as Fuel Arc*Active Fuel Height*Fuel Thickness, where Active Fuel Height = 24-in (60.96 cm) and Fuel Thickness = 0.02-in (0.0508 cm).

Table 6.2-2 – MURR Fuel Number Densities (maximum arc length)

Isotope	Number Density (atom/b-cm)
U-234	2.3171E-05
U-235	3.6147E-03
U-236	1.3402E-05
U-238	1.9174E-04
Al	5.0596E-02
Total	5.4439E-02

Table 6.2-3 – MITR-II Fuel Number Densities (maximum meat width)

Isotope	Number Density (atom/b-cm)
U-234	2.3613E-05
U-235	3.6835E-03
U-236	1.3657E-05
U-238	1.9539E-04
Al	5.0481E-02
Total	5.4398E-02

Table 6.2-4 – ATR Fuel Element Volume and Gram Densities (maximum arc length)

Plate	Fuel Meat Arc Length (cm)	Fuel Meat Volume (cm³)	U-235 Mass Per Plate (g)	U-235 density, ρ_1 (g/cm³)	Total UAl_x + Al Density, ρ_2 (g/cm³)
1	4.2247	26.2	27.1	1.04	3.44
2	5.0209	31.1	32.5	1.04	3.45
3	5.2764	32.7	43.2	1.32	3.69
4	5.5319	34.3	45.1	1.32	3.69
5	5.7873	35.8	58.2	1.62	3.95
6	6.0427	37.4	60.9	1.63	3.96
7	6.2982	39.0	63.6	1.63	3.96
8	6.5536	40.6	66.3	1.63	3.96
9	6.8090	42.2	69.0	1.64	3.96
10	7.0644	43.8	71.7	1.64	3.97
11	7.3198	45.3	74.3	1.64	3.97
12	7.5752	46.9	77.0	1.64	3.97
13	7.8306	48.5	79.7	1.64	3.97
14	8.0860	50.1	82.4	1.64	3.97
15	8.3414	51.7	85.2	1.65	3.98
16	8.5968	53.2	71.4	1.34	3.71
17	8.8521	54.8	73.6	1.34	3.71
18	9.0058	55.8	60.1	1.08	3.48
19	8.9039	55.1	58.7	1.06	3.47
Total	--	824.5	1200.0	--	--

Table 6.2-5 – ATR Fuel Density Equation

U-235 Density (g/cm ³)	Total Fuel Density (g/cm ³)
ρ_1	ρ_2
1.00	3.409
1.30	3.671
1.60	3.933
Linear Fit: $\rho_2 = 0.8733\rho_1 + 2.5357$	

Table 6.2-6 – ATR Fuel Number Densities (maximum arc length)

Plate	U-234 (atom/b-cm)	U-235 (atom/b-cm)	U-236 (atom/b-cm)	U-238 (atom/b-cm)	Aluminum (atom/b-cm)	Total (atom/b-cm)
1	1.7026E-05	2.6560E-03	9.8475E-06	1.4089E-04	5.2187E-02	5.5010E-02
2	1.7156E-05	2.6763E-03	9.9226E-06	1.4196E-04	5.2153E-02	5.4998E-02
3	2.1711E-05	3.3869E-03	1.2557E-05	1.7966E-04	5.0974E-02	5.4574E-02
4	2.1618E-05	3.3724E-03	1.2503E-05	1.7889E-04	5.0998E-02	5.4583E-02
5	2.6648E-05	4.1571E-03	1.5413E-05	2.2051E-04	4.9696E-02	5.4115E-02
6	2.6746E-05	4.1724E-03	1.5470E-05	2.2132E-04	4.9670E-02	5.4106E-02
7	2.6790E-05	4.1791E-03	1.5495E-05	2.2168E-04	4.9659E-02	5.4102E-02
8	2.6830E-05	4.1854E-03	1.5518E-05	2.2201E-04	4.9649E-02	5.4098E-02
9	2.6867E-05	4.1911E-03	1.5539E-05	2.2232E-04	4.9639E-02	5.4095E-02
10	2.6901E-05	4.1965E-03	1.5559E-05	2.2260E-04	4.9630E-02	5.4092E-02
11	2.6933E-05	4.2015E-03	1.5577E-05	2.2287E-04	4.9622E-02	5.4089E-02
12	2.6963E-05	4.2061E-03	1.5595E-05	2.2311E-04	4.9614E-02	5.4086E-02
13	2.6990E-05	4.2105E-03	1.5611E-05	2.2334E-04	4.9607E-02	5.4083E-02
14	2.7017E-05	4.2145E-03	1.5626E-05	2.2356E-04	4.9600E-02	5.4081E-02
15	2.7077E-05	4.2239E-03	1.5661E-05	2.2406E-04	4.9585E-02	5.4075E-02
16	2.2037E-05	3.4377E-03	1.2746E-05	1.8235E-04	5.0889E-02	5.4544E-02
17	2.2037E-05	3.4377E-03	1.2745E-05	1.8235E-04	5.0889E-02	5.4544E-02
18	1.7683E-05	2.7586E-03	1.0228E-05	1.4633E-04	5.2016E-02	5.4949E-02
19	1.7487E-05	2.7279E-03	1.0114E-05	1.4470E-04	5.2067E-02	5.4967E-02

Table 6.2-7 – TRIGA Fuel Characteristics

Parameter	Type 101	Type 103	Type 109	Type 117	Type 203
General Description	8 wt.% aluminum clad	8.5 wt.% stainless steel clad	8.5 wt.% stainless steel clad, HEU	20 wt.% stainless steel clad	8.5 wt.% instrumented stainless steel clad
Active Fuel Length (in)	14	15	15	15	15
Fuel Pellet OD (in)	1.41	1.44	1.44	1.44	1.44
U (wt.% in fuel)	8.0	8.5	8.5	20	8.5
U (g)	180	195	196	504	195
U-235 (wt.% in U)	20	20	70	20	20
U-235 (g)	36	39	137	101	39
H/Zr	1.0	1.7	1.6	1.6	1.7
Erbium (wt.%)	0	0	1.3	0.5	0
Zirconium Rod Length (in)	n/a	15.0	15.0	15.0	15.0
Overall Rod Length (in)	28.37	28.90	28.90	29.68	45.25
Cladding OD (in)	1.48	1.48	1.48	1.48	1.48
Cladding Thickness (in)	0.03	0.02	0.02	0.02	0.02
Graphite Reflector Length Top/Bottom (in)	4.0 / 4.0 ^①	2.6 / 3.7	2.6 / 3.7	2.6 / 3.7	3.1 / 3.4
Graphite Reflector OD (in)	1.4	1.4	1.4	1.4	1.4
Molybdenum Disc (Y/N)	No	Yes	Yes	Yes	Yes
Samarium Trioxide Disc (Y/N)	Yes (prior to 1964)	Yes (prior to 1964)	No	No	No
Zr Fuel Matrix Mass (g)	2,070	2,088	2,060	2,060	2,088

Notes:

① Graphite reflector dimensions provided for an active fuel length of 14-in. If the active fuel length is reduced, the top and bottom reflectors increase equally in length, and the overall column stackup of fuel and reflector remains fixed at 22-in.

Table 6.2-8 – TRIGA Fuel Number Densities

Isotope	Type 101 (atom/b-cm)	Type 103/203 (atom/b-cm)	Type 109 (atom/b-cm)	Type 117 (atom/b-cm)
H	3.8146E-02	6.0352E-02	5.6041E-02	5.6041E-02
Zr	3.8146E-02	3.5501E-02	3.5025E-02	3.5025E-02
U-235	2.5748E-04	2.5736E-04	9.0406E-04	6.6650E-04
U-238	1.0169E-03	1.0164E-03	3.8442E-04	2.6258E-03
Total	7.7566E-02	9.7128E-02	9.2354E-02	9.4358E-02

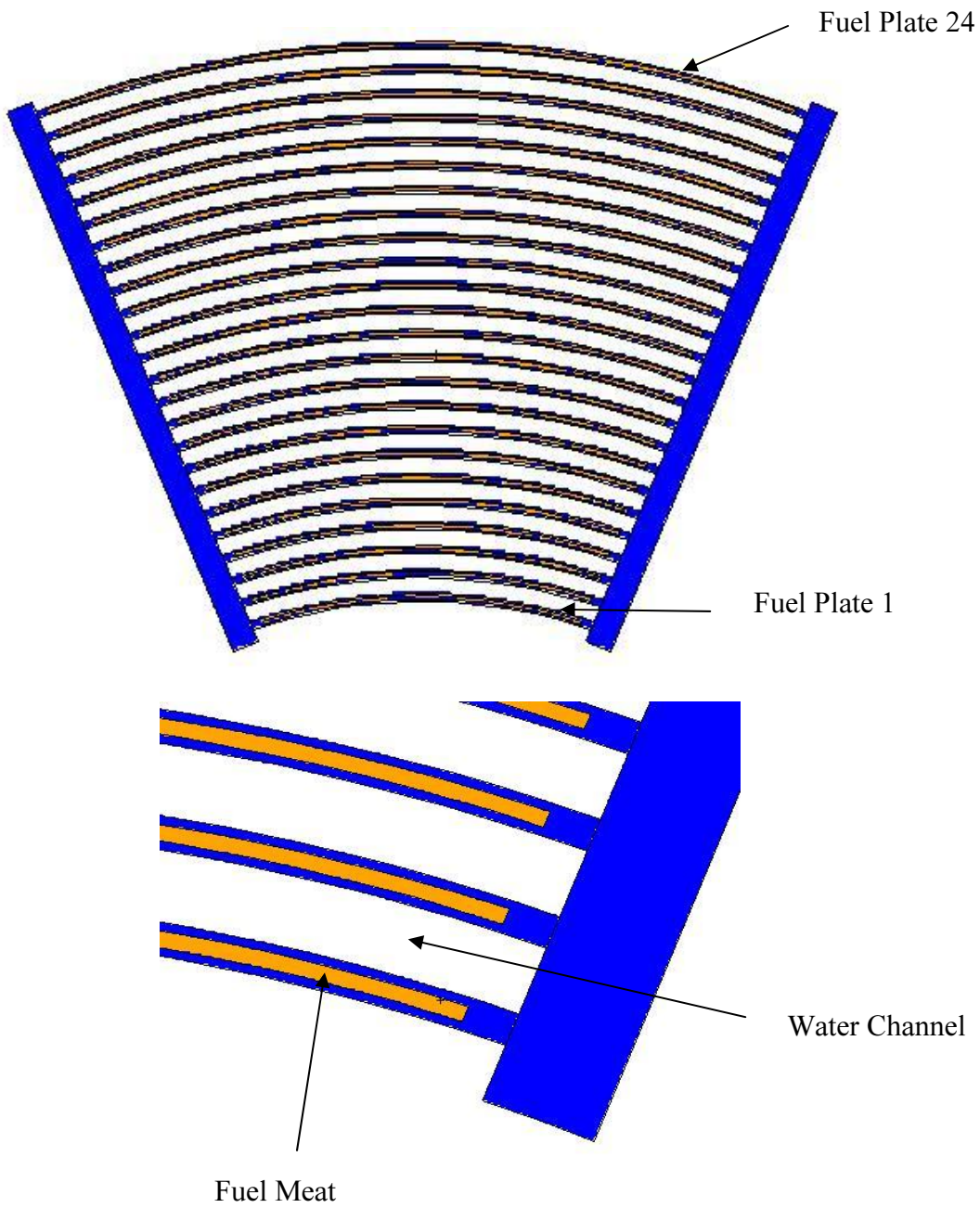


Figure 6.2-1 – MURR Fuel Element Model

Figure Withheld Under 10 CFR 2.390

Figure 6.2-2 – MURR Fuel Element Details

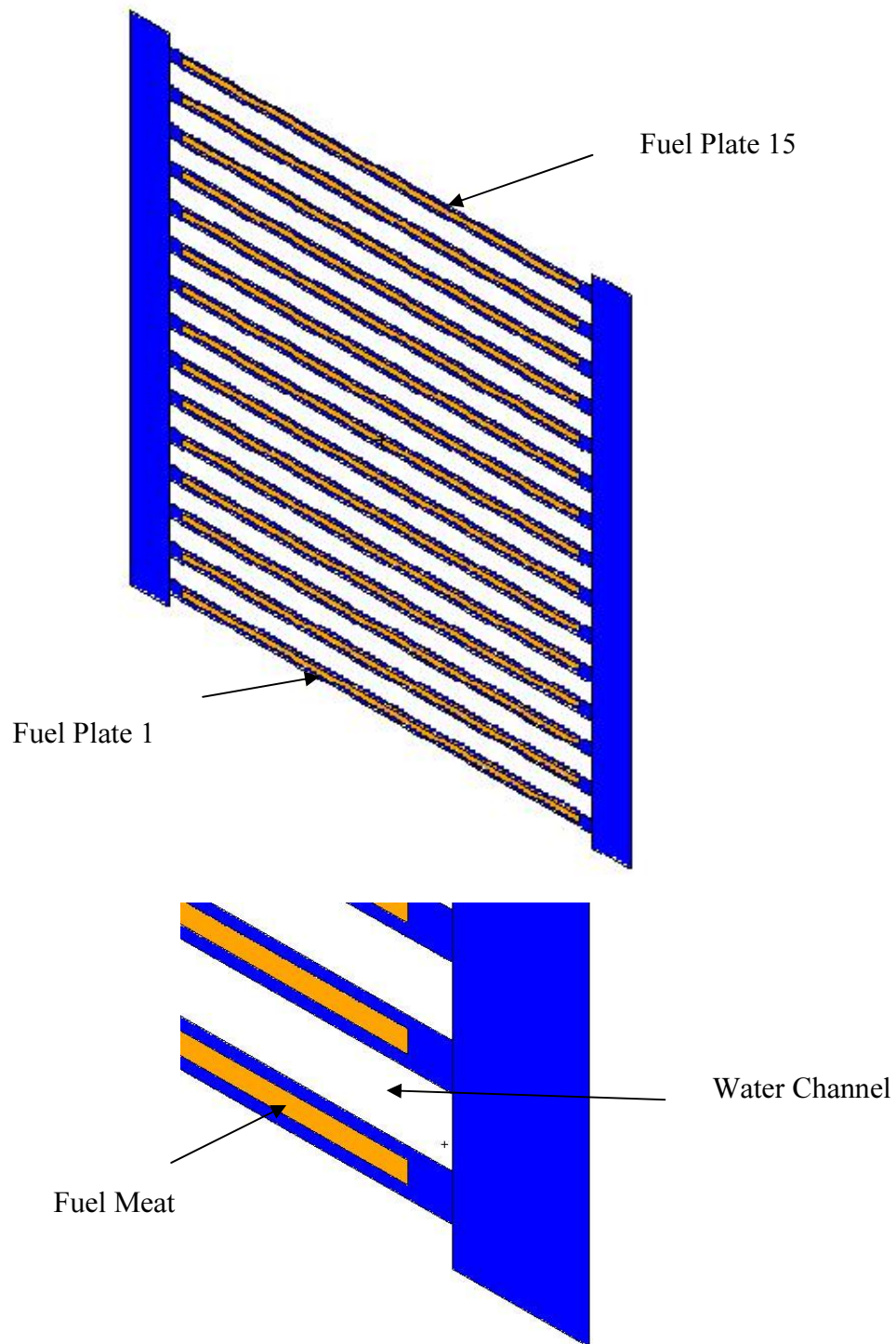


Figure 6.2-3 – MITR-II Fuel Element Model

Figure Withheld Under 10 CFR 2.390

Figure 6.2-4 – MITR-II Fuel Element Details

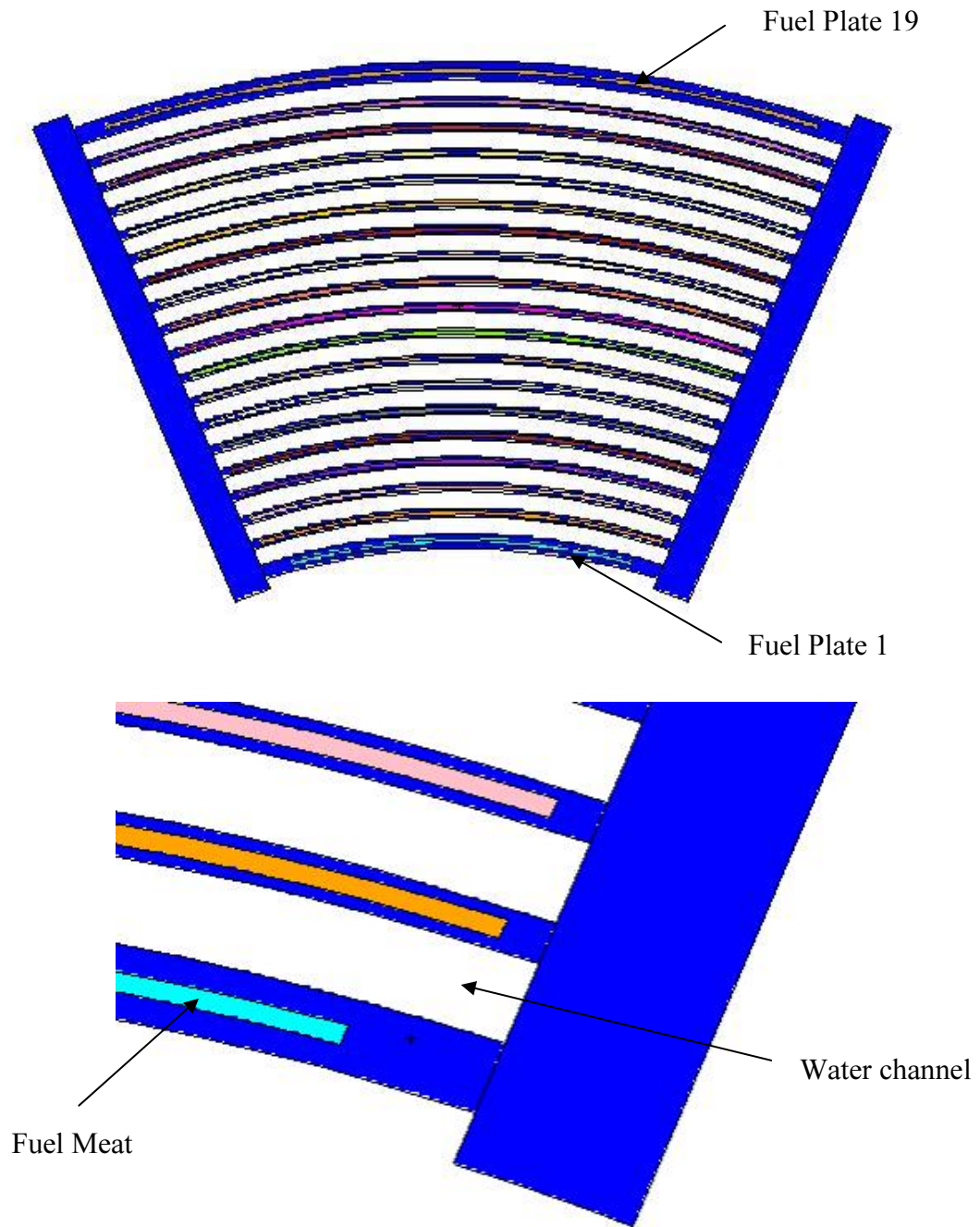


Figure 6.2-5 – ATR Fuel Element Model

Figure Withheld Under 10 CFR 2.390

Figure 6.2-6 – ATR Fuel Element Details

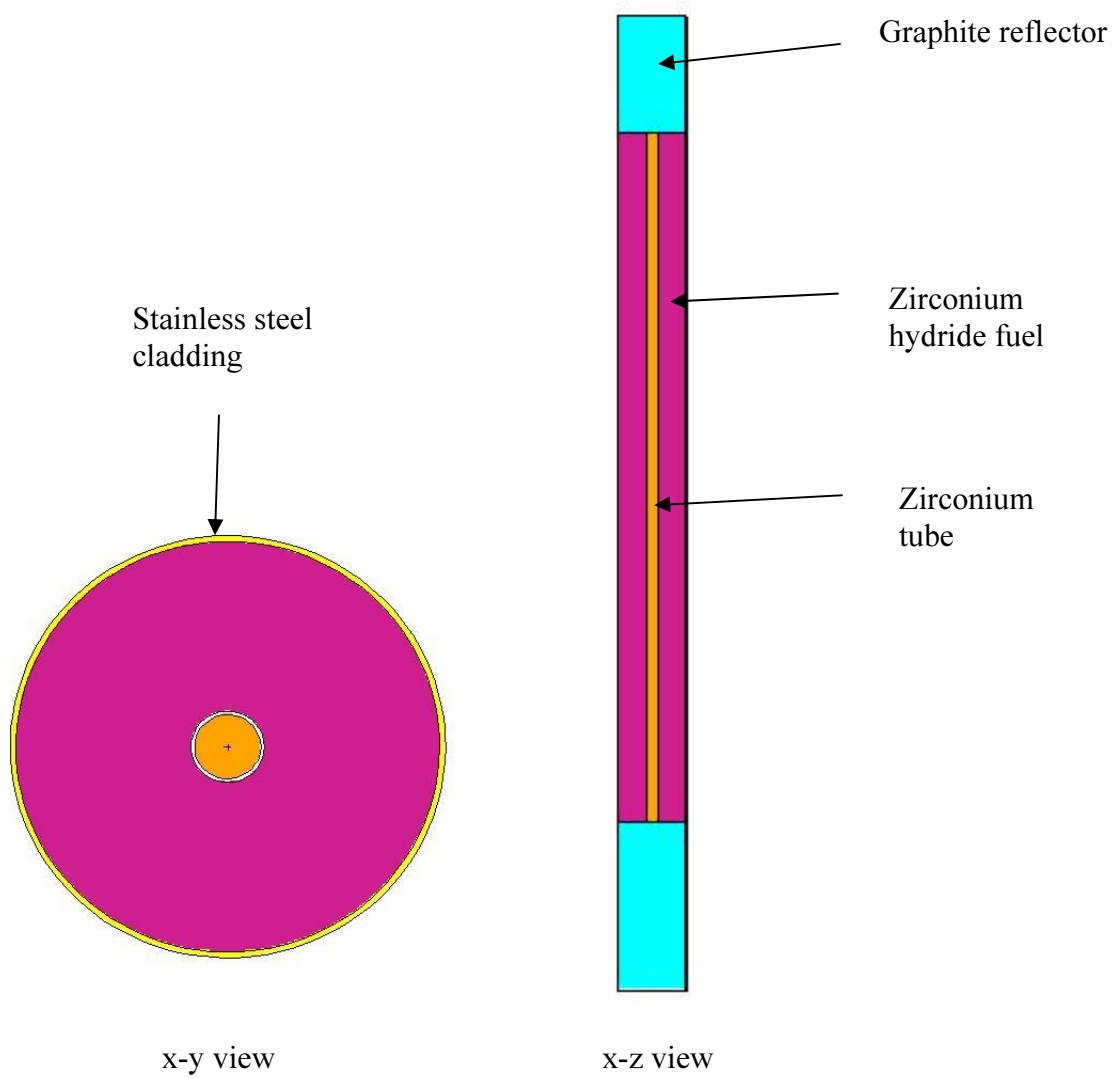


Figure 6.2-7 – Stainless Steel Clad TRIGA Fuel Element (Type 109)

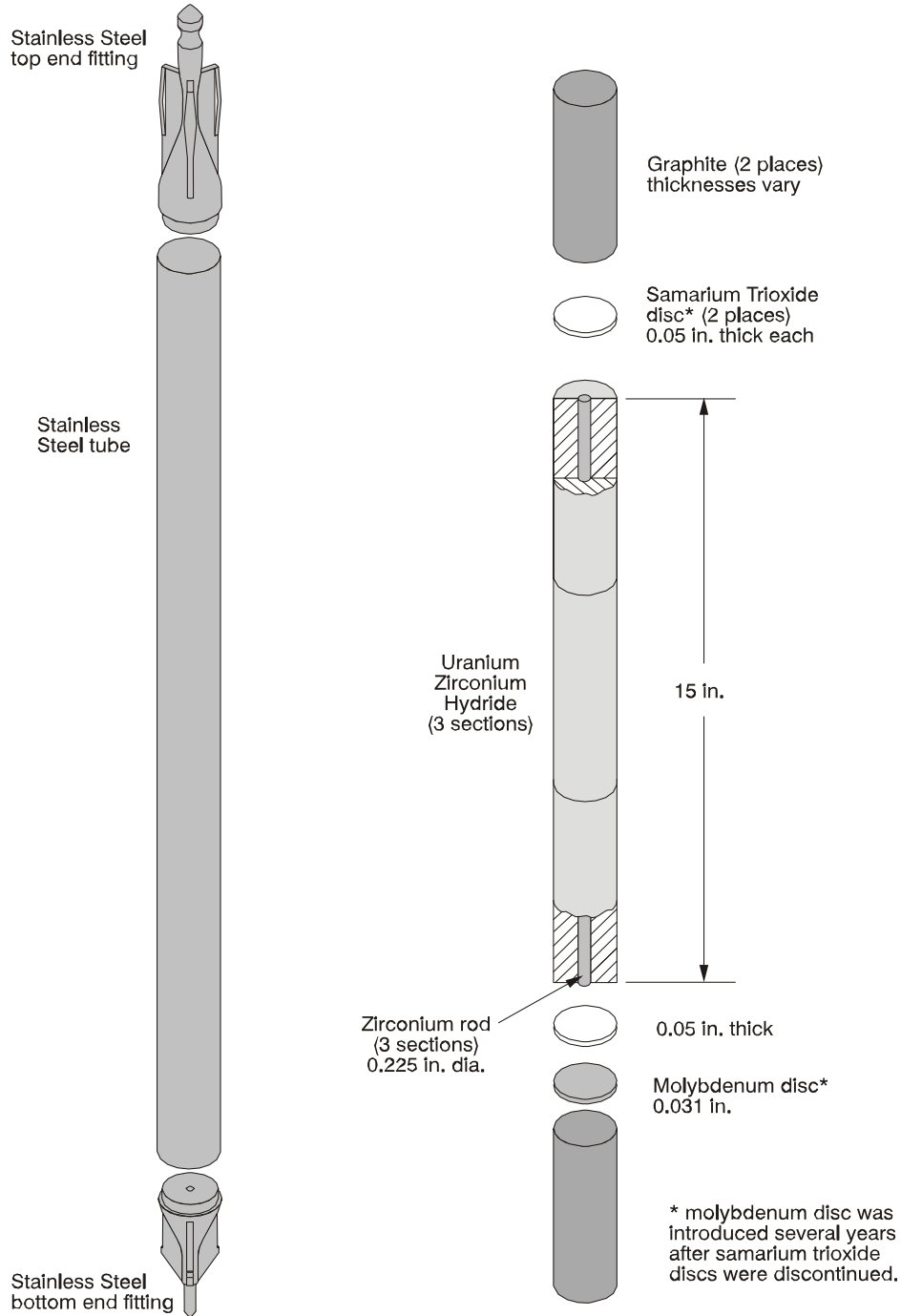


Figure 6.2-8 – Typical Stainless Steel Clad TRIGA Fuel Element

6.3 General Considerations

6.3.1 Model Configuration

The BRR cask is modeled using conservative simplifying assumptions. The impact limiters are not modeled, and in the single package cases the cask is reflected with 12-in of water. In the array cases, removing the impact limiters conservatively minimizes the separation between the packages and increases the reactivity. The cask body itself is simply modeled as cylinders of steel-lead-steel without modeling the minor cask details, as these minor details have a negligible effect on the system reactivity.

The modeled cask geometry is shown in Figure 6.3-1, and the key model dimensions are provided in Table 6.3-1. Cask dimensions are based on the drawings in Section 1.3.3, *Packaging General Arrangement Drawings*. Note that the cask model in the upper region is simply representative of the shield plug thicknesses and that the 2-in thick steel lid is not included in the model, thereby bring the casks closer together in the array configuration.

Each fuel type has its own unique basket design. The baskets are modeled in sufficient detail to capture the relevant criticality effects, which are primarily of interest near the active fuel region. The key basket dimensions are included in Table 6.3-2, and x-y and x-z views of the four basket designs are provided in Figure 6.3-2 and Figure 6.3-3, respectively. Basket dimensions are based on the drawings in Section 1.3.3, *Packaging General Arrangement Drawings*. Note that the axial and radial fuel positions shown in these figures do not reflect the most reactive configurations, which is determined in Section 6.4, *Single Package Evaluation*.

Minor differences exist between the as-modeled and packaging general arrangement drawing dimensions, as shown in Table 6.3-1 and Table 6.3-2. These differences are small and are within the uncertainty of the Monte Carlo method and may therefore be neglected.

The baskets are modeled as undamaged in all NCT and HAC models. The baskets have been shown to be elastic in all accident scenarios and maintain their geometry (see Section 2.7.1.5, *Fuel Basket Stress Analysis*). The fuel is also modeled as undamaged in all models (with end structures conservatively removed), as it has also been demonstrated that the fuel maintains its structural integrity during accident conditions (see Section 2.7.1.6, *Fuel Impact Deformation*).

In the NCT cases, credit is taken for the leaktight nature of the package, and the cask cavity is modeled as dry (void). Although the package has been shown to be leaktight under accident conditions, in the HAC cases, water is conservatively modeled in the cask cavity at the density that maximizes reactivity. If it is assumed that water is free to flow throughout the cask cavity and fuel elements (as the baskets are designed to drain freely), the moderator water density between the fuel plates may be modeled at the same value as the water density between the fuel elements. This assumption is utilized in all MCNP criticality models. However, it has been shown that when an ATR fuel element is removed from a spent fuel pool and allowed to drip dry, a small volume of water remains between the fuel plates due to the surface tension in the thin channels between the fuel plates. Because the quantity of residual water is relatively small, any minor surface tension effects have been neglected in the MCNP modeling. In addition, no models are developed in which the cask is partially filled with water with some fuel elements

uncovered (such as might be the case if the cask were on its side in an accident), because this scenario would be less reactive due to lack of moderation in the uncovered fuel elements.

In the array cases, a close-packed hexagonal array is modeled by adding a hexagonal reflective boundary condition. The water density between the casks in the array is adjusted to determine the most reactive condition.

6.3.2 Material Properties

The fuel meat compositions are provided in Table 6.2-2, Table 6.2-3, Table 6.2-6, and Table 6.2-8 for MURR, MITR-II, ATR, and TRIGA fuel, respectively. For all fuels, aluminum structural material is modeled as pure aluminum with a density of 2.7 g/cm^3 .

The TRIGA fuel contains materials not found in the aluminum plate fuels, such as stainless steel, graphite, and zirconium. For the stainless steel clad TRIGA fuel, the composition of stainless steel utilized is the standard composition provided in the SCALE material library [4] and is provided in Table 6.3-3. For the TRIGA fuels that contain a zirconium rod in the center of the fuel element, the zirconium is modeled as pure with a density of 6.5 g/cm^3 . The graphite reflectors in the TRIGA fuel elements is modeled as pure graphite with a density of 1.6 g/cm^3 . The density is obtained from the TRIGA benchmark experiments (IEU-COMP-THERM-003) listed in the *International Handbook of Evaluated Criticality Benchmark Experiments* [3]. The molybdenum disc is omitted in most models, but when present is modeled as pure molybdenum with a density of 10.22 g/cm^3 . The material properties of the remaining packaging and moderating materials are described as follows.

The inner and outer tubes of the package are constructed from stainless steel 304. The standard compositions for stainless steel 304 are obtained from the SCALE material library [4], which is a standard set accepted for use in criticality analyses. The stainless steel composition and density utilized in the MCNP models are provided in Table 6.3-3.

Water is modeled with a density ranging up to 1.0 g/cm^3 and the chemical formula H_2O .

6.3.3 Computer Codes and Cross-Section Libraries

MCNP5 v1.30 is used for the criticality analysis [1]. All cross sections utilized are at room temperature (293.6 K). The uranium isotopes utilize preliminary ENDF/B-VII cross section data that are considered by Los Alamos National Laboratory to be more accurate than ENDF/B-VI cross sections. ENDF/B-V cross sections are utilized for chromium, nickel, iron, and lead because natural composition ENDF/B-VI cross sections are not available for these elements. The remaining isotopes utilize ENDF/B-VI cross sections. Titles of the cross sections utilized in the models have been extracted from the MCNP output (when available) and provided in Table 6.3-4. The $S(\alpha,\beta)$ card LWTR.60T is used to simulate hydrogen bound to water in all models. For the TRIGA models only, the $S(\alpha,\beta)$ cards H/ZR.60T and ZR/H.60T are used to simulate hydrogen and zirconium in zirconium hydride, respectively.

All cases are run with 2500 neutrons per generation for 250 generations, skipping the first 50. The 1-sigma uncertainty is approximately 0.001 for the HAC cases, and somewhat less for the NCT cases.

6.3.4 Demonstration of Maximum Reactivity

The reactivities of the NCT single package and array cases are small (<0.6) because the package is leaktight and no water is present in the package cavity. The TRIGA fuel is the most reactive under NCT because hydrogen moderator is included in the zirconium hydride fuel matrix, although the reactivity is still relatively low.

Under HAC, water is allowed to enter the package cavity at the density that maximizes reactivity. For the plate fuels, the system is always the most reactive when full-density water is utilized because the system is undermoderated. For the TRIGA fuel, optimum reactivity is achieved for a reduced water density (0.6 or 0.7 g/cm³). All four fuels show an increase in reactivity when the fuel is axially shifted to the top of the cavity, as this configuration maximizes reflection from the lead in the shield plug. All four fuels also show an increase in reactivity when the fuel elements are moved to the radial center of the package. For the MITR-II fuel, which has an inner and outer row of fuel elements, reactivity is maximized by moving the inner row outward and the outer row inward, which decreases the distance between the fuel elements.

For the array cases, a hexagonal reflective boundary condition is placed around the cask, simulating a hexagonal lattice. The water density between the packages is varied between 0 and 1.0 g/cm³, and the array reactivities (both NCT and HAC) are maximized with no water between the packages.

It has been demonstrated in the structural analysis that the baskets and fuel elements maintain their structural integrity during accident condition. Therefore, no damaged basket or fuel models are developed.

The MITR-II fuel is the most reactive, with $k_s = 0.890$ (Case D21), which is below the USL of 0.9209 (see Table 6.1-1). The reason the MITR-II configuration is more reactive than either MURR or ATR configurations is due to the basket design. The MITR-II basket places three fuel elements in the center of the basket, while the MURR and ATR baskets do not allow fuel elements in the central region. The TRIGA configuration is less reactive than either the MURR or MITR-II configurations, although TRIGA is more reactive than ATR.

Table 6.3-1 – Key Cask Model Dimensions

Item	Dimension (in)
Cask Radial	
Cask inner diameter	16.0
Cask inner steel thickness	1.0
Cask lead thickness	8.0
Cask outer steel thickness	2.0
Cask outer diameter (w/o heat shield)	38.00
Cask Axial Top	
Shield plug bottom plate thickness	1.0
Shield plug lead thickness	9.7, modeled as 9.58
Shield plug top plate thickness	0.5
Shield plug overall height	11.2, modeled as 11.08
Cask Axial Bottom	
Bottom outer plate thickness	1.0
Bottom lead thickness at centerline	7.7, modeled as 7.72
Bottom casting inner thickness (after machining)	1.1, modeled as 1.22

Table 6.3-2 – Key Basket Model Dimensions

Item	Dimension (in)
MURR Basket	
Compartment separator width	1.0
Shell outer diameter	15.63
Shell thickness	0.25
Inner tube outer diameter	7.9, modeled as 7.938
Inner tube inner diameter	7.0
MITR-II Basket	
Compartment thickness	0.12
Compartment perpendicular width	2.7, modeled as 2.662
Outer row position diameter	10.6, modeled as 10.56
ATR Basket	
Compartment separator width	0.375
Shell outer diameter	13.5
Shell thickness	0.25
Inner tube outer diameter	7.2
Inner tube inner diameter	6.5
TRIGA Basket	
Tube outer diameter	2.0
Tube wall thickness	0.12, modeled as 0.11
Inner row position diameter	6.5
Outer row position diameter	11.5

Table 6.3-3 – SS304 Composition

Component	Wt.%
C	0.08
Si	1.0
P	0.045
Cr	19.0
Mn	2.0
Fe	68.375
Ni	9.5
Density (g/cm ³)	7.94

Table 6.3-4 – Cross Section Libraries Utilized

Isotope/Element	Cross Section Label (from MCNP output)
1001.62c	1-h-1 at 293.6K from endf-vi.8 njoy99.50
6000.66c	6-c-0 at 293.6K from endf-vi.6 njoy99.50
8016.62c	8-o-16 at 293.6K from endf-vi.8 njoy99.50
13027.62c	13-al-27 at 293.6K from endf-vi.8 njoy99.50
14000.60c	14-si-nat from endf/b-vi
15031.66c	15-p-31 at 293.6K from endf-vi.6 njoy99.50
17000.66c	17-cl-0 at 293.6K from endf-vi.0 njoy99.50
24000.50c	njoy
25055.62c	25-mn-55 at 293.6K from endf/b-vi.8 njoy99.50
26000.55c	njoy
28000.50c	njoy
40000.66c	40-zr-0 at 293.6K from endf-vi.1 njoy99.50
82000.50c	njoy
92234.69c	92-u-234 at 293.6K from t16 u234la4 njoy99.50
92235.69c	92-u-235 at 293.6K from t16 u235la9d njoy99.50
92236.69c	92-u-236 at 293.6K from t16 u236la2d njoy99.50
92238.69c	92-u-238 at 293.6K from t16 u238la8h njoy99.50

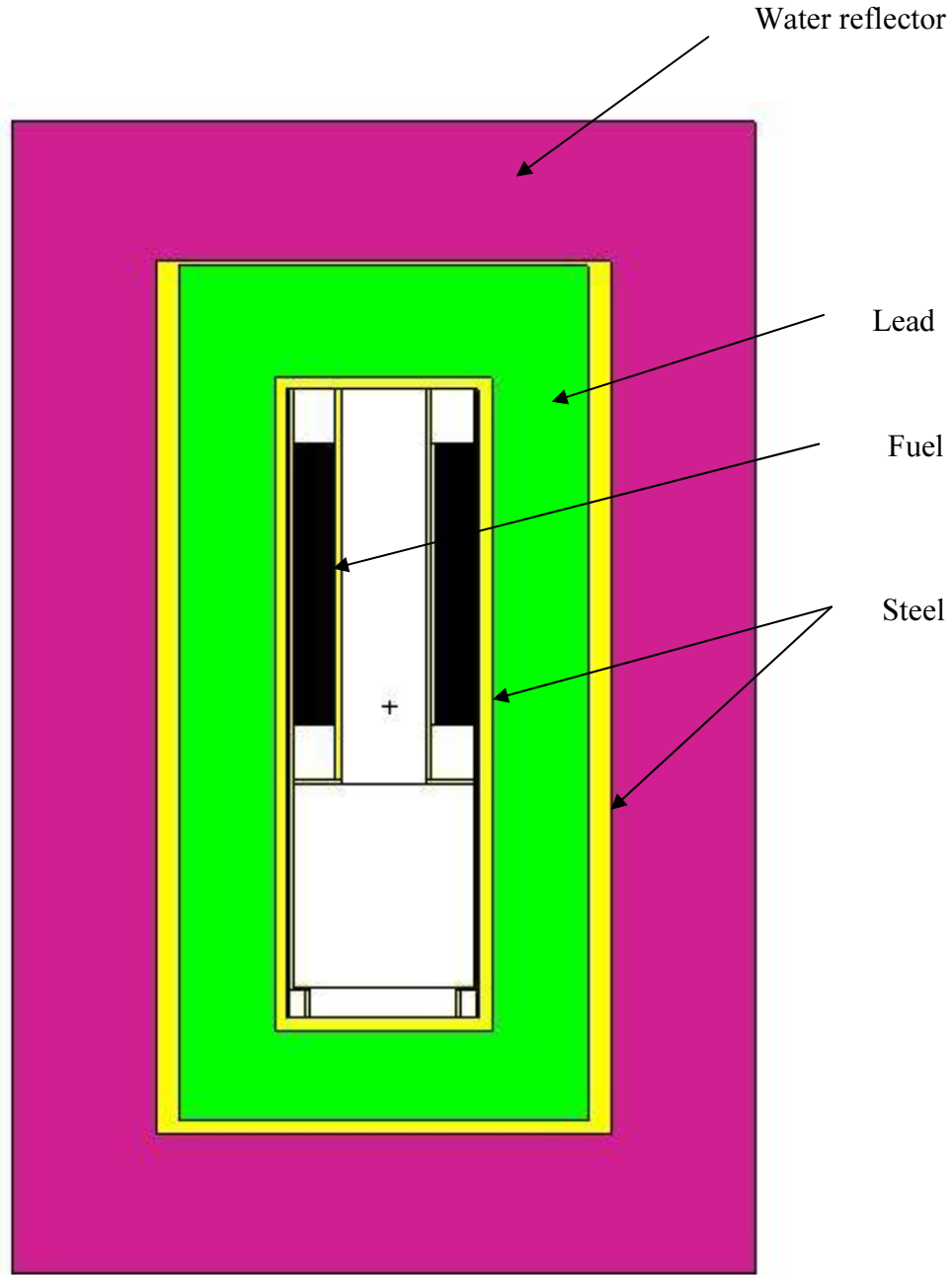
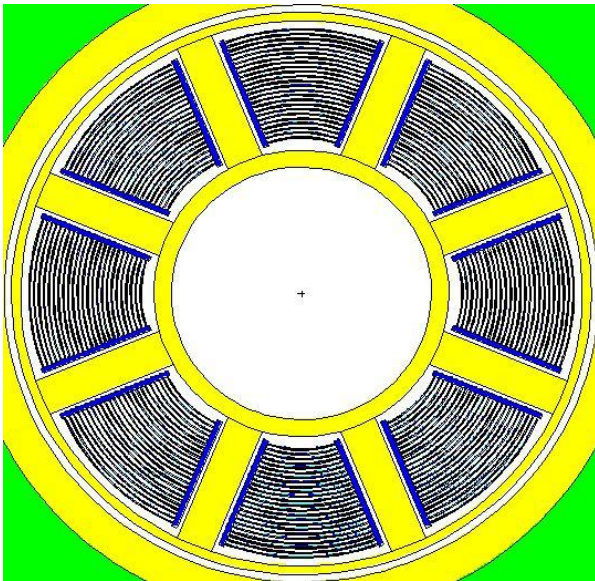
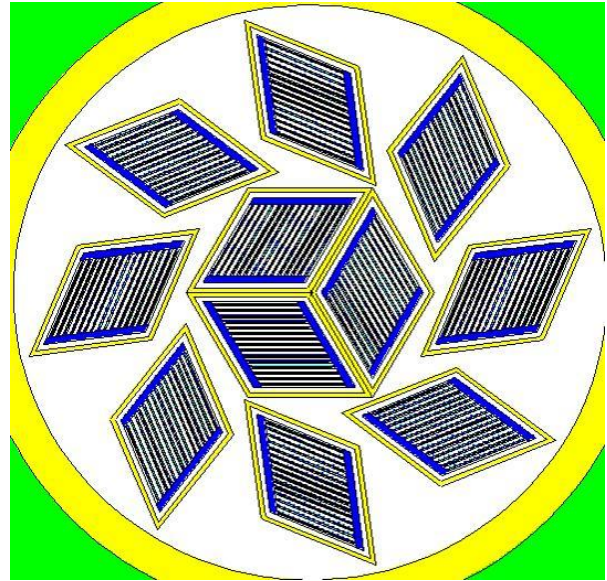


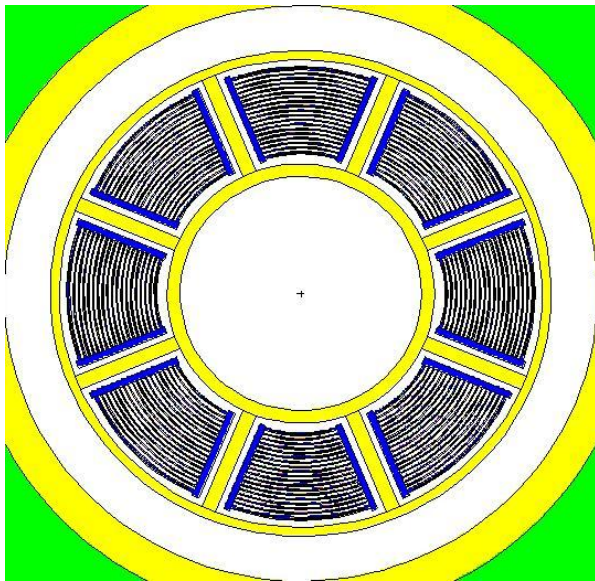
Figure 6.3-1 – NCT Single Package Model (x-z view)



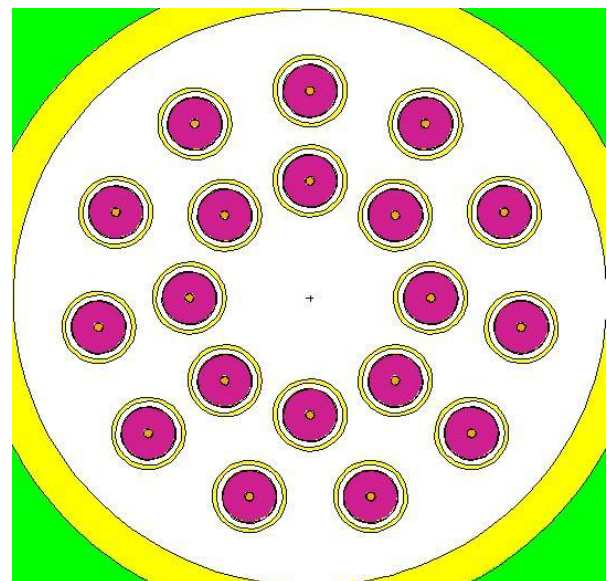
MURR



MITR-II



ATR



TRIGA

Figure 6.3-2 – Basket Models (x-y view)

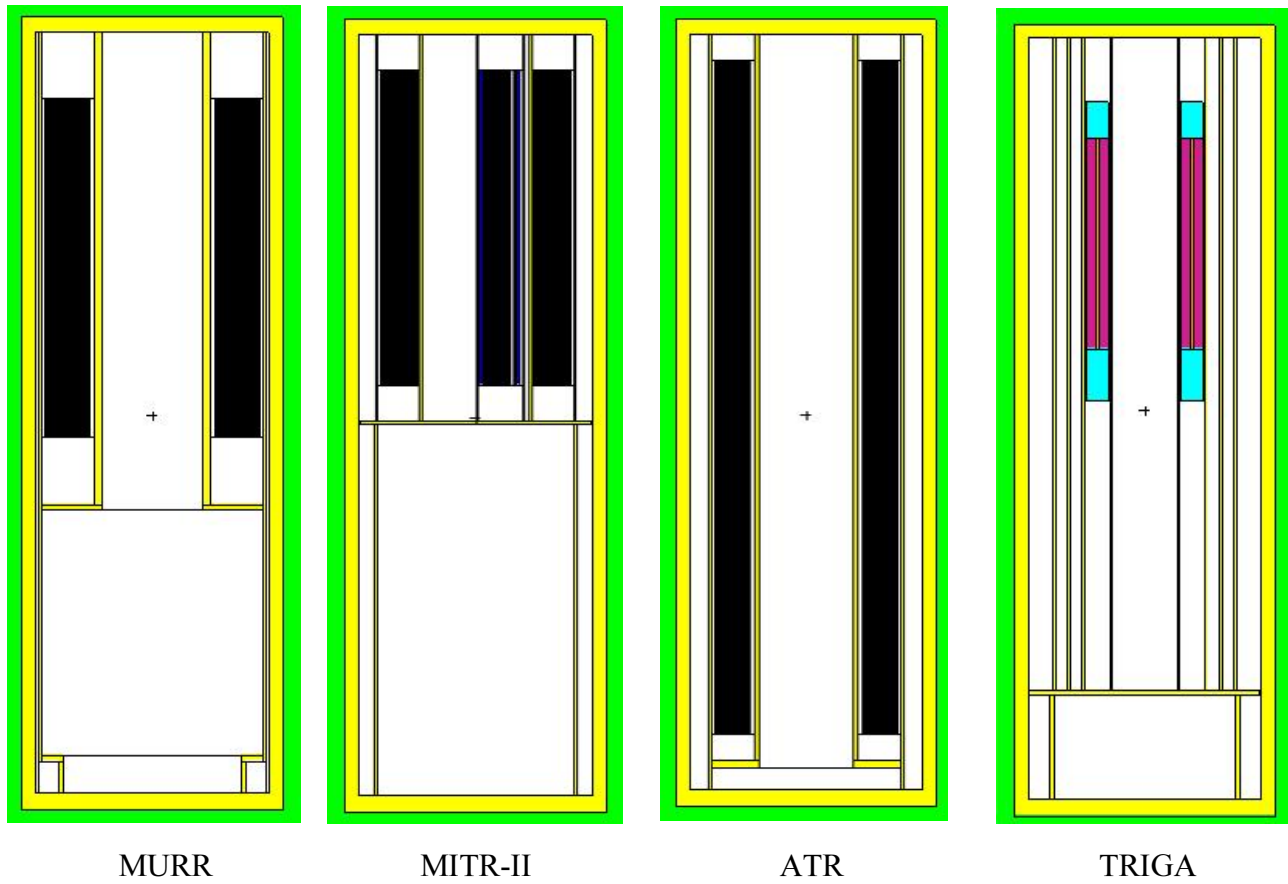


Figure 6.3-3 – Basket Models (x-z view)

6.4 Single Package Evaluation

6.4.1 Configuration

6.4.1.1 NCT Single Package Configuration

The geometry of the NCT single package configuration is discussed in Section 6.3.1, *Model Configuration*. The fuel element geometry is consistent with the most reactive fuel element models, including tolerances, as determined in Section 6.9.2, *Parametric Evaluations to Determine the Most Reactive Fuel Geometries*. For the TRIGA fuels, it is demonstrated in Section 6.9.2.4, *TRIGA Fuel Parametric Evaluation*, that the HEU fuel type (Type 109) is the most reactive of the five TRIGA fuel types under consideration. Therefore, all TRIGA models use this fuel type.

MURR

The MURR results are listed in Table 6.4-1 as Cases A1 through A3. In Case A1, the active fuel region is centered both axially and laterally within the basket compartments. In Case A2, all fuel elements are moved within the basket compartments towards the radial center. In Case A3, the fuel elements are moved radially inward (like Case A2) and shifted axially to the top of the package. In actual practice, it would not be possible to shift the active fuel all the way to the top due to the presence of the end fittings. This configuration is the most reactive, as reflection from the package shield plug is maximized. Therefore, Case A3 is the most reactive, with $k_s = 0.08545$. Clearly, the reactivity of unmoderated MURR fuel is very low.

MITR-II

The MITR-II results are listed in Table 6.4-1 as Cases A10 through A13. In Case A10, the active fuel region is centered both axially and laterally within the basket compartments. In Case A11, all fuel elements are moved within the basket compartments towards the radial center. In Case A12, the outer row of elements are moved radially inward, and the inner row is moved radially outward. Comparing Cases A10 through A12, Case A11 is the most reactive. In Case A13, the fuel elements are moved radially inward (like Case A11) and shifted axially to the top of the package. In actual practice, it would not be possible to shift the active fuel all the way to the top due to the presence of the end fittings. This configuration is the most reactive, as reflection from the package shield plug is maximized. Therefore, Case A13 is the most reactive, with $k_s = 0.07517$. Clearly, the reactivity of unmoderated MITR-II fuel is very low.

ATR

The ATR results are listed in Table 6.4-1 as Cases A20 through A22. In Case A20, the active fuel region is centered both axially and laterally within the basket compartments. In Case A21, all fuel elements are moved within the basket compartments towards the radial center. In Case A22, the fuel elements are moved radially inward (like Case A21) and shifted axially to the top of the package. All three configurations have similar reactivities, although Case A22 is the most reactive, with $k_s = 0.08849$. Clearly, the reactivity of unmoderated ATR fuel is very low.

BRR Package Safety Analysis ReportTRIGA

The TRIGA results are listed in Table 6.4-1 as Cases A30 through A33. In Case A30, the fuel elements are laterally centered in the basket compartments, and the fuel elements are offset from the package lid. In Case A31, the fuel elements are moved within the basket tubes towards the radial center. In Case A32, the outer row of elements are moved radially inward, and the inner row is moved radially outward. Comparing Cases A30 through A32, Case A31 is the most reactive. In Case A33, the fuel elements are moved radially inward (like Case A31) and shifted axially to the top of the package. In actual practice, it would not be possible to shift the active fuel all the way to the top due to the end fittings. This configuration is the most reactive, as reflection from the package shield plug is maximized. Therefore, Case A33 is the most reactive, with $k_s = 0.41671$. Clearly, the reactivity of unmoderated TRIGA fuel is very low and is significantly less than the USL, although the unmoderated TRIGA fuel results in the highest reactivity compared to the other fuel types (MURR, MITR-II and ATR).

6.4.1.2 HAC Single Package Configuration

The HAC single package configurations are similar to the NCT single package configurations except that water is allowed inside the package at the most reactive density.

MURR

The MURR results are summarized in Table 6.4-2 as Cases B1 through B5. In Cases B1 through B3, the package cavity is flooded with full-density water. In Case B1, the active fuel is centered both laterally and axially within the basket compartments. In Case B2, the active fuel is moved within the basket compartments towards the radial center. In Case B3, the radial configuration from Case B2 is maintained, and the fuel elements are shifted upward to the maximum possible extent, maximizing reflection from the shield plug. Case B3 is the most reactive of the three configurations examined.

In Cases B4 and B5, the configuration of Case B3 is modified so that the basket/fuel element water density is reduced to 0.8 and 0.9 g/cm³, respectively. Because the MURR fuel is undermoderated, reducing the water density will reduce the reactivity. As expected, the reactivity for Case B4 and B5 drops rapidly as the water density is reduced. Therefore, Case B3 is the most reactive, with $k_s = 0.76124$.

MITR-II

The MITR-II results are summarized in Table 6.4-2 as Cases B20 through B25. In Cases B20 through B23, the package cavity is flooded with full-density water. In Case B20, the active fuel is centered both laterally and axially within the basket compartments. In Case B21, the active fuel is moved within the basket compartments towards the radial center, and the reactivity increases somewhat. In Case B22, the outer row is moved radially inward, and the inner row moved radially outward, minimizing the distance between the fuel elements. This configuration is substantially more reactive than the centered fuel element case. In Case B23, the radial configuration from Case B22 is maintained, and the fuel elements are shifted upward to the maximum possible extent, maximizing reflection from the shield plug. Case B23 is the most reactive of the four configurations examined, although the reactivity effect of the axial shifting is small.

BRR Package Safety Analysis Report

In Cases B24 and B25, the configuration of Case B23 is modified so that the basket/fuel element water density is reduced to 0.8 and 0.9 g/cm³, respectively. Because the MITR-II fuel is undermoderated, reducing the water density will reduce the reactivity. As expected, the reactivity for Case B24 and B25 drops rapidly as the water density is reduced. Therefore, Case B23 is the most reactive, with $k_s = 0.87495$.

ATR

The ATR results are summarized in Table 6.4-2 as Cases B40 through B44. In Cases B40 through B42, the package cavity is fully flooded with full-density water. In Case B40, the fuel elements are centered both axially and laterally within the basket compartments. In Case B41, the fuel elements are moved within the basket compartments towards the radial center. In Case B42, the fuel is also shifted axially to the top of the package in addition to be moved toward the radial center. Comparing these three cases, Case B42 is the most reactive, although the reactivities are somewhat similar.

In Cases B43 and B44, the configuration of Case B42 is modified so that the basket/fuel element water density is reduced to 0.8 and 0.9 g/cm³, respectively. Because the ATR fuel is undermoderated, reducing the water density will reduce the reactivity. As expected, the reactivity for Case B43 and B44 drops rapidly as the water density is reduced. Therefore, Case B42 is the most reactive, with $k_s = 0.68525$.

TRIGA

The TRIGA results are summarized in Table 6.4-2 as Cases B60 through B70. In Cases B60 through B64, the package cavity is fully flooded with full-density water. In Case B60, the fuel elements are laterally centered within the basket tubes, at an arbitrary distance away from the package lid. In Case B61, the fuel elements are moved within the basket tubes towards the radial center, and the reactivity increases. In Case B62, the outer row is moved radially inward and the inner row is moved radially outward. Cases B63 and B64 are essentially repeats of Cases B60 and B61, respectively, except that the fuel elements are shifted upward until the top of the graphite reflector touches the bottom of the shield plug. Comparing these five cases, Case B64 is the most reactive. Therefore, the remaining HAC single package cases utilize this configuration (i.e., fuel elements moved to the radial center, shifted up to the maximum extent.)

In Cases B65 through B70, the configuration of Case B64 is modified so that the water density inside of the basket is allowed to vary between 0.4 and 0.9 g/cm³. The reactivity peaks at a density of 0.7 g/cm³ and then decreases with decreasing density. The maximum reactivity occurs for Case B68, with $k_s = 0.70869$.

6.4.2 Results

Following are the tabulated results for the single package cases. The most reactive configurations are listed in boldface.

Table 6.4-1 – NCT Single Package Results

Case ID	Filename	k_{eff}	σ	k_s ($k+2\sigma$)
MURR				
A1	NS_MURR	0.08167	0.00023	0.08213
A2	NS_MURR_IN	0.08152	0.00022	0.08196
A3	NS_MURR_INUP	0.08499	0.00023	0.08545
MITR-II				
A10	NS_MIT	0.07209	0.00019	0.07247
A11	NS_MIT_IN	0.07263	0.00020	0.07303
A12	NS_MIT_INOUT	0.07221	0.00020	0.07261
A13	NS_MIT_INUP	0.07481	0.00018	0.07517
ATR				
A20	NS_ATR	0.08689	0.00024	0.08737
A21	NS_ATR_IN	0.08759	0.00025	0.08809
A22	NS_ATR_INUP	0.08797	0.00026	0.08849
TRIGA				
A30	NS_TRIGA	0.39557	0.00089	0.39735
A31	NS_TRIGA_IN	0.40299	0.00092	0.40483
A32	NS_TRIGA_INOUT	0.40078	0.00092	0.40262
A33	NS_TRIGA_INUP	0.41493	0.00089	0.41671

Table 6.4-2 – HAC Single Package Results

Case ID	Filename	Water Density (g/cm ³)	k _{eff}	σ	k _s (k+2σ)
MURR					
B1	HS_MURR	1.0	0.75395	0.00115	0.75625
B2	HS_MURR_IN	1.0	0.75287	0.00123	0.75533
B3	HS_MURR_INUP	1.0	0.75898	0.00113	0.76124
B4	HS_MURR_C080INUP	0.8	0.69306	0.00108	0.69522
B5	HS_MURR_C090INUP	0.9	0.72871	0.00118	0.73107
MITR-II					
B20	HS_MIT_W100	1.0	0.84872	0.00110	0.85092
B21	HS_MIT_W100IN	1.0	0.85553	0.00118	0.85789
B22	HS_MIT_W100INOUT	1.0	0.86948	0.00126	0.87200
B23	HS_MIT_W100INOUTUP	1.0	0.87253	0.00121	0.87495
B24	HS_MIT_W080	0.8	0.82687	0.00113	0.82913
B25	HS_MIT_W090	0.9	0.85267	0.00122	0.85511
ATR					
B40	HS_ATR	1.0	0.67992	0.00113	0.68218
B41	HS_ATR_IN	1.0	0.68013	0.00110	0.68233
B42	HS_ATR_INUP	1.0	0.68279	0.00123	0.68525
B43	HS_ATR_C080INUP	0.8	0.64718	0.00105	0.64928
B44	HS_ATR_C090INUP	0.9	0.66179	0.00106	0.66391
TRIGA					
B60	HS_TRIGA_W100	1.0	0.66788	0.00108	0.67004
B61	HS_TRIGA_W100IN	1.0	0.69115	0.00097	0.69309
B62	HS_TRIGA_W100INOUT	1.0	0.67398	0.00098	0.67594
B63	HS_TRIGA_W100UP	1.0	0.66998	0.00112	0.67222
B64	HS_TRIGA_W100INUP	1.0	0.69348	0.00106	0.69560
B65	HS_TRIGA_W040INUP	0.4	0.67497	0.00119	0.67735
B66	HS_TRIGA_W050INUP	0.5	0.69534	0.00124	0.69782
B67	HS_TRIGA_W060INUP	0.6	0.70552	0.00104	0.70760
B68	HS_TRIGA_W070INUP	0.7	0.70661	0.00104	0.70869
B69	HS_TRIGA_W080INUP	0.8	0.70510	0.00099	0.70708
B70	HS_TRIGA_W090INUP	0.9	0.70164	0.00106	0.70376

6.5 Evaluation of Package Arrays under Normal Conditions of Transport

6.5.1 Configuration

In the NCT array configurations, the most reactive NCT single package configuration for each fuel type determined in Section 6.4.1.1, *NCT Single Package Configuration*, is utilized. A hexagonal reflective surface is added around the package, as shown in Figure 6.5-1. This simulates a close-packed infinite hexagonal array of packages. The reflective boundary is also present on the top and bottom surfaces.

Five cases are run for each fuel type. The initial case is simply the most reactive NCT single package case with reflective boundary conditions and no water between the packages. In the remaining four cases, the water density between the packages is varied between 0.25 and 1.0 g/cm³. In each case, the reactivity is maximized with no water between the packages.

The results are summarized in Table 6.5-1. Cases C1 through C5 are for MURR, Cases C10 through C14 are for MITR-II, Cases C20 through C24 are for ATR, and Cases C30 through C34 are for TRIGA. Of the four fuel types considered, the TRIGA fuel Case C30 with no water between the packages is the most reactive, with $k_s = 0.53939$. TRIGA fuel is significantly more reactive than the other fuels because hydrogen is included in the fuel matrix.

6.5.2 Results

The results for the NCT array cases are provided in the following table. The most reactive configuration for each fuel type is listed in boldface.

Table 6.5-1 – NCT Array Results

Case ID	Filename	External Water Density (g/cm ³)	k _{eff}	σ	k _s (k+2σ)
MURR					
C1	NA_MURR_INUP	0	0.19604	0.00037	0.19678
C2	NA_MURR_W025INUP	0.25	0.12467	0.00031	0.12529
C3	NA_MURR_W050INUP	0.50	0.11327	0.00029	0.11385
C4	NA_MURR_W075INUP	0.75	0.10858	0.00026	0.10910
C5	NA_MURR_W100INUP	1.0	0.10606	0.00027	0.10660
MITR-II					
C10	NA_MIT_W000	0	0.18595	0.00040	0.18675
C11	NA_MIT_W025	0.25	0.11474	0.00029	0.11532
C12	NA_MIT_W050	0.50	0.10296	0.00026	0.10348
C13	NA_MIT_W075	0.75	0.09822	0.00027	0.09876
C14	NA_MIT_W100	1.0	0.09531	0.00024	0.09579
ATR					
C20	NA_ATR_INUP	0	0.23274	0.00041	0.23356
C21	NA_ATR_W025INUP	0.25	0.13567	0.00032	0.13631
C22	NA_ATR_W050INUP	0.50	0.12103	0.00031	0.12165
C23	NA_ATR_W075INUP	0.75	0.11473	0.00029	0.11531
C24	NA_ATR_W100INUP	1.0	0.11116	0.00028	0.11172
TRIGA					
C30	NA_TRIGA_INUP	0	0.53733	0.00103	0.53939
C31	NA_TRIGA_W025INUP	0.25	0.46130	0.00099	0.46328
C32	NA_TRIGA_W050INUP	0.50	0.44977	0.00096	0.45169
C33	NA_TRIGA_W075INUP	0.75	0.44506	0.00096	0.44698
C34	NA_TRIGA_W100INUP	1.0	0.43997	0.00094	0.44185

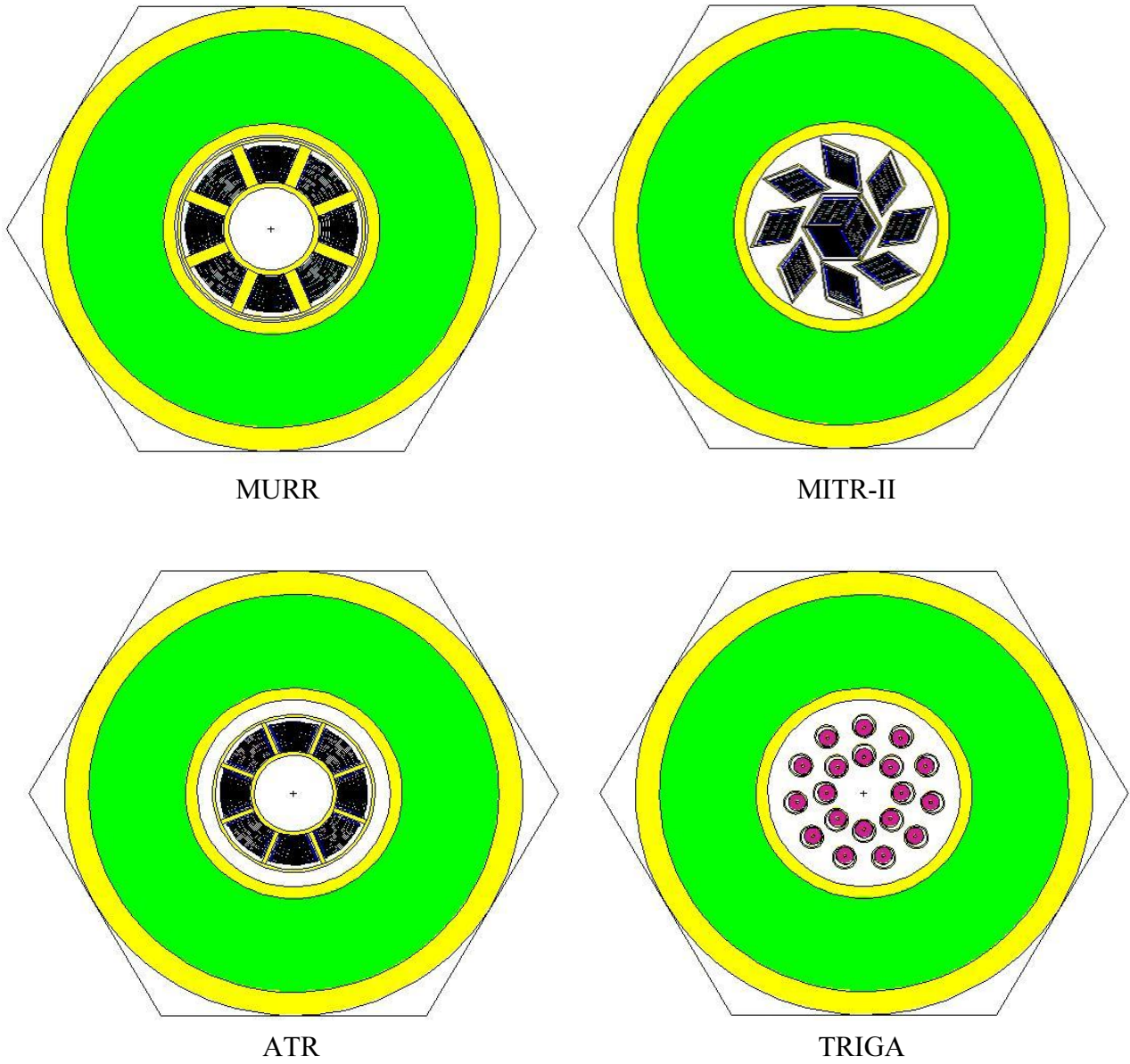


Figure 6.5-1 – NCT Array Geometry

6.6 Package Arrays under Hypothetical Accident Conditions

6.6.1 Configuration

In the HAC array configuration, an infinite hexagonal array of packages is modeled in the same manner as the NCT array. Various internal moderation conditions are examined, as well as various moderation conditions between packages.

MURR

The MURR results are reported in Table 6.6-1. In Case D1, the fuel elements are moved radially inward and shifted to the top of the package, which was determined to be the most reactive single package orientation. The package cavity is flooded with full-density water, and void is modeled between the packages.

In Cases D2 and D3, the configuration of Case D1 is modified so that all water inside the cavity is treated as variable density (0.8 and 0.9 g/cm³, respectively). Because the water density between the fuel plates is reduced in this configuration, moderation is decreased and the reactivity decreases.

In Cases D4 through D7, the most reactive case (Case D1) is run with variable water density between the packages. The reactivity decreases when water is added to this region. Therefore, Case D1 is the most reactive, with $k_s = 0.80658$.

MITR-II

The MITR-II results are reported in Table 6.6-2. Because the MITR-II configuration is significantly more reactive than the MURR, ATR, or TRIGA configurations, additional configurations and moderation conditions are examined for this fuel type compared to the other fuel types.

In all MITR-II models, the outer row is moved radially inward, and the inner row is moved radially outward, which was determined to be the most reactive single package orientation (Case B23). In Case D20, the fuel is modeled at the axial center of the basket compartment, the package cavity is flooded with full-density water, and void is modeled between the packages. Case D21 is the same as Case D20, except the fuel is shifted axially upward to the bottom of the shield plug. Consistent with the HAC single package results, the reactivity increases when the fuel is shifted upward.

In Cases D22 through D25, the basic configuration of Case D21 is modeled, except the water below the fuel elements is treated as variable density, while the water inside and between the fuel elements remains at full-density. Such a scenario could result from a partially filled cask, and could possibly increase neutron transmission between the casks in the axial direction due to the reduced water density. However, the cask is relatively long in proportion to the fuel length, and the effect on the reactivity is within statistical fluctuation. Therefore, the water in the cask cavity is modeled at a uniform density for all MURR, ATR, and TRIGA HAC array cases.

In Cases D26 and D27, the configuration of Case D21 is modified so that all water inside the cavity is treated as variable density (0.8 and 0.9 g/cm³, respectively). Because the water density

BRR Package Safety Analysis Report

between the fuel plates is reduced in this configuration, moderation is decreased and the reactivity decreases.

In Cases D28 through D31, the most reactive case (Case D21) is run with variable water density between the packages. The reactivity decreases when water is added to this region. Therefore, Case D21 is the most reactive, with $k_s = 0.88988$. Note that this is also the most reactive case of the four fuel types examined.

ATR

The ATR results are reported in Table 6.6-3. In Case D40, the fuel elements are moved radially inward and shifted to the top of the package, which was determined to be the most reactive single package orientation. The package cavity is flooded with full-density water, and void is modeled between the packages.

In Cases D41 and D42, the configuration of Case D40 is modified so that all water inside the cavity is treated as variable density (0.8 and 0.9 g/cm³, respectively). Because the water density between the fuel plates is reduced in this configuration, moderation is decreased and the reactivity decreases.

In Cases D43 through D46, the most reactive case (Case D40) is run with variable water density between the packages. The reactivity decreases when water is added to this region. Therefore, Case D40 is the most reactive, with $k_s = 0.69739$.

TRIGA

The TRIGA results are reported in Table 6.6-4. In all models, the fuel elements are moved radially inward and axially shifted to the top of the cask, which was determined to be the most reactive single package orientation. It is expected that the most reactive condition will occur at a reduced internal water density, consistent with the single package TRIGA results. Therefore, in Cases D60 through D67, the cavity water density is varied from 0.3 to 1.0 g/cm³, while void is modeled external to the package. The maximum reactivity occurs for Case D63, which has a water density of 0.6 g/cm³.

In Cases D68 through D71, the internal water density is modeled at 0.6 g/cm³ (Case D63 configuration) while the external water density is varied between 0.25 and 1.0 g/cm³. The reactivity decreases when water is modeled between the packages. Therefore, Case D63 is the most reactive, with $k_s = 0.72039$.

6.6.2 Results

Following are the tabulated results for the HAC array cases. The most reactive configuration in each series is listed in boldface.

Table 6.6-1 – HAC Array Results, MURR

Case ID	Filename	Internal Water Density (g/cm ³)	External Water Density (g/cm ³)	k _{eff}	σ	k _s (k+2σ)
D1	HA_MURR	1.0	0	0.80428	0.00115	0.80658
D2	HA_MURR_C080	0.8	0	0.74913	0.00111	0.75135
D3	HA_MURR_C090	0.9	0	0.77692	0.00116	0.77924
D4	HA_MURR_W025	1.0	0.25	0.77495	0.00125	0.77745
D5	HA_MURR_W050	1.0	0.50	0.77403	0.00106	0.77615
D6	HA_MURR_W075	1.0	0.75	0.77030	0.00115	0.77260
D7	HA_MURR_W100	1.0	1.0	0.76810	0.00131	0.77072

Table 6.6-2 – HAC Array Results, MITR-II

Case ID	Filename	Internal Water Density (upper) (g/cm ³)	Internal Water Density (lower) (g/cm ³)	External Water Density (g/cm ³)	k _{eff}	σ	k _s (k+2σ)
D20	HA_MIT_INOUT	1.0	1.0	0	0.87811	0.00129	0.88069
D21	HA_MIT_INOUTUP2	1.0	1.0	0	0.88740	0.00124	0.88988
D22	HA_MIT_B000	1.0	0	0	0.88391	0.00121	0.88633
D23	HA_MIT_B025	1.0	0.25	0	0.88655	0.00113	0.88881
D24	HA_MIT_B050	1.0	0.50	0	0.88439	0.00118	0.88675
D25	HA_MIT_B075	1.0	0.75	0	0.88584	0.00129	0.88842
D26	HA_MIT_C080	0.8	0.8	0	0.84732	0.00113	0.84958
D27	HA_MIT_C090	0.9	0.9	0	0.86850	0.00117	0.87084
D28	HA_MIT_W025	1.0	1.0	0.25	0.87884	0.00125	0.88134
D29	HA_MIT_W050	1.0	1.0	0.50	0.87825	0.00112	0.88049
D30	HA_MIT_W075	1.0	1.0	0.75	0.87704	0.00118	0.87940
D31	HA_MIT_W100	1.0	1.0	1.0	0.87644	0.00110	0.87864

Table 6.6-3 – HAC Array Results, ATR

Case ID	Filename	Internal Water Density (g/cm ³)	External Water Density (g/cm ³)	k _{eff}	σ	k _s (k+2σ)
D40	HA_ATR	1.0	0	0.69505	0.00117	0.69739
D41	HA_ATR_C080	0.8	0	0.66976	0.00104	0.67184
D42	HA_ATR_C090	0.9	0	0.68206	0.00109	0.68424
D43	HA_ATR_W025	1.0	0.25	0.68753	0.00115	0.68983
D44	HA_ATR_W050	1.0	0.50	0.68575	0.00111	0.68797
D45	HA_ATR_W075	1.0	0.75	0.68528	0.00106	0.68740
D46	HA_ATR_W100	1.0	1.0	0.68342	0.00110	0.68562

Table 6.6-4 – HAC Array Results, TRIGA

Case ID	Filename	Internal Water Density (g/cm ³)	External Water Density (g/cm ³)	k _{eff}	σ	k _s (k+2σ)
D60	HA_TRIGA_W0C030	0.3	0	0.68281	0.00107	0.68495
D61	HA_TRIGA_W0C040	0.4	0	0.70304	0.00102	0.70508
D62	HA_TRIGA_W0C050	0.5	0	0.71234	0.00113	0.71460
D63	HA_TRIGA_W0C060	0.6	0	0.71827	0.00106	0.72039
D64	HA_TRIGA_W0C070	0.7	0	0.71592	0.00107	0.71806
D65	HA_TRIGA_W0C080	0.8	0	0.71130	0.00109	0.71348
D66	HA_TRIGA_W0C090	0.9	0	0.70455	0.00107	0.70669
D67	HA_TRIGA_W0C100	1.0	0	0.69737	0.00112	0.69961
D68	HA_TRIGA_W025C060	0.6	0.25	0.70793	0.00125	0.71043
D69	HA_TRIGA_W050C060	0.6	0.50	0.70781	0.00097	0.70975
D70	HA_TRIGA_W075C060	0.6	0.75	0.70655	0.00110	0.70875
D71	HA_TRIGA_W100C060	0.6	1.0	0.70660	0.00105	0.70870

6.7 Fissile Material Packages for Air Transport

This section is not applicable, because air transport is not claimed.

6.8 Benchmark Evaluations

The Monte Carlo computer program MCNP5 v1.30 is utilized for this benchmark analysis [1]. MCNP has been used extensively in criticality evaluations for several decades and is considered a standard in the industry.

The ORNL USLSTATS code [2] is used to establish a USL for the analysis. USLSTATS provides a simple means of evaluating and combining the statistical error of the calculation, code biases, and benchmark uncertainties. The USLSTATS calculation uses the combined uncertainties and data to provide a linear trend and an overall uncertainty. Computed multiplication factors, k_{eff} , for the package are deemed to be adequately subcritical if the computed value of k_s is less than or equal to the USL as follows:

$$k_s = k_{\text{eff}} + 2\sigma \leq \text{USL}$$

The USL includes the combined effects of code bias, uncertainty in the benchmark experiments, uncertainty in the computational evaluation of the benchmark experiments, and an administrative margin. This methodology has accepted precedence in establishing criticality safety limits for transportation packages complying with 10 CFR 71.

6.8.1 Applicability of Benchmark Experiments

The four fuel types analyzed fall into two distinct categories (1) high-enriched aluminum plate fuel, which includes MURR, MITR-II, and ATR, and (2) zirconium hydride (TRIGA) fuel. A separate benchmark analysis is performed for these two categories. The critical experiment benchmarks are selected from the *International Handbook of Evaluated Criticality Safety Benchmark Experiments* [3] based upon their similarity to the packaging and contents.

6.8.1.1 Aluminum Plate Fuel

The important selection parameters are high-enriched uranium plate-type fuel with a thermal spectrum. Thirty-five (35) benchmarks that meet these criteria are selected from the *Handbook*. The titles for all utilized experiments are listed in Table 6.8-1. Note that the benchmark from experiment set HEU-MET-THERM-022 is for the Advanced Test Reactor itself, so the fuel configuration in this benchmark is essentially the same as the ATR fuel modeled in the packaging analysis.

Ideally, benchmarks would be limited to those with a fuel matrix of UAl_x and aluminum, aluminum cladding, and no absorbers, consistent with the aluminum plate fuel criticality models. Experiment set HEU-COMP-THERM-022 consists of 11 benchmark experiments that utilize UO_2 powder sintered with stainless steel, and stainless steel cladding. Experiments 1 through 5 (Cases BA1 through BA5) do not utilize control rods, while experiments 6 through 11 (Cases BA6 through BA11) utilize boron control rods. Experiment set HEU-MET-THERM-006 consists of 23 benchmark experiments. The first 16 experiments are directly applicable (Cases BA12 through BA27), although experiments 17 and 18 (Cases BA28 and BA29) utilize thin cadmium sheets, and experiments 19 through 23 (Cases BA30 through BA34) utilize uranium in solution in addition to the fuel plates. HEU-MET-THERM-022 (Case BA35) is a detailed model of the ATR core using explicit ATR fuel elements very similar to the ATR fuel element model

BRR Package Safety Analysis Report

utilized in the criticality analysis. However, this full-core model necessarily contains absorber materials. Despite the presence of absorbers, because this benchmark utilizes ATR fuel, it is considered directly applicable to the plate fuel criticality analysis.

Therefore, of these 35 benchmarks, 17 benchmarks are directly applicable, while 18 benchmarks are applicable to a lesser degree. To compensate for the benchmarks that are not directly applicable, trending will be performed both on all 35 benchmark experiments and on the subset of 17 directly applicable benchmark experiments. The USL selected is the minimum of both benchmark sets.

6.8.1.2 TRIGA Fuel

The important selection parameters are high-enriched (70%) zirconium hydride fuel with a thermal spectrum. No directly applicable benchmark experiments are available in the *Handbook*, although the *Handbook* does contain two intermediate-enriched (20%) TRIGA benchmarks. The available TRIGA benchmarks are for an entire Mark II core and hence contain absorber materials as well as a graphite reflector. While the BRR package TRIGA criticality analysis does not contain absorbers, these experiments are utilized because they represent the most similar available benchmarks.

Because a sample set of two benchmarks is not of sufficient size to obtain a statistical distribution, additional benchmarks are selected to supplement the two available TRIGA benchmarks. As zirconium hydride fuel contains moderator embedded in the fuel matrix, 10 high-enriched (93%) and 9 low-enriched (10%) uranium solution benchmarks are also utilized to simulate fuel intimately mixed with moderator. Therefore, a total of 21 benchmarks are utilized for benchmarking of TRIGA fuel. These 21 benchmarks are divided into three groups for trending: (1) all 21 benchmarks, (2) a subset of the 10 HEU benchmarks and two TRIGA benchmarks, and (3) a subset of the 9 LEU benchmarks and two TRIGA benchmarks. The USL selected is the minimum of all three benchmark sets.

6.8.2 Bias Determination

The USL is calculated by application of the USLSTATS computer program [2]. USLSTATS receives as input the k_{eff} as calculated by MCNP, the total 1- σ uncertainty (combined benchmark and MCNP uncertainties), and a trending parameter.

The uncertainty value, σ_{total} , assigned to each case is a combination of the benchmark uncertainty for each experiment, σ_{bench} , and the Monte Carlo uncertainty associated with the particular computational evaluation of the case, σ_{MCNP} , or:

$$\sigma_{\text{total}} = (\sigma_{\text{bench}}^2 + \sigma_{\text{MCNP}}^2)^{1/2}$$

These values are input into the USLSTATS program in addition to the following parameters, which are the values recommended by the USLSTATS user's manual [2]:

- P, proportion of population falling above lower tolerance level = 0.995 (note that this parameter is required input but is not utilized in the calculation of USL Method 1)
- 1- γ , confidence on fit = 0.95

BRR Package Safety Analysis Report

- α , confidence on proportion $P = 0.95$ (note that this parameter is required input but is not utilized in the calculation of USL Method 1)
- Δk_m , administrative margin used to ensure subcriticality = 0.05.

These data are followed by triplets of trending parameter value, computed k_{eff} , and uncertainty for each case. A confidence band analysis is performed on the data for each trending parameter using USL Method 1.

6.8.2.1 Aluminum Plate Fuel

Five trending parameters are selected for the aluminum plate fuel: (1) Energy of the Average neutron Lethargy causing Fission (EALF), (2) U-235 number density, (3) channel width, (4) ratio of the number of hydrogen atoms in a unit cell to the number of U-235 atoms in a unit cell (H/U-235), and (5) plate pitch.

The USL generated for each of the trending parameters utilized is provided in Table 6.8-2. All benchmark data used as input to USLSTATS are reported in Table 6.8-4.

Energy of the Average neutron Lethargy causing Fission (EALF)

The EALF is used as the first trending parameter for the benchmark cases. The EALF comparison provides a means to observe neutron spectral dependencies or trends. Over the range of applicability, the minimum USL is 0.9254 for the full benchmark set, and 0.9212 for the subset of directly applicable benchmarks.

The HAC MITR-II and ATR cases that are moderated with full-density water fall within the range of applicability, which includes the most reactive case (Case D21). For reduced water density MITR-II and ATR cases, the EALF sometimes exceeds the range of applicability, although the reactivity drops for these cases. None of the MURR cases fall within the range of applicability, even with full-density water, although the most reactive MURR case is only slightly outside the range of applicability ($1.74\text{E-}07$ MeV for Case D1 versus $1.59\text{E-}07$ MeV upper range). Because the MURR cases are not limiting, the margin to the USL is large, and the EALF is only slightly outside the range of applicability, this behavior is considered to be acceptable. All of the NCT models for MURR, MITR-II, and ATR fall outside the range of applicability for this parameter. This behavior is expected, because the NCT cases are unmoderated and the EALF is relatively large for these cases. Also, the NCT cases have very low reactivity and are not a concern. Therefore, this parameter is judged to be acceptable for the MURR, MITR-II, and ATR fuels.

U-235 Number Density

The U-235 number density is used as the second trending parameter for the benchmark cases. Over the range of applicability, the minimum USL is 0.9240 for the full benchmark set, and 0.9209 for the subset of directly applicable benchmarks.

The U-235 number densities for the three plate fuels are as follows:

- MURR: $3.65\text{E-}03$ atom/b-cm
- MITR-II: $3.68\text{E-}03$ atom/b-cm
- ATR: variable, see Table 6.2-6

BRR Package Safety Analysis Report

This parameter is within the range of applicability for both MURR and MITR-II fuel. For the ATR fuel element model, the U-235 number densities for plates 1 through 4 and 16 through 19 fall within the range of applicability, while the number densities for plates 5 through 15 exceed the range of applicability (maximum value = 4.22E-03 atom/b-cm). The maximum range of applicability is 3.92E-03 atom/b-cm, so range is exceeded only slightly. Also, the average U-235 number density for the fuel element is 3.73E-03 atom/b-cm, which is within the allowable range. Therefore, application of this USL to the ATR criticality models is considered acceptable.

Channel Width

The channel width is used as the third trending parameter for the benchmark cases. Over the range of applicability, the minimum USL is 0.9225 for the full benchmark set, and 0.9209 for the subset of directly applicable benchmarks.

The channel width for the three plate fuels are as follows:

- MURR: 0.088-in
- MITR-II: 0.094-in
- ATR: 0.085-in

The channel width for all three plate type fuels exceeds the maximum channel width of 0.078-in of the benchmark experiments. However, this parameter is only slightly larger than the maximum benchmark experiment channel width, and was maximized in order to maximize model reactivity. Extrapolation of the USL equation ($0.9218 - 1.1029E-02 * X$) to the maximum channel width of 0.094-in yields a USL of 0.9208, which is essentially identical to the non-extrapolated value of 0.9209. Therefore, application of the non-extrapolated USL (0.9209) to the criticality models is considered acceptable.

H/U-235 Atom Ratio

The H/U-235 atom ratio is used as the fourth trending parameter for the benchmark cases. The H/U-235 atom ratio is defined here as the ratio of hydrogen atoms to U-235 atoms in a unit cell. This parameter is computed by the following equation:

$$NH * C / (NU235 * M)$$

where,

NH is the hydrogen number density

C is the channel width

NU235 is the U-235 number density

M is the fuel meat width

Over the range of applicability, the minimum USL is 0.9257 for the full benchmark set, and 0.9209 for the subset of directly applicable benchmarks.

- MURR: The H/U-235 value may be computed as:
 $6.687E-02 * 0.088 / (3.6519E-03 * 0.02) = 80.6$

BRR Package Safety Analysis Report

Therefore, H/U-235 of the MURR models is acceptably within the range of applicability of the benchmarks.

- MITR-II: The H/U-235 atom ratio may be computed as:

$$6.687\text{E-}02 * 0.094 / (3.6835\text{E-}03 * 0.03) = 56.9$$

The minimum H/U-235 atom ratio of the benchmark models is 65.1. Therefore, this parameter is slightly outside the range of the benchmark experiments for the MITR-II fuel, although the difference is so small that this parameter is considered to be acceptable.

- ATR: Using the maximum ATR plate U-235 number density, the H/U-235 value may be computed as:

$$6.687\text{E-}02 * 0.085 / (4.224\text{E-}03 * 0.02) = 67.3$$

Therefore, H/U-235 of the ATR models is acceptably within the range of applicability of the benchmarks.

Pitch

The fuel plate pitch is used as the fifth trending parameter for the benchmark cases. Over the range of applicability, the minimum USL is 0.9225 for the full benchmark set, and 0.9209 for the subset of directly applicable benchmarks.

- MURR: The fuel plate pitch is fixed at 0.13-in for all fuel element models. This pitch falls within the range of the benchmark experiments.
- MITR-II: The fuel plate pitch is fixed at 0.16-in for all fuel element models. The maximum pitch of the benchmark models is 0.128-in, so the pitch in the models exceeds the range of the benchmarks. However, the pitch is directly related to system moderation, and the acceptability of the EALF indicator demonstrates that MCNP is performing acceptably for thermal conditions. Therefore, this parameter is considered to be acceptable.
- ATR: The fuel plate pitch is fixed at 0.128-in for all ATR models (excluding the pitch for plates 1 and 19, which is slightly bigger because these plates are thicker). This pitch falls within the range of the benchmark experiments.

Recommended USL

For the full benchmark set, the minimum USL is 0.9225, while for the subset of directly applicable benchmarks, the USL is 0.9209. Therefore, the USL is trending lower for the subset of directly applicable benchmarks. Note, however, that the average $k_{\text{eff}} = 0.992$ for both the full benchmark set and directly applicable subset. The USL could likely be improved by development of additional benchmark models, but given the large margins to the most reactive case, the lower value (0.9209) is conservatively selected as the USL for this analysis.

6.8.2.2 TRIGA Fuel

Three trending parameters are selected for the TRIGA fuel: (1) Energy of the Average neutron Lethargy causing Fission (EALF), (2) U-235 number density, and (3) ratio of the number of hydrogen atoms to U-235 atoms in the fuel matrix (H/U-235).

BRR Package Safety Analysis Report

The USL generated for each of the trending parameters utilized is provided in Table 6.8-3. All benchmark data used as input to USLSTATS are reported in Table 6.8-5.

Energy of the Average neutron Lethargy causing Fission (EALF)

The EALF is used as the first trending parameter for the benchmark cases. The EALF comparison provides a means to observe neutron spectral dependencies or trends. Over the range of applicability, the minimum USL is 0.9301 for the subset consisting of 10 HEU solution benchmarks and 2 TRIGA benchmarks.

All HAC TRIGA models fall within the range of applicability for this parameter, including the most reactive TRIGA case (Case D63). None of the NCT TRIGA models fall within the range of applicability, although this behavior is expected, because the NCT cases are unmoderated (except for the hydrogen in the fuel matrix). Also, because the NCT cases are much lower in reactivity than the HAC cases, this parameter is considered to be acceptable.

U-235 Number Density

The U-235 number density is used as the second trending parameter for the benchmark cases. Over the range of applicability, the minimum USL is 0.9306 for the subset consisting of 10 HEU solution benchmarks and 2 TRIGA benchmarks.

The U-235 number density in the BRR TRIGA models is $9.0406\text{E-}04$ atom/b-cm, which is only slightly outside the maximum range of applicability of the benchmark models (EALF = $8.5392\text{E-}04$ atom/b-cm). Therefore, this parameter is considered acceptable.

H/U-235 Atom Ratio

The H/U-235 atom ratio is used as the third trending parameter for the benchmark cases. Over the range of applicability, the minimum USL is 0.9318 for the subset consisting of 10 HEU solution benchmarks and 2 TRIGA benchmarks. The H/U-235 atom ratio is 62.0, which is only slightly outside the minimum range of applicability of the benchmark models (H/U-235 = 68.2). Therefore, this parameter is considered acceptable.

Recommended USL

The minimum USL of 0.9301 occurs for the EALF parameter over the subset of HEU solution and TRIGA benchmarks. Because the USL for the aluminum plate fuel is lower (0.9209), and only two TRIGA benchmarks are available, the USL of 0.9209 is recommended for use in the TRIGA analysis to add additional margin.

Table 6.8-1 – Benchmark Experiments Utilized

Series	Title
Aluminum Plate Fuel (MURR, MITR-II, ATR)	
HEU-COMP-THERM-022	SPERT III Stainless-Steel-Clad Plate-Type Fuel in Water
HEU-MET-THERM-006	SPERT-D Aluminum-Clad Plate-Type Fuel in Water, Dilute Uranyl Nitrate, or Borated Uranyl Nitrate
HEU-MET-THERM-022	Advanced Test Reactor: Serpentine Arrangement of Highly Enriched Water-Moderated Uranium-Aluminide Fuel Plates Reflected by Beryllium
TRIGA Fuel	
IEU-COMP-THERM-003	TRIGA Mark II Reactor: U(20) – Zirconium Hydride Fuel Rods in Water with Graphite Reflector
HEU-SOL-THERM-001	Minimally Reflected Cylinders of Highly Enriched Solutions of Uranyl Nitrate
LEU-SOL-THERM-003	Full and Truncated Bare Spheres of 10% Enriched Uranyl Nitrate Water Solutions

Table 6.8-2 – USL Results for Aluminum Plate Fuel

Trending Parameter (X)	Minimum USL Over Range of Applicability	Range of Applicability
35 Experiment Set		
EALF (MeV)	0.9254	5.22210E-08 <= X <= 1.58510E-07
U-235 Number Density (atom/b-cm)	0.9240	1.84900E-03 <= X <= 3.92600E-03
Channel width (in)	0.9225	6.45700E-02 <= X <= 7.80000E-02
H/U-235	0.9257	65.100 <= X <= 116.50
Pitch (in)	0.9225	0.12457 <= X <= 0.12800
17 Experiment Set		
EALF (MeV)	0.9212	5.22210E-08 <= X <= 1.58510E-07
U-235 Number Density (atom/b-cm)	0.9209	1.84900E-03 <= X <= 3.92600E-03
Channel width (in)	0.9209	6.45700E-02 <= X <= 7.80000E-02
H/U-235	0.9209	66.0 <= X <= 116.50
Pitch (in)	0.9209	0.12457 <= X <= 0.12800

Table 6.8-3 – USL Results for TRIGA Fuel

Trending Parameter (X)	Minimum USL Over Range of Applicability	Range of Applicability
21 Experiment Set		
EALF (MeV)	0.9320	$3.42760E-08 \leq X \leq 2.95740E-07$
U-235 Number Density (atom/b-cm)	0.9331	$4.33640E-05 \leq X \leq 8.53920E-04$
H/U-235	0.9350	$68.200 \leq X \leq 1437.5$
12 Experiment Set (HEU solution + TRIGA)		
EALF (MeV)	0.9301	$4.29310E-08 \leq X \leq 2.95740E-07$
U-235 Number Density (atom/b-cm)	0.9306	$1.31030E-04 \leq X \leq 8.53920E-04$
H/U-235	0.9318	$68.200 \leq X \leq 499.40$
11 Experiment Set (LEU solution + TRIGA)		
EALF (MeV)	0.9338	$3.42760E-08 \leq X \leq 8.71200E-08$
U-235 Number Density (atom/b-cm)	0.9339	$4.33640E-05 \leq X \leq 3.68010E-04$
H/U-235	0.9340	$150.10 \leq X \leq 1437.5$

Table 6.8-4 – Benchmark Experiment Data for Aluminum Plate Fuel

Case ID	Filename	k	σ_{mcnp}	σ_{bench}	σ_{total}	EALF (MeV)	U-235 (atom/b-cm)	Chanel Width (in)	H/U-235	Pitch (in)
BA1	HCT022_C01	0.98895	0.00060	0.0081	0.0081	9.528E-08	3.3155E-03	0.06457	65.1	0.12457
BA2	HCT022_C02	0.98980	0.00061	0.0081	0.0081	9.665E-08	3.3155E-03	0.06457	65.1	0.12457
BA3	HCT022_C03	0.98985	0.00063	0.0081	0.0081	9.809E-08	3.3155E-03	0.06457	65.1	0.12457
BA4	HCT022_C04	0.98856	0.00060	0.0081	0.0081	9.917E-08	3.3155E-03	0.06457	65.1	0.12457
BA5	HCT022_C05	0.98909	0.00063	0.0081	0.0081	9.587E-08	3.3155E-03	0.06457	65.1	0.12457
BA6	HCT022_C06	0.98902	0.00059	0.0081	0.0081	9.840E-08	3.3155E-03	0.06457	65.1	0.12457
BA7	HCT022_C07	0.98963	0.00056	0.0081	0.0081	9.890E-08	3.3155E-03	0.06457	65.1	0.12457
BA8	HCT022_C08	0.98908	0.00057	0.0081	0.0081	9.951E-08	3.3155E-03	0.06457	65.1	0.12457
BA9	HCT022_C09	0.98840	0.00056	0.0081	0.0081	9.589E-08	3.3155E-03	0.06457	65.1	0.12457
BA10	HCT022_C10	0.98845	0.00060	0.0081	0.0081	9.963E-08	3.3155E-03	0.06457	65.1	0.12457
BA11	HCT022_C11	0.98930	0.00060	0.0081	0.0081	1.001E-07	3.3155E-03	0.06457	65.1	0.12457
BA12	HMT006_C01	0.99240	0.00082	0.0044	0.0045	8.481E-08	1.8490E-03	0.06457	116.5	0.12457
BA13	HMT006_C02	0.99331	0.00088	0.0040	0.0041	7.044E-08	1.8490E-03	0.06457	116.5	0.12457
BA14	HMT006_C03	0.99740	0.00072	0.0040	0.0041	6.338E-08	1.8490E-03	0.06457	116.5	0.12457
BA15	HMT006_C04	0.99282	0.00081	0.0040	0.0041	6.185E-08	1.8490E-03	0.06457	116.5	0.12457
BA16	HMT006_C05	0.99230	0.00079	0.0040	0.0041	5.852E-08	1.8490E-03	0.06457	116.5	0.12457
BA17	HMT006_C06	0.99010	0.00071	0.0040	0.0041	5.615E-08	1.8490E-03	0.06457	116.5	0.12457
BA18	HMT006_C07	0.98783	0.00073	0.0040	0.0041	5.432E-08	1.8490E-03	0.06457	116.5	0.12457
BA19	HMT006_C08	0.98428	0.00076	0.0040	0.0041	5.245E-08	1.8490E-03	0.06457	116.5	0.12457
BA20	HMT006_C09	0.98657	0.00072	0.0040	0.0041	5.222E-08	1.8490E-03	0.06457	116.5	0.12457
BA21	HMT006_C10	0.99885	0.00085	0.0040	0.0041	8.220E-08	1.8490E-03	0.06457	116.5	0.12457
BA22	HMT006_C11	0.98965	0.00081	0.0040	0.0041	6.236E-08	1.8490E-03	0.06457	116.5	0.12457
BA23	HMT006_C12	0.99403	0.00070	0.0040	0.0041	5.415E-08	1.8490E-03	0.06457	116.5	0.12457

(continued)

Table 6.8-4 – Benchmark Experiment Data for Aluminum Plate Fuel (concluded)

Case ID	Filename	k	σ_{mcnp}	σ_{bench}	σ_{total}	EALF (MeV)	U-235 (atom/b-cm)	Chanel Width (in)	H/U-235	Pitch (in)
BA24	HMT006_C13	1.01283	0.00086	0.0040	0.0041	8.231E-08	1.8490E-03	0.06457	116.5	0.12457
BA25	HMT006_C14	0.98495	0.00071	0.0061	0.0061	5.715E-08	1.8490E-03	0.06457	116.5	0.12457
BA26	HMT006_C15	0.98128	0.00077	0.0040	0.0041	5.654E-08	1.8490E-03	0.06457	116.5	0.12457
BA27	HMT006_C16	0.99241	0.00078	0.0040	0.0041	6.330E-08	1.8490E-03	0.06457	116.5	0.12457
BA28	HMT006_C17	0.98934	0.00082	0.0040	0.0041	7.405E-08	1.8490E-03	0.06457	116.5	0.12457
BA29	HMT006_C18	0.99282	0.00087	0.0040	0.0041	8.003E-08	1.8490E-03	0.06457	116.5	0.12457
BA30	HMT006_C19	0.99360	0.00068	0.0040	0.0041	5.243E-08	1.8490E-03	0.06457	113.9	0.12457
BA31	HMT006_C20	0.99275	0.00076	0.0040	0.0041	6.471E-08	1.8490E-03	0.06457	113.7	0.12457
BA32	HMT006_C21	0.99469	0.00077	0.0040	0.0041	6.917E-08	1.8490E-03	0.06457	113.7	0.12457
BA33	HMT006_C22	0.99670	0.00080	0.0040	0.0041	7.407E-08	1.8490E-03	0.06457	113.6	0.12457
BA34	HMT006_C23	1.00132	0.00080	0.0040	0.0041	7.670E-08	1.8490E-03	0.06457	113.5	0.12457
BA35	HMT022_C01	0.99179	0.00013	0.0035	0.0035	1.585E-07	3.9260E-03	0.078	66.0	0.12800

Table 6.8-5 – Benchmark Experiment Data for TRIGA Fuel

Case ID	Filename	k	σ_{mcnp}	σ_{bench}	σ_{total}	EALF (MeV)	U-235 (atom/b-cm)	H/U-235
BT1	HST001_C01	0.99686	0.00068	0.0060	0.0060	8.147E-08	3.4777E-04	181.8
BT2	HST001_C02	0.99418	0.00072	0.0072	0.0072	2.763E-07	8.2771E-04	70.6
BT3	HST001_C03	1.00015	0.00067	0.0035	0.0036	8.014E-08	3.4118E-04	185.7
BT4	HST001_C04	0.99470	0.00069	0.0053	0.0053	2.957E-07	8.5392E-04	68.2
BT5	HST001_C05	0.99727	0.00059	0.0049	0.0049	4.293E-08	1.3103E-04	499.4
BT6	HST001_C06	1.00351	0.00057	0.0046	0.0046	4.450E-08	1.4240E-04	458.8
BT7	HST001_C07	0.99609	0.00071	0.0040	0.0041	7.710E-08	3.2800E-04	193.3
BT8	HST001_C08	0.99648	0.00067	0.0038	0.0039	8.174E-08	3.4777E-04	181.8
BT9	HST001_C09	0.99068	0.00068	0.0054	0.0054	2.954E-07	8.5392E-04	68.2
BT10	HST001_C10	0.99130	0.00055	0.0054	0.0054	4.609E-08	1.5266E-04	427.4
BT11	ICT003_C01	0.99699	0.00052	0.0056	0.0056	8.712E-08	3.6801E-04	150.1
BT12	ICT003_C02	1.00145	0.00052	0.0056	0.0056	8.678E-08	3.6801E-04	150.1
BT13	LST003_C01	0.99485	0.00044	0.0039	0.0039	4.098E-08	7.6403E-05	770.3
BT14	LST003_C02	0.99401	0.00042	0.0042	0.0042	3.921E-08	6.8143E-05	877.6
BT15	LST003_C03	0.99902	0.00041	0.0042	0.0042	3.886E-08	6.7111E-05	897.0
BT16	LST003_C04	0.99249	0.00039	0.0042	0.0042	3.875E-08	6.5820E-05	913.2
BT17	LST003_C05	0.99573	0.00035	0.0048	0.0048	3.593E-08	5.2398E-05	1173.4
BT18	LST003_C06	0.99694	0.00031	0.0049	0.0049	3.564E-08	5.0849E-05	1213.1
BT19	LST003_C07	0.99602	0.00031	0.0049	0.0049	3.554E-08	4.9817E-05	1239.8
BT20	LST003_C08	0.99930	0.00028	0.0052	0.0052	3.447E-08	4.4138E-05	1411.6
BT21	LST003_C09	0.99606	0.00027	0.0052	0.0052	3.428E-08	4.3364E-05	1437.5

6.9 Appendices

6.9.1 References

1. MCNP5, “MCNP – A General Monte Carlo N-Particle Transport Code, Version 5; Volume II: User’s Guide,” LA-CP-03-0245, Los Alamos National Laboratory, April 2003. MCNP5 is distributed by the Radiation Safety Information Computational Center (www-rsicc.ornl.gov), Release C00710MNYCP02 (Windows PC).
2. USLSTATS, “USLSTATS: A Utility To Calculate Upper Subcritical Limits For Criticality Safety Applications,” Version 1.4.2, Oak Ridge National Laboratory, April 23, 2003. Note: USLSTATS is described in Appendix C, *User’s Manual for USLSTATS V1.0*, in NUREG/CR-6361 *Criticality Benchmark Guide for Light-Water-Reactor Fuel in Transportation and Storage Packages*, March 1997. No new user’s manual has been developed for later updates to the program.
3. *International Handbook of Evaluated Criticality Safety Benchmark Experiments*, Nuclear Energy Agency, NEA/NSC/DOC(95)03, September 2006.
4. *Standard Composition Library*, ORNL/TM-2005/39, Version 5, Vol. III, Section M8, April 2005.

6.9.2 Parametric Evaluations to Determine the Most Reactive Fuel Geometries

6.9.2.1 ATR Fuel Parametric Evaluation

A parametric analysis is performed to determine the impacts of various fuel element tolerances on the reactivity. This parametric analysis considers the effects of a number of parameters, such as fuel meat arc length, fuel meat thickness, channel width, and active fuel length.

Because the ATR fuel element is complex, with 19 unique fuel plates and 19 unique fuel material descriptions, performing this parametric study on the actual fuel element geometry would be cumbersome. Rather, the approach utilized is to perform the parametric study on a system of 19 identical flat plates. This geometry mimics the ATR fuel element to determine trends in the data. Note that the reactivity of the 19 flat plate model is not identical to the reactivity of an actual ATR fuel element due to geometrical and material differences, although the trends are the same. The most reactive model variations are then incorporated into the ATR fuel element model.

In the parametric models, 1200 g U-235 is equally distributed between 19 identical flat plates. The base configuration consists of plates with a fuel meat width of 6.7355 cm (the average meat arc length for an ATR fuel element), active fuel height of 48-in, fuel meat thickness of 0.02-in, fuel cladding thickness of 0.015-in (total plate thickness of 0.050-in), and fuel channel thickness of 0.078-in. A total of 12 parametric models are developed, as summarized below.

Case ID	ATR Parametric Study Case Description
P1	Base case
P2	Increase width of fuel meat by 0.1-in
P3	Decrease width of fuel meat by 0.1-in
P4	Increase thickness of fuel meat by 0.002-in
P5	Decrease thickness of fuel meat by 0.002-in
P6	Increase thickness of fuel meat by 0.002-in but decrease the cladding thickness to maintain a nominal plate thickness
P7	Decrease thickness of fuel meat by 0.002-in but increase the cladding thickness to maintain a nominal plate thickness
P8	Increase water channel thickness to maximum of 0.085-in
P9	Increase water channel thickness to maximum of 0.085-in by reducing the cladding thickness
P10	Decrease active fuel length to 47.0-in
P11	Reduce cladding thickness to the minimum value of 0.008-in
P12	Combine cases P2 and P9

The geometry of Case P1 is shown in Figure 6.9-1. The fuel element is reflected by approximately 12-in of water.

In Cases P2 through P12, each case is identical to the base case P1 with the exception of the changes identified in the table above. The pitch, which is the sum of the plate thickness and channel thickness, is treated as a dependant variable and is allowed to vary as the independent parameters are changed. For example, in Case P5, decreasing the thickness of the fuel meat decreases the pitch, although the channel thickness remains constant. The detailed model description of the parametric cases is summarized in Table 6.9-1.

The results of the parametric analysis are summarized in Table 6.9-2. Because the uncertainty in the calculation is ~ 0.001 , a difference of at least 0.002 (2 milli-k, abbreviated mk) between the various cases is required in order to distinguish a real effect from statistical fluctuation. The results indicate a reactivity increase of 4.3 mk for Case P2, when the width of the fuel meat is increased, and a decrease of 5.4 mk for Case P3, when the width of the fuel meat is decreased. Therefore, reactivity increases when the width of the fuel meat is maximized.

The nominal thickness of the fuel meat is 0.02-in. No tolerance on the fuel meat is provided on the fuel fabrication drawings because the fuel plates are fabricated using a rolling process. A thickness tolerance of 0.002-in ($\pm 10\%$) is assumed for computational purposes. In Cases P4 and P5, the fuel meat thickness is adjusted for constant channel thickness and variable pitch, while for Cases P6 and P7 the fuel meat thickness is adjusted for constant plate thickness and nominal pitch. The reactivity fluctuations are within 2 mk in all four cases, and it is concluded that a nominal fuel meat thickness of 0.02-in is acceptable for modeling purposes.

BRR Package Safety Analysis Report

In Case P8, the water channel thickness is increased to the maximum value of 0.085-in (increase in pitch), while in Case P9 the water channel thickness is increased to the maximum by artificially reducing the cladding thickness (nominal pitch). Both cases P8 and P9 show large reactivity gains of 9.6 and 12.9 mk, respectively, indicating that reactivity is maximized when the water channel thickness is maximized.

In Case P10, the active fuel length is reduced to a lower bound value of 47.0-in. The reactivity increase is within statistical fluctuation. It may be inferred that increasing the active fuel length would also result in a reactivity effect within statistical fluctuation.

In Case P11, the cladding thickness is reduced to the minimum value of 0.008-in, and the reactivity increases by 5.5 mk. This reactivity gain is likely due to the more compact geometry, as the pitch reduces considerably. This scenario is not directly applicable to an ATR fuel element because the pitch is fixed by the side plates and such a configuration is not possible.

The only cases that show a statistically significant increase are P2, P8, P9, and P11. In Case P12, the increased fuel meat width of Case P2 and increased channel width of Case P9 are combined. This model geometry bounds Case P8, and Case P11 is incorporated in an approximate manner because the cladding thickness has been reduced to accommodate the larger channel. The reactivity of Case P12 represents an increase of 19.5 mk over base Case P1.

Based on the parametric evaluation, an optimized fuel model is developed with both increased channel width and increased meat arc length. In this model, a nominal pitch is utilized (i.e., the centerline radial locations of the 19 plates are the same in each model, as indicated in Table 6.2-4), and the channel width is increased by removing cladding. This approach is highly conservative, because it is unlikely (if not impossible) to maximize the channel width between each plate. In an actual fuel element, maximizing the channel width between two plates would likely minimize the channel width between the next two plates, as the overall plate thickness is held to a rather tight tolerance.

6.9.2.2 MURR Fuel Parametric Evaluation

A parametric analysis is performed to determine the impacts of various fuel element tolerances on the reactivity. In the parametric analysis for ATR fuel, it is determined that reactivity is maximized by maximizing the arc length of the fuel meat and the channel thickness. Because ATR and MURR are both plate-type and utilize similar enrichments, it is expected that MURR fuel will also experience maximum reactivity with these parameters maximized. Therefore, the parametric analysis considers the effects of only the following parameters: fuel meat arc length/width, channel width, and active fuel length.

The base configuration for MURR consists of plates with a nominal meat arc length/width, nominal active fuel length, and nominal channel width. In each parametric case, the indicated parameter is modified in comparison with the base case. The minimum, nominal, and maximum meat arc lengths are provided in Table 6.9-3. The minimum meat arc lengths are obtained directly from Figure 6.2-2 (see dimension B). The maximum meat arc lengths are computed by subtracting twice the fuel-free width (2×0.115 -in) from the maximized plate width (dimension C of Figure 6.2-2 + 0.010-in). The nominal value is computed as the average of the minimum and maximum values. The detailed model description of the parametric cases is summarized in Table 6.9-4. A total of 7 parametric models are developed, as summarized below.

Case ID	MURR Parametric Study Case Description
PM1	Base MURR case
PM2	Decrease active fuel length to minimum value
PM3	Increase active fuel length to maximum value
PM4	Increase channel width to maximum value
PM5	Decrease width of fuel meat to minimum value
PM6	Increase width of fuel meat to maximum value
PM7	Combine cases PM4 and PM6

The geometry of base MURR parametric Case PM1 is shown in Figure 6.9-1. The fuel element is reflected with approximately 12-in of water. Note that, unlike the ATR parametric model, the MURR parametric model is an explicit geometrical representation of the MURR fuel element. Although the ATR and MURR fuel elements appear to be rather similar, because all MURR plates utilize the same fuel number densities and fuel meat to side structure distance, performing the parametric study on the actual geometry for MURR fuel is relatively straightforward.

The results of the parametric analysis are summarized in Table 6.9-5. Because the uncertainty in the calculation is ~ 0.001 , a difference of at least 0.002 (2 milli-k, abbreviated mk) between the various cases is required in order to distinguish a real effect from statistical fluctuation. The variation of the active fuel length has a negligible effect on the results. Also, the fuel shows a positive reactivity increase of 23.8 mk when the fuel meat is widened and the channel width is increased (compare Case PM7 with Case PM1). This result is consistent with the results obtained in the ATR fuel parametric analysis. Therefore, in all MURR fuel models, the fuel is modeled with nominal active fuel length, maximum fuel width, and maximum channel width. The maximum channel width is achieved by artificially reducing the cladding thickness.

6.9.2.3 MITR-II Fuel Parametric Evaluation

A parametric analysis is performed to determine the impacts of various fuel element tolerances on the reactivity. In the parametric analysis for ATR and MURR fuel, it is determined that reactivity is maximized by maximizing the arc length of the fuel meat and the channel thickness. Because ATR, MURR, and MITR-II are all plate-type and utilize similar enrichments, it is expected that MITR-II fuel will also experience maximum reactivity with these parameters maximized. Therefore, the parametric analysis considers the effects of only the following parameters: fuel meat arc length/width, channel width, and active fuel length.

The base configuration for MITR-II consists of plates with a nominal meat arc length/width, nominal active fuel length, and nominal channel width. In each parametric case, the indicated parameter is modified in comparison with the base case. The detailed model description of the parametric cases is summarized in Table 6.9-6. A total of 7 parametric models are developed, as summarized below.

Case ID	MITR-II Parametric Study Case Description
PN1	Base MITR-II case
PN2	Decrease active fuel length to minimum value
PN3	Increase active fuel length to maximum value
PN4	Increase channel width to maximum value
PN5	Decrease width of fuel meat to minimum value
PN6	Increase width of fuel meat to maximum value
PN7	Combine cases PN4 and PN6

The geometry of base MITR-II parametric Case PN1 is shown in Figure 6.9-1. The fuel element is reflected with approximately 12-in of water. Note that, like the MURR parametric model, the MITR-II parametric model is an explicit geometrical representation of the MITR-II fuel element.

The results of the parametric analysis are summarized in Table 6.9-7. Because the uncertainty in the calculation is ~ 0.001 , a difference of at least 0.002 (2 milli-k, abbreviated mk) between the various cases is required in order to distinguish a real effect from statistical fluctuation. The variation of the active fuel length has a negligible effect on the results. Although Case PN2 shows a positive reactivity increase when the active fuel height is reduced, because the increase is less than 2 mk, it is concluded that the increase is simply statistical fluctuation. Also, the fuel shows a positive reactivity increase of 11.0 mk when the fuel meat is widened and the channel width is increased (compare Case PN7 with Case PN1). This result is consistent with the results obtained in the ATR and MURR fuel parametric analyses. Therefore, in all MITR-II fuel models, the fuel is modeled with nominal active fuel length, maximum fuel width, and maximum channel width. The maximum channel width is achieved by artificially reducing the cladding thickness.

6.9.2.4 TRIGA Fuel Parametric Evaluation

For the TRIGA fuels, the objective of the parametric analysis is to select the most reactive fuel type for use in the criticality analysis from the five types under consideration. To select the bounding fuel element type, simple moderated pin cell models with infinite square reflection are developed. The lattice pitch is varied for each model by adjusting the location of the reflective surfaces. The pin cell model for each of the fuel element types is shown in Figure 6.9-2. The pin cell models are based upon the data provided in Table 6.2-7. Note that the Type 203 fuel element is not modeled explicitly, since it is essentially the same as Type 103.

The pin cell results are summarized in Table 6.9-8. The most reactive TRIGA fuel type is Type 109 (Case PT20), which is the HEU fuel element. In these cases, the thin molybdenum disc between the fuel and bottom reflector is omitted. In Case PT23, Case PT20 is run with the molybdenum disc modeled explicitly. The reactivity is slightly less, but within the statistical uncertainty of the method. Therefore, this fuel type (without the molybdenum disc) is used for all TRIGA analysis in this calculation.

Table 6.9-1 – ATR Parametric Analysis Input Data

Parameter	P1	P2	P3	P4	P5	P6
Fuel Arc (cm)	6.7355	6.9895	6.4815	6.7355	6.7355	6.7355
Meat thickness (in)	0.02	0.02	0.02	0.022	0.018	0.022
Active fuel height (in)	48	48	48	48	48	48
Channel (in)	0.078	0.078	0.078	0.078	0.078	0.078
Cladding (in)	0.015	0.015	0.015	0.015	0.015	0.014
Total plate (in)	0.050	0.050	0.050	0.052	0.048	0.050
Pitch (in)	0.128	0.128	0.128	0.130	0.126	0.128
Volume (cm ³)	41.7164	43.2895	40.1432	45.8880	37.5447	45.8880
U-235 (g)	63.2	63.2	63.2	63.2	63.2	63.2
U-235 density (g/cm ³)	1.51	1.46	1.57	1.38	1.68	1.38
UAlx+Al density (g/cm ³)	3.86	3.81	3.91	3.74	4.00	3.74
N U-234	2.4865E-05	2.3962E-05	2.5840E-05	2.2605E-05	2.7628E-05	2.2605E-05
N U-235	3.8789E-03	3.7380E-03	4.0309E-03	3.5263E-03	4.3099E-03	3.5263E-03
N U-236	1.4382E-05	1.3859E-05	1.4945E-05	1.3074E-05	1.5980E-05	1.3074E-05
N U-238	2.0576E-04	1.9828E-04	2.1382E-04	1.8705E-04	2.2862E-04	1.8705E-04
N U-Al	5.0157E-02	5.0391E-02	4.9905E-02	5.0742E-02	4.9442E-02	5.0742E-02
Total	5.4281E-02	5.4365E-02	5.4190E-02	5.4491E-02	5.4024E-02	5.4491E-02

Parameter	P7	P8	P9	P10	P11	P12
Fuel Arc (cm)	6.7355	6.7355	6.7355	6.7355	6.7355	6.9895
Meat thickness (in)	0.018	0.02	0.02	0.02	0.02	0.02
Active fuel height (in)	48	48	48	47	48	48
Channel (in)	0.078	0.085	0.085	0.078	0.078	0.085
Cladding (in)	0.016	0.015	0.0115	0.015	0.008	0.0115
Total plate (in)	0.050	0.050	0.0430	0.050	0.036	0.0430
Pitch (in)	0.128	0.135	0.128	0.128	0.114	0.128
Volume (cm ³)	37.5447	41.7164	41.7164	40.8473	41.7164	43.2895
U-235 (g)	63.2	63.2	63.2	63.2	63.2	63.2
U-235 density (g/cm ³)	1.68	1.51	1.51	1.55	1.51	1.46
UAlx+Al density (g/cm ³)	4.00	3.86	3.86	3.89	3.86	3.81
N U-234	2.7628E-05	2.4865E-05	2.4865E-05	2.5394E-05	2.4865E-05	2.3962E-05
N U-235	4.3099E-03	3.8789E-03	3.8789E-03	3.9615E-03	3.8789E-03	3.7380E-03
N U-236	1.5980E-05	1.4382E-05	1.4382E-05	1.4688E-05	1.4382E-05	1.3859E-05
N U-238	2.2862E-04	2.0576E-04	2.0576E-04	2.1014E-04	2.0576E-04	1.9828E-04
N U-Al	4.9442E-02	5.0157E-02	5.0157E-02	5.0020E-02	5.0157E-02	5.0391E-02
Total	5.4024E-02	5.4281E-02	5.4281E-02	5.4232E-02	5.4281E-02	5.4365E-02

Table 6.9-2 – ATR Parametric Analysis Results

Case ID	Filename	k_{eff}	σ	k_s (k+2σ)	Δ from P1 (mk)
P1	HS_ATR_P1	0.46601	0.00096	0.46793	--
P2	HS_ATR_P2	0.47015	0.00102	0.47219	4.3
P3	HS_ATR_P3	0.46045	0.00102	0.46249	-5.4
P4	HS_ATR_P4	0.46403	0.00101	0.46605	-1.9
P5	HS_ATR_P5	0.46442	0.00111	0.46664	-1.3
P6	HS_ATR_P6	0.46753	0.00105	0.46963	1.7
P7	HS_ATR_P7	0.46683	0.00101	0.46885	0.9
P8	HS_ATR_P8	0.47528	0.00112	0.47752	9.6
P9	HS_ATR_P9	0.47879	0.00100	0.48079	12.9
P10	HS_ATR_P10	0.46704	0.00106	0.46916	1.2
P11	HS_ATR_P11	0.47123	0.00108	0.47339	5.5
P12	HS_ATR_P12	0.48534	0.00104	0.48742	19.5

Table 6.9-3 – MURR Meat Arc Lengths

Plate	Minimum (in)	Nominal (in)	Maximum (in)
1	1.643	1.708	1.773
2	1.745	1.810	1.875
3	1.847	1.912	1.977
4	1.950	2.015	2.080
5	2.052	2.117	2.182
6	2.154	2.219	2.284
7	2.256	2.321	2.386
8	2.358	2.423	2.488
9	2.460	2.525	2.590
10	2.562	2.627	2.692
11	2.664	2.729	2.794
12	2.766	2.831	2.896
13	2.868	2.933	2.998
14	2.971	3.036	3.101
15	3.073	3.138	3.203
16	3.175	3.240	3.305
17	3.277	3.342	3.407
18	3.379	3.444	3.509
19	3.481	3.546	3.611
20	3.583	3.648	3.713
21	3.685	3.750	3.815
22	3.787	3.852	3.917
23	3.889	3.954	4.019
24	3.992	4.057	4.122

Table 6.9-4 – MURR Parametric Analysis Input Data

Parameter	PM1/PM4	PM2	PM3	PM5	PM6/PM7
Fuel width (in)	nominal	nominal	nominal	nominal-0.065	nominal+0.065
Meat thickness (in)	0.02	0.02	0.02	0.02	0.02
Active fuel height (in)	24	23.25	24.75	24	24
Channel (in)	0.08/0.088	0.08	0.08	0.08	0.08/0.088
Cladding (in)	0.015/0.011	0.015	0.015	0.015	0.015/0.011
Total plate (in)	0.050/0.042	0.050	0.050	0.050	0.050/0.042
Pitch (in)	0.13	0.13	0.13	0.13	0.13
Meat volume (cm ³)	544.13	527.13	561.14	531.86	556.40
U-235 mass (g)	785	785	785	785	785
U-235 den (g/cm ³)	1.44	1.49	1.40	1.48	1.41
UAlx+Al den (g/cm ³)	3.80	3.84	3.76	3.82	3.77
N-234 (atom/b-cm)	2.3694E-05	2.4458E-05	2.2976E-05	2.4241E-05	2.3171E-05
N-235 (atom/b-cm)	3.6962E-03	3.8154E-03	3.5842E-03	3.7815E-03	3.6147E-03
N-236 (atom/b-cm)	1.3704E-05	1.4146E-05	1.3289E-05	1.4020E-05	1.3402E-05
N-238 (atom/b-cm)	1.9607E-04	2.0239E-04	1.9012E-04	2.0059E-04	1.9174E-04
N-Al (atom/b-cm)	5.0460E-02	5.0262E-02	5.0646E-02	5.0319E-02	5.0596E-02
Total (atom/b-cm)	5.4390E-02	5.4319E-02	5.4457E-02	5.4339E-02	5.4439E-02

Table 6.9-5 – MURR Parametric Analysis Results

Case ID	Filename	k_{eff}	σ	k_s ($k+2\sigma$)	Δ from PM1 (mk)
PM1	HS_MURR3_P1	0.50645	0.00110	0.50865	--
PM2	HS_MURR3_P2	0.50715	0.00099	0.50913	0.5
PM3	HS_MURR3_P3	0.50612	0.00109	0.50830	-0.3
PM4	HS_MURR3_P4	0.52638	0.00103	0.52844	19.8
PM5	HS_MURR3_P5	0.50314	0.00099	0.50512	-3.5
PM6	HS_MURR3_P6	0.50980	0.00106	0.51192	3.3
PM7	HS_MURR3_P7	0.53021	0.00114	0.53249	23.8

Table 6.9-6 – MITR-II Parametric Analysis Input Data

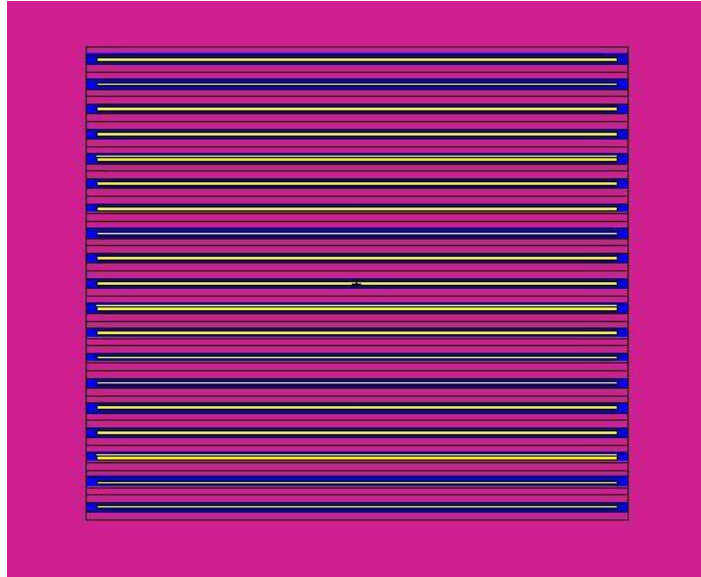
Parameter	PN1/PN4	PN2	PN3	PN5	PN6/PN7
Fuel width (in)	2.076	2.076	2.076	1.981	2.171
Meat thickness (in)	0.03	0.03	0.03	0.03	0.03
Active fuel height (in)	22.375	21.99	22.76	22.375	22.375
Channel (in)	0.090/0.094	0.090	0.090	0.090	0.090/0.094
Cladding (in)	0.019/0.017	0.019	0.019	0.019	0.019/0.017
Total plate (in)	0.068/0.064	0.068	0.068	0.068	0.068/0.064
Pitch (in)	0.158	0.158	0.158	0.158	0.158
Meat volume (cm ³)	342.53	336.64	348.43	326.86	358.21
U-235 mass (g)	515	515	515	515	515
U-235 den (g/cm ³)	1.503	1.530	1.478	1.576	1.438
UAlx+Al den (g/cm ³)	3.85	3.87	3.83	3.91	3.79
N-234 (atom/b-cm)	2.4693E-05	2.5125E-05	2.4275E-05	2.5877E-05	2.3613E-05
N-235 (atom/b-cm)	3.8521E-03	3.9195E-03	3.7869E-03	4.0368E-03	3.6835E-03
N-236 (atom/b-cm)	1.4282E-05	1.4532E-05	1.4040E-05	1.4967E-05	1.3657E-05
N-238 (atom/b-cm)	2.0433E-04	2.0791E-04	2.0088E-04	2.1413E-04	1.9539E-04
N-Al (atom/b-cm)	5.0202E-02	5.0090E-02	5.0310E-02	4.9895E-02	5.0481E-02
Total (atom/b-cm)	5.4297E-02	5.4257E-02	5.4336E-02	5.4187E-02	5.4398E-02

Table 6.9-7 – MITR-II Parametric Analysis Results

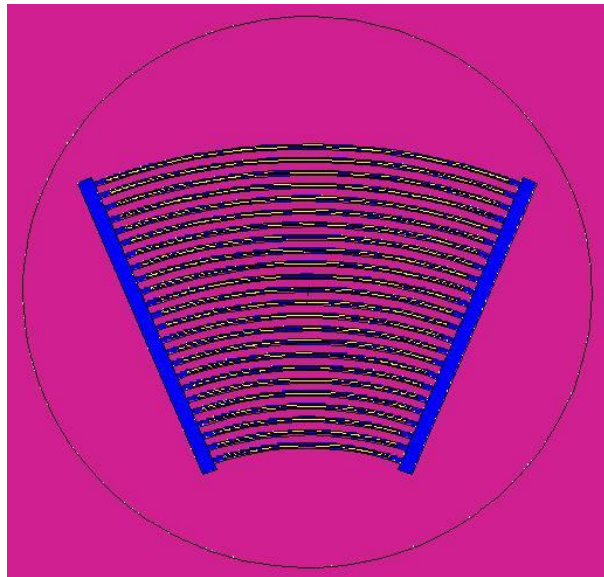
Case ID	Filename	k_{eff}	σ	k_s ($k+2\sigma$)	Δ from PN1 (mk)
PN1	HS_MIT2_P1	0.39975	0.00089	0.40153	
PN2	HS_MIT2_P2	0.40082	0.00093	0.40268	1.1
PN3	HS_MIT2_P3	0.39965	0.00088	0.40141	-0.1
PN4	HS_MIT2_P4	0.40562	0.00105	0.40772	6.2
PN5	HS_MIT2_P5	0.39724	0.00096	0.39916	-2.4
PN6	HS_MIT2_P6	0.40496	0.00087	0.40670	5.2
PN7	HS_MIT2_P7	0.41052	0.00098	0.41248	11.0

Table 6.9-8 – TRIGA Fuel Pin Cell Results

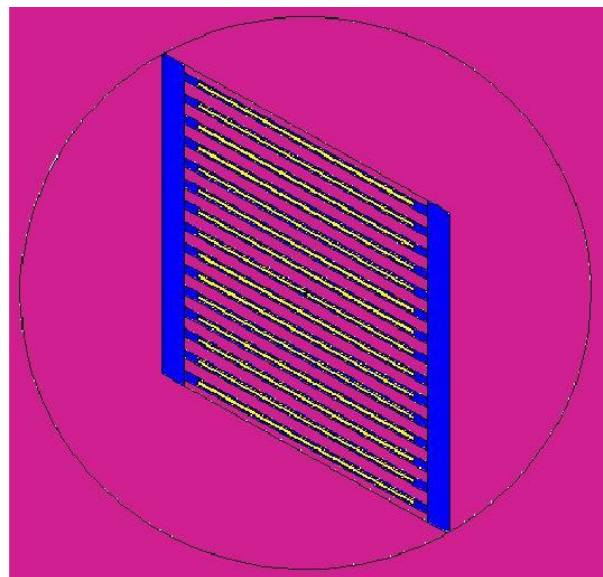
Case ID	Filename	Pitch (cm)	k_{eff}	σ	k_s ($k+2\sigma$)
Type 101 (8 wt.% aluminum clad)					
PT1	C101_P19	0.38	1.38089	0.00099	1.38287
PT2	C101_P22	0.44	1.31512	0.00086	1.31684
PT3	C101_P25	0.50	1.21166	0.00082	1.21330
Type 103/203 (8.5 wt.% stainless steel clad)					
PT10	C103_P19	0.38	1.31017	0.00085	1.31187
PT11	C103_P22	0.44	1.22796	0.00092	1.22980
PT12	C103_P25	0.50	1.13356	0.00080	1.13516
Type 109 (8.5 wt.% stainless steel clad, HEU)					
PT20	C109_P19	0.38	1.59214	0.00094	1.59402
PT21	C109_P22	0.44	1.55156	0.00095	1.55346
PT22	C109_P25	0.50	1.47780	0.00097	1.47974
PT23	C109_P19M	0.38	1.59058	0.00090	1.59238
Type 117 (20 wt.% stainless steel clad)					
PT30	C117_P19	0.38	1.45689	0.00095	1.45879
PT31	C117_P22	0.44	1.43108	0.00090	1.43288
PT32	C117_P25	0.50	1.36660	0.00093	1.36846



ATR



MURR



MITR-II

Figure 6.9-1 – ATR, MURR, and MITR-II Base Parametric Models

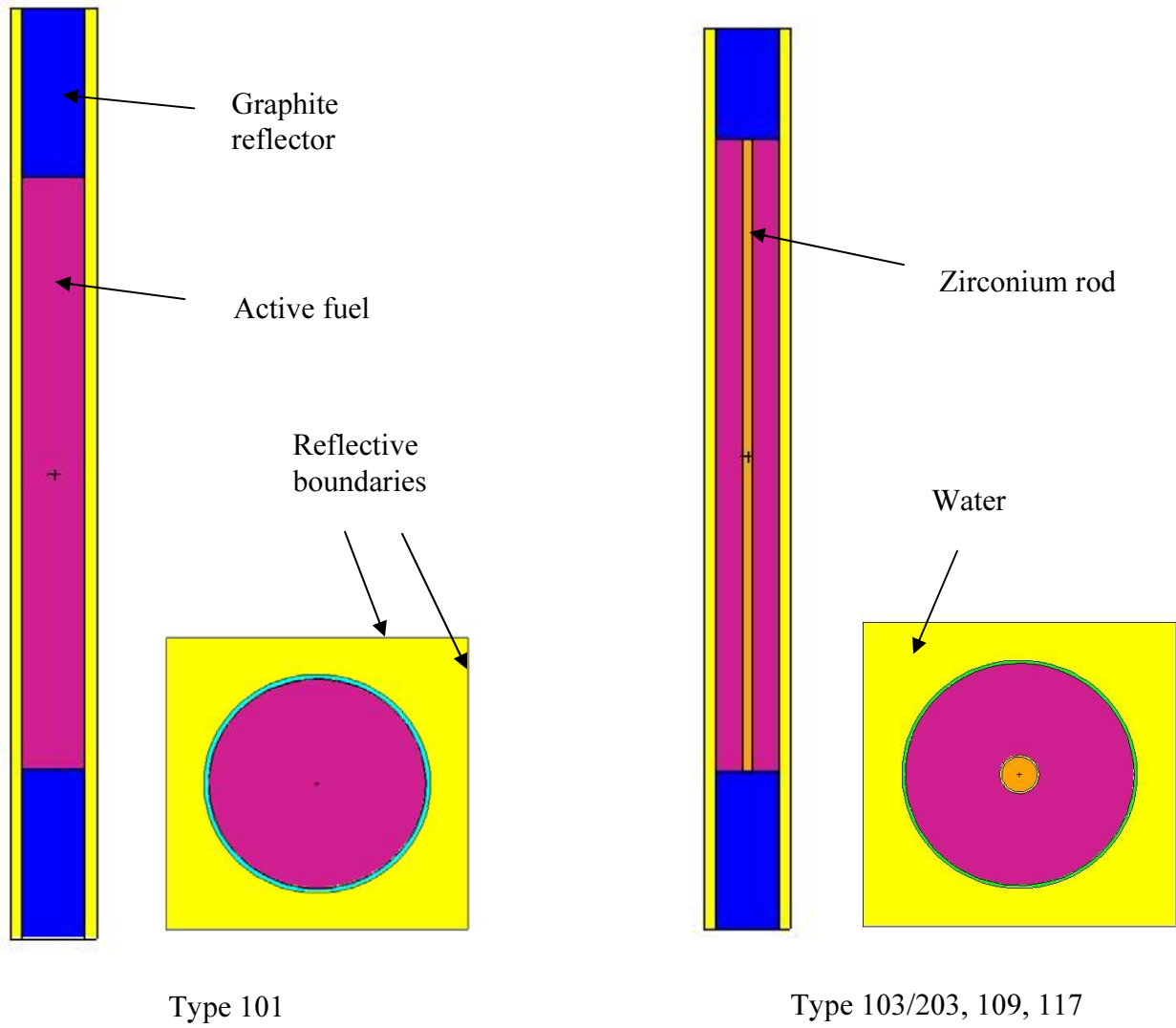


Figure 6.9-2 – TRIGA Pin Cell Models

6.9.3 Sample Input Files

A sample input file is provided for the most reactive case for each of the four fuel types.

MURR Case D1 (HA_MURR)

```

MURR
c
c      Basket
c
300    0          -400 424 -410 fill=6      imp:n=1 $ cavity
c
c      Cask
c
310    4 -7.94    (-424:410:400) 423 -411 -401 imp:n=1 $ inner steel
311    5 -11.35  (-423:411:401) 422 -412 -402 imp:n=1 $ lead
312    4 -7.94    (-422:412:402) 421 -413 -403 imp:n=1 $ outer steel
313    0          (-421:413:403) -405      imp:n=1 $ between
c
999    0          405                imp:n=0
c
c      Universe 1: MURR Fuel Element (infinitely long)
c
2      3 -2.7      -6 8 9 -10                u=1 imp:n=1 $ left Al piece
4      3 -2.7      -5 7 9 -10                u=1 imp:n=1 $ right Al piece
6      10 5.4439E-02 52 -53 -16 -15          u=1 imp:n=1 $ plate 1
8      3 -2.7      51 -54 -7 -8              #6  u=1 imp:n=1
10     2 -1.0      54 -55 -7 -8              u=1 imp:n=1
12     10 5.4439E-02 56 -57 -16 -15          u=1 imp:n=1 $ plate 2
14     3 -2.7      55 -58 -7 -8              #12 u=1 imp:n=1
16     2 -1.0      58 -59 -7 -8              u=1 imp:n=1
18     10 5.4439E-02 60 -61 -16 -15          u=1 imp:n=1 $ plate 3
20     3 -2.7      59 -62 -7 -8              #18 u=1 imp:n=1
22     2 -1.0      62 -63 -7 -8              u=1 imp:n=1
24     10 5.4439E-02 64 -65 -16 -15          u=1 imp:n=1 $ plate 4
26     3 -2.7      63 -66 -7 -8              #24 u=1 imp:n=1
28     2 -1.0      66 -67 -7 -8              u=1 imp:n=1
30     10 5.4439E-02 68 -69 -16 -15          u=1 imp:n=1 $ plate 5
32     3 -2.7      67 -70 -7 -8              #30 u=1 imp:n=1
34     2 -1.0      70 -71 -7 -8              u=1 imp:n=1
36     10 5.4439E-02 72 -73 -16 -15          u=1 imp:n=1 $ plate 6
38     3 -2.7      71 -74 -7 -8              #36 u=1 imp:n=1
40     2 -1.0      74 -75 -7 -8              u=1 imp:n=1
42     10 5.4439E-02 76 -77 -16 -15          u=1 imp:n=1 $ plate 7
44     3 -2.7      75 -78 -7 -8              #42 u=1 imp:n=1
46     2 -1.0      78 -79 -7 -8              u=1 imp:n=1
48     10 5.4439E-02 80 -81 -16 -15          u=1 imp:n=1 $ plate 8
50     3 -2.7      79 -82 -7 -8              #48 u=1 imp:n=1
52     2 -1.0      82 -83 -7 -8              u=1 imp:n=1
54     10 5.4439E-02 84 -85 -16 -15          u=1 imp:n=1 $ plate 9
56     3 -2.7      83 -86 -7 -8              #54 u=1 imp:n=1
58     2 -1.0      86 -87 -7 -8              u=1 imp:n=1
60     10 5.4439E-02 88 -89 -16 -15          u=1 imp:n=1 $ plate 10
62     3 -2.7      87 -90 -7 -8              #60 u=1 imp:n=1
64     2 -1.0      90 -91 -7 -8              u=1 imp:n=1
66     10 5.4439E-02 92 -93 -16 -15          u=1 imp:n=1 $ plate 11
68     3 -2.7      91 -94 -7 -8              #66 u=1 imp:n=1
70     2 -1.0      94 -95 -7 -8              u=1 imp:n=1
72     10 5.4439E-02 96 -97 -16 -15          u=1 imp:n=1 $ plate 12

```

BRR Package Safety Analysis Report

74	3	-2.7	95	-98	-7	-8	#72	u=1	imp:n=1	
76	2	-1.0	98	-99	-7	-8		u=1	imp:n=1	
78	10	5.4439E-02	100	-101	-16	-15		u=1	imp:n=1	\$ plate 13
80	3	-2.7	99	-102	-7	-8	#78	u=1	imp:n=1	
82	2	-1.0	102	-103	-7	-8		u=1	imp:n=1	
84	10	5.4439E-02	104	-105	-16	-15		u=1	imp:n=1	\$ plate 14
86	3	-2.7	103	-106	-7	-8	#84	u=1	imp:n=1	
88	2	-1.0	106	-107	-7	-8		u=1	imp:n=1	
90	10	5.4439E-02	108	-109	-16	-15		u=1	imp:n=1	\$ plate 15
92	3	-2.7	107	-110	-7	-8	#90	u=1	imp:n=1	
94	2	-1.0	110	-111	-7	-8		u=1	imp:n=1	
96	10	5.4439E-02	112	-113	-16	-15		u=1	imp:n=1	\$ plate 16
98	3	-2.7	111	-114	-7	-8	#96	u=1	imp:n=1	
100	2	-1.0	114	-115	-7	-8		u=1	imp:n=1	
102	10	5.4439E-02	116	-117	-16	-15		u=1	imp:n=1	\$ plate 17
104	3	-2.7	115	-118	-7	-8	#102	u=1	imp:n=1	
106	2	-1.0	118	-119	-7	-8		u=1	imp:n=1	
108	10	5.4439E-02	120	-121	-16	-15		u=1	imp:n=1	\$ plate 18
110	3	-2.7	119	-122	-7	-8	#108	u=1	imp:n=1	
112	2	-1.0	122	-123	-7	-8		u=1	imp:n=1	
114	10	5.4439E-02	124	-125	-16	-15		u=1	imp:n=1	\$ plate 19
116	3	-2.7	123	-126	-7	-8	#114	u=1	imp:n=1	
118	2	-1.0	126	-127	-7	-8		u=1	imp:n=1	
120	10	5.4439E-02	128	-129	-16	-15		u=1	imp:n=1	\$ plate 20
122	3	-2.7	127	-130	-7	-8	#120	u=1	imp:n=1	
124	2	-1.0	130	-131	-7	-8		u=1	imp:n=1	
126	10	5.4439E-02	132	-133	-16	-15		u=1	imp:n=1	\$ plate 21
128	3	-2.7	131	-134	-7	-8	#126	u=1	imp:n=1	
130	2	-1.0	134	-135	-7	-8		u=1	imp:n=1	
132	10	5.4439E-02	136	-137	-16	-15		u=1	imp:n=1	\$ plate 22
134	3	-2.7	135	-138	-7	-8	#132	u=1	imp:n=1	
136	2	-1.0	138	-139	-7	-8		u=1	imp:n=1	
138	10	5.4439E-02	140	-141	-16	-15		u=1	imp:n=1	\$ plate 23
140	3	-2.7	139	-142	-7	-8	#138	u=1	imp:n=1	
142	2	-1.0	142	-143	-7	-8		u=1	imp:n=1	
144	10	5.4439E-02	144	-145	-16	-15		u=1	imp:n=1	\$ plate 24
146	3	-2.7	143	-146	-7	-8	#144	u=1	imp:n=1	
150	2	-1.0	6:5:-9:10:9	-51	-8	-7:146	-10	-8	-7	u=1 imp:n=1

c

Universe 6: Basket

c

600	4	-7.94	600	-601	-620		u=6	imp:n=1	\$ bottom	
601	4	-7.94	600	-604	620	-621	u=6	imp:n=1	\$ bottom	
602	4	-7.94	604	-605	620		u=6	imp:n=1	\$ shell	
603	4	-7.94	602	-604	622	-623	u=6	imp:n=1	\$ shelf	
604	4	-7.94	602	-603	623		u=6	imp:n=1	\$ inner ring	
610	2	-1.0	-600	-621			u=6	imp:n=1	\$ bottom air	
611	2	-1.0	601	-620	-605		u=6	imp:n=1	\$ bottom air corner	
612	2	-1.0	605				u=6	imp:n=1	\$ side and top air	
613	2	-1.0	-604	621	-622		u=6	imp:n=1	\$ inner air	
614	2	-1.0	-602	622			u=6	imp:n=1	\$ inner air	
615	0		603	-604	623	637	-630	fill=20	u=6	imp:n=1 \$ basket loc
1 (top)										
616	0		603	-604	623	631	-634	fill=20(2)	u=6	imp:n=1 \$ basket loc
2										
617	0		603	-604	623	635	633	fill=20(3)	u=6	imp:n=1 \$ basket loc
3										
618	0		603	-604	623	637	-632	fill=20(4)	u=6	imp:n=1 \$ basket loc
4										

BRR Package Safety Analysis Report

```

619    0          603 -604 623    631 -636 fill=20(5) u=6 imp:n=1 $ basket loc
5
620    0          603 -604 623    -630  635 fill=20(6) u=6 imp:n=1 $ basket loc
6
621    0          603 -604 623    -632 -634 fill=20(7) u=6 imp:n=1 $ basket loc
7
622    0          603 -604 623    633 -636 fill=20(8) u=6 imp:n=1 $ basket loc
8
630    4  -7.94    603 -604 630 -631 623    u=6 imp:n=1 $ web
631    4  -7.94    603 -604 632 -633 623    u=6 imp:n=1 $ web
632    4  -7.94    603 -604 634 -635 623    u=6 imp:n=1 $ web
633    4  -7.94    603 -604 636 -637 623    u=6 imp:n=1 $ web
c
c      Universe 20: MURR fuel element moved +y
c
200    0          -203 24 -25    fill=1(11) u=20 imp:n=1 $ MURR
201    2 -1.0      203:-24:25    u=20 imp:n=1 $ water

5      p  2.4142136 -1 0 -0.13275    $ right Al outer
6      p -2.4142136 -1 0 -0.13275    $ left Al outer
7      p  2.4142136 -1 0 -1.09516    $ right Al inner
8      p -2.4142136 -1 0 -1.09516    $ left Al inner
9      cz 6.858    $ Al boundary
10     cz 14.884    $ Al boundary
c
15     p  2.4142136 -1 0 -1.39997    $ plate meat boundary
16     p -2.4142136 -1 0 -1.39997    $ plate meat boundary
c
24     pz  76.1821    $ bottom of fuel
25     pz  137.1421    $ top of fuel (24")
c
51     cz 7.0460 $ fuel plate 1
52     cz 7.0739
53     cz 7.1247
54     cz 7.1526
c
55     cz 7.3762 $ fuel plate 2
56     cz 7.4041
57     cz 7.4549
58     cz 7.4828
c
59     cz 7.7064 $ fuel plate 3
60     cz 7.7343
61     cz 7.7851
62     cz 7.8130
c
63     cz 8.0366 $ fuel plate 4
64     cz 8.0645
65     cz 8.1153
66     cz 8.1432
c
67     cz 8.3668 $ fuel plate 5
68     cz 8.3947
69     cz 8.4455
70     cz 8.4734
c
71     cz 8.6970 $ fuel plate 6
72     cz 8.7249
73     cz 8.7757
74     cz 8.8036

```

BRR Package Safety Analysis Report

c
75 cz 9.0272 \$ fuel plate 7
76 cz 9.0551
77 cz 9.1059
78 cz 9.1338
c
79 cz 9.3574 \$ fuel plate 8
80 cz 9.3853
81 cz 9.4361
82 cz 9.4640
c
83 cz 9.6876 \$ fuel plate 9
84 cz 9.7155
85 cz 9.7663
86 cz 9.7942
c
87 cz 10.0178 \$ fuel plate 10
88 cz 10.0457
89 cz 10.0965
90 cz 10.1244
c
91 cz 10.3480 \$ fuel plate 11
92 cz 10.3759
93 cz 10.4267
94 cz 10.4546
c
95 cz 10.6782 \$ fuel plate 12
96 cz 10.7061
97 cz 10.7569
98 cz 10.7848
c
99 cz 11.0084 \$ fuel plate 13
100 cz 11.0363
101 cz 11.0871
102 cz 11.1150
c
103 cz 11.3386 \$ fuel plate 14
104 cz 11.3665
105 cz 11.4173
106 cz 11.4452
c
107 cz 11.6688 \$ fuel plate 15
108 cz 11.6967
109 cz 11.7475
110 cz 11.7754
c
111 cz 11.9990 \$ fuel plate 16
112 cz 12.0269
113 cz 12.0777
114 cz 12.1056
c
115 cz 12.3292 \$ fuel plate 17
116 cz 12.3571
117 cz 12.4079
118 cz 12.4358
c
119 cz 12.6594 \$ fuel plate 18
120 cz 12.6873
121 cz 12.7381
122 cz 12.7660

BRR Package Safety Analysis Report

c
123 cz 12.9896 \$ fuel plate 19
124 cz 13.0175
125 cz 13.0683
126 cz 13.0962
c
127 cz 13.3198 \$ fuel plate 20
128 cz 13.3477
129 cz 13.3985
130 cz 13.4264
c
131 cz 13.6500 \$ fuel plate 21
132 cz 13.6779
133 cz 13.7287
134 cz 13.7566
c
135 cz 13.9802 \$ fuel plate 22
136 cz 14.0081
137 cz 14.0589
138 cz 14.0868
c
139 cz 14.3104 \$ fuel plate 23
140 cz 14.3383
141 cz 14.3891
142 cz 14.4170
c
143 cz 14.6406 \$ fuel plate 24
144 cz 14.6685
145 cz 14.7193
146 cz 14.7472
c
203 cz 100 \$ dummy
c
400 cz 20.32 \$ IR cask
401 cz 22.86 \$ IR lead
402 cz 43.18 \$ OR lead
403 cz 48.26 \$ OR cask
404 cz 78.74 \$ 1 foot water reflector
*405 hex 0 0 -25.25 0 0 190.5355 0 48.27 0
c
410 pz 137.1422 \$ bottom of lid
411 pz 139.6822 \$ steel
412 pz 164.0154 \$ lead
413 pz 165.2854 \$ steel
414 pz 195.7654 \$ 1 foot water reflector
c
420 pz -55.72 \$ 1 foot water reflector
421 pz -25.24 \$ bottom of cask
422 pz -22.7 \$ steel
423 pz -3.0912 \$ lead
424 pz 0 \$ steel
c
c basket surfaces
c
600 cz 15.4432
601 cz 16.3957
602 cz 8.89
603 cz 10.0813
604 cz 19.177
605 cz 19.812

BRR Package Safety Analysis Report

```

620      pz 5.715
621      pz 6.6675
622      pz 50.9778
623      pz 51.9303
630 12   px -1.27
631 12   px 1.27
632 12   py -1.27
633 12   py 1.27
634 13   px -1.27
635 13   px 1.27
636 13   py -1.27
637 13   py 1.27

m2      1001.62c 2          $ water
        8016.62c 1
mt2     lwtr.60t
m3      13027.62c 1        $ Al
m4      6000.66c -0.08     $ SS-304
        14000.60c -1.0
        15031.66c -0.045
        24000.50c -19.0
        25055.62c -2.0
        26000.55c -68.375
        28000.50c -9.5
m5      82000.50c 1        $ Pb
m10     92234.69c 2.3171E-05 $ fuel.
        92235.69c 3.6147E-03
        92236.69c 1.3402E-05
        92238.69c 1.9174E-04
        13027.62c 5.0596E-02
c       total 5.4439E-02
c
*tr2    0 0 0 45 135 90 45 45 90          $ loc 2
*tr3    0 0 0 90 180 90 0 90 90          $ loc 3
*tr4    0 0 0 135 225 90 45 135 90       $ loc 4
*tr5    0 0 0 180 90 90 90 180 90       $ loc 5
*tr6    0 0 0 135 45 90 225 135 90       $ loc 6
*tr7    0 0 0 90 0 90 180 90 90         $ loc 7
*tr8    0 0 0 45 45 90 135 45 90         $ loc 8
*tr11   0 3.4 0                          $ u=20
*tr12   0 0 0 22.5 112.5 90 67.5 22.5 90 $ rotate 22.5 deg
*tr13   0 0 0 67.5 157.5 90 22.5 67.5 90 $ rotate 67.5 deg
c
mode    n
kcode   2500 1.0 50 250
sdef    rad=d1 ext=d2 axs=0 0 1
si1     10 18.5
si2     76 137

```

MITR-II Case D21 (HA_MIT_INOUTUP2)

```

MIT
c
c      Basket
c
300    0          320 -321 323 -322 611 -410 fill=5 imp:n=1 $ basket
location 1
301    like 300 but trcl=2          imp:n=1 $ basket
location 2

```

BRR Package Safety Analysis Report

```

302      like 300 but trcl=3                      imp:n=1 $ basket
location 3
303      like 300 but trcl=4                      imp:n=1 $ basket
location 4
304      like 300 but trcl=5                      imp:n=1 $ basket
location 5
305      like 300 but trcl=6                      imp:n=1 $ basket
location 6
306      like 300 but trcl=7                      imp:n=1 $ basket
location 7
307      like 300 but trcl=8                      imp:n=1 $ basket
location 8
310      0                340 -341 343 -342 611 -410 fill=6 imp:n=1 $ inner
location 1
311      like 310 but trcl=16                     imp:n=1 $ inner
location 2
312      like 310 but trcl=15                     imp:n=1 $ inner
location 3
320      2 -1.0                -400 611 -410 #300 #301 #302 #303 #304
                #305 #306 #307 #310 #311 #312 imp:n=1 $ inside basket

c
c      Cask
c
410      4 -7.94      (-424:410:400) 423 -411 -401 imp:n=1 $ inner steel
411      5 -11.35    (-423:411:401) 422 -412 -402 imp:n=1 $ lead
412      4 -7.94      (-422:412:402) 421 -413 -403 imp:n=1 $ outer steel
413      0                (-421:413:403) -405                imp:n=1 $ between
c
600      2 -1.0      424 -610 -600                imp:n=1 $ water
601      2 -1.0      424 -610 601 -400            imp:n=1 $ water
602      2 -1.0      610 -611 602 -400            imp:n=1 $ water
604      4 -7.94      424 -610 600 -601            imp:n=1 $ basket
605      4 -7.94      610 -611 -602                imp:n=1 $ basket
c
999      0                405                imp:n=0
c
c      Universe 1: MIT Fuel Element (infinitely long)
c
10       3 -2.7                10 -11 18 -19                u=1 imp:n=1 $ right Al piece
11       3 -2.7                13 -12 18 -19                u=1 imp:n=1 $ left Al piece
12       2 -1.0                12 -10 18 -50                u=1 imp:n=1
20       10 5.4398E-02 40 -41 70 -90                u=1 imp:n=1 $ plate 1
21       3 -2.7                12 -10 50 -110 #20            u=1 imp:n=1
22       2 -1.0                12 -10 110 -51            u=1 imp:n=1
30       10 5.4398E-02 40 -41 71 -91                u=1 imp:n=1 $ plate 2
31       3 -2.7                12 -10 51 -111 #30            u=1 imp:n=1
32       2 -1.0                12 -10 111 -52            u=1 imp:n=1
40       10 5.4398E-02 40 -41 72 -92                u=1 imp:n=1 $ plate 3
41       3 -2.7                12 -10 52 -112 #40            u=1 imp:n=1
42       2 -1.0                12 -10 112 -53            u=1 imp:n=1
50       10 5.4398E-02 40 -41 73 -93                u=1 imp:n=1 $ plate 4
51       3 -2.7                12 -10 53 -113 #50            u=1 imp:n=1
52       2 -1.0                12 -10 113 -54            u=1 imp:n=1
60       10 5.4398E-02 40 -41 74 -94                u=1 imp:n=1 $ plate 5
61       3 -2.7                12 -10 54 -114 #60            u=1 imp:n=1
62       2 -1.0                12 -10 114 -55            u=1 imp:n=1
70       10 5.4398E-02 40 -41 75 -95                u=1 imp:n=1 $ plate 6
71       3 -2.7                12 -10 55 -115 #70            u=1 imp:n=1
72       2 -1.0                12 -10 115 -56            u=1 imp:n=1
80       10 5.4398E-02 40 -41 76 -96                u=1 imp:n=1 $ plate 7

```

BRR Package Safety Analysis Report

```

81      3 -2.7          12 -10 56 -116 #80      u=1 imp:n=1
82      2 -1.0          12 -10 116 -57      u=1 imp:n=1
90     10 5.4398E-02 40 -41 77 -97      u=1 imp:n=1 $ plate 8
91      3 -2.7          12 -10 57 -117 #90      u=1 imp:n=1
92      2 -1.0          12 -10 117 -58      u=1 imp:n=1
100    10 5.4398E-02 40 -41 78 -98      u=1 imp:n=1 $ plate 9
101    3 -2.7          12 -10 58 -118 #100     u=1 imp:n=1
102    2 -1.0          12 -10 118 -59      u=1 imp:n=1
110    10 5.4398E-02 40 -41 79 -99      u=1 imp:n=1 $ plate 10
111    3 -2.7          12 -10 59 -119 #110     u=1 imp:n=1
112    2 -1.0          12 -10 119 -60      u=1 imp:n=1
120    10 5.4398E-02 40 -41 80 -100     u=1 imp:n=1 $ plate 11
121    3 -2.7          12 -10 60 -120 #120     u=1 imp:n=1
122    2 -1.0          12 -10 120 -61      u=1 imp:n=1
130    10 5.4398E-02 40 -41 81 -101     u=1 imp:n=1 $ plate 12
131    3 -2.7          12 -10 61 -121 #130     u=1 imp:n=1
132    2 -1.0          12 -10 121 -62      u=1 imp:n=1
140    10 5.4398E-02 40 -41 82 -102     u=1 imp:n=1 $ plate 13
141    3 -2.7          12 -10 62 -122 #140     u=1 imp:n=1
142    2 -1.0          12 -10 122 -63      u=1 imp:n=1
150    10 5.4398E-02 40 -41 83 -103     u=1 imp:n=1 $ plate 14
151    3 -2.7          12 -10 63 -123 #150     u=1 imp:n=1
152    2 -1.0          12 -10 123 -64      u=1 imp:n=1
160    10 5.4398E-02 40 -41 84 -104     u=1 imp:n=1 $ plate 15
161    3 -2.7          12 -10 64 -124 #160     u=1 imp:n=1
162    2 -1.0          12 -10 124 -19      u=1 imp:n=1
170    2 -1.0          -13:11:-18:19      u=1 imp:n=1 $ water in pipe
c
c      Universe 5: Element rotated 7.5 degrees CCW and moved to wedge 1
location outer
c
500    0              330 -331 333 -332 24 -25 fill=1(12) u=5 imp:n=1
501    2 -1.0          330 -331 333 -332 -24      u=5 imp:n=1
502    2 -1.0          330 -331 333 -332 25      u=5 imp:n=1
503    4 -7.94        -330:331:-333:332      u=5 imp:n=1
c
c      Universe 6: Element rotated 30 degrees CCW and moved to wedge 1
location inner
c
510    0              350 -351 353 -352 24 -25 fill=1(14) u=6 imp:n=1
511    2 -1.0          350 -351 353 -352 -24      u=6 imp:n=1
512    2 -1.0          350 -351 353 -352 25      u=6 imp:n=1
513    4 -7.94        -350:351:-353:352      u=6 imp:n=1

10     px  2.5451      $ Al side
11     px  3.0226      $ Al side
12     px -2.5451     $ Al side
13     px -3.0226     $ Al side
18 10  py -3.02768    $ Al bottom
19 10  py  3.02768    $ Al top
c
24     pz  80.3096     $ bottom of fuel
25     pz 137.1421    $ top of fuel (22.375")
c
40     px -2.3878     $ meat width (w/2*cos(30))
41     px  2.3878     $ meat width
c
50 10  py -2.89052    $ cladding bottom
51 10  py -2.48920
52 10  py -2.08788

```

BRR Package Safety Analysis Report

53 10 py -1.68656
54 10 py -1.28524
55 10 py -0.88392
56 10 py -0.48260
57 10 py -0.08128
58 10 py 0.32004
59 10 py 0.72136
60 10 py 1.12268
61 10 py 1.52400
62 10 py 1.92532
63 10 py 2.32664
64 10 py 2.72796
c
70 10 py -2.84734 \$ meat bottom
71 10 py -2.44602
72 10 py -2.04470
73 10 py -1.64338
74 10 py -1.24206
75 10 py -0.84074
76 10 py -0.43942
77 10 py -0.03810
78 10 py 0.36322
79 10 py 0.76454
80 10 py 1.16586
81 10 py 1.56718
82 10 py 1.96850
83 10 py 2.36982
84 10 py 2.77114
c
90 10 py -2.77114 \$ meat top
91 10 py -2.36982
92 10 py -1.96850
93 10 py -1.56718
94 10 py -1.16586
95 10 py -0.76454
96 10 py -0.36322
97 10 py 0.03810
98 10 py 0.43942
99 10 py 0.84074
100 10 py 1.24206
101 10 py 1.64338
102 10 py 2.04470
103 10 py 2.44602
104 10 py 2.84734
c
110 10 py -2.72796 \$ cladding top
111 10 py -2.32664
112 10 py -1.92532
113 10 py -1.52400
114 10 py -1.12268
115 10 py -0.72136
116 10 py -0.32004
117 10 py 0.08128
118 10 py 0.48260
119 10 py 0.88392
120 10 py 1.28524
121 10 py 1.68656
122 10 py 2.08788
123 10 py 2.48920
124 10 py 2.89052

BRR Package Safety Analysis Report

```

c
c 200      cz 19.5      $ IR basket  dummy*****
c 201      cz 20       $ OR basket  dummy*****
c 202      cz 50       $ 12" water
c 203      cz 100      $ dummy
c
c 224      pz -60.96
c 225      pz 60.96
c
320  1  py -3.6855          $ outer nine
321  1  py 3.6855
322  1  p  -1.7321 -1 0  7.3711 $ left basket outer bound
323  1  p  -1.7321 -1 0 -7.3711 $ right basket outer bound
c
330  1  py -3.3807
331  1  py 3.3807
332  1  p  -1.7321 -1 0  6.7615 $ left basket inner bound
333  1  p  -1.7321 -1 0 -6.7615 $ right basket inner bound
c
340  13 py -3.6855          $ inner three
341  13 py 3.6855
342  13 p  -1.7321 -1 0  7.3711 $ left basket outer bound
343  13 p  -1.7321 -1 0 -7.3711 $ right basket outer bound
c
350  13 py -3.3807
351  13 py 3.3807
352  13 p  -1.7321 -1 0  6.7615 $ left basket inner bound
353  13 p  -1.7321 -1 0 -6.7615 $ right basket inner bound
c
c 350      py 7.2873
c 351      p  2.414214 -1 0 -0.7965
c 352      p -2.414214 -1 0 -0.7965
c 360      cz 16
c 361      cz 16.3048
c
400      cz 20.32 $ IR cask
401      cz 22.86 $ IR lead
402      cz 43.18 $ OR lead
403      cz 48.26 $ OR cask
404      cz 78.74 $ 1 foot water reflector
*405     hex 0 0 -25.25 0 0 190.5355 0 48.27 0
c
410      pz 137.1422 $ bottom of lid
411      pz 139.6822 $ steel
412      pz 164.0154 $ lead
413      pz 165.2854 $ steel
414      pz 195.7654 $ 1 foot water reflector
c
420      pz -55.72  $ 1 foot water reflector
421      pz -25.24  $ bottom of cask
422      pz -22.7   $ steel
423      pz -3.0912 $ lead
424      pz 0       $ steel
c
600      cz 17.145
601      cz 17.78
602      cz 20.0025
610      pz 66.8782
611      pz 67.5132

```

BRR Package Safety Analysis Report

```

m2      1001.62c  2          $ water
        8016.62c  1
mt2     lwtr.60t
m3      13027.62c 1          $ Al
m4      6000.66c  -0.08     $ SS-304
        14000.60c -1.0
        15031.66c -0.045
        24000.50c -19.0
        25055.62c -2.0
        26000.55c -68.375
        28000.50c -9.5
m5      82000.50c 1          $ Pb
m10     92234.69c 2.3613E-05 $ fuel
        92235.69c 3.6835E-03
        92236.69c 1.3657E-05
        92238.69c 1.9539E-04
        13027.62c 5.0481E-02
c       total 5.4398E-02
c
*tr1    0 13.4112 0 22.5 112.5 90 67.5 22.5 90 $ wedge 1
*tr2    0 0 0          45 135 90 45 45 90     $ wedge 2(8)
*tr3    0 0 0          90 180 90 0 90 90     $ wedge 3(7)
*tr4    0 0 0          135 225 90 45 135 90   $ wedge 4(6)
*tr5    0 0 0          180 90 90 90 180 90   $ wedge 5
*tr6    0 0 0          135 45 90 225 135 90  $ wedge 6
*tr7    0 0 0          90 0 90 180 90 90     $ wedge 7
*tr8    0 0 0          45 45 90 135 45 90    $ wedge 8
*tr10   0 0 0          30 120 90 60 30 90     $ rotate fuel surfaces 30 deg
CW
*tr12   0 13.059 0 7.5 82.5 90 97.5 7.5 90   $ rotate 30-22.5=7.5 CCW
*tr13   -2.1279 -3.6856 0                    $ inner wedge
*tr14   -2.3358 -4.0212 0 30 60 90 120 30 90 $ rotate 30 CCW
*tr15   0 0 0          120 210 90 30 120 90  $ inner wedge
*tr16   0 0 0          120 30 90 210 120 90  $ inner wedge
c
mode    n
kcode   2500 1.0 50 250
sdef    rad=d1 ext=d2 axs=0 0 1
sil     20
si2     80 137
rand    seed=746877864974

```

ATR Case D40 (HA_ATR)

```

ATR
300     0          -400 424 -410 fill=6      imp:n=1 $ cavity
c
c       Cask
c
310     4 -7.94     (-424:410:400) 423 -411 -401 imp:n=1 $ inner steel
311     5 -11.35    (-423:411:401) 422 -412 -402 imp:n=1 $ lead
312     4 -7.94     (-422:412:402) 421 -413 -403 imp:n=1 $ outer steel
313     0          (-421:413:403) -405          imp:n=1 $ between
c
999     0          405                          imp:n=0
c
c       Universe 1: ATR Fuel Element (infinitely long)
c
2       3 -2.7          -6 8 9 -10              u=1 imp:n=1 $ left Al piece
4       3 -2.7          -5 7 9 -10              u=1 imp:n=1 $ right Al piece

```

BRR Package Safety Analysis Report

6	10	5.5010E-02	52	-53	-14	-13		u=1	imp:n=1	\$	plate 1
8	3	-2.7	51	-54	-7	-8	#6	u=1	imp:n=1		
10	2	-1.0	54	-55	-7	-8		u=1	imp:n=1		
12	11	5.4998E-02	56	-57	-16	-15		u=1	imp:n=1	\$	plate 2
14	3	-2.7	55	-58	-7	-8	#12	u=1	imp:n=1		
16	2	-1.0	58	-59	-7	-8		u=1	imp:n=1		
18	12	5.4574E-02	60	-61	-16	-15		u=1	imp:n=1	\$	plate 3
20	3	-2.7	59	-62	-7	-8	#18	u=1	imp:n=1		
22	2	-1.0	62	-63	-7	-8		u=1	imp:n=1		
24	13	5.4583E-02	64	-65	-16	-15		u=1	imp:n=1	\$	plate 4
26	3	-2.7	63	-66	-7	-8	#24	u=1	imp:n=1		
28	2	-1.0	66	-67	-7	-8		u=1	imp:n=1		
30	14	5.4115E-02	68	-69	-16	-15		u=1	imp:n=1	\$	plate 5
32	3	-2.7	67	-70	-7	-8	#30	u=1	imp:n=1		
34	2	-1.0	70	-71	-7	-8		u=1	imp:n=1		
36	15	5.4106E-02	72	-73	-16	-15		u=1	imp:n=1	\$	plate 6
38	3	-2.7	71	-74	-7	-8	#36	u=1	imp:n=1		
40	2	-1.0	74	-75	-7	-8		u=1	imp:n=1		
42	16	5.4102E-02	76	-77	-16	-15		u=1	imp:n=1	\$	plate 7
44	3	-2.7	75	-78	-7	-8	#42	u=1	imp:n=1		
46	2	-1.0	78	-79	-7	-8		u=1	imp:n=1		
48	17	5.4098E-02	80	-81	-16	-15		u=1	imp:n=1	\$	plate 8
50	3	-2.7	79	-82	-7	-8	#48	u=1	imp:n=1		
52	2	-1.0	82	-83	-7	-8		u=1	imp:n=1		
54	18	5.4095E-02	84	-85	-16	-15		u=1	imp:n=1	\$	plate 9
56	3	-2.7	83	-86	-7	-8	#54	u=1	imp:n=1		
58	2	-1.0	86	-87	-7	-8		u=1	imp:n=1		
60	19	5.4092E-02	88	-89	-16	-15		u=1	imp:n=1	\$	plate 10
62	3	-2.7	87	-90	-7	-8	#60	u=1	imp:n=1		
64	2	-1.0	90	-91	-7	-8		u=1	imp:n=1		
66	20	5.4089E-02	92	-93	-16	-15		u=1	imp:n=1	\$	plate 11
68	3	-2.7	91	-94	-7	-8	#66	u=1	imp:n=1		
70	2	-1.0	94	-95	-7	-8		u=1	imp:n=1		
72	21	5.4086E-02	96	-97	-16	-15		u=1	imp:n=1	\$	plate 12
74	3	-2.7	95	-98	-7	-8	#72	u=1	imp:n=1		
76	2	-1.0	98	-99	-7	-8		u=1	imp:n=1		
78	22	5.4083E-02	100	-101	-16	-15		u=1	imp:n=1	\$	plate 13
80	3	-2.7	99	-102	-7	-8	#78	u=1	imp:n=1		
82	2	-1.0	102	-103	-7	-8		u=1	imp:n=1		
84	23	5.4081E-02	104	-105	-16	-15		u=1	imp:n=1	\$	plate 14
86	3	-2.7	103	-106	-7	-8	#84	u=1	imp:n=1		
88	2	-1.0	106	-107	-7	-8		u=1	imp:n=1		
90	24	5.4075E-02	108	-109	-16	-15		u=1	imp:n=1	\$	plate 15
92	3	-2.7	107	-110	-7	-8	#90	u=1	imp:n=1		
94	2	-1.0	110	-111	-7	-8		u=1	imp:n=1		
96	25	5.4544E-02	112	-113	-16	-15		u=1	imp:n=1	\$	plate 16
98	3	-2.7	111	-114	-7	-8	#96	u=1	imp:n=1		
100	2	-1.0	114	-115	-7	-8		u=1	imp:n=1		
102	26	5.4544E-02	116	-117	-16	-15		u=1	imp:n=1	\$	plate 17
104	3	-2.7	115	-118	-7	-8	#102	u=1	imp:n=1		
106	2	-1.0	118	-119	-7	-8		u=1	imp:n=1		
108	27	5.4949E-02	120	-121	-18	-17		u=1	imp:n=1	\$	plate 18
110	3	-2.7	119	-122	-7	-8	#108	u=1	imp:n=1		
112	2	-1.0	122	-123	-7	-8		u=1	imp:n=1		
114	28	5.4967E-02	124	-125	-14	-13		u=1	imp:n=1	\$	plate 19
116	3	-2.7	123	-126	-7	-8	#114	u=1	imp:n=1		
122	2	-1.0	6:5:-9:10:9	-51	-8	-7:126	-10	-8	-7	u=1	imp:n=1

c

c

Universe 6: Basket

c

BRR Package Safety Analysis Report

```

600    4  -7.94    602 -603 623          u=6 imp:n=1 $ inner ring
601    4  -7.94    602 -604 622 -623      u=6 imp:n=1 $ bottom plate
602    4  -7.94    604 -605          u=6 imp:n=1 $ outer ring
603    2  -1.0    -604 -622          u=6 imp:n=1 $ bottom void
604    2  -1.0    -602 622          u=6 imp:n=1 $ inner void
605    2  -1.0    605          u=6 imp:n=1 $ inf. water
614    0          603 -604 623    637 -630 fill=20    u=6 imp:n=1 $ basket loc
1 (top)
615    0          603 -604 623    631 -634 fill=20(2) u=6 imp:n=1 $ basket loc
2
616    0          603 -604 623    635 633 fill=20(3) u=6 imp:n=1 $ basket loc
3
617    0          603 -604 623    637 -632 fill=20(4) u=6 imp:n=1 $ basket loc
4
618    0          603 -604 623    631 -636 fill=20(5) u=6 imp:n=1 $ basket loc
5
619    0          603 -604 623    -630 635 fill=20(6) u=6 imp:n=1 $ basket loc
6
620    0          603 -604 623    -632 -634 fill=20(7) u=6 imp:n=1 $ basket loc
7
621    0          603 -604 623    633 -636 fill=20(8) u=6 imp:n=1 $ basket loc
8
630    4  -7.94    603 -604 630 -631 623    u=6 imp:n=1 $ web
631    4  -7.94    603 -604 632 -633 623    u=6 imp:n=1 $ web
632    4  -7.94    603 -604 634 -635 623    u=6 imp:n=1 $ web
633    4  -7.94    603 -604 636 -637 623    u=6 imp:n=1 $ web
c
c    Universe 20: ATR fuel element moved +y
c
200    0          -203 24 -25    fill=1(11) u=20 imp:n=1
201    2  -1.0    203:-24:25          u=20 imp:n=1 $ water

5      p  2.4142136 -1 0 -0.2665911 $ right Al outer
6      p -2.4142136 -1 0 -0.2665911 $ left Al outer
7      p  2.4142136 -1 0 -1.474587  $ right Al inner
8      p -2.4142136 -1 0 -1.474587  $ left Al inner
9      cz 7.52856          $ Al boundary
10     cz 14.015466       $ Al boundary
c
13     p  2.4142136 -1 0 -2.4370013 $ plate 1 & 19 meat
14     p -2.4142136 -1 0 -2.4370013 $ plate 1 & 19 meat
15     p  2.4142136 -1 0 -1.7732672 $ plate 2-17 meat
16     p -2.4142136 -1 0 -1.7732672 $ plate 2-17 meat
17     p  2.4142136 -1 0 -1.9060140 $ plate 18 meat
18     p -2.4142136 -1 0 -1.9060140 $ plate 18 meat
c
24     pz 15.2221          $ bottom of fuel
25     pz 137.1421        $ top of fuel (48")
c
51     cz 7.66699 $ fuel plate 1
52     cz 7.7343
53     cz 7.7851
54     cz 7.85241
c
55     cz 8.06831 $ fuel plate 2
56     cz 8.09752
57     cz 8.14832
58     cz 8.17753
c
59     cz 8.39343 $ fuel plate 3

```

BRR Package Safety Analysis Report

60 cz 8.42264
61 cz 8.47344
62 cz 8.50265
c
63 cz 8.71855 \$ fuel plate 4
64 cz 8.74776
65 cz 8.79856
66 cz 8.82777
c
67 cz 9.04367 \$ fuel plate 5
68 cz 9.07288
69 cz 9.12368
70 cz 9.15289
c
71 cz 9.36879 \$ fuel plate 6
72 cz 9.398
73 cz 9.4488
74 cz 9.47801
c
75 cz 9.69391 \$ fuel plate 7
76 cz 9.72312
77 cz 9.77392
78 cz 9.80313
c
79 cz 10.01903 \$ fuel plate 8
80 cz 10.04824
81 cz 10.09904
82 cz 10.12825
c
83 cz 10.34415 \$ fuel plate 9
84 cz 10.37336
85 cz 10.42416
86 cz 10.45337
c
87 cz 10.66927 \$ fuel plate 10
88 cz 10.69848
89 cz 10.74928
90 cz 10.77849
c
91 cz 10.99439 \$ fuel plate 11
92 cz 11.0236
93 cz 11.0744
94 cz 11.10361
c
95 cz 11.31951 \$ fuel plate 12
96 cz 11.34872
97 cz 11.39952
98 cz 11.42873
c
99 cz 11.64463 \$ fuel plate 13
100 cz 11.67384
101 cz 11.72464
102 cz 11.75385
c
103 cz 11.96975 \$ fuel plate 14
104 cz 11.99896
105 cz 12.04976
106 cz 12.07897
c
107 cz 12.29487 \$ fuel plate 15

BRR Package Safety Analysis Report

108 cz 12.32408
 109 cz 12.37488
 110 cz 12.40409
 c
 111 cz 12.61999 \$ fuel plate 16
 112 cz 12.6492
 113 cz 12.7
 114 cz 12.72921
 c
 115 cz 12.94511 \$ fuel plate 17
 116 cz 12.97432
 117 cz 13.02512
 118 cz 13.05433
 c
 119 cz 13.27023 \$ fuel plate 18
 120 cz 13.29944
 121 cz 13.35024
 122 cz 13.37945
 c
 123 cz 13.59535 \$ fuel plate 19
 124 cz 13.68806
 125 cz 13.73886
 126 cz 13.83157
 c
 203 cz 100 \$ dummy
 c
 400 cz 20.32 \$ IR cask
 401 cz 22.86 \$ IR lead
 402 cz 43.18 \$ OR lead
 403 cz 48.26 \$ OR cask
 404 cz 78.74 \$ 1 foot water reflector
 *405 hex 0 0 -25.25 0 0 190.5355 0 48.27 0
 c
 410 pz 137.1422 \$ bottom of lid
 411 pz 139.6822 \$ steel
 412 pz 164.0154 \$ lead
 413 pz 165.2854 \$ steel
 414 pz 195.7654 \$ 1 foot water reflector
 c
 420 pz -55.72 \$ 1 foot water reflector
 421 pz -25.24 \$ bottom of cask
 422 pz -22.7 \$ steel
 423 pz -3.0912 \$ lead
 424 pz 0 \$ steel
 c
 c basket surfaces
 c
 602 cz 8.255
 603 cz 9.144
 604 cz 16.51
 605 cz 17.145
 622 pz 4.0132
 623 pz 5.2832
 c 624 pz 135.763
 630 12 px -0.47625
 631 12 px 0.47625
 632 12 py -0.47625
 633 12 py 0.47625
 634 13 px -0.47625
 635 13 px 0.47625

BRR Package Safety Analysis Report

```

636 13 py -0.47625
637 13 py  0.47625

m2      1001.62c  2          $ water
        8016.62c  1
mt2     lwtr.60t
m3      13027.62c 1          $ Al
m4      6000.66c  -0.08     $ SS-304
        14000.60c -1.0
        15031.66c -0.045
        24000.50c -19.0
        25055.62c -2.0
        26000.55c -68.375
        28000.50c -9.5

m5      82000.50c 1          $ Pb
m10     92234.69c 1.7026E-05 $ fuel plate 1
        92235.69c 2.6560E-03
        92236.69c 9.8475E-06
        92238.69c 1.4089E-04
        13027.62c 5.2187E-02
c       total      5.5010E-02
m11     92234.69c 1.7156E-05 $ fuel plate 2
        92235.69c 2.6763E-03
        92236.69c 9.9226E-06
        92238.69c 1.4196E-04
        13027.62c 5.2153E-02
c       total      5.4998E-02
m12     92234.69c 2.1711E-05 $ fuel plate 3
        92235.69c 3.3869E-03
        92236.69c 1.2557E-05
        92238.69c 1.7966E-04
        13027.62c 5.0974E-02
c       total      5.4574E-02
m13     92234.69c 2.1618E-05 $ fuel plate 4
        92235.69c 3.3724E-03
        92236.69c 1.2503E-05
        92238.69c 1.7889E-04
        13027.62c 5.0998E-02
c       total      5.4583E-02
m14     92234.69c 2.6648E-05 $ fuel plate 5
        92235.69c 4.1571E-03
        92236.69c 1.5413E-05
        92238.69c 2.2051E-04
        13027.62c 4.9696E-02
c       total      5.4115E-02
m15     92234.69c 2.6746E-05 $ fuel plate 6
        92235.69c 4.1724E-03
        92236.69c 1.5470E-05
        92238.69c 2.2132E-04
        13027.62c 4.9670E-02
c       total      5.4106E-02
m16     92234.69c 2.6790E-05 $ fuel plate 7
        92235.69c 4.1791E-03
        92236.69c 1.5495E-05
        92238.69c 2.2168E-04
        13027.62c 4.9659E-02
c       total      5.4102E-02
m17     92234.69c 2.6830E-05 $ fuel plate 8
        92235.69c 4.1854E-03
        92236.69c 1.5518E-05

```

BRR Package Safety Analysis Report

	92238.69c	2.2201E-04	
	13027.62c	4.9649E-02	
c	total	5.4098E-02	
m18	92234.69c	2.6867E-05	\$ fuel plate 9
	92235.69c	4.1911E-03	
	92236.69c	1.5539E-05	
	92238.69c	2.2232E-04	
	13027.62c	4.9639E-02	
c	total	5.4095E-02	
m19	92234.69c	2.6901E-05	\$ fuel plate 10
	92235.69c	4.1965E-03	
	92236.69c	1.5559E-05	
	92238.69c	2.2260E-04	
	13027.62c	4.9630E-02	
c	total	5.4092E-02	
m20	92234.69c	2.6933E-05	\$ fuel plate 11
	92235.69c	4.2015E-03	
	92236.69c	1.5577E-05	
	92238.69c	2.2287E-04	
	13027.62c	4.9622E-02	
c	total	5.4089E-02	
m21	92234.69c	2.6963E-05	\$ fuel plate 12
	92235.69c	4.2061E-03	
	92236.69c	1.5595E-05	
	92238.69c	2.2311E-04	
	13027.62c	4.9614E-02	
c	total	5.4086E-02	
m22	92234.69c	2.6990E-05	\$ fuel plate 13
	92235.69c	4.2105E-03	
	92236.69c	1.5611E-05	
	92238.69c	2.2334E-04	
	13027.62c	4.9607E-02	
c	total	5.4083E-02	
m23	92234.69c	2.7017E-05	\$ fuel plate 14
	92235.69c	4.2145E-03	
	92236.69c	1.5626E-05	
	92238.69c	2.2356E-04	
	13027.62c	4.9600E-02	
c	total	5.4081E-02	
m24	92234.69c	2.7077E-05	\$ fuel plate 15
	92235.69c	4.2239E-03	
	92236.69c	1.5661E-05	
	92238.69c	2.2406E-04	
	13027.62c	4.9585E-02	
c	total	5.4075E-02	
m25	92234.69c	2.2037E-05	\$ fuel plate 16
	92235.69c	3.4377E-03	
	92236.69c	1.2746E-05	
	92238.69c	1.8235E-04	
	13027.62c	5.0889E-02	
c	total	5.4544E-02	
m26	92234.69c	2.2037E-05	\$ fuel plate 17
	92235.69c	3.4377E-03	
	92236.69c	1.2745E-05	
	92238.69c	1.8235E-04	
	13027.62c	5.0889E-02	
c	total	5.4544E-02	
m27	92234.69c	1.7683E-05	\$ fuel plate 18
	92235.69c	2.7586E-03	
	92236.69c	1.0228E-05	

BRR Package Safety Analysis Report

```

          92238.69c 1.4633E-04
          13027.62c 5.2016E-02
c        total      5.4949E-02
m28      92234.69c 1.7487E-05 $ fuel plate 19
          92235.69c 2.7279E-03
          92236.69c 1.0114E-05
          92238.69c 1.4470E-04
          13027.62c 5.2067E-02
c        total      5.4967E-02
c
*tr2     0 0 0 45 135 90 45 45 90          $ loc 2
*tr3     0 0 0 90 180 90 0 90 90          $ loc 3
*tr4     0 0 0 135 225 90 45 135 90        $ loc 4
*tr5     0 0 0 180 90 90 90 180 90        $ loc 5
*tr6     0 0 0 135 45 90 225 135 90        $ loc 6
*tr7     0 0 0 90 0 90 180 90 90          $ loc 7
*tr8     0 0 0 45 45 90 135 45 90          $ loc 8
*tr11    0 1.7 0                          $ u=20
*tr12    0 0 0 22.5 112.5 90 67.5 22.5 90  $ rotate 22.5 deg
*tr13    0 0 0 67.5 157.5 90 22.5 67.5 90  $ rotate 67.5 deg
c
mode     n
kcode    2500 1.0 50 250
sdef     rad=d1 ext=d2 axs=0 0 1
si1      9.5 16
si2      15 137

```

TRIGA Case D63 (HA_TRIGA_W0C060)

```

TRIGA
300      0          -400 424 -410  fill=1      imp:n=1 $ cavity
c
c        Cask
c
310      4 -7.94    (-424:410:400) 423 -411 -401 imp:n=1 $ inner steel
311      5 -11.35  (-423:411:401) 422 -412 -402 imp:n=1 $ lead
312      4 -7.94    (-422:412:402) 421 -413 -403 imp:n=1 $ outer steel
313      0          (-421:413:403) -405          imp:n=1 $ between
c
999      0          405          imp:n=0
c
c        Universe 1: Basket
c
601      0          601 -611  trcl=1 fill=2      u=1 imp:n=1
602      like 601 but trcl=2          u=1 imp:n=1
603      like 601 but trcl=3          u=1 imp:n=1
604      like 601 but trcl=4          u=1 imp:n=1
605      like 601 but trcl=5          u=1 imp:n=1
606      like 601 but trcl=6          u=1 imp:n=1
607      like 601 but trcl=7          u=1 imp:n=1
608      like 601 but trcl=8          u=1 imp:n=1
610      like 601 but trcl=9          u=1 imp:n=1
611      like 601 but trcl=10         u=1 imp:n=1
612      like 601 but trcl=11         u=1 imp:n=1
613      like 601 but trcl=12         u=1 imp:n=1
614      like 601 but trcl=13         u=1 imp:n=1
615      like 601 but trcl=14         u=1 imp:n=1
616      like 601 but trcl=15         u=1 imp:n=1
617      like 601 but trcl=16         u=1 imp:n=1
618      like 601 but trcl=17         u=1 imp:n=1

```

BRR Package Safety Analysis Report

```

619      like 601 but trcl=18                u=1 imp:n=1
620      like 601 but trcl=19                u=1 imp:n=1
625      2 -0.6          601 #601 #602 #603 #604 #605 #606 #607 #608
          #610 #611 #612 #613 #614 #615 #616 #617
          #618 #619 #620                u=1 imp:n=1
c 630    0          -600                u=1 imp:n=1 $ below
basket
631     4 -7.94          600 -601 -602        u=1 imp:n=1 $ basket plate
632     2 -0.6          600 -601 602        u=1 imp:n=1
633     4 -7.94          603 -604 -600        u=1 imp:n=1 $ bottom
support
634     2 -0.6          604 -600                u=1 imp:n=1
635     2 -0.6          -603 -600            u=1 imp:n=1
c
c      Universe 2: Fuel in tube
c
650     0          -610 fill=3(0 -0.38 111.488) u=2 imp:n=1 $ inside tube
651     4 -7.94          610                u=2 imp:n=1 $ tube
c
c      Universe 3: Fuel
c
200     7 -6.5          31 -32 -10      imp:n=1 u=3 $ zirc rod
201     2 -0.6          31 -32 10 -11  imp:n=1 u=3 $ gap
202     1 9.2354E-02    31 -32 11 -20  imp:n=1 u=3 $ fuel
203     6 -1.6          30 -31 -20      imp:n=1 u=3 $ bottom graphite
204     6 -1.6          32 -33 -20      imp:n=1 u=3 $ top graphite
205     4 -7.94          30 -33 20 -22  imp:n=1 u=3 $ cladding
206     2 -0.6          -30:33:22      imp:n=1 u=3 $ inf. water

10      cz 0.28575    $ zirc OR
11      cz 0.3175     $ fuel IR
20      cz 1.8288     $ fuel OR
22      cz 1.8796     $ cladding OR
c
30      pz -28.448    $ bottom graphite
31      pz -19.05     $ bottom fuel
32      pz 19.05      $ top fuel
33      pz 25.654     $ top graphite
c
400     cz 20.32      $ IR cask
401     cz 22.86      $ IR lead
402     cz 43.18      $ OR lead
403     cz 48.26      $ OR cask
404     cz 78.74      $ 1 foot water reflector
*405    hex 0 0 -25.25 0 0 190.5355 0 48.27 0
c
410     pz 137.1422    $ bottom of lid
411     pz 139.6822    $ steel
412     pz 164.0154    $ lead
413     pz 165.2854    $ steel
414     pz 195.7654    $ 1 foot water reflector
c
420     pz -55.72     $ 1 foot water reflector
421     pz -25.24     $ bottom of cask
422     pz -22.7      $ steel
423     pz -3.0912    $ lead
424     pz 0          $ steel
c
c      basket surfaces
c

```

BRR Package Safety Analysis Report

```

600      pz 18.5928      $ bottom of basket support plate
601      pz 19.2278      $ top of basket support plate
602      cz 20.0025      $ bottom plate
603      cz 15.875       $ IR bottom
604      cz 16.51        $ OR bottom
610      cz 2.2606       $ IR inner tube
611      cz 2.54         $ OR inner tube

m1       1001.62c  5.6041E-02 $ fuel
        40000.66c 3.5025E-02
        92235.69c 9.0406E-04
        92238.69c 3.8442E-04
c        Total      9.2354E-02
mt1      h/zr.60t
        zr/h.60t
m2       1001.62c  2          $ water
        8016.62c  1
mt2      lwtr.60t
m4       6000.66c  -0.08     $ SS-304
        14000.60c -1.0
        15031.66c -0.045
        24000.50c -19.0
        25055.62c -2.0
        26000.55c -68.375
        28000.50c -9.5
m5       82000.50c 1          $ Pb
m6       6000.66c  1          $ graphite
mt6      grph.60t
m7       40000.66c 1          $ Zr
c
*tr1     0 -8.255 0  j j j j j j j j j -1
*tr2     0 -8.255 0  45 135 90 45 45 90 j j j -1
*tr3     0 -8.255 0  90 180 90 0 90 90 j j j -1
*tr4     0 -8.255 0  135 225 90 45 135 90 j j j -1
*tr5     0 -8.255 0  180 270 90 90 180 90 j j j -1
*tr6     0 -8.255 0  135 45 90 225 135 90 j j j -1
*tr7     0 -8.255 0  90 0 90 180 90 90 j j j -1
*tr8     0 -8.255 0  45 45 90 135 45 90 j j j -1
c
*tr9     0 -14.605 0  j j j j j j j j j -1
*tr10    0 -14.605 0  32.7 122.7 90 57.3 32.7 90 j j j -1
*tr11    0 -14.605 0  65.5 155.5 90 24.5 65.5 90 j j j -1
*tr12    0 -14.605 0  98.1 188.1 90 8.1 98.1 90 j j j -1
*tr13    0 -14.605 0  130.8 220.8 90 40.8 130.8 90 j j j -1
*tr14    0 -14.605 0  163.5 253.5 90 73.5 163.5 90 j j j -1
*tr15    0 -14.605 0  163.5 73.5 90 253.5 163.5 90 j j j -1
*tr16    0 -14.605 0  130.8 40.8 90 220.8 130.8 90 j j j -1
*tr17    0 -14.605 0  98.1 8.1 90 188.1 98.1 90 j j j -1
*tr18    0 -14.605 0  65.5 24.5 90 155.5 65.5 90 j j j -1
*tr19    0 -14.605 0  32.7 57.3 90 122.7 32.7 90 j j j -1
c
mode     n
kcode    2500 1.0 50 250
sdef     rad=d1 ext=d2 axs=0 0 1
si1      5.5 16.2
si2      92 130

```

7.0 PACKAGE OPERATIONS

7.1 Procedures for Loading the Package

This section delineates the procedures for loading a payload from the BRR packaging. Hereafter, reference to specific BRR packaging components may be found in Appendix 1.3.3, *Packaging General Arrangement Drawings*.

7.1.1 Preparation for Loading

1. Remove the BRR package tie-down cover from the upper impact limiter.
2. Attach rigging to the upper impact limiter using the three (3) 1/2-13 UNC threaded holes marked as impact limiter lift points.
3. Remove the (8) eight Ø1-inch ball lock pins from each upper impact limiter attachment.
4. Using an overhead crane (or equivalent), lift and remove the upper impact limiter from the cask body.
5. Secure the lift adaptor to the cask body using the four (4) 1-8UNC bolts. Tighten the bolts to 220 ±20 ft-lb torque.
6. Remove the (8) eight Ø1-inch ball lock pins from each lower impact limiter attachment.
7. Lift the cask body from the lower impact limiter, and place it on the facility transport equipment.
8. Secure the cask body to the facility transport equipment, and remove the rigging from the lift adaptor.

7.1.2 Loading of Contents

1. Remove the twelve (12) 1-8UNC socket head cap screws (SHCSs) that retain the closure lid.
2. Install three (3) hoist rings (or equivalent) into the three (3) 1/2-13 UNC threaded holes in the closure lid.
3. Lift and remove the closure lid from the cask body. Store the closure lid in a manner to minimize potential damage to the O-ring seals and sealing surfaces.
4. Install and secure the sealing surface protector to the cask body.
5. Using the center 1/2-13 UNC threaded hole in the shield plug as a lift point, remove the shield plug from the cask body.
6. If not previously installed, install the appropriate fuel basket into the cask body cavity as follows:
 - a. For the MURR basket, use the 3/8-16UNC threaded hole.
 - b. For the MITR-II basket, use the two (2) 3/8-16UNC threaded holes.
 - c. For the ATR basket, use the 3/8-16UNC threaded hole.

- d. For the TRIGA basket, use the 3/8-16UNC threaded hole.
7. Remove the drain port dust cover and then the drain port plug. Install an appropriate fitting to the drain port.
8. Using an overhead crane (or equivalent), and attached to the lift adaptor, lift the cask body with the fuel basket from the facility transport equipment and position over the spent fuel pool staging area.
9. Slowly lower the cask body into the pool until the cavity is flooded, and the cask body is secure in the facility fuel loading station.
10. Load a fuel element into each fuel channel in the fuel basket.
 - a. Up to eight (8) MURR fuel elements may be loaded into the basket.
 - b. Up to eleven (11) MITR-II fuel elements may be loaded into the basket.
 - c. Up to eight (8) ATR fuel elements may be loaded into the basket.
 - d. Up to nineteen (19) TRIGA fuel elements may be loaded into the basket.
11. Using the center 1/2-13 UNC threaded hole as a lift point, lower the shield plug into the cask body cavity. Visually verify that the shield plug is properly seated, and reposition if necessary.
12. Install the shield plug restraint, or optionally, install the shield plug restraint once the cask body has been raised to the working level.
13. Lift the loaded cask body from the spent fuel pool while spraying exposed portions with clean demineralized water. Perform a radiological survey of the cask body as it is raised out of the pool.
14. Open the drain fitting to drain the pool water from the cavity. Continue draining the cavity until no appreciable water is noted. Optionally, the cavity may be drained after securing the cask body in the facility work area.
15. Close the drain fitting, and remove the connecting plumbing from the drain fitting.
16. Lift the loaded cask body out of the spent fuel pool area and secure it in the facility work area.
17. Perform a survey of the exterior surfaces of the cask body to determine that smearable surface contamination meets the requirements of 10 CFR §71.87(i) [1] and 49 CFR §173.443 [2]; decontaminate exposed exterior surfaces that exceed the allowable contamination levels.
18. Visually inspect both closure lid main O-ring seals. If necessary, remove the O-ring seal(s) and clean the seal(s) and the sealing surface(s) on the closure lid and cask body to remove contamination. If, during the visual examination, it is determined that damage to the O-ring seal(s) and/or sealing surface(s) is sufficient to impair containment integrity (e.g., cuts, tears, and/or joint separation in O-ring material, or scratches and/or indentations in sealing areas), replace the damaged seal(s) and/or repair the damaged sealing surface(s) per Section 8.2.3.2, *Sealing Area Routine Inspection and Repair*.
19. As an option, remove and sparingly apply vacuum grease to the O-ring seals and/or sealing surfaces. Reinstall O-ring seals into the appropriate seal grooves in the closure lid.

BRR Package Safety Analysis Report

20. Remove the sealing surface protector and shield plug restraint from the shield plug and cask body.
21. Visually inspect the cask body sealing surface, and clean of contamination or water as necessary. If damage sufficient to impair containment integrity is found, repair the damaged surface per Section 8.2.3.2, *Sealing Area Routine Inspection and Repair*.
22. Install the closure lid on the cask body, using the alignment pin to guide the closure lid into position.
23. Visually inspect the closure SHCSs for wear or damage that could impair their function and, if necessary, replace or repair per the requirements of the drawings in Appendix 1.3.3, *Packaging General Arrangement Drawings*.
24. Install the twelve (12) 1-8UNC SHCSs to secure the closure lid to the cask body. Using a star pattern, tighten the closure SHCSs to 220 ± 20 ft-lb torque (lubricated).
25. Remove the vent port dust cover and the vent port plug.
26. Remove the drain port fitting from the drain port.
27. Visually inspect the drain and vent port sealing surfaces and sealing washers. If necessary, clean the sealing surfaces on the drain and vent ports to remove contamination. If, during the visual examination, it is determined that damage to a sealing surface or a sealing washer is sufficient to impair containment integrity (e.g., cuts, tears, and/or joint separation in sealing material, or scratches and/or indentations in sealing areas), repair the damaged sealing surface per Section 8.2.3.2, *Sealing Area Routine Inspection and Repair*, and/or replace the sealing washers.
28. Install the drain port plug and sealing washer in the drain port. Tighten the drain port plug to 40 ± 4 ft-lb torque.
29. Install the vent port plug and sealing washer to the vent port tool, and then install the vent port tool into the vent port.
30. Connect a vacuum pump and a shutoff valve to the vent port tool and evacuate the cavity until the internal pressure is 1 – 2 torr. Isolate the vacuum pump from the cask body cavity by closing the shutoff valve and shutting off the vacuum pump, closing the shutoff valve and venting the suction line to atmosphere, or other appropriate means that does not maintain a vacuum on the outlet of the shutoff valve.
31. Monitor the cavity pressure for a minimum of 30 minutes. If the cavity pressure does not exceed 3 torr at the end of the time period, proceed to Step 35.
32. If the pressure exceeds 3 torr, open the port tool to re-pressurize the cask body cavity to atmospheric pressure. Repeat Steps 30 and 31.
33. If after eight (8) hours of vacuum drying with air and the pressure exceeds 3 torr, disconnect the vacuum pump from the vent port tool and connect a source of helium gas.
34. Provide a helium atmosphere inside the cask payload cavity by backfilling with helium gas to a pressure of slightly greater than atmospheric pressure, i.e., +1, -0 psig. Repeat Steps 30 and 31.
35. Disconnect the vacuum pump from the vent port tool and connect a source of helium gas.

BRR Package Safety Analysis Report

36. Provide a helium atmosphere inside the cask payload cavity by backfilling with helium gas to a pressure of slightly greater than atmospheric pressure, i.e., +1, -0 psig.
37. Disconnect the helium gas source from the vent port tool.
38. Using the vent port tool, install the vent port plug and sealing washer in the vent port. Tighten the vent port plug to 9 ± 1 ft-lb torque.
39. Leakage rate testing of the main containment O-ring seal, the drain port sealing washer, and the vent port sealing washer shall be performed based on the following criteria:
 - a. If the inner main O-ring seal (containment), the drain port sealing washer, and/or vent port sealing washer are replaced, or the corresponding sealing surface(s) were repaired, then perform the maintenance/periodic leakage rate test per Section 8.2.2.2, *Helium Leakage Rate Testing the Main Containment O-ring Seal*, Section 8.2.2.3, *Helium Leakage Rate Testing the Drain Port Sealing Washer*, or Section 8.2.2.4, *Helium Leakage Rate Testing the Vent Port Sealing Washer*, as appropriate.
 - b. If the inner main O-ring seal (containment), the drain port sealing washer, and/or vent port sealing washer are not replaced, nor the corresponding sealing surface(s) repaired, then perform preshipment leakage rate testing per Section 7.4, *Preshipment Leakage Rate Test*, or per Section 8.2.2.2, *Helium Leakage Rate Testing the Main Containment O-ring Seal*, or Section 8.2.2.3, *Helium Leakage Rate Testing the Drain Port Sealing Washer*, or Section 8.2.2.4, *Helium Leakage Rate Testing the Vent Port Sealing Washer*, as appropriate.
 - c. At the conclusion of all leakage rate testing, install the drain port dust cover and the vent port dust cover.

7.1.3 Preparation for Transport

1. Utilizing the lift adaptor, lift and lower the cask body into the lower impact limiter that is located on the transport trailer. Ensure that the cask body is aligned with the impact limiter alignment stripe for correct circumferential location.
2. Install the (8) eight $\varnothing 1$ -inch ball lock pins into each lower impact limiter attachment.
3. Remove the (4) four 1 – 8 UNC bolts that attach the lift adaptor to the cask body. Remove the lift adaptor. The lifting holes may be optionally plugged.
4. Lift and lower the upper impact limiter onto the cask body. Ensure that the upper impact limiter is aligned with the cask body stripe for correct circumferential location.
5. Install the (8) eight $\varnothing 1$ -inch ball lock pins into each upper impact limiter attachment.
6. Install the tamper-indicating device (security seal) in the appropriate upper impact limiter attachment location.
7. Remove the rigging from the upper impact limiter lift points.
8. Install the BRR package tie-down cover over the upper impact limiter, and secure the cover to the semi-trailer using the tie-down attachments.
9. Monitor external radiation for each loaded BRR package per the requirements of 49 CFR §173.441.

10. Determine that surface contamination levels for each loaded BRR package is per the requirements of 49 CFR §173.443.
11. Determine the transport index for each loaded BRR package per the requirements of 49 CFR §173.403.
12. Complete all necessary shipping papers in accordance with Subpart C of 49 CFR 172 [3].
13. BRR package marking shall be in accordance with 10 CFR §71.85(c) and Subpart D of 49 CFR 172. Package labeling shall be in accordance with Subpart E of 49 CFR 172. Package placarding shall be in accordance with Subpart F of 49 CFR 172.

7.2 Procedures for Unloading the Package

This section delineates the procedures for unloading a payload from the BRR packaging. Hereafter, reference to specific BRR packaging components may be found in Appendix 1.3.3, *Packaging General Arrangement Drawings*.

7.2.1 Receipt of Package from Carrier

1. Remove the BRR package tie-down cover from the upper impact limiter.
2. Verify that the tamper-indicating device (security seal) has not been tampered with or removed.
3. Attach rigging to the upper impact limiter using the three (3) 1/2–13 UNC threaded holes marked as impact limiter lift points.
4. Remove the tamper-indicating device (security seal) and the (8) eight Ø1-inch ball lock pins from each upper impact limiter attachment.
5. Using an overhead crane (or equivalent), lift and remove the upper impact limiter from the cask body.
6. Secure the lift adaptor to the cask body using the (4) four 1–8UNC bolts. Tighten the bolts to 220 ±20 ft-lb.
7. Remove the (8) eight Ø1-inch ball lock pins from each lower impact limiter attachment.
8. Lift the loaded cask body from the lower impact limiter, and place it on the facility transport equipment.
9. Secure the cask body to the facility transport equipment, and remove the rigging from the lift adaptor.

7.2.2 Removal of Contents

The BRR package is designed to be unloaded either in a pool of water (wet) or in a hot cell (dry), as delineated in the following sections.

7.2.2.1 Wet Unloading

1. Remove the vent port dust cover and connect a vent port tool to the vent port. Connect a gas sampling device to the vent port tool.
2. Loosen and remove the vent port plug using the vent port tool so that a gas sample may be extracted from the cavity .
3. Following verification of no contamination in the gas sample, vent the cavity to atmosphere to equalize cavity pressure.
4. Install three (3) hoist rings (or equivalent) into the three (3) 1/2–13 UNC threaded holes in the closure lid.

BRR Package Safety Analysis Report

5. Remove the twelve (12) 1-8UNC socket head cap screws (SHCSs) that secure the closure lid.
6. Lift and remove the closure lid from the cask body. Store the closure lid in a manner to minimize potential damage to the O-ring seals and sealing surfaces.
7. Install and secure the sealing surface protector to the cask body.
8. Install the shield plug restraint over the shield plug in the cask body.
9. Remove the drain port dust cover and then the drain port plug. Install an appropriate fitting to the drain port.
10. Using appropriate rigging and an overhead crane (or equivalent) attached to the lift adaptor, lift the loaded cask body from the facility transport equipment and position over the spent fuel pool staging area.
11. Remove the shield plug restraint, or optionally, remove the restraint after the cask body is secured in the facility fuel unloading station.
12. Slowly lower the cask body into the pool until the cavity is flooded, and secure the loaded cask body in the facility fuel unloading station.
13. Using the center 1/2-13 UNC threaded hole in the shield plug as a lift point, remove the shield plug from the cask body.
14. Remove the fuel elements from the basket and place in the facility's receiving station.
15. Using the center 1/2-13 UNC threaded hole as a lift point, lower the shield plug into the cask body cavity. Visually verify that the shield plug is properly seated, and reposition if necessary.
16. Install the shield plug restraint, or optionally, install the shield plug restraint once the cask body has been raised to the working level.
17. Lift the cask body from the spent fuel pool while spraying exposed portions with clean demineralized water. Perform a radiological survey of the cask body as it is raised out of the pool.
18. Open the drain fitting to drain the pool water from the cavity. Continue draining the cavity until no appreciable water is noted. Optionally, the cavity may be drained after securing the cask body in the facility work area.
19. Close the drain fitting, and remove the connecting plumbing from the drain fitting.
20. Lift the cask body out of the spent fuel pool area and secure it in the facility work area.
21. Perform a survey of the exterior surfaces of the cask body to determine that smearable surface contamination meets the requirements of 10 CFR §71.87(i) and 49 CFR §173.443; decontaminate exposed exterior surfaces that exceed the allowable contamination levels.
22. Remove the sealing surface protector and shield plug restraint from the shield plug and cask body.
23. Install the closure lid on the cask body, using the alignment pin to guide the closure lid into position.

BRR Package Safety Analysis Report

24. Install the twelve (12) 1-8UNC SHCSs to secure the closure to the cask body. Using a star pattern, tighten the closure SHCSs to 220 ± 20 ft-lb torque (lubricated).
25. Install the vent port plug and tighten to 9 ± 1 ft-lb torque. Install the vent port dust cover.
26. Install the drain port plug and tighten to 40 ± 4 ft-lb torque. Install the drain port dust cover.
27. Assemble the impact limiters onto the package and secure the package to the transport trailer as described in Section 7.1.3, *Preparation for Transport*. A tamper-indicating device is not required.

7.2.2.2 Dry Unloading

1. Remove the vent port dust cover and connect a vent port tool to the vent port. Connect a gas sampling device to the vent port tool.
2. Loosen and remove the vent port plug using the vent port tool so that a gas sample may be extracted from the cavity.
3. Following verification of no contamination in the gas sample, vent the cavity to atmosphere to equalize cavity pressure.
4. Install three (3) hoist rings (or equivalent) into the three (3) 1/2-13 UNC threaded holes in the closure lid.
5. Remove the twelve (12) 1-8UNC socket head cap screws (SHCSs) that retain the closure lid.
6. Lift and remove the closure lid from the cask body. Store the closure lid in a manner to minimize potential damage to the O-ring seals and sealing surfaces.
7. Install and secure the sealing surface protector to the cask body.
8. Install the shield plug restraint over the shield plug in the cask body.
9. Install a remote lift adaptor in the center 1/2-13 UNC threaded hole of the shield plug.
10. Place the loaded cask body into the hot cell.
11. Remove the shield plug restraint and lift the shield plug from the cask body.
12. Remove the fuel elements from the basket and place in the facility's receiving station.
13. Replace the shield plug into the cask body cavity and replace the shield plug restraint.
14. Remove the unloaded cask body from the hot cell.
15. Remove the remote lift adaptor from the shield plug.
16. Remove the shield plug restraint and remove the sealing surface protector.
17. Install the closure lid on the cask body, using the alignment pin to guide the closure lid into position.
18. Install the twelve (12) 1-8UNC SHCSs to secure the closure to the cask body. Using a star pattern, tighten the closure SHCSs to 220 ± 20 ft-lb torque (lubricated).
19. Install the vent port plug and tighten to 9 ± 1 ft-lb torque. Install the vent port dust cover.
20. If used, install the drain port plug and tighten to 40 ± 4 ft-lb torque. Install the drain port dust cover.

21. Assemble the impact limiters onto the package and secure the package to the transport trailer as described in Section 7.1.3, *Preparation for Transport*. A tamper-indicating device is not required.

7.3 Preparation of an Empty Package for Transport

Previously used and empty BRR packagings shall be prepared and transported per the requirements of 49 CFR §173.428.

7.4 Preshipment Leakage Rate Test

After the BRR package is assembled and prior to shipment, leakage rate testing shall be performed to confirm proper assembly of the package following the guidelines of Section 7.6, *Preshipment Leakage Rate Test*, and Appendix A.5.2, *Gas Pressure Rise*, of ANSI N14.5 [4].

7.4.1 Gas Pressure Rise Leakage Rate Test Acceptance Criteria

In order to demonstrate containment integrity in preparation for shipment, no leakage shall be detected when tested to a sensitivity of 1×10^{-3} reference cubic centimeters per second (ref-cm³/s) air, or less, per Section 7.6, *Preshipment Leakage Rate Test*, of ANSI N14.5.

7.4.2 Determining the Test Volume and Test Time

1. Assemble a leakage rate test apparatus that consists of, at a minimum, the components illustrated in Figure 7.4–1, using a calibrated volume with a range of 6 – 31 cubic inches, and a calibrated pressure transducer with a minimum sensitivity of 100 millitorr. Connect the test apparatus to the test volume (i.e., the seal test port, or vent port insert, as appropriate).
2. Set the indicated sensitivity on the digital readout of the calibrated pressure transducer, ΔP , to, at a minimum, the resolution (i.e., sensitivity) of the calibrated pressure transducer (e.g., $\Delta P = 1, 10, \text{ or } 100$ millitorr sensitivity).
3. Open all valves (i.e., the vent valve, calibration valve, and vacuum pump isolation valve), and record ambient atmospheric pressure, P_{atm} .
4. Isolate the calibrated volume by closing the vent and calibration valves.
5. Evacuate the test volume to a pressure less than the indicated sensitivity on the digital readout of the calibrated pressure transducer or 1.0 torr, whichever is less.
6. Isolate the vacuum pump from the test volume by closing the vacuum pump isolation valve. Allow the test volume pressure to stabilize and record the test volume pressure, P_{test} (e.g., $P_{\text{test}} < 1$ millitorr for an indicated sensitivity of 1 millitorr).
7. Open the calibration valve and, after allowing the system to stabilize, record the total volume pressure, P_{total} .
8. Knowing the calibrated volume, V_c , calculate and record the test volume, V_t , using the following equation:

$$V_t = V_c \left(\frac{P_{\text{atm}} - P_{\text{total}}}{P_{\text{total}} - P_{\text{test}}} \right)$$

9. Knowing the indicated sensitivity on the digital readout of the calibrated pressure transducer, ΔP , calculate and record the test time, t , using the following equation:

$$t = \Delta P(1.32)V_t$$

7.4.3 Performing the Gas Pressure Rise Leakage Rate Test

1. Isolate the calibrated volume by closing the calibration valve.
2. Open the vacuum pump isolation valve and evacuate the test volume to a pressure less than the test volume pressure, P_{test} , determined in Step 6 of Section 7.4.2, *Determining the Test Volume and Test Time*.
3. Isolate the vacuum pump from the test volume by closing the vacuum pump isolation valve. Allow the test volume pressure to stabilize and record the beginning test pressure, P_1 . After a period of time equal to “t” seconds, determined in Step 9 of Section 7.4.2, *Determining the Test Volume and Test Time*, record the ending test pressure, P_2 . To be acceptable, there shall be no difference between the final and initial pressures such that the requirements of Section 7.4.1, *Gas Pressure Rise Leakage Rate Test Acceptance Criteria*, are met.
4. If, after repeated attempts, the O-ring seal fails to pass the leakage rate test, replace the damaged seal and/or repair the damaged sealing surfaces per Section 8.2.3.2.1, *Seal Area Routine Inspection and Repair*. Perform verification leakage rate test per the applicable procedure delineated in Section 8.2.2, *Maintenance/Periodic Leakage Rate Tests*.

7.4.4 Optional Preshipment Leakage Rate Test

As an option to Section 7.4.3, *Performing the Gas Pressure Rise Leakage Rate Test*, Section 8.2.2, *Maintenance/Periodic Leakage Rate Tests*, may be performed.

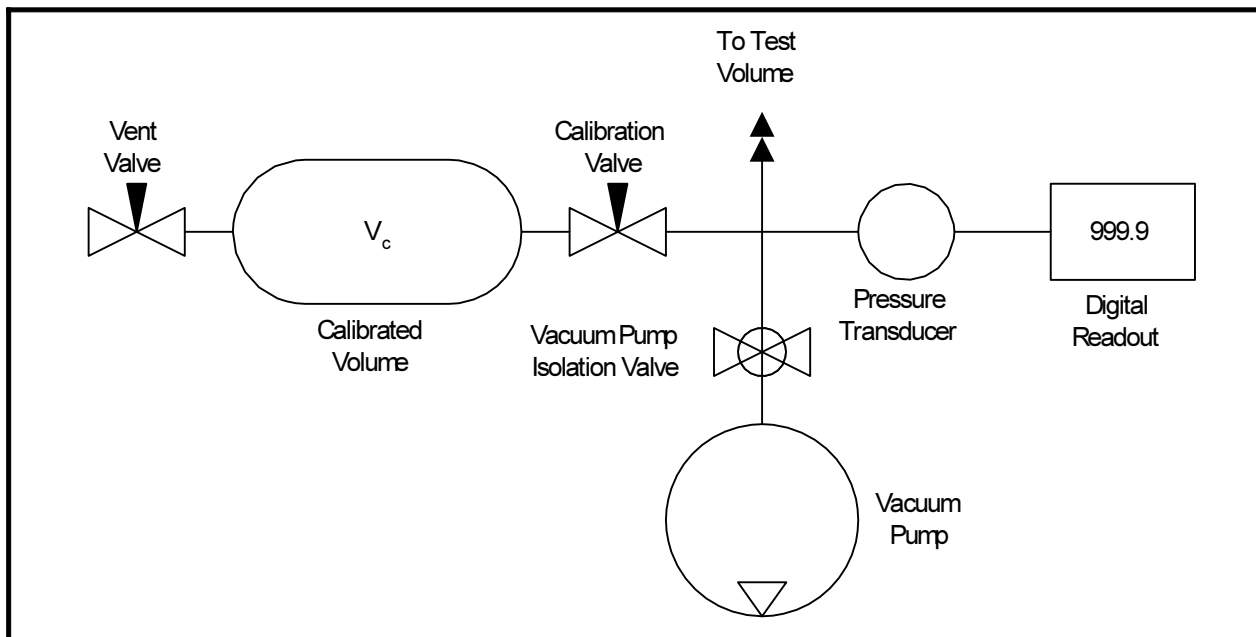


Figure 7.4-1 – Pressure Rise Leakage Rate Test Schematic

7.5 Appendix

7.5.1 References

1. Title 10, Code of Federal Regulations, Part 71 (10 CFR 71), *Packaging and Transportation of Radioactive Material*, 01–01–08 Edition.
2. Title 49, Code of Federal Regulations, Part 173 (49 CFR 173), *Shippers–General Requirements for Shipments and Packagings*, 10–01–08 Edition
3. Title 49, Code of Federal Regulations, Part 172 (49 CFR 172), *Hazardous Materials Tables and Hazardous Communications Regulations*, 10–01–08 Edition.
4. ANSI N14.5–1997, *American National Standard for Radioactive Materials – Leakage Tests on Packages for Shipment*, American National Standards Institute (ANSI), Inc.

8.0 ACCEPTANCE TESTS AND MAINTENANCE PROGRAM

This section describes the acceptance tests and the maintenance program that shall be used on the BRR package in compliance with Subpart G of 10 CFR 71 [1].

8.1 Acceptance Tests

Per the requirements of 10 CFR §71.85, this section discusses the inspections and tests to be performed prior to first use of the BRR packaging. Acceptance criteria for all inspections and tests are found either on the drawings in Appendix 1.3.3, *Packaging General Arrangement Drawings*, or in the sections that follow. Deviations from requirements will be recorded and dispositioned in accordance with the cognizant quality assurance program.

8.1.1 Visual Inspection and Measurements

Each BRR packaging will be visually inspected and measured to ensure that all of the requirements delineated on the drawings in Appendix 1.3.3, *Packaging General Arrangement Drawings*, are satisfied. This includes but is not limited to such items as materials, physical arrangement of components, quantities, dimensions, welds, and measurements.

8.1.2 Weld Examinations

The locations, types, and sizes of all welds will be identified and recorded to ensure compliance with the drawings in Appendix 1.3.3, *Packaging General Arrangement Drawings*. All welds are subject to visual examination per AWS D1.6 [2]. The welds between the inner containment shell and either end structure, the welds between the outer shell and either end structure, and the longitudinal weld(s) in the outer shell, if any, are examined by ultrasonic inspection in accordance with the ASME Code, Subsection NB, Article NB-5000, and Section V, Article 4 [4]. Optionally, the weld between the inner containment shell and the lower end structure may be examined by radiographic inspection in accordance with the ASME Code, Subsection NB, Article NB-5000, and Section V, Article 2 [3]. All welds on the BRR package, except seal welds, are liquid penetrant inspected on the final pass in accordance with the ASME Code, Subsection Nx, Article Nx-5000, and Section V, Article 6 [5]. The appropriate Subsection for the containment welds and outer shell welds is NB; for other cask body welds and the impact limiter shells, NF; and for the fuel baskets, NG.

8.1.3 Structural and Pressure Tests

8.1.3.1 Lifting Device Load Testing

The BRR package does not contain any lifting devices that require load testing.

8.1.3.2 Containment Boundary Pressure Testing

The BRR package containment boundary shall be pressure tested to the greater of 125% of the design pressure per the requirements of ASME Code, Subsection NB, Article NB-6220 [6], or

150% of the maximum normal operating pressure (MNOP), per 10 CFR §71.85(b). Since the MNOP of the BRR package is 10 psig, and the design pressure is 25 psig, the test pressure shall be a minimum of $1.25 \times 25 = 31.25$ psig.

Following pressure testing of the containment boundary, welds directly related to the pressure testing and accessible base material adjacent to the welds shall be visually inspected for plastic deformation or cracking in accordance with AWS D1.6, and liquid penetrant inspected per ASME Code, Subsection NB, Article NB-5000, and Section V, Article 6, as delineated on the drawings in Appendix 1.3.3, *Packaging General Arrangement Drawings*. Indications of cracking or distortion shall be recorded and evaluated in accordance with the cognizant quality assurance program.

Except for the leakage rate testing of the containment body structure prior to lead pour, leakage rate testing per Section 8.1.4, *Fabrication Leakage Rate Tests*, shall be performed after completion of pressure testing to verify package configuration and performance to design criteria.

8.1.4 Fabrication Leakage Rate Tests

This section provides the generalized procedure for fabrication leakage rate testing of the containment vessel boundaries and penetrations during and following the completion of fabrication. Fabrication leakage rate testing shall follow the guidelines of Section 7.3, *Fabrication Leakage Rate Test*, of ANSI N14.5 [7].

Prior to leakage rate testing, internal components that are not permanently affixed to the containment boundary, such as shield plug and spent fuel baskets, shall be removed. For ease of leakage rate testing, the interior surfaces of the containment boundary should be thoroughly cleaned.

Fabrication leakage rate testing shall be performed on the containment boundary. Four separate tests comprise the series. Each test shall meet the acceptance criteria delineated in Section 8.1.4.1, *Fabrication Leakage Rate Test Acceptance Criteria*.

8.1.4.1 Fabrication Leakage Rate Test Acceptance Criteria

1. To be acceptable, each leakage rate test shall demonstrate a “leaktight” leakage rate of 1×10^{-7} reference cubic centimeters per second (ref-cm³/s), air, or less, per Section 6.3, *Application of Reference Air Leakage Rate (L_R)*, of ANSI N14.5.
2. In order to demonstrate the leaktight leakage rate, the sensitivity of the leakage rate test procedure shall be 5×10^{-8} cm³/s, air, or less, per Section 8.4, *Sensitivity*, of ANSI N14.5.
3. Failure to meet the stated leakage rate shall be recorded and evaluated in accordance with the cognizant quality assurance program.

8.1.4.2 Helium Leakage Rate Testing the Containment Structure Integrity

Fabrication leakage rate testing of the containment structure integrity is performed in two stages: prior to lead pour, and following lead pour. These two stages are necessitated by the in-situ lead shielding surrounding the cylindrical containment shell between the upper and lower end structures, which would prevent helium gas from reaching the surface of the steel.

8.1.4.2.1 Containment Body Structure (Prior to Lead Pour)

This leakage rate test verifies the leak tightness of the upper and lower end forgings/castings, and the inner shell that comprise the primary metallic containment boundary of the BRR packaging.

1. The fabrication leakage rate test shall be performed following the guidelines of Section A.5.3, *Gas Filled Envelope – Gas Detector*, of ANSI N14.5.
2. The BRR packaging shall be assembled with a test lid and seal in place of the closure lid onto the partially fabricated cask, consisting of the upper and lower end structures, inner containment shell, and outer structural shell.
3. Connect a port tool to the drain port in the lower end forging.
4. Install a helium mass spectrometer leak detector (MSLD) to the port tool. Evacuate through the drain port until the vacuum is sufficient to operate the MSLD.
5. Surround the outer surface of the containment body with an envelope filled with helium gas (99% purity or better) to a minimum concentration of 50%, and to a pressure slightly greater than atmospheric pressure. The final leakage rate shall be adjusted for the helium concentration in the envelope.
6. Perform the helium leakage rate test to the requirements of Section 8.1.4.1, *Fabrication Leakage Rate Test Acceptance Criteria*. If, after repeated attempts, the containment structure fails to pass the leakage rate test, isolate the leak path and, prior to repairing the leak path and repeating the leakage rate test, record on a nonconformance report and disposition prior to final acceptance in accordance with the cognizant quality assurance program.
7. Disconnect the port tool from the drain port in the lower end forging.

8.1.4.2.2 Containment Body Structure (Following Lead Pour)

This leakage rate test verifies the leak tightness of the closure lid, and the final machined configuration of the upper end structure that comprise the balance of the metallic containment boundary of the BRR packaging.

1. The fabrication leakage rate test shall be performed following the guidelines of Section A.5.3, *Gas Filled Envelope – Gas Detector*, of ANSI N14.5.
2. The BRR packaging shall be assembled with the two O-ring seals installed in the closure lid, and the vent and seal test port plugs installed with their associated sealing washers. If not previously tightened, tighten the closure lid bolts to 200 – 240 ft-lb torque (lubricated). Assembly is as shown in Appendix 1.3.3, *Packaging General Arrangement Drawings*.
3. Connect a port tool to the drain port in the lower end of the packaging.
4. Install a helium mass spectrometer leak detector (MSLD) to the port tool. Evacuate through the drain port until the vacuum is sufficient to operate the MSLD.
5. Surround the outer surface of the closure lid and upper end structure with an envelope filled with helium gas (99% purity or better) to a minimum concentration of 50%, and to a pressure slightly greater than atmospheric pressure. The final leakage rate shall be adjusted for the helium concentration in the envelope.

BRR Package Safety Analysis Report

6. Perform the helium leakage rate test to the requirements of Section 8.1.4.1, *Fabrication Leakage Rate Test Acceptance Criteria*. If, after repeated attempts, the containment structure fails to pass the leakage rate test, isolate the leak path and, prior to repairing the leak path and repeating the leakage rate test, record on a nonconformance report and disposition prior to final acceptance in accordance with the cognizant quality assurance program.
7. Remove the port tool and re-install the drain port plug. Tighten to 36 – 44 ft-lb torque.

8.1.4.3 Helium Leakage Rate Testing the Main Containment O-ring Seal

1. The fabrication leakage rate test of the BRR package containment O-ring seal integrity shall be performed following the guidelines of Section A.5.4, *Evacuated Envelope – Gas Detector*, of ANSI N14.5.
2. Assemble the BRR package with the two O-ring seals installed in the closure lid. Ensure the vent and seal test ports are installed with their associated sealing washers. Assembly is as shown in Appendix 1.3.3, *Packaging General Arrangement Drawings*.
3. Utilizing a port tool, attach a vacuum pump and a source of helium gas, in parallel, to the vent port.
4. Close the valve to the source of helium gas and open the valve to the vacuum pump.
5. Utilizing a port tool, rotate the vent port plug to the open position.
6. Evacuate the system to a 90% vacuum or better ($\leq 10\%$ ambient atmospheric pressure). Isolate the vacuum pump from the system.
7. Provide a helium atmosphere inside the evacuated cavity by backfilling with helium gas (99% purity or better) to ambient atmospheric pressure (+1 psi, -0 psi).
8. Utilizing the port tool, rotate the vent port plug to the closed position, and remove the helium-contaminated port tool from the vent port.
9. Install a clean (helium-free) port tool into the seal test port.
10. Utilizing appropriate fittings, attach a helium MSLD to the port tool.
11. Utilizing the port tool, rotate the seal test port plug to the open position.
12. Evacuate the cavity between the containment O-ring seal and the test O-ring seal until the vacuum is sufficient to operate the leak detector per the manufacturer's recommendations.
13. Perform the helium leakage rate test to the requirements of Section 8.1.4.1, *Fabrication Leakage Rate Test Acceptance Criteria*. If, after repeated attempts, the BRR package containment O-ring seal fails to pass the leakage rate test, isolate the leak path and, prior to repairing the leak path and repeating the leak test, record on a nonconformance report and disposition prior to final acceptance in accordance with the cognizant quality assurance program.

8.1.4.4 Helium Leakage Rate Testing the Drain Port Sealing Washer

1. The fabrication leakage rate test of the drain port plug containment sealing washer integrity shall be performed following the guidelines of Section A.5.4, *Evacuated Envelope – Gas Detector*, of ANSI N14.5.

BRR Package Safety Analysis Report

2. The BRR package shall be assembled with the two O-ring seals installed on the closure lid. Ensure the vent and seal test port plugs are installed with their associated sealing washers. Assembly is as shown in Appendix 1.3.3, *Packaging General Arrangement Drawings*.
3. Verify the presence of a helium atmosphere below the vent port plug containment sealing washer, as specified above in Steps 3 – 8 of Section 8.1.4.3, *Helium Leakage Rate Testing the Main Containment O-ring Seal*.
4. Install a port tool into the drain port.
5. Utilizing appropriate fittings, attach a helium MSLD to the port tool.
6. Evacuate the cavity above the drain port plug containment sealing washer until the vacuum is sufficient to operate the leak detector per the manufacturer's recommendations.
7. Perform the helium leakage rate test to the requirements of Section 8.1.4.1, *Fabrication Leakage Rate Test Acceptance Criteria*. If, after repeated attempts, the drain port plug containment sealing washer fails to pass the leakage rate test, isolate the leak path and, prior to repairing the leak path and repeating the leak test, record on a nonconformance report and disposition prior to final acceptance in accordance with the cognizant quality assurance program.

8.1.4.5 Helium Leakage Rate Testing the Vent Port Sealing Washer

The fabrication leakage rate test of the vent port sealing washer may also be performed during the leakage rate testing of the metallic containment boundary following lead pour per Section 8.1.4.2.2, *Containment Body Structure (Following Lead Pour)*.

1. The fabrication leakage rate test of the vent port plug containment sealing washer integrity shall be performed following the guidelines of Section A.5.4, *Evacuated Envelope – Gas Detector*, of ANSI N14.5.
2. The BRR package shall be assembled with the two O-ring seals installed on the closure lid. Ensure the vent and seal test port plugs are installed with their associated sealing washers. Assembly is as shown in Appendix 1.3.3, *Packaging General Arrangement Drawings*.
3. Verify the presence of a helium atmosphere below the vent port plug containment sealing washer, as specified above in Steps 3 – 8 of Section 8.1.4.3, *Helium Leakage Rate Testing the Main Containment O-ring Seal*.
4. Install a port tool into the vent port.
5. Utilizing appropriate fittings, attach a helium MSLD to the port tool.
6. Evacuate the cavity above the vent port plug containment sealing washer until the vacuum is sufficient to operate the leak detector per the manufacturer's recommendations.
7. Perform the helium leakage rate test to the requirements of Section 8.1.4.1, *Fabrication Leakage Rate Test Acceptance Criteria*. If, after repeated attempts, the vent port plug containment sealing washer fails to pass the leakage rate test, isolate the leak path and, prior to repairing the leak path and repeating the leak test, record on a nonconformance report and disposition prior to final acceptance in accordance with the cognizant quality assurance program.

8.1.5 Component and Material Tests

8.1.5.1 Polyurethane Foam

This section establishes the requirements and acceptance criteria for installation, inspection, and testing of the rigid, closed-cell, polyurethane foam utilized within the BRR packaging impact limiters.

8.1.5.1.1 Introduction and General Requirements

The polyurethane foam used within the BRR packaging is comprised of a specific “formulation” of foam constituents that, when properly apportioned, mixed, and reacted, produce a polyurethane foam material with physical characteristics consistent with the requirements given in Section 8.1.5.1.2, *Physical Characteristics*. In practice, the chemical constituents are batched into multiple parts (e.g., parts A and B) for later mixing in accordance with a formulation. Therefore, a foam “batch” is considered to be a specific grouping and apportionment of chemical constituents into separate and controlled vats or bins for each foam formulation part. Portions from each batch part are combined in accordance with the foam formulation requirements to produce the liquid foam material for pouring into a component or box. Thus, a foam “pour” is defined as apportioning and mixing the batch parts into a desired quantity for subsequent installation (pouring). Finally, all contiguous pours into a single mold are termed a “bun”.

The following sections describe the general requirements for constituent storage, and foam pour and test data records.

8.1.5.1.1.1 Polyurethane Foam Constituent Storage

The foam supplier shall certify that the polyurethane foam constituents have been properly stored prior to use, and that the polyurethane foam constituents have been used within their shelf life.

8.1.5.1.1.2 Impact Limiter Shell Preparation

Prior to installing foam into the impact limiter shells, the interior surfaces of the shells shall be treated with an antibonding agent, such as a paste wax.

8.1.5.1.1.3 Polyurethane Foam Installation

The foam shall be installed while the longitudinal axis of the impact limiter shell is vertical. The walls of the shell where the liquid foam material is to be installed shall be between 55 °F and 95 °F prior to foam installation. Measure and record the shell temperature to an accuracy of ± 2 °F prior to foam installation.

In the case of multiple pours into a single impact limiter, the cured level of each pour shall be measured and recorded to an accuracy of ± 1 inch.

Measure and record the weight of liquid foam material installed during each pour to an accuracy of ± 10 pounds.

All test samples shall be poured into disposable containers at the same time as the actual pour it represents, clearly marking the test sample container with the pour date and a unique pour

identification number. All test samples shall be cut from a larger block to obtain freshly cut faces. Prior to physical testing, each test sample shall be cleaned of superfluous foam dust.

8.1.5.1.1.4 Polyurethane Foam Pour and Test Data Records

A production pour and testing record shall be compiled by the foam supplier during the foam pouring operation and subsequent physical testing. Upon completion of production and testing, the foam supplier shall issue a certification referencing the production record data and test data pertaining to each foamed component. At a minimum, relevant pour and test data shall include:

- formulation, batch, and pour numbers, with foam material traceability, and pour date,
- instrumentation description, serial number, and calibration due date,
- pour and test data (e.g., date, temperature, dimensional, and/or weight measurements, compressive stress, etc., as applicable), and
- technician and Quality Assurance/Quality Control (QA/QC) sign-off.

8.1.5.1.2 Physical Characteristics

The following subsections define the required physical characteristics of the polyurethane foam material.

Testing for the various polyurethane foam physical characteristics is based on a “formulation”, “batch”, or “pour”, as appropriate, as defined in Section 8.1.5.1.1, *Introduction and General Requirements*. The physical characteristics determined for a specific foam formulation are relatively insensitive to small variations in chemical constituents and/or environmental conditions, and therefore include physical testing only for leachable chlorides, thermal conductivity, and specific heat. Similarly, the physical characteristics determined for a batch are only slightly sensitive to small changes in formulation and/or environmental conditions during batch mixing, and therefore include physical testing only for flame retardancy. Finally, the physical characteristics determined for a pour are also only slightly sensitive to small changes in formulation and slightly more sensitive to variations in environmental conditions during pour mixing, and therefore include physical testing for density and compressive stress.

8.1.5.1.2.1 Physical Characteristics Determined for a Foam Formulation

8.1.5.1.2.1.1 Leachable Chlorides

The leachable chloride physical characteristic shall be determined once for a particular foam formulation. If multiple components are to utilize a specific foam formulation, then additional physical testing, as defined below, need not be performed.

1. The leachable chlorides test shall be performed using an ion chromatograph (IC) apparatus. The IC measures inorganic anions of interest (i.e., chlorides) in water. Description of a typical IC is provided in EPA Method 300.0 [8]. The IC shall be calibrated against a traceable reference specimen per the IC manufacturer’s operating instructions.
2. One test sample shall be taken from a pour for each foam formulation. The test sample shall be a cube with dimensions of 2.00 ± 0.06 in.

BRR Package Safety Analysis Report

3. Place the test sample in a room (ambient) temperature environment (i.e., 68 °F to 86 °F) for sufficient time to thermally stabilize the test sample. Measure and record the room temperature to an accuracy of ± 2 °F.
4. Obtain a minimum of 550 mL of distilled or de-ionized water for testing. The test water shall be from a single source to ensure consistent anionic properties for testing control.
5. Obtain a 400 mL, or larger, contaminant free container that is capable of being sealed. Fill the container with 250 ± 3 mL of test water. Fully immerse the test sample inside the container for a duration of 72 ± 3 hours. If necessary, use an inert standoff to ensure the test sample is completely immersed for the full test duration. Seal the container prior to the 72-hour duration.
6. Obtain a second, identical container to use as a “control”. Fill the control container with 250 ± 3 mL of the same test water. Seal the control container prior to the 72-hour duration.
7. At the end of the test period, measure and record the leachable chlorides in the test water per the IC manufacturer’s operating instructions. The leachable chlorides in the test water shall not exceed one part per million (1 ppm).
8. Should leachable chlorides in the test water exceed 1 ppm, measure and record the leachable chlorides in the test water from the “control” container. The difference in leachable chlorides from the test water and “control” water sample shall not exceed 1 ppm.

8.1.5.1.2.1.2 Thermal Conductivity

1. The thermal conductivity test shall be performed using a heat flow meter (HFM) apparatus. The HFM establishes steady state unidirectional heat flux through a test specimen between two parallel plates at constant but different temperatures. By measurement of the plate temperatures and plate separation, Fourier’s law of heat conduction is used by the HFM to automatically calculate thermal conductivity. Description of a typical HFM test method is provided in ASTM C518 [9]. The HFM shall be calibrated against a traceable reference specimen per the HFM manufacturer’s operating instructions.
2. Three test samples shall be taken from the sample pour. Each test sample shall be of sufficient size to enable testing per the HFM manufacturer’s operating instructions.
3. Place the test samples in a room (ambient) temperature environment (i.e., 68 °F to 86 °F) for sufficient time to thermally stabilize the test samples.
4. Measure and record the necessary test sample parameters as input data to the HFM apparatus per the HFM manufacturer’s operating instructions.
5. Perform thermal conductivity testing and record the measured thermal conductivity for each test sample following the HFM manufacturer’s operating instructions.
6. Determine and record the average thermal conductivity of the three test samples. The numerically averaged thermal conductivity of the three test samples shall be within the range between 0.17 and 0.25 (BTU-in)/(hr-ft²-°F).

8.1.5.1.2.1.3 Specific Heat

1. The specific heat test shall be performed using a differential scanning calorimeter (DSC) apparatus. The DSC establishes a constant heating rate and measures the differential heat flow into both a test specimen and a reference specimen. Description of a typical DSC is provided in ASTM E1269 [10]. The DSC shall be calibrated against a traceable reference specimen per the DSC manufacturer's operating instructions.
2. Three test samples shall be taken from the sample pour. Each test sample shall be of sufficient size to enable testing per the DSC manufacturer's operating instructions.
3. Place the test samples in a room (ambient) temperature environment (i.e., 68 °F to 86 °F) for sufficient time to thermally stabilize the test samples.
4. Measure and record the necessary test sample parameters as input data to the DSC per the DSC manufacturer's operating instructions.
5. Perform specific heat testing and record the measured specific heat for each test sample following the DSC manufacturer's operating instructions.
6. Determine and record the average specific heat of the three test specimens. The numerically averaged specific heat of the three test samples shall be within the range between 0.28 and 0.42 Btu/lb_m-°F.

8.1.5.1.2.2 Physical Characteristics Determined for a Foam Batch

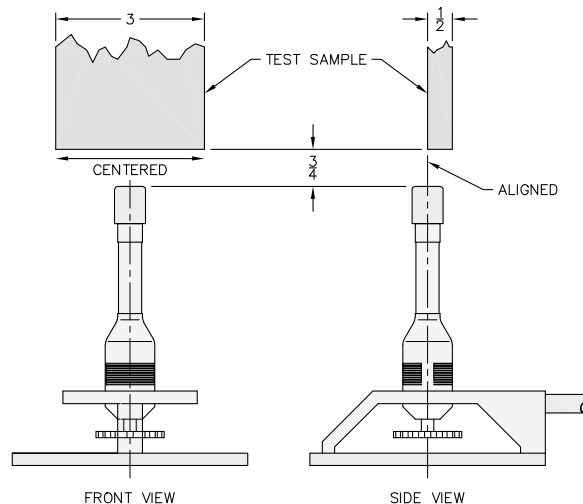
Polyurethane foam material physical characteristics for flame retardancy shall be determined once for a particular foam batch based on the batch definition in Section 8.1.5.1.1, *Introduction and General Requirements*. If single or multiple components are to utilize a single foam batch, then additional flame retardancy testing, as defined below, need not be performed for each foam pour.

Polyurethane foam shall be tested for flame retardancy as follows:

1. Three test samples shall be taken from a pour from each foam batch. Each test sample shall be a rectangular prism with nominal dimensions of 0.5 inches thick, 3.0 inches wide, and a minimum length of 7.0 inches. In addition, individual sample lengths must not be less than the total burn length observed for the sample when tested.
2. Place the test samples in a room (ambient) temperature environment (i.e., 68 °F to 86 °F) for sufficient time to thermally stabilize the test samples. Measure and record the room temperature to an accuracy of ± 2 °F.
3. Measure and record the length of each test sample to an accuracy of ± 0.15 in.

BRR Package Safety Analysis Report

4. Install an approximately 3/8-inch, or larger, Bunsen or Tirrill burner inside an enclosure of sufficient size to perform flame retardancy testing. Adjust the burner flame height to 1 1/2 ± 1/4 inch. Verify that the burner flame temperature is 1,550 °F, minimum.
5. Support the test sample with the long axis oriented vertically within the enclosure such that the test sample's bottom edge will be 3/4 ± 1/8 inch (see adjacent figure) above the top edge of the burner.



6. Move the burner flame under the test sample for an elapsed time of 60 ± 2 seconds. As illustrated, align the burner flame with the front edge of the test sample thickness and the center of the test sample width.
7. Immediately after removal of the test sample from the burner flame, measure and record the following data:
 - a. Measure and record, to the nearest second, the elapsed time until flames from the test sample extinguish.
 - b. Measure and record, to the nearest second, the elapsed time from the occurrence of drips, if any, until drips from the test sample extinguish.
 - c. Measure and record, to the nearest 0.15 inch, the burn length following cessation of all visible burning and smoking.
8. Flame retardancy testing acceptance is based on the following criteria:
 - a. The numerically averaged flame extinguishment time of the three test samples shall not exceed fifteen seconds.
 - b. The numerically averaged flame extinguishment time of drips from the three test samples shall not exceed three seconds.
 - c. The numerically averaged burn length of the three test samples shall not exceed 6.0 in.

8.1.5.1.2.3 Physical Characteristics Determined for a Foam Pour

8.1.5.1.2.3.1 Density

Polyurethane foam material physical characteristic for density shall be determined for each foam pour based on the pour definition in Section 8.1.5.1.1, *Introduction and General Requirements*.

1. Three test samples shall be taken from the foam pour. Each test sample shall be a rectangular prism with minimum nominal dimensions of 1.0 inch thick (T) × 2.0 inch wide (W) × 2.0 inch long (L).

BRR Package Safety Analysis Report

2. Place the test samples in a room (ambient) temperature environment (i.e., 68 °F to 86 °F) for sufficient time to thermally stabilize the test samples. Measure and record the room temperature to an accuracy of ± 2 °F.
3. Measure and record the weight of each test sample to an accuracy of ± 1 gram.
4. Measure and record the thickness, width, and length of each test sample to an accuracy of ± 0.03 in.
5. Determine and record the room temperature density of each test sample utilizing the following formula:

$$\rho_{foam} = \frac{\text{Weight, g}}{453.6 \text{ g/lb}_m} \times \frac{1,728 \text{ in}^3/\text{ft}^3}{T \times W \times L, \text{ in}^3}, \text{ lb}_m/\text{ft}^3$$

6. Determine and record the average density of the three test samples. The numerically averaged density of the three test samples shall be within $\pm 15\%$ of the specified nominal foam density, i.e., within the range of 7.7 to 10.4 lb_m/ft^3 for a nominal 9 lb_m/ft^3 foam.

8.1.5.1.2.3.2 Compressive Stress

1. Three test samples shall be taken from each foam pour. Each test sample shall be a rectangular prism with minimum nominal dimensions of 1.0 inch thick (T) \times 2.0 inch wide (W) \times 2.0 inch long (L). The thickness dimension shall be the parallel-to-rise direction (for the perpendicular-to-rise direction, see below).
2. Place the test samples in a room (ambient) temperature environment (i.e., 68 °F to 86 °F) for sufficient time to thermally stabilize the test samples. Measure and record the room temperature to an accuracy of ± 2 °F.
3. Measure and record the thickness, width, and length of each test sample to an accuracy of ± 0.03 inch.
4. Compute and record the surface area of each test sample by multiplying the width by the length (i.e., $W \times L$).
5. Place a test sample in a Universal Testing Machine. Lower the machine's crosshead until it touches the test sample. Set the machine's parameters for the thickness of the test sample.
6. Determine and record the average parallel-to-rise compressive stress of the three test samples from each batch pour for each foam density. As shown in Table 8.1-1, the average parallel-to-rise compressive stress for each foam pour shall be the nominal compressive stress $\pm 15\%$ at strains of 20%, 40%, and 70%.
7. Determine and record the average parallel-to-rise compressive stress of all test samples from each foamed component. As shown in Table 8.1-1, the average parallel-to-rise compressive stress for all foam pours used in a single bun shall be the nominal compressive stress $\pm 10\%$ at strains of 20%, 40%, and 70%.
8. Data for compressive stress in the perpendicular-to-rise direction shall be obtained in an identical manner, using three additional test samples, except that the thickness dimension of the test samples shall be perpendicular to the foam rise direction. As shown in Table 8.1-2, the average perpendicular-to-rise compressive stress for each foam pour shall be the nominal compressive stress $\pm 15\%$ at strains of 20%, 40%, and 70%. As further shown in

Table 8.1-2, the average perpendicular-to-rise compressive stress for all foam pours used in a single bun shall be the nominal compressive stress $\pm 10\%$ at strains of 20%, 40%, and 70%.

8.1.5.2 Butyl Rubber O-rings

Physical characteristics of the butyl rubber containment O-ring seals and sealing washers for the following parameters shall be determined for each lot based on the following acceptance tests. All material shall conform to the following ASTM D2000 [11] designation:

M4AA710 A13 B13 F17 F48 Z Trace Element.

8.1.5.2.1 Durometer

The durometer of each lot of the butyl rubber material shall be determined in accordance with ASTM D2240 [12]. Each lot of butyl rubber material shall have a hardness of 70 ± 5 Shore A durometer (i.e., within the range of 65 to 75 Shore A durometer).

8.1.5.2.2 Tensile Strength and Elongation

The tensile strength of each lot of the butyl rubber material shall be determined in accordance with ASTM D412 [13]. Each lot of butyl rubber material shall have a minimum tensile strength of 10 MPa and a minimum elongation of 250%.

8.1.5.2.3 Heat Resistance

The heat resistance of each lot of the butyl rubber material shall be determined in accordance with ASTM D573 [14]. Each lot of butyl rubber material shall experience a maximum 10 Shore A durometer hardness increase, a maximum reduction in tensile strength of 25%, and a maximum reduction in ultimate elongation of 25%, when tested at 70 °C.

8.1.5.2.4 Compression Set

The compression set of each lot of the butyl rubber material shall be determined in accordance with Method B of ASTM D395 [15]. After 22 hours at 70 °C, each lot of butyl rubber material shall have a maximum compression set of 25%.

8.1.5.2.5 Cold Temperature Resistance

The cold temperature resistance of each lot of the butyl rubber material shall be determined in accordance with Method A, 9.3.2 of ASTM D2137 [16]. After 3 minutes at -40 °C, each lot of butyl rubber material shall be non-brittle.

8.1.5.2.6 Cold Temperature Resiliency

The cold temperature resiliency of each lot of the butyl rubber material shall be determined in accordance with the TR-10 test of ASTM D1329 [17]. Each lot of butyl rubber material shall be resilient at a test temperature of -50 °C or less.

8.1.6 Shielding Integrity Tests

8.1.6.1 In-Situ Lead Shielding

In-situ or poured lead shielding integrity shall be confirmed via gamma scanning. Two gamma scan techniques are utilized. The primary difference is in the method used to determine acceptance criteria. Both gamma scan techniques are exactly the same in all other respects and are conducted as discussed below.

A gamma probe is used to scan the outer cask surface while a Cobalt-60 or similar gamma source of sufficient strength is positioned within a collimator or guide tube along the centerline of the cask cavity. The cask outer surface is marked with a grid and a chart is made to reflect the gridded surface. The source is first placed on the bottom of the cask cavity while the surface is scanned around its circumference. The source is then moved up the predetermined distance to the next gridline and the circumference scanned again. This sequence is repeated until the entire cask outer surface is scanned. Dose rates are recorded from each grid square by scanning every point in the grid and recording the maximum dose rates in the corresponding grid on the chart. This data then serves as the raw gamma scan results.

The dose rates are evaluated by comparing them to predetermined dose rate values for nominal lead thickness and nominal-less-10% lead thickness. The two methods utilized to determine acceptance criteria for this data are as follows:

The first method, the *Laboratory Calibration Method*, utilizes test blocks of the cask wall made up of lead and steel plates. The test blocks simulate nominal and nominal-less-10% lead thicknesses. The source is placed behind the nominal test block assembly at a distance equal to the inside radius of the cask. The probe is then placed on the outside of the test block assembly and the dose rate recorded. This test sequence is repeated on the nominal-less-10% test block assembly. The resultant dose rate values are then utilized as acceptance criteria for the actual cask gamma scan. Additionally, the expected dose rate values for nominal and reduced (nominal-less-10%) thickness shielding are calculated utilizing attenuation values for steel and lead as correlation verification.

The second, the *Field Calibration Method*, utilizes a specially fabricated test lid that incorporates a holder for various lead and steel plate thicknesses. The fixture is installed onto the cask with the test lid set up to simulate the nominal lead thickness. The source is placed below the test lid, inside the cask, at a distance equal to the inside radius of the cask, along the centerline of the cask body. The dose rate is then measured and recorded. The test lid is adjusted to establish the nominal-less-10% lead thickness configuration. The source is again placed below the test lid at a distance equal to the inside radius of the cask, and the dose rate is again measured and recorded. The value for nominal-less-10% lead thickness is utilized as the maximum acceptable dose rate value for the BRR packaging.

8.1.6.2 Plate or Sheet Lead Shielding

Plate or sheet lead is utilized in the bottom end of the cask body and in the removable shield plug. Ultrasonic examination of each plate or sheet is performed prior to installation to ensure that no voids exist in excess of 10% of the lead plate or sheet thickness.

8.1.7 Thermal Tests

Tests to demonstrate the heat transfer capability of the packaging are not required because the thermal evaluations presented in Chapter 3, *Thermal Evaluation*, are based on well established heat transfer properties and methodologies and demonstrate relatively large thermal margins for all components. As such, the uncertainties in the predicted temperature levels are small. Further, since the thermal modeling incorporates several conservative assumptions, it is expected that the peak temperatures achieved will be less than predicted. See Chapter 3, *Thermal Evaluation*, for further discussions.

Table 8.1-1 – Compressive Strength (psi) Parallel-to-Foam Rise at 65°F to 85°F

Strain	Minimum		Nominal	Maximum	
	Nom. -15%	Nom. -10%		Nom. +10%	Nom. +15%
20%	234	248	275	303	316
40%	252	267	297	327	342
70%	644	682	758	834	872

Table 8.1-2 – Compressive Strength (psi) Perpendicular-to-Foam Rise at 65°F to 85°F

Strain	Minimum		Nominal	Maximum	
	Nom. -15%	Nom. -10%		Nom. +10%	Nom. +15%
20%	225	239	265	292	305
40%	250	265	294	323	338
70%	652	690	767	844	882

8.2 Maintenance Program

This section describes the maintenance program used to ensure continued performance of the BRR packaging.

8.2.1 Structural and Pressure Tests

No structural or pressure tests are necessary to ensure continued performance of the packaging.

8.2.2 Maintenance/Periodic Leakage Rate Tests

This section provides the generalized procedure for maintenance/periodic leakage rate testing of the containment boundary penetrations during routine maintenance, or at the time of seal replacement or sealing area repair. Maintenance leakage rate testing shall follow the guidelines of Section 7.4, *Maintenance Leakage Rate Test*, and Section 7.5, *Periodic Leakage Rate Test*, of ANSI N14.5.

Maintenance/periodic leakage rate testing shall be performed on the main O-ring seal, the vent port sealing washer, and the drain port sealing washer for the containment boundary in accordance with Section 8.2.2.2, *Helium Leakage Rate Testing the Main Containment O-ring Seal*, 8.2.2.3, *Helium Leakage Rate Testing the Drain Port Sealing Washer*, and 8.2.2.4, *Helium Leakage Rate Testing the Vent Port Sealing Washer*. Each leakage rate test shall meet the acceptance criteria delineated in Section 8.2.2.1, *Maintenance/Periodic Leakage Rate Test Acceptance Criteria*.

Prior to leakage rate testing, internal components that are not permanently affixed to the containment boundary, such as shield plug and spent fuel baskets, shall be removed. For ease of leakage rate testing, the interior surfaces of the containment boundary should be thoroughly cleaned.

8.2.2.1 Maintenance/Periodic Leakage Rate Test Acceptance Criteria

Maintenance/periodic leakage rate test acceptance criteria are identical to the criteria delineated in Section 8.1.4.1, *Fabrication Leakage Rate Test Acceptance Criteria*.

8.2.2.2 Helium Leakage Rate Testing the Main Containment O-ring Seal

1. The maintenance/periodic leakage rate test of the BRR package containment O-ring seal integrity shall be performed following the guidelines of Section A.5.4, *Evacuated Envelope – Gas Detector*, of ANSI N14.5.
2. The BRR package shall be assembled with the two O-ring seals installed in the closure lid, and the vent and seal test ports are installed with their associated sealing washers. If not previously tightened, tighten the closure lid bolts to 200 – 240 ft-lb torque. Assembly is as shown in Appendix 1.3.3, *Packaging General Arrangement Drawings*.
3. Utilizing a port tool, attach a vacuum pump and a source of helium gas, in parallel, to the vent port.
4. Close the valve to the source of helium gas and open the valve to the vacuum pump.
5. Utilizing a port tool, rotate the vent port plug to the open position.

BRR Package Safety Analysis Report

6. Evacuate the system to a 90% vacuum or better ($\leq 10\%$ ambient atmospheric pressure). Isolate the vacuum pump from the system.
7. Provide a helium atmosphere inside the evacuated cavity by backfilling with helium gas (99% purity or better) to ambient atmospheric pressure (+1 psi, -0 psi).
8. Utilizing the port tool, rotate the vent port plug to the closed position, and remove the helium-contaminated port tool from the vent port.
9. Install a clean (helium-free) port tool into the seal test port.
10. Utilizing appropriate fittings, attach a helium MSLD to the port tool.
11. Utilizing the port tool, rotate the seal test port plug to the open position.
12. Evacuate the cavity between the containment O-ring seal and the test O-ring seal until the vacuum is sufficient to operate the leak detector per the manufacturer's recommendations.
13. Perform the helium leakage rate test to the requirements of Section 8.2.2.1, *Maintenance/Periodic Leakage Rate Test Acceptance Criteria*. If, after repeated attempts, the BRR package containment O-ring seal fails to pass the leakage rate test, isolate the leak path and, prior to repairing the leak path and repeating the leak test, record on a nonconformance report and disposition prior to final acceptance in accordance with the cognizant quality assurance program.

8.2.2.3 Helium Leakage Rate Testing the Drain Port Sealing Washer

1. The maintenance/periodic leakage rate test of the drain port plug containment sealing washer integrity shall be performed following the guidelines of Section A.5.4, *Evacuated Envelope – Gas Detector*, of ANSI N14.5.
2. The BRR package shall be assembled with the two O-ring seals installed on the closure lid. Ensure the vent and seal test port plugs are installed with their associated sealing washers. Assembly is as shown in Appendix 1.3.3, *Packaging General Arrangement Drawings*.
3. Verify the presence of a helium atmosphere below the vent port plug containment sealing washer, as specified above in Steps 3 – 8 of Section 8.2.2.2, *Helium Leakage Rate Testing the Main Containment O-ring Seal*.
4. Install a port tool into the drain port.
5. Utilizing appropriate fittings, attach a helium MSLD to the port tool.
6. Evacuate the cavity above the drain port plug containment sealing washer until the vacuum is sufficient to operate the leak detector per the manufacturer's recommendations.
7. Perform the helium leakage rate test to the requirements of Section 8.2.2.1, *Maintenance/Periodic Leakage Rate Test Acceptance Criteria*. If, after repeated attempts, the drain port plug containment sealing washer fails to pass the leakage rate test, isolate the leak path and, prior to repairing the leak path and repeating the leak test, record on a nonconformance report and disposition prior to final acceptance in accordance with the cognizant quality assurance program.

8.2.2.4 Helium Leakage Rate Testing the Vent Port Sealing Washer

1. The maintenance/periodic leakage rate test of the vent port plug containment sealing washer integrity shall be performed following the guidelines of Section A.5.4, *Evacuated Envelope – Gas Detector*, of ANSI N14.5.
2. The BRR package shall be assembled with the two O-ring seals installed on the closure lid. Ensure the vent and seal test port plugs are installed with their associated sealing washers. Assembly is as shown in Appendix 1.3.3, *Packaging General Arrangement Drawings*.
3. Verify the presence of a helium atmosphere below the vent port plug containment sealing washer, as specified above in Steps 3 – 8 of Section 8.2.2.2, *Helium Leakage Rate Testing the Main Containment O-ring Seal*.
4. Install a port tool into the vent port.
5. Utilizing appropriate fittings, attach a helium MSLD to the port tool.
6. Evacuate the cavity above the vent port plug containment sealing washer until the vacuum is sufficient to operate the leak detector per the manufacturer's recommendations.
7. Perform the helium leakage rate test to the requirements of Section 8.2.2.1, *Maintenance/Periodic Leakage Rate Test Acceptance Criteria*. If, after repeated attempts, the vent port plug containment sealing washer fails to pass the leakage rate test, isolate the leak path and, prior to repairing the leak path and repeating the leak test, record on a nonconformance report and disposition prior to final acceptance in accordance with the cognizant quality assurance program.

8.2.3 Component and Material Tests

8.2.3.1 Fasteners

All threaded components shall be visually inspected before installation for deformed or stripped threads. Damaged threaded components shall be repaired or replaced prior to further use. The threaded components to be visually inspected include the closure lid bolts, vent port plug, and drain port plug.

8.2.3.2 Sealing Area Routine Inspection and Repair

Before each use and at the time of seal replacement, containment sealing surfaces shall be visually inspected for damage that could impair the sealing capabilities of the packaging. Perform surface finish inspections for the closure lid O-ring grooves, the mating sealing area on the cask body, and the surfaces that mate with the sealing washer in the vent port and drain port. Damage shall be repaired prior to further use (e.g., using emery cloth or other surface finishing techniques) to restore the sealing surfaces to the value specified on the drawings in Appendix 1.3.3, *Packaging General Arrangement Drawings*.

Upon completion of any surface finish repairs, perform a leakage rate test per Section 8.2.2, *Maintenance/Periodic Leakage Rate Tests*.

8.2.3.3 Impact Limiters

Before each use, the impact limiters shall be inspected for tears or perforations in the stainless steel sheets, and for the presence of the fire-consumable plastic plugs. The ball-lock pins that retain the impact limiters shall be visually inspected for any damage that could reduce their effectiveness. Any damage shall be repaired prior to further use.

8.2.3.4 Seals

The containment boundary O-ring seal, the vent port sealing washer, and the drain port sealing washer shall be replaced within the 12-month period prior to shipment or when damaged (whichever is sooner), per the size and material requirements delineated on the drawings in Appendix 1.3.3, *Packaging General Arrangement Drawings*. Following seal replacement and prior to a loaded shipment, the new seals shall be leakage rate tested to the requirements of Section 8.2.2, *Maintenance/Periodic Leakage Rate Tests*.

8.2.4 Thermal Tests

No thermal tests are necessary to ensure continued performance of the BRR packaging.

8.3 Appendix

8.3.1 References

1. Title 10, Code of Federal Regulations, Part 71 (10 CFR 71), Packaging and Transportation of Radioactive Material, 01–01–08 Edition.
2. ANSI/AWS D1.6/D.6M:2007, *Structural Welding Code–Stainless Steel*, American Welding Society (AWS).
3. American Society of Mechanical Engineers (ASME) Boiler and Pressure Vessel Code, Section III, *Rules for Construction of Nuclear Facility Components*, Division 1 – Subsection NB, *Class 1 Components*, and Section V, *Nondestructive Examination*, Article 2, *Radiographic Examination*, 2007 Edition.
4. American Society of Mechanical Engineers (ASME) Boiler and Pressure Vessel Code, Section III, *Rules for Construction of Nuclear Facility Components*, Division 1 – Subsection NB, *Class 1 Components*, and Section V, *Nondestructive Examination*, Article 4, *Ultrasonic Examination Methods for Welds*, 2007 Edition.
5. American Society of Mechanical Engineers (ASME) Boiler and Pressure Vessel Code, Section III, *Rules for Construction of Nuclear Facility Components*, Division 1 – Subsection NB, *Class 1 Components*, and Section V, *Nondestructive Examination*, Article 6, *Liquid Penetrant Examination*, 2007 Edition.
6. American Society of Mechanical Engineers (ASME) Boiler and Pressure Vessel Code, Section III, *Rules for Construction of Nuclear Facility Components*, Division 1 – Subsection NB, *Class 1 Components*, Article NB–6220, 2007 Edition.
7. ANSI N14.5–1997, *American National Standard for Radioactive Materials – Leakage Tests on Packages for Shipment*, American National Standards Institute (ANSI), Inc.
8. EPA Method 300.0, Revision 2.2 (October 1999), *Determination of Inorganic Anions by Ion Chromatography*, U.S. Environmental Protection Agency.
9. ASTM C518–04, *Standard Test Method for Steady–State Thermal Transmission Properties by Means of the Heat Flow Meter Apparatus*, American Society for Testing and Materials (ASTM).
10. ASTM E1269, *Standard Test Method for Determining Specific Heat Capacity by Differential Scanning Calorimetry*, American Society for Testing and Materials (ASTM).
11. ASTM D2000–05, *Standard Classification System for Rubber Products in Automotive Applications*, American Society for Testing and Materials (ASTM).
12. ASTM D2240–05, *Standard Test Method for Rubber Property – Durometer Hardness*, American Society for Testing and Materials (ASTM).
13. ASTM D412–98a(2002)e1, *Standard Test Methods for Vulcanized Rubber and Thermoplastic Rubbers and Thermoplastic Elastomers – Tension*, American Society for Testing and Materials (ASTM).

14. ASTM D573-04, *Standard Test Method for Rubber – Deterioration in an Air Oven*, American Society for Testing and Materials (ASTM).
15. ASTM D395-03, *Standard Test Methods for Rubber Property – Compression Set*, American Society for Testing and Materials (ASTM).
16. ASTM D2137-94(2000), *Standard Test Methods for Rubber Property – Brittleness Point of Flexible Polymers and Coated Fabrics*, American Society for Testing and Materials (ASTM).
17. ASTM D1329-02, *Standard Test Method for Evaluating Rubber Property – Retraction at Lower Temperatures (TR Test)*, American Society for Testing and Materials (ASTM).